frontiers | Research Topics

Acetogens - From the origin of life to biotechnological applications

Edited by
Mirko Basen and Volker Müller

Published in
Frontiers in Microbiology

ISSN 1664-8714
ISBN 978-2-83251-594-5
DOI 10.3389/978-2-83251-594-5

About Frontiers

Frontiers is more than just an open access publisher of scholarly articles: it is a pioneering approach to the world of academia, radically improving the way scholarly research is managed. The grand vision of Frontiers is a world where all people have an equal opportunity to seek, share and generate knowledge. Frontiers provides immediate and permanent online open access to all its publications, but this alone is not enough to realize our grand goals.

Frontiers journal series

The Frontiers journal series is a multi-tier and interdisciplinary set of open-access, online journals, promising a paradigm shift from the current review, selection and dissemination processes in academic publishing. All Frontiers journals are driven by researchers for researchers; therefore, they constitute a service to the scholarly community. At the same time, the *Frontiers journal series* operates on a revolutionary invention, the tiered publishing system, initially addressing specific communities of scholars, and gradually climbing up to broader public understanding, thus serving the interests of the lay society, too.

Dedication to quality

Each Frontiers article is a landmark of the highest quality, thanks to genuinely collaborative interactions between authors and review editors, who include some of the world's best academicians. Research must be certified by peers before entering a stream of knowledge that may eventually reach the public - and shape society; therefore, Frontiers only applies the most rigorous and unbiased reviews. Frontiers revolutionizes research publishing by freely delivering the most outstanding research, evaluated with no bias from both the academic and social point of view. By applying the most advanced information technologies, Frontiers is catapulting scholarly publishing into a new generation.

What are Frontiers Research Topics?

Frontiers Research Topics are very popular trademarks of the *Frontiers journals series*: they are collections of at least ten articles, all centered on a particular subject. With their unique mix of varied contributions from Original Research to Review Articles, Frontiers Research Topics unify the most influential researchers, the latest key findings and historical advances in a hot research area.

Find out more on how to host your own Frontiers Research Topic or contribute to one as an author by contacting the Frontiers editorial office: frontiersin.org/about/contact

Acetogens - From the origin of life to biotechnological applications

Topic editors

Mirko Basen — University of Rostock, Germany

Volker Müller — Goethe University Frankfurt, Germany

Citation

Basen, M., Müller, V., eds. (2023). *Acetogens - From the origin of life to biotechnological applications*. Lausanne: Frontiers Media SA.

doi: 10.3389/978-2-83251-594-5

Table of contents

frontiers | Frontiers in Microbiology

TYPE Editorial
PUBLISHED 20 April 2023
DOI 10.3389/fmicb.2023.1186930

OPEN ACCESS

EDITED BY
Biswarup Mukhopadhyay,
Virginia Tech, United States

REVIEWED BY
Wolfgang Buckel,
University of Marburg, Germany

*CORRESPONDENCE
Mirko Basen
✉ mirko.basen@uni-rostock.de
Volker Müller
✉ vmueller@bio.uni-frankfurt.de

RECEIVED 15 March 2023
ACCEPTED 03 April 2023
PUBLISHED 20 April 2023

CITATION
Basen M and Müller V (2023) Editorial: Acetogens - from the origin of life to biotechnological applications.
Front. Microbiol. 14:1186930.
doi: 10.3389/fmicb.2023.1186930

Editorial: Acetogens - from the origin of life to biotechnological applications

Mirko Basen[1]* and Volker Müller[2]*

[1]Microbiology, Institute of Biological Sciences, University of Rostock, Rostock, Germany, [2]Department of Molecular Microbiology and Bioenergetics, Institute of Molecular Biosciences, Johann Wolfgang Goethe University, Frankfurt, Germany

KEYWORDS

acetogens, origin of life, synthesis gas fermentation, Wood-Ljungdahl pathway, CODH/ACS, acetyl-CoA pathway, CO_2 fixation, hydrogenase

Editorial on the Research Topic
Acetogens - from the origin of life to biotechnological applications

Acetogenic bacteria are a fascinating group of strict anaerobic bacteria characterized by a pathway, the Wood-Ljungdahl pathway (WLP), in which two molecules of carbon dioxide (CO_2) are reduced and condensed to one molecule of acetyl-CoA. This product of CO_2 fixation is the key intermediate in anabolism since it is the precursor of every cellular component in acetogens. Acetyl-CoA also is the key intermediate in catabolism, where it is further converted to acetate via acetyl-phosphate, which is the only ATP-generating reaction of CO_2 reduction. Since one ATP is consumed in the activation of the intermediate formate in the WLP, the overall ATP gain is zero. Therefore, acetogens need an additional way to conserve energy. Hydrogen is used as reductant in the WLP. It is activated by hydrogenases, and subsequently, the electrons are transferred to electron carriers (e.g., NAD^+, ferredoxin, $NADP^+$) that differ from species to species by an array of soluble and membrane-bound transhydrogenases. The reduced electron carriers in turn provide the electrons to the WLP. The secret of energy conservation in acetogens growing on H_2+CO_2 is the excess of reduced ferredoxin (Fd_{red}) from H_2 oxidation, that is in turn re-oxidized by membrane-bound enzymes complexes, the Rnf complex or Ech hydrogenases. These enzymes at the same time provide NADH, NADPH or H_2 to the WLP, and conserve energy by sodium ion or proton translocation. Of the known seven pathways of CO_2 fixation, the WLP has the most favorable ATP balance (one ATP needed for the synthesis of acetyl-CoA) and therefore, is considered the oldest biochemical pathway on Earth, and the starting point for the synthesis of living matter from CO_2 and H_2 or carbon monoxide (CO), gaseous compounds present on Early Earth. Indeed, acetogens grow by acetogenesis from H_2 + CO_2 and they have additional, chemiosmotic mechanisms of energy conservation that ensure a net synthesis of ATP, as mentioned above. CO_2 reduction to acetyl-CoA with H_2 as reductant is also performed by methanogenic archaea in their anabolism, but in catabolism, the methyl group is released as methane. William Martin discusses the possible evolution of methanogenesis and acetogenesis, highlights similarities and differences and critically elaborates on the question whether the WLP indeed was the first CO_2 fixation pathway. Along the same lines, Lemaire et al. discuss on a more biochemical level the different strategies

involved in CO_2 fixation in acetogens and methanogens, with a particular focus on energy conservation mechanisms. They use the editors' favorite terms of "energy extremophiles" for organisms that only conserve a fraction of an ATP per substrate turnover. Indeed, acetogens grow close to the thermodynamic limit of life ($\Delta G_0' < -30$ kJ mol^{-1}). The authors highlight the importance and mechanistics of electron bifurcation in the energy metabolism of both groups. This mechanism links redox homeostasis e.g., the concomitant reduction of $NAD^+$and Fd by electron bifurcating hydrogenase, to energy conservation, since Fd_{red} can be used for chemiosmotic energy conservation, or to drive reactions at low potential such as CO_2 reduction, "saving ATP". Methanogenesis is thermodynamically preferred over acetogenesis and thus methanogens outcompete acetogens during growth on $H_2 + CO_2$. Fu et al. demonstrate a preference of chemolithotrophic acetogenesis at 15°C and 50°C while hydrogenotrophic methanogenesis dominated at 30°C. Under certain conditions, however, acetogens prevail. Fazi et al. report, that in a natural environment with a high CO_2 concentration acetogens are enriched and outcompete methanogens. Methanogens are archaea and acetogens are bacteria, but use the same pathway for CO_2 fixation to acetyl-CoA, the WLP. The long-standing assumption that acetogenesis should also be present in archaea was found to be true in the last decade. Here, Loh et al. discuss the WLP in a bathyarchaeon isolated from the termite hind gut that is different from the bacterial one. Different gas availabilities influence the prevalence of certain acetogens as well. In her review, Philips discusses the different mechanisms of cathodic electron uptake by acetogens in the light of thermodynamics and kinetics of H_2 uptake. She suggests that the ability of acetogens to thrive on cathodes correlates with the ability to maintain low H_2 partial pressures.

The WLP is not only used by acetogens for CO_2 reduction but also for oxidation of more reduced carbon compounds such as formate or methyl groups (derived, for example, from methanol). And some acetogens can even oxidize acetate to CO_2, and produce H_2. One such organisms is *Thermoacetogenium phaeum*. Keller et al. have addressed the enzymes involved in the reverse WLP and the energetics of acetate oxidation; they present interesting data on reverse electron transport in energy coupling, and metabolic schemes for the bioenergetics of acetate oxidation.

The WLP enabled growth of first life forms on Earth and is used by many bacteria for chemolithoautotrophic growth on $H_2 + CO_2$ and by some for chemoorganoheterotrophic growth on acetate. However, the metabolism of acetogens is much more interesting and diverse. They can grow on sugars, carboxylic acids, aldehydes as well as on primary, and secondary alcohols. Many of these substrates can only be oxidized by acetogens because electrons derived from the oxidation are transferred to CO_2 that is used as electron acceptor; under these conditions the WLP acts as an electron sink. This was experimentally demonstrated by Jain et al. They used a novel genetic system to knock out the genes encoding a key enzyme in the WLP in the thermophilic acetogenic bacterium *Thermoanaerobacter kivui* and found that cells are no longer able to grow on organic substrates. Addition of formate restored growth, reinforcing the importance of the WLP for redox balancing. Similarly, Moon et al. show that oxidation of the reduced sugar alcohol mannitol is dependent on external CO_2 as electron acceptor.

The diverse metabolism of acetogens is a consequence of their phylogenetic diversity. Acetogenesis is not a phylogenetic trait but found in many different phylogenetic lineages. Valk et al. found acetate formation form galacturonate by a new species of the family *Lachnospiraceae* using the WLP; however, the metagenome sequences lack a canonical acetyl-CoA synthase/CO dehydrogenase (ACS/CODH) gene cluster and the authors suggest a novel ACS/CODH in this species. Merino et al. isolated the microbiota of a hot spring in Japan and found novel actinobacteria. Based on metabolic pathway predictions, these actinobacteria are anaerobes, capable of glycolysis, dissimilatory nitrate reduction and CO_2 fixation via the WLP. Even within the genus *Moorella*, there are surprises. Redl et al. provide a comprehensive genome analysis of all *Moorella* strains and question the difference of the previously acknowledged strains *Moorella thermoacetica* and *Moorella thermoautotrophica*.

Acetogens are prime candidates as production platforms in a CO_2-based economy, but the products that can be formed from CO_2 may be limited due to energetic constraints. Some acetogens can use electron acceptors other than CO_2 such as nitrate or dimethylsulfoxide, and the simultaneous use of two different electron acceptors may chance carbon flow to more reduced end products. Klask et al. report that addition of nitrate not only enhances growth of *Clostridium ljungdahlii* but also shifts the product spectrum to ethanol. Along those lines, Zhu et al. report that addition of carbon monoxide increases the cellular ATP level and thus enables ethanol formation in *Clostridium ljungdahlii*. The redox potential of CO allows for more ferredoxin reduction, the fuel of chemiosmotic energy conservation, leading to more ATP. CO, however, is highly toxic, and toxicity of CO on a whole cell level is poorly understood. Kang et al. report on the *Adaptive Laboratory Evolution of Eubacterium limosum ATCC 8486 on Carbon Monoxide*. Genome analyses of the evolved strain revealed mutations in the ACS/CODH and when these mutations were generated in the wild type, the same phenotype was observed, highlighting the role of ACS/CODH in CO toxicity. Arantes et al. isolated a novel strain of *Acetobacterium wieringae* able to grow on CO, a trait not common for *Acetobacterium* species. Genome analyses suggest the formate dehydrogenase as reason for the apparent CO insensitivity.

In summary, the 16 publications in this Research Topic are as diverse as the physiological group itself, reflecting the importance of acetogens for understanding fundamental and ancient principles of Life that are as well widespread in nature and of biotechnological interest.

Author contributions

MB and VM wrote and edited the editorial. All authors contributed to the article and approved it for publication.

Acknowledgments

VM and MB are grateful to Deutsche Forschungsgemeinschaft (DFG) for funding. We acknowledge all authors, reviewers, and editors who contributed to the Research Topic.

Conflict of interest

The authors declare that the research was conducted in the absence of any commercial or financial relationships that could be construed as a potential conflict of interest.

Publisher's note

frontiers in Microbiology

ORIGINAL RESEARCH
published: 04 October 2019
doi: 10.3389/fmicb.2019.02238

Microbiomes in Soils Exposed to Naturally High Concentrations of CO_2 (Bossoleto Mofette Tuscany, Italy)

Stefano Fazi[1], Fabrizio Ungaro[2], Stefania Venturi[3,4], Lara Vimercati[5], Carolina Cruz Viggi[1], Silvia Baronti[2], Francesca Ugolini[2], Costanza Calzolari[2], Franco Tassi[3,4], Orlando Vaselli[3,4], Antonio Raschi[2] and Federico Aulenta[1]*

[1] Water Research Institute, National Research Council (IRSA-CNR), Rome, Italy, [2] Institute of BioEconomy – National Research Council (IBE-CNR), Florence, Italy, [3] Institute of Geosciences and Earth Resources, National Research Council (IGG-CNR), Florence, Italy, [4] Department of Earth Sciences, University of Florence, Florence, Italy, [5] Department of Ecology and Evolutionary Biology, University of Colorado Boulder, Boulder, CO, United States

OPEN ACCESS

Edited by:
Mirko Basen, University of Rostock, Germany

Reviewed by:
Roey Angel, Academy of Sciences of the Czech Republic, Czechia
Kristof Brenzinger, Netherlands Institute of Ecology (NIOO-KNAW), Netherlands

***Correspondence:**
Stefano Fazi
fazi@irsa.cnr.it

Specialty section:
This article was submitted to Extreme Microbiology, a section of the journal Frontiers in Microbiology

Received: *22 March 2019*
Accepted: *12 September 2019*
Published: *04 October 2019*

Citation:
Fazi S, Ungaro F, Venturi S, Vimercati L, Cruz Viggi C, Baronti S, Ugolini F, Calzolari C, Tassi F, Vaselli O, Raschi A and Aulenta F (2019) Microbiomes in Soils Exposed to Naturally High Concentrations of CO_2 (Bossoleto Mofette Tuscany, Italy). Front. Microbiol. 10:2238. doi: 10.3389/fmicb.2019.02238

Direct and indirect effects of extremely high geogenic CO_2 levels, commonly occurring in volcanic and hydrothermal environments, on biogeochemical processes in soil are poorly understood. This study investigated a sinkhole in Italy where long-term emissions of thermometamorphic-derived CO_2 are associated with accumulation of carbon in the topsoil and removal of inorganic carbon in low pH environments at the bottom of the sinkhole. The comparison between interstitial soil gasses and those collected in an adjacent bubbling pool and the analysis of the carbon isotopic composition of CO_2 and CH_4 clearly indicated the occurrence of CH_4 oxidation and negligible methanogenesis in soils at the bottom of the sinkhole. Extremely high CO_2 concentrations resulted in higher microbial abundance (up to 4×10^9 cell g^{-1} DW) and a lower microbial diversity by favoring bacteria already reported to be involved in acetogenesis in mofette soils (i.e., Firmicutes, Chloroflexi, and Acidobacteria). Laboratory incubations to test the acetogenic and methanogenic potential clearly showed that all the mofette soil supplied with hydrogen gas displayed a remarkable CO_2 fixation potential, primarily due to the activity of acetogenic microorganisms. By contrast, negligible production of acetate occurred in control tests incubated with the same soils, under identical conditions, without the addition of hydrogen. In this study, we report how changes in diversity and functions of the soil microbial community – induced by high CO_2 concentration – create peculiar biogeochemical profile. CO_2 emission affects carbon cycling through: (i) inhibition of the decomposition of the organic carbon and (ii) promotion of CO_2-fixation via the acetyl-CoA pathway. Sites naturally exposed to extremely high CO_2 levels could potentially represent an untapped source of microorganisms with unique capabilities to catalytically convert CO_2 into valuable organic chemicals and fuels.

Keywords: mofette, CO_2, bacteria, soil, acetogenesis

INTRODUCTION

Natural diffuse gas emitting areas, emanating almost pure volcanic or thermometamorphic CO_2 to the atmosphere, commonly result in CO_2 concentrations (>90% v/v) in the soil markedly higher than typical soil CO_2 contents (ranging from near atmospheric levels to 100-fold higher values and generally <10% v/v; e.g., Amundson and Davidson, 1990; Oh et al., 2005; Schaetzl and Anderson, 2005), which are likely on par with CO_2 concentrations in the Earth's atmosphere when photosynthesis evolved (Beulig et al., 2016).

Soil biogeochemical processes in areas affected by direct and indirect influence of extremely high CO_2 levels are poorly studied although they could potentially have significant ecological, environmental and biotechnological implications. Despite the fact that responses to high CO_2 emissions were mainly studied on plants and on their capacity of carbon fixation, recent investigations clearly pointed out the pivotal role played by naturally occurring microbial communities on the utilization of volcanic CO_2 and its incorporation into the soil organic matter (Beulig et al., 2016). Microbially driven CO_2 utilization is a ubiquitous process in soils, carried out by different microbial metabolic pathways. Under chemical-physical conditions typical of venting spots (e.g., acidic pH and absence of oxygen), strictly anaerobic autotrophic prokaryotes, such as acetogenic bacteria (using hydrogen to reduce carbon dioxide into acetic acid) and hydrogenotrophic methanogenic archaea (using hydrogen to reduce carbon dioxide to methane), were reported to be the dominant members of the soil microbiome (Beulig et al., 2015). Both acetogens and methanogens use molecular hydrogen as electron donor and CO_2 as terminal electron acceptor in their energy metabolism, producing acetate or methane as end-products. Several environmental parameters (e.g., temperature, pH, hydrogen partial pressure) influence competitive interactions between these two trophic groups, ultimately shaping the flow of carbon and electrons, since either acetate or methane can be produced. At low temperatures (i.e., <15°C) and acidic pH (i.e., <5), acetogenic bacteria can outcompete methanogens for hydrogen use, due to their higher growth rates (Cord-Ruwisch et al., 1988; Kotsyurbenko et al., 2001). By contrast, due to their higher affinity for hydrogen, documented by a lower half-saturation Michaelis-Menten constant and lower minimal hydrogen threshold concentration, methanogens can have a competitive advantage over acetogens in environments characterized by a low hydrogen availability (Cord-Ruwisch et al., 1988; Kotsyurbenko et al., 2001). To date, the competition between methanogens and acetogens was primarily investigated in laboratory-scale bioreactors typically operating under highly controlled, steady-state conditions, whereas only limited information is available on its relevance in natural ecosystems.

Sites naturally exposed to extremely high CO_2 levels could potentially represent an untapped source of microorganisms with unique capabilities to catalytically convert CO_2 (at levels as high as those typically occurring in flue gasses emissions of industries or even anaerobic digestion plants) into valuable organic chemicals and fuels. Such microorganisms have recently received attention in the context of microbial electrosynthesis, i.e., a novel technology in which electric current, ideally produced from renewable energy sources (e.g., solar, wind), is supplied to living microorganisms via a cathode to reduce CO_2 to yield industrially relevant products, such as methane, volatile fatty acids, and alcohols (Rabaey and Rozendal, 2010). One of the most attractive aspects of microbial electrosynthesis is the remarkable conversion efficiency (> 80%) of electricity to chemicals (e.g., acetate). On the other hand, the relatively low production rates and costly product separation processes reported so far, still largely challenge the commercial exploitation of the technology.

Microbial processes at extremely high CO_2 soil concentration levels are also relevant within the broader context of carbon capture and storage (CCS) technologies. The urgent need for large-scale solutions to reduce atmospheric levels of greenhouse gasses has indeed prompted the interest toward CO_2 storage in deep saline aquifers or exhausted gas and oil reservoirs. However, before underground CO_2 storage can be implemented at large scale, it is necessary to determine the potential environmental risks associated with the leakage of CO_2 from the reservoir to the near surface environment, to minimize possible environmental impacts. In principle, leakage of large volumes of CO_2 can remarkably affect structures and functions of soil microbial communities, and the overall biogeochemical processes they mediate (McFarland et al., 2013). Sites characterized by CO_2-rich gas discharges represent unique natural analogs of engineered carbon storage sites experiencing steady CO_2 leakage events. These sites could therefore provide the unique opportunity for studying the potential impacts of CO_2 on near-surface ecosystems and groundwater and developing monitoring strategies and possibly preventing CO_2 leakage events.

Natural CO_2-rich reservoirs commonly occur worldwide (Pearce et al., 2004; Pearce, 2006) and their distribution is mainly controlled by Cenozoic rift systems, e.g., East African Rift System (Vaselli et al., 2002; Smets et al., 2010), Tertiary volcanism and hydrothermal and volcanic systems related to both Quaternary to recent volcanic activity and sedimentary basins.

The Bossoleto hydrothermal area at Rapolano (Tuscany, Italy), where fluxes of gas originated by both thermometamorphic processes on limestone and mantle degassing flow up to the surface in correspondence of deep fractures connected to the faults system (Minissale et al., 2002; Guerra and Raschi, 2004; Brogi et al., 2007), represents a typical example of natural CO_2 storage site.

The objective of this study was to investigate the specific interactions between soil CO_2 concentration changes and the microbial community dynamics in terms of structure and function to improve our understanding of microbially mediated C cycle, including the potential impact of CO_2 on near-surface ecosystems. Onsite investigations in natural CO_2 vents were integrated with laboratory experimental approaches in order to: (i) examine the diversity of soil microbial communities (both bacteria and archaea) in natural environments with extremely high CO_2 concentration by 16S rRNA gene sequencing and by *in situ* hybridization approach (CARD-FISH) and (ii) use laboratory incubations to test the acetogenic and methanogenic

potential of the microbial communities differently exposed to natural CO_2 enrichment.

MATERIALS AND METHODS

Site Description and Soil Sampling Strategy

The Bossoleto mofette belongs to the Rapolano hydrothermal area (**Figure 1**). It is a round shaped sinkhole characterized by gaseous emissions primarily consisting of CO_2. In this sinkhole, a CO_2 lake forms every night due to the combination of site topography and CO_2 accumulation. Typically, CO_2 concentrations range from 0.04 to 80% (v/v) over a 24-h period. During the night, the concentrations build up, reaching a maximum of about 80% at around 7:00 AM; afterward (typically after 9:00 AM), a rapid decrease occurs when direct radiation is incident on the bottom of the mofette (Van Gardingen et al., 1995; Kies et al., 2015). Due to infrared absorption by CO_2, the temperature inside the sinkhole can be up to 30°C, i.e., higher than the corresponding air temperature (Kies et al., 2015). Inside the Bossoleto area, plant populations have therefore existed at elevated CO_2 for hundreds of years (Miglietta et al., 1993; Körner and Miglietta, 1994; Raschi et al., 1997), an ample time for the occurrence of evolutionary changes in microorganisms with short generation times (Collins and Bell, 2006).

Soil sampling was carried out at six locations along a geomorphological gradient spanning from the peak of the sink-rim (site 3), to the back-slope (sites 4-5-6) and to the toe-slope at the bottom of the sinkhole (sites 7-8) (**Figure 1**). At each sampling site in the sink-rim and at the back-slope, soil samples were collected from the topsoil (0–10 cm, named "Sur") and the subsurface layers (35–45 cm, hereafter named "Sub"). At the bottom of the sinkhole in sites 7 and 8 the "Sub" samples were collected at 20–30 cm depth. Only at site 7 an additional subsurface sample was collected at −60 cm depth (hereafter named "Deep"). A free-gas sample was collected from one of the bubbling pools (named "BP") located at the bottom of the Bossoleto sinkhole close to the soil gas sampling sites.

Soil Analyses

In three selected sites (site 3, site 4 and site 7 - **Figure 1**), soils were characterized in both the field and laboratory from the surface to a depth of approximately 60 cm depth, for a number of parameters including pH, HCl reaction, micro- and macro-nutrients and C-N content. Soil horizons were identified, described and sampled in the field following standard soil survey protocol (USDA, 2017). The pH was measured in a soil/water suspension (1:2.5 mass ratio). HCl reaction was observed in

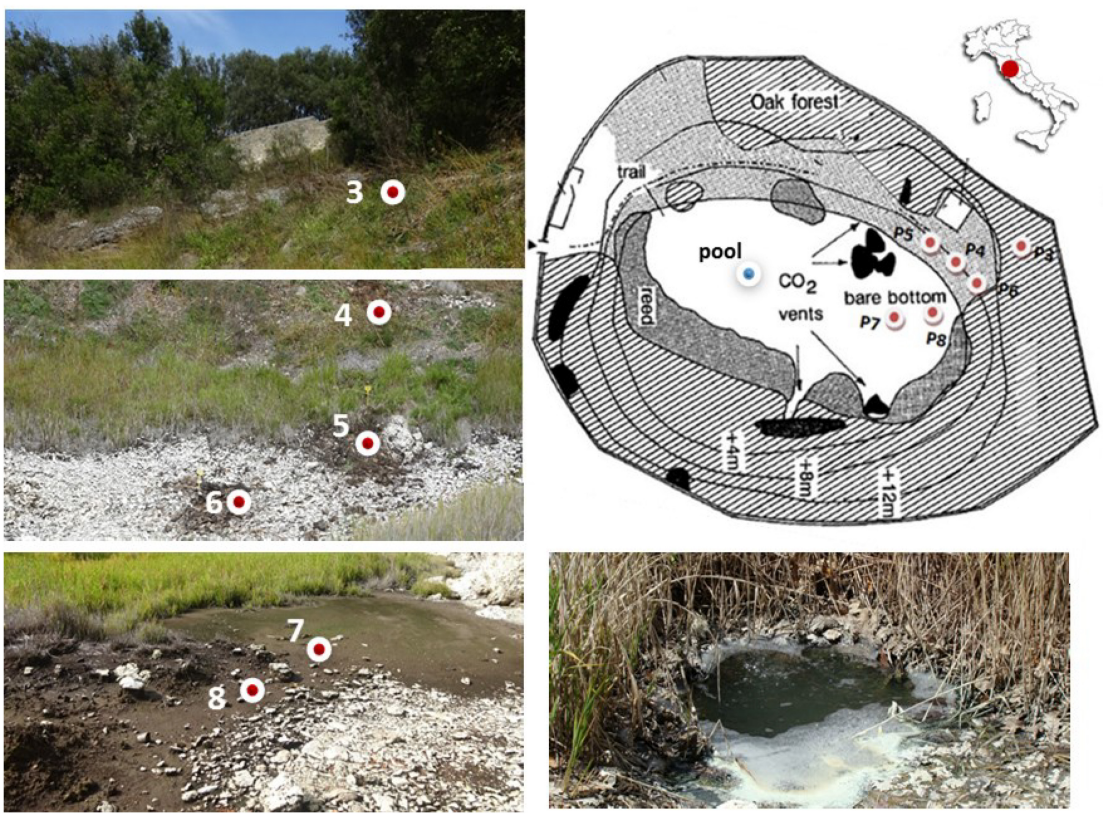

FIGURE 1 | Sampling sites along the geomorphological gradient of the Bossoleto mofette (Rapolano, Tuscany, Italy) (Photos by S. Fazi, Site map modified after Körner and Miglietta, 1994).

the field by using a 1M solution for determining effervescence class as a relative index of the carbonate amount in the soil matrix (USDA, 2017). Soil C and N contents were measured in laboratory using a CHN Elemental Analyzer (Carlo Erba Instruments, mod 1500 series 2). Dry sub-samples were also digested with a microwave oven (CEM, MARSXpress) according to the EPA method 3052 (U. S. Environmental Protection Agency, 2004). The solutions obtained after the mineralization were filtered (0.45 μm PTFE) and diluted. Micro- and macro-nutrients were determined by an ICP optical spectrometer (Varian Inc., Vista MPX) using scandium as internal standard.

Gas Sampling and Analysis

Interstitial soil gasses were sampled from 5 sites (i.e., sites 3, 4, 5, 6 and 8) along vertical profiles from −10 to −50 cm, at regular depth intervals of 10 cm, except at site 8 where the maximum sampling depth was 20 cm, due to the presence of a shallow water table (**Figure 1**). Gas sampling was carried out using a stainless-steel tube (internal diameter: 0.4 cm) as described in Tassi et al. (2015). The gas from the pool was collected in a pre-evacuated glass vial (60 cm^3) equipped with a thorion© valve and containing 20 mL of 4 M NaOH (Giggenbach, 1975). During sampling, CO_2 and H_2S dissolved in the alkaline solution, whereas non-condensable gasses (N_2, O_2, Ar, CH_4, C_2H_6) were stored in the flask headspace. A glass vial for the analysis of $^{13}C/^{12}C$ ratios in CO_2 ($\delta^{13}C$-CO_2) was also collected.

Inorganic gasses in both vials (CO_2, H_2S, N_2 and O_2 + Ar) and the flask headspace (N_2 and O_2 + Ar) were analyzed using a Shimadzu 15A gas chromatograph (GC) and a Thermo Focus gas chromatograph, was used to separate the Ar and O_2 peaks, as described in Tassi et al. (2015). CH_4 and C_2H_6 were analyzed using a Shimadzu 14A gas chromatograph equipped with flame ionization detector (FID) and a 10 m stainless steel column packed with 80/100 mesh Chromosorb PAW coated with 23% SP 1700 as described in Tassi et al. (2015). The $\delta^{13}C$-CO_2 values were measured by a Finnigan MAT 252 mass spectrometer after the extraction and purification of the gas mixtures (Evans et al., 1998; Vaselli et al., 2006). The $\delta^{13}C$-CH_4 were analyzed using MS (Varian MAT 250) according to the procedure reported by Schoell (1980).

Bacteria and Archaea Abundance and Diversity

The total bacteria and archaea cell abundances were assessed by Catalyzed Reported Deposition-Fluorescence *in situ* Hybridization (CARD-FISH) following extraction and detection procedures described elsewhere (Fazi et al., 2007; Amalfitano and Fazi, 2008). Subsamples of the purified cell suspension (1 mL) were filtered onto 0.2 μm-pore size polycarbonate membranes (47 mm diameter) and frozen at −20°C until analysis. Filter sections were then cut and hybridized in duplicate by rRNA-target HRP-labeled probes (Biomers, Ulm, Germany) targeting most Bacteria (EUB338, EUB338-II, EUB338- III) and Archaea (ARCH 915). The stained cells were quantified using an epifluorescence microscope (Leica, DM LB 30). At least 300 cells were counted in each filter section. Data are expressed as a percentage of total DAPI stained prokaryotes cells (%) and as abundance (cells/g of DW).

Sequencing approaches were employed to study microbial diversity across the environmental gradient. Samples of fresh soil from each site at two depths (three in site 7) were frozen directly in the field in dry ice and kept at −80°C until DNA extraction. DNA was extracted from each sample using the approach described in Fierer et al. (2012). To determine the diversity and composition of the bacterial communities, the protocol described in Leff et al. (2015) for amplicon 16S rRNA gene sequencing was used. Specifically, the 16S rRNA gene from isolated DNA was PCR-amplified using the 515f/806r primer pair. To prepare amplicons for sequencing, amplicon purification and normalization was done with Invitrogen SequalPrep Normalization Kit (Invitrogen Inc., CA, United States). Amplicons were combined into a single pool and sequenced using the Illumina MiSeq platform (BioFrontiers Institute, Boulder, CO, United States) using pair-end 2 × 150 bp chemistry.

Data Processing and Statistical Analysis

Forward-oriented sequences were demultiplexed, quality filtered and processed using the Quantitative Insights into Microbial Ecology (QIIME) v1.9.1 bioinformatics package (Caporaso et al., 2010b). 16S rRNA gene paired-end reads were joined and singletons were excluded from further analysis and sequences with >97% identity were clustered into an OTU via UCLUST (Edgar, 2010). Representative sequences for each OTU were chosen for classification and the Greengenes 13.5 database (DeSantis et al., 2006) was employed to assign taxonomy identification to each single OTU. Based on this classification, all mitochondrial and chloroplast OTUs based on this classification were removed from the bacterial data set. The taxonomic assignments of the top OTUs from each treatment were verified by using BLAST to search NCBI, and refined as needed. Sequences were aligned with the PyNAST (Caporaso et al., 2010a) and a phylogeny was built with the FastTree algorithm (Price et al., 2009). OTU tables were rarefied to the lowest number of sequences in the lowest populated sample to make more robust comparisons and were used to assess alpha diversity and relative abundance of all taxa. A community-level Bray-Curtis distance matrix was generated and analyzed with a permutational multivariate analysis of variance (PERMANOVA) using an ADONIS model (Oksanen et al., 2013) to partition the variance in community composition. Principal Coordinate Analysis (PCoA) ordination was constructed based on the basis of the Bray-Curtis distance matrix and Hellinger transformed in order to visualize differences in community composition between low and high CO_2 concentrations. Similarity percentage analysis (SIMPER) was used to determine the OTUs that contributed most to the observed dissimilarity between communities of low and high CO_2 concentrations. All statistical tests, unless otherwise stated, were performed using the "vegan" R package (Oksanen et al., 2013).

The chemical variables were incorporated into a Non-metric MultiDimensional Scaling (NMDS) ordination plot in order to graphically synthesize the Bray-Curtis dissimilarity among

samples. Chemical and microbial data were then projected onto the NMDS ordination using a vector-fitting procedure, in which the length of the arrow is proportional to the correlation between NMDS axes and each variable. This method allowed determining the variation pattern of each projected variable discriminating the samples (Foulquier et al., 2013; Amalfitano et al., 2014).

The 16S rRNA gene sequences from Illumina MiSeq libraries from this study were deposited in the SRA (Short Read Archive) database under Bioproject ID PRJNA548940.

Assessment of the Acetogenic and Methanogenic Potential

To evaluate the acetogenic and methanogenic potential of the mofette microbial communities, a set of anoxic incubations was set up. Incubations were prepared in 120 mL (total volume) serum bottles, incubated statically, in the dark, at room temperature (20–25°C). Each bottle contained about 10 g (wet weight) of mofette soil (site 7sup, 7sub, 7deep, and site 3sub) and 40 mL of anaerobic mineral medium. The medium contained the following components: NH_4Cl (0.5 g/L), $MgCl_2 \times 6H_2O$ (0.1 g/L), K_2HPO_4 (0.4 g/L), and $CaCl_2 \times 2H_2O$ (0.05 g/L). Upon preparation, all bottles were sealed with Teflon-faced butyl rubber stoppers, flushed with a N_2/CO_2 (70:30 v/v) gas mixture. H_2 was added to half of the bottles to reach a final headspace concentration of 60:15 (v/v) H_2:CO_2. Upon setup, the pH value was in the range 5.5–6.0, hence close to typical pH values measured in the field.

Once all the bottles completely converted the initial dose of H_2 (1st feeding cycle), they were flushed with the N_2/CO_2 gas mixture and then re-spiked with another dose of H_2 (2nd feeding cycle). At the end of the first feeding cycle, the liquid volume cumulatively removed during incubation (i.e., for organic acids and pH analyses) was replaced with freshly prepared anaerobic medium. Each incubation experiment was set up in duplicate to ensure reproducibility.

Organic acids were analyzed by injecting 1 μL of filtered (0.22 μm porosity) liquid sample into a PerkinElmer Auto System gas-chromatograph equipped with a Flame Ionization Detector (FID). Gasses (H_2, CH_4 and CO_2) were analyzed by injecting 50 μL of headspace sample into a Perkin-Elmer Auto System gas-chromatograph, equipped with a Thermal Conductivity Detector (TCD).

The percentage of reducing equivalents from the electron donor (i.e., H_2) used in acetogenesis or methanogenesis was calculated at the end of each incubation from the measured levels of acetate and methane formed and the electron donor consumed. Molar equivalents factors used were: 8 eq/mol for acetate, 8 eq/mo1 for methane, and 2 eq/mol for hydrogen.

RESULTS

Soil Characterization and Geochemical Analysis

Soils from the Bossoleto sinkhole represent a toposequence with some typical aspects of soil formation in semiarid Mediterranean environments developed on travertine parent materials. Shallow skeletal soils are more developed on the summit of the sinkhole (site 3; 270 m a.s.l.) under oak forest (*Quercus ilex* L.*; Quercus pubescens* L.*; Fraxinus ornus* L.) and scanty herbaceous vegetation cover (*Cyclamen repandum* Sibth & Sm.; *Festuca inops* De Not., *Teucrium chamaedrys* L.). Under these conditions, a thick litter develops and the soil is characterized by the presence of a Bk horizon (i.e., with accumulation of calcium carbonate). The horizons sequence observed in the field is O-A-Bk-BC-Cr (**Figure 2**) and the soil is classified as Typic Calcixerept according to Soil Taxonomy (USDA, 2010) or as Skeletic Haplic Calcisol (IUSS Working Group Wrb, 2015). Soils along the slope are shallower and less developed: in the back-slope position (site 4; 264 m a.s.l) with uneven grass cover (*Sanguisorba minor* Scop., *Plantago lanceolata* L., *Centaurea deusta* Ten. subsp. deusta), water erosion is more active and only a less developed transitional BC horizon is observed along the soil profile. The horizons sequence observed in the field is O-A-BC-Cr and the soil is classified as (Lithic) Typic Xerorthent (USDA, 2010) or as a Skeletic Regosol (humic) (IUSS Working Group Wrb, 2015). The bottom of the sinkhole (site 7; 258 m a.s.l.) has scant herbaceous cover (*Agrostis stolonifera* L., *Phragmites australis* (Cav.) Trin. ex Steud.). Soil profile is formed on colluvial materials whose development is strongly affected by: (i) the rate of delivery of organic and mineral materials from the slopes of the sinkhole, (ii) the presence of high CO_2 concentrations and (iii) the shallow fluctuating groundwater. Under these conditions, organic matter accumulates at the top of the soil profile (Oa and O organic topsoil horizons) and strongly anaerobic conditions lead to the formation of deeper Cg horizons with undecomposed root materials. The soil is classified as Thapto-Histic Fluvaquents (USDA, 2010) or Histic Gleyic Fluvisol (IUSS Working Group Wrb, 2015). Soil pH (field, lab and HCl reaction) exhibited a clear decrease along the toposequence (range 4.68–7.60) due to increasing CO_2 concentrations in the pedosphere (along soil depth and along the toposequence), which resulted in the complete exploitation of the soil buffer capacity despite the calcareous nature of the parent material (**Table 1**). In terms of macro-nutrients such as C and N, the soil in site 3 showed intermediate content of N with a positive trend toward the bottom of the sinkhole (range 0.08–1.46%). Sites 3 and 7 also recorded high content of total C (range 2.31–16.61%), with site 5 showing the highest C:N ratio (range 10.32–149.02).

In terms of micro- and macro-nutrients (**Supplementary Table 1**), a loss of Ca (−93%) and other bases (e.g., Mg, Li) was observed in site 7 with respect to both sites 3 and 4. This was coupled with an increase in total P (+ 604%) and K (+ 113%) and Cu, Pb, Fe, Al and other microelements, likely because of the effect of the pH on element mobility.

Chemical Composition of Gasses and δ^{13}C-CO_2 and δ^{13}C-CH_4 Values

The chemical composition (CO_2, N_2, H_2S, O_2, Ar in mmol/mol; CH_4 and C_2H_6 in μmol/mol) and the δ^{13}C-CO_2 and δ^{13}C-CH_4 (in ‰ vs. V-PDB) of both soil gasses and bubbling pool is reported in **Table 2**. Interstitial soil gasses from profiles at

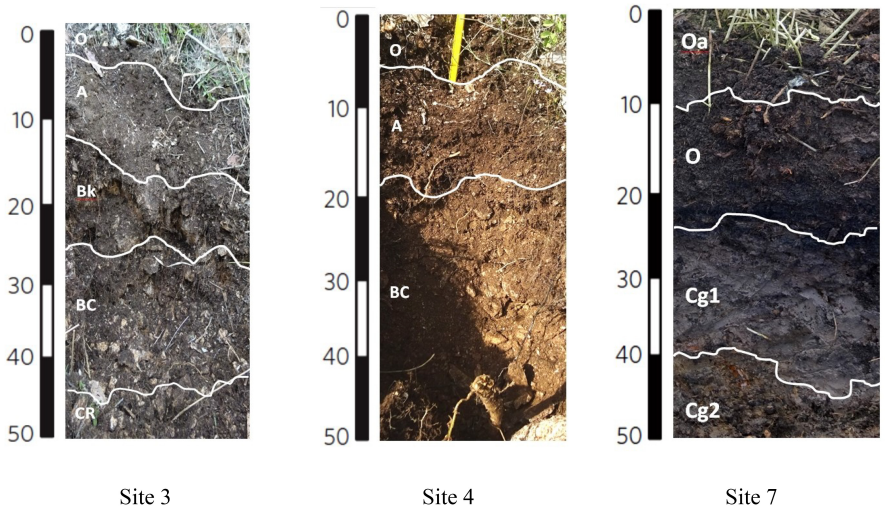

FIGURE 2 | Soil profiles for sites 3, 4 and 7. The sequence of soil horizons along each soil profile is reported. Capital letters designate the master horizons and layers (O, horizons or layers dominated by organic soil materials; A, mineral soil horizon or layers at the soil surface or below an O horizon; B, subsurface mineral horizons that typically formed below an A or O horizon; C, subsurface mineral horizons or layers, excluding strongly cemented and harder bedrock, that are little affected by pedogenic processes and lack properties of O, A, and B horizons; R, strongly cemented to indurated bedrock). Two capital-letter symbols are used for transitional horizons, dominated by properties of one master horizon but have subordinate properties of another. Lowercase letters are used as suffixes to indicate specific characteristics of master horizons and layer (a, highly decomposed organic material; k, accumulation of carbonates; g, strong gleying due to saturation with stagnant water). Arabic numbers as suffixes indicate vertical subdivisions within a horizon or layer.

sites 3, 4 and 5 were mainly consisting of N_2 (from 744 to 821 mmol/mol) with variable concentrations of O_2 (from 19 to 183 mmol/mol), CO_2 (from 9.0 to 226 mmol/mol) and minor amounts of Ar (from 10 to 13 mmol/mol). Methane and C_2H_6 concentrations were up to 16 and 6.1 μmol/mol, respectively, whereas no H_2S was detected (<0.05 mmol/mol). Sites 3, 4 and 5 were hereafter named LC: Low CO_2 concentration sites.

The soil gasses from profile at site 6 had CO_2 and N_2 at comparable concentrations (up to 601 and 730 mmol/mol, respectively), relatively low O_2 (≤27 mmol/mol), with Ar from 6.5 to 14 mmol/mol, and CH_4 and C_2H_6 concentrations (up to 28 and 11 μmol/mol, respectively) slightly higher than those measured at sites 3, 4 and 5. At the maximum depth of profile at site 6, CO_2 reached a concentration of 730 mmol/mol and H_2S was detected (0.10 mmol/mol). Soil gasses from profile at sites 7-8 were characterized by dominant CO_2 (up to 807 mmol/mol), whereas N_2 and Ar concentrations were up to 190 and 4.9 mmol/mol, respectively. Oxygen was below the detection limit (<0.5 mmol/mol), H_2S (up to 0.18 mmol/mol) and CH_4 and C_2H_6 were up to 41 and 4.5 μmol/mol. Sites 6sub, 7 and 8 were hereafter named HC: High CO_2 concentration sites.

TABLE 1 | pH, HCl reaction and C-N content in soil from Bossoleto mofette.

		pH	HCl reaction	N%	C%	C/N
Site 3	Sup	7.32	Strong	0.52	14.23	27.61
	Sub	7.31	Strong	0.25	10.98	44.03
Site 4	Sup	7.31	Strong	0.75	11.69	15.50
	Sub	7.60	Strong	0.29	10.14	35.46
Site 5	Sub	7.14	Strong	0.08	11.89	149.02
Site 6	Sub	6.68	Strong	0.49	12.88	26.33
Site 7	Sup	4.68	None	1.46	15.11	10.32
	Sub	5.76	None	0.16	2.31	14.54
	Deep	5.83	None	0.25	4.87	19.41
Site 8	Sup	5.36	None	1.38	16.61	12.05
	Sub	5.76	None	0.61	7.77	12.68

The bubbling gas was marked by the highest CO_2 (983 mmol/mol), H_2S (0.25 mmol/mol), CH_4 (125μmol/mol) and C_2H_6 (7.9 μmol/mol) concentrations and the lowest N_2 and Ar contents (16 and 1.1 mmol/mol, respectively). The chemical composition of the interstitial soil gasses collected at 10 and 20 cm depth at site 8 resembled that of the gas sample collected at the bubbling pool (BP) (**Figure 3**). The N_2 vs. CH_4 and CO_2 binary diagrams (**Figure 4**) show that the interstitial gasses from sites 3 and 4 and those from 10 to 40 cm depth in site 5 were characterized by N_2 concentrations higher than those expected for air-BP mixing. The interstitial gas sample from site 5 and those collected at 10–30 cm depth from site 6 showed CO_2 content higher with respect to the air-BP mixing curves. The interstitial soil gasses from sites 6 at depth >30 cm and 8 were depleted in CH_4 with respect to the air-BP mixing line (**Figure 4**).

The $\delta^{13}C$-CO_2 values ranged from −11.5 to −6.06‰ vs. V-PDB, showing increasing trends from profiles at site 3 to site 8 and at increasing depth along each profile. The $\delta^{13}C$-CO_2 value of the bubbling gas (−6.41‰ vs. V-PDB) was similar to those of profile at site 8. The $\delta^{13}C$-CH_4 value measured in profile 6 at

TABLE 2 | Chemical and isotopic composition of interstitial soil gasses and bubbling gasses (pool) from Bossoleto mofette.

Site	Depth	CO_2	H_2S	N_2	O_2	Ar	CH_4	C_2H_6	$\delta^{13}C$-CO_2	$\delta^{13}C$-CH_4
	cm	mmol/mol	mmol/mol	mmol/mol	mmol/mol	mmol/mol	μmol/mol	μmol/mol	‰ vs. V-PDB	‰ vs. V-PDB
Slope peak of the sink-rim										
3	10	43	<0.05	799	147	11	0.5	0.5	−10.79	Nd
	20	67	<0.05	788	133	11	1.4	1.2	−10.11	nd
	30	101	<0.05	805	84	11	1.9	2.0	−11.50	nd
	40	143	<0.05	802	45	10	3.0	2.7	−8.50	nd
	50	183	<0.05	783	24	11	5.0	2.9	−7.82	nd
Back-slope										
4	10	9	<0.05	798	183	10	<0.1	< 0.1	nd	nd
	20	11	<0.05	812	166	11	<0.1	< 0.1	−10.45	nd
	30	13	<0.05	820	155	12	<0.1	< 0.1	nd	nd
	40	17	<0.05	821	149	13	0.5	0.5	−11.87	nd
	50	18	<0.05	821	148	13	1.1	1.0	nd	nd
5	10	64	<0.05	820	106	10	1.6	2.0	−8.64	nd
	20	96	<0.05	804	89	12	2.4	2.0	−7.64	nd
	30	137	<0.05	814	38	11	5.0	4.4	−7.65	nd
	40	173	<0.05	791	25	12	11	5.9	−7.45	nd
	50	226	<0.05	744	19	12	16	6.1	−7.13	nd
6	10	397	<0.05	568	27	8.4	21	9.0	−7.10	nd
	20	404	<0.05	567	20	8.9	26	9.5	−7.83	−23.3
	30	373	<0.05	601	12	14	28	11	−8.05	nd
	40	670	<0.05	322	<0.5	8.3	18	6.3	−7.20	nd
	50	730	0.10	264	<0.5	6.5	19	5.9	−8.14	nd
Toe-slope at the bottom of the sinkhole										
7-8	10	805	0.11	190	<0.5	4.9	41	4.5	−6.06	nd
	20	807	0.18	188	<0.5	4.6	41	4.2	−6.38	−31.7
Pool		983	0.25	16	<0.5	1.1	125	7.9	−6.41	−38.5

20 cm depth was −23.3‰ vs. V-PDB, whereas those at site 8 (at 20 cm depth) and the bubbling gas were −31.7 and −38.5‰ vs. V-PDB, respectively.

Bacterial and Archaea Abundance and Diversity

The average prokaryotic abundance showed higher values in the surface ($2.7 \times 10^9 \pm 1.3 \times 10^9$ cell/g DW) than in the subsurface ($1.2 \times 10^9 \pm 3.7 \times 10^8$ cell/g DW) samples, with an overall increase passing from site 3 to sites 7 and 8. The highest abundances were observed at the surface from sites 7 and 8 ($4.5 \times 10^9 \pm 1.2 \times 10^9$ cell/g DW and $3.9 \times 10^9 \pm 7.6 \times 10^7$ cell/g DW, respectively). The deep sample at site 7 showed an average abundance of $1.3 \times 10^9 \pm 1.3 \times 10^8$ cell/g DW (**Figure 5**). Overall, Bacteria (probe EUB338 I-III) represented about 80% of total DAPI stained cells. Archaea (probe ARCH 915) were on average 6% of total cells, with the highest values (12%) measured at site 8 subsurface samples.

The number of OTUs retrieved in each sample was in the range of 1000–1700 and 2200–2600 at sites with high (HC) and low (LC) CO_2 concentration, respectively. Rarefaction curves show that the LC samples harbor significantly higher diversity than HC samples, regardless of rarefaction depth and the two communities were significantly different from each other (PERMANOVA $p = 0.002$, $R^2 = 0.38$) (**Supplementary Figure 1**).

The relative abundances of the 13 dominant phyla are shown in **Figure 6**, revealing the main differences between microbial communities inhabiting soils at the two CO_2 concentration levels. Overall, the NMDS ordination plots, showing the variation patterns of the chemical and microbiological variables are reported in **Figure 7**. Proteobacteria dominated the community in all sampling sites with members within the Xanthomonadaceae (Gammaproteobacteria), being the most abundant family in HC soils. The closest un-cultured match for the most abundant Xanthomonadaceae phylotype is from a sludge reactor for toluene degradation (LC336110, 100% identity).

The second most abundant Proteobacteria in HC samples was within the genus *Geobacter*, whose closest environmental match was from paddy soils (MG101255, 100% identity). This anaerobic genus was already reported in similar environments exposed to high CO_2 fluxes (Oppermann et al., 2010). Acidobacteria, Actinobacteria, Planctomycetes and Verrucomicrobia showed significantly higher abundances in LC samples. It is worth noting that Chloroflexi, Firmicutes, WPS2 and Cyanobacteria were more abundant in HC samples. Moreover, HC samples showed a higher percentage of undefined sequences when compared to LC samples. The closest environmental match in the NCBI database of the most abundant Unclassified OTU

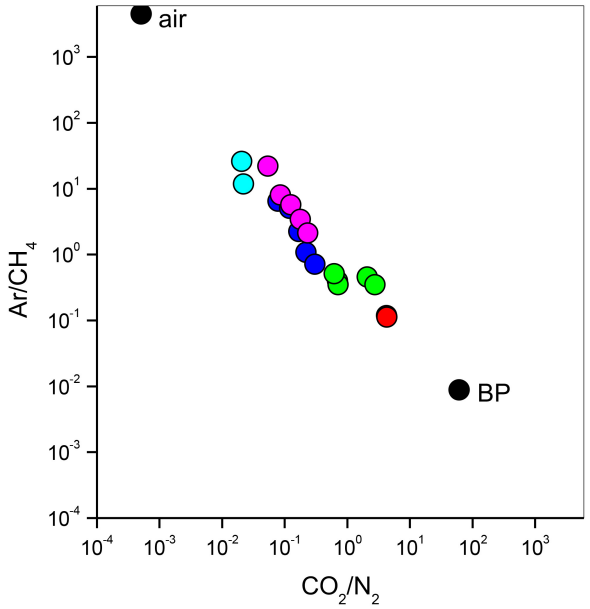

FIGURE 3 | Ar/CH_4 vs. CO_2/N_2 binary diagram for the interstitial soil gasses from site 3 (magenta circles), site 4 (cyan circles), site 5 (blue circles), site 6 (green circles) and site 8 (red circles). Air and gas from the bubbling pool (BP) are also reported (black circles).

in HC samples is an OTU retrieved in an acid mine drainage (HQ322903, 96% identity).

Chloroflexi classes, Ktedonobacteria and Anaerolineae were abundant only in HC samples. The most abundant Ktedonobacteria OTU, within the Thermogemmatisporaceae family, had a 97% match to an uncultured bacterium from Antarctic soils (EF221335, 97% identity), while the most abundant Anaerolineae phylotype retrieved from HC samples had closest matches with uncultured bacteria from marine sediments (MG637761, 97% identity) and from subfloor sediments in methane hydrate fields (AB540881, 97% identity). Chloroflexi class Dehalococcoidia was only retrieved in one of the HC samples (7deep) and had closest matches with uncultured bacteria from a groundwater aquifer (KC606861, 97% identity) and from sediment from high arsenic groundwater (KF632458, 97% identity).

Thaumarcheota were abundant in all sites except site 3. They made up ∼6% of total community in both LC and HC samples. Two different orders of Thaumarcheota were found in LC and HC samples, respectively: (i) Nitrosospherales (this group also showed to be more abundant in "reference soils (low CO_2)" (Beulig et al., 2015) (*N. gargensis* and Candidatus Nitrososphaera) and (ii) Cenarcheales (SAGMA-X). The most abundant Nitrosospherales phylotype retrieved from LC samples had a closest match with uncultured bacteria from paddy soils (KP328055, 100% identity), while the closest environmental matches for the most abundant Thaumarchaeota phylotypes in HC samples were from bottled mineral water (JX458345, 99% identity), subtropical forest soil (MH016249, 100% identity) and landfill leachate (KM870444, 100% identity). Our results showed the nearly complete absence from soils of Methanogens that were found only in the most extreme conditions (1.5% only in one HC sample 7deep, data not shown).

Hierarchical clustering for the dataset was generated on the basis of a distance matrix calculated by using the Bray-Curtis distance (**Supplementary Figure 2A**). This clustering shows a clear profile of the core microbiome with soil samples at high (HC: sites 3-4-5) and low (LC: sites 6sub-7-8) CO_2 concentrations in different groups. HC samples showed a more dissimilar composition (based on counts on each sample) among each other than the LC samples, as also shown by PCoA plot (**Supplementary Figure 2B**). The top 10 OTUs that explained the most variance between low and high CO_2 concentrations according to SIMPER analysis are reported in **Table 3** and the mean dissimilarity of the bacterial communities between them was 95%.

Acetogenic Potential

All the mofette soil incubations supplied with hydrogen gas displayed a remarkable CO_2 fixation potential, primarily due to the activity of acetogenic (i.e., acetate-producing) microorganisms originally present in the soil. By contrast, negligible production of acetate occurred in control tests incubated with the same soils, under identical conditions, without addition of hydrogen gas. As an example, **Figure 8** shows the time course of hydrogen, carbon dioxide, and acetate in a representative incubation experiment setup with soil taken from site 7. Hydrogen and CO_2 utilization, as well as acetate formation, commenced without any significant lag phase. Upon depletion of hydrogen (on day 28), both acetate production and CO_2 consumption almost ceased. These latter processes, however, resumed as soon as H_2 was re-spiked to the bottles (on day 40). Throughout the entire incubation period, the pH remained in the range of 5.5–6.5 and negligible formation of methane and/or of other reduced organic metabolites was detected. **Figure 9A** compares the observed H_2-dependent specific acetate formation rates for the different mofette soils. Unexpectedly, the highest values, up to 6.7 ± 0.9 μmol of acetate produced per g of soil (dry weight) per day, were observed in the soil exposed to relatively lower CO_2 levels. This finding may be due to the lower natural pH of soils exposed to higher CO_2 levels, which may have resulted in a lower abundance of acetogenic microorganisms. By contrast, the mofette soils exposed to remarkably higher CO_2 levels displayed a lower and similar acetogenic formation rate, ranging from 1.8 to 3.4 μmol/g · d. A mass balance indicated that acetate production accounted for 50–80% of consumed H_2 (**Figure 9B**), possibly suggesting that other (still not identified) anaerobic H_2 consuming processes such as sulfate reduction occurred during incubations.

DISCUSSION

Origin of Interstitial Gases

The interstitial soil gasses collected at 10 and 20 cm depth at site 8 showed chemical composition similar to that recorded for the gas sample collected from the bubbling pool (BP). The latter, basically

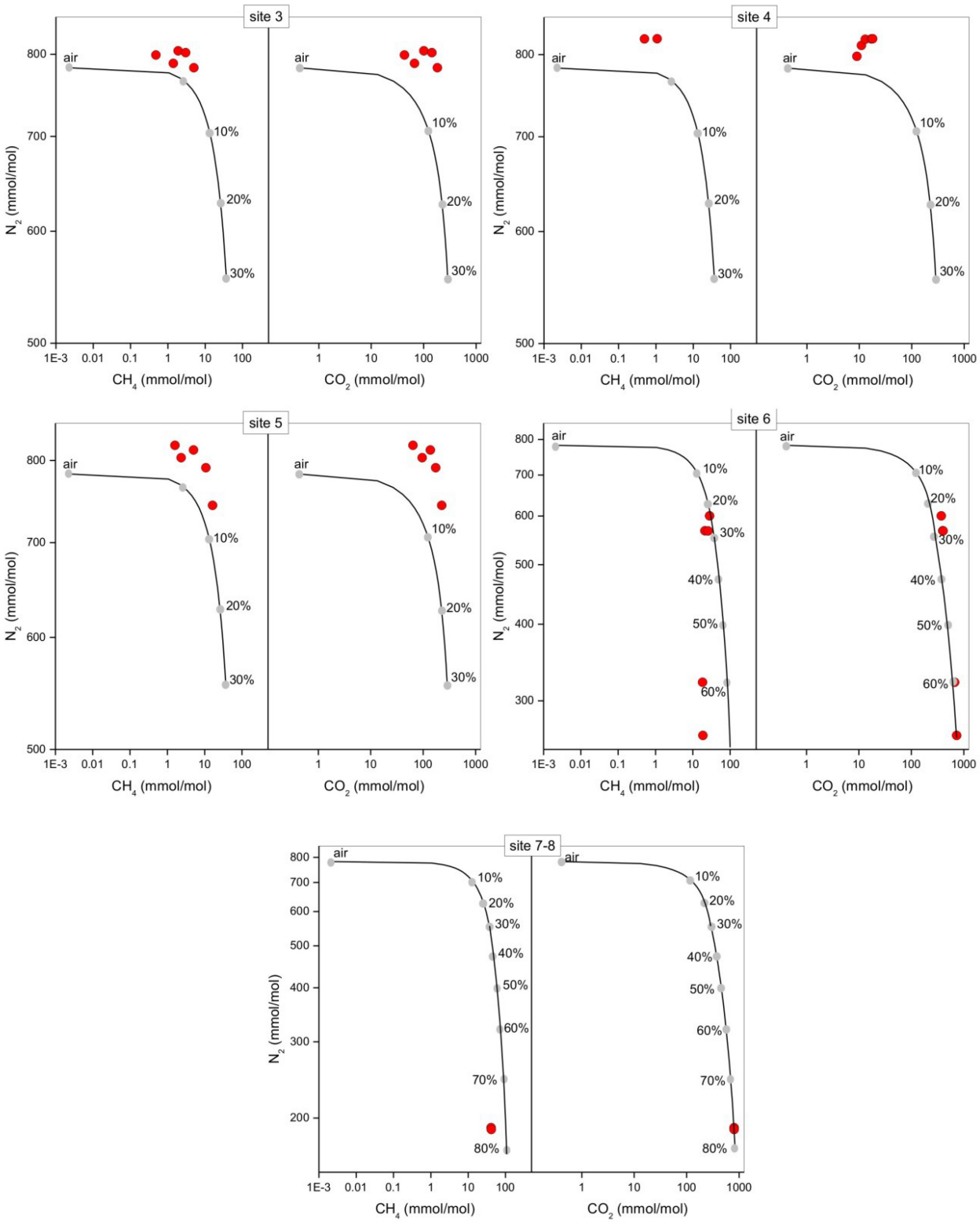

FIGURE 4 | N_2 vs. CH_4 and N_2 vs. CO_2 binary diagrams for the interstitial soil gasses (red circles) from each sampling site at the different depths (data are shown in **Table 2**). The expected composition of soil gasses resulting from mixing of air with variable amounts of geogenic gas. The geogenic gas characteristics were obtained by analyzing a free-gas sample collected from one of the bubbling pools (named "BP"). The expected composition of soil gasses then obtained using a simple mass balance modeling approach, is shown (black line and gray dots). The fraction (in percentage) of the deep gas involved in the mixture is also reported.

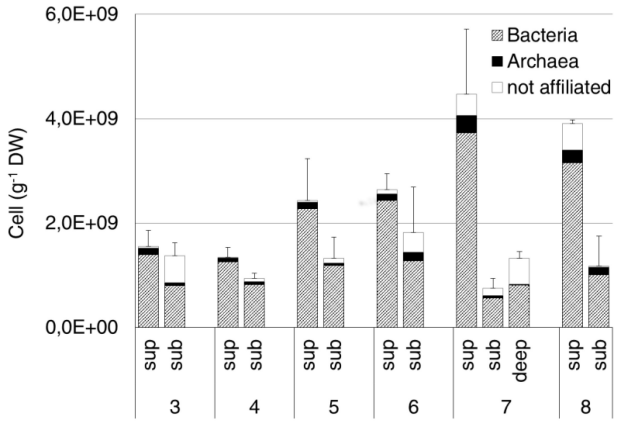

FIGURE 5 | Bacteria and Archaea abundance estimated by CARD-FISH in the original soil samples. Data are expressed as number of cells per gram of dry weight (DW). Cells were hybridized by the specific probes EUB338 I-III and ARCH915 for Bacteria and Archaea, respectively. Error bars represent the standard deviation.

dominated by CO_2 produced at depth by thermometamorphic reactions on carbonates and partially originating from mantle degassing, is to be considered typical of the thermal fluid emission of this area (e.g., Minissale et al., 2002). A moderate increase of the atmospheric inert gasses (N_2 and Ar), characterizing the interstitial soil gasses with respect to the gas sample from the pool, can likely be related to soil permeability that allowed a significant air contamination of the deep-originated gasses. The atmospheric gas concentrations showed a significant decrease in interstitial gasses from the sites located at decreasing distance from the crater bottom, since air in the soil was counteracted by the flux of the deep-originated gasses, which achieved their highest concentrations in correspondence of the bubbling pool area (**Figure 1**). Hence, the chemical composition of the interstitial gasses was produced, at a first approximation, by air dilution of the BP-type gas (**Figure 3**). The consumption of O_2, a process that typically occurs as fluids circulate underground where reducing conditions are dominating, may have produced an indirect N_2 increase with respect to that in the air for those samples having a low deep gas contribution such as 3, 4 and 5 (10–40 cm) (**Figure 4**). The interstitial gas sample from site 5 and those collected at 10–30 cm depth from site 6 show CO_2 concentrations higher with respect to the curves (Fig. 4) that were constructed considering a simple binary mixing between air and a gas phase having the BP composition. As suggested to explain the indirect N_2 increase, such a CO_2-excess was the result of O_2 depletion affecting the air end-member during its diffusion within the soil, producing a relative enrichment in the other gasses. However, a

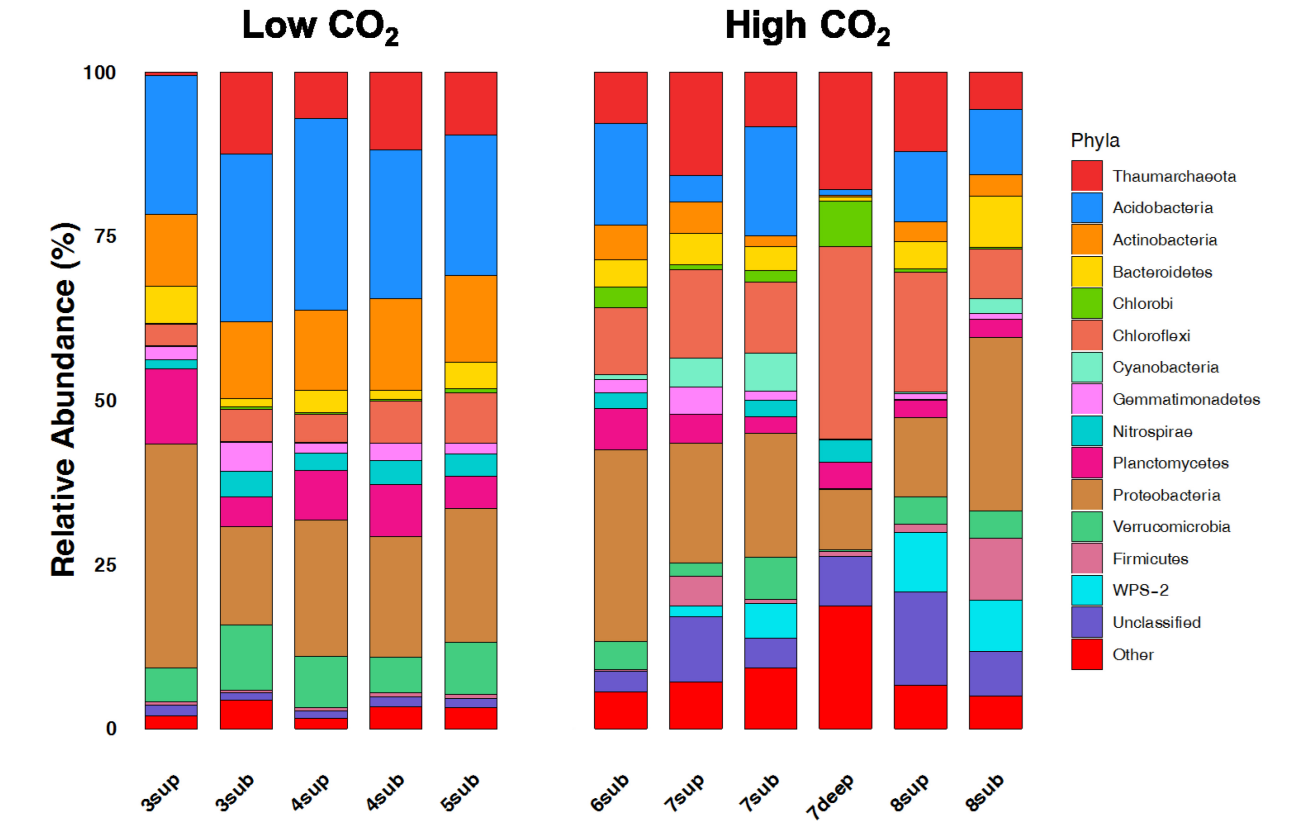

FIGURE 6 | Broad taxonomic affiliation of 16S rRNA gene sequences obtained from environmental samples from high CO_2 (HC) and low CO_2 (LC) concentration sites. The relative abundances of the 13 dominant phyla of OTUs belonging to the domain of Bacteria and Archaea are shown as% of total OTUs.

TABLE 3 | Similarity percentage analysis (SIMPER) between environmental samples collected from high CO_2 (HC) and low CO_2 (LC) concentration sites.

OTU ID	Phylum	Closest known taxonomic classification	%Con	%Cum
OTU_1	Thaumarchaeota	Nitrososphaeraceae (Family)	2.35	2.35
OTU_3	Thaumarchaeota	Cenarchaeales (SAGMA-X) (Order)	1.69	4.04
OTU_19	Deltaproteobacteria	Syntrophobacteraceae (Family)	1.27	5.31
OTU_12	Chloroflexi	Thermogemmatisporaceae (Family)	1.01	6.33
OTU_6	Gammaproteobacteria	Xanthomonadaceae (Family)	0.94	7.27
OTU_13	Verrucomicrobia	Chthoniobacteraceae (Family)	0.92	8.19
OTU_5	WPS-2		0.72	8.91
OTU_16	Verrucomicrobia	Chthoniobacteraceae (Family)	0.68	9.59
OTU_7	Alphaproteobacteria	Rhizobiales (Order)	0.66	10.24
OTU_68	Acidobacteria	Acidobacteria-6 (Class)	0.63	10.88

%Con, Contribution; %Cum, Cumulative.

minor contribution from CH_4 oxidation cannot be ruled out, as apparently supported by the δ^{13}C-CO_2 values of the interstitial gasses, which were more negative than those of the CO_2 from the pool, especially those collected at the shallower sampling depths (**Table 3**). The occurrence of CH_4 oxidation was confirmed by (i) the composition of the interstitial soil gasses from sites 6 at depth >30 cm and 8 which were depleted in CH_4 with respect to the air-BP mixing line, and (ii) the δ^{13}C-CH_4 values that were less negative than that of BP, as a result of isotopic fractionation during CH_4 consumption that typically produces a significant ^{13}C-enrichment in the residual CH_4 (e.g., Tassi et al., 2015; Venturi et al., 2019).

Microbiome Profiling

The long-term abiotic selection pressure represented by high CO_2 concentrations is known to drive compositional changes in soil microbial communities (Oppermann et al., 2010; Krüger et al., 2011; Frerichs et al., 2013; Šibanc et al., 2014). However, whether soil CO_2 concentration itself directly impact soil microbes or whether microbial organisms respond indirectly to co-varying factors such as local hypoxia or elevated soil pH is less clear. O_2 concentration and pH were among the main co-varying factors that differed between soils with different CO_2 exposure, both being negatively correlated with CO_2 (**Figure 7**). Since O_2 and pH are major abiotic factors known to affect microbial communities, it is possible that these and not the direct exposure to CO_2 levels would determine the microbial community composition at the mofette sites (Maček et al., 2011). Nevertheless, it must be considered that the observed variations in both the O_2 contents and pH were ultimately controlled by the supply of geogenic CO_2, the latter hindering diffusion of atmospheric O_2 into the soil and enhancing soil acidification due to increased concentrations of H^+ and H_2CO_3*.

The variation patterns of major physicochemical parameters differentiated those samples positioned intermediately between the less affected by CO_2 emission (sites 3–5) and the most affected ones (sites 6–8), as revealed by NMDS analysis (**Figure 7**, Left Panel). The high species richness in the CO_2-rich soils (1000 to 2600 16S OTUs) puts them on a par with many soils from different environments (Solon et al., 2018). However, the presence of high CO_2 concentration levels resulted in much lower species richness (16S rRNA gene) and significantly different communities than in sites characterized by lower CO_2 content, regardless of the depth at which samples were taken. These results corroborate the findings of Beulig et al. (2015), where mofettes exhibited substantially lower prokaryotic diversity than the reference sites. In particular, Chloroflexi, Firmicutes, WPS2 and Cyanobacteria were associated to high CO_2 conditions, whereas Acidobacteria, Actinobacteria, Planctomycetes and Verrucomicrobia showed higher percentages in Low CO_2 samples (**Figure 7**, Right Panel). Most of OTUs retrieved were not identified at the genus level, suggesting that this environment harbors novel bacterial and archaeal diversity, which deserves further investigation to allow fine-scale phylogeny of these communities.

WPS2, initially described in a study on polluted soil in Germany, branch off from either Cyanobacteria or Deinococcus phylum (Nogales et al., 2001). Representatives of this group were already recorded in acidic environments (Grasby et al., 2013; Trexler et al., 2014; Bragina et al., 2015) and a recent study showed that WPS2 is likely an anoxygenic phototroph capable of carbon fixation (Holland-Moritz et al., 2018). Soils exposed to high CO_2 concentrations could confer an advantage to this group, which would explain its higher abundance relative to lower CO_2 concentrations.

Chloroflexi have been identified in many environments, including freshwater and marine sediments. Nonetheless, Chloroflexi remain a relatively understudied bacterial lineage. The phylum shows different metabolic lifestyles, including photoautotrophs (e.g., *Chloroflexus aurantiacus*), fermentative (e.g., *Anaerolinea thermophila* UNI-1), organohalide respiring organisms in the Dehalococcoidia, and aerobic thermophiles (e.g., *Thermomicrobium*) (Hug et al., 2013). Although members of Chloroflexi were not directly reported to grow acetogenically, previous studies (e.g., Chan et al., 2013; Hug et al., 2013; Wasmund et al., 2014) suggested that members of Chloroflexi can have the potential to utilize CO_2 via the acetyl-CoA pathway. Beulig et al. (2015), by SIP analysis of mofette soil incubations, suggested that Chloroflexi perform acetogenesis. Moreover, two Chloroflexi genomes (RBG-2 and RBG-1351), closely related to the Dehalococcoidia, are described to be putative acetogens, utilizing a pathway for the formation of acetate less common in bacteria. For the first time, the complete acetyl-CoA pathway for carbon fixation was described in the Chloroflexi (Hug et al., 2013). In Dehalococcoidia, genes encoding enzymes of the reductive acetyl-CoA pathway were identified, which may enable the fixation of CO_2 or complete oxidation of organics completely to CO_2 (Wasmund et al., 2014).

Chloroflexi have been found in high abundance in similar sites exposed to high CO_2 concentration (Fernández-Montiel et al., 2016; Crognale et al., 2018) and sequences retrieved in this study were affiliated with two classes associated

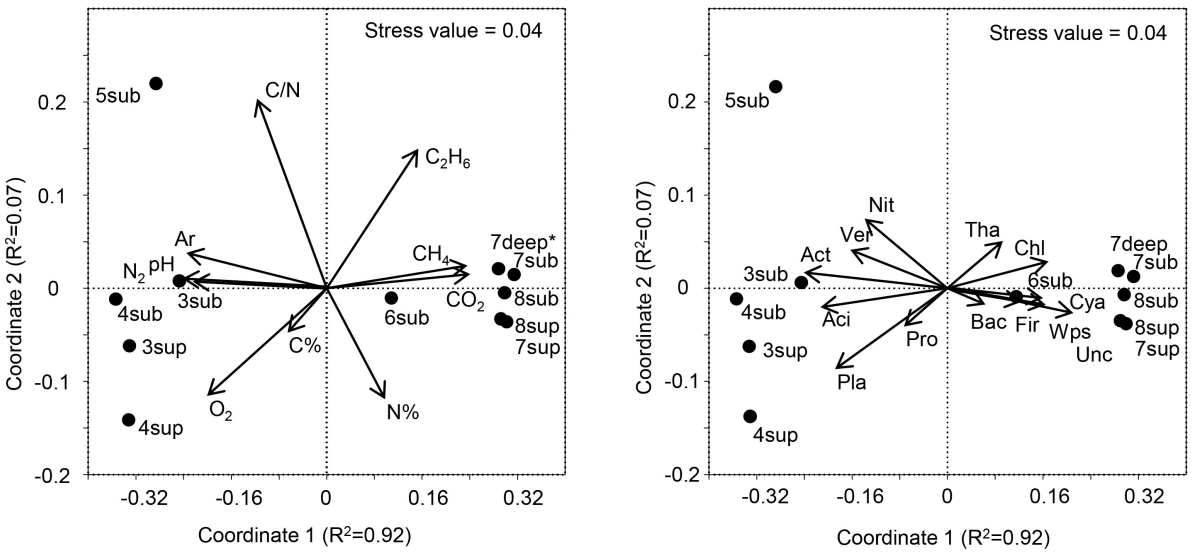

FIGURE 7 | Left panel: NMDS ordination plot, based on the Bray Curtis distance matrix, showing the variation patterns of chemical variables. The vector length is proportional to the correlation between the NMDS axes and each chemical variable. **Right panel:** The typifying microbial composition revealed by 16S rRNA gene sequencing projected onto the NMDS ordination synthesizing the chemical dissimilarity between areas. The vector length is proportional to the correlation between the NMDS axes and relative abundance of each microbial phylum. The stress value (value 0.04) provides an accurate representation of the dissimilarity among areas affected or not affected by hydrothermal fluids. Wps, WPS; Chl, Chloroflexi; Ver, Verrucomicrobia; Cya, Cyanobacteria; Aci, Acidobacteria; Act, Actinobacteria; Pla, Planctomycetes; Tha, Thaumarchaeota; Pro, Proteobacteria; Bac, Bacteroidetes; Fir, Firmicutes; Nit, Nitrospira; Unc, Unclassified. *Gas profile for site 7deep was estimated from the values of sites 7-8sub.

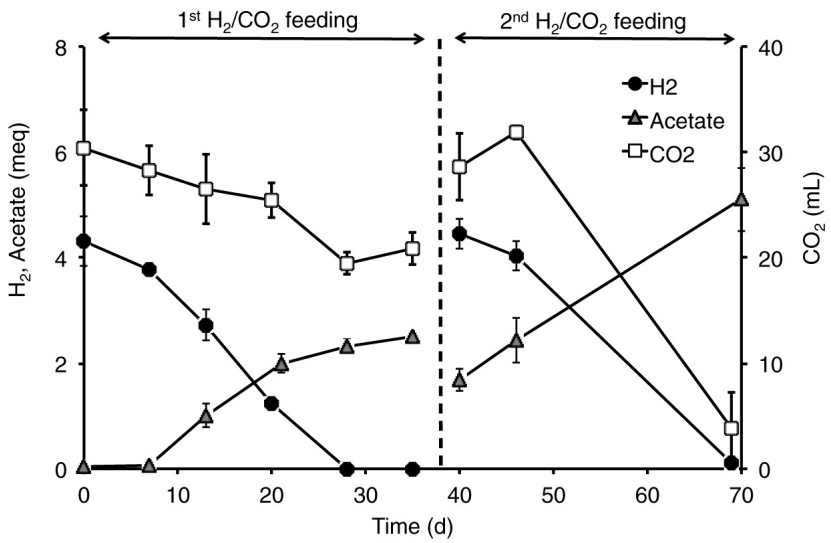

FIGURE 8 | Time course of H_2, acetate, and CO_2 in the incubations setup with mofette soil (10 g wet weight in 40 mL anaerobic mineral medium buffered at pH 5.5-6-0) 7sup sampled from a high CO_2 area. At the start of each feeding cycle, the headspace composition of the bottles consisted of H_2 (60%, vol/vol), CO_2 (15%, vol/vol), and N_2 (25%, vol/vol). The total pressure was around 1 atm. Bottles were incubated statically, in the dark, at room temperature (20–25°C). Error bars represent the standard error of duplicate incubations.

with hypoxic and microhypoxic niches: Ktedonobacteria and Anaerolinea. Ktedonobacteria can thrive in microaerophilic conditions (Chang et al., 2011). Anaerolineae have been reported to grow under strictly anaerobic conditions with isolates found in anaerobic sludge and hot spring (Yamada et al., 2006). Previous studies reported that Ktedonobacteria are prominent in extreme environments such as volcanic, Antarctic, and cave ecosystems (Tebo et al., 2015; Yabe et al., 2017; Schmidt et al., 2018). They comprises only five described species and a large number of uncultured environmental clone sequences (Cavaletti et al., 2006; Yabe et al., 2011; King and King, 2014). Several other strains were isolated, but not formally described, from soil (genus

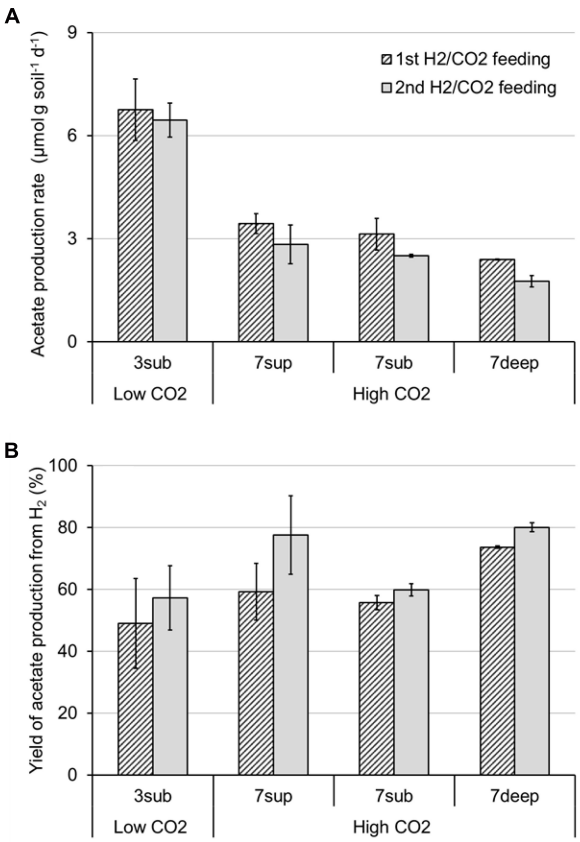

FIGURE 9 | Maximum rate of acetate production **(A)** and yield of acetate production **(B)** from H_2 in bottles incubated with the different mofette soils (3sub, 7sup, 7sub, and 7deep). Error bars represent the standard error of duplicate incubations.

Ktedonobacter), geothermal soils or compost (Stott et al., 2008; Yabe et al., 2011). Moreover, The genome of *K. racemifer* SOSP1-21 T was sequenced and contains a cox operon that confers the potential for carbon monoxide oxidation (Chang et al., 2011; King and King, 2014).

Anaerolineae class comprises only a few cultured strains and a large number of environmental 16S rRNA gene sequences. Since Anaerolineae were frequently found within various ecosystems, they were considered to be ubiquitous (Yamada and Sekiguchi, 2009). Two thermophilic, filamentous organisms (i.e., *Anaerolinea thermophila* and *Caldilinea aerophila*) were isolated from an anaerobic granular sludge and a hot spring (Sekiguchi et al., 2003). Moreover, thermophilic and mesophilic filamentous strains were isolated from anaerobic sludge blanket at a temperature range of 25–50°C (Yamada et al., 2005) and in hydrothermal vents in the Yaeyama Archipelago in Japan (Nunoura et al., 2013).

Acidobacteria were more abundant in low CO_2 samples than in those exposed to high CO_2 fluxes, a pattern previously reported in similar environments (Crognale et al., 2018). Members of the phylum Acidobacteria represent one of the predominant bacterial groups in soil but their ecological functions are still poorly understood (Jones et al., 2009; Foesel et al., 2014; Kielak et al., 2016). Acidobacteria were abundantly found in volcanic craters (Glamoclija and Garrel, 2004; Crognale et al., 2018), in marine vents (Sievert et al., 2000; López-García et al., 2003) and in the Yellowstone National Park geothermal areas (Norris et al., 2002).

In both LC and HC samples (except site 3), the archaeal OTUs were mainly affiliated to Thaumarchaeota, a deep-branching phylum within Archaea domain. An increase in Thaumarchaeota associated sequences was recorded in other mofettes with high CO_2 concentrations (Frerichs et al., 2013; Šibanc et al., 2014; Crognale et al., 2018) and it was proposed that this could be an "indicator taxa" of high CO_2 enriched soils (Frerichs et al., 2013), which could be connected to the CO_2 soil acidification and the obligate acidophilic nature of these taxa (Lehtovirta-Morley et al., 2011). Thaumarchaeota are among the most abundant Archaea on Earth and are believed to significantly contribute to the global N-cycle and C-cycle. This phylum includes not only all known Ammonia-Oxidizing Archaea (AOA) but also several clusters with unknown energy metabolism (Pester et al., 2011; Stieglmeier et al., 2014). Previous studies suggested that ammonia-oxidizing Thaumarchaeota can be adapted to both low ammonia availability and an autotrophic or mixotrophic lifestyle (Zhang et al., 2008; Schleper and Nicol, 2010; Pratscher et al., 2011). It has also been suggested that members of this phylum may be involved in methane oxidation (Crognale et al., 2018) since ammonia monooxygenase and methane monooxygenase enzymes are evolutionarily linked (Holmes et al., 1995), enabling both methanotrophy and ammonia oxidation (O'Neill and Wilkinson, 1977; Jones and Morita, 1983). The presence of the two different clades in different CO_2 concentrations, Nitrosospherales and Cenarcheales in LC and HC, respectively, suggests strong selection by local environmental conditions: Cenarcheales found at high CO_2 may not be ammonia-oxidizers and have a different metabolic pathway for energy production or may have extremely high affinity for O_2, which allows their survival as ammonia oxidizers at very high CO_2 concentrations. At higher O_2 concentrations they may be outcompeted by Nitrosospherales. The circadian Oxygen oscillation could also justify the presence of ammonia-oxidizing archaea. Interestingly, Methanobacteria class, belonging to the South African Gold Mine Euryarchaeotic Group (SAGMEG), was only found in the most extreme conditions (1.5% only in the sample 7deep). OTUs affiliated with archaeal groups that include methanogens were nearly absent from this site, as previously reported in similar acidic soils exposed to natural CO_2 fluxes (Crognale et al., 2018). The nearly complete absence of methanogens in the study soils could be due to the fact that these microorganisms were outcompeted by either acetogens, as also discussed in the following paragraph, or the fluctuating oxygen concentration during daytime. This suggests that methanogenesis marginally contributes to the overall metabolic features of the microbial communities in such an environment.

Acetogenic Bacteria

Acetogenic bacteria are ubiquitous in nature and are a specialized group of strictly anaerobic bacteria.

Acetogens were isolated from diverse environments, including soils, hypersaline waters and sediments (Liu and Conrad, 2011). In these ecosystems, chemolithoautotrophic acetogenic bacteria can directly compete with methanogenic archaea (hydrogenotrophic) or syntrophically interact with acetoclastic methanogens (Chassard and Bernalier-Donadille, 2006; Liu and Conrad, 2011). Acetogens include Firmicutes, Spirochaetes, Delta-Proteobacteria and Acidobacteria (Drake et al., 2006). Recently Beulig et al. (2015) speculated that Chloroflexi might be involved in acetogenesis in wetland mofette. Comparing the community composition in the environmental samples from sites at low (LC) and at high CO_2 concentration (HC), our results suggest a major role of Acidobacteria in LC sites whereas in HC sites Chloroflexi and Firmicutes are likely the predominant acetogens. This could also explain the difference in yield of acetate production observed in the incubation experiments with soil from low and at high CO_2 concentration sites. Under standard conditions, H_2-CO_2-dependent methanogenesis ($\Delta G^{o'} = -130$ kJ/reaction) is more energetically favorable than H_2-CO_2-dependent acetogenesis ($\Delta G^{o'} = -95$ kJ/reaction). At low H_2 concentrations, typically found in many anoxic environments, methanogenesis is energetically more favorable than acetogenesis, and hydrogenotrophic methanogens outcompete chemolithoautotrophic acetogens (Drake et al., 2006). However, acetogens have a kinetic advantage over methanogens at acidic pH and low temperature (Conrad et al., 1989; Kotsyurbenko et al., 1993), hence providing a likely explanation for the remarkable acetogenic potential observed in the incubation experiments, together with the lack of methanogenic activity, further confirmed by the absence of methanogens in sequencing analyses. In spite of that, it should be considered that the herein described incubation tests would have likely resulted in the selective enrichments of acetogens (e.g., Firmicutes), thereby overestimating the actual acetogenic potential of the natural communities.

CONCLUDING REMARKS

Gas discharges, characterized by extremely high CO_2 concentrations, are significantly affecting soil formation processes interacting with the geomorphological gradient observed in the mofette. Consequently, low pH values at the bottom of the Bossoleto sinkhole, as well as increased organic carbon accumulation in the topsoil and removal of inorganic carbon, were recorded. Similarly, variations in macro and micro-elements concentrations were also observed, likely due to the effect of the pH on element mobility. The comparison between interstitial soil gasses and those collected in an adjacent bubbling pool and the isotopic carbon fractionation, clearly indicated an increase in CO_2 due to CH_4 oxidation at the bottom of the sinkhole. The extremely high CO_2 concentrations resulted in higher microbial abundance and a lowered microbial diversity by favoring bacteria already reported to be involved in acetogenesis in mofette soils (i.e., Chloroflexi, Acidobacteria and Firmicutes). All the mofette soils supplied with hydrogen gas, in experimental incubations, displayed a remarkable CO_2 fixation potential, primarily due to the activity of acetogenic (i.e., acetate-producing) microorganisms. By contrast, negligible production of acetate occurred in control tests incubated with the same soils, under identical conditions, without the addition of H_2. Our results suggest that the composition of microbial communities at high CO_2 concentrations affects carbon cycling through inhibition of organic carbon decomposition and increases CO_2-fixation via the acetyl-CoA pathway. These acetogenic organisms, outcompeting methanogens, might determine considerable changes in carbon cycling leading to the accumulation of organic carbon in soils at the bottom of the mofette. Sites naturally exposed to extremely high CO_2 levels could, therefore, potentially represent an untapped source of microorganisms with unique capabilities to catalytically convert CO_2 into valuable organic chemicals for industrial applications.

DATA AVAILABILITY STATEMENT

The 16S rRNA gene sequences from Illumina MiSeq libraries from this study were deposited in the SRA (Short Read Archive) database under Bioproject ID PRJNA548940.

AUTHOR CONTRIBUTIONS

SF conceived the study. SF, FUn, FT, OV, AR, and FA contributed to the conception and design of the study. All authors performed the sampling campaign and the field and laboratory analysis, wrote the sections of the manuscript, contributed to manuscript revision, and read and approved the submitted version. LV and SV organized the database and performed the statistical analysis. SF wrote the first draft of the manuscript.

FUNDING

This research was supported by the CNR Short Term Mobility fellowship assigned to SF and by the Italian Ministry of Education, University and Research (MIUR) in the frame of the WE-MET Project (ERANETMED_NEXUS-14-035).

ACKNOWLEDGMENTS

The authors wish to deeply thank Noah Fierer of University of Colorado Boulder for the continuous support to the project and valuable suggestions and Tess Brewer, Teal Potter, and Smets Wenke for help with the analyses. Enrico Calvi (CNR-IGG Pisa) is warmly thanked for analyzing the carbon isotopic ratios of CO_2 in the soil gasses, Ilaria Pizzetti and Adita Bandra for the assistance during sampling.

SUPPLEMENTARY MATERIAL

The Supplementary Material for this article can be found online at: https://www.frontiersin.org/articles/10.3389/fmicb.2019.02238/full#supplementary-material

REFERENCES

Amalfitano, S., Del Bon, A., Zoppini, A., Ghergo, S., Fazi, S., Parrone, D., et al. (2014). Groundwater geochemistry and microbial community structure in the aquifer transition from volcanic to alluvial areas. *Water Res.* 65, 384–394. doi: 10.1016/j.watres.2014.08.004

Amalfitano, S., and Fazi, S. (2008). Recovery and quantification of bacterial cells associated with streambed sediments. *J. Microbiol. Methods.* 75, 237–243. doi: 10.1016/j.mimet.2008.06.004

Amundson, R. G., and Davidson, E. A. (1990). Carbon dioxide and nitrogenous gases in the soil atmosphere. *J. Geochem. Explor.* 38, 13–41. doi: 10.1016/0375-6742(90)90091-N

Beulig, F., Heuer, V. B., Akob, D. M., Viehweger, B., Elvert, M., Herrmann, M., et al. (2015). Carbon flow from volcanic CO2 into soil microbial communities of a wetland mofette. *ISME J.* 9, 746–759. doi: 10.1038/ismej.2014.148

Beulig, F., Urich, T., Nowak, M., Trumbore, S. E., Gleixner, G., Gilfillan, G. D., et al. (2016). Altered carbon turnover processes and microbiomes in soils under long-term extremely high CO2 exposure. *Nat. Microbiol.* 1:15025. doi: 10.1038/nmicrobiol.2015.25

Bragina, A., Berg, C., and Berg, G. (2015). The core microbiome bonds the Alpine bog vegetation to a transkingdom metacommunity. *Mol. Ecol.* 24, 4795–4807. doi: 10.1111/mec.13342

Brogi, A., Capezzuoli, E., and Gandin, A. (2007). I travertini delle terme di s. giovanni (rapolano terme, appennino settentrionale) e loro implicazione neotettonica. *Italian J. Neurol. Sci.* 20, 107–124.

Caporaso, J. G., Bittinger, K., Bushman, F. D., Desantis, T. Z., Andersen, G. L., and Knight, R. (2010a). PyNAST: a flexible tool for aligning sequences to a template alignment. *Bioinformatics* 26, 266–267. doi: 10.1093/bioinformatics/btp636

Caporaso, J. G., Kuczynski, J., Stombaugh, J., Bittinger, K., Bushman, F. D., Costello, E. K., et al. (2010b). QIIME allows analysis of high-throughput community sequencing data. *Nat. Methods* 7, 335–336. doi: 10.1038/nmeth.f.303

Cavaletti, L., Monciardini, P., Bamonte, R., Schumann, P., Rohde, M., Sosio, M., et al. (2006). New lineage of filamentous, spore-forming, gram-positive bacteria from soil. *Appl. Environ. Microbiol.* 72, 4360–4369. doi: 10.1128/aem.00132-136

Chan, Y., Van Nostrand, J. D., Zhou, J., Pointing, S. B., and Farrell, R. L. (2013). Functional ecology of an antarctic dry valley. *Proc. Natl. Acad. Sci. U.S.A.* 110, 8990–8995. doi: 10.1073/pnas.1300643110

Chang, Y. J., Land, M., Hauser, L., Chertkov, O., del Rio, T. G., Nolan, M., et al. (2011). Non-contiguous finished genome sequence and contextual data of the filamentous soil bacterium Ktedonobacter racemifer type strain (SOSP1-21 T). *Stand. Genomic Sci.* 5, 97–111. doi: 10.4056/sigs.2114901

Chassard, C., and Bernalier-Donadille, A. (2006). H2 and acetate transfers during xylan fermentation between a butyrate-producing xylanolytic species and hydrogenotrophic microorganisms from the human gut. *FEMS Microbiol. Lett.* 254, 116–122. doi: 10.1111/j.1574-6968.2005.00016.x

Collins, S., and Bell, G. (2006). Evolution of natural algal populations at elevated CO2. *Ecol. Lett.* 9, 129–135. doi: 10.1111/j.1461-0248.2005.00854.x

Conrad, R., Bak, F., Seitz, H. J., Thebrath, B., Mayer, H. P., and Schütz, H. (1989). Hydrogen turnover by psychrotrophic homoacetogenic and mesophilic methanogenic bacteria in anoxic paddy soil and lake sediment. *FEMS Microbiol. Lett.* 62, 285–293. doi: 10.1016/0378-1097(89)90010-90014

Cord-Ruwisch, R., Seitz, H. J., and Conrad, R. (1988). The capacity of hydrogenotrophic anaerobic bacteria to compete for traces of hydrogen depends on the redox potential of the terminal electron acceptor. *Arch. Microbiol.* 149, 350–357. doi: 10.1007/BF00411655

Crognale, S., Venturi, S., Tassi, F., Rossetti, S., Rashed, H., Cabassi, J., et al. (2018). Microbiome profiling in extremely acidic soils affected by hydrothermal fluids: the case of the solfatara crater (campi flegrei, southern italy). *FEMS Microbiol. Ecol.* 94, 1–17. doi: 10.1093/femsec/fiy190

DeSantis, T. Z., Hugenholtz, P., Larsen, N., Rojas, M., Brodie, E. L., Keller, K., et al. (2006). Greengenes, a chimera-checked 16S rRNA gene database and workbench compatible with ARB. *Appl. Environ. Microbiol.* 72, 5069–5072. doi: 10.1128/AEM.03006-3005

Drake, H. L., Küsel, K., and Matthies, C. (2006). "Acetogenic prokaryotes," in *The Prokaryotes Ecophysiology and Biochemistry*, eds E. Dworkin, M. Rosenberg, E. Schleifer, and K. H. Stackebrandt, (New York, NY: Springer), 354–420. doi: 10.1007/0-387-30742-7_13

Edgar, R. C. (2010). Search and clustering orders of magnitude faster than BLAST. *Bioinformatics* 26, 2460–2461. doi: 10.1093/bioinformatics/btq461

Evans, W. C., White, L. D., and Rapp, J. B. (1998). Geochemistry of some gases in hydrothermal fluids from the southern Juan de Fuca ridge. *J. Geophys. Res.* 15, 305–313.

Fazi, S., Amalfitano, S., Pizzetti, I., and Pernthaler, J. (2007). Efficiency of fluorescence in situ hybridization for bacterial cell identification in temporary river sediments with contrasting water content. *Syst. Appl. Microbiol.* 30, 463–470. doi: 10.1016/j.syapm.2007.03.003

Fernández-Montiel, I., Sidrach-Cardona, R., Gabilondo, R., Pedescoll, A., Scheu, S., and Bécares, E. (2016). Soil communities are affected by CO2 belowground emissions at a natural vent in Spain. *Soil Biol. Biochem.* 97, 92–98. doi: 10.1016/j.soilbio.2016.02.007

Fierer, N., Lauber, C. L., Ramirez, K. S., Zaneveld, J., Bradford, M. A., and Knight, R. (2012). Comparative metagenomic, phylogenetic and physiological analyses of soil microbial communities across nitrogen gradients. *ISME J.* 6, 1007–1017. doi: 10.1038/ismej.2011.159

Foesel, B. U., Nägele, V., Naether, A., Wüst, P. K., Weinert, J., Bonkowski, M., et al. (2014). Determinants of Acidobacteria activity inferred from the relative abundances of 16S rRNA transcripts in German grassland and forest soils. *Environ. Microbiol.* 16, 658–675. doi: 10.1111/1462-2920.12162

Foulquier, A., Volat, B., Neyra, M., Bornette, G., and Montuelle, B. (2013). Long-term impact of hydrological regime on structure and functions of microbial communities in riverine wetland sediments. *FEMS Microbiol. Ecol.* 85, 211–226. doi: 10.1111/1574-6941.12112

Frerichs, J., Oppermann, B. I., Gwosdz, S., Möller, I., Herrmann, M., and Krüger, M. (2013). Microbial community changes at a terrestrial volcanic CO2 vent induced by soil acidification and anaerobic microhabitats within the soil column. *FEMS Microbiol. Ecol.* 84, 60–74. doi: 10.1111/1574-6941.12040

Giggenbach, W. F. (1975). A simple method for the collection and analysis of volcanic gas samples. *Bull. Volcanol.* 39, 132–145. doi: 10.1007/BF02596953

Glamoclija and Garrel, L.L.G.P. (2004). "The solfatara crater, italy: characterization of hydrothermal deposits, biosignatures and their astrobiological implication," in *Proceedings of the 5th Lunar and Planetary Science Conference*, League, TX.

Grasby, S. E., Richards, B. C., Sharp, C. E., Brady, A. L., Jones, G. M., and Dunfield, P. F. (2013). The paint pots, kootenay national park, canada — a natural acid spring analogue for Mars. *Can. J. Earth Sci.* 50, 94–108. doi: 10.1139/e2012-060

Guerra, M., and Raschi, A. (2004). "Field trip guide book D03 field sight near rapolano terme (siena, tuscany). relationship between tectonics and fluid circulation," in *Proceedings of the 32nd International Geological Congress*, Florence.

Holland-Moritz, H., Stuart, J., Lewis, L. R., Miller, S., Mack, M. C., McDaniel, S. F., et al. (2018). Novel bacterial lineages associated with boreal moss species. *Environ. Microbiol.* 20, 2625–2638. doi: 10.1111/1462-2920.14288

Holmes, A. J., Costello, A., Lidstrom, M. E., and Murrell, J. C. (1995). Evidence that participate methane monooxygenase and ammonia monooxygenase may be evolutionarily related. *FEMS Microbiol. Lett.* 132, 203–208. doi: 10.1016/0378-1097(95)00311-R

Hug, L. A., Castelle, C. J., Wrighton, K. C., Thomas, B. C., Sharon, I., Frischkorn, K. R., et al. (2013). Community genomic analyses constrain the distribution of metabolic traits across the Chloroflexi phylum and indicate roles in sediment carbon cycling. *Microbiome* 1:22. doi: 10.1186/2049-2618-1-22

IUSS Working Group Wrb, (2015). *World Reference Base for Soil Resources 2014, Update 2015. International Soil Classification System for Naming Soils and Creating Legends for Soil Maps*. Rome: FAO.

Jones, R. D., and Morita, R. Y. (1983). Methane oxidation by nitrosococcus oceanus and nitrosomonas europaea. *Appl. Environ. Microbiol.* 45, 401–410.

Jones, R. T., Robeson, M. S., Lauber, C. L., Hamady, M., Knight, R., and Fierer, N. (2009). A comprehensive survey of soil acidobacterial diversity using pyrosequencing and clone library analyses. *ISME J.* 3, 442–453. doi: 10.1038/ismej.2008.127

Kielak, A. M., Barreto, C. C., Kowalchuk, G. A., van Veen, J. A., and Kuramae, E. E. (2016). The ecology of acidobacteria: moving beyond genes and genomes. *Front. Microbiol.* 7:744. doi: 10.3389/fmicb.2016.00744

Kies, A., Hengesch, O., Tosheva, Z., Raschi, A., and Pfanz, H. (2015). Diurnal CO2-cycles and temperature regimes in a natural CO2 gas lake. *Int. J. Greenh. Gas Control.* 37, 142–145. doi: 10.1016/j.ijggc.2015.03.012

King, C. E., and King, G. M. (2014). Description of thermogemmatispora carboxidivorans sp. nov., a carbon-monoxideoxidizing member of the class ktedonobacteria isolated from a geothermally heated biofilm, and analysis of carbon monoxide oxidation by members of the class ktedonobacteria. *Int. J. Syst. Evol. Microbiol.* 64(Pt 4), 1244–1251. doi: 10.1099/ijs.0.059675-59670

Körner, C., and Miglietta, F. (1994). Long term effects of naturally elevated CO2 on mediterranean grassland and forest trees. *Oecologia* 99, 343–351. doi: 10.1007/BF00627748

Kotsyurbenko, O. R., Glagolev, M. V., Nozhevnikova, A. N., and Conrad, R. (2001). Competition between homoacetogenic bacteria and methanogenic archaea for hydrogen at low temperature. *FEMS Microbiol. Ecol.* 38, 153–159. doi: 10.1016/S0168-6496(01)00179-179

Kotsyurbenko, O. R., Nozhevnikova, A. N., and Zavarzin, G. A. (1993). Methanogenic degradation of organic matter by anaerobic bacteria at low temperature. *Chemosphere* 27, 1745–1761. doi: 10.1016/0045-6535(93)90155-X

Krüger, M., Jones, D., Frerichs, J., Oppermann, B. I., West, J., Coombs, P., et al. (2011). Effects of elevated CO 2 concentrations on the vegetation and microbial populations at a terrestrial CO 2 vent at Laacher See. Germany. *Int. J. Greenh. Gas Control.* 2, 1093–1098. doi: 10.1016/j.ijggc.2011.05.002

Leff, J. W., Jones, S. E., Prober, S. M., Barberán, A., Borer, E. T., Firn, J. L., et al. (2015). Consistent responses of soil microbial communities to elevated nutrient inputs in grasslands across the globe. *Proc. Natl. Acad. Sci. U.S.A.* 112, 10967–10972. doi: 10.1073/pnas.1508382112

Lehtovirta-Morley, L. E., Stoecker, K., Vilcinskas, A., Prosser, J. I., and Nicol, G. W. (2011). Cultivation of an obligate acidophilic ammonia oxidizer from a nitrifying acid soil. *Proc. Natl. Acad. Sci. U.S.A.* 108, 15892–15897. doi: 10.1073/pnas.1107196108

Liu, F., and Conrad, R. (2011). Chemolithotrophic acetogenic H2/CO2 utilization in Italian rice field soil. *ISME J.* 5, 1526–1539. doi: 10.1038/ismej.2011.17

López-García, P., Duperron, S., Philippot, P., Foriel, J., Susini, J., and Moreira, D. (2003). Bacterial diversity in hydrothermal sediment and epsilonproteobacterial dominance in experimental microcolonizers at the Mid-Atlantic Ridge. *Environ. Microbiol.* 5, 961–976. doi: 10.1046/j.1462-2920.2003.00495.x

Maček, I., Dumbrell, A. J., Nelson, M., Fitter, A. H., Vodnik, D., and Helgason, T. (2011). Local adaptation to soil hypoxia determines the structure of an arbuscular mycorrhizal fungal community in roots from natural CO 2 springs. *Appl. Environ. Microbiol.* 77, 4770–4777.

McFarland, J. W., Waldrop, M. P., and Haw, M. (2013). Extreme CO2 disturbance and the resilience of soil microbial communities. *Soil Biol. Biochem.* 65, 274–286. doi: 10.1016/j.soilbio.2013.04.019

Miglietta, F., Raschi, A., Bettarini, I., Resti, R., and Selvi, F. (1993). Natural CO2 springs in Italy: a resource for examining long-term response of vegetation to rising atmospheric CO2 concentrations. *Plant. Cell Environ.* 16, 873–878. doi: 10.1111/j.1365-3040.1993.tb00510.x

Minissale, A., Vaselli, O., Tassi, F., Magro, G., and Grechi, G. P. (2002). Fluid mixing in carbonate aquifers near Rapolano (central Italy): chemical and isotopic constraints. *Appl. Geochem.* 17, 1329–1342. doi: 10.1016/s0883-2927(02)00023-9

Nogales, B., Moore, E. R. B., Llobet-Brossa, E., Rossello-Mora, R., Amann, R., and Timmis, K. N. (2001). Combined use of 16S ribosomal DNA and 16S rRNA to Study the bacterial community of polychlorinated biphenyl-polluted soil. *Appl. Environ. Microbiol.* 67, 1874–1884. doi: 10.1128/AEM.67.4.1874-1884.2001

Norris, T. B., Wraith, J. M., Castenholz, R. W., and McDermott, T. R. (2002). Soil microbial community structure across a thermal gradient following a geothermal heating event. *Appl. Environ. Microbiol.* 68, 6300–6309. doi: 10.1128/AEM.68.12.6300-6309.2002

Nunoura, T., Hirai, M., Miyazaki, M., Kazama, H., Makita, H., Hirayama, H., et al. (2013). Isolation and characterization of a thermophilic, obligately anaerobic and heterotrophic marine chloroflexi bacterium from a chloroflexi-dominated microbial community associated with a japanese shallow hydrothermal system, and proposal for thermomarinilin. *Microbes Environ.* 28, 228–235. doi: 10.1264/jsme2.me12193

Oh, N.-H., Kim, H.-S., and Richter, D. D. (2005). What regulates soil CO 2 concentrations? A modeling approach to CO 2 diffusion in deep soil profiles. *Environ. Eng. Sci.* 22, 38–45. doi: 10.1089/ees.2005.22.38

Oksanen, J., Blanchet, F. G., Kindt, R., Oksanen, M. J., and Suggests, M. (2013). *Package 'vegan.' Community Ecol. Packag. Version*.

O'Neill, J. G., and Wilkinson, J. F. (1977). Oxidation of ammonia by methane-oxidizing bacteria and the effects of ammonia on methane oxidation. *J. Gen. Microbiol.* 100, 407–412. doi: 10.1099/00221287-100-2-407

Oppermann, B. I., Michaelis, W., Blumenberg, M., Frerichs, J., Schulz, H. M., Schippers, A., et al. (2010). Soil microbial community changes as a result of long-term exposure to a natural CO2 vent. *Geochim. Cosmochim. Acta.* 74, 2697–2716. doi: 10.1016/j.gca.2010.02.006

Pearce, J. M. (2006). "What can we learn from natural analogues? an overview of how analogues can benefit the geological storage of CO2," in *Advances in the Geological Storage of Carbon Dioxide*, eds S. Lombardi, L. K. Altunina, and S. E. Beaubien, (Netherlands: Springer), 129–139.

Pearce, J. M., Czernichowski-Lauriol, I., Lombardi, S., Brune, S., Nador, A., Baker, J., et al. (2004). "A review of natural CO2 accumulations in europe as analogues for geological sequestration," in *Geological Storage of Carbon Dioxide*, eds R. H. Baines, and S. Worden, (Amsterdam: Elsevier), 29–42.

Pester, M., Schleper, C., and Wagner, M. (2011). The Thaumarchaeota: an emerging view of their phylogeny and ecophysiology. *Curr. Opin. Microbiol.* 14, 300–306. doi: 10.1016/j.mib.2011.04.007

Pratscher, J., Dumont, M. G., and Conrad, R. (2011). Ammonia oxidation coupled to CO2 fixation by archaea and bacteria in an agricultural soil. *Proc. Natl. Acad. Sci. U.S.A.* 108, 4170–4175. doi: 10.1073/pnas.1010981108

Price, M. N., Dehal, P. S., and Arkin, A. P. (2009). FastTree: computing large minimum evolution trees with profiles instead of a distance matrix. *Mol. Biol. Evol.* 26, 1641–1650. doi: 10.1093/molbev/msp077

Rabaey, K., and Rozendal, R. A. (2010). Microbial electrosynthesis - revisiting the electrical route for microbial production. *Nat. Rev. Microbiol.* 8, 706–716. doi: 10.1038/nrmicro2422

Raschi, A., Miglietta, F., Tognetti, R., and Van Gardingen, P. R. (1997). *Plant Responses to Elevated CO2*. Cambridge: Cambridge University Press.

Schaetzl, R. J., and Anderson, S. (2005). *Soils: Genesis and Geomorphology*. Cambridge: Cambridge University Press.

Schleper, C., and Nicol, G. W. (2010). Ammonia-oxidising archaea - physiology, ecology and evolution. *Adv. Microb. Physiol.* 57, 1–41. doi: 10.1016/B978-0-12-381045-8.00001-1

Schmidt, S. K., Gendron, E. M. S., Vincent, K., Solon, A. J., Sommers, P., Schubert, Z. R., et al. (2018). Life at extreme elevations on atacama volcanoes: the closest thing to mars on earth? antonie van leeuwenhoek. *Int. J. Gen. Mol. Microbiol.* 111, 1389–1401. doi: 10.1007/s10482-018-1066-1060

Schoell, M. (1980). The hydrogen and carbon isotopic composition of methane from natural gases of various origins. *Geochim. Cosmochim. Acta.* 26, 399–407. doi: 10.1016/0016-7037(80)90155-90156

Sekiguchi, Y., Yamada, T., Hanada, S., Ohashi, A., Harada, H., and Kamagata, Y. (2003). *Anaerolinea thermophila* gen. nov., sp. nov. and *Caldilinea aerophila* gen. nov., sp. nov., novel filamentous thermophiles that represent a previously uncultured lineage of the domain bacteria at the subphylum level. *Int. J. Syst. Evol. Microbiol.* 53(Pt 6), 1843–1851. doi: 10.1099/ijs.0.02699-2690

Šibanc, N., Dumbrell, A. J., Mandić-Mulec, I., and Maček, I. (2014). Impacts of naturally elevated soil CO 2 concentrations on communities of soil archaea and bacteria. *Soil Biol. Biochem.* 68, 348–356. doi: 10.1016/j.soilbio.2013.10.018

Sievert, S. M., Kuever, J., and Muyzer, G. (2000). Identification of 16s ribosomal DNA-defined bacterial populations at a shallow submarine hydrothermal vent near Milos island (Greece). *Appl. Environ. Microbiol.* 66, 3102–3109. doi: 10.1128/AEM.66.7.3102-3109.2000

Smets, B., Tedesco, D., Kervin, F., Kies, A., Vaselli, O., and Yalire, M. M. (2010). Dry gas vents ("mazuku") in goma region (north-kivu, democratic republic of congo): formation and risk assessment. *J. African Earth Sci.* 58, 787–798. doi: 10.1016/j.jafrearsci.2010.04.008

Solon, A. J., Vimercati, L., Darcy, J. L., Arán, P., Porazinska, D., Dorador, C., et al. (2018). Microbial communities of high-elevation fumaroles, penitentes, and dry tephra "Soils" of the puna de atacama volcanic zone. *Microb. Ecol.* 76, 340–351. doi: 10.1007/s00248-017-1129-1121

Stieglmeier, M., Klingl, A., Alves, R. J. E., Rittmann, S. K. M. R., Melcher, M., Leisch, N., et al. (2014). Nitrososphaera viennensis gen. nov., sp. nov., an aerobic and mesophilic, ammonia-oxidizing archaeon from soil and a member

of the archaeal phylum Thaumarchaeota. *Int. J. Syst. Evol. Microbiol.* 64(Pt 8), 2738–2752. doi: 10.1099/ijs.0.063172-63170

Stott, M. B., Crowe, M. A., Mountain, B. W., Smirnova, A. V., Hou, S., Alam, M., et al. (2008). Isolation of novel bacteria, including a candidate division, from geothermal soils in New Zealand. *Environ. Microbiol.* 10, 2030–2041. doi: 10.1111/j.1462-2920.2008.01621.x

Tassi, F., Venturi, S., Cabassi, J., Vaselli, O., Gelli, I., Cinti, D., et al. (2015). Biodegradation of CO_2, CH_4 and volatile organic compounds (VOCs) in soil gas from the Vicano-Cimino hydrothermal system (central Italy). *Org. Geochem.* 86, 81–93.

Tebo, B. M., Davis, R. E., Anitori, R. P., Connell, L. B., Schiffman, P., and Staudigel, H. (2015). Microbial communities in dark oligotrophic volcanic ice cave ecosystems of Mt. Erebus, Antarctica. *Front. Microbiol.* 6:179. doi: 10.3389/fmicb.2015.00179

Trexler, R., Solomon, C., McClure, E. E., Brislawn, C. J., Grube, A. M., Wright, J. R., et al. (2014). Assessing impacts of unconventional natural gas extraction on microbial communities in headwater stream ecosystems in northwestern Pennsylvania. *Front. Microbiol.* 5:522. doi: 10.3389/fmicb.2014.00522

U. S. Environmental Protection Agency, (2004). *Method 3052: Microwave Assisted Acid Digestion of Siliceous and Organically Based Matrices*. Washington, D.C: U. S. Environmental Protection Agency.

USDA, (2010). *Keys to Soil Taxonomy*, 11th Edn. Washington DC: Soil Survey Staff, United States Department of Agriculture - Natural Resources Conservation Service.

USDA, (2017). *Soil Survey Manual – Handbook No. 18*. Washington DC: Soil Survey Staff, United States Department of Agriculture - Natural Resources Conservation Service.

Van Gardingen, P. R., Grace, J., Harkness, D. D., Miglietta, F., and Raschi, A. (1995). Carbon dioxide emission at an Italian mineral spring result in local greenhouse effect. *Agric. For. Meteorol.* 73, 17–27.

Vaselli, O., Capaccioni, B., Tedesco, D., Tassi, F., Yalire, M. M., and Kasareka, M. C. (2002). The "Evils winds" (Mazukus) at nyiragongo volcano (democratic republic of congo). *Acta Vulcanol.* 1, 123–128.

Vaselli, O., Tassi, F., Montegrossi, G., Capaccioni, B., and Giannini, L. (2006). Sampling and analysis of volcanic gases. *Acta Vulcanol.* 18, 65–76.

Venturi, S., Tassi, F., Magi, F., Cabassi, J., Ricci, A., Capecchiacci, F., et al. (2019). Carbon isotopic signature of interstitial soil gases reveals the potential role of ecosystems in mitigating geogenic greenhouse gas emissions: case studies from hydrothermal systems in Italy. *Sci. Total Environ.* 655, 887–898. doi: 10.1016/j.scitotenv.2018.11.293

Wasmund, K., Schreiber, L., Lloyd, K. G., Petersen, D. G., Schramm, A., Stepanauskas, R., et al. (2014). Genome sequencing of a single cell of the widely distributed marine subsurface dehalococcoidia, phylum chloroflexi. *ISME J.* 8, 383–397. doi: 10.1038/ismej.2013.143

Yabe, S., Aiba, Y., Sakai, Y., Hazaka, M., and Yokota, A. (2011). Thermogemmatispora onikobensis gen. nov., sp. nov. and Thermogemmatispora foliorum sp. nov., isolated from fallen leaves on geothermal soils, and description of *Thermogemmatisporaceae* fam. nov. and Thermogemmatisporales ord. nov. within the class Ktedonob. *Int. J. Syst. Evol. Microbiol.* 61(Pt 4), 903–910. doi: 10.1099/ijs.0.024877-24870

Yabe, S., Sakai, Y., Abe, K., and Yokota, A. (2017). Diversity of *Ktedonobacteria* with Actinomycetes-Like Morphology in Terrestrial Environments. *Microbes Environ. Environ.* 32, 61–70. doi: 10.1264/jsme2.me16144

Yamada, T., and Sekiguchi, Y. (2009). Cultivation of uncultured chloroflexi subphyla: significance and ecophysiology of formerly uncultured chloroflexi "Subphylum I" with natural and biotechnological relevance. *Microbes Environ.* 24, 205–216. doi: 10.1264/jsme2.me09151s

Yamada, T., Sekiguchi, Y., Hanada, S., Imachi, H., Ohashi, A., Harada, H., et al. (2006). *Anaerolinea thermolimosa* sp. nov., *Levilinea saccharolytica* gen. nov., sp. nov. and Leptolinea tardivitalis gen. nov., sp. nov., novel filamentous anaerobes, and description of the new classes Anaerolineae classis nov. And Caldilineae classis nov. In the bacterial phylum chloroflexi. *Int. J. Syst. Evol. Microbiol.* 56(Pt 6), 1331–1340. doi: 10.1099/ijs.0.64169-64160

Yamada, T., Sekiguchi, Y., Imachi, H., Kamagata, Y., Ohashi, A., and Harada, H. (2005). Diversity, localization, and physiological properties of filamentous microbes belonging to Chloroflexi subphylum I in mesophilic and thermophilic methanogenic sludge granules. *Appl. Environ. Microbiol.* 71, 7493–7503. doi: 10.1128/AEM.71.11.7493-7503.2005

Zhang, C. L., Ye, Q., Huang, Z., Li, W. J., Chen, J., Song, Z., et al. (2008). Global occurrence of archaeal amoA genes in terrestrial hot springs. *Appl. Environ. Microbiol.* 74, 6417–6426. doi: 10.1128/AEM.00843-848

Conflict of Interest: The authors declare that the research was conducted in the absence of any commercial or financial relationships that could be construed as a potential conflict of interest.

frontiers in Microbiology

ORIGINAL RESEARCH
published: 23 October 2019
doi: 10.3389/fmicb.2019.02418

Competition Between Chemolithotrophic Acetogenesis and Hydrogenotrophic Methanogenesis for Exogenous H_2/CO_2 in Anaerobically Digested Sludge: Impact of Temperature

*Bo Fu[1,2,3], Xin Jin[1], Ralf Conrad[2], Hongbo Liu[1,3] and He Liu[1,3]**

[1] Jiangsu Key Laboratory of Anaerobic Biotechnology, School of Environmental and Civil Engineering, Jiangnan University, Wuxi, China, [2] Department of Biogeochemistry, Max Planck Institute for Terrestrial Microbiology, Marburg, Germany, [3] Jiangsu Collaborative Innovation Center of Technology and Material of Water Treatment, Suzhou, China

OPEN ACCESS

Edited by:
Mirko Basen,
University of Rostock, Germany

Reviewed by:
Oliver Schmidt,
University of Bayreuth, Germany
Alfons Stams,
Wageningen University & Research, Netherlands

***Correspondence:**
He Liu
liuhe@jiangnan.edu.cn

Specialty section:
This article was submitted to Microbial Physiology and Metabolism, a section of the journal Frontiers in Microbiology

Received: 12 July 2019
Accepted: 07 October 2019
Published: 23 October 2019

Citation:
Fu B, Jin X, Conrad R, Liu H and Liu H (2019) Competition Between Chemolithotrophic Acetogenesis and Hydrogenotrophic Methanogenesis for Exogenous H_2/CO_2 in Anaerobically Digested Sludge: Impact of Temperature. Front. Microbiol. 10:2418. doi: 10.3389/fmicb.2019.02418

Anaerobic digestion is a widely applied technology for sewage sludge treatment. Hydrogen and CO_2 are important degradation products, which serve as substrates for both hydrogenotrophic methanogenesis and chemolithotrophic acetogenesis. In order to understand the competition between these processes for H_2/CO_2, sludge samples were incubated under H_2/CO_2 headspace at different temperatures, and analyzed with respect to turnover of H_2, CO_2, CH_4 and acetate including their $\delta^{13}C$ values. At 15°C, ^{13}C-depleted acetate ($\delta^{13}C$ of −41 to −43‰) and transient acetate accumulation were observed under H_2/CO_2, and CH_4 accumulated with $\delta^{13}C$ values increasing from −53 to −33‰. The copy numbers of the *fhs* gene, which is characteristic for acetogenic bacteria, were at 15°C one order of magnitude higher in the H_2/CO_2 incubations than the N_2 control. At 30°C, however, acetate did not accumulate in the H_2/CO_2 incubation and the $\delta^{13}C$ of CH_4 was very low (−100 to −77‰). At 50°C, isotopically enriched acetate was transiently formed and subsequently consumed followed by the production of ^{13}C-depleted CH_4. Collectively, the results indicate a high contribution of chemolithotrophic acetogenesis to H_2/CO_2 utilization at 15°C and 50°C, while H_2/CO_2 was mainly consumed by hydrogenotrophic methanogenesis at 30°C. Fermentative production and methanogenic consumption of acetate were active at 50°C.

Keywords: methanogenesis, acetogenesis, carbon isotope, temperature, H_2/CO_2 utilization

INTRODUCTION

Anaerobic digestion has been widely used for stabilization and energy recovery of sewage sludge (Kelessidis and Stasinakis, 2012). Anaerobic digestion of organic matter is achieved in four steps: hydrolysis, fermentation, acetogenesis, and methanogenesis (Adekunle and Okolie, 2015). Acetate and CH_4 are the respective products of chemolithotrophic acetogensis ($4\ H_2 + 2\ CO_2 \rightarrow CH_3COOH + 2\ H_2O$) and hydrogenotrophic methanogenesis ($4\ H_2 + CO_2 \rightarrow CH_4 + 2\ H_2O$). Chemolithotrophic acetogenic bacteria normally compete

directly with hydrogenotrophic methanogens for H_2/CO_2 as substrates (Lopes et al., 2015; Liu et al., 2016). Meanwhile, the emission of CO_2 and CH_4 during anaerobic digestion of sewage sludge has received attention because of the greenhouse effect (Niu et al., 2013). The generation of acetate instead of CH_4 from sewage sludge is a promising technology for waste recycling and reduction of greenhouse gas emission (Agler et al., 2011).

Temperature is one of the key variables in anaerobic sludge digestion and has an important effect on H_2/CO_2 utilization (Conrad and Wetter, 1990; Kotsyurbenko et al., 2001; Shanmugam et al., 2014). Studies on rice field soils indicate that acetogenic bacteria can outcompete methanogens for H_2 at low temperature (Conrad et al., 1989; Liu and Conrad, 2011). Thermophilic anaerobic digestion processes offer kinetic advantages when compared with mesophilic conditions. Compared to 35°C, rates of methanogenesis increase at 55°C, but the methanogenic pathway also changes by replacing acetoclastic methanogesis with syntrophic acetate oxidation coupled to hydrogenotrophic methanogenesis (Zábranská et al., 2000; Hao et al., 2011; Ho et al., 2013). Their respective contribution to the overall anaerobic degradation of organic matter in sewage sludge may be different due to different temperatures. Some studies reported the competition between acetogenic bacteria and methanogens in lake sediments and rice field soils (Chin and Conrad, 2010; Liu and Conrad, 2011; Olivier, 2016), however, the effect of temperature on the contribution of acetogenesis and methanogenesis to chemolithotrophic H_2/CO_2 utilization in anaerobic digested sludge is not well understood.

However, the differentiation of chemolithotrophic acetogenesis and hydrogenotrophic methanogenesis in H_2/CO_2 utilization is complex. Acetate is not only produced by chemolithotrophic acetogenesis but also by fermentation and heterotrophic acetogenesis. Methane is the end product of both acetoclastic methanogenesis and hydrogenotrophic methanogenesis. Isotope technique is a reasonable approach, since studies have shown that the stable carbon isotope fractionation of chemolithotrophic acetogenesis (−38 to −68‰) and hydrogenotrophic methanogenesis (−21 to −71‰) is strong (Galand et al., 2010; Blaser et al., 2013; Gehring et al., 2015; Ji et al., 2018), which imprints a signature on the stable carbon isotope composition ($^{13}C/^{12}C$) of acetate and CH_4.

In this study, we aimed to specify the competition between chemolithotrophic acetogenesis and hydrogenotrophic methanogenesis for H_2/CO_2 in anaerobic digested sludge. Incubation under H_2/CO_2 at different temperatures served for determining the potential of the chemolithotrophic acetogenesis and hydrogenotrophic methanogenesis. Incubation in the presence of bromoethanesulfonate (BES) was used to inhibit methanogenesis.

MATERIALS AND METHODS

Sewage Sludge Incubation

Sewage sludge was obtained from secondary settling tank sludge of Wuxi Shuofang sewage treatment plant. The physicochemical characteristics of sewage sludge were: pH (7.65); dry weight (DW; 14.3%); volatile substances (72g/L); water content (85.6%); total N (15.8 mg g^{-1} DW); and total phosphorus (17.0 mg g^{-1} DW). Sludge slurries were prepared in 26-mL pressure tubes by mixing 3.9 g sewage sludge and 6.1 mL of anoxic sterile water. The tubes were closed with black rubber stoppers, flushed with N_2, pressurized to 0.5 bar overpressure, and then pre-incubated at 25°C for about 5 days to deplete alternative electron acceptors and initiate methanogenesis. After pre-incubation, three treatments were all incubated under 15°C, 30°C, 50°C: (1) control, the sludge slurry was incubated under N_2 headspace; (2) H_2/CO_2 treatment, the sludge slurry was incubated under H_2/CO_2 (80/20, v/v) headspace to stimulate both chemolithotrophic acetogenesis and hydrogenotrophic methanogenesis; and (3) H_2/CO_2 + BES treatment, the sludge slurry was incubated under H_2/CO_2 (80/20, v/v) headspace and methanogenesis was inhibited by 100 mM BES. The headspace pressures of the three treatments were all adjusted to 1.5 bar. The tubes with sewage sludge slurry were prepared in numerous parallels (about 108 tubes), of which triplicates were sacrificed for chemical analyses of liquid samples and molecular analyses. Gas samples were taken from 27 tubes during the incubation at few days' intervals to measure the concentrations of CH_4, CO_2, H_2 and the $\delta^{13}C$ values of CH_4 and CO_2. The other tubes were opened to retrieve liquid samples for analysis of volatile fatty acids (VFAs) concentration and the $\delta^{13}C$ of acetate, and were stored frozen at −20°C for later molecular analyses. The $\delta^{13}C$ of the organic carbon in the sewage sludge was −29.8‰.

Chemical Analysis

Analytical methods for CH_4, CO_2, H_2 in gas samples and acetate in liquid samples were as described before (Fu et al., 2018). Simply, the partial pressures of CH_4 and CO_2 were analyzed by gas chromatography (GC). The partial pressures were converted into molar quantities by using the ideal gas volume formula at different temperatures. The small amount of dissolved CH_4 was neglected, and the amount of dissolved CO_2 was calculated from the Henry constants at different temperatures. The concentrations of bicarbonate were calculated from the CO_2 partial pressures and the pH using the equations listed in Stumm and Morgan (1981). The ^{13}C content of CH_4 and CO_2 was measured using a Finnigan Gas Chromatography Combustion Isotope Ratio Mass Spectrometry System. Concentrations of acetate and other VFAs were analyzed by high-pressure liquid chromatography (HPLC). An HPLC system (Spectra System P1000, Thermo Fisher Scientific, San Jose, CA, United States; Mistral, Spark, Emmen, Netherlands) equipped with an ion-exclusion column (Aminex HPX-87-H) and a Finnigan LC IsoLink (Thermo Fisher Scientific, Bremen, Germany) was used to measure the $\delta^{13}C$ values of acetate.

DNA Extraction and Quantification of Gene Copy

DNA was extracted from the sewage sludge sample using the PowerSoil® DNA Isolation kit. Frozen sewage sludge samples were thawed at 4°C. In order to ensure homogeneity, sludge samples were vortexed prior to DNA extraction. Quality and

concentration of the extracted DNA were detected by UV spectrophotometer (NanoDrop ND 2000).

All the oligonucleotide primers were synthesized by Shanghai Bio-Engineering Co., Ltd. (China), and all the qPCR reaction components were purchased from Shanghai Bio-Engineering Co., Ltd. (China). The qPCR was conducted in a Rotor-Gene Q fluorescence quantitative PCR instrument. For all assays, the standard was a sample containing known numbers of DNA copies of the target gene. Standards were continuously diluted and used in each reaction to construct calibration curves. Methanogenic archaea and acetogenic bacteria were quantified by amplification of the *mcrA and fhs* genes, respectively using primers listed in *fhs-f*/*fhs-r* **Table 1** (Angel et al., 2011; Xu et al., 2015). The *mcrA* and *fhs* gene qPCR conditions included an initial denaturation at 94°C for 4 min, followed 30 cycles at 94°C for 30s at the specific annealing temperature shown in **Table 1**. In order to know the relative abundance of acetogenic bacteria, we also used the universal primers 519f/907r to quantify the 16S rRNA gene copies of the domain Bacteria (**Table 1**) (Imachi et al., 2008).

RESULTS

H_2/CO_2 Utilization at Low Temperature

The time courses of accumulation of CH_4, CO_2, acetate and H_2, as well as the temporal change of $\delta^{13}C$ values of CH_4, acetate, and CO_2 of the treatments control, H_2/CO_2, and H_2/CO_2 + BES are shown in **Figures 1–3** for the incubation temperatures 15, 30, and 50°C, respectively. At 15°C CH_4 concentrations increased with time in the control and H_2/CO_2 treatments but not in the presence of BES, which inhibited CH_4 production completely (**Figure 1A**). At the same time, CO_2 (**Figure 1E**) and H_2 (**Figure 1G**) concentrations decreased in the H_2/CO_2 treatments both in the presence and absence of BES. Later on, CO_2 slightly increased in the absence of BES presumably because of the conversion of acetate to CO_2 and CH_4 (**Figure 1E**). In the N_2 incubations H_2 transiently accumulated to 104 μmol/gDW and then decreased to very low concentration at low temperature (**Figure 1G**).

The two major products of consumption of H_2 and CO_2 were CH_4 (**Figure 1A**) and acetate (**Figure 1B**). In the H_2/CO_2 incubations, acetate concentrations accumulated to a maximum on day 17, and then gradually decreased to nearly zero with time (**Figure 1B**). Acetate was then presumably converted to CH_4, which was inhibited in the BES-treated samples (**Figure 1A**). There was almost no acetate accumulation in the N_2 controls (**Figure 1C**). Formate, propionate, and butyrate concentrations were always lower than 14, 21, and 23 μmol/g DW, respectively (**Supplementary Figure S1**).

The amounts of consumed H_2 and produced acetate and CH_4 are summarized in **Table 2**. With exogenous H_2/CO_2 and the methanogenic inhibitor BES, about 800–916 μmol/g DW of H_2 were consumed and about 212–258 μmol/g DW acetate were produced, indicating a stoichiometry of 4 to 1 as expected for chemolithotrophic acetogenesis. Without BES, the transiently accumulated acetate was finally converted to less than 215 μmol/g DW CH_4, taking into account that CH_4 was also produced from the sewage sludge without exogenous H_2/CO_2.

The $\delta^{13}C$ values of acetate under H_2/CO_2 treatments showed transiently very low values ($< -40‰$) on day 10 (**Figure 1D**). Based on the isotopic signature of acetogenic pure cultures, this ^{13}C-depleted acetate was apparently produced from chemolithotrophic acetogenesis (Blaser et al., 2013). These values were much lower than the $\delta^{13}C$ of sludge organic matter ($-29.8‰$), indicating that acetate was produced by chemolithotrophic acetogenesis. Later on, $\delta^{13}C$ values of acetate increased to values $> -30‰$, especially in the absence of BES, indicating conversion by acetoclastic methanogenesis (**Figure 1D**). Only little CH_4 (8–18 μmol/g DW) with a $\delta^{13}C$ of about $-54‰$ was observed in in the presence of BES due to the inhibition of methanogenesis. In the absence of BES, the $\delta^{13}C$ values of CH_4 under H_2/CO_2 increased to about $-33‰$, but in the N_2 controls only to about $-47‰$ (**Figure 1B**). In the N_2 control, the $\delta^{13}C$ values of CO_2 accordingly increased from initially $-31‰$ to about $-18.6‰$ (**Figure 1F**). However, in the H_2/CO_2 treatments, the $\delta^{13}C$ values of CO_2 initially increased to about 0‰, irrespectively of the presence of BES. This increase is consistent with the conversion of CO_2 to either CH_4 or acetate. Later on, the $\delta^{13}C$ values of CO_2 decreased again, especially in the absence of BES, presumably due to methanogenic consumption of acetate (**Figure 1F**).

H_2/CO_2 Utilization at Mesophilic Temperature

At 30°C, the time courses of accumulation of CH_4, CO_2, acetate and H_2 are shown in **Figure 2**. The time courses were similar as at 15°C with the following remarkable exceptions: Methane production rates were larger. Acetate only accumulated in the BES treatment, when CH_4 production was inhibited

TABLE 1 | Oligonucleotide sequences used for quantitative PCR (qPCR) approaches.

Target	Primer (reference)	DNA sequence (bp)	Annealing temperature (°C)
mcrA gene	mlas-mod (Angel et al., 2011)	5′-GGYGGTGTMGGDTTCACMCARTA-3′	57
	mcrA-rev (Angel et al., 2011)	5′-CGTTCATBGCGTAGTTVGGRTAGT-3′	
fhs gene	fhs-f (Xu et al., 2009)	5′-gTWTgggAAAAggYggMgAAgg-3′	55
	fhs-r (Xu et al., 2009)	5′-gTATTgDgTYTTRgCCATACA-3′	
Bacteria	519f (Imachi et al., 2008)	5′-CAGCMGCCGCGGTAANWC-3′	50
	907r (Imachi et al., 2008)	5′-CCGTCAATTCMTTTRAGTTT-3′	

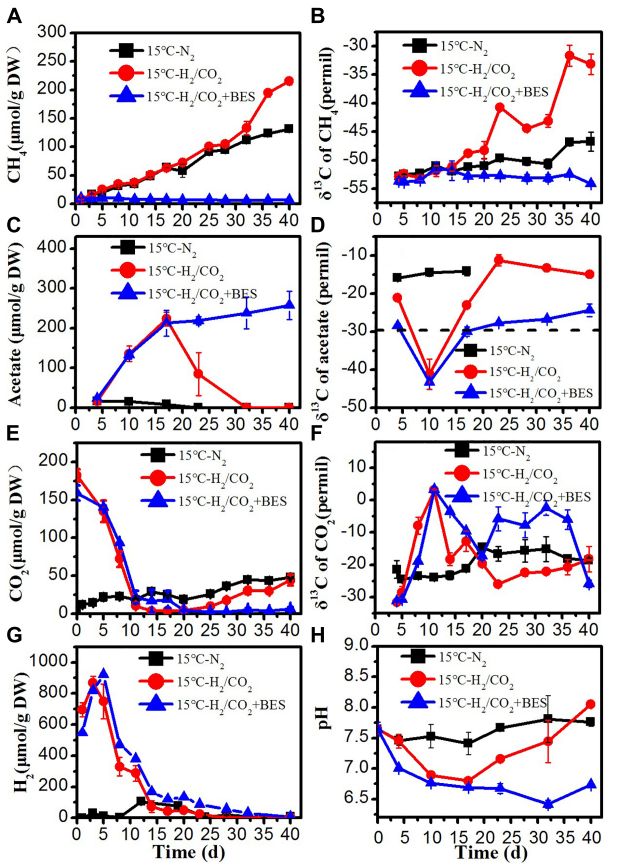

FIGURE 1 | Time course of accumulated **(A)** CH_4, **(B)** $\delta^{13}C$ of CH_4, **(C)** acetate, **(D)** $\delta^{13}C$ of acetate, **(E)** CO_2, **(F)** $\delta^{13}C$ of CO_2, **(G)** H_2 concentration, and **(H)** pH during the treatment of sewage sludge at 15°C, BES as an inhibiter of methanogenesis. The $\delta^{13}C$ of the sludge organic matter (−29.8‰) was represented by dotted line. Mean ± SD, $n = 3$.

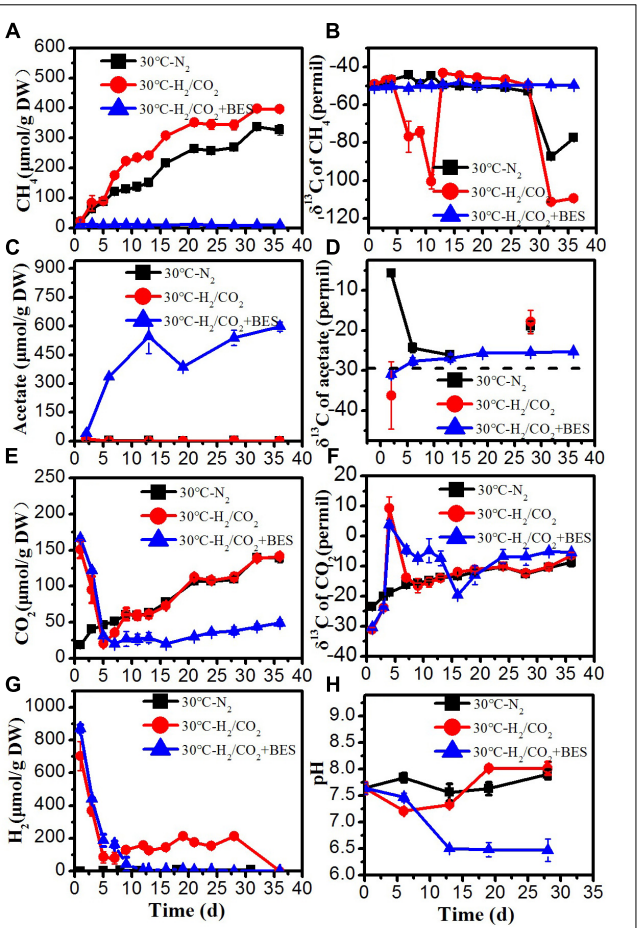

FIGURE 2 | Time course of accumulated **(A)** CH_4, **(B)** $\delta^{13}C$ of CH_4, **(C)** acetate, **(D)** $\delta^{13}C$ of acetate, **(E)** CO_2, **(F)** $\delta^{13}C$ of CO_2, **(G)** H_2 concentration, and **(H)** pH during the treatment of sewage sludge at 30°C, BES as an inhibiter of methanogenesis. The $\delta^{13}C$ of the sludge organic matter (−29.8‰) was represented by dotted line. Mean ± SD, $n = 3$.

by BES (**Figure 2B**). Similarly, formate, propionate and butyrate accumulated in the H_2/CO_2 incubations transiently but only in the presence of BES (**Supplementary Figure S2**). These observations indicate that any produced VFA was instantaneously consumed and did not accumulate when acetoclastic methanogenesis was operating in the absence of BES. In the N_2 controls only traces of H_2 (<7 μmol/g DW) were detected (**Figure 2G**). The concentrations of H_2 and CO_2 both decreased initially in the H_2/CO_2 treatments. Although H_2 and CO_2 later on gradually increased again but slightly increased H_2 was completely consumed after Day 28 in the absence of BES (**Figure 2E**). Initially, H_2 and CO_2 was consumed by hydrogenotrophic methanogenesis to produce CH_4, as indicated by the very low $\delta^{13}C$ value of CH_4 (−100.6‰) (**Figure 2B**). At the end of the incubation, $\delta^{13}C$ of CH_4 again decreased to −111.3‰ and $\delta^{13}C$ of CO_2 gradually and slightly increased indicating dominance of hydrogenotrophic methanogenesis. The slight increase of H_2 and CO_2 concentration in the middle of incubation could be due to the fermentation of organic matter in the sludge, which is consistent with a similar trend and similar values in the N_2 controls and the decrease of $\delta^{13}C$ of CO_2 and the absence of acetate accumulation (**Figures 2C,E–G**).

The amounts of acetate production (about 500–550 μmol/g DW) were larger than expected from the amounts of H_2 consumed (about 870 μmol/g DW) and the assumed stoichiometry of 1:4 (**Table 2**). Accumulation of CH_4 in the presence of exogenous H_2/CO_2 was not much larger (396 μmol/g DW) than in the absence (326 μmol/g DW) (**Table 2**). Therefore, it is likely that both CH_4 and acetate were to a large extent produced from the sewage sludge rather than from the exogenous H_2/CO_2, which would imply a stoichiometry of 4:1 as characteristic for hydrogenotrophic methanogenesis.

H_2/CO_2 Utilization at Thermophilic Temperature

At 50°C, the rates of CH_4 production were higher than at 30 and 15°C (**Figure 3**). The added H_2 was only slowly consumed when BES was present. The concentrations of H_2 decreased initially in the H_2/CO_2 treatments, but H_2 later on gradually increased

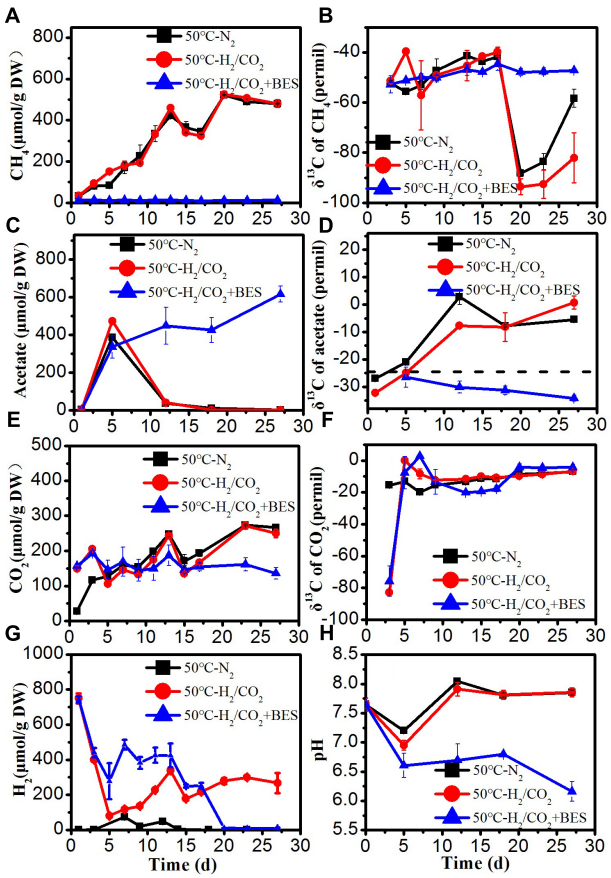

FIGURE 3 | Time course of accumulated **(A)** CH_4, **(B)** $\delta^{13}C$ of CH_4, **(C)** acetate, **(D)** $\delta^{13}C$ of acetate, **(E)** CO_2, **(F)** $\delta^{13}C$ of CO_2, **(G)** H_2 concentration, and **(H)** pH during the treatment of sewage sludge at 50°C, BES as an inhibiter of methanogenesis. The $\delta^{13}C$ of the sludge organic matter (−29.8‰) was represented by dotted line. Mean ± SD, n = 3.

again to the final concentrations of about 280 μmol/g DW, which were higher than at the other temperatures (**Figure 3G**). The added CO_2 was also hardly consumed at 50°C, and in the N_2 control CO_2 eventually increased to a similar concentration (**Figure 3E**). The detected H_2 concentrations in the N_2 controls were generally lower than 73 μmol/gDW (**Figure 3G**). Acetate, however, was transiently produced in all the treatments including the N_2 control, but was later on consumed again except when CH_4 production was inhibited by BES (**Figure 3C**). Accumulated formate of 173–206 μmol/g was finally consumed to very low concentration except in the H_2/CO_2 treatments where finally about 68 μmol/g DW formate remained (**Supplementary Figure S3**). In the N_2 controls and the H_2/CO_2 treatments, propionate and butyrate were transiently accumulated to about 87 and 32 μmol/g DW and subsequently consumed (**Supplementary Figure S3**). Propionate and butyrate concentrations reached 82 and 63 μmol/g DW in the BES treatments (**Supplementary Figure S3**). The $\delta^{13}C$ of acetate substantially increased to about − 7‰ due to the consumption, except in the presence of BES (**Figure 3D**). The $\delta^{13}C$ of CO_2 initially increased and then stayed relatively constant at about −15 to −5‰ (**Figure 3F**), and that of CH_4 was about −50‰, but decreased significantly at the end of incubation, except in the presence of BES (**Figure 3B**).

The produced amounts of both acetate and CH_4 were much larger than the amounts of exogenous H_2 consumed, assuming a stoichiometry of 1:4 as characteristic for chemolithotrophic acetogenesis and hydrogenotrophic methanogenesis (**Table 2**). Consequently, it is likely that most of the acetogenic and methanogenic substrates were produced from the anaerobic sewage sludge.

Quantification of Methanogens and Acetogenic Bacteria

The copy numbers of the *mcrA* gene, coding for a subunit of the methyl coenzyme M reductase, was measured as equivalent for the number of methanogens in the sewage sludge (**Figure 4**). In BES treatments *mcrA* was not quantified. The copy numbers of *mcrA* gene at 50 and 30°C were one order of magnitude higher than those of 15°C during the whole incubation (**Figure 4A**). At 15°C, the final copy numbers of *mcrA* gene under H_2/CO_2 were one order of magnitude higher than that of the controls, which indicated H_2/CO_2 stimulated the growth of methanogens (**Figure 4**). The copy numbers of *mcrA* gene at 30°C were always one order of magnitude higher than those of the N_2 control during the whole incubation. However, the copy numbers of *mcrA* gene in the H_2/CO_2

TABLE 2 | Accumulated (positive μmol/g DW) or consumed (negative μmol/g DW) metabolites in the different incubations.

	At time of maximum acetate accumulation						At the end					
Incubation	**H_2**	**Acetate**	**Formate**	**Propionate**	**butyrate**	**CH_4**	**H_2**	**Acetate**	**Formate**	**Propionate**	**butyrate**	**CH_4**
15°C, N_2	–	8	10	8	0	64	–	0	0	0	0	131
15°C, H_2/CO_2	−825	223	3	20	0	64	−866	0	0	1	0	216
15°C, H_2/CO_2, BES	−801	212	14	21	1	8	−916	258	0	23	6	6
30°C, N_2	–	2	0	0	0	129	–	0	0	0	0	326
30°C, H_2/CO_2	−575	0	23	0	0	222	−700	0	0	0	0	395
30°C, H_2/CO_2, BES	−829	335	306	310	71	10	−870	598	0	0	45	10
50°C, N_2	–	386	0	83	28	84	–	2	0	0	2	479
50°C, H_2/CO_2	−669	473	0	86	32	151	−483	2	68	0	2	481
50°C, H_2/CO_2, BES	−465	336	11	92	0	11	−734	616	1	82	63	12

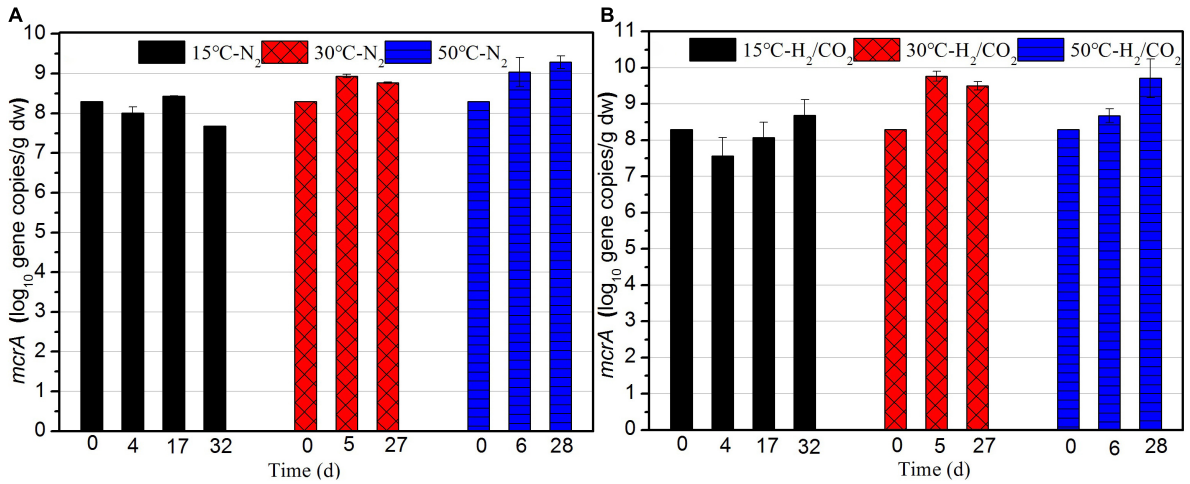

FIGURE 4 | Copy numbers of *mcrA* gene during the **(A)** N_2 controls and **(B)** H_2/CO_2 treatments of sewage sludge at 15, 30, and 50°C. Mean ± SD, $n = 3$.

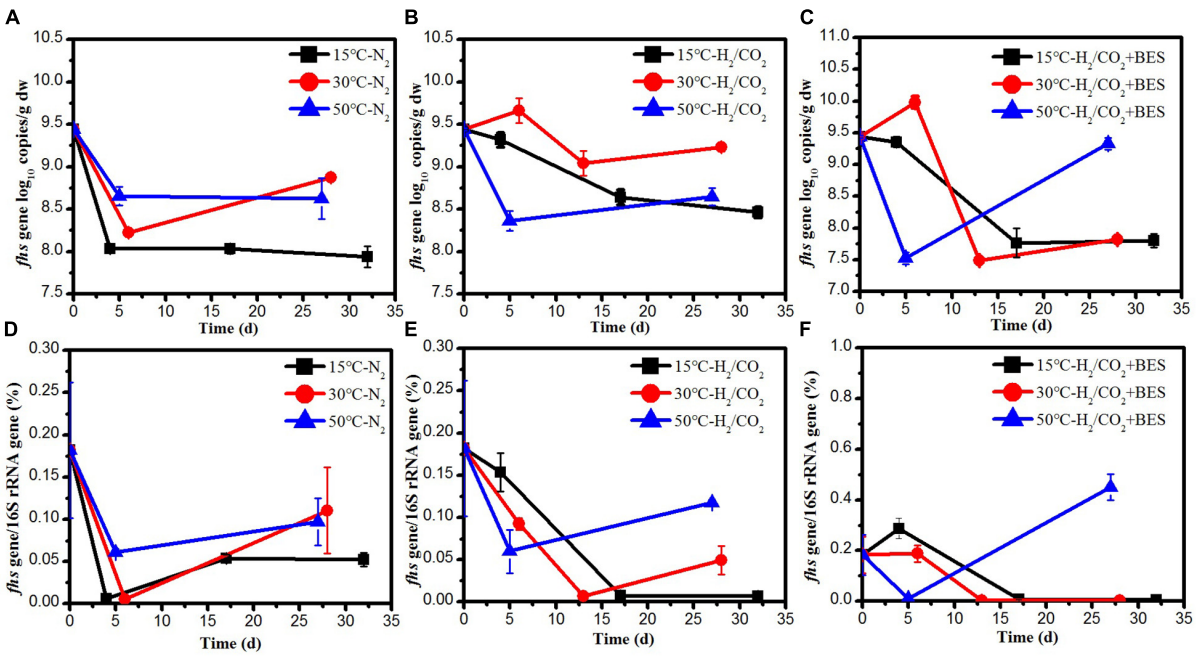

FIGURE 5 | Copy numbers of **(A–C)** *fhs* gene and **(D–F)** *fhs* gene/16S gene during the treatment of sewage sludge at 15, 30, and 50°C, BES as an inhibiter of methanogenesis. Mean ± SD, $n = 3$.

incubation at 50°C were at a similar level than those of the N_2 controls (**Figure 4**).

The *fhs* gene, coding for the formyl tetrahydrofolate synthetase, was quantified as equivalent of the number of acetogens, and compared to the number of bacterial 16S rRNA gene copies. At low temperature, the initial copy numbers of *fhs* gene in the H_2/CO_2 incubations were one order of magnitude higher than those of the N_2 control (**Figure 5**). The copy numbers of *fhs* gene at 30°C showed a same trend as at 15°C and the relative abundance under H_2/CO_2 was 19–40 times higher than that of the N_2 control (**Figure 5**). At 50°C, addition of H_2/CO_2 did not affect the copy numbers and abundance of *fhs* gene (**Figure 5**).

Chemolithotrophic Acetogenesis Versus Hydrogenotrophic Methanogenesis Under Elevated H_2/CO_2 Concentration at Different Temperature

In order to interpret the competition for H_2/CO_2 between acetogens and methanogens at different temperatures, we determined the percentage of methane to the total products

(methane + acetate) at the time of maximum acetate accumulation (**Table 3**). Methanogenesis contributed only marginally (3–4%) in presence of BES due to the inhibition of methanogenesis. However, hydrogenotrophic methanogenesis may has been the exclusive process (98–100%) for H_2/CO_2 consumption at 30°C, especially in the treatment with H_2/CO_2 (**Table 3**), which was also indicated by the initial and transient decrease of the $\delta^{13}C$ of CH_4 to values of −100.6‰ and final decrease again to −111.3‰ (**Figure 2B**). By contrast, acetogenesis contributed substantially at 15 and 50°C (**Table 3**). At 15°C, acetogenesis contributed only in the H_2/CO_2 treatment (78%), but at 50°C it also contributed much (82%) without exogenous H_2/CO_2 (**Table 3**). The transient accumulation of acetate at 50°C (especially in the N_2 control) indicates that at the beginning of the incubation fermentative acetate production (in addition to chemolithotrophic acetogenesis) was faster than the consumption of acetate.

DISCUSSION

The Effect of Temperature on Competition Between Chemolithotrophic Acetogenesis and Hydrogenotrophic Methanogenesis

The competition of acetogens and methanogens for H_2 is of great importance in many anoxic systems. However, the investigation of the competition between them is very complex. As the product of acetogens, acetate is also produced by fermentation and consumed by different metabolic pathways at the same time. Isotope technique is a reasonable approach to study the competition between acetogens and methanogens for H_2 since chemolithotrophic acetogenesis and hydrogenotrophic methanogenesis result in a distinct ^{13}C depletion of acetate and methane, respectively (Conrad, 2005; Ho et al., 2014; Gehring et al., 2016). Unfortunately, a complication arises from the fact that acetate concentrations in the anoxic environment are often too low for detection and isotopic analysis. Stimulation of chemolithotrophic acetogenesis and hydrogenotrophic methanogenesis by addition of H_2 apparently allowed determination of reasonable ^{13}C values of acetate and methane. Although the experiment set-up of exogenous H_2 addition may not represent *in situ* condition, it still provides a maximum of further insight into the potential competition between acetogens and methanogens for H_2.

The results of our study showed that the outcome of the competition between chemolithotrophic acetogenesis and hydrogenotrophic methanogenesis strongly depended on the incubation temperature. Collectively, our results suggest the following pathways for consumption of H_2/CO_2 (**Figure 6**). Chemolithotrophic acetogenesis consumed most of the added H_2/CO_2 at low temperature (15°C) and high (50°C) temperature. Hydrogenotrophic methanogenesis was the dominant pathway at middle (30°C) temperature. At high temperature, acetate was not only produced from H_2/CO_2 but also greatly from organic matter. Subsequently, the acetate was probably degraded by thermotolerant acetoclastic methanogens. A conversion of acetate to H_2/CO_2 (by the reversal of chemolithotrophic acetogenesis) was unlikely due to the relatively high H_2 concentrations in the 50°C treatment, rendering this reaction thermodynamically endergonic.

At 15°C, the addition of H2/CO2 stimulated the production of acetate with isotopically low value (−41.1 to −43.3‰) indicating the operation of chemolithotrophic acetogenesis (**Figure 1D**). Furthermore, the decrease in $\delta^{13}C$ values of acetate was paralleled by an increase of copy numbers of the *fhs* gene (**Figure 5**). The accumulated acetate was gradually exhausted, accompanied by a significant increase of $\delta^{13}C$-enriched CH_4 and an increase of $\delta^{13}C_{acetate}$ value (**Figures 1B,D**). Typically, the acetate-derived CH_4 shows a smaller fractionation than the CO_2-derived CH_4 (Conrad, 2005; Gehring et al., 2015). Hence, the formed acetate from chemolithotrophic acetogenesis was mainly consumed by acetoclastic methanogens to produce CH_4.

At 30°C, the ratios of methane to the total products in the treatments with H_2/CO_2 and the N_2 controls were almost 100% (**Table 3**). The methane production under H_2/CO_2

TABLE 3 | Percentage of methane relative to total products (acetate + methane) formed at the time of maximum acetate accumulation.

Treatment	15°C	30°C	50°C
N_2	89	98	18
H_2/CO_2	22	100	24
H_2/CO_2 + BES	4	3	3

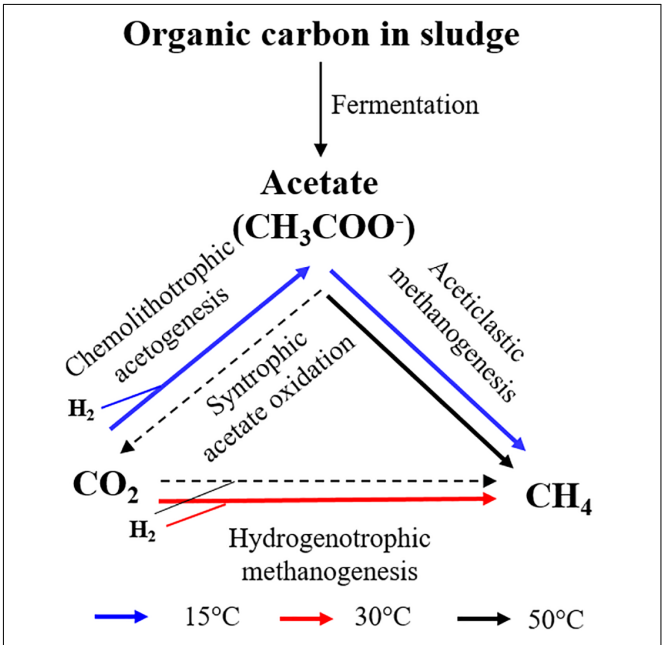

FIGURE 6 | The pathways for consumption of H_2/CO_2 during the anaerobic digestion of sewage sludge at 15, 30, and 50°C.

was accompanied by very low $\delta^{13}C$ values (−100.5 to −76.8‰) and increased copy numbers of the *mcrA* gene (**Figures 2B**, **4**). This indicated that elevated H_2/CO_2 exclusively stimulated the formation of methane via hydrogenotrophic methanogenesis at mesophilic temperature.

At 50°C, the ratios of methane to the total products in the H_2/CO_2 incubations and N_2 controls were only 24 and 18%, respectively. Hence much of the H_2/CO_2 was converted to acetate similarly as at 15°C. However, the stoichiometry of acetate production indicated that an additional part was produced from fermentation of organic matters (Heuer et al., 2010). The copy numbers of the *fhs* gene were similar with those in the N_2 controls. The acetate was transiently produced and paralleled by an increase in $\delta^{13}C$ values of acetate due to acetate consumption (**Figures 3C,D**). The isotopically enriched acetate was eventually and completely consumed, followed by the production of ^{13}C-depleted CH_4, which was produced after day 16 until the end of incubation (**Figure 3B**). Collectively, these observations can be explained by chemolithotrophic acetogenesis from H_2/CO_2, followed by aceticlastic methanogenesis. However, the relatively high and constant H_2 concentrations during the latter incubation are not easily explained. Perhaps, they were caused by small H_2 production from aceticlastic methanogens (Kulkarni et al., 2018).

Compared to the N_2 controls, the presence of exogenous H_2 significantly affected the percentage of methane relative to the total products formed only at 15°C (**Table 3**), which indicated that chemolithotrophic acetogenesis was more favored at low than at medium and high temperatures. This has also been shown in our previous study of rice field soils (Liu and Conrad, 2011; Fu et al., 2018). Acetogens have at low temperatures higher growth rates than most methanogens (Kotsyurbenko et al., 2001). Under mesophilic conditions, however, methanogenesis is generally energetically more beneficial than acetogenesis, and also exhibits a higher cell-specific affinity for substrate, resulting in much stronger H_2/CO_2 utilization via hydrogenotrophic methanogenesis than via homoacetogenesis (Hoehler et al., 2002; Conrad et al., 2008). At thermophilic temperatures, acetate production from H_2/CO_2 was augmented by heterotrophic acetate production.

Implication for Sludge Digestion Operation

This study illuminates the carbon flow in sludge anaerobic digestion under elevated H_2/CO_2 concentrations at different temperatures. This understanding deepens our knowledge of methanogenesis pathways involved in anaerobic digestion of sewage sludge, which are fundamental for improvement or regulation of the anaerobic digestion process. Temperature regulation strategy may be used for sludge digestion operation. Thermophilic digestion facilitates syntrophic acetate oxidization, which helps relieve methanogens from substrate inhibition such as high ammonia and high acetate concentration (Hao et al., 2011; Wang et al., 2015; Westerholm et al., 2019). As such, thermophilic digestion could potentially apply to ammonia-rich wastes such as cattle and pig manure or easily degradable wastes such as food waste for methane production.

Methane has a low monetary value. Therefore, more and more attention has been paid to the promises and challenges of an undefined-mixed-culture process to generate a mixture of carboxylates as intermediate platform chemicals toward generation of complex fuels from wastes (Agler et al., 2011). As useful chemical, acetate can be generated from fermentation and homoacetogenesis during anaerobic digestion. Thermophilic digestion enables high hydrolysis and fermentation efficiencies, which could allow efficient acetate accumulation from organic wastes. Additionally, elevated H_2/CO_2 concentrations at low temperatures is beneficial to homoacetogenesis, enabling higher production of acetate than methane. Our previous study has reported a novel system coupling glucose fermentation and homoacetogenesis for elevated acetate production (Nie et al., 2008; Ni et al., 2010). When aiming at higher acetate production from sludge, a two-stage thermophilic-psychrophilic AD process coupling fermentation and homoacetogenesis is an alternative approach, with the first stage operated at high temperature (50–55°C) to enable fast hydrolysis and fermentation, and the second stage at 10–15°C under elevated H_2/CO_2 concentration derived from the first stage to enable efficient acetogenesis.

DATA AVAILABILITY STATEMENT

The datasets generated for this study are available on request to the corresponding author.

AUTHOR CONTRIBUTIONS

BF planned, designed, and performed the experiments as well as revised the manuscript. XJ participated in performing the experiments and wrote the manuscript. RC designed the experiments and analyzed the results as well as revised the manuscript. HoL assisted in the performance of experiments and revisions of the final manuscript. HeL conceived and coordinated the study, and revised the final manuscript. All authors read and approved the final version of the manuscript.

FUNDING

This research was supported by the Natural Science Foundation of Jiangsu Province (BK20181344), the National Natural Science Foundation of China (51678280), and the Jiangsu Key Laboratory of Anaerobic Biotechnology (JKLAB201711).

SUPPLEMENTARY MATERIAL

The Supplementary Material for this article can be found online at: https://www.frontiersin.org/articles/10.3389/fmicb.2019.02418/full#supplementary-material

REFERENCES

Adekunle, F. K., and Okolie, A. J. (2015). A review of biochemical process of anaerobic digestion. *Adv. Biosci. Biotechnol.* 6, 205–212. doi: 10.4236/abb.2015.63020

Agler, T. M., Wrenn, A. B., Zinder, H. S., and Angenent, T. L. (2011). Waste to bioproduct conversion with undefined mixed cultures: the carboxylate platform. *Trends Biotechnol.* 29, 70–78. doi: 10.1016/j.tibtech.2010.11.006

Angel, R., Claus, P., and Conrad, R. (2011). Methanogenic archaea are globally ubiquitous in aerated soils and become active under wet anoxic conditions. *ISME J.* 6, 847–862. doi: 10.1038/ismej.2011.141

Blaser, M. B., Dreisbach, L. K., and Conrad, R. (2013). Carbon isotope fractionation of 11 acetogenic strains grown on H2 and CO2. *Appl. Environ. Microb.* 79, 1787–1794. doi: 10.1128/AEM.03203-12

Chin, K. J., and Conrad, R. (2010). Intermediary metabolism in methanogenic paddy soil and the influence of temperature. *FEMS Microbiol. Ecol.* 18, 85–102. doi: 10.1016/0168-6496(95)00042-9

Conrad, R. (2005). Quantification of methanogenic pathways using stable carbon isotopic signatures: a review and a proposal. *Org. Geochem.* 36, 739–752. doi: 10.1016/j.orggeochem.2004.09.006

Conrad, R., Bak, F., Seitz, H. J., Thebrath, B., Mayer, H. P., and Schütz, H. (1989). Hydrogen turnover by psychrotrophic homoacetogenic and mesophilic methanogenic bacteria in anoxic paddy soil and lake sediment. *FEMS Mocrobiol. Ecol.* 62, 285–294. doi: 10.1016/0378-1097(89)90010-4

Conrad, R., Liu, S., and Drake, H. (2008). "Temperature effects on methanogenic microbial communities," in *Microbes and the Environment: Perspectives and Challenges*, eds S. J. Liu, and H. L. Drake, (Beijing: Science Press), 35–40.

Conrad, R., and Wetter, B. (1990). Influence of temperature on energetics of hydrogen metabolism in homoacetogenic, methanogenic, and other anaerobic bacteria. *Arch. Microbiol.* 155, 94–98. doi: 10.1007/bf00291281

Fu, B., Conrad, R., and Blaser, M. (2018). Potential contribution of acetogenesis to anaerobic degradation in methanogenic rice field soils. *Soil Biol. Biochem.* 119, 1–10. doi: 10.1016/j.soilbio.2017.10.034

Galand, P., Yrjälä, K., and Conrad, R. (2010). Stable carbon isotope fractionation during methanogenesis in three boreal peatland ecosystems. *Biogeosciences* 7, 3893–3900. doi: 10.5194/bg-7-3893-2010

Gehring, T., Klang, J., Niedermayr, A., Berzio, S., Immenhauser, A., Klocke, M., et al. (2015). Determination of methanogenic pathways through carbon isotope (δ13C) analysis for the two-stage anaerobic digestion of high-solids substrates. *Environ. Sci. Technol.* 49, 4705–4714. doi: 10.1021/es505665z

Gehring, T., Niedermayr, A., Berzio, S., Immenhauser, A., Wichern, M., and Lübken, M. (2016). Determination of the fractions of syntrophically oxidized acetate in a mesophilic methanogenic reactor through an 12C and 13C isotope based kinetic model. *Water Res.* 102, 362–373. doi: 10.1016/j.watres.2016.06.038

Hao, L. P., Lü, F., He, P. J., Li, L., and Shao, L. M. (2011). Predominant contribution of syntrophic acetate oxidation to thermophilic methane formation at high acetate concentrations. *Environ. Sci. Technol.* 45, 508–513. doi: 10.1021/es102228v

Heuer, V. B., Krüger, M., Elvert, M., and Hinrichs, K. U. (2010). Experimental studies on the stable carbon isotope biogeochemistry of acetate in lake sediments. *Org. Geochem.* 41, 22–30. doi: 10.1016/j.orggeochem.2009.07.004

Ho, D. P., Jensen, P. D., and Batstone, D. J. (2013). Methanosarcinaceae and acetate-oxidizing pathways dominate in high-rate thermophilic anaerobic digestion of waste-activated sludge. *Appl. Environ. Microb.* 79, 6491–6500. doi: 10.1128/AEM.01730-13

Ho, D., Jensen, P., and Batstone, D. (2014). Effects of temperature and hydraulic retention time on acetotrophic pathways and performance in high-rate sludge digestion. *Environ. Sci. Technol.* 48, 6468–6476. doi: 10.1021/es500074j

Hoehler, T. M., Albert, D. B., Alperin, M. J., Bebout, B. M., Martens, C. S., and Des Marais, D. J. (2002). Comparative ecology of H2 cycling in sedimentary and phototrophic ecosystems. *Antonie Van Leeuwenhoek* 81, 575–585.

Imachi, H., Sakai, S., Sekiguchi, Y., Hanada, S., Kamagata, Y., Ohashi, A., et al. (2008). *Methanolinea* tarda gen. nov., sp. nov., a methane-producing archaeon isolated from a methanogenic digester sludge. *Int. J. Syst. Evol. Microbiol.* 58, 294–301. doi: 10.1099/ijs.0.65394-0

Ji, Y., Liu, P., and Conrad, R. (2018). Change of the pathway of methane production with progressing anoxic incubation of paddy soil. *Soil Biol. Biochem.* 121, 177–184. doi: 10.1016/j.soilbio.2018.03.014

Kelessidis, A., and Stasinakis, S. A. (2012). Comparative study of the methods used for treatment and final disposal of sewage sludge in European countries. *Waste Manage.* 32, 1186–1195. doi: 10.1016/j.wasman.2012.01.012

Kotsyurbenko, O. R., Glagolev, M. V., Nozhevnikova, A. N., and Conrad, R. (2001). Competition between homoacetogenic bacteria and methanogenic archaea for hydrogen at low temperature. *FEMS Microbiol. Ecol.* 38, 153–159. doi: 10.1016/s0168-6496(01)00179-9

Kulkarni, G., Mand, D. T., and Metcalf, W. W. (2018). Energy conservation via hydrogen cycling in the methanogenic archaeon *Methanosarcina barkeri*. *Mbio* 9, e01256-18. doi: 10.1128/mBio.01256-18

Liu, F., and Conrad, R. (2011). Chemolithotrophic acetogenic H2/CO2 utilization in Italian rice field soil. *ISME J.* 5, 1526–1539. doi: 10.1038/ismej.2011.17

Liu, R., Hao, X., and Wei, J. (2016). Function of homoacetogenesis on the heterotrophic methane production with exogenous H2/CO2 involved. *Chem. Eng. J.* 284, 1196–1203. doi: 10.1016/j.cej.2015.09.081

Lopes, M., Alves, J. I., Arantes, A. L., Belo, I., Sousa, D. Z., and Alves, M. M. (2015). Hydrogenotrophic activity under increased H2/CO2 pressure: effect on methane production and microbial community. *J. Biotechnol.* 208:S57.

Ni, B. J., He, L., Nie, Y. Q., Zeng, R. J., Du, G. C., Chen, J., et al. (2010). Coupling glucose fermentation and homoacetogenesis for elevated acetate production: experimental and mathematical approaches. *Biotechnol. Bioeng.* 108, 345–353. doi: 10.1002/bit.22908

Nie, Y. Q., Liu, H., Du, G. C., and Chen, J. (2008). Acetate yield increased by gas circulation and fed-batch fermentation in a novel syntrophic acetogenesis and homoacetogenesis coupling system. *Bioresour. Technol.* 99, 2989–2995.

Niu, D. J., Hui, H., Dai, X. H., and Zhao, Y. C. (2013). Greenhouse gases emissions accounting for typical sewage sludge digestion with energy utilization and residue land application in China. *Waste Manage.* 33, 123–128. doi: 10.1016/j.wasman.2012.06.024

Olivier, M. F. (2016). *Temperature and Salinity Controls on Methanogenesis in an Artificial Freshwater Lake*. Cardiff Bay: Cardiff University.

Shanmugam, S. R., Chaganti, S. R., Lalman, J. A., and Heath, D. D. (2014). Statistical optimization of conditions for minimum H2 consumption in mixed anaerobic cultures: effect on homoacetogenesis and methanogenesis. *Int. J. Hydrogen Energy* 39, 15433–15445.

Stumm, W., and Morgan, J. J. (1981). *Aquatic Chemistry: An Introduction Emphasizing Chemical Equilibria in Natural Waters*. New York: Wiley.

Wang, H., Fotidis, A. I., and Angelidaki, I. (2015). Ammonia effect on hydrogenotrophic methanogens and syntrophic acetate-oxidizing bacteria. *FEMS Microbiol. Ecol.* 91, 1–8. doi: 10.1093/femsec/fiv130

Westerholm, M., Dolfing, J., and Schnürer, A. (2019). Growth characteristics and thermodynamics of syntrophic acetate oxidizers. *Environ. Sci. Technol.* 53, 5512–5520. doi: 10.1093/femsec/fiv130

Xu, S., Fu, B., Zhang, L., and Liu, H. (2015). Bioconversion of H2/CO2 by acetogen enriched cultures for acetate and ethanol production: the impact of pH. *World J. Microbiol. Biotechn.* 31, 941–950. doi: 10.1007/s11274-015-1848-8

Xu, K., Liu, H., Du, G., and Chen, J. (2009). Real-time PCR assays targeting formyltetrahydrofolate synthetase gene to enumerate acetogens in natural and engineered environments. *Anaerobe* 15, 204–213. doi: 10.1016/j.anaerobe.2009.03.005

Zábranská, J., Štěpová, J., Wachtl, R., Jenlček, P., and Dohányos, M. (2000). The activity of anaerobic biomass in thermophilic and mesophilic digesters at different loading rates. *Water Sci. Technol.* 42, 49–56.

Conflict of Interest: The authors declare that the research was conducted in the absence of any commercial or financial relationships that could be construed as a potential conflict of interest.

frontiers in Microbiology

ORIGINAL RESEARCH
published: 29 November 2019
doi: 10.3389/fmicb.2019.02785

Energy-Conserving Enzyme Systems Active During Syntrophic Acetate Oxidation in the Thermophilic Bacterium *Thermacetogenium phaeum*

Anja Keller[1,2], *Bernhard Schink*[1,2] *and Nicolai Müller*[1]*

[1] Department of Biology, Universität Konstanz, Konstanz, Germany, [2] Konstanz Research School Chemical Biology, Konstanz, Germany

The thermophilic acetogen *Thermacetogenium phaeum* uses the Wood-Ljungdahl pathway (WLP) in both directions, either for the production of acetate from various compounds or for the oxidation of acetate in syntrophic cooperation with methanogens. In this study, energy–conserving enzyme systems in *T. phaeum* were investigated in both metabolic directions. A gene cluster containing a membrane-bound periplasmically oriented formate dehydrogenase directly adjacent to putative menaquinone synthesis genes was identified in the genome. The protein products of these genes were identified by total proteome analysis, and menaquinone MK-7 had been found earlier as the dominant quinone in the membrane. Enzyme assays with membrane preparations and anthraquinone-2,6-disulfonate as electron acceptor verified the presence of a quinone-dependent formate dehydrogenase. A quinone-dependent methylene–THF reductase is active in the soluble fraction and in the membrane fraction. From these results we conclude a reversed electron transport system from methyl-THF oxidation to CO_2 reduction yielding formate as reduced product which is transferred to the methanogenic partner. The redox potential difference between methyl-THF (E_o' = −200 mV) and formate (E_o' = −432 mV) does not allow electron transfer through syntrophic formate removal alone. We postulate that part of the ATP conserved by substrate-level phosphorylation has to be invested into the generation of a transmembrane proton gradient by ATPase. This proton gradient could drive the endergonic oxidation of methyl-THF in an enzyme reaction similar to the membrane-bound reversed electron transport system previously observed in the syntrophically butyrate-oxidizing bacterium *Syntrophomonas wolfei*. To balance the overall ATP budget in acetate oxidation, we postulate that acetate is activated through an ATP-independent path via aldehyde:ferredoxin oxidoreductase (AOR) and subsequent oxidation of acetaldehyde to acetyl-CoA.

Keywords: syntrophic acetate oxidation, acetogenesis, methylene-THF reductase, membrane–bound formate dehydrogenase, Wood-Ljungdahl pathway

OPEN ACCESS

Edited by:
Mirko Basen,
University of Rostock, Germany

Reviewed by:
Wolfgang Buckel,
University of Marburg, Germany
Johann Heider,
University of Marburg, Germany

***Correspondence:**
Nicolai Müller
Nicolai.Mueller@uni-konstanz.de

Specialty section:
This article was submitted to Microbial Physiology and Metabolism, a section of the journal Frontiers in Microbiology

Received: *27 August 2019*
Accepted: *15 November 2019*
Published: *29 November 2019*

Citation:
Keller A, Schink B and Müller N (2019) Energy-Conserving Enzyme Systems Active During Syntrophic Acetate Oxidation in the Thermophilic Bacterium Thermacetogenium phaeum. Front. Microbiol. 10:2785. doi: 10.3389/fmicb.2019.02785

INTRODUCTION

The Wood-Ljungdahl pathway (WLP) or reductive acetyl-CoA pathway is the central pathway in acetogens and most strictly anaerobic acetate-oxidizing bacteria (AOB). Although the WLP was investigated in depth the mechanism of energy conservation of most acetogens and AOB remained unclear since no net ATP is gained in this pathway by substrate level phosphorylation (Schuchmann and Müller, 2014). For *Acetobacterium woodii,* the mechanism of energy conservation was elucidated completely (Biegel et al., 2009, 2011; Biegel and Müller, 2010; Hess et al., 2013; Bertsch et al., 2015) and also the one in *Moorella thermoacetica* was studied in detail (Huang et al., 2012; Wang et al., 2013; Mock et al., 2014). *A. woodii* conserves energy with the help of a *Rhodobacter* nitrogen fixation (Rnf) complex which pumps sodium ions across the membrane while reduced ferredoxin (Fd^{2-}) is oxidized with NAD^+ in an exergonic reaction (Biegel and Müller, 2010). Other modes of energy conservation were hypothesized before. The thermophile *M. thermoacetica* was shown to have a heterohexameric methylene-THF reductase (MTHFR) (Mock et al., 2014) which does not catalyze the reduction of methylene-THF with NADH. The genes for this enzyme are located in a cluster containing genes annotated as a heterodisulfide reductase (Hdr) enzyme complex. In the same study, it was proposed that the MTHFR could be coupled via formate dehydrogenase to the Ech hydrogenase, similar to a membrane-bound formate hydrogenlyase complex found in *Escherichia coli*. This system could be used to create a proton gradient across the membrane and thus conserve energy during acetogenesis (Mock et al., 2014). In contrast, *A. woodii* lacks this putatively proton translocating system and instead has a heterotrimeric NADH-oxidizing methylene-tetrahydrofolate (THF) reductase which is not coupled to energy conservation (Bertsch et al., 2015).

Only little is known so far about the biochemistry of syntrophic acetate-oxidizing bacteria (SAOB). SAOB are hard to isolate and to cultivate. To date only six defined cultures are known (Schnürer et al., 1996; Hattori et al., 2000; Balk et al., 2002; Westerholm et al., 2010, 2011; Timmers et al., 2018). These cultures do not reach high cell densities, and investigations in cell-free systems are challenged with the problem that the SAOB have to be separated from their methanogenic partners to obtain cell suspensions containing only the bacterial component. One of the strains whose physiology was investigated in more detail is *Clostridium ultunense*, a mesophilic bacterium that oxidizes acetate in a triculture with a hydrogen- and formate-utilizing methanogen MAB1 and a further bacterium, strain TRX1 (Schnürer et al., 1996). The difficulties of mass cultivation for enzyme assays of syntrophic acetate oxidizers can be overcome by using proteomic and genomic approaches. A recent study compared the genomes of all defined SAOB co-cultures that have been sequenced so far (Manzoor et al., 2018).

For the present study, *Thermacetogenium phaeum* was chosen as a model organism for SAOB as its genome sequence is available. It poses a special case of SAOB due to its thermophilic lifestyle, with a temperature range between 40 and 65°C and an optimum growth temperature of 58°C, that facilitates acetate conversion to CO_2 and CH_4 (Hattori et al., 2000; Oehler et al., 2012). *T. phaeum* is able to revert the WLP and thus oxidizes acetate in syntrophic cooperation with *Methanothermobacter thermautotrophicus* strain TM but uses as well hydrogen plus CO_2 to form acetate in axenic cultures (Hattori et al., 2000, 2005). Recently, growth of *T. phaeum* with acetate, ethanolamine, methanol, and ethanol was characterized by proteomic analysis and enzyme assays (Keller et al., 2019). In the current study, the focus will be on syntrophic growth with acetate, and on axenic growth with formate or hydrogen plus CO_2. Enzyme systems that are possibly involved in energy conservation such as membrane-bound formate dehydrogenases or hydrogenases as well as the MTHFR are studied in detail.

MATERIALS AND METHODS

Origin of Organisms and Culture Conditions

Axenic cultures of *T. phaeum* strain PB (DSM 26808) as well as the syntrophic co-culture with *M. thermautotrophicus* strain TM were obtained from the German Culture Collection (DSMZ, Braunschweig, Germany). Cultures were grown anaerobically in modified freshwater medium DSM880 as described before (Keller et al., 2019) at 55°C in the dark without shaking. The axenic culture of *T. phaeum* was grown with formate or hydrogen/CO_2, whereas the syntrophic co-culture was grown with acetate as substrate. Cultivation with hydrogen/CO_2 (79%/21% v/v) was performed by flushing the headspace (70 ml) of 150 ml bottles for 1 min at an overpressure of 1 bar. Formate and acetate were autoclaved in 3 M stock solutions and then added to the cultures to 40 mM final concentration. Cultures were transferred at least 10 times [corresponding to approximately 22 (H_2/CO_2) or 30 (formate) cell generations] with the respective substrates to assure complete adaptation before growth curves were recorded and proteome analysis was performed. For quantification of growth, four bottles were filled each with 45 ml medium and 5 ml pre-culture. Increase in optical density was monitored with a Jenway 6300 spectrophotometer (Staffordshire, United Kingdom) at 600 nm. Substrate depletion and product formation was monitored by HPLC with a Shimadzu system as described before (Keller et al., 2019). Compounds were separated at 60°C on a Rezex™ RHM-Monosaccharide H^+ (8%) ion exchange resin column (LC column 300 × 7.8 mm, 00H-0132-K0, Phenomenex, Los Angeles, CA, United States).

Preparation of Cell-Free Extract and Subcellular Fractions

The preparation of cell-free extracts and subcellular fractions for enzyme activity measurements was carried out under strictly anoxic conditions in an anoxic glove box (Coy, Ann Arbor, MI, United States). Centrifugation was performed in air-tight vessels, and buffers were made anoxic by alternately applying vacuum and 100% N_2 three times under vigorous stirring.

Cultures were harvested by centrifugation at 7,000 × *g* for 15 min at 4°C and washed once with 50 mM Tris–HCl buffer, pH 7.5, containing 3 mM dithiothreitol (DTT). The co-culture was separated by a self-assembling Percoll gradient (70% Percoll in distilled water containing 250 mM sucrose) adapted from Luo et al. (2002) and Enoki et al. (2011) as described before (Keller et al., 2019). The gradient tubes were centrifuged for 1 h at 4°C at 45,000 × *g* in a type 70-Ti rotor in an Optima LE-80K ultracentrifuge (Beckman Coulter, Brea, CA, United States). Cells of *T. phaeum* were enriched in the upper one of the two bands and the cells were collected and washed with 50 mM Tris–HCl, pH 7.5, containing 3 mM DTT. Percoll-separated *T. phaeum* cells of syntrophic cultures or *T. phaeum* cells of axenic cultures were suspended in 3 ml Tris–HCl buffer, pH 7.5, containing 3 mM DTT, and disrupted by at least three passages through a French pressure cell (Aminco, Silver Spring, MD, United States) operated at 137 MPa. The crude extract was centrifuged at room temperature at 11,300 × *g* for 5 min to clear it from cell debris and unopened cells. The soluble fraction containing cytoplasmic and periplasmic enzymes was obtained by ultracentrifugation at 100,000 × *g* in an Optima TL-ultracentrifuge using a TLA110-rotor (Beckman Coulter, Brea, CA, United States) for 1 h. The pellet was washed once with 50 mM Tris–HCl, pH 7.5, containing 3 mM DTT, and after the second centrifugation the pellet was suspended in 0.8 ml and defined as membrane fraction. The soluble fraction was further separated via an anion exchange column (Q-sepharose, HiTrapQ HP column, 5 ml, GE Healthcare, Pittsburgh, PA, United States) manually operated with syringes as described by Keller et al. (2019). First, 0.8 ml of the soluble fraction was applied and the column was washed with five column volumes of 50 mM Tris–HCl, pH 7.5, containing 3 mM DTT. Fraction 1 was eluted with two column volumes of Tris–HCl buffer containing additional 200 mM NaCl and then fraction 2 was eluted with Tris–HCl buffer containing 1 M NaCl.

Mass Spectrometry

Mass spectrometry was performed at the Proteomics facility of the University of Konstanz as described before (Keller et al., 2019). The membrane fraction was cleared from interfering lipids by suspending the membrane pellet in 10% SDS. The solubilized membrane pellet was mixed with loading dye (0.125 M Tris–HCl, pH 6.8, 2% (w/v) SDS, 25% glycerol, 0.01% (w/v) bromophenolblue and 5% β-mercaptoethanol) at a ratio of 1:1, heated to 98°C for 10 min, and was run about 2 cm into a 12% SDS gel (Laemmli, 1970). The gel was stained with colloidal Coomassie (Neuhoff et al., 1988; Schmidt et al., 2013) and the band containing the protein was excised. Samples were digested by trypsin treatment and analyzed by liquid chromatography nanospray tandem mass spectrometry (LC-MS/MS) using an Eksigent nano–HPLC and an LTQ–Orbitrap mass spectrometer (Thermo Fisher, Waltham, MA, United States) as described before (Keller et al., 2019). The ion chromatogram was analyzed using the Proteome Discoverer software (Thermo Fisher, Waltham, MA, United States) and the areas of the respective peaks were integrated for semi-quantitative analysis of relative protein abundances.

Enzyme Activity Measurements

All enzyme activity measurements were performed anoxically in glass cuvettes sealed with rubber stoppers which were flushed with 100% N_2. Activity measurements were carried out at least in triplicate in a Jasco V630 or V730 spectrophotometer (Tokyo, Japan) at 55°C with 50 mM Tris–HCl buffer, pH 7.5, containing 3 mM DTT if not stated otherwise.

Formate Dehydrogenase

Formate dehydrogenase was assayed according to Schmidt et al. (2014) and Keller et al. (2019). Electron acceptors used were either 0.5 mM anthraquinone-2,6-disulfonate (AQDS) [ε_{408} = 7.2 mM^{-1} cm^{-1} (Liu et al., 2007; Shi et al., 2012)], 1 mM benzyl viologen (BV) [BV: ε_{578} = 8.65 $mM^{-1}cm^{-1}$ (McKellar and Sprott, 1979)], 0.25 mM NAD^+ [ε_{340} = 6.3 mM^{-1} cm^{-1} (Ziegenhorn et al., 1976)] or 16 μM oxidized ferredoxin (Fd_{ox}) [ε_{390} = 30 mM^{-1} cm^{-1} (Gersonde et al., 1971)]. Reduction of AQDS was monitored at 408 nm, of BV at 578 nm, of NAD^+ at 340 nm and of Fd_{ox} at 390 nm. Reactions were started by addition of 5 mM sodium formate.

Hydrogenases

Hydrogenases were measured analogous to formate dehydrogenase with the electron acceptors 0.5 mM AQDS, 1 mM BV, 0.25 mM NAD^+ and 16 μM Fd_{ox}. The reaction was started by injection of 100 μl hydrogen into the head space according to Keller et al. (2019).

NADH:Acceptor Oxidoreductase

NADH:acceptor oxidoreductase was measured with 0.5 mM NADH and 0.5 mM AQDS. To monitor the reaction, reduction of AQDS was followed at 408 nm. Formate dehydrogenase, hydrogenase and NADH:acceptor oxidoreductase activity were measured in soluble and membrane fractions of *T. phaeum* cells grown in syntrophic co-culture with acetate.

Methylene-THF Reductase (MTHFR)

Methylene-THF reductase was measured with 0.25 mM NADH or 0.25 mM NADPH as electron donor and methylene-THF as electron acceptor which was synthesized directly in the buffer as described in detail in Bertsch et al. (2015). For this purpose, 1.5 mM formaldehyde and 0.5 mM THF were mixed in 50 mM Tris buffer, pH 7.0, containing 3 mM DTT. Controls with formaldehyde alone were performed to rule out side reactions such as methanol dehydrogenase. To examine an electron bifurcation function of the MTHFR 16 μM Fd_{ox} was added to 0.25 mM NADH and oxidation of NADH was monitored. Oxidation of NADH and NADPH was followed at 365 nm [ε_{365} = 3.441 mM^{-1} cm^{-1} (Ziegenhorn et al., 1976)]. Furthermore, the MTHFR was assayed with 0.2 mM methyl-THF and 0.5 mM NAD^+, 1 mM BV and 0.5 mM AQDS as electron acceptors modified after (Rosner and Schink, 1995; Bertsch et al., 2015). The enzyme was assayed in 50 mM Tris buffer, pH 7.5, containing 3 mM DTT, and the reaction was started by addition of methyl-THF. NAD^+ reduction was monitored at 340 nm [ε_{340} = 6.3 mM^{-1} cm^{-1} (Ziegenhorn et al., 1976)], BV reduction at 578 nm [BV: ε_{578} = 8.65 $mM^{-1}cm^{-1}$

(McKellar and Sprott, 1979)], and AQDS reduction at 408 nm [ε_{408} = 7.2 mM^{-1} cm^{-1} (Liu et al., 2007; Shi et al., 2012)].

Methylene-THF Dehydrogenase (MTHFD)

Methylene-THF dehydrogenase was assayed with 0.25 mM NAD^+ and 0.25 mM $NADP^+$ as electron acceptors and methylene-THF as electron donor, which was synthesized as described above. The reduction of NAD^+ and $NADP^+$ was monitored at 365 nm. Activities of MTHFR and MTHFD were assayed in the soluble fraction and its subfractions 1 and 2, as well as in the membrane fractions of acetate-grown cells.

Comparison of Gene Clusters

The methylene-THF encoding gene clusters of *A.* woodii WB1 (DSM 1030), *M. thermoacetica* (ATCC 39073) and *T. phaeum* PB (DSM12270) as well as the gene cluster containing the periplasmically oriented formate dehydrogenase of *T. phaeum* and *Syntrophomonas wolfei* Goettingen (DSM2245B) were compared with the help of the IMG genome BLAST tool[1] using the blastp program comparing amino acid sequences. Transmembrane domains were predicted with TMHMM (v.2.0, URL)[2], and signal peptides were predicted with SignalP 5.0[3]. Selenocysteine insertion motifs were identified using the bSECISearch tool (Zhang and Gladyshev, 2005)[4].

RESULTS

Growth With Formate or Hydrogen/CO_2

Axenic cultures of *T. phaeum* were grown with 40 mM formate or hydrogen/CO_2, respectively. For growth with hydrogen/CO_2 (79%/21%) the headspace of the bottles was flushed for 1 min. As described earlier (Keller et al., 2019), syntrophic cultures of *T. phaeum* with *M. thermautotrophicus* grown with 40 mM acetate needed 21 days to reach early stationary phase with a doubling time of 42 h as described before (Keller et al., 2019). Cultures grown with formate needed 8 days and with hydrogen/CO_2 5 days to reach stationary phase, with doubling times of 25 to 30 h during exponential growth phases. Growth was very poor and the average change in OD_{600} was 0.042 for hydrogen/CO_2 which, however, could be increased by flushing the headspace again with hydrogen/CO_2. Cultures grown with formate reached an average OD_{600} of 0.07 (**Figure 1**).

Total Proteome Analysis

Total proteome analysis was done with both the soluble fraction and the membrane fraction after syntrophic growth with acetate and growth with formate or hydrogen/CO_2 (**Supplementary Table S1**). All four hydrogenase systems and one formate hydrogenlyase system (FHL) encoded in the genome (Oehler et al., 2012) were identified in the proteome at different levels of abundance (**Figure 2**). Non-F_{420}–reducing hydrogenase (gene locus tags Tph_c26910-26930), membrane-bound Ech hydrogenase (Tph_c21310-21360), NAD(P)-dependent iron-only hydrogenase (Tph_c18430- 18460) and a periplasmic [NiFeSe] hydrogenase (Tph_c06350- 06370) were identified in the proteome during growth with acetate, formate, and hydrogen/CO_2 (**Figure 2**). A FHL was present during growth with hydrogen/CO_2. This FHL system comprises 9 subunits (Tph_c26250- c26370). These subunits are two formate dehydrogenase subunits (Tph_c26250- c_26260), two FHL subunits (Tph_c26270, Tph_c26330) and five hydrogenase-4 (FHL) subunits (Tph_c26280- c26300, Tph_c26340- c26350). Besides the formate dehydrogenase genes present in the FHL cluster, there are five more formate dehydrogenase genes encoded in the genome of *T. phaeum*. The formate dehydrogenase (Tph_18420) whose gene is located next to the one of an NAD(P)-dependent iron-only hydrogenase was present in the proteome during growth with all three substrates. Two formate dehydrogenase gene clusters (Tph_c21680- 21660, Tph_c08060- 08040) were found to be located next to genes annotated as a putative NADH:quinone oxidoreductase. One of the latter formate dehydrogenase gene clusters (Tph_c21680-21660) was apparently not expressed under the applied growth conditions as the respective proteins were not identified in the proteome. The gene cluster of the other formate dehydrogenase (Tph_c08060-08040) was only partially expressed during growth with acetate but constitutively expressed during growth with formate and hydrogen/CO_2 as judged from the presence of the respective proteins. Another formate dehydrogenase (Tph_c27290) was present only during growth with acetate at a very low level, however, in an earlier study, this protein was found to be moderately abundant during syntrophic growth with ethanol or ethanolamine (Keller et al., 2019). Membrane-bound formate dehydrogenase (Tph_c15380- 15410) was identified in the proteome during growth with acetate and not during growth with formate or hydrogen. Enzymes of the WLP were present in the proteome during growth with formate or hydrogen/CO_2 (**Figure 3**). The presence of all enzymes of the WLP during growth with acetate was shown before (Keller et al., 2019).

Analysis of the Methylene-THF Reductase Gene Cluster

The genes for the enzymes of the WLP were found to be clustered in two different locations in the genome of *T. phaeum*. The first cluster contains genes for MTHFD and cyclohydrolase (Tph_c16310- Tph_16320). The amino acid sequence of the two subunits of the enzyme combining MTHFD and cyclohydrolase activity exhibit 50% (Tph_c16320) and 54% identity (Tph_c16310) compared to the ones of *M. thermoacetica*. Identities with the homologs in *A. woodii* are substantially lower, with 35% and 29%, respectively. The second cluster contains the genes encoding CODH/ACS (structural precursor genes and their maturation factors; Tph_c15140- Tph_c15190), methyl-tetrahydrofolate-corrinoid iron-sulfur protein Co-methyltransferase (Tph_c15130) and MTHFR (Tph_c15100- Tph_c15110). MTHFR subunits of *T. phaeum* show high similarity to the MetF (Tph_c15100, 39%

[1]https://img.jgi.doe.gov/cgi-bin/m/main.cgi
[2]http://www.cbs.dtu.dk/services/TMHMM/
[3]http://www.cbs.dtu.dk/services/SignalP/
[4]http://genomics.unl.edu/bSECISearch

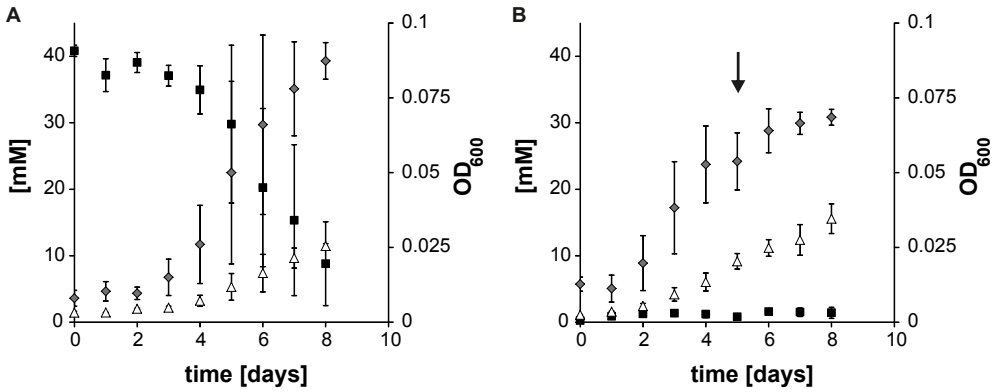

FIGURE 1 | Growth curves of *Thermacetogenium phaeum* depicting substrate depletion, product formation, and OD_{600} increase. **(A)** Axenic growth with formate. **(B)** Axenic growth with hydrogen/CO_2. The arrow marks the time point when the culture was refed with H_2/CO_2. Gray diamonds depict OD_{600}, black squares depict formate concentration and white triangles depict acetate. All concentrations are given in mM ± standard deviation.

identity) and MetV (Tph_c15110 34% identity) of *A. woodii* (**Table 1**; Keller et al., 2019). When comparing the gene clusters of *A. woodii* and *M. thermoacetica,* differences in the composition of this gene cluster can be observed (**Figure 4**). Compared to *A. woodii*, *T. phaeum* lacks the gene that is annotated as *rnfC2* and its product was postulated as the NADH-binding subunit of the MTHFR in *A. woodii* (Bertsch et al., 2015; Keller et al., 2019). Analogous to *M. thermoacetica*, in *T. phaeum,* an *hdrA* gene is located in the gene cluster directly adjacent to the MTHFR. The amino acid sequences of HdrA are identical to 31%. Furthermore, there is a coenzyme F_{420}-reducing hydrogenase subunit (Tph_c15120) that shows 40% identity to the one of *M. thermoacetica*. These two enzymes are not present in *A. woodii*. The genes for the subunits HdrB and HdrC present in *M. thermoacetica* are not located in the methylene-THF containing gene cluster of *T. phaeum*. However, there is a gene coding for an HdrB (Tph_c15470) subunit whose amino acid sequence has an identity of 42% and a gene for an HdrC (Tph_c15480) subunit whose amino acid sequence has an identity of 36% to the one of *M. thermoacetica* in a different gene cluster next to a formate dehydrogenase gene and to the quinone synthesis genes.

Analysis of a Putatively Periplasmically Oriented Formate Dehydrogenase Gene Cluster

During growth with acetate, the genes coding for a membrane-bound formate dehydrogenase (Tph_c15370- c15410) were expressed. Genes coding for this enzyme system were found to be located next to quinone synthesis genes (Tph_c15430-c15460), to two genes of subunits of a heterodisulfide reductase (*hdrB* and *hdrC*, Tph_c15470- Tph_c15480) and to one gene of a subunit of a sec-independent TAT translocase (*tatC*, Tph_c15420) (**Figure 4**). Another gene for a subunit of the TAT translocase complex can be found elsewhere in the genome and is located next to the gene coding for Ech hydrogenase (*tatA*, Tph_c21300). The formate dehydrogenase complex consists of two genes coding for subunits containing *trans*-membrane helices; first a formate dehydrogenase gamma subunit gene (Tph_c15380) and second a quinone-dependent subunit gene (Tph_c15390). One of the remaining two subunit genes (*fdhA2*, Tph_c15410) carries a signal sequence for the Twin-arginine translocation pathway which is lacking in the other subunit (analyzed with SignalP 5.0 and automatic annotation in IMG). A selenocysteine insertion sequence (SECIS)-search of the nucleotide sequence of *fdhA2* (Tph_c15410) revealed that the proteins of this gene and the protein of the adjacent gene *fdhA1* coding for a large formate dehydrogenase subunit (Tph_c15400) are linked through selenocysteine incorporation, meaning that these two genes are translated into one single protein (Zhang and Gladyshev, 2005). In contrast to Oehler et al. (2012), we therefore suggest that this formate dehydrogenase complex is membrane bound, and that the fused protein of the genes *fdhA1* and *fdhA2* (Tph_c15400 and Tph_c15410) is located at the periplasmically oriented side of the enzyme complex. Consequently, the complete formate dehydrogenase complex consists of three protein subunits, namely two proteins with transmembrane helices (Tph_c15380 and fdh subunit gamma, Tph_c15390) and one large periplasmic subunit. The protein of the gene annotated as *fdhE* (Tph_c15370) is responsible for maturation of the formate dehydrogenase complex. Analysis of the gene neighborhood of the quinone-dependent formate dehydrogenase (Tph_c15390) with the same COG hit in IMG showed similarity with the respective gene neighborhood in *S. wolfei* and *Syntrophomonas zehnderi*. Yet, these strains do not have a heterodisulfide reductase encoded in the same gene cluster. In an IMG gene neighborhood search with this heterodisulfide reductase beta subunit, *Syntrophaceticus schinkii* shows the highest similarity. If the amino acid sequence of heterodisulfide reductase is searched against the genome of *S. wolfei* with the IMG BLAST tool, it shows 47% identity for the beta subunit and 43% for the HdrC subunit. The amino acid sequences of the formate dehydrogenase subunits FdhA1 (Tph_c15400, Swol_0799) showed 56% similarity and FdhA2 (Tph_c15410, Swol_0800) showed 53%, the iron-sulfur

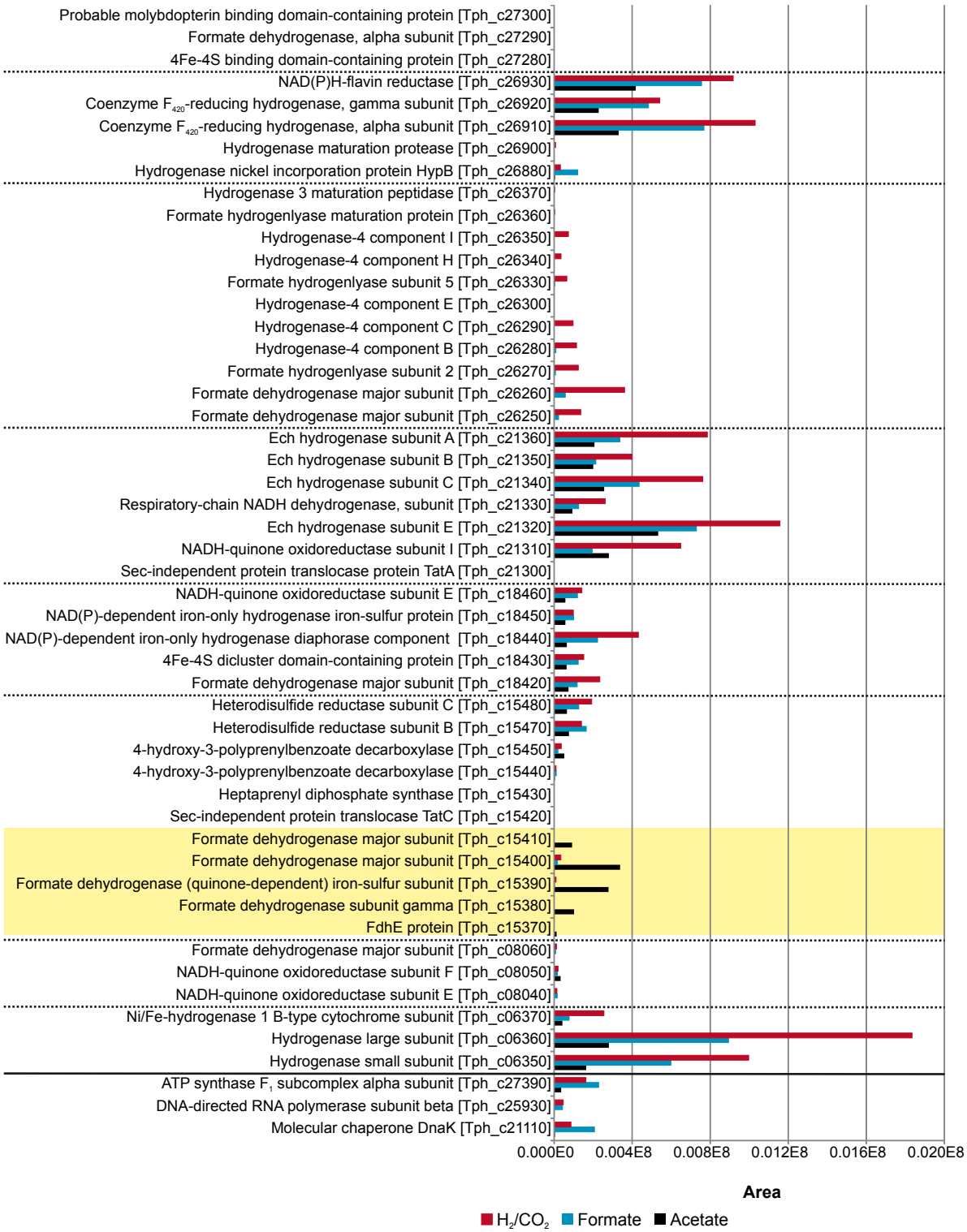

FIGURE 2 | Proteome data of all formate hydrogenases and hydrogenases obtained during growth of *T. phaeum* with formate, hydrogen/CO_2, and acetate. All expressed genes of the different gene clusters are shown in the graph. The clusters are separated by dashed lines. Proteins of the membrane bound, periplasmically oriented formate dehydrogenase that are dominantly present during syntrophic growth with acetate are highlighted in yellow. Housekeeping proteins are depicted beneath the solid line. The proteome data for cultivation with acetate is taken from Keller et al. (2019). The relative abundance of the respective proteins was semi-quantitatively analyzed using the area values of the corresponding peaks of the ion chromatogram and using the Proteome Explorer software (Thermo Fisher). Shown are non-normalized area values in relation to area values of housekeeping proteins (ATPase, RNA-polymerase and molecular chaperone DnaK).

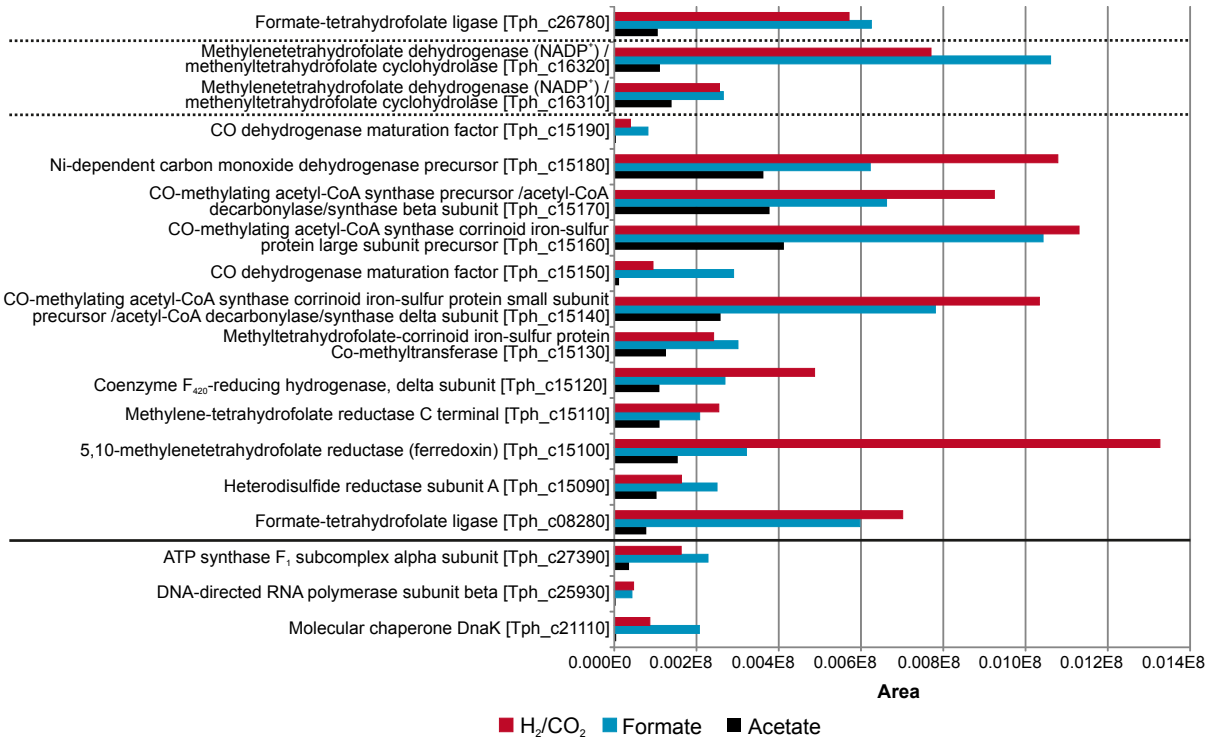

FIGURE 3 | Proteome data of all enzymes of the Wood-Ljungdahl pathway (WLP) obtained during growth of *T. phaeum* with formate, hydrogen/CO_2, and acetate. The clusters are separated by dashed lines. Housekeeping proteins are depicted beneath the solid line. The proteome data for cultivation with acetate is taken from Keller et al. (2019). The relative abundance of the respective proteins was semi-quantitatively analyzed using the area values of the corresponding peaks of the ion chromatogram and using the Proteome Explorer software (Thermo Fisher). Shown are non-normalized area values in relation to area values of housekeeping proteins (ATPase, RNA-polymerase and molecular chaperone DnaK).

subunit (Tph_c15390, Swol_0798) had 54%, the gamma subunit (Tph_c15380, Swol_0797) 46% and the formate accessory protein (Tph_c15370, Swol_0796) had only 28% identity. In contrast to the iron-sulfur subunit (Tph_c15390), its homolog in *S. wolfei* (Swol_0796) does not have transmembrane helices. *M. thermoacetica* was shown to have a periplasmically oriented formate dehydrogenase (gene locus tags Moth_0450-0452) as well. The amino acid sequences of the major subunit (Moth_0450) showed 23 to 30% identity to the major subunits (Tph_c15400-15410) of the periplasmically oriented formate dehydrogenase of *T. phaeum*. The iron-sulfur complex containing subunit (Moth_0451) exhibits 30% identity with the quinone-dependent subunit (Tph_c15390) of *T. phaeum* and the gamma subunit (Moth_0452) shows 33% identity to the gamma subunit (Tph_c15380) of *T. phaeum*.

Activities of Key Enzymes

Methylene-THF Reductase (MTHFR) and Methylene-THF Dehydrogenase (MTHFD)

Activities of MTHFR and MTHFD were assayed photometrically in the following subcellular fractions: membrane fraction, soluble fraction, and fraction 1 and 2 which were soluble fractions eluted from an anion exchange column with 200 mM NaCl or 1 M NaCl, respectively. MTHFR was measured with methylene-THF and NADH or NADPH as electron donors in the direction of methyl-THF formation. Activity with NADH was observed only in fraction 2 (**Table 2**), which is most likely due to the presence of MTHFD in the soluble fraction which immediately reduces the produced NAD^+ through oxidation of methylene-THF. Therefore, both MTHFR and MTHFD have to be separated to properly assess their individual activity with methylene-THF. No activity was observed with NADPH. Addition of Fd_{ox} that was purified from *Clostridium pasteurianum* did not lead to increased activity. This test was run to check for a possible bifurcating enzyme reaction that could enable endergonic oxidation of methyl-THF with NAD^+ by exergonic oxidation of reduced ferredoxin with another molecule of NAD^+. MTHFR was measured also in the oxidative direction with methyl-THF and NAD^+, benzyl viologen (BV) or anthraquinone-2,6-disulfonate (AQDS) as electron acceptor. No activity of the MTHFR was observed for methyl-THF oxidation with NAD^+ in the soluble or membrane fraction. Instead, methyl-THF oxidizing enzyme activity was found with the artificial electron acceptors BV and AQDS and can therefore be considered as NAD^+-independent. The highest activity with benzyl viologen was detected in the membrane fraction with 2598 mU/mg protein and the second highest one in fraction 2 with 477 mU/mg protein. Activities with the artificial quinone-analogous acceptor AQDS were generally lower and in the range of 4 mU/mg protein (membrane fraction) to 24 mU/mg protein (soluble fraction).

TABLE 1 | Comparison of genes of the cluster coding for CODH and MTHFR of *Thermacetogenium phaeum* to genes of *Moorella thermoacetica* and *Acetobacterium woodii*.

Gene name	*T. phaeum*	*M. thermoacetica*		*A. woodii*	
	Locus tag Tph_c	Locus tag Moth_	Identity [%]	Locus tag Awo_c	Identity [%]
Hypothetical protein	15080	No identity		No identity	
Heterodisulfide reductase subunit A	15090	1194	31	No identity	
5,10-methylene-tetrahydrofolate reductase (ferredoxin)	15100	1191	66	09310	39
Methylene-tetrahydrofolate reductase C terminal	15110	1192	55	09290 09300	38 34
Coenzyme F_{420}-reducing hydrogenase, delta subunit	15120	1193	40	10560	31
Methyl-tetrahydrofolate-corrinoid iron-sulfur protein Co-methyltransferase	15130	1197	62	10730	39
CO-methylating acetyl-CoA synthase corrinoid iron-sulfur protein small subunit precursor/acetyl-CoA decarbonylase/synthase delta subunit	15140	1198	57	10710	37
CO dehydrogenase maturation factor	15150	1199	57	10670 10750	46 32
CO-methylating acetyl-CoA synthase corrinoid iron-sulfur protein large subunit precursor	15160	1201	58	10720	42
CO-methylating acetyl-CoA synthase precursor/acetyl-CoA decarbonylase/synthase beta subunit	15170	1202	59	10760	44
Ni-dependent carbon monoxide dehydrogenase precursor	15180	1203	57	10740	40
CO dehydrogenase maturation factor	15190	1204	56	10750	42

Comparison was performed with the IMG genome BLAST tool.

MTHFD was measured with methylene-THF and NAD^+ and $NADP^+$ as electron acceptors. Here, the activity with NAD^+ was 10,000 fold higher than with $NADP^+$ and was mainly found in fraction 1. A control experiment with formaldehyde was performed since methylene-THF was synthesized directly in the buffer by addition of THF and formaldehyde. The highest activity here was 5 mU/mg protein in the soluble fraction with NADH.

Electron-Carrier Re-oxidizing Enzyme Systems

In an attempt to identify enzyme systems that terminally transfer electrons to protons to release hydrogen or transfer electrons to protons and CO_2 to release formate, activities of NADH:acceptor oxidoreductase, formate dehydrogenase, and hydrogenase were tested with photometric enzyme assays. An NADH:acceptor oxidoreductase was measured only in the soluble fraction with an activity of 95 mU/mg protein and with the quinone-like artificial electron acceptor AQDS. Activities of formate dehydrogenase and hydrogenase were measured with various electron acceptors (**Table 3**). Formate dehydrogenase showed very little activity with NAD^+ (5 mU/mg protein) only in the soluble fraction and not in the membrane fraction. There was no reaction with Fd_{ox}. Activity of formate dehydrogenase with AQDS was distributed evenly between soluble fraction (554 mU/mg protein) and membrane fraction (283 mU/mg protein), whereas activity with benzyl viologen was found mainly in the soluble fraction (12234 mU/mg protein in the soluble fraction and 1866 mU/mg protein in the membrane fraction). From these results, formate dehydrogenase can be considered an NAD^+-independent enzyme. Activity of hydrogenase with NAD^+ was almost evenly distributed between soluble and membrane fraction. No activity of the hydrogenase was observed with Fd_{ox}. When tested with benzyl viologen and AQDS, activities of hydrogenase were found to be enriched in the membrane fraction compared to the soluble fraction.

DISCUSSION

In the present study, *T. phaeum* was grown axenically with hydrogen/CO_2 or formate as well as in a syntrophic co-culture with acetate. All genes of the WLP were found to be expressed during growth with the used substrates. Thus, we confirm that in *T. phaeum* the WLP is used in both directions, depending on the substrate provided (Hattori et al., 2005). In the following part we discuss the enzymes which were prominently induced and thus were putatively connected to energy conservation under the respective growth condition.

Acetogenic Growth With Hydrogen/CO_2 or Formate

The only acetogen for which the mechanism of energy conservation during growth with hydrogen/CO_2 was unraveled

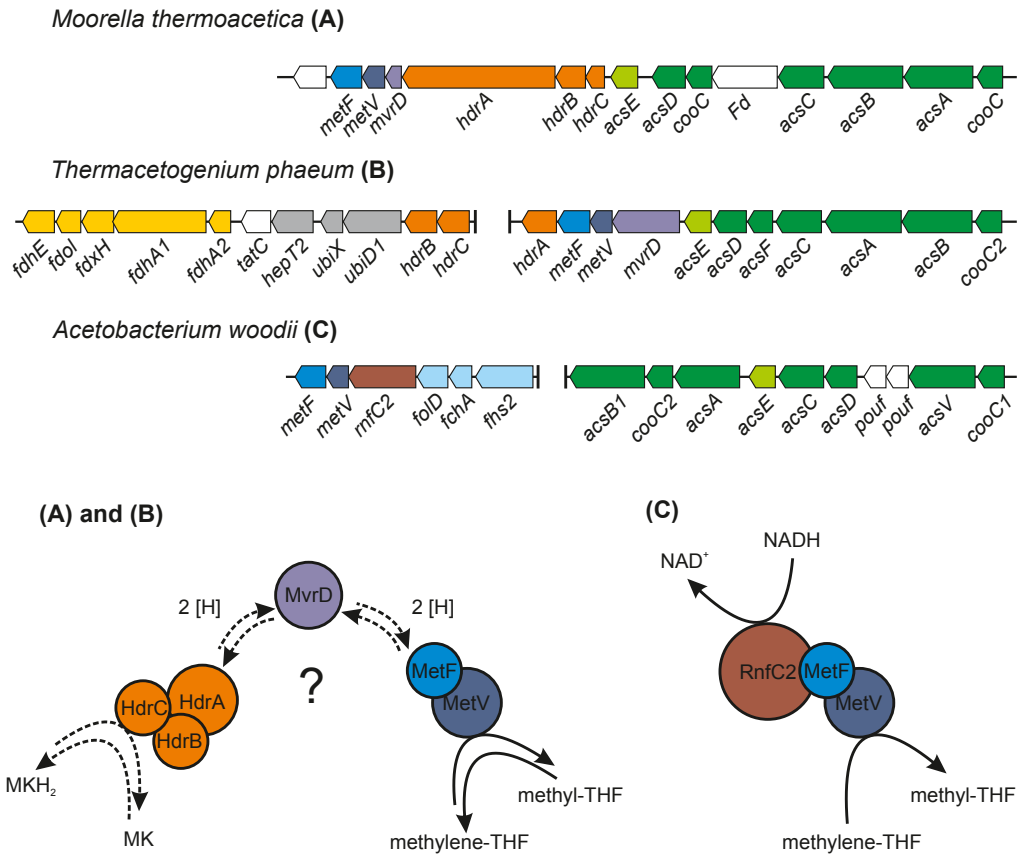

FIGURE 4 | Comparison of the organization of the gene cluster containing the CODH/ACS–encoding genes and the genes for MTHFR of *T. phaeum* with the corresponding gene clusters of *M. thermoacetica* and *Acetobacterium woodii*. The proposed system for the electron transfer of the MTHFR in *T. phaeum* and *M. thermoacetica* is depicted in **(A)** and **(B)** and the protein complex responsible for methylene-THF reduction in *A. woodii* is depicted in **(C)** [adapted from Bertsch et al. (2015)]. MK, oxidized menaquinone; MKH_2, menaquinol; MvrD, methyl-viologen-reducing hydrogenase subunit D; the native electron carrier is still unknown and MvrD is one potential candidate (labeled with a question mark). Activities of MTHFR described in this study were measured with artificial electron acceptors.

TABLE 2 | Activities of methylene-THF reductase and methylene-THF dehydrogenase measured with various electron acceptors in different subcellular fractions of cells grown syntrophically with acetate.

Substrate	Electron carrier	Activity [mU/mg protein]			
		SF	Fraction 1	Fraction 2	MF
Methylene-THF reductase					
Methylene-THF	NADH	bd[a]	bd[a]	169 ± 9	bd[a]
Formaldehyde	NADH	5 ± 0	bd[a]	bd[a]	bd[a]
Methylene-THF	NADPH	–[b]	–[b]	bd[a]	–[b]
Formaldehyde	NADPH	–[b]	–[b]	bd[a]	–[b]
Methyl-THF	NAD^+	bd	–[b]	–[b]	bd
Methyl-THF	BV	16 ± 9	bd[a]	477 ± 84	2598 ± 350
Methyl-THF	AQDS	24 ± 11	bd[a]	5 ± 0	4 ± 2
Methylene-THF dehydrogenase					
Methylene-THF	NAD^+	–[b]	2757304 ± 409024	717 ± 19	–[b]
Formaldehyde	NAD^+	–[b]	bd[a]	bd[a]	–[b]
Methylene-THF	$NADP^+$	–[b]	275 ± 35	–[b]	–[b]
Formaldehyde	$NADP^+$	–[b]	bd[a]	–[b]	–[b]

Activities were measured in soluble fraction (SF), membrane fraction (MF) or in SF separated by anion exchange chromatography with a HiTrapQ column (Fraction 1, elution with 200 mM NaCl and Fraction 2, elution with 1 M NaCl). This was done to separate and individually assay the activities of MTHFR and MTHFD. All enzyme assays were performed in triplicates and are given in mU per mg protein. bd[a], below detection limit (<1 mU per mg protein). –[b], not measured.

TABLE 3 | Activities of formate dehydrogenase and hydrogenase measured with various electron acceptors in the soluble and the membrane fraction of cells grown syntrophically with acetate.

	Electron carrier	SF	MF
Formate DH	AQDS	554 ± 27	283 ± 36
	BV	12234 ± 1161	1866 ± 205
	NAD^+	5 ± 2	bd[a]
	Fd_{ox}	bd[a]	bd[a]
Hydrogenase	AQDS	14 ± 2	254 ± 57
	BV	418 ± 40	1576 ± 116
	NAD^+	248 ± 34	109 ± 28
	Fd_{ox}	bd[a]	bd[a]
NADH:acceptor oxidoreductase	AQDS	95 ± 2	bd[a]

An NADH: acceptor oxidoreductase was measured with AQDS. Activities were measured in soluble fraction (SF), membrane fraction (MF). All enzyme assays were performed in triplicates and are given in mU per mg protein. bd[a], below detection limit (<1 mU per mg protein).

completely so far is *A. woodii*. In this organism, the energy-conserving enzyme system is the Rnf complex which generates a sodium ion gradient by oxidation of reduced Fd with NAD^+, thus driving ATP formation (Biegel et al., 2009, 2011; Biegel and Müller, 2010). However, *T. phaeum*, like *M. thermoacetica,* does not contain genes for an Rnf complex in its genome. Another enzyme which was examined as a potential candidate participating in energy conservation is MTHFR. During acetogenesis, the MTHFR reduces methylene-THF to methyl-THF and uses electrons at a potential of −200 mV which can be delivered by NADH [E_0'(NAD^+/NADH) = −320 mV] in an exergonic reaction (Schuchmann and Müller, 2014). Indeed, activity of the MTHFR with methylene-THF and NADH was observed in the soluble fraction 2. At first sight, this might appear as evidence that MTHFR is NAD^+-dependent. Considering the presence of an NADH:AQDS oxidoreductase, this could also mean that NADH is oxidized with quinones or other yet unknown electron acceptors by an NADH:acceptor oxidoreductase (**Figure 5**). It was suggested that MTHFR could have a bifurcating function and could couple the reduction of Fd_{ox} with NADH to the reduction of methylene-THF. The ΔG_0' of the total reaction would be −12 to +2 kJ per mole, depending on the redox potential of the ferredoxin (Köpke et al., 2010; Schuchmann and Müller, 2014). The concept was disproven in *M. thermoacetica* (Mock et al., 2014), and also in the present study such a bifurcating reaction with NADH and Fd_{ox} was not observed. Instead, the observed activity with NADH and methylene-THF can be interpreted as a combined reaction of NADH:acceptor oxidoreductase and MTHFR, i.e., electron transfer from NADH via quinones to methylene-THF. Comparison of MTHFR of *M. thermoacetica* with MTHFR of *T. phaeum* shows high similarity of 55 to 66% (**Table 1**), but also the whole gene cluster exhibits a similar organization (**Figure 4**). MTHFR consists of two subunits MetV and MetF whose genes are located next to genes of a hydrogenase. Different from *M. thermoacetica* where all *hdrABC*-genes for the three subunits of the HdrABC complex are located in the same gene cluster, in *T. phaeum* only *hdrA* is located in the *metFV*-gene cluster. Genes *hdrB* and *hdrC* are located next to genes for a putatively periplasmically oriented formate dehydrogenase in a separate gene cluster. Genes *hdrB* and *hdrC* were constitutively expressed during growth with all substrates employed. This indicates that the HdrABC complex functions as a linker between MTHFR and the quinone pool during methylene-THF oxidation and reduction. It was proposed for *M. thermoacetica* that the MTHFR reaction can be coupled to a complex containing Ech hydrogenase plus formate dehydrogenase, similar to the formate hydrogenlyase complex of *E. coli* (Mock et al., 2014). However, no biochemical evidence was provided yet for this concept with *M. thermoacetica* (Mock et al., 2014). During growth with hydrogen/CO_2, genes coding for a formate hydrogenlyase system were expressed in *T. phaeum* which were not expressed during growth with formate or acetate. It was proposed that the formate hydrogenlyase system of *E. coli* could couple reduction of CO_2 with hydrogen with the formation of a proton gradient via the membranous HyfBDF subunits (Andrews et al., 1997). Expression of this gene cluster was observed before with *T. phaeum* during growth with ethanol or ethanolamine in axenic cultures (Keller et al., 2019). Under these conditions, CO_2 reduction via the WLP is used as a sink for electrons derived from ethanol or ethanolamine oxidation to acetate. Under standard conditions, the reduction of CO_2 to formate with electrons from hydrogen is slightly endergonic which makes it implausible that energy is conserved in this step. During growth with formate, the genes for formate hydrogenlyase system are not expressed, indicating that this system is responsible only for CO_2-fixation and not for energy conservation. The energy conserving systems during acetogenesis are still unknown. The genes for Ech hydrogenase (Tph_c21310-21360) as a putatively proton-translocating enzyme system are expressed during all growth conditions. Thus this enzyme system is a possible candidate for energy conservation. However, no hydrogenase activity could be measured with Fd_{ox} and hydrogen. A formate dehydrogenase whose gene (Tph_c08060) is located in a gene cluster together with genes of a NADH:quinone oxidoreductase (Tph_c08040- Tph_c08050) was present during growth with formate. The electrons derived in this reaction could be coupled via a quinone pool to the reduction of methylene-THF (**Figure 5**). However, at least one more formate dehydrogenase needs to be present to deliver low-potential electrons for the CO dehydrogenase. A possible candidate is the constitutively present Tph_c18420.

Syntrophic Acetate Oxidation

In the direction of acetate oxidation, MTHFR poses an energetic barrier as it releases electrons at a redox potential of −200 mV, which cannot be transferred directly to NADH (−320 mV). This thermodynamic situation is comparable to ethanol oxidation with NAD^+ by alcohol dehydrogenase and is thus hardly possible at high product concentrations (Schmidt et al., 2014). However, the MTHFR in *T. phaeum* appears to be NAD^+-independent, at least in the direction of methyl-THF oxidation. For growth of *T. phaeum* with hydrogen/CO_2, it was suggested that MTHFR could be linked

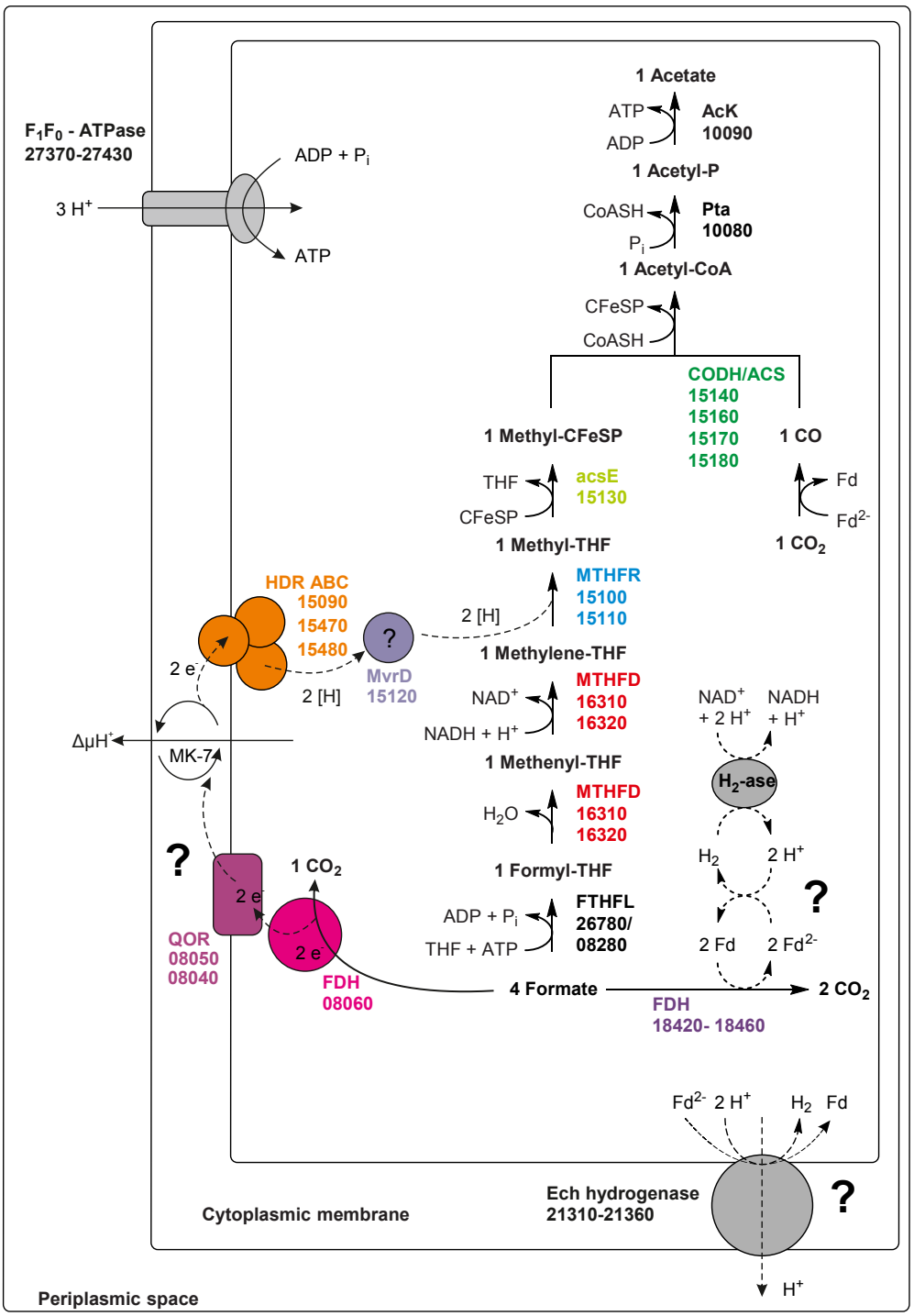

FIGURE 5 | Proposed pathway of formate utilization in *T. phaeum*. Colored squares and circles represent key enzyme systems using the same color coding as in **Figure 4**. Numbers represent the IMG gene locus tags of proteome-identified enzyme systems. Abbreviations: FeS, iron-sulfur cluster; 4Fe-4S, four-iron-four-sulfur cluster; MoPt, molybdopterin; MK-7, menaquinone-7; Fd, ferredoxin; Fd^{2-}, reduced ferredoxin; AcK, acetate kinase; pta, Phosphotransacetylase; CFeSP, corrinoid iron sulfur protein; CODH/ACS, carbon monoxide dehydrogenase/acetyl-coenzyme A synthase-complex; THF, tetrahydrofolate; MTHFR, methylene-THF reductase; MTHFD, methylene-THF dehydrogenase; FTHFL, formyl-THF lyase; HDR, heterodisulfide reductase; FDH, formate dehydrogenase; QOR, quinone:acceptor oxidoreductase; MvrD, methyl-viologen-reducing hydrogenase subunit D; H_2-ase, hydrogenase. Question marks indicate enzyme systems, whose activities were not detected.

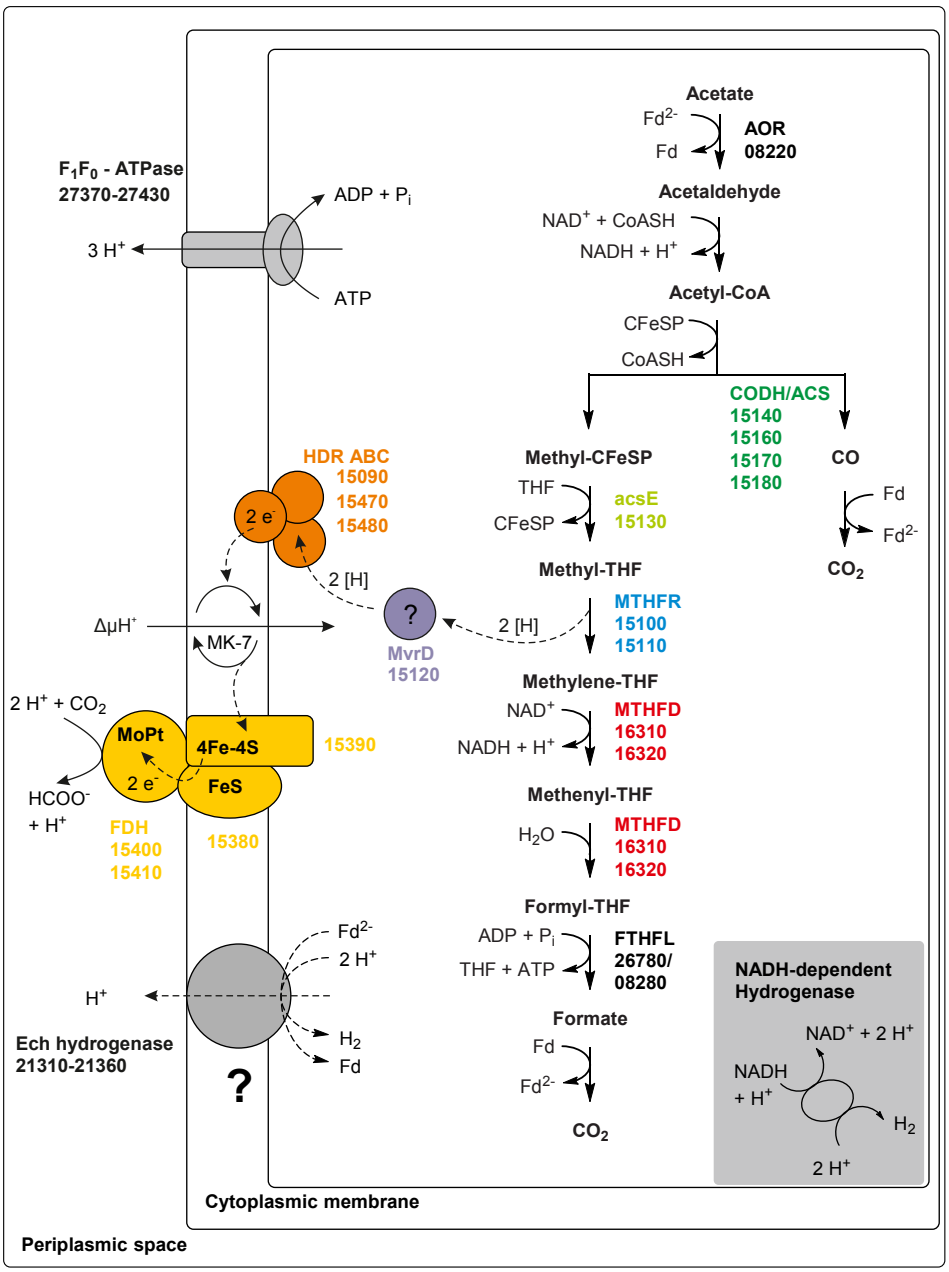

FIGURE 6 | Proposed pathway of acetate oxidation in *T. phaeum*. Colored squares and circles represent key enzyme systems using the same color coding as in **Figure 4**. Numbers represent the IMG gene locus tags of proteome-identified enzyme systems. Abbreviations: FeS, iron-sulfur cluster; 4Fe-4S, four-iron-four-sulfur cluster; MoPt, molybdopterin; MK-7, menaquinone-7; Fd, ferredoxin; Fd^{2-}, reduced ferredoxin; AOR, aldehyde:ferredoxin oxidoreductase; CFeSP, corrinoid iron sulfur protein; CODH/ACS, carbon monoxide dehydrogenase/acetyl-coenzyme A synthase-complex; THF, tetrahydrofolate; MTHFR, methylene-THF reductase; MTHFD, methylene-THF dehydrogenase; FTHFL, formyl-THF lyase; HDR, heterodisulfide reductase; FDH, formate dehydrogenase; MvrD, methyl-viologen-reducing hydrogenase subunit D. Question marks indicate enzyme systems, whose activities were not detected.

to a quinone pool by an HdrABC system. The HdrB and HdrC subunits are encoded in a gene cluster together with genes for a periplasmically oriented formate dehydrogenase. This formate dehydrogenase is present only during growth with acetate, and it reveals high similarity to a previously described periplasmically oriented formate dehydrogenase in *S. wolfei* (Schmidt et al., 2013; Crable et al., 2016). In *S. wolfei*, this gene cluster is expressed during syntrophic butyrate oxidation. The electrons from butyryl-CoA oxidation to crotonyl–CoA have a comparably high electron potential of $E_o' = -10$ mV or −125 mV depending on the literature (Gustafson et al., 1986; Sato et al., 1999) and thus cannot be used directly for NAD^+ reduction. In *S. wolfei,* an electron transfer flavoprotein (EtfAB) carries the electrons from butyryl-CoA dehydrogenase

to a membrane-bound FeS-containing oxidoreductase which reduces the quinone pool in the membrane (Schmidt et al., 2013; Crable et al., 2016). In *T. phaeum,* the MTHFR activity with BV and AQDS as artificial electron acceptors was found in washed membrane fractions indicating that MTHFR is associated with the membrane, yet not membrane-integral as it lacks transmembrane helices. Probably the enzyme whose gene is annotated as coenzyme F_{420}-reducing hydrogenase (Tph_c15120) transfers the electrons to the HdrABC system which subsequently reduces a quinone, most likely menaquinone, as menaquinone MK-7 is the predominant quinone in *T. phaeum* (Hattori et al., 2000; Oehler et al., 2012). This system thus produces methylene-THF and menaquinol. The latter could then be re-oxidized at the gamma subunit of the formate dehydrogenase. The electrons are transferred to an iron-sulfur cluster-containing subunit and finally to the active site of the formate dehydrogenase (**Figure 6**). We show here that *in vitro* activity of a quinone-dependent formate dehydrogenase can be measured with BV or with AQDS as an artificial quinone. Similar enzyme assay results were obtained for hydrogenase, which is apparently also NAD^+-independent, quinone-dependent and membrane bound. One potential candidate could be a complex of three hydrogenase subunits, which were constitutively present in the proteome (**Figure 2**, Tph_c06350 – Tph_c06370). One subunit (Tph_c06350) carries a TAT-signal sequence and another subunit (Tph_c06370) has transmembrane helices and is annotated as b-type cytochrome subunit that is most likely responsible for redox communication with menaquinone. This protein complex hence possibly resembles a membrane-bound, periplasmically oriented and quinone-dependent hydrogenase analogous to the described formate dehydrogenase. Therefore, besides formate, electrons derived from methyl-THF oxidation could alternatively be released as hydrogen via menaquinone similar to the system in *S. wolfei* (Crable et al., 2016). Yet, proteome data of *T. phaeum* obtained in the current study indicates, that membrane-bound formate dehydrogenase is of greater importance, as it is the only enzyme system that is almost exclusively present during syntrophic growth with acetate (**Figure 2**). Coupling MTHFR to the putatively periplasmically oriented formate dehydrogenase could overcome the energetic barrier that this reaction sets in the reversed WLP. However, this reaction would need to be pulled by a proton gradient and a low formate concentration. The low formate concentration can be achieved only in syntrophic cooperation with *M. thermautotrophicus* strain TM as partner that uses both formate and hydrogen as electron donors (Hattori et al., 2001). This could explain why *T. phaeum* has difficulties to oxidize acetate with a methanogen that uses only hydrogen as electron donor (Hattori et al., 2001). Unfortunately, formation of a proton gradient coupled to methyl-THF oxidation by quenching of the fluorescent dye ACMA in inverted membrane vesicles according to Schoelmerich and Müller (2019) could not yet be demonstrated in *T. phaeum* (data not shown). The postulated reversed electron transport from methyl-THF to formate would require a proton gradient to be established by ATP hydrolysis. This would mean that acetate cannot be activated to acetyl-phosphate with acetate kinase as typical of the acetate-forming WLP (Schuchmann and Müller, 2014). Alternatively, acetate could be activated by an acetaldehyde oxidoreductase without ATP investment as it was described before for *Clostridium ljungdahlii* (Köpke et al., 2010; Bengelsdorf et al., 2013; Keller et al., 2019). The ATP thus "saved" could be partly invested into the described reversed electron transport system. In cell-free extracts of *T. phaeum*, the activity of acetaldehyde oxidoreductase was proven with benzyl viologen as electron acceptor in the direction of acetaldehyde oxidation (Keller et al., 2019). In the physiological direction of acetate reduction, no activity could be measured yet. A reason for this failure could be the presumably low activity of the enzyme in the direction of acetaldehyde formation. Experiments with a purified aldehyde:ferredoxin oxidoreductase (AOR) of *M. thermoacetica* indicate that acetate (K_m = 5.6 mM) is turned over at an about 500 times higher K_m than acetaldehyde (K_m = 10 μM) (Huber et al., 1995). With this, an accumulation of toxic acetaldehyde inside the cell is avoided. Attempts were made to purify the acetaldehyde:oxidoreductase of *T. phaeum*, however, no active protein fraction was obtained so far (data not shown).

Recently, a genomic comparison of the five AOB sequenced to that date, i.e., *C. ultunense* (Schnürer et al., 1996), *T. phaeum* (Hattori et al., 2000), *Pseudothermotoga lettingae* (Balk et al., 2002), *S. schinkii* (Westerholm et al., 2010) and *Tepidanaerobacter acetatoxydans* (Westerholm et al., 2011) was published (Manzoor et al., 2018). This study revealed that not all SAOBs use the WLP. Even *P. lettingae* and *C. ultunense* lack central enzymes of the WLP such as the CODH/ACS and MTHFR in their genomes, thus more than one pathway of acetate oxidation must exist (Manzoor et al., 2018). Only *S. schinkii* and *T. phaeum* encode the entire WLP, but *S. schinkii* is not able to grow with hydrogen/CO_2 or formate. According to Manzoor et al. (2018), *T. phaeum* is the only SAOB that encodes a formate hydrogenlyase system and only *S. schinkii* encodes also a membrane-bound formate dehydrogenase (Ssch_1490003-1490006). The periplasmically oriented formate dehydrogenase and the formate hydrogenlyase complex, both representing two membrane-bound enzyme systems, could be the key for the reversibility of the WLP in *T. phaeum*. However, the exact mechanism of these systems is unclear, and it is indispensable to provide further biochemical data additional to genomic and proteomic studies to support the proposed fermentation pathways.

DATA AVAILABILITY STATEMENT

The raw data supporting the conclusion of this manuscript will be made available by the authors, without undue reservation, to any qualified researcher.

AUTHOR CONTRIBUTIONS

AK conducted the experiments designed by AK and NM. AK, NM, and BS wrote and approved the final manuscript.

FUNDING

This work was funded by the Deutsche Forschungsgemeinschaft, project number MU 3953/1-1.

ACKNOWLEDGMENTS

We thank Julia Schmidt for technical assistance and Andreas Marquardt of the Proteomics Facility of the University of Konstanz for proteome analysis. We also thank Alexander Schmidt for helpful ideas and discussions especially in the beginning of the project.

SUPPLEMENTARY MATERIAL

The Supplementary Material for this article can be found online at: https://www.frontiersin.org/articles/10.3389/fmicb.2019.02785/full#supplementary-material

TABLE S1 | Total Proteomics analysis of cells of *Thermacetogenium phaeum* grown with formate (Formiat), hydrogen/CO_2 (H_2CO_2), or acetate (Acetat). Shown are the results of mass spectrometry analysis using the Proteome Discoverer software (Thermo Fisher). Identified proteins are presented along with the accession numbers of their genes as well as the MASCOT-scores and the area values of the Proteome Discoverer software (Thermo Fisher). Area values were used for semi-quantitatively presenting the abundances of the identified proteins. The data for cells grown with acetate are the same as used in (Keller et al., 2019).

REFERENCES

Andrews, S. C., Berks, B. C., McClay, J., Ambler, A., Quail, M. A., Golby, P., et al. (1997). A 12-cistron *Escherichia coli* operon (hyf) encoding a putative proton-translocating formate hydrogenlyase system. *Microbiology* 143, 3633–3647. doi: 10.1099/00221287-143-11-3633

Balk, M., Weijma, J., and Stams, A. J. M. (2002). *Thermotoga lettingae* sp. nov., a novel thermophilic, methanol-degrading bacterium isolated from a thermophilic anaerobic reactor. *Int. J. Syst. Evol. Microbiol.* 52, 1361–1368. doi: 10.1099/ijs.0.02165-0

Bengelsdorf, F. R., Straub, M., and Dürre, P. (2013). Bacterial synthesis gas (syngas) fermentation. *Environ. Technol.* 34, 1639–1651. doi: 10.1080/09593330.2013.827747

Bertsch, J., Öppinger, C., Hess, V., Langer, J. D., and Müller, V. (2015). Heterotrimeric NADH-oxidizing methylenetetrahydrofolate reductase from the acetogenic bacterium *Acetobacterium woodii*. *J. Bacteriol.* 197, 1681–1689. doi: 10.1128/JB.00048-15

Biegel, E., and Müller, V. (2010). Bacterial Na+-translocating ferredoxin:NAD+ oxidoreductase. *Proc. Natl. Acad. Sci. U.S.A.* 107, 18138–18142. doi: 10.1073/pnas.1010318107

Biegel, E., Schmidt, S., González, J., and Müller, V. (2011). Biochemistry, evolution and physiological function of the Rnf complex, a novel ion-motive electron transport complex in prokaryotes. *Cell. Mol. Life Sci.* 68, 613–634. doi: 10.1007/s00018-010-0555-8

Biegel, E., Schmidt, S., and Müller, V. (2009). Genetic, immunological and biochemical evidence for a Rnf complex in the acetogen *Acetobacterium woodii*. *Environ. Microbiol.* 11, 1438–1443. doi: 10.1111/j.1462-2920.2009.01871.x

Crable, B. R., Sieber, J. R., Mao, X., Alvarez-Cohen, L., Gunsalus, R., Ogorzalek Loo, R. R., et al. (2016). Membrane complexes of *Syntrophomonas wolfei* involved in syntrophic butyrate degradation and hydrogen formation. *Front. Microbiol.* 7:1795. doi: 10.3389/fmicb.2016.01795

Enoki, M., Shinzato, N., Sato, H., Nakamura, K., and Kamagata, Y. (2011). Comparative proteomic analysis of *Methanothermobacter themautotrophicus* ΔH in pure culture and in co-culture with a butyrate-oxidizing bacterium. *PLoS One* 6:e24309. doi: 10.1371/journal.pone.0024309

Gersonde, K., Trittelvitz, E., Schlaak, H.-E., and Stabel, H.-H. (1971). The influence of the dimerisation on the stoichiometry of the active center in ferredoxin from *Clostridium pasteurianum*. *Eur. J. Biochem.* 22, 57–65. doi: 10.1111/j.1432-1033.1971.tb01514.x

Gustafson, W. G., Feinberg, B. A., and McFarland, J. T. (1986). Energetics of β-oxidation. Reduction potentials of general fatty acyl-CoA dehydrogenase, electron transfer flavoprotein and fatty acyl-CoA substrates. *J. Biol. Chem.* 261, 7733–7741.

Hattori, S., Galushko, A. S., Kamagata, Y., and Schink, B. (2005). Operation of the CO dehydrogenase/acetyl coenzyme a pathway in both acetate oxidation and acetate formation by the syntrophically acetate-oxidizing bacterium *Thermacetogenium phaeum*. *J. Bacteriol.* 187, 3471–3476. doi: 10.1128/jb.187.10.3471-3476.2005

Hattori, S., Kamagata, Y., Hanada, S., and Shoun, H. (2000). *Thermacetogenium phaeum* gen. nov., sp. nov., a strictly anaerobic, thermophilic, syntrophic acetate-oxidizing bacterium. *Int. J. Syst. Evol. Microbiol.* 50(Pt 4), 1601–1609. doi: 10.1099/00207713-50-4-1601

Hattori, S., Luo, H., Shoun, H., and Kamagata, Y. (2001). Involvement of formate as an interspecies electron carrier in a syntrophic acetate-oxidizing anaerobic microorganism in coculture with methanogens. *J. Biosci. Bioeng.* 91, 294–298. doi: 10.1263/jbb.91.294

Hess, V., Schuchmann, K., and Müller, V. (2013). The ferredoxin:NAD+ oxidoreductase (Rnf) from the acetogen *Acetobacterium woodii* requires Na+ and is reversibly coupled to the membrane potential. *J. Biol. Chem.* 288, 31496–31502. doi: 10.1074/jbc.M113.510255

Huang, H., Wang, S., Moll, J., and Thauer, R. (2012). Electron Bifurcation Involved in the Energy Metabolism of the acetogenic bacterium *Moorella thermoacetica* growing on glucose or H2 plus CO2. *J. Bacteriol.* 194, 3689–3699. doi: 10.1128/jb.00385-12

Huber, C., Skopan, H., Feicht, R., White, H., and Simon, H. (1995). Pterin cofactor, substrate specificity, and observations on the kinetics of the reversible tungsten-containing aldehyde oxidoreductase from *Clostridium thermoaceticum*. *Arch. Microbiol.* 164, 110–118. doi: 10.1007/s002030050242

Keller, A., Schink, B., and Müller, N. (2019). Alternative pathways of acetogenic ethanol and methanol degradation in the thermophilic anaerobe *Thermacetogenium phaeum*. *Front. Microbiol.* 10:423. doi: 10.3389/fmicb.2019.00423

Köpke, M., Held, C., Hujer, S., Liesegang, H., Wiezer, A., Wollherr, A., et al. (2010). *Clostridium ljungdahlii* represents a microbial production platform based on syngas. *Proc. Natl. Acad. Sci. U.S.A.* 107, 13087–13092. doi: 10.1073/pnas.1004716107

Laemmli, U. K. (1970). Cleavage of structural proteins during the assembly of the head of bacteriophage T4. *Nature* 227, 680–685. doi: 10.1038/227680a0

Liu, C., Zachara, J. M., Foster, N. S., and Strickland, J. (2007). Kinetics of Reductive dissolution of hematite by bioreduced anthraquinone-2,6-disulfonate. *Environ. Sci. Technol.* 41, 7730–7735. doi: 10.1021/es070768k

Luo, H.-W., Zhang, H., Suzuki, T., Hattori, S., and Kamagata, Y. (2002). Differential expression of methanogenesis genes of *Methanothermobacter thermoautotrophicus* (formerly *Methanobacterium thermoautotrophicum*) in pure culture and in cocultures with fatty acid-oxidizing syntrophs. *Appl. Environ. Microbiol.* 68, 1173–1179. doi: 10.1128/aem.68.3.1173-1179.2002

Manzoor, S., Schnürer, A., Bongcam-Rudloff, E., and Müller, B. (2018). Genome-guided analysis of *Clostridium ultunense* and comparative genomics reveal different strategies for acetate oxidation and energy conservation in syntrophic acetate-oxidising bacteria. *Genes* 9:E225. doi: 10.3390/genes9040225

McKellar, R. C., and Sprott, G. D. (1979). Solubilization and properties of a particulate hydrogenase from *Methanobacterium* strain G2R. *J. Bacteriol.* 139, 231–238.

Mock, J., Wang, S., Huang, H., Kahnt, J., and Thauer, R. K. (2014). Evidence for a hexaheteromeric methylenetetrahydrofolate reductase in *Moorella thermoacetica*. *J. Bacteriol.* 196, 3303–3314. doi: 10.1128/JB.01839-14

Neuhoff, V., Arold, N., Taube, D., and Ehrhardt, W. (1988). Improved staining of proteins in polyacrylamide gels including isoelectric focusing gels with clear background at nanogram sensitivity using Coomassie brilliant blue G-250 and R-250. *Electophoresis* 9, 255–262. doi: 10.1002/elps.1150090603

Oehler, D., Poehlein, A., Leimbach, A., Müller, N., Daniel, R., Gottschalk, G., et al. (2012). Genome-guided analysis of physiological and morphological traits of the fermentative acetate oxidizer *Thermacetogenium phaeum*. *BMC Genomics* 13:723. doi: 10.1186/1471-2164-13-723

Rosner, B. M., and Schink, B. (1995). Purification and characterization of acetylene hydratase of *Pelobacter acetylenicus*, a tungsten iron-sulfur protein. *J. Bacteriol.* 177, 5767–5772. doi: 10.1128/jb.177.20.5767-5772.1995

Sato, K., Nishina, Y., Setoyama, C., Miura, R., and Shiga, K. (1999). Unusually high standard redox potential of Acrylyl-CoA/Propionyl-CoA couple among Enoyl-CoA/Acyl-CoA couples: a reason for the distinct metabolic pathway of propionyl-CoA from longer Acyl-CoAs. *J. Biochem.* 126, 668–675. doi: 10.1093/oxfordjournals.jbchem.a022501

Schmidt, A., Frensch, M., Schleheck, D., Schink, B., and Müller, N. (2014). Degradation of acetaldehyde and its precursors by *Pelobacter carbinolicus* and *P. acetylenicus*. *PLoS One* 9:e115902. doi: 10.1371/journal.pone.0115902

Schmidt, A., Müller, N., Schink, B., and Schleheck, D. (2013). A proteomic view at the biochemistry of syntrophic butyrate oxidation in *Syntrophomonas wolfei*. *PLoS One* 8:e56905. doi: 10.1371/journal.pone.0056905

Schnürer, A., Schink, B., and Svensson, B. (1996). *Clostridium ultunense* sp. nov., a mesophilic bacterium oxidizing acetate in syntrophic association with a hydrogenotrophic methanogenic bacterium. *Int. J. Syst. Bacterioleriol.* 46, 1145–1152. doi: 10.1099/00207713-46-4-1145

Schoelmerich, M. C., and Müller, V. (2019). Energy conservation by a hydrogenase-dependent chemiosmotic mechanism in an ancient metabolic pathway. *Proc. Natl. Acad. Sci. U.S.A.* 116, 6329–6334. doi: 10.1073/pnas.1818580116

Schuchmann, K., and Müller, V. (2014). Autotrophy at the thermodynamic limit of life: a model for energy conservation in acetogenic bacteria. *Nat. Rev. Microbiol.* 12, 809–821. doi: 10.1038/nrmicro3365

Shi, Z., Zachara, J. M., Shi, L., Wang, Z., Moore, D. A., Kennedy, D. W., et al. (2012). Redox reactions of reduced flavin mononucleotide (FMN), riboflavin (RBF), and anthraquinone-2,6-disulfonate (AQDS) with ferrihydrite and lepidocrocite. *Environ. Sci. Technol.* 46, 11644–11652. doi: 10.1021/es301544b

Timmers, P. H. A., Vavourakis, C. D., Kleerebezem, R., Damsté, J. S. S., Muyzer, G., Stams, A. J. M., et al. (2018). Metabolism and occurrence of methanogenic and sulfate-reducing syntrophic acetate oxidizing communities in haloalkaline environments. *Front. Microbiol.* 9:3039. doi: 10.3389/fmicb.2018.03039

Wang, S., Huang, H., Kahnt, J., and Thauer, R. K. (2013). A reversible electron-bifurcating ferredoxin- and NAD-dependent [FeFe]-hydrogenase (HydABC) in *Moorella thermoacetica*. *J. Bacteriol.* 195, 1267–1275. doi: 10.1128/JB.02158-12

Westerholm, M., Roos, S., and Schnürer, A. (2010). *Syntrophaceticus schinkii* gen. nov., sp. nov., an anaerobic, syntrophic acetate-oxidizing bacterium isolated from a mesophilic anaerobic filter. *FEMS Microbiol. Lett.* 309, 100–104. doi: 10.1111/j.1574-6968.2010.02023.x

Westerholm, M., Roos, S., and Schnürer, A. (2011). *Tepidanaerobacter acetatoxydans* sp. nov., an anaerobic, syntrophic acetate-oxidizing bacterium isolated from two ammonium-enriched mesophilic methanogenic processes. *Syst. Appl. Microbiol.* 34, 260–266. doi: 10.1016/j.syapm.2010.11.018

Zhang, Y., and Gladyshev, V. N. (2005). An algorithm for identification of bacterial selenocysteine insertion sequence elements and selenoprotein genes. *Bioinformatics* 21, 2580–2589. doi: 10.1093/bioinformatics/bti400

Ziegenhorn, J., Senn, M., and Bücher, T. (1976). Molar absorptivities of beta-NADH and beta-NADPH. *Clin. Chem.* 22, 151–160.

Conflict of Interest: The authors declare that the research was conducted in the absence of any commercial or financial relationships that could be construed as a potential conflict of interest.

frontiers in Microbiology

HYPOTHESIS AND THEORY
published: 10 January 2020
doi: 10.3389/fmicb.2019.02997

Extracellular Electron Uptake by Acetogenic Bacteria: Does H_2 Consumption Favor the H_2 Evolution Reaction on a Cathode or Metallic Iron?

*Jo Philips**

Department of Engineering, Aarhus University, Aarhus, Denmark

OPEN ACCESS

Edited by:
Mirko Basen,
University of Rostock, Germany

Reviewed by:
Rashmi Chandra,
Monterrey Institute of Technology and Higher Education (ITESM), Mexico
Amelia-Elena Rotaru,
University of Southern Denmark, Denmark

***Correspondence:**
Jo Philips
jo.philips@eng.au.dk

Specialty section:
This article was submitted to Microbiotechnology, Ecotoxicology and Bioremediation, a section of the journal Frontiers in Microbiology

Received: *05 July 2019*
Accepted: *11 December 2019*
Published: *10 January 2020*

Citation:
Philips J (2020) Extracellular Electron Uptake by Acetogenic Bacteria: Does H_2 Consumption Favor the H_2 Evolution Reaction on a Cathode or Metallic Iron? Front. Microbiol. 10:2997. doi: 10.3389/fmicb.2019.02997

Some acetogenic bacteria are capable of using solid electron donors, such as a cathode or metallic iron [Fe(0)]. Acetogens using a cathode as electron donor are of interest for novel applications such as microbial electrosynthesis, while microorganisms using Fe(0) as electron donor cause detrimental microbial induced corrosion. The capacity to use solid electron donors strongly differs between acetogenic strains, which likely relates to their extracellular electron transfer (EET) mechanism. Different EET mechanisms have been proposed for acetogenic bacteria, including a direct mechanism and a H_2 dependent indirect mechanism combined with extracellular hydrogenases catalyzing the H_2 evolution reaction on the cathode or Fe(0) surface. Interestingly, low H_2 partial pressures often prevail during acetogenesis with solid electron donors. Hence, an additional mechanism is here proposed: the maintenance of low H_2 partial pressures by microbial H_2 consumption, which thermodynamically favors the H_2 evolution reaction on the cathode or Fe(0) surface. This work elaborates how the H_2 partial pressure affects the H_2 evolution onset potential and the H_2 evolution rate on a cathode, as well as the free energy change of the anoxic corrosion reaction. In addition, the H_2 consumption characteristics, i.e., H_2 threshold (thermodynamic limit for H_2 consumption) and H_2 consumption kinetic parameters, of acetogenic bacteria are reviewed and evidence is discussed for strongly different H_2 consumption characteristics. Different acetogenic strains are thus expected to maintain different H_2 partial pressures on a cathode or Fe(0) surface, while those that maintain lower H_2 partial pressures (lower H_2 threshold, higher H_2 affinity) more strongly increase the H_2 evolution reaction. Consequently, I hypothesize that the different capacities of acetogenic bacteria to use solid electron donors are related to differences in their H_2 consumption characteristics. The focus of this work is on acetogenic bacteria, but similar considerations are likely also relevant for other hydrogenotrophic microorganisms.

Keywords: acetogenesis, extracellular electron transfer mechanisms, energy conservation, ATP gain, Butler-Volmer equation, zero valent iron, biocathode, HER reaction

INTRODUCTION

Acetogenic bacteria are a phylogenetically diverse group of microorganisms that share a unique metabolism for energy conservation and carbon fixation, i.e., the Wood–Ljungdahl pathway (Drake et al., 2008). This pathway reduces the electron acceptor CO_2 with the electron donor H_2 to acetyl-CoA for carbon fixation or to acetate or other organic compounds (e.g., ethanol) for energy conservation:

$$2\,CO_2 + 4\,H_2 \rightarrow CH_3COO^- + H^+ + 2\,H_2O \quad \text{(Reaction 1)}$$

$$\Delta G^0{}_{acetogenesis} = -55.8\ \text{kJ} \cdot \text{mol}^{-1}$$

With $\Delta G^0{}_{acetogenesis}$ the Gibbs free energy change of acetogenesis in standard conditions (pH 0, all concentrations 1 M and all partial pressures 1 atm), in contrast to $\Delta G^{0\prime}{}_{acetogenesis}$ (-95.6 kJ · mol^{-1}) in physiological standard conditions (pH 7).

Intriguingly, some acetogens can use solid electron donors, including a cathode (Nevin et al., 2010, 2011), metallic iron [Fe(0)] (Kato et al., 2015; Philips et al., 2019) and possibly reduced minerals. The use of a cathode as electron donor is of high interest for the development of innovative bioelectrochemical technologies. Microbial electrosynthesis, for instance, is a promising process for the conversion of excess renewable electricity and CO_2 into biofuels or other valuable organic compounds using acetogenic bacteria as biocatalysts (Rabaey and Rozendal, 2010; Lovley and Nevin, 2013). In contrast, microorganisms using Fe(0) as electron donor cause microbial induced corrosion, resulting in severe damage to steel infrastructure (Enning and Garrelfs, 2014). Finally, the oxidation of reduced minerals by acetogens could have a still unknown impact on global biogeochemical cycles.

Not all tested acetogens are capable of using a cathode or Fe(0) as electron donor (**Table 1**). The highest electron uptake rates from cathodes have been reported for *Sporomusa ovata* strains (Nevin et al., 2010; Aryal et al., 2017). In contrast, the well-studied strain *Acetobacterium woodii* is not capable of withdrawing electrons from cathodes poised at a potential of −0.4 V vs. Standard Hydrogen Electrode (SHE) (potential slightly more positive than the standard potential for H_2 evolution at pH 7, see calculations below). At more negative cathode potentials (< -0.6 V vs. SHE), almost all tested acetogenic strains withdraw cathodic electrons, with the exception of *Sporomusa aerivorans* (**Table 1**). Acetogenic communities enriched on cathodes (potentials usually ≤ -0.6 V vs. SHE) are often dominated by *Acetobacterium* species (**Table 2**). Only one study has performed a metagenome analysis to identify their cathode-dominating acetogen and found a *Acetobacterium wieringae* strain (Marshall et al., 2017). Interestingly, similar acetogenic genera are found in enrichments using Fe(0) as electron donor (**Table 2**) and acetogenic strains related to *Sporomusa sphaeroides* and *A. wieringae* have been isolated with Fe(0) (Kato et al., 2015; Philips et al., 2019; **Table 1**). Moreover, a limited to no Fe(0) corrosion enhancement was found for *A. woodii* (**Table 1**). Consequently, acetogenic strains likely use a similar mechanism to withdraw extracellular electrons from a cathode as from Fe(0), while not all acetogens have such a mechanism.

This work first reviews the different extracellular electron transfer (EET) mechanisms that have been proposed for acetogenic bacteria. Next, an additional EET mechanism is proposed: the maintenance of low H_2 partial pressures by H_2 consumption, favoring H_2 evolution by the cathode or Fe(0) surface. The H_2 consumption characteristics of acetogens are further described using thermodynamic and kinetic calculations and a literature review. Finally, this work hypothesizes that the

TABLE 1 | Overview of acetogenic strains and their capacity to withdraw electrons from Fe(0) or a cathode.

Strain	Fe(0)	Cathode
Acetobacterium carbinolicum	No (Kato et al., 2015)	n.d.
Acetobacterium malicum	Yes (Philips et al., 2019)	n.d.
Acetobacterium woodii	Yes (Philips et al., 2019), No (Mand et al., 2014; Kato et al., 2015)	−0.4 V: No (Nevin et al., 2011), −0.71 V: Yes (Arends, 2013)
Clostridium aceticum	n.d.	−0.4 V: Yes (Nevin et al., 2011)
Clostridium ljungdahlii	n.d.	−0.4 V: Yes (Nevin et al., 2011), No (personal communication Miriam Rosenbaum), −0.7 V: Yes (personal communication Miriam Rosenbaum; Bajracharya et al., 2015)
Moorella thermoacetica	n.d.	−0.3V: Yes (Faraghiparapari and Zengler, 2017), −0.4 V: Yes (Nevin et al., 2011)
Moorella thermoautotrophica	n.d.	−0.3V: Yes (Faraghiparapari and Zengler, 2017), −0.4 V: Yes (Yu et al., 2017)
Sporomusa acidovorans	n.d.	−0.69 V: Yes (Aryal et al., 2017)
Sporomusa aerivorans	n.d.	−0.69 V: No (Aryal et al., 2017)
Sporomusa malonica	n.d.	−0.69 V: Yes (Aryal et al., 2017)
Sporomusa ovata	No (Kato et al., 2015)	−0.3V: Yes (Faraghiparapari and Zengler, 2017), −0.4 V: Yes (Nevin et al., 2010), −0.69 V: Yes (Aryal et al., 2017)
Sporomusa silvacetica	n.d.	−0.4 V: Yes (Nevin et al., 2011)
Sporomusa sphaeroides	Yes (Kato et al., 2015; Philips et al., 2019)	−0.4 V: Yes (Nevin et al., 2011), −0.5 V: Yes (Deutzmann et al., 2015)
Thermoanaerobacter kivui	n.d.	−0.3 V: No (Faraghiparapari and Zengler, 2017)

The cathode potential (expressed vs. SHE) at which the electron uptake from a cathode was tested is indicated. n.d., not yet determined.

TABLE 2 | (Putative) acetogenic genera in acetogenic enrichments on Fe^0 or cathodes.

Solid electron donor	(Putative) acetogenic genera	References
Fe(0)	*Acetobacterium*	Mand et al., 2014
Fe(0)	*Sporomusa, Clostridium*	Kato et al., 2015
Fe(0)	*Acetobacterium, Sporomusa, Clostridium, Acetoanaerobium*	Philips et al., 2019
Cathode (−0.6 V)	*Acetobacterium*	Marshall et al., 2012, 2013; LaBelle et al., 2014
Cathode (−0.7 V)	*Acetobacterium*	Su et al., 2013
Cathode (−0.85 V)	*Acetoanaerobium*	Jourdin et al., 2016
Cathode (−1.0 V)	*Acetobacterium*	Patil et al., 2015; Arends et al., 2017
Cathode (−1.0 V)	*Acetobacterium, Acetoanaerobium*	Xafenias and Mapelli, 2014
Cathode (−0.65 V)	*Acetobacterium*	Saheb-Alam et al., 2018

Cathode potentials are expressed vs. SHE.

different capacities of acetogenic bacteria to use solid electron donors are related to differences in their H_2 consumption characteristics. This work mainly focuses on acetogenic bacteria, but similar considerations are likely also valid for other hydrogenotrophic microorganisms.

EXTRACELLULAR ELECTRON TRANSFER MECHANISMS OF ACETOGENS

An overview of the different EET mechanisms that have been proposed for acetogenic bacteria is shown in **Figure 1**. Direct EET (**Figure 1A**) is a mechanism that is well-studied in microorganisms using solid electron acceptors, as for instance *Geobacter* spp. (Philips et al., 2016). Other microorganisms, e.g., *Acidithiobacillus ferrooxidans*, use a direct EET mechanism to withdraw electrons from solid electron donors (Valdes et al., 2008). A direct EET mechanism typically involves outer-membrane bound cytochromes, transporting extracellular electrons from the inside to the outside of the cell or the other way around (Philips et al., 2016). A direct extracellular electron uptake has been proposed for acetogenic bacteria (Nevin et al., 2011; Kato et al., 2015), but clear evidence is still lacking. Moreover, *Moorella* and *Sporomusa* spp. have cytochromes, but most other acetogens have not (Moller et al., 1984; Schuchmann and Müller, 2014).

Some microorganisms excrete redox shuttles to mediate EET (**Figure 1B**). *Shewanella oneidensis* and *Pseudomonas aeruginosa*, for instance, use respectively flavins and phenazines to mediate the transport of electrons to an anode (Philips et al., 2016). Artificial mediators have been applied to improve the EET of acetogens from cathodes (Song et al., 2011), but acetogens were not found to excrete redox mediators to mediate EET from Fe(0) (Philips et al., 2019).

Another possibility is an indirect EET mechanism relying on the evolution of H_2 on the cathode or Fe(0). All acetogens are capable of using H_2 as electron donor. In addition, a cathode at a sufficiently low potential (calculated in detail below) generates H_2 through proton reduction:

$$2\,H^+ + 2\,e^- \rightarrow H_2 \qquad \text{(Reaction 2)}$$

Moreover, the presence of Fe(0) in anoxic conditions always leads to H_2 generation through the anoxic corrosion reaction:

$$Fe(0) + 2\,H^+ \leftrightarrow Fe^{2+} + H_2 \qquad \text{(Reaction 3)}$$

Nevertheless, an indirect EET mechanism depending on H_2 has often been disregarded, because the acetate levels in biological treatments are often higher than can be explained by the H_2 levels in abiotic controls. For instance, no H_2 evolution was recorded for an abiotic cathode poised at −0.4 V vs. SHE, while several acetogenic strains consumed current and produced acetate at the same potential (Nevin et al., 2011). Similarly, some acetogens have a higher acetate production rate with Fe(0) as electron donor than can be explained just by chemically generated H_2 (Kato et al., 2015; Philips et al., 2019). Consequently, an H_2-dependent EET mechanism can only explain the extracellular electron uptake by acetogens, if the microorganisms somehow increase the H_2 evolution on the cathode or Fe(0) surface.

Acetogens could increase H_2 evolution on a cathode or Fe(0) through a syntrophic association with an electrotrophic microorganism, which produces H_2 using a direct EET mechanism (**Figure 1C**). Such a mechanism was proposed for a cathodic microbial community dominated by *Acetobacterium* and *Desulfovibrio* spp. (Marshall et al., 2017). In addition, acetate production by *A. woodii* on a cathode poised at −0.4 V vs. SHE was facilitated through H_2 generation by strain IS4 (Deutzmann and Spormann, 2017), i.e., a sulfate reducer isolated with Fe(0) as electron donor (Dinh et al., 2004) and possibly using cytochromes for a direct EET (Beese-Vasbender et al., 2015b).

Interestingly, some acetogenic strains can increase H_2 evolution on a cathode or Fe(0), also without a syntrophic partner. Deutzmann et al. (2015) found that cell-free spent medium of *S. sphaeroides* increased the H_2 evolution rate on a cathode poised at −0.5 V vs. SHE, while similar results were reported with Fe(0) for *Sporomusa* and *Acetobacterium* strains (Philips et al., 2019). Tremblay et al. (2019) detected H_2 already at a cathode potential of −0.3 V vs. SHE with cell-free spent medium of *S. ovata*, while H_2 could only be detected at −0.5 V vs. SHE in fresh medium. Deutzmann et al. (2015) suggested that spent medium contains extracellular enzymes, such as hydrogenases, that absorb on the cathode or Fe(0) surface and catalyze the H_2 evolution reaction (**Figure 1D**). For the methanogen *Methanococcus maripaludis*,

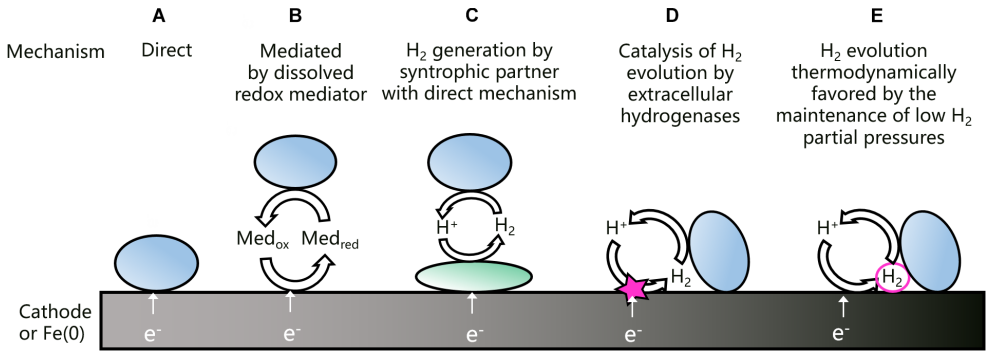

FIGURE 1 | Schematic overview of the different EET mechanisms that have been proposed for the uptake of electrons from a cathode or Fe(0) by acetogenic bacteria (adjusted from Philips et al., 2019). Previously proposed EET mechanisms are direct **(A)**, mediated by dissolved redox mediators **(B)**, depended on H_2 generation by a syntrophic partner with a direct mechanism **(C)**, or depended on H_2 generation catalyzed by extracellular hydrogenases **(D)**. The last mechanism **(E)** is proposed and elaborated in this work.

a heterodisulfide reductase supercomplex was isolated, which catalyzes the reduction of CO_2 to formate at a cathode and Fe(0) surface (Lienemann et al., 2018). In addition, this methanogen excretes a [NiFe] hydrogenase to stimulate the anoxic corrosion reaction (Reaction 3) (Tsurumaru et al., 2018). So far, the H_2 catalyzing components in the spent medium of acetogens have not yet been identified.

The recent evidence discussed above (Deutzmann et al., 2015; Philips et al., 2019; Tremblay et al., 2019), suggests that H_2 plays an important role in the EET mechanism of acetogenic bacteria. Nevertheless, H_2 can often not be detected during acetogenesis with a cathode or Fe(0) as electron donor (Jourdin et al., 2016; Philips et al., 2019). For that reason, this work proposes that the maintenance of low H_2 partial pressures is an additional mechanism by which acetogens favor H_2 evolution on a cathode or Fe(0) surface (**Figure 1E**). The importance of the H_2 partial pressure for the H_2 evolution reaction on a cathode or Fe(0) is elaborated next.

LOW H_2 PARTIAL PRESSURES FAVOR THE H_2 EVOLUTION REACTION ON A CATHODE AND FE(0)

Effect of the H_2 Partial Pressure on Cathodic H_2 Evolution

The cathode potential below which H_2 evolution (Reaction 2) is thermodynamically favorable, i.e., the H_2 evolution onset potential (E_{H^+/H_2}) (V), is given by the Nernst equation:

$$E_{H^+/H_2} = E^{\circ}_{H^+/H_2} - \frac{R \cdot T}{2 \cdot F} \cdot ln\left(\frac{p_{H_2}}{[H^+]^2}\right) \quad (1)$$

With R the ideal gas constant (8.314 10^{-3} kJ · mol^{-1} · K^{-1}), T the temperature (K), F the Faraday constant (96.485 kJ · V^{-1}) and p_{H_2} the H_2 partial pressure (atm) and $[H^+]$ is the proton concentration (M). Equation 1 further neglects activity coefficients, assuming that activities can be approached by concentrations. The H_2 partial pressure (atm) is used throughout this work even for conditions in solution (such as at the cathode or Fe(0) surface), but can be related to the dissolved H_2 concentration using the Henri constant. $E^{\circ}{}_{H+/H_2}$ is the standard potential (pH 0, 1 atm H_2) for H_2 evolution, which is 0 V (i.e., the potential of the SHE), while $E^{\circ\prime}{}_{H^+/H_2}$ is −0.414 V (pH 7, 1 atm H_2).

Equation 1 demonstrates that the H_2 evolution onset potential depends on the H_2 partial pressure and the pH at the cathode surface (**Figure 2A**; Vincent et al., 2007; May et al., 2016). For instance, at a H_2 partial pressure of 50 Pa (5×10^{-4} atm), the H_2 evolution onset potential becomes – 0.316 V (pH 7), while at pH 5.5 [optimal pH for some acetogens (Liew et al., 2016)], the H_2 evolution onset potential is – 0.325 V (1 atm H_2). Consequently, H_2 evolution can thermodynamically be favorable at cathode potentials less negative than −0.4 V vs. SHE, even though this potential is often used in bioelectrochemical studies to avoid H_2 evolution.

The H_2 evolution onset potential, and thus the H_2 partial pressure (Equation 1), also affects the kinetics of the cathodic H_2 evolution (Rheinlander et al., 2014), which can be described by the Butler–Volmer equation (Bard and Faulkner, 2001):

$$j = j_0 \cdot \left(e^{\frac{-\alpha \cdot 2 \cdot F}{R \cdot T} \cdot (E_{electrode} - E_{H^+/H_2})} - e^{\frac{(1-\alpha) \cdot 2 \cdot F}{R \cdot T} \cdot (E_{electrode} - E_{H^+/H_2})}\right) \quad (2)$$

With j the current density (A · cm^{-2}), j_0 the exchange current density (A · cm^{-2}), α the transfer coefficient (-) (usually approximated by 0.5) (Bard and Faulkner, 2001) and $E_{electrode}$ the potential at which the electrode is poised. The left exponential expresses the cathodic reaction (H^+ to H_2 reduction), while the right exponential expresses the anodic reaction (H_2 to H^+ oxidation). When $E_{electrode}$ is E_{H^+/H_2}, (thermodynamic equilibrium) both the anodic and the cathodic current density become j_0, hence the net current density is zero. Remark that Equation 2 is only valid if mass transfer is not limiting, e.g., when the concentrations at the electrode surface are the same as in the bulk liquid, which is only true at electrode potentials close to E_{H^+/H_2} or, in other words, at very low currents.

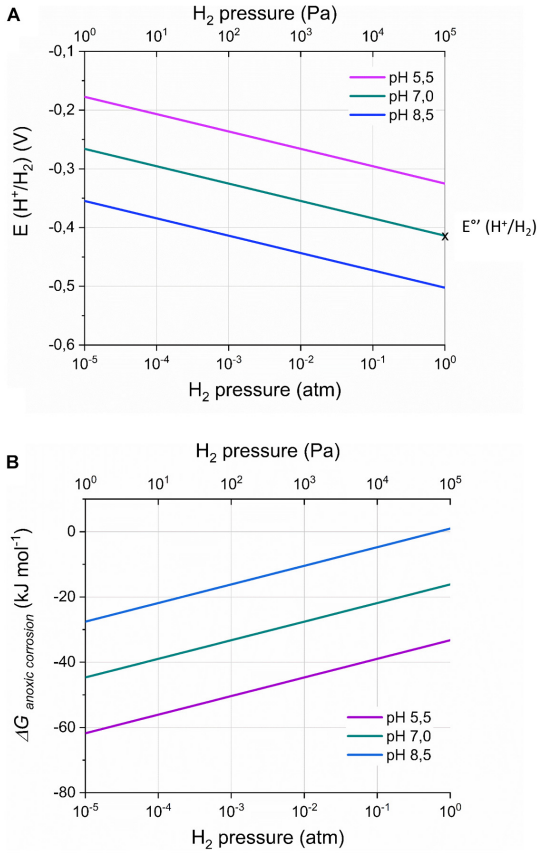

FIGURE 2 | The onset potential for H_2 evolution by a cathode $E(H^+/H_2)$ (V) **(A)** and the Gibbs free energy change ($\Delta G_{anoxic\ corrosion}$; kJ mol^{-1}) of the anoxic corrosion reaction **(B)** in function of the H_2 partial pressure and the pH, according to respectively Equations 1 and 3. The standard H_2 potential at pH 7 [$E°'(H^+/H_2)$] is indicated on the graph. $\Delta G_{anoxic\ corrosion}$ was calculated assuming a Fe^{2+} concentration of 1 mM. Remark the logarithmic scale for the H_2 partial pressures.

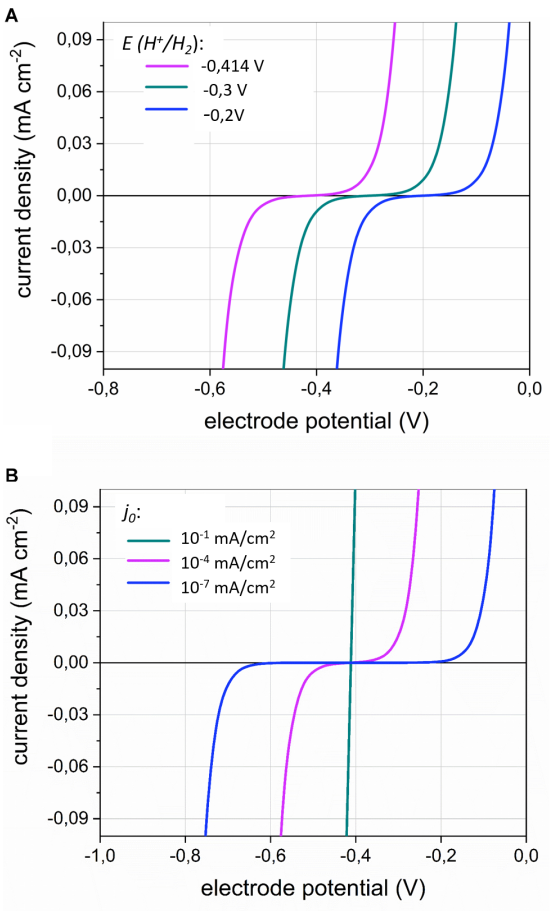

FIGURE 3 | The current density j (mA · cm^{-2}) in function of the electrode potential (V) according to the Butler–Volmer Equation (Equation 2) for **(A)** different values of the H_2 evolution onset potential $E(H^+/H_2)$; (with $j_0 = 1 \cdot 10^{-7}$ mA · cm^{-2}) and **(B)** different values of the exchange current density j_0 (with $E(H^+/H_2) = -0.414$V). The transfer coefficient α was set to 0.5. The inflection point of the curves represents $E(H^+/H_2)$.

The importance of the H_2 evolution onset potential for the current density (equivalent to the H_2 evolution rate) is illustrated in **Figure 3A**. A less negative E_{H^+/H_2} value, for instance due to a lower H_2 partial pressure, allows cathodic current at less negative potentials.

In addition, the effect the exchange current density j_0 is illustrated in **Figure 3B**. The exchange current density inversely relates to the activation overpotential (Bard and Faulkner, 2001), as a smaller exchange current density entails that a more negative electrode potential is needed to enable a substantial cathodic current (**Figure 3B**). In bioelectrochemical studies, the overpotentials for cathodic H_2 evolution are often high (0.2 V more negative than $E°'_{H^+/H_2}$), due to the low reactivity of the often used carbon-based electrode materials. Choosing for more reactive cathode materials (materials with high j_0) strongly reduces the activation overpotential of the H_2 evolution reaction (Jeremiasse, 2011). Such materials facilitate the cathodic electron uptake by acetogens at less negative cathode potentials than are required with unreactive electrode materials (Kracke et al., 2019; Tian et al., 2019). Moreover, cell-free spent medium of *S. ovata* was also found to decrease the overpotential for cathodic H_2 evolution (Tremblay et al., 2019), likely because it contains hydrogenase enzymes or other components catalyzing the H_2 evolution (**Figure 1D**).

In summary, Equation 2 demonstrates that the current density (H_2 evolution rate) depends both on the H_2 evolution onset potential (and thus the H_2 partial pressure; thermodynamic effect) and on the exchange current density (kinetic effect, related to the electrode material and catalysis by enzymes), when mass transfer is not limiting.

Effect of the H_2 Partial Pressure on Anoxic Fe(0) Corrosion

The H_2 partial pressure also affects the anoxic chemical corrosion reaction, as the Gibbs free energy change of Reaction 3 ($\Delta G_{anoxic\ corrosion}$) depends on the H_2 partial pressure and pH at

the Fe(0) surface (**Figure 2B**):

$$\Delta G_{anoxic\ corrosion} = \Delta G^{\circ}_{anoxic\ corrosion} + R \cdot T \cdot ln\left(\frac{p_{H_2} \cdot [Fe^{2+}]}{[H^+]^2}\right) \quad (3)$$

With $[Fe^{2+}]$ the dissolved Fe^{2+} concentration (M) and $\Delta G^{\circ}_{anoxic\ corrosion}$ the standard Gibbs free energy change (-78.9 kJ · mol^{-1}, pH 0). Consequently, hydrogenotrophic microorganisms can thermodynamically favor H_2 evolution on Fe(0) by maintaining low H_2 partial pressures on the Fe(0) surface. For instance, *A. woodii* maintained a H_2 partial pressure on Fe(0) of 150 Pa (1.5×10^{-3} atm) (Philips et al., 2019), leading to $\Delta G_{anoxic\ corrosion}$ of -32 kJ · mol^{-1}, while this is only -22 kJ · mol^{-1} in abiotic conditions (0.1 atm or 10.000 Pa H_2; assuming $[Fe^{2+}]$ of 1 mM) (Philips et al., 2019). All other strains tested in the same study maintained lower H_2 partial pressures on Fe(0) than *A. woodii* [below the detection limit of a TCD detector (40 Pa)] (Philips et al., 2019), thus leading to a $\Delta G_{anoxic\ corrosion}$ value at least as negative as -36 kJ · mol^{-1}.

Also the rate of the anoxic chemical corrosion reaction likely depends on the H_2 partial pressure. In addition, Reaction 3 was found to be catalyzed by hydrogenase enzymes (Bryant and Laishley, 1990; Da Silva et al., 2004; Rouvre and Basseguy, 2016). Consequently, the rate of the anoxic corrosion reaction likely depends both on the H_2 partial pressure (thermodynamic effect) and on enzymatic catalysis (kinetic effect), similar as for a cathode.

In general, the H_2 partial pressure at the cathode or Fe(0) surface results from the balance (steady-state) between the H_2 evolution rate on the cathode or Fe(0) and the H_2 consumption rate by the microorganisms. For that reason, the H_2 consumption characteristics of acetogenic bacteria are discussed next.

H_2 CONSUMPTION CHARACTERISTICS OF ACETOGENIC BACTERIA

The consumption of H_2 by any microorganism is described by its H_2 threshold (the thermodynamic limit of H_2 consumption) and its H_2 consumption kinetics. Below, the theoretical H_2 threshold is calculated for acetogens and experimentally determined values for the H_2 threshold and H_2 consumption kinetic parameters of acetogens are reviewed.

The Theoretical H_2 Threshold of Acetogens

Microorganisms do not completely consume their substrates due to bioenergetic constraints. The theoretical limit for H_2 consumption by acetogenic bacteria is the H_2 partial pressure at which Reaction 1 reaches its thermodynamic equilibrium:

$$\Delta G_{acetogenesis} = \Delta G^{0}_{acetogenesis} + R \cdot T \cdot ln\left(\frac{[CH_3COO^-] \cdot [H^+]}{p^2_{CO_2} \cdot p^4_{H_2}}\right) = 0 \quad (4)$$

With $[CH_3COO^-]$ and $[H^+]$ respectively the acetate and proton concentrations (M) and p_{CO_2} and p_{H_2} respectively the CO_2 and H_2 partial pressures (atm). The minimum H_2 partial pressure at which a reaction is thermodynamically feasible is called the H_2 threshold (θ_{H_2}; atm) (Cord-Ruwisch et al., 1988) and can for acetogens be derived as:

$$\theta_{H_2} = e^{\left(\frac{1}{4} \cdot \left(\frac{\Delta G^{\circ}_{acetogenesis}}{R \cdot T} + ln\left(\frac{[CH_3COO^-] \cdot [H^+]}{p^2_{CO_2}}\right)\right)\right)} \quad (5)$$

Using pH 7, a temperature of 298 K, a CO_2 partial pressure of 0.2 atm and an acetate concentration of 2 mM [i.e., relevant physiological conditions for acetogens using a cathode or Fe(0) as electron donor (Nevin et al., 2010; Kato et al., 2015; Aryal et al., 2017; Philips et al., 2019)], the H_2 threshold becomes $3 \cdot 10^{-5}$ atm or 3 Pa (30 ppm or 0.003%, assuming 1 atm total pressure). Experimental H_2 thresholds for acetogens are always higher than this value (discussed below). This is likely because Reaction 1 does not account for the coupling of acetogenesis to energy conservation. Indeed, calculations of the Gibbs free energy change at experimentally derived H_2 thresholds found a critical Gibbs free energy change, which was not zero but slightly negative (Seitz et al., 1990). This critical Gibbs free energy change likely reflects the energy needed for the microbial metabolism. Accordingly, Reaction 1 should be written as (Poehlein et al., 2012):

$$2\ CO_2 + 4\ H_2 + n\ ADP + n\ P_i \rightarrow CH_3COO^- + H^+ + n\ ATP + 2\ H_2O \quad \text{(Reaction 4)}$$

With n the number of ATP molecules gained per molecule of acetate (i.e., the ATP gain). Consequently, the expression for the H_2 threshold becomes:

$$\theta_{H_2} = e^{\left(\frac{1}{4} \cdot \left(\frac{\Delta G^{\circ}_{acetogenesis} + n \cdot \Delta G_{ADP/ATP}}{R \cdot T} + ln\left(\frac{[CH_3COO^-] \cdot [H^+]}{p^2_{CO_2}}\right)\right)\right)} \quad (6)$$

with $\Delta G_{ADP/ATP}$ the Gibbs free energy change for the phosphorylation of ADP to ATP in physiological conditions (also called the phosphorylation potential). Reported values for $\Delta G_{ADP/ATP}$ range between 30 and 80 kJ · mol^{-1} (Thauer et al., 1977; Atkins and De Paula, 2011). For *A. woodii*, a phosphorylation potential of only 32 kJ · mol^{-1} has been measured (Spahn et al., 2015), but for other acetogens this value is unknown. For the calculation of the H_2 threshold of different acetogens described here, a value for $\Delta G^{\circ}_{ADP/ATP}$ of 50 kJ · mol^{-1} (Poehlein et al., 2012) was used, in order not to underestimate the H_2 threshold.

Equation 6 shows that the H_2 threshold depends on the ATP gain n, which is maximally 1.9 ($\Delta G^{0\prime}_{acetogenesis}$ divided by $\Delta G_{ADP/ATP}$), but depends on the energy conservation mechanism of the acetogenic strain (Schuchmann and Müller, 2014).

All acetogenic bacteria share the Wood–Ljungdahl pathway, as the enzymes forming this pathway are highly conserved among acetogens (Schuchmann and Müller, 2014). However, the carbon flow through the Wood–Ljungdahl pathway does not

TABLE 3 | Comparison of theoretical H_2 thresholds of three model acetogens.

Strain	*Acetobacterium woodii*	*Clostridium autoethanogenum*	*Moorella thermoacetica*
Temperature optimum (°C)	25	37	55
pH optimum	7.0	5.5	7.0
ATP gain *n* (mole ATP/mole acetate)[a]	0.3[b]	1[c]	0.5[d]
Hydrogen threshold (Pa)[e]	**14**	**1160**	**51**

[a]*Only ATP gains for the formation of acetate are considered here, ATP gains for the formation of other products are different (Bertsch and Müller, 2015; Mock et al., 2015).* [b]*The energy conservation mechanism of A. woodii is completely unraveled and the exact ATP gain known (Schuchmann and Müller, 2014).* [c]*This ATP gain is an assumed value (Mock et al., 2015), as the energy conservation mechanism of C. autoethanogenum is not yet completely unraveled.* [d]*This ATP gain is an assumed value (Schuchmann and Müller, 2014; Basen and Müller, 2017), as the energy conservation mechanism of M. thermoacetica is not yet completely unraveled.* [e]*Calculated using Equation 6 and the ATP gain n and the pH and temperature given in the table and assuming an acetate concentration of 2 mM and CO_2 partial pressure of 0.2 atm. The effect of the temperature on $\Delta G^0_{acetogenesis}$ and $\Delta G_{ADP/ATP}$ was neglected, as the temperature effect on $\Delta G_{ADP/ATP}$ is not known.*

lead to energy conservation. Acetogens conserve energy using chemiosmotic ion gradient-driven phosphorylation. The cation generating this gradient (Na^+ or H^+), the energy-conserving module (Rnf or Ech complex), as well as other components (electron bifurcating enzymes) creating the electron flow, differ between acetogenic bacteria (Schuchmann and Müller, 2014). So far, only for few model acetogenic strains the energy conservation machinery is (almost) fully unraveled and the theoretical ATP gain *n* has become available (**Table 3**). This ATP gain ranges between 0.3 for *A. woodii* to 1 for *Clostridium autoethanogenum*. Based on Equation 6, this entails that the H_2 thresholds for these model strains range from 14 to 1160 Pa (including different optimal temperatures and pH) (**Table 3**). Moreover, based on recently sequenced genomes, it is plausible that a wide variability in the energy conservation mechanism of acetogenic strains exists (Poehlein et al., 2016). In theory, the ATP gain *n* could range from 0.15 (Mock et al., 2015) to maximally 1.9, entailing H_2 thresholds ranging over five order of magnitudes (**Figure 4**). Consequently, acetogenic bacteria strongly differ in the lowest H_2 partial pressure they can use. Strains with a high H_2 threshold (high ATP gain) obtain high energy by performing acetogenesis, but cannot grow at low H_2 partial pressures. In contrast, strains with a low H_2 threshold (low ATP gain) gain low energy from acetogenesis, but have the advantage of being able to grow at low H_2 partial pressures.

Previously, differences in the H_2 threshold of methanogens were similarly linked to different ATP gains (Thauer et al., 2008). The above analysis, however, only holds as long as the metabolism is coupled to energy generation, as it does not incorporate the possibility that acetogenesis continues decoupled from energy generation (Schuchmann and Müller, 2014). Moreover, the above reactions do not incorporate the consumption of H_2 and CO_2 for biomass formation. Furthermore, different energy conservation strategies could exist in a single strain (Mock et al., 2015) and be expressed depending on the H_2 partial pressure. Consequently, further investigations of the energy conservation mechanisms of acetogenic bacteria will be highly important to better understand their H_2 threshold.

Experimental H_2 Thresholds of Acetogens

Experimental H_2 thresholds have been reported for several acetogenic strains (**Table 4**). These values are usually measured as the constant H_2 partial pressure that remains after H_2 depletion (other nutrients not limiting) (Cord-Ruwisch et al., 1988; Poehlein et al., 2012). Reported H_2 thresholds range over two orders of magnitudes (**Table 4**), but strong value variability was reported even for the same strain, as experimental H_2 thresholds for *A. woodii* for instance range from 14 to 250 Pa (**Table 4**). This variability is likely due to varying experimental conditions, as the H_2 threshold depends in theory on the CO_2 partial pressure, the acetate concentration, the pH, the total pressure and the temperature (Equations 5 and 6). Conrad and Wetter (1990) and Kotsyurbenko et al. (2001) nicely demonstrated that experimental H_2 thresholds followed the theoretical temperature dependence (Equation 5), as long as the temperature remained in the strain's optimal temperature range. The effect of the other parameters on the experimental H_2 thresholds has much less been studied and often these parameters are not reported together with the experimental H_2 threshold values. Fortunately, some studies have used the same experimental conditions to determine the H_2 threshold of different acetogenic strains and demonstrated significant differences in experimental H_2 thresholds between strains (Cord-Ruwisch et al., 1988; Leclerc et al., 1997; Le Van et al., 1998).

This work advocates the reporting of experimental H_2 thresholds (as well as of the experimental conditions of the measurements) of H_2 consuming anaerobic microorganisms, as this parameter can easily be determined and forms a highly valuable measure to assess bioenergetics, and possibly also the energy conservation mechanism, of new and already-known strains.

H_2 Consumption Kinetics of Acetogens

Very limited information on the H_2 consumption kinetics of acetogenic bacteria is available in literature, except for frequently reported doubling times (overview in Bengelsdorf et al., 2018). The kinetic parameters for H_2 consumption were previously reported only for four acetogenic strains (**Table 5**). These strains strongly differ in their H_2 consumption kinetics, as the maximum cell specific growth rate (μ_{max}) differs one order of magnitude between these strains, while the Monod or half saturation constant (K_{H_2}), i.e., a measure for the affinity of the strains for H_2, ranges over more than two orders of magnitude. The importance of these different kinetic parameters becomes clear in **Figure 5**, plotting the cell specific growth rate (μ) in function of the H_2

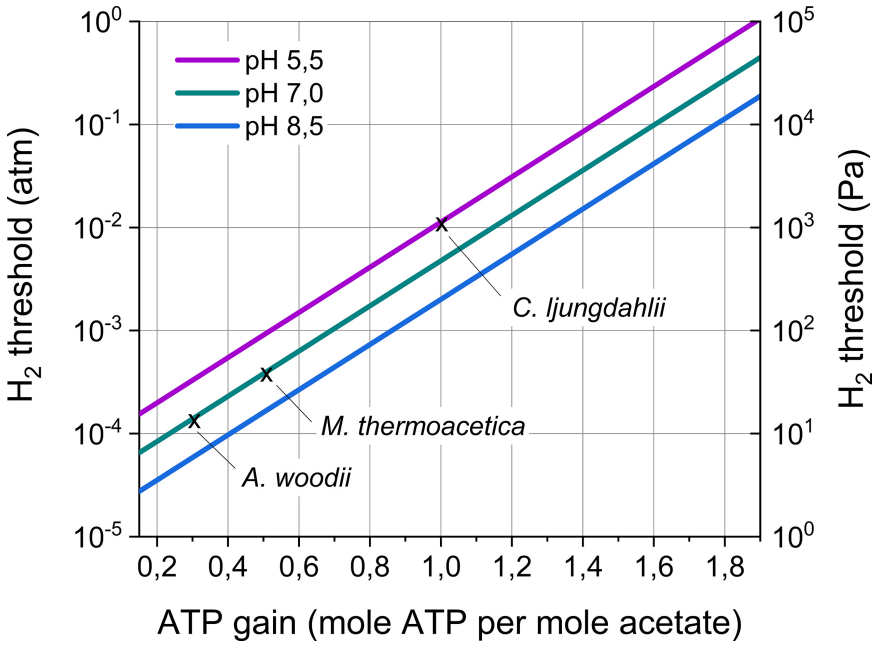

FIGURE 4 | H_2 threshold in function of the ATP gain of acetogenesis and the pH. The H_2 threshold was calculated according to Equation 6 assuming an acetate concentration of 2 mM and a CO_2 partial pressure of 0.2 atm. Temperature effects were not included in this graph. The H_2 thresholds for three model acetogens (as in **Table 3**) are indicated. Remark the logarithmic scale for the H_2 threshold.

TABLE 4 | Experimental H_2 thresholds for different acetogens performing acetogenesis from CO_2 and H_2.

Strain	H_2 threshold (Pa)	Conditions[a]	References
Acetitomaculum ruminis	384[b]	38°C, 24% CO_2	Le Van et al., 1998
Acetobacterium bakii	8–80	4–30°C, 20% CO_2	Kotsyurbenko et al., 2001
Acetobacterium carbinolicum	96[b]	28–34°C, 20% CO_2, 1 bar	Cord-Ruwisch et al., 1988
	5–20	5–25°C, 2 mM acetate, pH 7, 28 kPa CO_2	Conrad and Wetter, 1990
Acetobacterium fimetarium	15–80	4–30°C, 20% CO_2	Kotsyurbenko et al., 2001
Acetobacterium paludosum	15–150	4–30°C, 20% CO_2	Kotsyurbenko et al., 2001
Acetobacterium psammolithicum	53[c]	30°C	Krumholz et al., 1999
Acetobacterium tundrae	10–100	4–30°C, 20% CO_2	Kotsyurbenko et al., 2001
Acetobacterium woodii	53[b]	28–34°C, 20% CO_2, 1 bar	Cord-Ruwisch et al., 1988
	250	30°C, 20% CO_2	Poehlein et al., 2012
	14–55	15–30°C, 2 mM acetate, pH 7, 28 kPa CO_2	Conrad and Wetter, 1990
	37[b]	30°C, 24% CO_2	Le Van et al., 1998
	18[b]	30°C, 20% CO_2, 1 atm	Leclerc et al., 1997
Moorella thermoacetica	156[b]	30°C, 20% CO_2, 1 atm	Leclerc et al., 1997
Sporomusa termitida	84[b]	28–34°C, 20% CO_2, 1 bar	Cord-Ruwisch et al., 1988
	88[b]	30°C, 24% CO_2	Le Van et al., 1998
Thermoanaerobacter kivui	300–600	50–60°C, 2 mM acetate, pH 7, 28 kPa CO_2	Conrad and Wetter, 1990
Treponema primitia	50[b]	30°C, 20% CO_2	Graber and Breznak, 2004

[a]*Conditions are mentioned as far as they are reported in the cited reference.* [b]*H_2 thresholds were converted from ppm values assuming a total pressure of 1 atm.* [c]*The H_2 threshold was converted using a Henri coefficient for H_2 of 7.78 10^{-3} mol m^{-3} kPa^{-1}.*

partial pressure according to the Monod Equation:

$$\mu = \frac{\mu_{max} \cdot p_{H_2}}{K_{H_2} + p_{H_2}} \quad (7)$$

This figure shows that strains with a high μ_{max}, such as *C. ljungdahlii*, have the highest growth rate and thus a competitive advantage at high H_2 partial pressures (> 0.25 atm). In contrast, at intermediate H_2 partial pressures, strains with an intermediate K_{H_2} value, such as *S. termitida*, have a competitive advantage, while at very low H_2 partial pressures (< 0.0015 atm), strains with a strong affinity for H_2 (low K_{H_2}), such as *A. woodii*, have the highest growth rate.

TABLE 5 | Monod kinetic parameters for H_2 consumption by acetogenic strains with K_{H_2} (Pa) the Monod or half saturation constant (i.e., a measure for the affinity of the strains for H_2) and μ_{max} the maximum cell specific growth rate (h^{-1}).

Strain	K_{H_2} (Pa)	μ_{max} (h^{-1})	Temperature (°C)	References
Acetobacterium woodii	94	0.024	30	Peters et al., 1998
Acetobacterium bakii	520	n.d.[a]	30	Kotsyurbenko et al., 2001
Sporomusa termitida	770[b]	0.09[c]	30	Breznak et al., 1988
Clostridium ljungdahlii	42000	0.195	37	Mohammadi et al., 2014

[a]A value of 760 nmol · h^{-1} was reported by Kotsyurbenko et al. (2001), but could not be converted to μ_{max}, as no growth yield was reported. [b]Converted using a Henri coefficient for H_2 of 7.78 10^{-3} mol m^{-3} kPa^{-1}. [c]Converted from the doubling time g (h) using $\mu_{max} = ln\ 2 \cdot g^{-1}$.

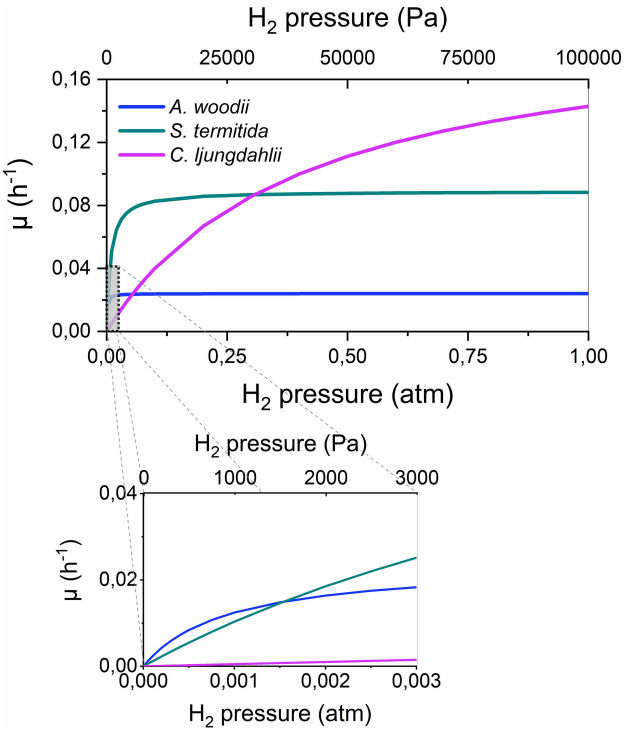

FIGURE 5 | The cell specific growth rate (μ, h^{-1}) in function of the H_2 partial pressure for three acetogens, according to Equation 7 and the kinetic parameters of **Table 5**. The H_2 threshold was not incorporated in this graph.

Possibly, these differences explain why acetogenic *Clostridium* spp. are well suited for gas fermentations (Liew et al., 2016), while *Acetobacterium* and *Sporomusa* species are often found on cathodes or Fe(0), where low H_2 partial pressures prevail (**Table 2**). Importantly, **Figure 5** also shows that the highest growth rates are only obtained at high H_2 partial pressures, possibly impeding the production rates attainable with microbial electrosynthesis in comparison to gas fermentation.

Equation 7 can further be extended to also include the H_2 threshold (Kotsyurbenko et al., 2001):

$$\mu = \frac{\mu_{max} \cdot (p_{H_2} - \theta_{H_2})}{K_{H_2} + (p_{H_2} - \theta_{H_2})} \quad (8)$$

This equation was not used for **Figure 5**, as for none of the strains, all three parameters (μ_{max}, K_{H_2} and θ_{H_2}) are reported.

DISCUSSION

Several acetogenic bacteria are capable of using solid electron donors (**Tables 1**, **2**), implying that these strains have an extracellular electron uptake mechanism. Different EET mechanisms have been proposed for acetogenic bacteria (**Figure 1**). Recent evidence suggests that an H_2-dependent indirect EET mechanism is combined with a mechanism to increase the H_2 evolution reaction rate on the cathode or Fe(0) surface (Deutzmann et al., 2015; Jourdin et al., 2016; Tremblay et al., 2019). In addition, low H_2 partial pressures often prevail during acetogenesis with a solid electron donor (< 50 Pa) (Nevin et al., 2010; Deutzmann et al., 2015; Jourdin et al., 2016; Philips et al., 2019). This work explained that the H_2 partial pressure affects the H_2 evolution onset potential (Equation 1 and **Figure 2A**) and the H_2 evolution rate (current) (Equation 2 and **Figure 3A**) at a cathode, as well the Gibbs free energy change of the anoxic corrosion reaction (Equation 3 and **Figure 2B**) and likely also the rate of the corrosion reaction. Consequently, hydrogenotrophic microorganisms could favor the H_2 evolution reaction by maintaining low H_2 partial pressures at the cathode or Fe(0) surface (**Figure 1E**).

The steady-state H_2 partial pressure at the material surface results from the balance between the H_2 evolution reaction and microbial H_2 consumption. Here, the H_2 consumption characteristics of acetogenic bacteria were reviewed, which suggested that acetogens differ in their H_2 threshold (thermodynamic limit for H_2 consumption) (**Figure 4** and **Tables 3**, **4**) and their H_2 consumption kinetics (**Figure 5** and **Table 5**). This entails that different acetogens likely maintain different H_2 partial pressures on the surface of a cathode or Fe(0). Therefore, I hypothesize that acetogens that maintain lower H_2 pressures (strains with a lower H_2 threshold and/or higher H_2 affinity) more strongly increase the H_2 evolution reaction on a cathode or Fe(0). Consequently, the differences in the capacities of acetogenic bacteria to use solid electron donors (**Table 1**) could be related to differences in their H_2 consumption characteristics.

The lowest theoretical H_2 threshold and highest H_2 affinity (lowest K_{H_2}) was reported for *A. woodii* (**Tables 3**, **5**). This contradicts with my hypothesis, as *A. woodii* is not capable

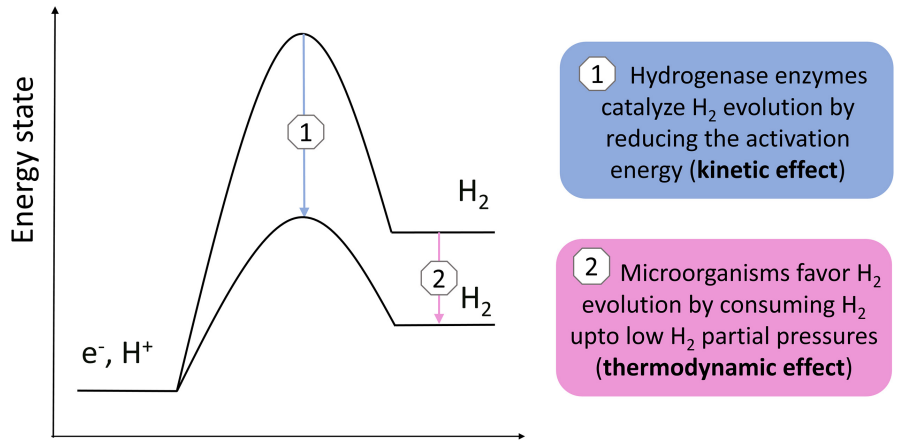

FIGURE 6 | Simple scheme illustrating the two different mechanisms by which H_2 consuming microorganisms possibly increase the H_2 evolution reaction on a cathode or Fe(0).

of withdrawing cathodic electrons at a cathode potential of −0.4 V vs. SHE and does not increase Fe(0) corrosion or just to a limited extent (**Table 1**). However, information on the H_2 consumption characteristics of acetogens is limited to just a few strains (**Tables 3–5**), not including the acetogenic strains most capable of using a cathode or Fe(0) as electron donor, i.e., *S. ovata*, *S. sphaeroides,* and *A. wieringae* (Kato et al., 2015; Aryal et al., 2017; Marshall et al., 2017; Philips et al., 2019). These and other acetogenic strains could have a lower H_2 threshold and/or a lower K_{H_2} than *A. woodii* (**Figure 4**). *A. woodii* maintained a H_2 partial pressure on Fe(0) of 150 Pa, while all other strains tested in the same study maintained H_2 partial pressures on Fe(0) below the detection limit (40 Pa) (Philips et al., 2019), indicating that the other strains have better H_2 consumption characteristics to maintain low H_2 partial pressures on the Fe(0) surface than *A. woodii*. Experimental studies are needed to determine the H_2 consumption characteristics (H_2 threshold and kinetic parameters) of more acetogenic strains and to investigate if those H_2 consumption characteristics relate to the capacity of acetogens to use solid electron donors.

It should be noted that H_2 consumption depends on more factors than just the H_2 threshold and the H_2 consumption kinetic parameters. The number of cells on the surface also affects the H_2 consumption rate, thus attachment and biofilm formation properties are important. In addition, several components, such as dissolved Fe(II), and a pH deviating from the optimal pH could inhibit H_2 consumption. Future studies assessing also these factors will be important to fundamentally understand the role of H_2 consumption in increasing the H_2 evolution reaction.

This work suggests that microbial H_2 consumption favors cathodic H_2 evolution. Interestingly, the increase of the anoxic corrosion reaction by microbial H_2 scavenging is a well-known theory, often referred to as "cathodic depolarization", initially proposed in 1934 (von Wolzogen Kühr and van der Vlugt, 1934). This theory was thought to be disproven by studies showing that only microorganisms isolated with Fe(0) as sole electron donor were capable of increasing anoxic corrosion, while strains isolated with H_2 as electron donor were not (Dinh et al., 2004; Mori et al., 2010; Uchiyama et al., 2010; Enning and Garrelfs, 2014; Kato et al., 2015). Those studies, however, did not consider that hydrogenotrophic microorganisms can differ strongly in their H_2 consumption characteristics, as explained in this work for acetogens. Moreover, it is very likely that enrichments with Fe(0) as electron donor select for strains with a low H_2 threshold and high H_2 affinity, while isolations with H_2 (often high H_2 partial pressure) select for strains with a high growth yield and growth rate, but a high H_2 threshold and low H_2 affinity.

Previous studies demonstrated that acetogens stimulate H_2 evolution on a cathode and Fe(0) through the excretion of hydrogenases or other components catalyzing the H_2 evolution reaction (Deutzmann et al., 2015; Philips et al., 2019; Tremblay et al., 2019). This work used the Butler–Volmer Equation (Equation 2) to demonstrate that the H_2 evolution rate (current) on a cathode depends both on the exchange current density (kinetic effect, related to catalysis by enzymes) (**Figure 3B**) and the H_2 partial pressure (thermodynamic effect) (**Figure 3A**). Consequently, there are two mechanisms by which hydrogenotrophic microorganisms could increase the H_2 evolution rate on a cathode or Fe(0) (**Figure 6**): (1) catalysis of the H_2 evolution reaction by extracellular hydrogenases or other components; and (2) the maintenance of low H_2 partial pressures by H_2 consumption. These two mechanisms are not mutually exclusive, but likely reinforce each other. The relative importance of each mechanism possibly depends on the reactivity of the material (higher for Fe(0) than for carbon-based cathodes), as well as on the H_2 consumption characteristics and enzyme secretion mechanisms of the involved strains.

In addition, more EET mechanism than presented in **Figure 1** could exist, while strains could combine different EET mechanisms or adjust their EET mechanism depending on the conditions (for instance cathode potential). Moreover, the presence of cytochromes in the acetogenic *Sporomusa* and *Moorella* spp. definitely warrants further investigation of a possible direct EET mechanism.

The focus here was solely on acetogenic bacteria, but also other hydrogenotrophic microorganisms, e.g., methanogens and sulfate reducers, could favor the H_2 evolution reaction on a cathode or Fe(0) by maintaining low H_2 partial pressures. Methanogens differ in their H_2 threshold and H_2 affinity (Thauer et al., 2008) and a correlation between their H_2 threshold and Fe(0) corrosion rate was already suggested (Palacios Jaramillo, 2019). In addition, some methanogens were found to excrete hydrogenase enzymes to catalyze the H_2 evolution reaction (Deutzmann et al., 2015; Tsurumaru et al., 2018), while evidence exist that some methanogenic strains have a direct EET mechanism (Beese-Vasbender et al., 2015a; Rowe et al., 2019; Yee et al., 2019). Also the sulfate reducing IS4 strain likely has a direct EET mechanism (Beese-Vasbender et al., 2015b). Consequently, different strategies to obtain extracellular electrons from solid electron donors probably occur in the microbial world (**Figure 1**).

Acetogens and other hydrogenotrophic microorganisms capable of using a solid electron donors are of interest for biotechnological applications (e.g., microbial electrosynthesis), while they could also cause microbial induced corrosion and impact biogeochemical cycles. A good understanding of the role of microorganisms in those processes requires fundamental insights into their EET mechanism. I hypothesize here that the EET mechanism of acetogenic bacteria depends on their H_2 consumption characteristics. Hence, assessment of the H_2 consumption characteristics of various acetogenic strains could be valuable to select the optimal strain for microbial electrosynthesis applications. Genetic engineering cannot change the H_2 consumption characteristics as easy as it changes the resulting end-products (Humphreys and Minton, 2018), so target strains should be chosen based on their H_2 consumption characteristics. In addition, a good understanding of strain related differences in the EET mechanism will improve the assessment of microbial influenced corrosion based on microbial community compositions.

CONCLUSION

This work explained that the H_2 partial pressure affects the H_2 evolution reaction on a cathode or Fe(0) surface. This led to the assumption that the maintenance of low H_2 partial pressures by hydrogenotrophic microorganisms is a mechanism to increase the H_2 evolution reaction on a cathode or Fe(0), in addition to the catalysis by extracellular hydrogenases or other components (**Figure 6**). The H_2 consumption characteristics of acetogenic bacteria were further discussed, which suggested that acetogens differ in their H_2 threshold and H_2 consumption kinetic parameters. Consequently, I hypothesize that the differences in the capacity of acetogens to use a solid electron donors, e.g., cathode and Fe(0), are related to the differences in their H_2 consumption characteristics. The focus here was on acetogenic bacteria, but similar considerations are likely also relevant for other hydrogenotrophic microorganisms capable of using a cathode or Fe(0) as electron donor.

DATA AVAILABILITY STATEMENT

The raw data supporting the conclusions of this article will be made available by the authors, without undue reservation, to any qualified researcher.

AUTHOR CONTRIBUTIONS

The author confirms being the sole contributor of this work and has approved it for publication.

FUNDING

JP was supported by a Starting Grant of the Aarhus Universitets Forskningsfond.

ACKNOWLEDGMENTS

The initial idea for this work originates from the visit of Prof. Em. Rolf Thauer (Max Planck Institute for Terrestrial Microbiology, Marburg, Germany) to Ghent University (Belgium) in 2015. I also acknowledge Dr. Jan B.A. Arends and Prof. Korneel Rabaey (Ghent University) for their support in developing the ideas of this work. I thank Assis. Prof. Jacopo Catalano (Aarhus University) for his advice on the electrochemical aspects of this work. The reviewers and editor's comments were very helpful to improve this work.

REFERENCES

Arends, J. B. A. (2013). *Optimizing the Plant Microbial Fuel Cell: Diversifying Applications and Product Outputs*. Ph.D. thesis, Ghent University, Belgium.

Arends, J. B. A., Patil, S. A., Roume, H., and Rabaey, K. (2017). Continuous long-term electricity-driven bioproduction of carboxylates and isopropanol from CO_2 with a mixed microbial community. *J. CO_2 Util.* 20, 141–149. doi: 10.1016/j.jcou.2017.04.014

Aryal, N., Tremblay, P. L., Lizak, D. M., and Zhang, T. (2017). Performance of different *Sporomusa* species for the microbial electrosynthesis of acetate from carbon dioxide. *Bioresour. Technol.* 233, 184–190. doi: 10.1016/j.biortech.2017.02.128

Atkins, P., and De Paula, J. (2011). *Physical Chemistry for the Life Sciences*. Oxford: Oxford University Press.

Bajracharya, S., ter Heijne, A., Benetton, X. D., Vanbroekhoven, K., Buisman, C. J. N., Strik, D., et al. (2015). Carbon dioxide reduction by mixed and pure cultures in microbial electrosynthesis using an assembly of graphite felt and stainless steel as a cathode. *Bioresour. Technol.* 195, 14–24. doi: 10.1016/j.biortech.2015.05.081

Bard, A. J., and Faulkner, L. R. (2001). *Electrochemical Methods: Fundamentals and Applications*. Hoboken, NJ: John Wiley & Sons.

Basen, M., and Müller, V. (2017). "Hot" acetogenesis. *Extremophiles* 21, 15–26. doi: 10.1007/s00792-016-0873-3

Beese-Vasbender, P. F., Grote, J. P., Garrelfs, J., Stratmann, M., and Mayrhofer, K. J. J. (2015a). Selective microbial electrosynthesis of methane by a pure culture of a marine lithoautotrophic archaeon. *Bioelectrochemistry* 102, 50–55. doi: 10.1016/j.bioelechem.2014.11.004

Beese-Vasbender, P. F., Nayak, S., Erbe, A., Stratmann, M., and Mayrhofer, K. J. J. (2015b). Electrochemical characterization of direct electron uptake in electrical microbially influenced corrosion of iron by the lithoautotrophic SRB *Desulfopila corrodens* strain IS4. *Electrochim. Acta* 167, 321–329. doi: 10.1016/j.electacta.2015.03.184

Bengelsdorf, F. R., Beck, M. H., Erz, C., Hoffmeister, S., Karl, M. M., Riegler, P., et al. (2018). "Bacterial anaerobic synthesis gas (syngas) and CO_2+H_2 fermentation," in *Advances in Applied Microbiology*, Vol. 103, eds S. Sariaslani, and G. M. Gadd (San Diego, CA: Elsevier Academic Press Inc), 143–221. doi: 10.1016/bs.aambs.2018.01.002

Bertsch, J., and Müller, V. (2015). Bioenergetic constraints for conversion of syngas to biofuels in acetogenic bacteria. *Biotechnol. Biofuels* 8:210. doi: 10.1186/s13068-015-0393-x

Breznak, J. A., Switzer, J. M., and Seitz, H. J. (1988). *Sporomusa termitida* sp. nov., an H_2/CO_2-utilizing acetogen isolated from termites. *Arch. Microbiol.* 150, 282–288. doi: 10.1007/bf00407793

Bryant, R. D., and Laishley, E. J. (1990). The role of hydrogenase in anaerobic biocorrosion. *Can. J. Microbiol.* 36, 259–264. doi: 10.1139/m90-045

Conrad, R., and Wetter, B. (1990). Influence of temperature on energetics of hydrogen metabolism in homoacetogenic, methanogenic and other anaerobic bacteria. *Arch. Microbiol.* 155, 94–98. doi: 10.1007/bf00291281

Cord-Ruwisch, R., Seitz, H.-J., and Conrad, R. (1988). The capacity of hydrogenotrophic anaerobic bacteria to compete for traces of hydrogen depends on the redox potential of the terminal electron acceptor. *Arch. Microbiol.* 149, 350–357. doi: 10.1007/bf00411655

Da Silva, S., Basseguy, R., and Bergel, A. (2004). Electron transfer between hydrogenase and 316L stainless steel: identification of a hydrogenase-catalyzed cathodic reaction in anaerobic mic. *J. Electroanal. Chem.* 561, 93–102. doi: 10.1016/j.jelechem.2003.07.005

Deutzmann, J. S., Merve, S., and Spormann, A. M. (2015). Extracellular enzymes facilitate electron uptake in biocorrosion and bioelectrosynthesis. *mBio* 6:e00496-15. doi: 10.1128/mBio.00496-15

Deutzmann, J. S., and Spormann, A. M. (2017). Enhanced microbial electrosynthesis by using defined co-cultures. *ISME J.* 11, 704–714. doi: 10.1038/ismej.2016.149

Dinh, H. T., Kuever, J., Mussmann, M., Hassel, A. W., Stratmann, M., and Widdel, F. (2004). Iron corrosion by novel anaerobic microorganisms. *Nature* 427, 829–832. doi: 10.1038/nature02321

Drake, H. L., Gossner, A. S., and Daniel, S. L. (2008). "Old acetogens, new light," in *Incredible Anaerobes: from Physiology to Genomics to Fuels*, Vol. 1125, eds J. Wiegel, R. J. Maier, and M. W. W. Adams (Oxford: Blackwell Publishing), 100–128. doi: 10.1196/annals.1419.016

Enning, D., and Garrelfs, J. (2014). Corrosion of iron by sulfate-reducing bacteria: new views of an old problem. *Appl. Environ. Microbiol.* 80, 1226–1236. doi: 10.1128/AEM.02848-13

Faraghiparapari, N., and Zengler, K. (2017). Production of organics from CO_2 by microbial electrosynthesis (MES) at high temperature. *J. Chem. Technol. Biotechnol.* 92, 375–381. doi: 10.1002/jctb.5015

Graber, J. R., and Breznak, J. A. (2004). Physiology and nutrition of *Treponema primitia,* an H_2/CO_2-acetogenic spirochete from termite hindguts. *Appl. Environ. Microbiol.* 70, 1307–1314. doi: 10.1128/aem.70.3.1307-1314.2004

Humphreys, C. M., and Minton, N. P. (2018). Advances in metabolic engineering in the microbial production of fuels and chemicals from C1 gas. *Curr. Opin. Biotechnol.* 50, 174–181. doi: 10.1016/j.copbio.2017.12.023

Jeremiasse, A. W. (2011). *Cathode Innovations for Enhanced H_2 Production through Microbial Electrolysis*. Ph.D. thesis, Wageningen University, Wageningen.

Jourdin, L., Yang, L., Flexer, V., Keller, J., and Freguia, S. (2016). Biologically induced hydrogen production drives high rate/high efficiency microbial electrosynthesis of acetate from carbon dioxide. *Chemelectrochem* 3, 581–591. doi: 10.1002/celc.201500530

Kato, S., Yumoto, I., and Kamagata, Y. (2015). Isolation of acetogenic bacteria that induce biocorrosion by utilizing metallic iron as the sole electron donor. *Appl. Environ. Microbiol.* 81, 67–73. doi: 10.1128/AEM.02767-14

Kotsyurbenko, O. R., Glagolev, M. V., Nozhevnikova, A. N., and Conrad, R. (2001). Competition between homoacetogenic bacteria and methanogenic Archaea for hydrogen at low temperature. *FEMS Microbiol. Ecol.* 38, 153–159. doi: 10.1016/s0168-6496(01)00179-9

Kracke, F., Wong, A. B., Maegaard, K., Deutzmann, J. S., Hubert, M. A., Hahn, C., et al. (2019). Robust and biocompatible catalysts for efficient hydrogen-driven microbial electrosynthesis. *Commun. Chem.* 2:45.

Krumholz, L. R., Harris, S. H., Tay, S. T., and Suflita, J. M. (1999). Characterization of two subsurface H_2-utilizing bacteria, *Desulfomicrobium hypogeium* sp nov and *Acetobacterium psammolithicum* sp nov., and their ecological roles. *Appl. Environ. Microbiol.* 65, 2300–2306.

LaBelle, E. V., Marshall, C. W., Gilbert, J. A., and May, H. D. (2014). Influence of acidic pH on hydrogen and acetate production by an electrosynthetic microbiome. *PLoS One* 9:e109935. doi: 10.1371/journal.pone.0109935

Le Van, T. D., Robinson, J. A., Ralph, J., Greening, R. C., Smolenski, W. J., Leedle, J. A. Z., et al. (1998). Assessment of reductive acetogenesis with indigenous ruminal bacterium populations and *Acetitomaculum ruminis*. *Appl. Environ. Microbiol.* 64, 3429–3436.

Leclerc, M., Bernalier, A., Donadille, G., and Lelait, M. (1997). H_2/CO_2 metabolism in acetogenic bacteria isolated from the human colon. *Anaerobe* 3, 307–315. doi: 10.1006/anae.1997.0117

Lienemann, M., Deutzmann, J. S., Sahin, M., and Spormann, A. M. (2018). Mediator-free enzymatic electrosynthesis of formate by the *Methanococcus maripaludis* heterodisulfide reductase supercomplex. *Bioresour. Technol.* 254, 278–283. doi: 10.1016/j.biortech.2018.01.036

Liew, F., Martin, M. E., Tappel, R. C., Heijstra, B. D., Mihalcea, C., and Kopke, M. (2016). Gas fermentation - A flexible platform for commercial scale production of low-carbon-fuels and chemicals from waste and Renewable feedstocks. *Front. Microbiol.* 7:694. doi: 10.3389/fmicb.2016.00694

Lovley, D. R., and Nevin, K. P. (2013). Electrobiocommodities: powering microbial production of fuels and commodity chemicals from carbon dioxide with electricity. *Curr. Opin. Biotechnol.* 24, 385–390. doi: 10.1016/j.copbio.2013.02.012

Mand, J., Park, H. S., Jack, T. R., and Voordouw, G. (2014). The role of acetogens in microbially influenced corrosion of steel. *Front. Microbiol.* 5:268. doi: 10.3389/fmicb.2014.00268

Marshall, C. W., Ross, D. E., Fichot, E. B., Norman, R. S., and May, H. D. (2012). Electrosynthesis of commodity chemicals by an autotrophic microbial community. *Appl. Environ. Microbiol.* 78, 8412–8420. doi: 10.1128/AEM.02401-12

Marshall, C. W., Ross, D. E., Fichot, E. B., Norman, R. S., and May, H. D. (2013). Long-term operation of microbial electrosynthesis systems improves acetate production by autotrophic microbiomes. *Environ. Sci. Technol.* 47, 6023–6029. doi: 10.1021/es400341b

Marshall, C. W., Ross, D. E., Handley, K. M., Weisenhorn, P. B., Edirisinghe, J. N., Henry, C. S., et al. (2017). Metabolic reconstruction and modeling microbial electrosynthesis. *Sci. Rep.* 7:8391. doi: 10.1038/s41598-017-08877-z

May, H. D., Evans, P. J., and LaBelle, E. V. (2016). The bioelectrosynthesis of acetate. *Curr. Opin. Biotechnol.* 42, 225–233. doi: 10.1016/j.copbio.2016.09.004

Mock, J., Zheng, Y. N., Mueller, A. P., Ly, S., Tran, L., Segovia, S., et al. (2015). Energy conservation associated with ethanol formation from H_2 and CO_2 in *Clostridium autoethanogenum* involving electron bifurcation. *J. Bacteriol.* 197, 2965–2980. doi: 10.1128/JB.00399-15

Mohammadi, M., Mohamed, A. R., Najafpour, G. D., Younesi, H., and Uzir, M. H. (2014). Kinetic studies on fermentative production of biofuel from synthesis gas using *Clostridium ljungdahlii*. *Sci. World J.* 2014:910590. doi: 10.1155/2014/910590

Moller, B., Ossmer, R., Howard, B. H., Gottschalk, G., and Hippe, H. (1984). *Sporomusa*, a new genus of gram-negative anaerobic bacteria including *Sporomusa sphaeroides* spec-nov and *Sporomusa ovata* spec-nov. *Arch. Microbiol.* 139, 388–396. doi: 10.1007/bf00408385

Mori, K., Tsurumaru, H., and Harayama, S. (2010). Iron corrosion activity of anaerobic hydrogen-consuming microorganisms isolated from oil facilities. *J. Biosci. Bioeng.* 110, 426–430. doi: 10.1016/j.jbiosc.2010.04.012

Nevin, K. P., Hensley, S. A., Franks, A. E., Summers, Z. M., Ou, J., Woodard, T. L., et al. (2011). Electrosynthesis of organic compounds from carbon dioxide is catalyzed by a diversity of acetogenic microorganisms. *Appl. Environ. Microbiol.* 77, 2882–2886. doi: 10.1128/AEM.02642-10

Nevin, K. P., Woodard, T. L., Franks, A. E., Summers, Z. M., and Lovley, D. R. (2010). Microbial electrosynthesis: feeding microbes electricity to convert carbon dioxide and water to multicarbon extracellular organic compounds. *mBio* 1:e00103-10. doi: 10.1128/mBio.00103-10

Palacios Jaramillo, P. A. (2019). *Microbial Induced Corrosion by Methanogens and other Associated Microbial Groups*. Ph.D. thesis, University of Southern Denmark, Odense.

Patil, S. A., Arends, J. B. A., Vanwonterghem, I., van Meerbergen, J., Guo, K., Tyson, G. W., et al. (2015). Selective enrichment establishes a stable performing community for microbial electrosynthesis of acetate from CO_2. *Environ. Sci. Technol.* 49, 8833–8843. doi: 10.1021/es506149d

Peters, V., Janssen, P. H., and Conrad, R. (1998). Efficiency of hydrogen utilization during unitrophic and mixotrophic growth of *Acetobacterium woodii* on hydrogen and lactate in the chemostat. *FEMS Microbiol. Ecol.* 26, 317–324. doi: 10.1016/s0168-6496(98)00047-6

Philips, J., Monballyu, E., Georg, S., De Paepe, K., Prévoteau, A., Rabaey, K., et al. (2019). An *Acetobacterium* strain isolated with metallic iron as electron donor enhances iron corrosion by a similar mechanism as *Sporomusa sphaeroides*. *FEMS Microbiol. Ecol.* 95:fiy222. doi: 10.1093/femsec/fiy222

Philips, J., Verbeeck, K., Rabaey, K., and Arends, J. B. A. (2016). "Electron transfer mechanisms in biofilms," in *Microbial Electrochemical and Fuel Cells: Fundamentals and Applications*, eds K. Scott, and E. Yu (Amsterdam: Elsevier), 67–113. doi: 10.1016/b978-1-78242-375-1.00003-4

Poehlein, A., Bengelsdorf, F. R., Schiel-Bengelsdorf, B., Daniel, R., and Dürre, P. (2016). Genome sequence of the acetogenic bacterium *Acetobacterium wieringae* DSM 1911(T). *Genome Announc.* 4:e01430-16. doi: 10.1128/genomeA.01430-16

Poehlein, A., Schmidt, S., Kaster, A. K., Goenrich, M., Vollmers, J., Thürme, A., et al. (2012). An ancient pathway combining carbon dioxide fixation with the generation and utilization of a sodium ion gradient for ATP synthesis. *PLoS One* 7:e33439. doi: 10.1371/journal.pone.0033439

Rabaey, K., and Rozendal, R. A. (2010). Microbial electrosynthesis - revisiting the electrical route for microbial production. *Nat. Rev. Microbiol.* 8, 706–716. doi: 10.1038/nrmicro2422

Rheinlander, P. J., Herranz, J., Durst, J., and Gasteiger, H. A. (2014). Kinetics of the hydrogen oxidation/evolution reaction on polycrystalline platinum in alkaline electrolyte reaction order with respect to hydrogen pressure. *J. Electrochem. Soc.* 161, F1448–F1457.

Rouvre, I., and Basseguy, R. (2016). Exacerbation of the mild steel corrosion process by direct electron transfer between Fe-Fe -hydrogenase and material surface. *Corros. Sci.* 111, 199–211. doi: 10.1016/j.corsci.2016.05.005

Rowe, A. R., Xu, S., Gardel, E., Bose, A., Girguis, P., Amend, J. P., et al. (2019). Methane-linked mechanisms of electron uptake from cathodes by *Methanosarcina barkeri*. *mBio* 10:e02448-18. doi: 10.1128/mBio.02448-18

Saheb-Alam, S., Singh, A., Hermansson, M., Persson, F., Schnurer, A., Wilen, B. M., et al. (2018). Effect of start-up strategies and electrode materials on carbon dioxide reduction on biocathodes. *Appl. Environ. Microbiol.* 84:e02242-17. doi: 10.1128/AEM.02242-17

Schuchmann, K., and Müller, V. (2014). Autotrophy at the thermodynamic limit of life: a model for energy conservation in acetogenic bacteria. *Nat. Rev. Microbiol.* 12, 809–821. doi: 10.1038/nrmicro3365

Seitz, H. J., Schink, B., Pfennig, N., and Conrad, R. (1990). Energetics of syntrophic ethanol oxidation in defined chemostat cocultures: 1. Energy requirement of H_2 production and H_2 oxidation. *Arch. Microbiol.* 155, 82–88. doi: 10.1007/bf00291279

Song, J., Kim, Y., Lim, M., Lee, H., Lee, J. I., and Shin, W. (2011). Microbes as electrochemical CO_2 conversion catalysts. *Chemsuschem* 4, 587–590. doi: 10.1002/cssc.201100107

Spahn, S., Brandt, K., and Müller, V. (2015). A low phosphorylation potential in the acetogen *Acetobacterium woodii* reflects its lifestyle at the thermodynamic edge of life. *Arch. Microbiol.* 197, 745–751. doi: 10.1007/s00203-015-1107-2

Su, M., Jiang, Y., and Li, D. (2013). Production of acetate from carbon dioxide in bioelectrochemical systems based on autotrophic mixed culture. *J. Microbiol. Biotechnol.* 23, 1140–1146. doi: 10.4014/jmb.1304.04039

Thauer, R. K., Jungermann, K., and Decker, K. (1977). Energy conservation in chemotrophic anaerobic bacteria. *Bacteriol. Rev.* 41, 100–180.

Thauer, R. K., Kaster, A. K., Seedorf, H., Buckel, W., and Hedderich, R. (2008). Methanogenic archaea: ecologically relevant differences in energy conservation. *Nat. Rev. Microbiol.* 6, 579–591. doi: 10.1038/nrmicro1931

Tian, S. H., Wang, H. Q., Dong, Z. W., Yang, Y., Yuan, H., Huang, Q., et al. (2019). Mo2C-induced hydrogen production enhances microbial electrosynthesis of acetate from CO_2 reduction. *Biotechnol. Biofuels* 12:71. doi: 10.1186/s13068-019-1413-z

Tremblay, P. L., Faraghiparapari, N., and Zhang, T. (2019). Accelerated H_2 evolution during microbial electrosynthesis with *Sporomusa ovata*. *Catalysts* 9:166. doi: 10.3390/catal9020166

Tsurumaru, H., Ito, N., Mori, K., Wakai, S., Uchiyama, T., Iino, T., et al. (2018). An extracellular NiFe hydrogenase mediating iron corrosion is encoded in a genetically unstable genomic island in *Methanococcus maripaludis*. *Sci. Rep.* 8:15149. doi: 10.1038/s41598-018-33541-5

Uchiyama, T., Ito, K., Mori, K., Tsurumaru, H., and Harayama, S. (2010). Iron-corroding methanogen isolated from a crude-oil storage tank. *Appl. Environ. Microbiol.* 76, 1783–1788. doi: 10.1128/AEM.00668-09

Valdes, J., Pedroso, I., Quatrini, R., Dodson, R. J., Tettelin, H., Blake, R., et al. (2008). *Acidithiobacillus ferrooxidans* metabolism: from genome sequence to industrial applications. *BMC Genomics* 9:597. doi: 10.1186/1471-2164-9-597

Vincent, K. A., Parkin, A., and Armstrong, F. A. (2007). Investigating and exploiting the electrocatalytic properties of hydrogenases. *Chem. Rev.* 107, 4366–4413. doi: 10.1021/cr050191u

von Wolzogen Kühr, C. A. H., and van der Vlugt, L. S. (1934). The graphitization of cast iron as an electrobiochemical process in anaerobic soil. *Water* 18, 147–165.

Xafenias, N., and Mapelli, V. (2014). Performance and bacterial enrichment of bioelectrochemical systems during methane and acetate production. *Int. J. Hydrogen Energy* 39, 21864–21875. doi: 10.1016/j.ijhydene.2014.05.038

Yee, M. O., Snoeyenbos-West, O. L., Thamdrup, B., Ottosen, L. D. M., and Rotaru, A. E. (2019). Extracellular electron uptake by two *Methanosarcina* species. *Front. Energy Res.* 7:29. doi: 10.3389/fenrg.2019.00029

Yu, L. P., Yuan, Y., Tang, J. H., and Zhou, S. G. (2017). Thermophilic *Moorella thermoautotrophica*-immobilized cathode enhanced microbial electrosynthesis of acetate and formate from CO_2. *Bioelectrochemistry* 117, 23–28. doi: 10.1016/j.bioelechem.2017.05.001

Conflict of Interest: The author declares that the research was conducted in the absence of any commercial or financial relationships that could be construed as a potential conflict of interest.

frontiers in Microbiology

ORIGINAL RESEARCH
published: 17 January 2020
doi: 10.3389/fmicb.2019.03070

Genome-Based Comparison of All Species of the Genus *Moorella*, and Status of the Species *Moorella thermoacetica* and *Moorella thermoautotrophica*

Stephanie Redl[1†], Anja Poehlein[2†], Carola Esser[3], Frank R. Bengelsdorf[3], Torbjørn Ø. Jensen[1], Christian B. Jendresen[1], Brian J. Tindall[4], Rolf Daniel[2], Peter Dürre[3] and Alex T. Nielsen[1]*

[1] Novo Nordisk Foundation Center for Biosustainability, Technical University of Denmark, Lyngby, Denmark, [2] Genomic and Applied Microbiology & Göttingen Genomics Laboratory, Georg-August University, Göttingen, Germany, [3] Institut für Mikrobiologie und Biotechnologie, Universität Ulm, Ulm, Germany, [4] Leibniz-Institut DSMZ-Deutsche Sammlung von Mikroorganismen und Zellkulturen GmbH, Brunswick, Germany

OPEN ACCESS

Edited by:
Martin G. Klotz,
Washington State University,
United States

Reviewed by:
Charles Lovell,
University of South Carolina,
United States
Alexander V. Lebedinsky,
Winogradsky Institute of Microbiology (RAS), Russia
Aharon Oren,
Hebrew University of Jerusalem, Israel

***Correspondence:**
Peter Dürre
peter.duerre@uni-ulm.de

[†] These authors have contributed equally to this work

Specialty section:
This article was submitted to Microbial Physiology and Metabolism, a section of the journal Frontiers in Microbiology

Received: 22 August 2019
Accepted: 19 December 2019
Published: 17 January 2020

Citation:
Redl S, Poehlein A, Esser C, Bengelsdorf FR, Jensen TØ, Jendresen CB, Tindall BJ, Daniel R, Dürre P and Nielsen AT (2020) Genome-Based Comparison of All Species of the Genus Moorella, and Status of the Species Moorella thermoacetica and Moorella thermoautotrophica. Front. Microbiol. 10:3070. doi: 10.3389/fmicb.2019.03070

Fermentation of gases provides a promising opportunity for the production of biochemicals from renewable resources, which has resulted in a growing interest in acetogenic bacteria. Thermophilic organisms provide potential advantages for the fermentation of, e.g., syngas into for example volatile compounds, and the thermophiles *Moorella thermoacetica* and *Moorella thermoautotrophica* have become model organisms of acetogenic metabolism. The justification for the recognition of the closely related species *M. thermoautotrophica* has, however, recently been disputed. In order to expand knowledge on the genus, we have here genome sequenced a total of 12 different *M. thermoacetica* and *M. thermoautotrophica* strains. From the sequencing results, it became clear that *M. thermoautotrophica* DSM 1974^T consists of at least two different strains. Two different strains were isolated in Lyngby and Ulm from a DSM 1974^T culture obtained from the DSMZ (Leibniz-Institut DSMZ-Deutsche Sammlung von Mikroorganismen und Zellkulturen GmbH, Brunswick, Germany). Phylogenetic analysis revealed a close relationship between all the sequenced genomes, suggesting that the two strains detected in the type strain of the species *M. thermoautotrophica* could not be distinguished at the species level from *M. thermoacetica*. Despite genetic similarities, differences in genomic features were observed between the strains. Differences in compounds that can serve as carbon and energy sources for selected strains were also identified. On the contrary, strain DSM 21394, currently still named *M. thermoacetica*, obviously represents a new *Moorella* species. In addition, based on genome analysis and comparison *M. glycerini* NMP, *M. stamsii* DSM 26217^T, and *M. perchloratireducens* An10 cannot be distinguished at the species level. Thus, this comprehensive analysis provides a significantly increased knowledge of the genetic diversity of *Moorella* strains.

Keywords: anaerobic, thermophile, acetogen, gas fermentation, syngas fermentation, phylogenetic analysis, *Moorella*, *Moorella thermoacetica*

Abbreviations: ANI, average nucleotide identity; ATCC, American Type Culture Collection; CRISPR: clustered regularly interspaced short palindromic repeats; DSM(Z), Deutsche Sammlung von Mikroorganismen (und Zellkulturen); MLSA, multi locus sequence analysis; OG, orthologous groups.

INTRODUCTION

Interest from the research community and industry in acetogenic bacteria has grown within recent years due to their potential to produce valuable compounds from syngas (Latif et al., 2014). Thermophilic acetogens are of significance, since their use would reduce gas cooling requirements, allow for cost-efficient recovery of products with relatively low boiling point (Henstra et al., 2007; Redl et al., 2017), and decrease the risk of contamination.

A well-studied syngas-fermenting thermophile is *Moorella thermoacetica*. The species was isolated from horse feces in 1942 and named *Clostridium thermoaceticum* (Fontaine et al., 1942). The taxonomy of the genus *Clostridium* was restructured in 1994 and *C. thermoaceticum* was transferred to a new genus *Moorella* as *M. thermoacetica* (Collins et al., 1994). Several strains originating from the cultures isolated by Fontaine et al. (1942) are deposited in strain collections. The type strain DSM 521^T and the strain ATCC 39073 have primarily served to elucidate the primary metabolism of *M. thermoacetica* (synonym *C. thermoaceticum*): they were used in experiments to study carbohydrate utilization (Andreesen et al., 1973), the acetate kinase (Schaupp and Ljungdahl, 1974), cytochromes and menaquinones (Gottwald et al., 1975), the formate dehydrogenase (Ljungdahl and Andreesen, 1977), and the utilization of CO (Diekert and Thauer, 1978). The genome of the non-type strain ATCC 39073 was sequenced in 2008 (Pierce et al., 2008) and the genome sequence of the type strain DSM 521^T followed in 2015 (Poehlein et al., 2015). A spore sample of the original *M. thermoacetica* strain isolated in 1942 was deposited by Kerby and Zeikus (1983) as a second representative of the type strain (DSM 2955^T) in the DSMZ (Leibniz-Institut DSMZ-Deutsche Sammlung von Mikroorganismen und Zellkulturen GmbH, Brunswick, Germany). It was shown to utilize H_2/CO_2 as substrate and was also adapted to growth on CO (Kerby and Zeikus, 1983). The ability to utilize gaseous substrates was not shown for ATCC 39073 and DSM 521^T until 1990 (Daniel et al., 1990). Another *M. thermoacetica* strain (Y72) with higher transformation efficiency than ATCC 39073 was described and its draft genome published in 2014 (Tsukahara et al., 2014).

Wiegel et al. (1981) described the isolation of strains closely related to the already known *C. thermoaceticum* (*M. thermoacetica*) strains. The novel strains were shown to grow chemolithotrophically on H_2/CO_2 and chemoheterotrophically on several carbon sources. At that time, the aforementioned strains of *C. thermoaceticum* (*M. thermoacetica*) were not known to utilize H_2/CO_2 and CO. Furthermore, Wiegel et al. (1981) described differences in the cell shape in comparison to *M. thermoacetica.* In addition to *C. aceticum* and *Acetobacterium woodii,* this new strain was the third species known to grow autotrophically using H_2 and CO_2 while producing acetate. Therefore, a new species was proposed and a strain isolated from a Yellowstone hot spring (strain JW 701/3) was deposited as *Clostridium thermoautotrophicum* DSM 1974^T (Wiegel et al., 1981). *C. thermoautotrophicum* was later re-classified as *Moorella thermoautotrophica* in the extensive study of Collins et al. (1994). In addition to *M. thermoautotrophica* DSM 1974^T, which is the designated type strain, a second *M. thermoautotrophica* strain, DSM 7417, is available. This strain (DSM 7417) was first described in Rijssel et al. (1992) when it appeared as a contamination in a continuous culture. The authors based their decision to place the newly described strain in the species of *M. thermoautotrophica* instead of *M. thermoacetica* mainly on observations regarding the cell shape (Rijssel et al., 1992). Recently, Kimura et al. (2016) requested an opinion regarding the taxonomic status of *M. thermoautotrophica*. Based on DNA–DNA hybridization experiments and 16S rRNA gene sequence analysis, Kimura et al. (2016) concluded that the species *M. thermoautotrophica* should be reclassified as *M. thermoacetica*. Over time, phenotypic differences between *M. thermoacetica* and *M. thermoautotrophica* were described, but often with partly conflicting results (Cato et al., 1986; Das et al., 1989; Yamamoto et al., 1998; Carlier and Bedora-Faure, 2006).

Here, we report that *M. thermoautotrophica* DSM 1974^T is a mixed culture of at least two strains, which we isolated. We sequenced the genome of those two strains as well as the genome of DSM 7417 and nine other *M. thermoacetica* strains, thereby considerably adding to the genomic information of this group of bacteria. We compared the genomes of the strains with the genome of the *M. thermoacetica* strain ATCC 39073 (Pierce et al., 2008) and the type strains DSM 2955^T (Bengelsdorf et al., 2015) and DSM 521^T (Poehlein et al., 2015). In addition, we performed genome comparison with all other genomes of the genus *Moorella*. Furthermore, differences in carbon utilization of the aforementioned strains were characterized. Based on this study, we conclude that the classification of the two strains isolated from DSM 1974^T as a separate species, *M. thermoautotrophica*, is not justified and that based on the data collected both strains should be reclassified as strains of the species *M. thermoacetica*. However, a problem arises due to the fact that the designated type strain deposited in the DSMZ, as DSM 1974^T, appears to be a mixture of two strains. The implications of these findings within the context of the rules of the International Code of Nomenclature (Parker et al., 2019) together with the content of the recent Request for an Opinion of Kimura et al. (2016) are discussed.

MATERIALS AND METHODS

Strains

The strains DSM 521^T, DSM 2955^T, DSM 7417, DSM 21394, DSM 11768, DSM 12797, DSM 12993, DSM 6867, and DSM 11254^T were purchased from DSMZ (Leibniz-Institut DSMZ-Deutsche Sammlung von Mikroorganismen und Zellkulturen GmbH, Brunswick, Germany). The strains isolated from the culture of DSM 1974^T obtained from the DSMZ were deposited at the DSMZ with the numbers DSM 103284 (DSM 1974-Ulm) and DSM 103132 (DSM 1974-HH). Strain ATCC 39073 was purchased from the ATCC (Manassas, VA, United States) and was maintained by a series of transfers (here labeled as ATCC 39073-HH). Prior to extracting DNA for genome sequencing, a single colony was isolated on solid medium.

Cultivation

Strains were cultivated in 50-ml serum bottles (50% filled) closed with butyl rubber stoppers (bottles and stoppers: Ochs, Germany) containing a magnetic stirring bar and medium with the following composition (in g/l) [13]: KH_2PO_4 (0.5); NH_4Cl (0.4); NaCl (0.4); $NaHCO_3$ (3.5); yeast extract (0.5); 1% trace element solution was added to the medium. The trace element solution was prepared with 2 g/l nitrilotriacetic acid; the pH adjusted to 6.0 with KOH, and the following compounds added (in mg/l): $MnSO_4 \cdot H_2O$ (1000); $Fe(SO_4)_2(NH_4)_2 \cdot 6\ H_2O$ (800); $CoCl_2 \cdot 6\ H_2O$ (200); $ZnSO_4 \cdot 7\ H_2O$ (200); $CuCl_2 \cdot 2\ H_2O$ (20); $NiCl_2 \cdot 6\ H_2O$ (20); $Na_2MoO_4 \cdot 2\ H_2O$ (20); Na_2SeO_4 (20); Na_2WO_4 (20) mg. The pH of the culture medium was adjusted to 6.5, flushed with N_2:CO_2 (80:20) and autoclaved at 140°C for 40 min. Solid medium contained 1% Gelzan™ and the medium was sterilized at 120°C for 20 min. The following sterile stock solutions were added after autoclaving: $CaCl_2$ (50 mg/l final), $MgCl_2$ (330 mg/l final), vitamin solution (1%), cysteine-HCl (1 mM final). The vitamin solution contained (mg/l): biotin (2); folic acid (2); pyridoxine-HCl (10); thiamine HCl (5); riboflavin (5); nicotinic acid (5); calcium D-(+)-pantothenate (5); vitamin B_{12} (0.5); *p*-aminobenzoic acid (5); thioctic acid (5). The medium was pre-warmed before inoculation. The strains were cultivated at 60°C with stirring at 350 rpm. Fructose as carbon and energy source was added at a final concentration of 60 mM to the medium. The headspace was pressurized with N_2:CO_2 (80:20) to 3 bar. When gases served as carbon and energy sources, the headspace was flushed for several minutes before inoculation with the gas mixture, and the headspace pressurized to 3 bar after inoculation. H_2:CO_2 (80:20) served as gaseous substrates. Strain DSM 103132 was isolated from DSM 1974^T using the medium described above solidified with 1% Gelzan™ and using 60 mM fructose as the substrate. Strain DSM 103284 was isolated from DSM 1974^T using the DSMZ medium 135, the solid medium contained 1.5% agar. In both cases, single colonies were picked and used for further cultivation.

Extraction of Genomic DNA

Cultures in mid-exponential phase were sampled, the cells were spun down, and DNA was extracted using the Wizard® Genomic DNA Purification Kit (Promega, Madison, WI, United States) and the MasterPure™ Gram Positive DNA Purification Kit (Epicentre, Madison, WI, United States) according to the manufacturer's protocol. DNA was quantified using the Qubit dsDNA HS Assay Kit with the Qubit 2.0 fluorometer (Thermo Fisher Scientific, Waltham, MA, United States).

Genome Sequencing

ATCC 39073-HH and DSM 103132 were sequenced using a PacBio RSII instrument (Pacific Biosciences, Menlo Park, CA, United States). SMRTbells™ libraries were constructed and sequenced following the recommended Pacific Biosciences template preparation protocol. Following SMRTbell™ construction, v2 primers and P4 polymerase were annealed and enzyme bound complexes attached to magnetic beads for loading. Each SMRTbell™ library was loaded onto a SMRT cell and sequenced on the PacBio RSII. The average reference coverage was above 500 for both strains, resulting from 129,760 and 134,994 reads of ATCC 39073-HH and DSM 103132, respectively, with an average read length of approximately 12,000 bp. Isolated DNA from all remaining strains was used to generate Illumina shotgun sequencing libraries. Sequencing was performed by employing a MiSeq system using MiSeq Reagent Kit v3 (600 cycles), as recommended by the manufacturer (Illumina, San Diego, CA, United States), resulting in 2 × 300 bp paired end reads. Strain DSM 103284 was sequenced with the Genome Analyzer IIx (Illumina, San Diego, CA, United States) resulting in 2 × 112 bp paired end reads. Quality filtering of the raw reads was done using Trimmomatic version 0.32 (Bolger et al., 2014). The *de novo* assembly was performed with the SPAdes genome assembler software (Bankevich et al., 2012). The assembly was validated and the read coverage determined with QualiMap (García-Alcalde et al., 2012). For scaffolding the contigs of strain DSM 103284, we used the Move Contigs tool of the Mauve Genome Alignment Software (Darling et al., 2010). Additionally, contigs that could not be ordered with Mauve were examined via Gene Ortholog Neighborhoods based on bidirectional best hits implemented at the IMG-ER (Integrated Microbial Genomes-Expert Review) system (Markowitz et al., 2013). For contig ordering, the genomes of *M. thermoacetica* DSM 521^T (CP012369) and DSM 2955^T (CP012370) were used as references. Sequence gaps were closed by PCR-based techniques and primer walking with conventional Sanger sequencing, using BigDye 3.0 chemistry on an ABI3730XL capillary sequencer (Applied Biosystems, Life Technologies GmbH, Darmstadt, Germany), and employing the Gap4 (v.4.11) software of the Staden Package (Staden et al., 1999). *M. glycerini* DSM 11254^T has been sequenced using a combined approach with Illumina short read and Oxford Nanopore long read technology. Therefore, high molecular weight DNA (HWD) was isolated with the MasterPure Complete DNA & RNA Purification Kit (Biozym, Hessisch Oldendorf, Germany) as recommended by the manufacturer. Quality of isolated DNA was initially checked by agarose gel electrophoresis and validated on an Agilent Bioanalyzer 2100 using an Agilent DNA 12000 Kit as recommended by the manufacturer (Agilent Technologies, Waldbronn, Germany). Concentration and purity of the isolated DNA was first checked with a Nanodrop ND-1000 (PeqLab Erlangen, Germany), and exact concentration was determined using the Qubit® dsDNA HS Assay Kit as recommended by the manufacturer (Life Technologies GmbH, Darmstadt, Germany). Illumina shotgun libraries were prepared using the Nextera XT DNA Sample Preparation Kit and subsequently sequenced on a MiSeq system with the reagent kit v3 with 600 cycles (Illumina, San Diego, CA, United States) as recommended by the manufacturer resulting in 1,694,377 paired end reads. For Nanopore sequencing, 1.5 μg HWD was used for library preparation using the Ligation Sequencing Kit 1D (SQK-LSK109) and the Native Barcode Expansion Kit (EXP-NBD104) as recommended by the manufacturer. Sequencing was performed on a MinION device Mk1B using a SpotON Flow Cell R9.4.1 as recommended by the manufacturer for 72 h. This resulted in 162,721 reads with a mean read length of 4,155 bp.

Unicycler v0.4.8 (Wick et al., 2017) was used with default settings to perform a hybrid assembly.

Genome Annotation

The genomes were annotated using the Prokka automatic annotation software (Seemann, 2014). Protein coding, rRNA, and tRNA sequences were annotated using Prodigal (Hyatt et al., 2010), RNAmmer (Lagesen et al., 2007), and Aragorn (Laslett and Canback, 2004) against databases using BLAST (Camacho et al., 2009) and HMMER (Finn et al., 2011). Prediction of non-coding RNAs and CRISPR repeats were done by infernal (Nawrocki and Eddy, 2013) and MinCED[1] based on CRISPR Recognition Tool (Bland et al., 2007). Signal peptides were searched using SignalP (Petersen et al., 2011). Protein coding genes were analyzed for COG (Tatusov et al., 1997; Galperin et al., 2014) functional annotation using Batch CD-search tool (Marchler-Bauer and Bryant, 2004). No secondary metabolite clusters were predicted in an analysis using antiSMASH 2.0 (Medema et al., 2011). The genome sequences and annotation data of all *M. thermoacetica* strains have been deposited in DDBJ/ENA/GenBank, for detailed information see **Table 1**.

Genome Analysis

For MLSA and gene content analysis, total protein sequences from the 24 genomes were extracted from the corresponding GenBank files using cds_extractor.pl v0.6[2] and used for downstream analysis with an in-house pipeline at the Göttingen Genomics Laboratory. In detail, proteinortho version 4.25 (default specification: blast = blastp v2.2.24, E-value = 1e-10, alg.-conn. = 0.1, coverage = 0.5, percent_identity = 50, adaptive_similarity = 0.95, inc_pairs = 1, inc_singles = 1, selfblast = 1, unambiguous = 0) (Lechner et al., 2011) was used to generate clusters of orthologs groups, inparalogs were removed. MUSCLE (Edgar, 2004) was employed to align the remaining sequences and poorly aligned positions were automatically filtered from the alignments using Gblocks (Castresana, 2000). A maximum likelihood tree from 1,177 orthologs groups was inferred with 500 bootstraps with RAxML

[1]https://github.com/ctSkennerton/minced

[2]https://github.com/aleimba/bac-genomics-scripts

TABLE 1 | Genome features of *Moorella* species.

Organism	Accession number	Size [bp]	GC-content [%]	Coding percentage [%]	CDS	Genes	rRNA	tRNA	Contigs	References
M. glycerini DSM 11254^T	CP046244 (chromosome) CP046245 (plasmid)	3,559,463	54,74	88.26	3,509	3,564	3	52	2	This study
M. glycerini NMP	CELZ01000000	3,577,805	53.80	88.48	3,636	3,697	4	57	73	Liebensteiner et al., 2015
M. humiferrea DSM 23265^T	PVXM00000000	2,628,568	53.52	89.51	2,668	2721	3	49	63	Poehlein et al., 2018b
M. mulderi DSM 14980^T	LTBC00000000	3,307,499	54.54	87.26	3,042	3,099	3	53	72	Castillo Villamizar and Poehlein, 2016
M. perchloratireducens An10	Gp0011525[a]	3,307,499	53.84	88.69	3,349	3,423	3	52	133	Markowitz et al., 2013
M. stamsii DSM 26217^T	PVXL00000000	3,328,173	53.81	87.87	3,306	3,358	3	49	82	Poehlein et al., 2018a
M. thermoacetica ATCC 31490	VCDV00000000	2,616,798	55.81	87.94	2,621	2,676	3	51	26	This study
M. thermoacetica ATCC 33924[b]	VCDY00000000	2,914,842	55.12	87.81	2,959	3,020	3	57	47	This study
M. thermoacetica ATCC 35608	VCDW00000000	2,611,625	55.83	87.96	2,605	2,661	3	52	26	This study
M. thermoacetica ATCC 39073	CP000232	2,628,784	55.79	86.39	2,465	2,634	3	51	1	Pierce et al., 2008
M. thermoacetica ATCC 49707	VCDX00000000	2,616,845	55.83	87.92	2,619	2,676	4	52	28	This study
M. thermoacetica DSM 103132	CP017019	2,976,077	55.10[c]	87.94	3,026	3,091	6	58	1	This study
M. thermoacetica DSM 103284	CP017237	2,560,375	55.94[c]	87.94	2,525	2,58	3	51	1	This study
M. thermoacetica DSM 11768	MIHH00000000	2,851,436	55.66	86.40	2,806	2,865	3	55	92	This study
M. thermoacetica DSM 12797	MIIF00000000	2,746,010	55.54	86.51	2,716	2,774	3	54	83	This study
M. thermoacetica DSM 12993	MDDD00000000	2,648,948	55.74	87.10	2,6	2,659	3	55	40	This study
M. thermoacetica DSM 21394	MDDC00000000	2,567,468	56.95	85.80	2,499	2,559	3	56	30	This study
M. thermoacetica DSM 2955^T	CP012370	2,623,349	55.81	88.17	2,624	2,68	3	52	1	Bengelsdorf et al., 2015
M. thermoacetica DSM 512^T	CP012369	2,527,564	55.95[d]	88.06	2,553	2,609	3	52	1	Poehlein et al., 2015
M. thermoacetica DSM 6867	MDDB00000000	2,617,097	55.83	87.80	2,62	2,676	3	52	42	This study
M. thermoautotrophica DSM 7417	MDDE00000000	2,585,122	55.87	87.59	2,558	2,62	6	55	26	This study
M. thermoacetica Y72	BARR00000000	2,603,418	55.89	88.05	2,629	2,715	3	51	95	Tsukahara et al., 2014

[a]*GOLD Sequencing Project ID (no accession number available).* [b]*DNA isolated and sequenced from a single colony.* [c]*Wiegel et al. (1981) stated a GC content of 53–55% in the DNA of strain DSM 1974^T.* [d]*Matteuzzi et al. (1978) stated a GC content of 54% in the DNA of strain DSM 521^T.*

(Stamatakis, 2014). The script PO_2_MLSA.py is available at github[3]. Visualization of the tree was performed using Dendroscop (Huson and Scornavacca, 2012).

Average Nucleotide Identity (ANIm) analyses were performed using pyani.py[4]. Briefly, nucleotide sequences were extracted from the corresponding GenBank files using seq_format-converter.pl v0.2[5] and subsequently used to run pyani in ANIm mode (uses MUMmer/NUCmer) to align input sequences. PHASTER (PHAge Search Tool Enhanced Release, Arndt et al., 2016) has been used for the detection of prophage regions. The analysis of genomic islands was performed using IslandViewer 4 (Bertelli et al., 2017).

RESULTS

Strain DSM 1974^T was purchased from DSMZ by our labs (University of Ulm and Technical University of Denmark) separately in 2015. Genome sequencing of the strain in the Göttingen Genomics Laboratory and at the Technical University of Denmark suggested that DSM 1974^T is a mixed culture. After suspecting cross-contamination in our labs, new DSM 1974^T cultures were ordered from DSMZ, however, with the same result. We independently isolated single clones after cultivation of DSM 1974^T on solid medium: DSM 103284 (DSM 1974-Ulm) at the University of Ulm and DSM 103132 (DSM 1974-HH) at the Technical University of Denmark as described in Section "Materials and Methods." We sequenced the genome of both strains which were derived from the DSM 1974^T culture, as well as the genome of DSM 7417 and the genome of another ATCC 39073 strain, here designated ATCC 39073-HH. In order to determine whether DSM 1947^T is a mixed culture we ordered ATCC 33924^T (that is derived from DSM 1974^T) from the ATCC and sequenced the DNA directly isolated from the freeze-dried culture (data not shown) and from a single colony isolated with the same procedure as for strain DSM 103132. Sequencing results confirmed that ATCC 33924^T = DSM 1974^T deposited at the ATCC is also a mixed culture and the strain isolated from that culture is identical to DSM 103132. The differences between DSM 103132 (isolated in Denmark) and DSM 103284 (isolated in Germany) suggest that slightly different cultivation conditions may favor the selection of different strains from the original mixed culture of DSM 1974^T. In addition, the genomes of 10 different *M. thermoacetica* strains, *M. thermoautotrophica* DSM 7417, and *M. glycerini* DSM 11254^T were sequenced.

Genome Features

Table 1 shows an overview of the *de novo* sequenced genomes of the DSM 1974^T-derived strains (DSM 103284 and DSM 103132) and all other strain sequences in this study compared to the published genomes of type strains DSM 521^T, DSM 2955^T, as well as ATCC 39073, *M. thermoacetica* Y72, *M. glycerini* DSM 11254^T, *M. glycerini* NMP, *M. humiferrea* DSM 23268^T, *M. mulderi* DSM 14980^T, *M. perchloratireducens* An10, and *M. stamsii* DSM 26217^T. In order to investigate the phylogeny of the strains, we first compared the 16S rRNA gene sequences of the type strains, ATCC 39073-HH, DSM 103132, and DSM 103284. The sequence similarity between the strains in the 16S rRNA gene region is at least 99.74%, as no more than 3 nucleotide mismatches could be found. In strains DSM 103284 and ATCC 39073-HH, the gene regions are identical. According to Stackebrandt and Goebel (1994), bacteria showing less than 97% similarity in their 16S rRNA gene sequences belong to different species, while additional methods must be taken into consideration when the 16S rRNA similarity values are above 97%. All strains were analyzed with respect to prophages and interestingly none of the strains harbors a complete prophage. In all strains, a different number of incomplete phages (between 1 and 5; for details see **Supplementary Table S2**) were detected. Six strains, *M. thermoacetica* DSM 103132 and DSM 103284, *M. glycerini* DSM 11254^T and NMP, *M. perchloratireducens* An10, and *M. stamsii* DSM 26217^T contain putative phages, marked as "questionable." These DNA regions show similarity to different *Bacillus* phages or to a Stx2-converting phage (**Supplementary Table S2**). We also checked some completely sequenced strains for the presence of genomic islands and found 9 such regions in strains DSM 103284 and DSM 2955^T as well as 10 genomic islands in strain DSM 521^T and ATCC 39073. Strain DSM 103132 harbors 36 genomic islands in total and one of these regions has a size of 166 kbp (**Supplementary Table S3**). All genomic islands contain mainly hypothetical proteins, transposases, or transcriptional regulators and only a few genes coding for enzymes (for details see **Supplementary Table S3**). With respect to plasmids, a 50-kbp plasmid was found in *M. glycerini* DSM 11254^T. None of the *M. thermoacetica* or *M. thermoautotrophica* strains was found to carry a plasmid. All other *Moorella* species could not be analyzed in detail, as they are draft genomes and there is no evidence for plasmid replication genes in these genomes.

Phylogenetic Analysis

We used MLSA based on the detected core genome (1,177 OGs excluding paralogs) to perform phylogenetic analysis of our strains (**Figure 1**) and an average nucleotide identity analysis (ANIm) (**Figure 2**). The phylogenetic tree yielded two main clades, one consisting of all *M. thermoacetica* and *M. thermoautotrophica* strains and the second of *M. glycerini* DSM 11254^T, *M. glycerini* NMP, *M. humiferrea* DSM 23268^T, *M. mulderi* DSM 14980^T, *M. perchloratireducens* An10, and *M. stamsii* DSM 26217^T. The first main clade shows three distinct subclades, one consisting of the different versions of *M. thermoacetica* ATCC 39079, DSM 521^T, DSM 2955^T, ATCC 49707, ATCC 31490, ATCC 35608^T, DSM 12993 and DSM 6867. It should be noted that DSM 521^T, DSM 2955^T, ATCC 35608^T, and ATCC 49707 are all derived from the same original strain. The second subclade consists of strains DSM 12797, DSM 11786, Y72, and DSM 7417. Strains ATCC 33924 and DSM 103132 form the third subclade. Strain DSM 103284, isolated from the mixed culture of DSM 1974^T and strain DSM 21394 cluster outside of the three subclades. Interestingly, DSM 21394

[3]https://github.com/jvollme

[4]https://github.com/widdowquinn/pyani

[5]https://github.com/aleimba/bac-genomics-scripts

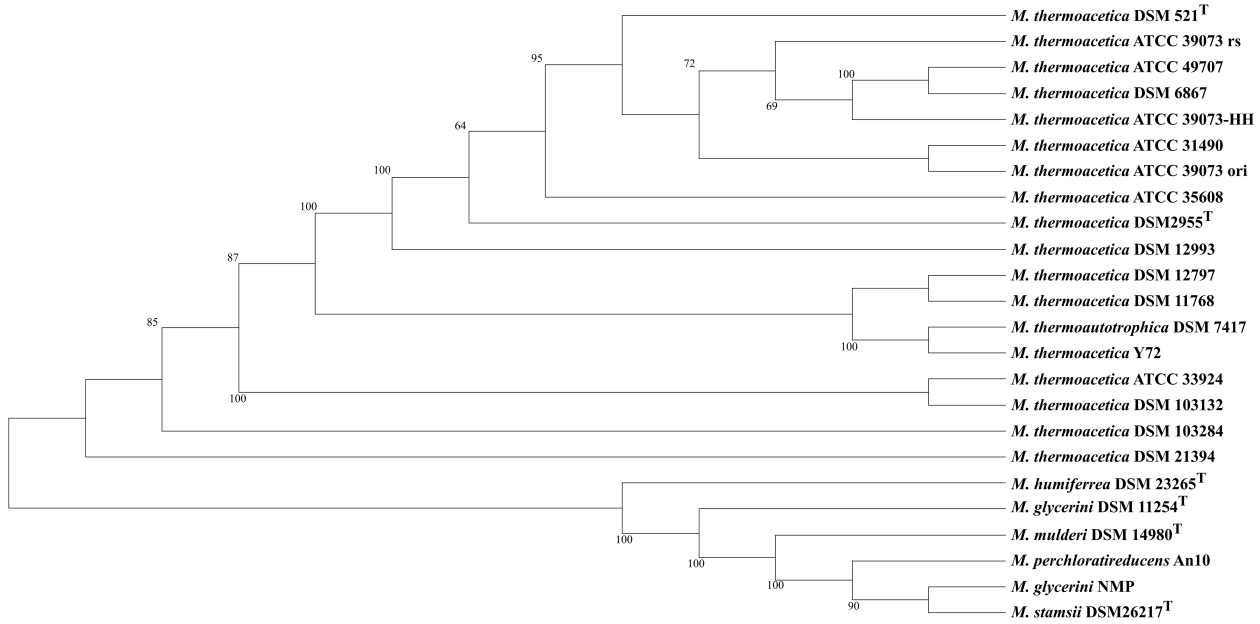

FIGURE 1 | MLSA tree of 24 sequenced *Moorella* strains: maximum likelihood trees of 24 *Moorella* genome sequences were inferred with 500 repetitions with RAxML (Stamatakis, 2014) and visualized with Dendroscope (Huson and Scornavacca, 2012). *M. thermoactica* marked with ATCC 39073 ori is the original sequence of this strain, ATCC 39073 rs is a sequenced version of the genome performed by the JGI and ATCC 39073-HH is a sequenced version of the genome performed by Technical University of Denmark.

is the strain with the third highest number of singletons (300 OGs). Whilst MLSA can provide insight into the phylogenetic relationship of organisms, for taxonomic studies there is a requirement for other methods, such as ANI analysis (Richter and Rosselló-Móra, 2009), which is a suitable *in silico* alternative for DNA–DNA hybridization (Goris et al., 2007). We performed an ANI analysis based on MUMmer alignment (ANIm) of the 24 genomes to define species and their complexes (**Figure 2**). We identified a large cluster comprising all *M. thermoacetica* and *M. thermoautotrophica* strains including DSM 103132 and DSM 103284, which have been both re-isolated from DSM 1974^T as well as DSM 7417. The latter two strains are currently considered to be *M. thermoautotrophica* strains. However, our analysis clearly shows that these strains would be more appropriately classified as *M. thermoacetica* isolates, since we identified ANIm values between 98 and 99% compared to *M. thermoacetica* DSM 512^T and DSM 2955^T, the two independent deposits of the type strain of this species in the DSMZ (**Supplementary Table S1**). Richter and Rosselló-Móra (2009) proposed a threshold for the species boundary of 95% ANI, making reference to both ANIb and ANIm values. However, careful examination of their original data suggests that ANIb and ANIm do not give the same values and the species boundary for the two may be different. ANIm values of 98–99% are clearly above this threshold, but values of 95–96% need to be taken with caution. Our analysis also revealed that strain DSM 21394 has an ANIm value of 94% (**Supplementary Table S1**) compared to the other *M. thermoacetica* strains, which is below the threshold for the species boundary and further studies would be needed to determine whether this strain should also be re-classified. This is also depicted in **Figure 2**, where all strains belonging to one species are marked in red tones. Interestingly, *M. stamsii* DSM 26217^T, *M. glycerini* NMP, and *M. perchloratireducens* An10 showed an ANIm value of 100% and they should therefore belong to the same species. However, the name *M. perchloratireducens* has not been validly published and *M. glycerini* NMP is not the nomenclatural type of the species so no formal nomenclatural action is required under the International Code of Nomenclature of Prokaryotes (Parker et al., 2019), since the names *M. glycerini* and *M. perchloratireducens* can only be formally considered to be heterotypic synonyms if both are validly published and are the corresponding nomenclatural types. The ANIm value of the type strain of *M. stamsii* to the other two strains is also 100%, indicating that all three should be placed in the same species, i.e., *M. stamsii*, which has been validly published. These results are in contrast to the published viewpoint that *M. stamsii* and *M. perchloratireducens* represent distinct species. It is common practice to determine the 16S rRNA gene sequence of a novel isolate and initially investigate the similarity value to the 16S rRNA gene sequences of other type strains before deciding how to further characterize a strain. In the case of 16S rRNA gene sequence similarity values of 97% and greater it is common practice to determine DNA–DNA hybridization values (which is now being replaced by ANI or digital DNA–DNA hybridization studies) to evaluate whether one is dealing with a new species. Where the 16S rRNA gene sequence similarity values are less than 97%, it is generally assumed that one has a novel species. Key discrepancies in the study of *M. glycerini, M. stamsii,* and

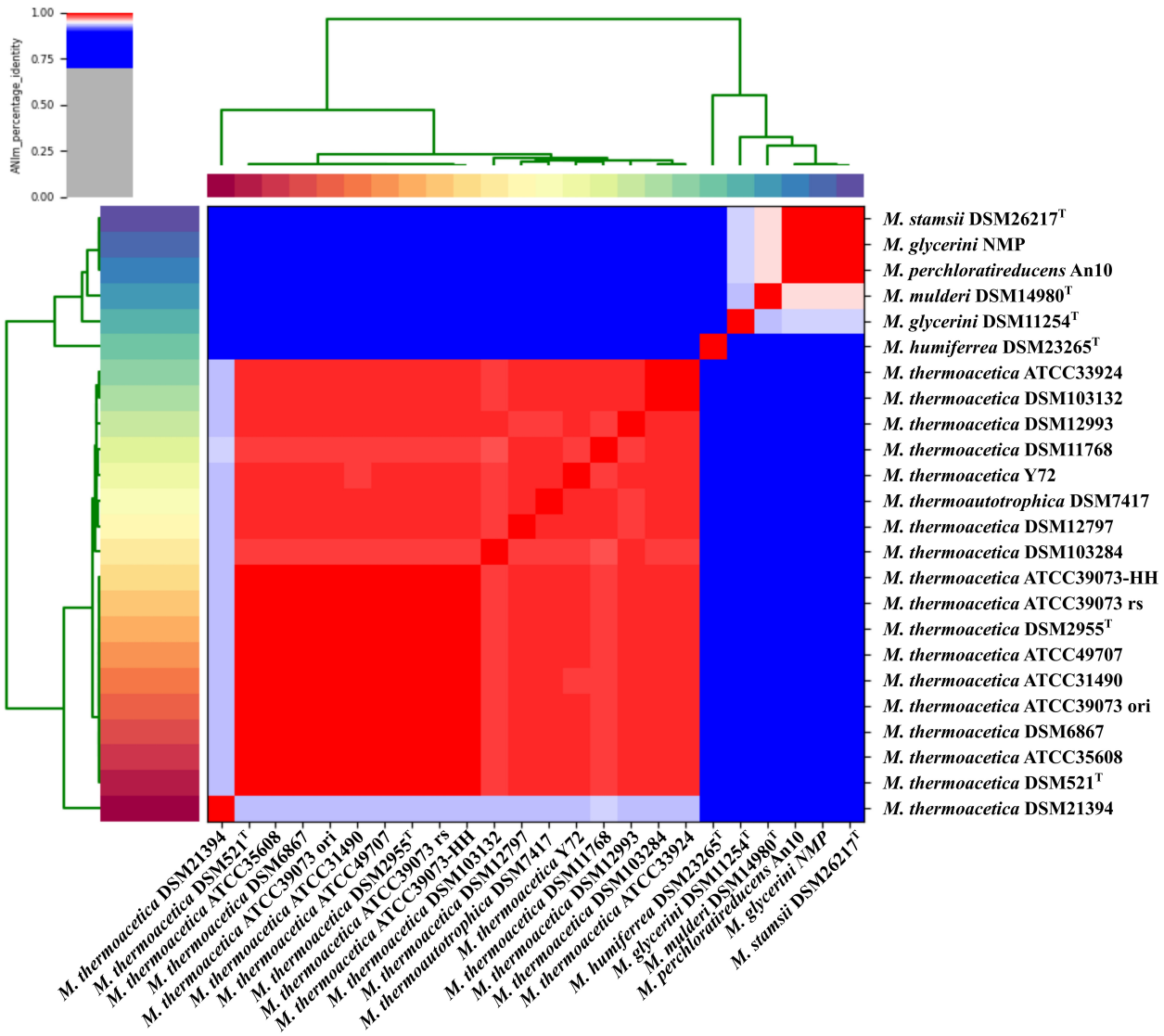

FIGURE 2 | Average nucleotide identity analysis of the 24 sequenced strains: ANIm analysis based on MUMmer alignment (Delcher et al., 2002) of the genome sequences was performed and visualized using PYANI (https://github.com/widdowquinn/pyani). *M. thermoactica* marked with ATCC 39073 ori is the original sequence of this strain, ATCC 39073 rs is a sequenced version of the genome performed by the JGI and ATCC 39073-HH is a sequenced version of the genome performed by Technical University of Denmark.

M. perchloratireducens are the 16S rRNA gene sequences and the genomic similarity. In the case of *M. glycerini,* the 16S rRNA gene sequence determined in the original study (Slobodkin et al., 1997), U82327, showed a pairwise similarity of 99.3% to the 16S rRNA sequence determined in the genome (CP046244). The 16S rRNA gene sequence determined in the original study of *M. stamsii* (Alves et al., 2013), HF563589, showed a pairwise similarity of 99.3% to the 16S rRNA sequence determined in the genome contig PVXL01000051. When U82327 and HF563589 were compared by Alves et al. (2013), the similarity values were 97%, but comparison of the 16S rRNA gene sequences obtained from the genomes (CP046244 and PVXL01000051) now gives 99.2% similarity and 100% similarity to CELZ01000013. In the case of DNA–DNA hybridization between these two strains the value was 51.1–53.3% (duplicated measurements). The 16S rRNA gene sequence from the genome of *M. glycerini* DSM 11254^T contains a large deletion that does not occur in U82327 or any of the other PCR-amplified 16S rRNA gene sequences or those determined via genome sequencing of the same strain (**Supplementary Figure S1**). The PCR-amplified 16S rRNA gene from *M. stamsii* (HF563589) also appears to contain numerous additional bases.

In the case of *M. perchloratireducens,* comparison of the 16S rRNA gene sequence determined in the original study, EF060194 (Balk et al., 2008), with that extracted from the genome (Gp0011525) showed 95.1% similarity. While EF060194

showed 97% sequence similarity with the 16S rRNA gene sequence from the genome of *M. thermoacetica* ATCC 39073 (CP00232), comparisons with the 16S rRNA gene sequence from Gp0011525 indicated that the genome-derived sequences showed 95% sequence similarity. In contrast, comparisons between EF060194 (*M. perchloratireducens*) and U82327 (*M. glycerini*)/HF563589 (*M. stamsii*) gave sequence similarity values of 93.9 and 93.1%, respectively. However, comparisons based on the 16S rRNA gene sequences extracted from the genomes Gp0011525 (*M. perchloratireducens*), CP046244 (*M. glycerini*), and PVXL01000051 (*M. stamsii*) gave pairwise similarities of 99.2–100%. No DNA–DNA hybridization studies were carried out by Balk et al. (2008), because they used a 16S rRNA gene sequence "threshold" of 98% 16S rRNA similarity. These results suggest significant discrepancies between the 16S rRNA gene sequence EF060194 obtained by primer amplified sequencing and that determined by genome sequencing that are evident in the alignments (**Supplementary Figure S1**) and are difficult to attribute to experimental error without further confirmatory work. It is interesting to note that of the two deposits of *M. perchloratireducens* An10, ATCC BAA-1531 and JCM 14829 only ATCC BAA-1531 is currently available and is the source strain for the genome Gp0011525. In the case of *M. mulderi* DSM 14980, the genome-derived 16S rRNA gene sequence (LTBC01000042.1) contains a large insert not present in sequence of the original PCR-amplified gene deposited as AF487538.1 (**Supplementary Figure S1**).

The ANIm values between *M. glycerini* (strain NMP), *M. stamsii*, and *M. perchloratireducens* indicate that they belong to the same species. Although the 16S rRNA gene sequence of the type strains of *M. glycerini* and *M. stamsii* are 99.3%, the AMIm value of 94% indicates that they are different species. In the case of *M. mulderi* DSM 14980 the genome-based 16S rRNA gene sequence similarity to *M. glycerini* DSM 11254 is 98.8% and the AMIm value 93%, indicating that they are different species. When compared to the genome-based 16S rRNA gene sequences of *M. glycerini* (strain NMP), *M. stamsii*, and *M. perchloratireducens* the value is 99.3% and the ANIm value 96%; this would appear to indicate that *M. mulderi* DSM 14980 is a member of the same species as *M. stamsii* DSM 26217. However, the original work of Richter and Rosselló-Móra (2009) indicate that an ANI cut-off of 95% ANIb is equivalent to an ANIm value of 96.5%, indicating that *M. mulderi* DSM 14980 and *M. stamsii* DSM 26217 are not members of the same species. This work also indicates the importance of examining the data beyond simple similarity values, where examination of the individual 16S rRNA gene sequence alignments, the differences in gene content and genome size provide extra valuable detail.

Genome Comparison

Until recently, only the sequence of the non-type strains *M. thermoacetica* ATCC 39079 and *M. thermoacetica* Y72 were publicly available, but many other strains, including the two independently deposited type strains of the species (DSM 521^T and DSM 2955^T), and several other strains are available at the German Collection of Microorganisms and Cell Cultures (DSMZ Brunswick), including strain DSM 1974^T. We sequenced the genomes of all these strains and performed whole genome comparison of all *M. thermoacetica* strains, and comparison with the genomes of five other species, namely *M. stamsii* DSM 26217^T, *M. humiferrea* DSM 23265^T, *M. glycerini* DSM 11254^T, M. *glycerini* NMP, *M. perchloratireducens* An10, and *M. mulderi* DSM 14980^T (**Figure 3**). All *M. thermoacetica* strains have a comparable genome size of 2.52–2.64 Mb, except the two closely clustering strains DSM 103132 and ATCC 33924, which have larger genomes (2.98 and 2.91 Mb). *M. glycerini* NMP has the largest genome size in our comparison with 3.58 Mb, followed by *M. glycerini* DSM 11254^T with 3.56 Mb. A whole genome comparison based on protein encoding genes revealed a core genome shared by all 24 strains of 1,297 OGs including paralogs and a pan genome of 8,042 OGs (**Figure 4**). The pan genome includes the core and the flexible genome, OGs shared by at least two genomes, but not by all genomes in the comparison. The size of the core genomes is half the size of the complete genome of the *M. thermoacetica* strains, due to the high proportion of *M. thermoacetica* strains in our comparison. We found a broad range of singletons, meaning genome-specific genes, varying between 15 and 275 OGs in the *M. thermoacetica* group. The highest number of singletons (674 OGs) was found in the genome of *M. glycerini* DSM 11254^T. The flexible genome harbors for example a complete gene cluster encoding a pyruvate:ferredoxin oxidoreductase, which is only present in DSM 103284, DSM 11768, DSM 512^T, DSM 2955^T, DSM 12797, and all ATCC 39073 genomes. A cluster encoding an anaerobic dimethylsulfoxide reductase (DSMO reductase) is present in all genomes compared here, except of *M. mulderi* DSM 14980 and *M. thermoacetica* DSM 103132, which has been re-isolated from the mixed culture DSM 1974. We also identified OGs that are specific for the above-mentioned phylogenetic clades. We identified, for example, a gene cluster coding for a carbohydrate-specific ABC transport system, which is exclusively present in the first main clade comprising all *M. thermoacetica* strains, but which is absent in the second main clade consisting of *M. stamsii* DSM 26217^T, *M. humiferrea* DSM 23265^T, *M. glycerini* DSM 11254^T, *M. perchloratireducens* An10, and *M. mulderi* DSM 14980^T. We also identified gene clusters specific for the first main clade, for example a cluster encoding, amongst other genes, a ribose permease, L-rhamnose mutarotase, and a L-fucose isomerase probably involved in rhamnose and fucose metabolism. There are also genome-specific genes. *M. thermoacetica* DSM 103284 for example harbors a hydrogenase gene cluster that could not be identified in any other genome analyzed in this study.

Phenotypical and Physiological Differences Between *M. thermoacetica* and *M. thermoautotrophica* Strains

Several phenotypical and physiological differences between *M. thermoacetica* and *M. thermoautotrophica* strains regarding compounds that can serve as carbon and energy source have been described in the literature. Those results are sometimes contradictory to each other. We therefore tested whether there are differences between the strains regarding carbon source utilization and whether the results can give a hint toward

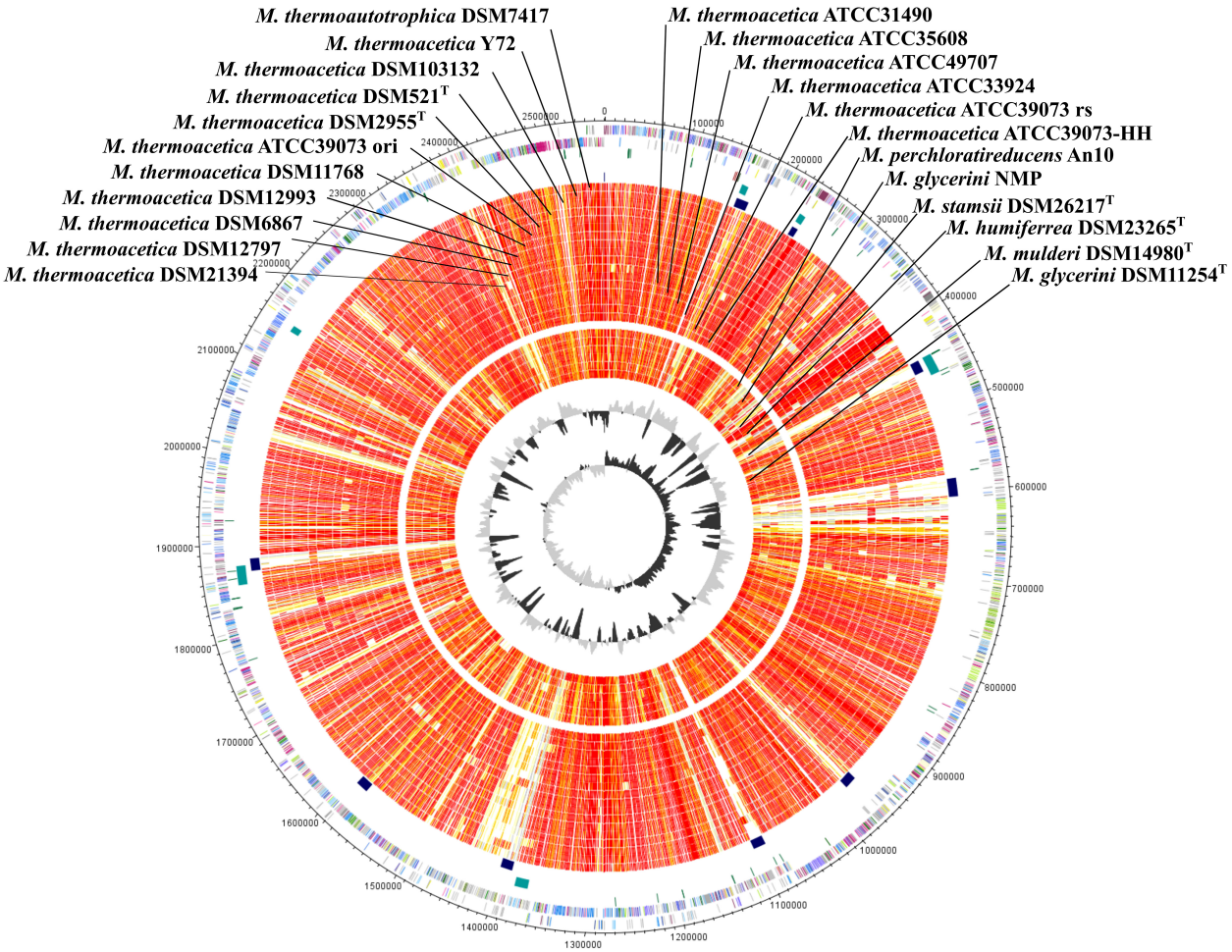

FIGURE 3 | Circular representation of the genome comparison of *M. thermoacetica* DSM 103284 with other *Moorella* strains. The genes encoded by the leading and the lagging strand (outer circles 1 and 2) of *M. thermoacetica* DSM 103284 are marked in COG colors in the artificial chromosome map. tRNA (green) and rRNA (pink) genes were plotted on circle 3. Detected prophage regions (petrol) and genomic islands (dark blue) are shown on circles 4 and 5, respectively. The presence of orthologous genes (red, high similarity; orange, medium similarity; yellow, low similarity (see color code below) is indicated for the genomes in comparison to *M. thermoacetica* DSM 103284. The two innermost plots represent the GC content and the GC skew (circles 29 and 30). Visualization was done using Proteinortho (Lechner et al., 2011) results and DNAPlotter (Carver et al., 2009). COG categories of the genes were extracted from IMG database (Galperin et al., 2014) entries of *M. thermoacetica* DSM 103284. Color code according to E-values of the blastp analysis performed using Proteinortho4.26. Gray, $1e^{-20}$ to 1; light yellow, $1e^{-21}$ to $1e^{-50}$; gold, $1e^{-51}$ to $1e^{-90}$; light orange, $1e^{-91}$ to 1e-100; orange, $1e^{-101}$ to $1e^{-120}$; red, > $1e^{-120}$ *M. thermoactica* marked with ATCC 39073 ori is the original sequence of this strain, ATCC 39073 rs is a sequenced version of the genome performed by the JGI and ATCC 39073-HH is a sequenced version of the genome performed by Technical University of Denmark.

the identity of strain DSM 1974^T. Our results largely agree with the results reported in the literature. Within the tested strains, only DSM 103132 can utilize arabinose (**Table 2**). As already published, *M. thermoacetica* (DSM 521^T or ATCC 39073) (Fontaine et al., 1942; Andreesen et al., 1973; Cato et al., 1986) and DSM 1974^T (Wiegel et al., 1981; Cato et al., 1986) are not able to utilize arabinose. DSM 103132 was also found to be the only strain that could utilize formate, but only reaching low optical densities. DSM 1974^T has been reported to utilize formate (Wiegel et al., 1981; Fröstl et al., 1996), like ATCC 39073 (Fröstl et al., 1996). All tested strains were able to grow on fructose and glucose, and these substrates led to the highest cell density, which is in agreement with literature on *M. thermoacetica* (DSM 521^T or ATCC 39073) (Fontaine et al., 1942; Andreesen et al., 1973). DSM 521^T was the only strain that did not utilize $H_2 + CO_2$ as carbon and energy source in our experiments. ATCC 39073 (Daniel et al., 1990; Fröstl et al., 1996) and DSM 1974^T (Wiegel et al., 1981; Savage and Drake, 1986; Fröstl et al., 1996) have been reported to utilize methanol. In agreement with our results, DSM 521^T has been reported not to grow on methanol (Cato et al., 1986). All strains tested in this study grew with pyruvate as energy and carbon source. Interestingly, Cato et al. (1986) indicated that pyruvate does not serve as a growth-supportive substrate for DSM 1974^T (Wiegel et al., 1981). None of the tested strains, except for DSM 103284, could utilize rhamnose, which is in line with DSM 1974^T being

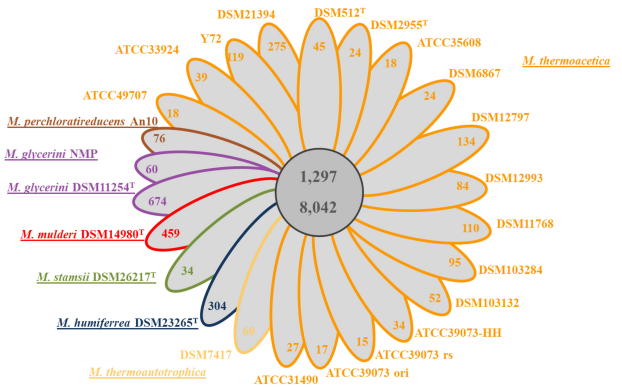

FIGURE 4 | Core/Pan genome analysis of 24 *Moorella* genomes: a simplified Venn diagram showing the core and the pan genome of all 24 *Moorella* strains. The number of genome-specific OGs is depicted in the respective ellipse. Ortholog detection was done with blastp and the Proteinortho software (Lechner et al., 2011) with a similarity cut off of 50% and an E-value of $1e^{-10}$. *M. thermoacetica* marked with ATCC 39073 ori is the original sequence of this strain, ATCC 39073 rs is a sequenced version of the genome performed by the JGI and ATCC 39073-HH is a sequenced version of the genome performed by the Technical University of Denmark.

the only *M. thermoacetica/thermoautotrophica* strain previously reported to utilize rhamnose (Cato et al., 1986). According to the literature, *M. thermoacetica* (DSM 521^T or ATCC 39073) (Fontaine et al., 1942; Andreesen et al., 1973; Cato et al., 1986) and DSM 1974^T (Wiegel et al., 1981; Cato et al., 1986) are not capable of utilizing sucrose, however, we observed growth for ATCC 39073-HH and DSM 103132 on that substrate. All tested strains, except DSM 103132, utilized xylose. In the case of DSM 1974^T, contradictory results have been reported: according to Cato et al. (1986), in 61–89% of the tests, cultures were able to utilize xylose. Some of the differences in substrate utilization can be explained by comparison of the genomes. For example, the arabinose operon in the genome of DSM 103132 is not present in the genome of ATCC 39073-HH. The pathway for xylose utilization is encoded in the ATCC 39073-HH genome, but not in the DSM 103132 genome. Other differences in carbon source utilization between the various studies may be due to the fact that strains might have adapted to different substrates or that the substrate utilization depends on the growth stage of the inoculum (Wiegel et al., 1981), which may be caused by differences in transcriptional regulators between the strains (Marcellin et al., 2016). Our results do not allow an unambiguous conclusion to be drawn whether one of the strains (DSM 103132 and DSM 103284) corresponds to the strain originally studied by Wiegel et al. (1981) and deposited as DSM 1974^T in the DSMZ. In addition to carbon source utilization, other phenotypical and physiological differences between the *M. thermoacetica/thermoautotrophica* strains have been described, such as differences in motility [DSM 1974^T is motile (Cato et al., 1986), DSM 521^T is not (Carlier and Bedora-Faure, 2006)] and growth temperature [DSM 1974^T can grow at 70°C (Cato et al., 1986), while DSM 521^T cannot (Carlier and Bedora-Faure, 2006)].

DISCUSSION

Strains of *M. thermoacetica* and *M. thermoautotrophica* have become model organisms of the acetogenic metabolism. Due to the observation of conflicting phenotypic traits that have been connected with the two different species, the scientific community has already questioned the taxonomic status of the two species *M. thermoautotrophica* and *M. thermoacetica* (Carlier and Bedora-Faure, 2006; Kimura et al., 2016). In addition to the high similarity of the genomes' 16S rRNA gene sequence, there are further similarities described for *M. thermoacetica/thermoautotrophica* strains such as a similar fatty acid and peptidoglycan profile (Yamamoto et al., 1998) and presence of the same menaquinone (Das et al., 1989). However, these features are generally conserved in "closely related" taxa and one would not expect significant differences between strains showing such a high degree of genetic similarity (Tindall, unpublished). Until a few years ago, only the sequence of the non-type strains *M. thermoacetica* ATCC 39079 and *M. thermoacetica* Y72 were publicly available, but many other strains, including the two type strains of the species (DSM 521^T and DSM 2955^T), and several other strains are available at the German Collection of Microorganisms and Cell Cultures (DSMZ Brunswick), including strain DSM 1974^T. We wished to broaden knowledge of the genetic diversity of this group of organisms and therefore sequenced the genome of both strains which were derived from the DSM 1974^T culture (DSM 103132 and DSM 103284), as well as the genome of DSM 7417 and the genome of another sub-culture of ATCC 39073 (ATCC 39073-HH). In addition, the genomes of eight different *M. thermoacetica* strains were sequenced. Comparison of the 16S rRNA gene sequences of the strains, ATCC 39073(-HH), DSM 103132, and DSM 103284, showed a sequence similarity between the strains higher than 99.74%. We used MLSA, gene content analysis, and ANI analysis to get insights into the phylogeny of the genus *Moorella*. With ANIm values between 98 and 99% compared to the other *M. thermoacetica* strains DSM 512^T and DSM 2955^T, the strains derived from DSM 1974^T (DSM 103132 and DSM 103284) are clearly *M. thermoacetica* isolates. Through genome sequencing of different *M. thermoacetica* and *M. thermoautotrophica* strains, it was evident that *M. thermoautotrophica* DSM 1974^T consists of at least two different strains, which are both very closely related to each other and to *M. thermoacetica*. Since phylogenetic analysis showed that all *M. thermoacetica/thermoautotrophica* strains described to date belong to the same species, there would appear to be no justification based on the currently available data for considering *M. thermoautotrophica* to be a separate species. Consequently, the strains DSM 103132 and DSM 103284 (both derived from DSM 1974^T, the designated type strain of *M. thermoautotrophica*) must be designated as *M. thermoacetica*. Based on the current study, the observed phenotypic differences are likely to be due to strain variations within one species, as already indicated by Wiegel et al. (1981) and Cato et al. (1986). Furthermore, observed differences in carbon source utilization cannot serve as a suitable measure to distinguish species, since the substrate acceptance may be dependent on cultivation conditions. However, the picture is

TABLE 2 | Substrate utilization by selected *Moorella* strains.

		ATCC 39073-HH	DSM 103132	DSM 2955^T	DSM 521^T	DSM 103284	DSM 7417	Data for original strain DSM 1974^T (Wiegel et al., 1981)
Arabinose	60 mM	NG	0.42	NG	NG	NG	NG	NG
Formate	10 mM	NG	0.12	NG	NG	NG	NG	+
Fructose	60 mM	1.65	1.30	1.66	0.67	1.24	1.29	+ +
Glucose	60 mM	1.50	0.22	1.90	0.59	0.25	0.23	+ +
H_2/CO_2	30 psi	0.11	0.22	0.45	NG	0.28	0.36	+
Methanol	60 mM	0.22	0.10	0.49	NG	0.50	0.26	+
Pyruvate	60 mM	0.39	0.33	0.28	0.33	0.56	0.27	NG
Rhamnose	60 mM	NG	NG	NG	NG	0.60	NG	NR
Sucrose	60 mM	1.60	0.26	NG	NG	NG	NG	NG
Xylose	60 mM	1.50	NG	0.88	0.44	0.70	0.70	NG

The highest optical densities are reported that were measured for the respective carbon sources. NG, no growth; NR, not reported; +, slow growth or low optical density; + +, fast growth, optical density at 600 nm above 1.0 with 0.5% (wt/vol) carbon source after 4 days.

complicated by the fact that DSM 1974^T, the strain which led to the proposal of the new species *C. thermoautotrophicum* (Wiegel et al., 1981) and was later transferred to the genus *Moorella* as *M. thermoautotrophica* (Collins et al., 1994) was consistently shown by genome sequencing to consist of two different strains. The isolation of two different strains that have subsequently been deposited as DSM 103132 and DSM 103284 confirms these observations. However, taking the original data of Wiegel et al. (1981) and comparing them with the data collected in this study for DSM 103132 and DSM 103284 does not show a large number of significant differences in the physiology of the strains. Based on the current data and taking into consideration the methods originally used by Wiegel et al. (1981) it is not possible to determine whether the original strain of Wiegel, JW 701/3, was a mixture of two different strains of the same species, whether the original strain was a pure culture, but a mixed culture was submitted for deposit (that methods used at the time would not have detected), or whether a second strain was introduced into the culture subsequent to accession to the DSMZ. Cross-contamination of strains is one possible explanation: the spores of *Moorella* species are highly heat-resistant and are not sufficiently inactivated by a standard autoclaving at 121°C (Fontaine et al., 1942). Byrer et al. (2000) for example described the strains JW/DB-2 and JW/DB-4 (ATCC number BAA-48) that show unusually heat-resistant spores. However, given the resolution of methods used at the time, one also cannot exclude with certainty that the original culture did not consist of more than one strain. One interesting aspect is that Wiegel et al. (1981) report that DNA–DNA hybridization supported the recognition of strains JW 701/3 and strain KIVU as members of the same species, but distinct from *C. thermoaceticum* (*M. thermoacetica*). Kimura et al. (2016) have previously reported a similar problem with the designated type strain of *M. thermoautotrophica.* Formulated as a Request for an Opinion, this limits any action that can be taken to a formal ruling by that body. However, their work concentrates largely on the interpretation of 16S rRNA gene sequences that appear to have been obtained by both cloning and the isolation of strains from the culture supplied. Representative partial sequences of the 16S rRNA genes of the seven groups obtained by cloning and sequencing of the isolates have been deposited as LC133084–LC133087 and designated in the publication as representing OUT-1 to OUT-4 in that order, respectively. Kimura et al. (2016) concentrate on a single 16S rRNA gene sequence deposited as L09168 (from DSM 1974) and do not mention that additional sequences are available, X58353 and X77849. X58353 (strain JW 701/3; 1155 bases, but with numerous Ns) was deposited in 1990 from the University of Kiel and will not be considered further. X77849 was deposited in 1994 from the University of Reading in co-operation with Dr. Hippe (DSMZ curator of the strain at the time) and is derived from DSM 1974 and presumably directly from stocks held in the DSMZ. L09168 was deposited in 1993 from The University of Queensland. A direct alignment of the two sequences L09168 and X77849 indicates that, ignoring a small number of Ns in X77849, the two are not identical making it difficult to conclude whether either of the two can be considered to be a 100% accurate reflection of the original gene sequences from the same strain. Similarly, a comparison with the 16S rRNA sequences from Kimura et al. (2016) also indicate that neither of the two sequences (X77849 and L09168) (**Supplementary Figure S2**) show 100% similarity with those obtained by Kimura et al. (2016). It should also be remembered that the sequences X77849 and L09168 are only one part of the evidence that were not obtained directly when the type strain was originally described and "verification" of X77849 vs. L09168 does not allow one to conclude that one sequence is "correct" and the other in error. If one were to extend the reasoning of Kimura et al. (2016) to other similar cases one would conclude that given the differences between the 16S rRNA gene sequence obtained by direct amplification and that extracted from the genome of *M. stamsii* that the type strain does not exist. An even more dramatic example is the case of *Alterococcus agarolyticus* (Shieh and Jean, 1998) that started its taxonomic career as an atypical member of the *Enterobacteriaceae* (Shieh and Jean, 1998) under the 16S rRNA gene sequence AF075271.1 (deposited 19th June 1998) that was substituted for by AF075271.2 (deposited 21st August 2002) and is widely accepted as a member of the *Verrucomicrobia*. Under these circumstances, the nomenclatural type currently available certainly does not correspond to the 16S rRNA gene sequence originally deposited as AF075271.1

and one would have to conclude that the type strain no longer exists. However, put in context other data in the original publication clearly indicates that *Alterococcus agarolyticus* was an atypical member of the *Enterobacteriaceae* and that the original 16S rRNA gene sequence AF075271.1 is in error and should have been verified.

In the case of *M. thermoautotrophica,* comparison with the 16S rRNA gene sequence deposited as X77849 and L09168 also needs to be treated with caution if the original source culture (DSM 1974^T) was not a pure culture or where the quality/accuracy of gene sequencing technologies may have changed over the decades. No attempt was made to compare the physiological/biochemical properties of the strains studied by Kimura et al. (2016) with the original work of Wiegel et al. (1981) and relies solely on one older gene sequence (L09168) that is not corroborated by another sequence (X77849) obtained at about the same time from the same source culture, DSM 1974^T. Examining the 16S rRNA sequences deposited by Kimura et al. (2016) (LC133084-LC133087) against L09168, X77849 and those extracted from the genomes derived from subcultures of DSM 1974 and ATCC 33924 (including re-deposits as DSM 103132 and DSM 103284), i.e., CP017019.1 (positions 154745–156300 and 147549–149104), CP017237.1 (positions 144877–146432), and VCDX01000030.1 (positions 1667–112) indicates that toward the end of the single primer amplified partial sequences LC133085 and LC133086 gaps are present that are not otherwise present in any of the other sequences in a region that could be considered to be conserved (**Supplementary Figure S2**). These gaps have, therefore, not been taken into consideration in the analysis here. Kimura et al. (2016) do not provide alignments of sequences in support of their work and make it impossible to determine why they consider "none of the sequences were similar to *M. thermoautotrophica* DSM 1974T (L09168)," when in fact they show only minimal differences in the alignments presented here. Although alignments are critical steps in the evaluation of sequence-based data (both nucleotide and amino acid based) they are rarely given, contrary to recommendations (Tindall et al., 2010), making the direct verification of the resulting interpretation via this critical step impossible and are therefore included in **Supplementary Figures S1, S2**. The sequence LC133087 appears to belong to a strain having the most similar 16S rRNA sequence to *M. humiferrea* strain 64_FGQ^T (GQ872425) and will not be considered further. In the alignment shown, CP017019.1 (positions 154745–156300), CP017019.1 (positions 147549–149104), VCDX01000030.1 (positions 1667–112), and LC133086.1 have a "T" at position 280 (alignment numbering, **Supplementary Figure S2**) while CP017237.1 (positions 144877–146432), LC133084.1, and LC133085.1 have a "C" at the same position. LC133086. 1 differs from CP017019.1 (positions 154745–156300), CP017019.1 (positions 147549–149104), and VCDX01000030.1 (positions 1667–112) in having a "T" position 435 rather than a "C" that is present in all other sequences (**Supplementary Figure S2**). LC133084.1 appears to be identical in the aligned bases to CP017237.1 (positions 144877–146432), but LC133085.1 has an "A" at position 745 rather than a "G" that is present in all other sequences (**Supplementary Figure S2**). Based on these observations, the only organism recovered in this study and that of Kimura et al. (2016) is that represented by LC133084.1 and CP017237.1 (DSM 103284). While this demonstrates the care that has to be taken in evaluating the interpretation of the data used by Kimura et al. (2016), the major problem that arises centers on the fact that the strains isolated by Kimura et al. (2016) have not been deposited in a culture collection and comparison with the original physiological and biochemical data published by Wiegel et al. (1981) cannot be made. Based on an evaluation of the 16S rRNA sequences determined previously and those determined here it is not possible to conclude that the type strain no longer exists, since it was deposited as DSM 1974 and ATCC 33924 and the 16S rRNA sequences deposited as X77849 and L09168 do not appear to be fully accurate.

The Request for an Opinion of Kimura et al. (2016) also misinterprets the wording of Rule 18c and draws incorrect conclusions. Tindall (2016) provided a detailed discussion of the incorrect interpretation of Rule 18c that was also applied by Kimura et al. (2016). Based on the evidence presented by Kimura et al. (2016) and that obtained in this work one cannot conclude that the nomenclatural type no longer exists, but rather there may be an issue with the purity of the culture deposited/currently available. The current study covers the physiological/biochemical properties of strains isolated from DSM 1974^T and expands on the genomic characterization of the strains studied. While it is clear that DSM 103132 and DSM 103284 (both derived from DSM 1974^T, the designated type strain of *M. thermoautotrophica*) are more appropriately considered to be members of the species *M. thermoacetica*, there is a formal nomenclatural issue that also needs to be addressed that requires reference to be made to the International Code of Nomenclature of Prokaryotes (Parker et al., 2019). Typically, the nomenclatural type of a species as defined in Rule 18a is an axenic culture, but there are instances where one component part of a syntrophic co-culture has been named and the co-culture accepted as the nomenclatural type (type strain). However, when mixed cultures or consortia are considered (see Rule 31a and 31b) and these are treated as a "single" biological entity, the names associated with them are not validly published and could be applied to *M. thermoautotrophica*. In the case of DSM 1974^T and ATCC 33924^T, although the strains currently in circulation appear to be a mixed culture, there is no unambiguous evidence that the parent culture, strain JW 701/3, was also a mixed culture. In contrast to the study of Kimura et al. (2016), it has been possible to study in greater detail pure cultures of strains isolated from DSM 1974^T (that is the parent deposit for all other culture collection strains) and subsequently deposited as DSM 103132 and DSM 103284. In both cases, the strains appear to be members of the species *M. thermoacetica*. One possible solution would be to designate one of them as a neotype, although based on the physiological and biochemical data presented here neither of the two strains (DSM 103132 or DSM 103284) can unambiguously be shown to be more similar in its properties than the other to the data originally published by Wiegel et al. (1981). Irrespective of which course of action is taken, it is clear that the culture of DSM 1974^T made available to the current authors contains strains that should be classified in the species *M. thermoacetica* leading to the logical conclusion that

DSM 103132 and DSM 103284 should be assigned to that species. This nomenclatural conclusion is inescapable, irrespective of whether one follows the arguments of Kimura et al. (2016), where the name *M. thermoautotrophica* would eventually be rejected, declared to not have been validly published, or whether one considers the names *M. thermoacetica* (Fontaine et al., 1942; Collins et al., 1994) and *M. thermoautotrophica* (Wiegel et al., 1981; Collins et al., 1994) to be heterotypic synonyms. In the latter case, priority is governed by Rule 23a, 38 and 42 where the dates of valid publication of the epithets are taken into consideration, i.e., *thermoacetica* Fontaine et al. (1942) has priority over *thermoautotrophica* Wiegel et al. (1981). This also leads to the use of the name *M. thermoacetica* (Fontaine et al., 1942; Collins et al., 1994) and recognition of *M. thermoautotrophica* (Wiegel et al., 1981; Collins et al., 1994) as the later heterotypic synonym when their respective nomenclatural types are considered to members of the same taxon. The current authors favor the latter course of action, but the Judicial Commission may also decide otherwise. Also, *M. thermoautotrophica* DSM 7417 should be reclassified as *M. thermoacetica* as well.

In addition to resolving the *M. thermoacetica/thermoautotrophica* problem, this comprehensive analysis of the genus *Moorella* by the study of a significant number of novel genome sequences and knowledge of phenotypic differences led to two other important conclusions. First, strain DSM 21394, currently still named *M. thermoacetica*, clearly does not belong to this species. Reclassification and renaming as a new species are required. Secondly, *M. glycerini* NMP, *M. stamsii* DSM 26217^T, and *M. perchloratireducens* cannot be distinguished at species level. Furthermore, *M. glycerini* NMP has been wrongly assigned as *M. glycerini* as this strain shows an ANIm value of 94% similarity compared to the type strain DSM 11254^T and is clearly a different species despite the high 16S rRNA gene sequence pairwise similarity of 99.7%. Based on the data presented here, *M. glycerini* NMP, *M. stamsii* DSM 26217^T, and *M. perchloratireducens* are all members of the same species. Although reclassification of these three strains may be required, caution needs to be exercised when one considers differences between the data reported here and that previously reported in the literature (Slobodkin et al., 1997; Balk et al., 2008; Alves et al., 2013), especially with regards to the 16S rRNA gene sequences and the genomic similarity inferred from DNA–DNA hybridization experiments vs. *in silico* comparisons.

DATA AVAILABILITY STATEMENT

The datasets generated for this study can be found in the IMG, GenBank, NCBI.

AUTHOR CONTRIBUTIONS

SR, AP, FB, TJ, CJ, PD, and AN conceived and designed the experiments. SR, AP, CE, FB, and TJ performed the experiments. SR, AP, CE, FB, TJ, CJ, PD, and AN analyzed the data. SR, AP, FB, TJ, CJ, BT, RD, PD, and AN wrote the manuscript.

FUNDING

This work was supported by The Novo Nordisk Foundation to the Technical University of Denmark (grant number NNF10CC1016517) and a Ph.D. grant to SR from the People Programme (Marie Curie Actions) of the European Union Seventh Framework Programme FP7-People-2012-ITN, under grant agreement number 317058, "BACTORY." TJ was supported by EU H2020's Research and Innovation Programme under grant agreement number 731263 "AMBITION." CJ was supported by a grant from the Novo Nordisk Foundation (grant number NNF15OC0015246). Support was also provided by the ERA-IB 7 Project "OBAC" (FKZ 031B0274) to the groups of RD and PD. Independent Research Fund Denmark under grant number 7026-00025B.

ACKNOWLEDGMENTS

We acknowledge the support for the PacBio sequencing given by Björn Hallström, Science for Life Laboratory (KTH) and conducted by Christian Tellgren-Roth (UGC, NGI). We thank Melanie Heinemann and Sarah Teresa Schüßler for technical support and Richard Egelkamp for help with graphic tools.

SUPPLEMENTARY MATERIAL

The Supplementary Material for this article can be found online at: https://www.frontiersin.org/articles/10.3389/fmicb.2019.03070/full#supplementary-material

REFERENCES

Alves, J. I., van Gelder, A. H., Alves, M. M., Sousa, D. Z., and Plugge, C. M. (2013). *Moorella stamsii* sp. nov., a new anaerobic thermophilic hydrogenogenic carboxydotroph isolated from digester sludge. *Int. J. Syst. Evol. Microbiol.* 63, 4072–4076. doi: 10.1099/ijs.0.050369-0

Andreesen, J. R., Schaupp, A., Neurauter, C., Brown, A., and Ljungdahl, L. G. (1973). Fermentation of glucose, fructose, and xylose by *Clostridium thermoaceticum*: effect of metals on growth yield, enzymes, and the synthesis of acetate from CO_2. *J. Bacteriol.* 114, 743–751.

Arndt, D., Grant, J. R., Marcu, A., Sajed, T., Pon, A., Liang, Y., et al. (2016). PHASTER: a better, faster version of the PHAST phage search tool. *Nucleic Acids Res.* 44, W16–W21. doi: 10.1093/nar/gkw387

Balk, M., van Gelder, T., Weelink, S. A., and Stams, A. J. M. (2008). (Per)chlorate reduction by the thermophilic bacterium *Moorella perchloratireducens* sp. nov., isolated from underground gas storage. *Appl. Environ. Microbiol.* 74, 403–409. doi: 10.1128/AEM.01743-07

Bankevich, A., Nurk, S., Antipov, D., Gurevich, A. A., Dvorkin, M., Kulikov, A. S., et al. (2012). SPAdes: a new genome assembly algorithm and its applications to single-cell sequencing. *J. Comp. Biol.* 19, 455–477. doi: 10.1089/cmb.2012.0021

Bengelsdorf, F. R., Poehlein, A., Esser, C., Schiel-Bengelsdorf, B., Daniel, R., and Dürre, P. (2015). Complete genome sequence of the acetogenic bacterium *Moorella thermoacetica* DSM 2955^T. *Genome Announc.* 3:e1157-15. doi: 10.1128/genomeA.01157-15

Bertelli, C., Laird, M. R., Williams, K. P., Simon Fraser University Research Computing Group, Lau, B. Y., Hoad, G., et al. (2017). IslandViewer 4: expanded

prediction of genomic islands for larger-scale datasets. *Nucleic Acids Res.* 45, W30–W35. doi: 10.1093/nar/gkx343

Bland, C., Ramsey, T. L., Sabree, F., Lowe, M., Brown, K., Kyrpides, N. C., et al. (2007). CRISPR recognition tool (CRT): a tool for automatic detection of clustered regularly interspaced palindromic repeats. *BMC Bioinform.* 8:209. doi: 10.1186/1471-2105-8-209

Bolger, A. M., Lohse, M., and Usadel, B. (2014). Trimmomatic: a flexible trimmer for Illumina sequence data. *Bioinformatics* 30, 2114–2120. doi: 10.1093/bioinformatics/btu170

Byrer, D. E., Rainey, F. A., and Wiegel, J. (2000). Novel strains of *Moorella thermoacetica* form unusually heat-resistant spores. *Arch. Microbiol.* 174, 334–339. doi: 10.1007/s002030000211

Camacho, C., Coulouris, G., Avagyan, V., Ma, N., Papadopoulos, J., Bealer, K., et al. (2009). BLAST+: architecture and applications. *BMC Bioinform.* 10:1. doi: 10.1186/1471-2105-10-421

Carlier, J.-P., and Bedora-Faure, M. (2006). Phenotypic and genotypic characterization of some *Moorella* sp. strains isolated from canned foods. *Syst. Appl. Microbiol.* 29, 581–588. doi: 10.1016/j.syapm.2006.01.002

Carver, T., Thomson, N., Bleasby, A., Berriman, M., and Parkhill, J. (2009). DNAPlotter: circular and linear interactive genome visualization. *Bioinformatics* 25, 119–120. doi: 10.1093/bioinformatics/btn578

Castillo Villamizar, G. A., and Poehlein, A. (2016). Genome sequence of the acetogenic bacterium *Moorella mulderi* DSM 14980^{T}. *Genome Announc.* 4:e444-16. doi: 10.1128/genomeA.00444-16

Castresana, J. (2000). Selection of conserved blocks from multiple alignments for their use in phylogenetic analysis. *Mol. Biol. Evol.* 17, 540–552. doi: 10.1093/oxfordjournals.molbev.a026334

Cato, E. P., George, W. L., and Finegold, S. M. (1986). Genus *Clostridium*. *Bergeys Manual of Syst. Bacteriol.* 2, 1141–1200.

Collins, M. D., Lawson, P. A., Willems, A., Cordoba, J. J., Fernandez-Garayzabal, J., Garcia, P., et al. (1994). The phylogeny of the genus *Clostridium*: proposal of five new genera and eleven new species combinations. *Int. J. Syst. Bacteriol.* 44, 812–826. doi: 10.1099/00207713-44-4-812

Daniel, S. L., Hsu, T., Dean, S. I., and Drake, H. L. (1990). Characterization of the H_2-and CO-dependent chemolithotrophic potentials of the acetogens *Clostridium thermoaceticum* and *Acetogenium kivui*. *J. Bacteriol.* 172, 4464–4471. doi: 10.1128/jb.172.8.4464-4471.1990

Darling, A. E., Mau, B., and Perna, N. T. (2010). progressiveMauve: multiple genome alignment with gene gain, loss and rearrangement. *PLoS One* 5:e11147. doi: 10.1371/journal.pone.0011147

Das, A., Hugenholtz, J., van Halbeek, H., and Ljungdahl, L. G. (1989). Structure and function of a menaquinone involved in electron transport in membranes of *Clostridium thermoautotrophicum* and *Clostridium thermoaceticum*. *J. Bacteriol.* 171, 5823–5829. doi: 10.1128/jb.171.11.5823-5829.1989

Delcher, A. L., Phillippy, A., Carlton, J., and Salzberg, S. L. (2002). Fast algorithms for large-scale genome alignment and comparison. *Nucleic Acids Res.* 30, 2478–2483. doi: 10.1093/nar/30.11.2478

Diekert, G. B., and Thauer, R. K. (1978). Carbon monoxide oxidation by *Clostridium thermoaceticum* and *Clostridium formicoaceticum*. *J. Bacteriol.* 136, 597–606.

Edgar, R. C. (2004). MUSCLE: multiple sequence alignment with high accuracy and high throughput. *Nucleic Acids Res.* 32, 1792–1797. doi: 10.1093/nar/gkh340

Finn, R. D., Clements, J., and Eddy, S. R. (2011). HMMER web server: interactive sequence similarity searching. *Nucleic Acids Res.* 39, W29–W37. doi: 10.1093/nar/gkr367

Fontaine, F. E., Peterson, W. H., McCoy, E., Johnson, M. J., and Ritter, G. J. (1942). A new type of glucose fermentation by *Clostridium thermoaceticum*. *J. Bacteriol.* 43, 701–715.

Fröstl, J. M., Seifritz, C., and Drake, H. L. (1996). Effect of nitrate on the autotrophic metabolism of the acetogens *Clostridium thermoautotrophicum* and *Clostridium thermoaceticum*. *J. Bacteriol.* 178, 4597–4603. doi: 10.1128/jb.178.15.4597-4603.1996

Galperin, M. Y., Makarova, K. S., Wolf, Y. I., and Koonin, E. V. (2014). Expanded microbial genome coverage and improved protein family annotation in the COG database. *Nucleic Acids Res.* 43, D261–D269. doi: 10.1093/nar/gku1223

García-Alcalde, F., Okonechnikov, K., Carbonell, J., Cruz, L. M., Götz, S., Tarazona, S., et al. (2012). Qualimap: evaluating next-generation sequencing alignment data. *Bioinformatics* 28, 2678–2679. doi: 10.1093/bioinformatics/bts503

Goris, J., Konstantinidis, K. T., Klappenbach, J. A., Coenye, T., Vandamme, P., and Tiedje, J. M. (2007). DNA–DNA hybridization values and their relationship to whole-genome sequence similarities. *Int. J. Syst. Evol. Microbiol.* 57, 81–91. doi: 10.1099/ijs.0.64483-0

Gottwald, M., Andreesen, J. R., LeGall, J., and Ljungdahl, L. G. (1975). Presence of cytochrome and menaquinone in *Clostridium formicoaceticum* and *Clostridium thermoaceticum*. *J. Bacteriol.* 122, 325–328.

Henstra, A. M., Sipma, J., Rinzema, A., and Stams, A. J. M. (2007). Microbiology of synthesis gas fermentation for biofuel production. *Curr. Opin. Biotechnol.* 18, 200–206. doi: 10.1016/j.copbio.2007.03.008

Huson, D. H., and Scornavacca, C. (2012). Dendroscope 3: an interactive tool for rooted phylogenetic trees and networks. *Syst. Biol.* 61, 1061–1067. doi: 10.1093/sysbio/sys062

Hyatt, D., Chen, G.-L., LoCascio, P. F., Land, M. L., Larimer, F. W., and Hauser, L. J. (2010). Prodigal: prokaryotic gene recognition and translation initiation site identification. *BMC Bioinform.* 11:1. doi: 10.1186/1471-2105-11-119

Kerby, R., and Zeikus, J. G. (1983). Growth of *Clostridium thermoaceticum* on H_2/CO_2 or CO as energy source. *Curr. Microbiol.* 8, 27–30. doi: 10.1007/bf01567310

Kimura, Z.-I., Hoshino, T., and Murakami, K. (2016). The status of the species *Moorella thermoautotrophica* Wiegel et al., 1981. Request for an Opinion. *Int. J. Syst. Evol. Microbiol.* 66, 3249–3251. doi: 10.1099/ijsem.0.001163

Lagesen, K., Hallin, P., Rødland, E. A., Stærfeldt, H.-H., Rognes, T., and Ussery, D. W. (2007). RNAmmer: consistent and rapid annotation of ribosomal RNA genes. *Nucleic Acids Res.* 35, 3100–3108. doi: 10.1093/nar/gkm160

Laslett, D., and Canback, B. (2004). ARAGORN, a program to detect tRNA genes and tmRNA genes in nucleotide sequences. *Nucleic Acids Res.* 32, 11–16. doi: 10.1093/nar/gkh152

Latif, H., Zeidan, A. A., Nielsen, A. T., and Zengler, K. (2014). Trash to treasure: production of biofuels and commodity chemicals via syngas fermenting microorganisms. *Curr. Opin. Biotechnol.* 27, 79–87. doi: 10.1016/j.copbio.2013.12.001

Lechner, M., Findeiß, S., Steiner, L., Marz, M., Stadler, P. F., and Prohaska, S. J. (2011). Proteinortho: detection of (co-) orthologs in large-scale analysis. *BMC Bioinform.* 12:1. doi: 10.1186/1471-2105-12-124

Liebensteiner, M. G., Pinkse, M. W., Nijsse, B., Verhaert, P. D., Tsesmetzis, N., Stams, A. J., et al. (2015). Perchlorate and chlorate reduction by the Crenarchaeon *Aeropyrum pernix* and two thermophilic Firmicutes. *Environ. Microbiol. Rep.* 7, 936–945. doi: 10.1111/1758-2229.12335

Ljungdahl, L. G., and Andreesen, J. R. (1977). Formate dehydrogenase, a selenium-tungsten enzyme from *Clostridium thermoaceticum*. *Methods Enzymol.* 53, 360–372. doi: 10.1016/s0076-6879(78)53042-5

Marcellin, E., Behrendorff, J. B., Nagaraju, S., DeTissera, S., Segovia, S., Palfreyman, R. W., et al. (2016). Low carbon fuels and commodity chemicals from waste gases–systematic approach to understand energy metabolism in a model acetogen. *Green Chem.* 18, 3020–3028. doi: 10.1039/c5gc02708j

Marchler-Bauer, A., and Bryant, S. H. (2004). CD-Search: protein domain annotations on the fly. *Nucleic Acids Res.* 32, W327–W331.

Markowitz, V. M., Chen, I.-M. A., Palaniappan, K., Chu, K., Szeto, E., Pillay, M., et al. (2013). IMG 4 version of the integrated microbial genomes comparative analysis system. *Nucleic Acids Res.* 42, D560–D567. doi: 10.1093/nar/gkt963

Matteuzzi, D., Hollaus, F., and Biavati, B. (1978). Proposal of neotype for *Clostridium thermohydrosulfuricum* and the merging of *Clostridium tartarivorum* with *Clostridium thermosaccharolyticum*. *Int. J. Syst. Evol. Microbiol.* 28, 528–531. doi: 10.1099/00207713-28-4-528

Medema, M. H., Blin, K., Cimermancic, P., Jager, V., de, Zakrzewski, P., et al. (2011). antiSMASH: rapid identification, annotation and analysis of secondary metabolite biosynthesis gene clusters in bacterial and fungal genome sequences. *Nucleic Acids Res.* 39, W339–W346. doi: 10.1093/nar/gkr466

Nawrocki, E. P., and Eddy, S. R. (2013). Infernal 1.1: 100-fold faster RNA homology searches. *Bioinformatics* 29, 2933–2935. doi: 10.1093/bioinformatics/btt509

Parker, C. T., Tindall, B. J., and Garrity, G. M. (2019). International Code of Nomenclature of Prokaryotes (2008 revision). *Int. J. Syst. Evol. Microbiol.* 69, S1–S111.

Petersen, T. N., Brunak, S., Heijne, G., von, and Nielsen, H. (2011). SignalP 4.0: discriminating signal peptides from transmembrane regions. *Nat. Methods* 8, 785–786. doi: 10.1038/nmeth.1701

Pierce, E., Xie, G., Barabote, R. D., Saunders, E., Han, C. S., Detter, J. C., et al. (2008). The complete genome sequence of *Moorella thermoacetica* (f. *Clostridium thermoaceticum*). *Environ. Microbiol.* 10, 2550–2573. doi: 10.1111/j.1462-2920.2008.01679.x

Poehlein, A., Bengelsdorf, F. R., Esser, C., Schiel-Bengelsdorf, B., Daniel, R., and Dürre, P. (2015). Complete genome sequence of the type strain of the acetogenic bacterium *Moorella thermoacetica* DSM 521^T. *Genome Announc.* 3:e1159-15. doi: 10.1128/genomeA.01159-15

Poehlein, A., Böer, T., Steensen, K., and Daniel, R. (2018a). Draft genome sequence of the hydrogenogenic carboxydotroph *Moorella stamsii* DSM 26271. *Genome Announc.* 6:e345-18. doi: 10.1128/genomeA.00345-18

Poehlein, A., Keyl, A., Milsch, J. C., and Daniel, R. (2018b). Draft genome sequence of the thermophilic acetogen *Moorella humiferrea* DSM 23265. *Genome Announc.* 6:e357-18. doi: 10.1128/genomeA.00357-18

Redl, S., Sukumara, S., Ploeger, T., Wu, L., Jensen, T. O., Nielsen, A. T., et al. (2017). Thermodynamics and economic feasibility of acetone production from syngas using the thermophilic production host *Moorella thermoacetica*. *Biotechnol. Biofuels* 10:150. doi: 10.1186/s13068-017-0827-8

Richter, M., and Rosselló-Móra, R. (2009). Shifting the genomic gold standard for the prokaryotic species definition. *Proc. Natl. Acad. Sci. U.S.A.* 106, 19126–19131. doi: 10.1073/pnas.0906412106

Rijssel, M., Veen, I., and Hansen, T. A. (1992). A lithotrophic *Clostridium* strain with extremely thermoresistant spores isolated from a pectin-limited continuous culture of *Clostridium thermosaccharolyticum* strain Haren. *FEMS Microbiol. Lett.* 91, 171–175. doi: 10.1016/0378-1097(92)90679-i

Savage, M. D., and Drake, H. L. (1986). Adaptation of the acetogen *Clostridium thermoautotrophicum* to minimal medium. *J. Bacteriol.* 165, 315–318. doi: 10.1128/jb.165.1.315-318.1986

Schaupp, A., and Ljungdahl, L. G. (1974). Purification and properties of acetate kinase from *Clostridium thermoaceticum*. *Arch. Microbiol.* 100, 121–129. doi: 10.1007/bf00446312

Seemann, T. (2014). Prokka: rapid prokaryotic genome annotation. *Bioinformatics* 30, 2068–2069. doi: 10.1093/bioinformatics/btu153

Shieh, W. Y., and Jean, W. D. (1998). *Alterococcus agarolyticus*, gen.nov., sp.nov., a halophilic thermophilic bacterium capable of agar degradation. *Can. J. Microbiol.* 44, 637–645. doi: 10.1139/w98-051

Slobodkin, A., Reysenbach, A. L., Mayer, F., and Wiegel, J. (1997). Isolation and characterization of the homoacetogenic thermophilic bacterium *Moorella glycerini* sp. nov. *Int. J. Syst. Bacteriol.* 47, 969–974. doi: 10.1099/00207713-47-4-969

Stackebrandt, E., and Goebel, B. M. (1994). Taxonomic note: a place for DNA-DNA reassociation and 16S rRNA sequence analysis in the present species definition in bacteriology. *Int. J. Syst. Evol. Microbiol.* 44, 846–849. doi: 10.1099/00207713-44-4-846

Staden, R., Beal, K. F., and Bonfield, J. K. (1999). The Staden package, 1998. *Methods Mol. Biol.* 132, 115–130. doi: 10.1385/1-59259-192-2:115

Stamatakis, A. (2014). RAxML version 8: a tool for phylogenetic analysis and post-analysis of large phylogenies. *Bioinformatics* 30, 1312–1313. doi: 10.1093/bioinformatics/btu033

Tatusov, R. L., Koonin, E. V., and Lipman, D. J. (1997). A genomic perspective on protein families. *Science* 278, 631–637. doi: 10.1126/science.278.5338.631

Tindall, B. J. (2016). What does rule 18c of the international code of nomenclature of bacteria really say? *Int. J. Syst. Evol. Microbiol.* 66, 3622–3624. doi: 10.1099/ijsem.0.001245

Tindall, B. J., Rosselló-Móra, R., Busse, H. J., Ludwig, W., and Kämpfer, P. (2010). Notes on the characterization of prokaryote strains for taxonomic purposes. *Int. J. Syst. Evol. Microbiol.* 60, 249–266. doi: 10.1099/ijs.0.016949-0

Tsukahara, K., Kita, A., Nakashimada, Y., Hoshino, T., and Murakami, K. (2014). Genomeguided analysis of transformation efficiency and carbon dioxide assimilation by *Moorella thermoacetica* Y72. *Gene* 535, 150–155. doi: 10.1016/j.gene.2013.11.045

Wick, R. R., Judd, L. M., Gorrie, C. L., and Holt, K. E. (2017). Unicycler: resolving bacterial genome assemblies from short and long sequencing reads. *PLoS Comput. Biol.* 13:e1005595. doi: 10.1371/journal.pcbi.1005595

Wiegel, J., Braun, M., and Gottschalk, G. (1981). *Clostridium thermoautotrophicum* species novum, a thermophile producing acetate from molecular hydrogen and carbon dioxide. *Curr. Microbiol.* 5, 255–260. doi: 10.1007/bf01571158

Yamamoto, K., Murakami, R., and Takamura, Y. (1998). Isoprenoid quinone, cellular fatty acid composition and diaminopimelic acid isomers of newly classified thermophilic anaerobic Gram-positive bacteria. *FEMS Microbiol. Lett.* 161, 351–358. doi: 10.1016/s0378-1097(98)00094-9

Conflict of Interest: BT was employed by company Leibniz-Institut DSMZ-Deutsche Sammlung von Mikroorganismen und Zellkulturen GmbH, Brunswick, Germany.

The remaining authors declare that the research was conducted in the absence of any commercial or financial relationships that could be construed as a potential conflict of interest.

frontiers in Microbiology

ORIGINAL RESEARCH
published: 29 January 2020
doi: 10.3389/fmicb.2020.00063

"*Candidatus* Galacturonibacter soehngenii" Shows Acetogenic Catabolism of Galacturonic Acid but Lacks a Canonical Carbon Monoxide Dehydrogenase/Acetyl-CoA Synthase Complex

Laura C. Valk[1], Martijn Diender[2], Gerben R. Stouten[1], Jette F. Petersen[3], Per H. Nielsen[3], Morten S. Dueholm[3], Jack T. Pronk[1] and Mark C. M. van Loosdrecht[1]*

[1] Department of Biotechnology, Delft University of Technology, Delft, Netherlands, [2] Laboratory of Microbiology, Wageningen University and Research, Wageningen, Netherlands, [3] Department of Chemistry and Bioscience, Centre for Microbial Communities, Aalborg University, Aalborg, Denmark

OPEN ACCESS

Edited by:
Mirko Basen, University of Rostock, Germany

Reviewed by:
Daan R. Speth, California Institute of Technology, United States
Emma Jayne Gagen, University of Queensland, Australia

***Correspondence:**
Laura C. Valk
l.c.valk@tudelft.nl;
lcv@bio.aau.dk

Specialty section:
This article was submitted to Microbial Physiology and Metabolism, a section of the journal Frontiers in Microbiology

Received: *26 September 2019*
Accepted: *13 January 2020*
Published: *29 January 2020*

Citation:
Valk LC, Diender M, Stouten GR, Petersen JF, Nielsen PH, Dueholm MS, Pronk JT and van Loosdrecht MCM (2020) "Candidatus Galacturonibacter soehngenii" Shows Acetogenic Catabolism of Galacturonic Acid but Lacks a Canonical Carbon Monoxide Dehydrogenase/Acetyl-CoA Synthase Complex. Front. Microbiol. 11:63. doi: 10.3389/fmicb.2020.00063

Acetogens have the ability to fixate carbon during fermentation by employing the Wood-Ljungdahl pathway (WLP), which is highly conserved across Bacteria and Archaea. In a previous study, product stoichometries in galacturonate-limited, anaerobic enrichment cultures of "*Candidatus* Galacturonibacter soehngenii," from a novel genus within the *Lachnospiraceae*, suggested the simultaneous operation of a modified Entner-Doudoroff pathway for galacturonate fermentation and a WLP for acetogenesis. However, a draft metagenome-assembled genome (MAG) based on short reads did not reveal homologs of genes encoding a canonical WLP carbon-monoxide-dehydrogenase/acetyl-Coenzyme A synthase (CODH/ACS) complex. In this study, $NaH^{13}CO_3$ fed to chemostat-grown, galacturonate-limited enrichment cultures of "*Ca.* G. soehngenii" was shown to be incorporated into acetate. Preferential labeling of the carboxyl group of acetate was consistent with acetogenesis via a WLP in which the methyl group of acetate was predominately derived from formate. This interpretation was further supported by high transcript levels of a putative pyruvate-formate lyase gene and very low transcript levels of a candidate gene for formate dehydrogenase. Reassembly of the "*Ca.* G. soehngenii" MAG with support from long-read nanopore sequencing data produced a single-scaffold MAG, which confirmed the absence of canonical CODH/ACS-complex genes homologs. However, high CO-dehydrogenase activities were measured in cell extracts of "*Ca.* G. soehngenii" enrichment cultures, contradicting the absence of corresponding homologs in the MAG. Based on the highly conserved amino-acid motif associated with anaerobic Ni-CO dehydrogenase proteins, a novel candidate was identified which could be responsible for the observed activities. These results demonstrate operation of an acetogenic pathway, most probably as a yet unresolved variant of the Wood-Ljungdahl pathway, in anaerobic, galacturonate-limited cultures of "*Ca.* G. soehngenii."

Keywords: acetogenesis, ^{13}C-labeling, meta-transcriptomics, chemostat enrichment culture, Wood-Ljungdahl pathway

INTRODUCTION

Over the course of multiple decades, seven carbon-fixing pathways capable of supporting autotrophic growth have been identified and intensively studied; the Calvin-Benson-Bassham (CCB) reductive pentose-phosphate cycle, the reductive citric-acid cycle (Arnon-Buchanan (AB) cycle), the hydroxypropionate (Fuchs-Holo) bi-cycle, the 3-hydroxypropionate/4-hydroxybutyrate cycle, dicarboxylate/hydroxybutyrate cycle, the reductive acetyl-CoA (Wood-Ljungdahl) pathway and the reductive glycine pathway (Berg, 2011; Fuchs, 2011; Figueroa et al., 2018). The first five pathways are primarily used for carbon fixation and the reductive glycine pathway for recycling of electron carriers. Only the Wood-Ljungdahl pathway (WLP) also acts as a primary pathway for energy conservation in anaerobes (Fuchs, 2011; Bar-Even et al., 2012b; Schuchmann and Müller, 2014).

The WLP is highly conserved across Archaea and Bacteria, with only two known variations, one found predominantly in methanogenic archaea and one in acetogenic bacteria. The first has formyl-methanofuran rather than formate as first intermediate, and uses ATP-independent formyl-MFR:tetrahydromethanopterin formyltransferase instead of ATP-consuming formyl-tetrahydrofolate ligase (consuming an ATP). Moreover, methanogens use methanofuran (MFR), tetrahydromethanopterin and coenzyme-F_{420} as cofactors while acetogens rely on NAD(P)H, tetrahydrofolate (THF) and ferredoxin (Fd) (Fuchs, 2011; Adam et al., 2018). Reduction of CO_2 to acetate via the WLP requires 8 electrons (Equation 1, Ragsdale and Pierce, 2008; Schuchmann and Müller, 2014).

$$2CO_2 + 8H^+ + 8e^- + nADP + nP_i \rightarrow CH_3COOH + nATP + (2+n)H_2O \quad (1)$$

The WLP consists of two branches. In acetogens, the WLP methyl branch reduces CO_2 to a methyl group by first reducing CO_2 to formate via formate dehydrogenase (*fdhA*; EC 1.17.1.9), after which formate is bound to tetrahydrofolate (THF) by formate-tetrahydrofolate ligase (*fhs*, EC 6.3.4.3). Formyl-THF is then further reduced to methenyl-THF, methylene-THF and lastly to methyl-THF by formyl-THF cyclohydrolase and methylene-THF dehydrogenase (*folD*; EC 3.5.4.9 and EC 1.5.1.5) and methylene-THF reductase (*metF*, EC 1.5.1.20), respectively (Ragsdale, 2008; Ragsdale and Pierce, 2008). A methyl transferase then transfers the methyl group from THF to a corrinoid iron–sulfur protein (*acsE*, EC 2.3.1.258), which is a subunit of the carbon monoxide (CO) dehydrogenase/acetyl-CoA synthase complex. The carbonyl branch of the WLP reduces CO_2 to CO in a reaction catalyzed by another subunit of the canonical WLP, the CO dehydrogenase/acetyl-CoA synthase complex (CODH/ACS, EC 2.3.1.169). Alternatively, CO can be formed by a separate CO dehydrogenase (CODH, EC 1.2.7.4) (Ragsdale and Kumar, 1996; Doukov et al., 2002; Jeoung and Dobbek, 2011). The CODH/ACS complex then links the two WLP branches by coupling the CO- and CH_3-groups with CoA, yielding acetyl-CoA (Menon and Ragsdale, 1996a; Ragsdale and Kumar, 1996; Ragsdale, 2008). The high degree of conservation of WLP genes and their genomic co-localization suggests that their evolution involved interspecies gene transfer events (Techtmann et al., 2012; Adam et al., 2018). However, two recent studies suggested carbon fixation occurred in the absence of a full complement of structural genes for canonical WLP enzymes (Figueroa et al., 2018; Valk et al., 2018). These observations suggest that variants of the canonical WLP may still await discovery.

In a recent study on D-galacturonate-limited, anaerobic enrichment cultures, we identified the dominant bacterium as a species from a novel genus within the *Lachnospiraceae*, for which we proposed the name "*Candidatus* Galacturonibacter soehngenii." The *Lachnospiraceae* family is part of the phylum Firmicutes, which includes several genera that harbor acetogens (Drake et al., 2008; Ragsdale and Pierce, 2008; Schuchmann and Muller, 2013; Valk et al., 2018). Fermentation product stoichiometries of the enrichment cultures were consistent with an acetogenic dissimilation of galacturonate. The overall stoichiometry is shown in Equation (2) (Valk et al., 2018).

$$1C_6H_{10}O_7 \rightarrow 2.5C_2H_4O_2 + 1CO_2 \quad (2)$$

Metagenome analysis of the enrichment culture revealed homologs of most structural genes for WLP enzymes, but no homologs were found for genes encoding subunits of the canonical CODH/ACS complex (EC 2.3.1.169) (Valk et al., 2018).

The goal of the present study was to further investigate the presence of a possible alternative configuration of the WLP in "*Ca.* G. soehngenii." To analyze *in vivo* activity of the WLP, D-galacturonate-limited enrichment cultures were co-fed with ^{13}C-labeled bicarbonate, followed by analysis of ^{13}C in the methyl and carboxyl groups of acetate. To investigate whether canonical WLP genes might have been overlooked in the initial metagenomics analysis, a fully closed metagenome-assembled genome (MAG) sequence of "*Ca.* G. soehngenii" was constructed using long-read nanopore sequencing, and meta-transcriptome analysis was performed to analyze the expression levels of genes of interest. Additionally, CO dehydrogenase activity was analyzed in cell extracts.

MATERIALS AND METHODS

Reactor Setup and Operation

Chemostat cultures were grown in 1.2 L laboratory bioreactors (Applikon, Delft, The Netherlands), which were stirred at 300 rpm and kept at 30°C. Anaerobic conditions were maintained by flushing the headspace with nitrogen gas, at a flow rate of 120 mL min^{-1}. Culture pH was controlled at 8 ± 0.1 by automatic titration (ADI 1030 Biocontroller, Applikon, Delft, The Netherlands) of 1 M NaOH. The dilution rate was 0.09 ± 0.01 h^{-1} and the working volume of 0.5 L was kept constant by peristaltic effluent pumps (Masterflex, Cole-Parmer, Vernon Hills, IL, United States) coupled to electrical level sensors. Bioreactors were inoculated (10% v/v) with 50 mL samples of D-galacturonate-limited, anaerobic chemostat enrichment cultures (Valk et al., 2018), stored in 30% v/v glycerol at –20°C. Cultures were run in continuous mode and after at least

6 days (18 generations) stable product composition and biomass concentration were established. System stability was assessed by online monitoring of CO_2 production and offline monitoring of fermentation products and optical density. When measurements varied by less than 10% over multiple volume changes, without a clear upward or downward trend, samples were taken during subsequent cycles.

Medium

The cultivation medium contained (g L^{-1}): D-galacturonate 4.3; NH_4Cl 1.34; KH_2PO_4 0.78; $Na_2SO_4.10H_2O$ 0.130; $MgCl_2.6H_2O$ 0.120; $FeSO_4.7H_2O$ 0.0031; $CaCl_2$ 0.0006; H_3BO_4 0.0001; Na_2MoO_4. $2H_2O$ 0.0001; $ZnSO_4.7H2O$ 0.0032; $CoCl_2.H_2O$ 0.0006; $CuCl_2.2H_2O$ 0.0022; $MnCl_2.4H_2O$ 0.0025; $NiCl_2.6H_2O$ 0.0005; EDTA 0.10. Nineteen liter of mineral solution (mineral concentration adjusted to the final volume, 20 L) was autoclaved for 20 min at 121°C after which 1 L (86 g L^{-1}) D-galacturonate solution was filter sterilized (0.2 μm Mediakap Plus, Spectrum Laboratories, Rancho Dominguez, CA, United States) into the media. 1.5 mL Pluronic PE 6100 antifoam (BASF, Ludwigshafen, Germany) was added per 20 L of mineral solution to avoid excessive foaming.

Analysis of Substrate and Extracellular Metabolite Concentrations

To determine substrate and extracellular metabolite concentration, reactor sample supernatant was obtained by centrifugation of culture samples (Heraeus Pico Microfuge, Thermo Fisher Scientific, Waltham, MA, United States). Concentrations of D-galacturonate and extracellular metabolites were analyzed with an Agilent 1100 Affinity HPLC (Agilent Technologies, Amstelveen, The Netherlands) equipped with an Aminex HPX-87H ion-exchange column (BioRad, Hercules, CA, United States) operated at 60°C with a mobile phase of 5 mM H_2SO_4 and a flow rate of 0.6 mL min^{-1}. CO_2 and H_2 concentrations in the bioreactor exhaust gas were measured using a Prima BT Bench Top mass spectrometer (Thermo Fisher Scientific, Waltham, MA, United States) after the gas was cooled by a condenser (4°C).

Biomass Dry Weight

Twenty milliliter of culture broth samples were filtered over pre-dried and pre-weighed membrane filters (0.2 μm Supor-200, Pall Corporation, New York, NY, United States), which were then washed with demineralized water, dried in a microwave oven (Robert Bosch GmbH, Gerlingen, Germany) for 20 min at 360 W and reweighed. Carbon and electron balances were constructed based on the number of carbon atoms and electrons per mole, while biomass composition was assumed to be $CH_{1.8}O_{0.5}N_{0.2}$ (Roels, 1983).

Quantitative Fluorescent *in situ* Hybridization (qFISH) Analysis

Fluorescent *in situ* hybridization was performed as described previously (Daims et al., 2005), using a hybridization buffer containing 35% (v/v) formamide. Probes were synthesized and 5′ labeled with either 5(6)-carboxyfluorescein-N-hydroxysuccinimide ester (FLUOS) or with one of the sulfoindocyanine dyes (Cy3 and Cy5; Thermo Hybaid Interactiva, Ulm, Germany) (**Table 1**). The general probe EUB338mix, labeled at both 3′ and 5′ ends with Cy5, was used to identify all eubacteria in the sample. Microscopic analysis was performed with a LSM510 Meta laser scanning confocal microscope (Carl Zeiss, Oberkochen, Germany). The qFISH analysis was based on at least 29 fields of view at 6730 × magnification, using DAIME (version 2.1) software (DOME, Vienna, Austria; Daims et al., 2006). The bio-volume fractions of "*Ca.* G. soehngenii" and *Enterobacteriaceae* populations were calculated as the ratio of the area hybridizing with specific probes relative to the total area hybridizing with the universal EUBmix probe set (Amann et al., 1990; Daims et al., 1999).

Labeling Experiment ^{13}C-Labeled Sodium Bicarbonate Addition

A 1 M $NaH^{13}CO_3$ solution was used to replace the regular 1 M NaOH solution as a pH titrant in steady-state D-galacturonate-limited enrichment cultures (pH 7.8 ± 0.1, D = 0.1 h^{-1}, T = 30°C). Broth was collected on ice every 2 h for 8 consecutive hours and centrifuged (12,000 × *g*, Heraeus Pico Microfuge, Thermo Fisher Scientific, Waltham, MA, United States) before the supernatant was collected and stored at –20°C until analysis by NMR. CO_2, H_2 and $^{13}CO_2$ concentrations in the exhaust gas were measured by MS (Prima BT Bench Top MS, Thermo Fisher Scientific, Waltham, MA, United States) after the gas had been cooled by a condenser (4°C).

Illumina and Nanopore Sequencing, Metagenome Assembly, and Genome Binning DNA

The metagenomic-assembled genome of "*Candidatus* Galacturonibacter soehngenii" described by Valk et al. (2018) was used as template for preparing the metagenome libraries. The DNA extraction, Illumina sequencing, metagenomic assembly and binning process is described

TABLE 1 | Oligonucleotide probes used for the quantitative fluorescence *in situ* hybridization analysis.

Probe	Sequence (5′–3′)	Specificity	References
EUB338mix	GCWGCCWCCCGTAGGWGT	All bacteria	Daims et al., 1999
ENT	CTCTTTGGTCTTGCGACG	*Enterobacteriaceae*	Kempf et al., 2000
Lac87	GTGGCGATGCAAGTCTGA	*"Ca.* G. soehngenii"	This study

With W indicating A or T.

in Valk et al. (2018). Long-read genomic DNA sequencing was conducted using 1D nanopore sequencing (Oxford Nanopore Technologies, Oxford, United Kingdom), following the manufacturer's protocol (LSK-108), omitting the optional DNA shearing and DNA repair steps. The library was loaded on a flow cell (FLO-MIN106) and the MinION Mk1B DNA sequencer (Oxford Nanopore Technologies, Oxford, United Kingdom) was used for sequencing combined with the MinKNOW v. 1.7.3 (Oxford Nanopore Technologies, Oxford, United Kingdom) software with the 48 h sequencing workflow (NC_48h_Sequencing_Run_FLO_MIN106_SQK-LSK108.py). Albacore v. 1.2.1 (Oxford Nanopore Technologies, Oxford, United Kingdom) was used to base-call the sequencing reads.

Genome Assembly

The assembling of the contigs from the "*Candidatus* Galacturonibacter soehngenii" genome bin into a single scaffold based on the long Nanopore reads was done using SSPACE-LongRead scaffolder v. 1.1 (Boetzer and Pirovano, 2014). GapFiller v. 1.11 (Boetzer and Pirovano, 2012) or by manual read mapping and extension in CLC Genomics Workbench v. 9.5.2 (Qiagen, Hilden, Germany) were used to close gaps in the draft genome with the previously assembled Illumina data. Finally, manual polishing of the complete genome was done to remove SNPs and ensure a high-quality assembly. The meta-genome has been submitted to the sequence read archive (SRA)[1] with accession number SRR10674409, under the BioProject ID PRJNA566068.

Genome Annotation and Analysis

The metagenome-assembled genome was uploaded to the automated Microscope platform (Vallenet et al., 2006, 2017). Manual assessment of pathway annotations was assisted by the MicroCyc (Caspi et al., 2008), KEGG (Kyoto Encyclopedia of Genes and Genomes; Kanehisa et al., 2014) and SwissProt alignment (BLASTP version 2.2.28+; Altschul et al., 1997) databases. The predicted proteome of "*Ca.* G. soehngenii" was submitted to InterProScan (version 5.25-64.0), to identify predictive Pfam domains (El-Gebali et al., 2018). The annotated genome sequence of "*Candidatus* Galacturonibacter soehngenii" has been submitted to the European Nucleotide Archive (ENA) under the BioProject ID PRJNA566068.

Genome-Centric Meta-Transcriptomic Analyses; RNA Extraction and Purification

During pseudo-steady state, broth samples were taken from the enrichment culture, directly frozen in liquid nitrogen and subsequently stored at −80°C. Five hundred microliter samples were thawed on ice, pelleted by centrifugation (21,000 × *g*, 2 min, 4°C) and used for total RNA extraction with the RNeasy PowerMicrobiome Kit (Qiagen, Hilden, Germany), following the manufacturer's instruction with the addition of phenol:chloroform:isoamy alcohol (25:25:1) and β-mercaptoethanol (10 μL mL^{-1} final concentration). Cell lysis was with a FastPrep-24 bead beater (MP Biomedicals, Fisher Scientific, Hampton, VA, United States, four successive cycles of 40 s at 6.0 m s^{-1}, 2 min incubation on ice between cycles). Total RNA extracts were subjected to DNase treatment to remove DNA contaminants by using the DNase Max Kit (Qiagen, Hilden, Germany) and further cleaned up and concentrated with the Agencourt AMpure XP magnetic beads (Beckman Coulter, Brea, CA, United States) before rRNA depletion. Integrity and quality of purified total RNA were assessed on a Tapestation 2200 (Agilent, Santa Clara, CA, United States) with the Agilent RNA screen-tapes (Agilent, Santa Clara, CA, United States) and the concentration was measured using Qubit RNA HS Assay Kit (Thermo Scientific Fisher, Waltham, MA, United States).

rRNA Depletion, Library Preparation, and Sequencing

Five hundred nanogram of total RNA from each sample was obtained after rRNA was depleted using the Ribo-Zero rRNA Removal (Bacteria) Kit (Illumina, San Diego, CA, United States), with 2 μg total RNA as input. Quality of extracted mRNA was checked with Agilent RNA HS screen-tapes (Agilent, Santa Clara, CA, United States) and RNA concentration was determined with a Qubit RNA HS Assay Kit (Thermo Scientific Fisher, Waltham, MA, United States). The TruSeq Stranded mRNA Sample Preparation Kit (Illumina, San Diego, CA, United States) was used to prepare cDNA sequencing libraries according to the manufacturer's instruction. Libraries were sequenced on an Illumina HiSeq2500 using the TruSeq PE Cluster Kit v3-cBot-HS and TruSeq SBS kit v.3-HS sequencing kit (1 × 50 bp; Illumina, San Diego, CA, United States). The raw meta-transcriptome reads have been submitted to the sequence read archive (SRA)[1] with accession number SRR10674118-23, under the BioProject ID PRJNA566068.

Trimming and Mapping of rRNA Reads

Raw RNA reads in FASTQ format were imported into CLC Genomics Workbench v. 9.5.5 and trimmed for quality, requiring a minimum phred score of 20 and a read length of 45. Reads from each sample were hereafter mapped to CDSs obtained from the MAG of "*Ca.* G. soehngenii" with a minimum similarity of 98% over 80% of the read length. Reads per kilobase of transcript per million mapped reads (RPKM) were calculated based on raw read-counts and the length of each CDS. The meta-transcriptome mapped to the genome of "*Ca.* G. soehngenii" are shown in **Supplementary Data Sheet S2**.

Plasmid and Strain Construction

Gene F7O84_RS11645 was codon optimized for expression in *Escherichia coli* with the GeneArt online tool and integrated behind the TEV recognition site of the pET151/D-TOPO expression vector by GeneArt (GeneArt GmbH, Regensburg, Germany). The resulting plasmid was transformed into a chemically competent *E. coli* strain BL21 according to manufacturer's instructions (NEBuilder HiFi DNA Assembly Master Mix chemical transformation protocol (E2621),

[1] https://www.ncbi.nlm.nih.gov/sra/

New England Biolabs, Ipswich, MA, United States) and named pUD1074. The plasmid sequence of pUD1074 has been deposited at the NCBI GenBank[2] with the corresponding accession number MN498128.

Heterologous Expression of the Putative CO Dehydrogenase Candidate

All *E. coli* cultures were performed in 120 mL capped bottles with 50 mL of mineral medium (Diender et al., 2016). Prior to inoculation, the bottles were autoclaved at 120°C after which the mineral media was supplemented with autoclaved (120°C, 20 min); glucose 5 g L^{-1}, peptone (BD Bacto Difco, Thermo Fisher Scientific, Waltham, MA, United States) 1 g L^{-1}, yeast extract (BD Bacto Difco, Thermo Fisher Scientific, Waltham, MA, United States) 2 g L^{-1} and cysteine 1 g L^{-1}. Additionally, 0.05 g L^{-1} ampicillin was added and the gas phase was exchanged with air, with a final pressure of 170 kPa. All *E. coli* cultures used for measurements were inoculated with overnight grown pre-cultures (1:50 v/v) and incubated at 37°C and shaken (300 rpm) until oxygen was depleted (2–3 h). Subsequently 1 mL (250 g L^{-1}) glucose, 1 mL reducing agent (0.4 M cysteine) and 1 mL IPTG (40 mM) were added.

After 3 h (at 30°C, unshaken) of incubation, the cells were harvested and processed anaerobically according to Diender et al. (2016). Enzymatic activity analysis was conducted using a modified method initially described by Diender et al. (2016). The essays were performed in an anaerobic environment using 100–300 μL of cell extract with both CO and hydroxylamine as substrate. To increase metal cofactor availability, 1:200 (v/v) metals solution was added to the assay buffer which contained in (g L^{-1}); HCl 1.8, H_3BO_3 0.0618, $MnCl_2$ 0.06125, $FeCl_2$ 0.9435, CoC_{l2} 0.0645, $NiCl_2$ 0.01286, $ZnCl_2$ 0.0677, $CuCl_2$ 0.01335.

Homology Protein BLAST Analysis

The sequence of the putative CODH (F7O84_RS11645) was blasted with the BLASTp (version 2.2.28+; Altschul et al., 1997) tool of the JGI-IMG/M database (Markowitz et al., 2012), with default parameter settings. Finished genomes from members of the *Lachnospiraceae* family in the public JGI-IMG/M database (Markowitz et al., 2012) were selected for analysis, **Supplementary Table S4**. The stains identified in the BLAST search, or closely related strains (**Supplementary Table S5**) were subsequently analyzed in KEGG (Kanehisa et al., 2014) for presences of the CODH/ACS complex with pathway map 1200.

RESULTS

Physiological Characterization of D-Galacturonate-Limited Enrichment Cultures Dominated by "*Ca.* G. soehngenii"

Anaerobic, galacturonate-limited chemostat enrichment cultures were used to study the physiology of "*Ca.* G. soehngenii" cultures. In a previous study (Valk et al., 2018), the relative abundance of "*Ca.* G. soehngenii" in such cultures did not exceed 65%, based on metagenomic analysis, and formate and H_2 were detected in the liquid and gas phases, respectively. It was hypothesized that, in these experiments, a low *in situ* hydrogen partial pressure limited *in vivo* WLP activity, as it was expected that hydrogen was used as reductant for the production of acetate from formate or CO_2. To investigate this possibility, head space flushing instead of sparging was applied, using N_2 gas. This caused an increase in the hydrogen partial pressure in the media broth (De Kok et al., 2013). Additionally, the dilution rate was decreased from 0.125 to 0.1 h^{-1}. Analysis of the abundance of "*Ca.* G. soehngenii" in the resulting enrichment cultures by quantitative fluorescence *in situ* hybridization (qFISH) indicated that 86.5 ± 2.6% of the bio-volume of qFISH-detectable cells consisted of "*Ca.* G. soehngenii." The major side population *Enterobacteriaceae* represented 13.8 ± 2.4% of the bio-volume. As these two subpopulations together accounted for 100.2 ± 5.0% of the bio-volume, it was assumed that any other, minor, subpopulations did not significantly influence the stoichiometry of catabolic fluxes.

Product yields and biomass-specific conversion rates of the D-galacturonate-limited anaerobic enrichment cultures dominated by "*Ca.* G. soehngenii" (**Table 2**) showed acetate as dominant catabolic product (0.57 ± 0.03 Cmol (Cmol galacturonate^{-1}). Carbon and electron recoveries were 94 and 92%, respectively, indicating that all major fermentation products were identified. As observed previously (Valk et al., 2018), this acetate yield on galacturonic acid was significantly higher than the combined yields of formate and hydrogen. This difference was interpreted as indicative for acetogenesis by one of the dominant organisms, of which only the "*Ca.* G. soehngenii" MAG was shown to harbor homologs for most WLP structural genes (Ragsdale and Pierce, 2008; Valk et al., 2018). Yields of hydrogen

TABLE 2 | Yields (in Cmol (Cmol galacturonate)$^{-1}$, unless stated otherwise) and biomass- specific conversion rates (q; mmol $g_x{}^{-1}$ h^{-1}) of anaerobic, galacturonate-limited chemostat enrichment cultures dominated by "*Ca.* Galacturonibacter soehngenii."

	Yield ($Cmol_i$ $Cmol_s{}^{-1}$)	Biomass specific conversion rates (mmol $(g_x)^{-1}$ h^{-1})
D-galacturonate	–	−4.0 ± 0.2
Biomass	0.17 ± 0.02	–
Acetate	0.57 ± 0.03	6.9 ± 0.4
Formate	0.02 ± 0.01	0.4 ± 0.2
CO_2	0.18 ± 0.02	4.3 ± 0.3
H_2 (mol $Cmol^{-1}$)	0.02 ± 0.01	0.2 ± 0.1
H_2 + Formate (mol $Cmol_s{}^{-1}$)	0.04 ± 0.02	
Acetyl-CoA derivatives (mol $Cmol_s{}^{-1}$)	0.29 ± 0.02	

Chemostat cultures were operated at dilution rate of 0.1 h^{-1}, pH, 8 and at 30°C, with galacturonate the sole carbon-source. Data are presented as average ± mean deviations, derived from nine measurements each on duplicate steady-state enrichment cultures.

[2]www.ncbi.nlm.nih.gov/genbank

and formate on galacturonate (0.02 ± 0.01 mol Cmol galacturonate^{-1}) and 0.02 ± 0.01 (Cmol galacturonate^{-1}), respectively were significantly lower than found in a previous study on "*Ca.* G. soehngenii" (Valk et al., 2018). This observation is consistent with a higher *in vivo* contribution of the WLP as a result of a higher hydrogen partial pressure and/or lower specific growth rate in the present study.

Incorporation of ^{13}C-Labeled Bicarbonate Into Acetate Corroborates Acetogenic Fermentation

A simple model was constructed to predict formation of labeled acetate, using biomass-specific conversion rates measured in pseudo-steady state enrichment cultures as inputs (**Supplementary Calculations S1, S2** and **Supplementary Figure S1**). Model simulations predicted that, after 8 h, approximately 15% of the acetate produced by the enrichment culture should be labeled. To investigate if CO_2 was indeed incorporated into acetate via acetogenic fermentation, ^{13}C-labeled bicarbonate was fed to a "*Ca.* G. soehngenii" enrichment chemostat culture. However, after 8 h, the fraction of ^{13}C in the methyl group of acetate increased to 2.0%. This increase represented only a small increase relative to the 1% natural abundance of ^{13}C (**Table 3**; Rumble et al., 2017). In contrast, after 8 h of ^{13}C-bicarbonate feeding, the enrichment culture showed a 21.5% abundance of ^{13}C in the carbonyl-group of acetate (**Table 3**).

Significant Activity of CO Dehydrogenase in Cell Extracts of "*Ca.* G. soehngenii" Enrichment Cultures

In the WLP, ^{13}C-labeled CO_2 incorporation into the carbonyl-group of acetate involves activity of CO dehydrogenase (COOS, EC 1.2.7.4). To investigate the presence of this key enzyme in "*Ca.* G. soehngenii," an anaerobic enzyme activity assay was performed on cell extracts of enrichment cultures, using CO as electron donor and methyl viologen (MV) as electron acceptor (Diender et al., 2016). These assays revealed a CO dehydrogenase activity of 2.1 ± 0.6 μmol min^{-1} (mg protein) $^{-1}$. Reduction of MV in the absence of either CO or cell extract was below detection limit [<0.05 μmol min^{-1} (mg protein) $^{-1}$].

TABLE 3 | Percentages of ^{13}C-labeled methyl and carbonyl groups in total-culture acetate, calculated from proton and carbon NMR spectra.

	Time (h)	% ^{13}C
Methyl (CH_3)	0	1.0
	4	1.6
	8	2.0
Carbonyl (CO)	8	21.8

Samples were taken from the "Ca. G. soehngenii" chemostat enrichment cultures in bioreactor 2 after switching the alkali supply line from 1 M NaOH to 1 M NaH$^{13}CO_3$ (Time = 0 h).

Identification of Two Putative Novel CO Dehydrogenase Genes in a Newly Obtained Single-Scaffold MAG of "*Ca*. G. soehngenii"

Previous analysis of the "*Ca.* G. soehngenii" MAG (Valk et al., 2018) was based on an assembly made with short-read DNA sequencing data. To identify if putative CODH/ACS complex genes had been missed in this analysis due to incomplete assembly, long-read Oxford Nanopore sequencing (Deamer et al., 2016; Jain et al., 2016) was used to improve the previously assembled "*Ca.* G. soehngenii" MAG. The resulting genome assembly consisted of 8 contigs and was estimated to have a 98% completeness and contained no genetic contamination with sequences from other organisms according to checkM (**Table 4**). As in the previous study, homologs were detected for most structural genes associated with the WLP (**Table 5**), but none of the annotated genes in the predicted proteome showed homology with known CODH/ACS genes (Vallenet et al., 2006; Ragsdale, 2008; Valk et al., 2018). A search in the newly assembled "*Ca*. G. soehngenii" MAG sequence for homologs of signature genes of the six other known pathways for inorganic carbon fixation did not point toward their involvement in carbon metabolism (**Supplementary Table S2**).

CO dehydrogenases contain highly conserved amino-acid motifs (Pfam or protein-family domains) associated with their nickel-iron-sulfur clusters (Eggen et al., 1991, 1996; Maupin-Furlow and Ferry, 1996; Jeoung and Dobbek, 2011; Techtmann et al., 2012; El-Gebali et al., 2018). The newly assembled "*Ca*. G. soehngenii" MAG sequence did not reveal hits for the Pfam domain of the CO dehydrogenase α-subunit of the CODH/ACS complex (PF18537) (Darnault et al., 2003). However, two open reading frames F7O84_RS02405 and F7O84_RS11645, harbored the PF03063 Pfam domain, which is associated with the hybrid cluster protein (HCP) and the catalytic center of the Ni-CODH family (van den Berg et al., 2000; Wolfe et al., 2002). Although HCP has been associated with hydroxylamine reductase activity, its catalytic activity has

TABLE 4 | Statistics of the metagenome-assembled genome (MAG) of "*Ca.* Galacturonibacter soehngenii."

	***"Candidatus* Galacturonibacter soehngenii"**
Genome size (Mbp)	4.1
Scaffolds	1
Contigs	8
Contigs N50	1033779
Max contig size	1514059
Completeness (%)	98
Contamination (%)	0
GC content (%)	34.4
Protein coding density (%)	89
CDS	3924
rRNA copies	5

Completeness and contamination were estimated with CheckM (Parks et al., 2015).

TABLE 5 | Genes of the Wood-Ljungdahl pathway from the predictive proteome of the MAG "*Ca.* G. soehngenii" with gene names, EC number, gene or homolog and *E*-value based on SwissProt alignment (BLASTP version 2.2.28+, MicroScope platform v3.13.2).

Encoded protein	EC	Gene name	*E*-value	Gene ID
Formate dehydrogenase	1.17.1.9	*fdhA*	$1\ e^{-60}$	F7O84_ RS07405
Formate–tetrahydrofolate ligase	6.3.4.3	*fhs*	0.0	F7O84_RS05385
Methenyl-tetrahydrofolate cyclohydrolase/methylene–tetrahydrofolate dehydrogenase	3.5.4.9 and 1.5.1.5	*folD*	$5\ e^{-152}$	F7O84_RS05380
Methyl–tetrahydrofolate reductase	1.5.1.20	*metF*	$1\ e^{-87}$	F7O84_RS08335
5-Methyl-tetrahydrofolate:corrinoid/iron-sulfur protein methyltransferase	2.1.1.258	*acsE*	$5\ e^{-37}$	F7O84_RS02745
CO-Methylating acetyl-CoA synthase	2.3.1.169	*acsBCD*	>10	
Carbon-monoxide dehydrogenase	1.2.7.4	*cooS*	>10	

not been experimentally confirmed and, moreover, sequence motifs in HCP showed high similarity with the functional domain of Ni-CODHs making it an interesting candidate genes for the CODH function of the WLP in "*Ca.* G. soehngenii" (Heo et al., 2002; Wolfe et al., 2002; Aragão et al., 2003; Almeida et al., 2006). A closer inspection of the genetic context of both genes showed many flanking genes encoding hypothetical proteins in their close vicinity, but no genes previously associated with acetogenesis.

Homologs of Acetogenesis Genes Are Transcribed in D-Galacturonate-Limited "*Ca.* G. soehngenii" Enrichment Cultures

A meta-transcriptome analysis of the enrichment cultures showed significant transcript levels of most homologs of known WLP genes, which were approximately 10-fold lower than those of homologs of structural genes encoding Entner-Doudoroff-pathway enzymes involved in galacturonate catabolism (**Table 6**). A notable exception was the extremely low transcript level of a putative formate dehydrogenase gene (F7O84_RS07405; EC 1.17.1.9). A candidate gene for pyruvate-formate lyase (PFL, EC 6.2.1.3) was highly transcribed (F7O84_03160, **Table 6**). These observations suggested that formate generated by PFL, rather than CO_2, was the major substrate for the methyl branch of the WLP in "*Ca.* G. soehngenii."

Homologs of Rnf cluster (F7O84_03275-3295; EC 7.2.1.2) and hydrogenase (F7O84_0945-50, F7O84_04820; EC 1.12.7.2) genes, which were previously implicated in acetogenesis (Biegel and Müller, 2010; Schuchmann and Müller, 2014, 2016), showed high transcript levels (**Table 6**). Of the two candidate genes for CO dehydrogenase, F7O84_RS11645 showed the highest transcript level (**Table 6**). As, under the experimental conditions, no hydroxylamine reductase activity was expected, this result reinforced the candidature of F7O84_RS11645 as possible CO dehydrogenase gene. In an attempt to directly investigate if F7O84_RS11645 encoded a functional CO dehydrogenase, its open reading frame was cloned into high-copy-number *E. coli* expression vector. However, enzyme assays with cell extracts of the resulting *E. coli* strain did not yield consistent evidence for either CO dehydrogenase or hydroxylamine dehydrogenase activity (**Supplementary Table S3**).

Identification of Proteins With a High Homology of the Putative CODH Within Other Members of the *Lachnospiraceae* Species

A protein BLAST search (Altschul et al., 1997) of the putative CODH (F7O84_RS11645) was done to investigate if presence of the putative CODH gene also coincided with an apparently incomplete WLP in other members of the *Lachnospiraceae* family. Indeed, 13 sequenced members of the *Lachnospiraceae* family showed predicted proteins with a high homology with the putative CODH (**Supplementary Table S4**). 9 of the 13 *Lachnospiraceae* members were present in the KEGG database (Kanehisa et al., 2014; **Supplementary Table S5**), and subsequently analyzed on the presence or absence of the CODH/ACS complex. All organisms contained only a partial WLP, with the ACS genes not identified. In seven of the members, respectively *Lachnoclostridium saccharolyticum*, *Lachnoclostridium phytofermentans, Pseudobutyrivibrio xylanivorans*, *Butyrivibrio fibrisolvens, Pseudobutyrivibrio xylanivorans,* and both *Roseburia* species the full CODH/ACS complex was not identified. Further study is required to elucidate the relevance of the putative CODH for acetogenic metabolism.

DISCUSSION

Incorporation of carbon from ^{13}C labeled bicarbonate into the carbonyl group of acetate supported our previous conclusion, based on product profiles, that acetogenesis occurs in anaerobic, galacturonate-limited enrichment culture of "*Ca.* G. soehngenii" (Valk et al., 2018). A much lower labeling of the methyl group of acetate indicated that, instead of carbon dioxide, the methyl branch of the WLP in the "*Ca.* G. soehngenii" enrichment cultures predominantly used formate as a substrate, generated in the anaerobic fermentation of galacturonate (**Figure 1**). This conclusion is consistent with the low transcript levels of the only putative formate dehydrogenase gene (F7O84_RS07405; EC 1.17.1.9; **Table 6**) identified in the "*Ca.* G. soehngenii" MAG, the high transcript level of a putative pyruvate-formate lyase gene (F7O84_RS03160, EC 6.2.1.3; **Table 5**) and the low net production rates of formate in the anaerobic enrichment cultures (**Table 2**). In contrast, previous labeling studies on acetogens

TABLE 6 | Transcript levels of putative key genes of the adapted Entner-Doudoroff pathway for galacturonate metabolism and the Wood-Ljungdahl pathway for acetogenesis in meta-transcriptome samples of the "*Ca.* G. soehngenii" chemostat enrichment cultures expressed as reads per kilobase million (RPKM, average ± average deviation) based on technical triplicates of duplicate enrichment cultures.

Protein function	EC number	Gene ID	RPKM
Adapted entner-doudoroff pathway			
Uronate isomerase	5.3.1.12	F7O84_RS17360	5852 ± 2398
Tagaturonate reductase	1.1.1.58	F7O84_RS17370	3067 ± 1236
Altronate dehydratase	4.2.1.7	F7O84_RS17375	8426 ± 3296
2-Dehydro-3-deoxygluconokinase	2.7.1.45	F7O84_RS17390	3863 ± 1343
2-Dehydro-3-deoxyphosphogluconate aldolase	4.1.2.14	F7O84_RS17395	1752 ± 245
Acetate production			
Pyruvate:ferredoxin oxidoreductase	1.2.7.1	F7O84_RS03200	4145 ± 278
Pyruvate formate lyase	6.2.1.3	F7O84_RS03160	1893 ± 651
Phosphate acetyltransferase	2.3.1.8	F7O84_RS05985	1500 ± 176
Acetate kinase	2.7.2.1	F7O84_RS05980	1625 ± 200
Wood-Ljungdahl pathway			
Formate dehydrogenase	1.17.1.9	F7O84_RS07405	14 ± 3
Formate–tetrahydrofolate ligase	6.3.4.3	F7O84_RS05385	256 ± 58
Methenyl-tetrahydrofolate cyclohydrolase/methylene–tetrahydrofolate dehydrogenase	3.5.4.9 and 1.5.1.5	F7O84_RS05385	236 ± 9
Methyl–tetrahydrofolate reductase	1.5.1.20	F7O84_RS08335	126 ± 13
5-methyl-tetrahydrofolate:corrinoid/iron-sulfur protein methyltransferase	2.1.1.258	F7O84_RS02745	144 ± 19
CO-methylating acetyl-CoA synthase	2.3.1.169		n.d.
CO dehydrogenase	1.2.7.4		n.d.
Prismane/CO dehydrogenase family	1.7.99.1	F7O84_RS02405	40 ± 8
Prismane/CO dehydrogenase family	1.7.99.1	F7O84_RS11645	315 ± 51
Energy-metabolism associated genes			
Electron transport complex protein A	7.2.1.2	F7O84_RS03295	58 ± 5
Electron transport complex protein B	7.2.1.2	F7O84_RS03300	261 ± 40
Electron transport complex protein C	7.2.1.2	F7O84_RS03275	329 ± 22
Electron transport complex protein DG	7.2.1.2	F7O84_RS03290	101 ± 13
Electron transport complex protein E	7.2.1.2	F7O84_RS03285	143 ± 9
Ferredoxin hydrogenase subunit A	1.12.7.2	F7O84_RS09545	196 ± 100
Ferredoxin hydrogenase subunit B	1.12.7.2	F7O84_RS09550	356 ± 32
Ferredoxin hydrogenase subunit C	1.12.7.2	F7O84_RS04820	124 ± 86

N.d., not detected.

harboring the WLP showed marginal preferential labeling of the carboxyl moiety of acetate (Wood and Harris, 1952; O'Brien and Ljungdahl, 1972; Schulman et al., 1972), indicating the use of extracellular CO_2 as substrate for both the methyl- and carbonyl-groups of acetate.

While the observed labeling pattern was consistent with acetogenic metabolism of galacturonate via a WLP, this did not rule out involvement of another pathway for carbon fixation in acetate. Involvement of the hydroxypropionate bi-cycle, 3-hydroxypropionate/4-hydroxybutyrate cycle and dicarboxylate/hydroxybutyrate cycle were excluded since no homologs were found in the "*Ca.* G. soehngenii" MAG for the majority of genes associated with these three pathways (**Supplementary Table S2**). Key genes were also missing for the reductive pentose phosphate cycle (rPPP) and reductive citric acid cycle (rTCA) (**Supplementary Table S2**) and, moreover, neither of these pathways could explain preferential labeling of the carboxyl group of acetate (Alberts et al., 2002; Shimizu et al., 2015). No gene candidates were identified for the glycine cleavage (GCV) system (**Supplementary Table S2** and **Supplementary Figure S2**) and ^{13}C-labeled bicarbonate fed into this pathway should result in equal labeling of the methyl and carbonyl groups of acetate (Figueroa et al., 2018; **Supplementary Figure S2**). Additionally, none of the routes would require the high CO dehydrogenase enzyme activity measured in cell extracts of the "*Ca.* G. soehngenii" enrichment culture. This analysis leaves the WLP as the only known carbon fixation pathway consistent with the observed stoichiometry of fermentation products, the labeling pattern of acetate and, with the notable exception of the CODH complex, genome and transcriptome analysis of "*Ca.* G. soehngenii."

Homologs of structural genes encoding enzymes of an adapted Entner-Doudoroff pathway for galacturonate metabolism were highly expressed in the galacturonate-limited, anaerobic "*Ca.* G. soehngenii" enrichment cultures (**Table 6**). Since conversion of one mole of galacturonate into two moles of pyruvate via this pathway is redox-cofactor neutral, redox equivalents for acetogenesis needed to be derived from pyruvate dissimilation (van Maris et al., 2006; Kuivanen et al., 2019). Pyruvate:ferredoxin oxidoreductase (F7O84_RS03200,

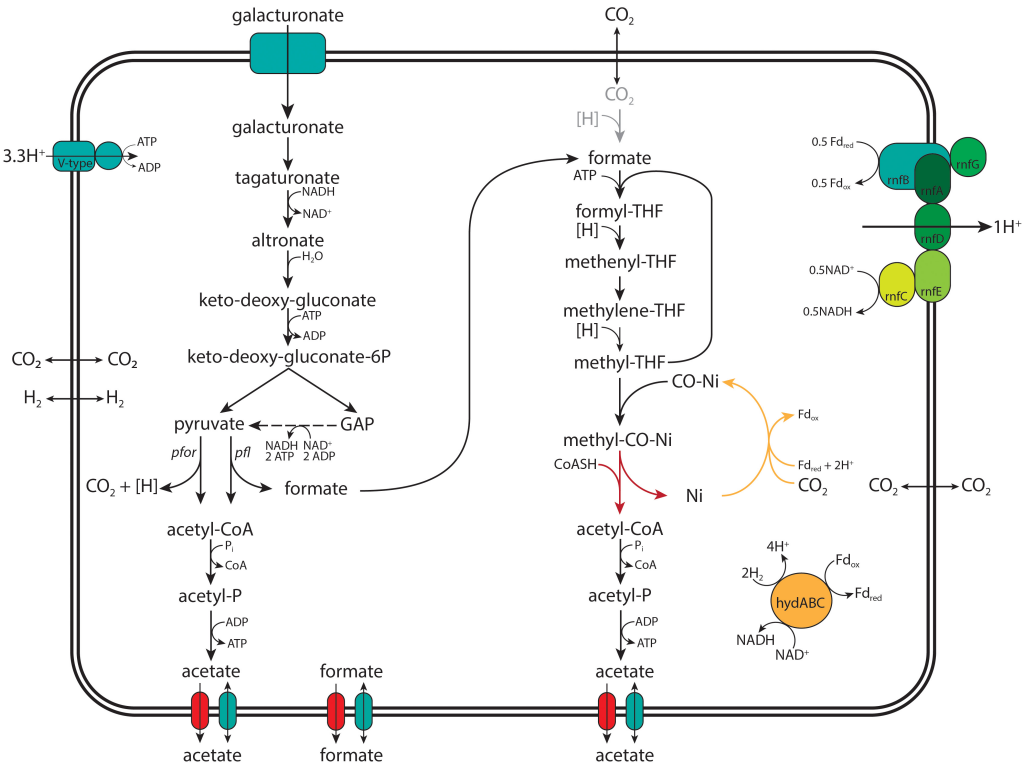

FIGURE 1 | Graphical representation of the proposed pathway for acetogenic D-galacturonate catabolism in "*Candidatus* Galacturonibacter soehngenii." The conversions of known and annotated genes identified in the MAG and transcribed in the meta-transcriptomic analysis "*Ca.* G. soehngenii" are colored black, the proposed CO dehydrogenase candidate colored yellow and the unidentified acetyl-CoA synthase colored red. With pyruvate:ferredoxin oxidoreductase (*pfor*, EC 1.2.7.1), pyruvate formate lyase (*pfl*, EC 6.2.1.3), ferredoxin hydrogenase (*hydABC*, EC 1.12.7.1) and the Rnf-cluster (*rnfABCDEG*, EC 7.2.1.2) explicitly shown.

EC 1.2.7.1) has been reported to couple fermentation and WLP in other anaerobes (Drake et al., 1981; Menon and Ragsdale, 1996b; Schuchmann and Müller, 2014). Strong, highly transcribed homologs of structural genes for PFOR and for a ferredoxin hydrogenase (EC 1.12.7.2) (**Table 6**; F7O84_RS03200 and F7O84_0945-50, F7O84_04820 respectively) indicated that it also fulfils this role in "*Ca.* G. soehngenii."

The significant CO dehydrogenase (CODH) (Weghoff and Müller, 2016) activities in cell extracts enrichment cultures, combined with the incorporation of ^{13}C from bicarbonate in acetate strongly suggested the presence of a functional CODH enzyme in "*Ca.* G. soehngenii." Two highly conserved classes of CODH enzymes have been described (King and Weber, 2007; Techtmann et al., 2012). Aerobic CODH enzymes (*coxSML* complex; EC 1.2.5.3) have a Mo-Cu-Se associated active site and only use CO as substrate (Schübel et al., 1995; Dobbek et al., 1999). Strictly anaerobic Ni-Fe-S associated CODH (*cooS*, EC 1.2.7.4) can use also CO_2 as substrate (Doukov et al., 2002; Ragsdale, 2008; Techtmann et al., 2012). A close functional relationship between Ni-CO dehydrogenases and hydroxylamine reductases was shown when a single amino-acid substitution was shown to change a Ni-CO dehydrogenase into a hydroxylamine reductase (Heo et al., 2002). Since no strong homologs of canonical aerobic or anaerobic CODH genes were identified, the HCP homolog F7O84_RS11645 is therefore the best candidate for the observed CODH activity. Our inability to demonstrate stable CODH activity in cell extracts upon expression of F7O84_RS11645 in *E. coli* could have many causes, including improper folding, metal or co-factor requirements (Ensign et al., 1990; Kerby et al., 1997) or requirement of additional subunits or other proteins (Bonams and Ludden, 1987; Bonam et al., 1989; Ensign and Ludden, 1991; Aragão et al., 2008; Bar-Even et al., 2012a). The immediate genetic context of F7O84_RS11645 showed many ORFs encoding predicted conserved proteins with unknown function. Co-expression of fosmid libraries (Shizuya et al., 1992; Ho et al., 2018) of the "*Ca.* G. soehngenii" MAG together with the plasmid used in this study in an *E. coli* strain, may be helpful in resolving the genetic requirements for CODH activity in this organism.

It remains unclear how the CODH-dependent carbonyl branch and formate-dependent methyl branch of a WLP pathway in "*Ca.* G. soehngenii" organism are linked. The present study is not the first in which carbon fixation linked to the WLP was observed in the absence of a full complement of canonical WLP structural genes (Zhuang et al., 2014; Figueroa et al., 2018). However, no clear physiological nor phylogenetic connections were detected between "*Ca.* G. soehngenii" and the organisms studied previously, a strict dehalogenide-respiring *Dehalococcoides mccartyi* strain from the Chloroflexi phylum

and the phosphite-oxidizing Deltaproteobacterium "*Candidatus* Phosphitivorax anaerolimi" Phox-21, respectively.

This study illustrates how quantitative analysis of metabolite formation by chemostat enrichment cultures, combined with ^{13}C-labeling, (meta-)genome assembly and annotation, meta-transcriptome analysis and biochemical assays can raise new and surprising questions about intensively studied metabolic pathways. Based on our results, involvement of a novel inorganic carbon assimilation pathway, which produces a similar labeling and product profile as the WLP, cannot be fully excluded. However, despite the wide distribution of the CODH/ACS complex in Bacteria and Archaea (Schuchmann and Müller, 2016), the available evidence appears to point in the direction of an as yet unidentified link between the methyl and carbonyl branches of the WLP. Further research to resolve this issue may benefit from additional labeling studies with ^{13}C-bicarbonate, ^{13}C-formate or partially labeled D-galacturonate combined with metabolome analysis and *in vitro* enzyme activity studies of formate dehydrogenase. Such studies are complicated by our current inability to grow "*Ca.* G. soehngenii" in pure cultures (Valk et al., 2018). The organisms shown in the **Supplementary Table S4** might be interesting alternative organisms to study in more detail, as they are available in pure culture. It would therefore be relevant to identify if any of these organisms exhibit a similar acetogenic metabolism, with an incomplete complement of WLP enzymes, to further explore this intriguing metabolic conundrum.

DATA AVAILABILITY STATEMENT

The datasets generated for this study can be found in the European Nucleotide Archive (ENA) under the BioProject ID PRJNA566068, NCBI GenBank accession number MN498128.

AUTHOR CONTRIBUTIONS

ML, JTP, and LV designed the experiments, interpreted the results, and wrote the manuscript. LV did all cultivations and labeling study. LV and MD performed the enzyme activity assays and heterologous experiment. LV and JFP performed the qFISH analysis. GS made the model. MSD performed the experimental work for the meta-transcriptomic and meta-genomic analysis. MSD, LV, and PN analyzed the data. All authors read and approved of the final manuscript.

FUNDING

This research was supported by the SIAM Gravitation Grant 024.002.002, the Netherlands Organisation for Scientific Research.

ACKNOWLEDGMENTS

We thank J. L. Rombouts for the design of the FISH probe Lac87 used in this study and P. de Waard for the assistance with NMR analysis. We additionally thank Dr. A. M. Vos and Dr. M. D. Verhoeven for critical reading of the manuscript.

SUPPLEMENTARY MATERIAL

The Supplementary Material for this article can be found online at: https://www.frontiersin.org/articles/10.3389/fmicb.2020.00063/full#supplementary-material

REFERENCES

Adam, P. S., Borrel, G., and Gribaldo, S. (2018). Evolutionary history of carbon monoxide dehydrogenase/acetyl-CoA synthase, one of the oldest enzymatic complexes. *Proc. Natl. Acad. Sci. U.S.A.* 115, E1166–E1173. doi: 10.1073/pnas.1716667115

Alberts, B., Johnson, A., Lewis, J., Raff, M., Roberts, K., and Walter, P. (2002). *Molecular Biology of the Cell*, 4th Edn. New York, NY: Garland Science.

Almeida, C. C., Romão, C. V., Lindley, P. F., Teixeira, M., and Saraiva, L. M. (2006). The role of the hybrid cluster protein in oxidative stress defense. *J. Biol. Chem.* 281, 32445–32450. doi: 10.1074/jbc.M605888200

Altschul, S. F., Madden, T. L., Schäffer, A. A., Zhang, J., Zhang, Z., Miller, W., et al. (1997). Gapped BLAST and PSI-BLAST: a new generation of protein database search programs. *Nucleic Acids Res.* 25, 3389–3402. doi: 10.1093/nar/25.17.3389

Amann, R. I., Binder, B. J., Olson, R. J., Chisholm, S. W., Devereux, R., and Stahl, D. A. (1990). Combination of 16S rRNA-targeted oligonucleotide probes with flow cytometry for analyzing mixed microbial populations. *Appl. Environ. Microbiol.* 56, 1919–1925. doi: 10.1128/aem.56.6.1919-1925.1990

Aragão, D., Macedo, S., Mitchell, E. P., Romão, C. V., Liu, M. Y., Frazão, C., et al. (2003). Reduced hybrid cluster proteins (HCP) from *Desulfovibrio desulfuricans* ATCC 27774 and *Desulfovibrio vulgaris* (Hildenborough): X-ray structures at high resolution using synchrotron radiation. *J. Biol. Inorg. Chem.* 8, 540–548. doi: 10.1007/s00775-003-0443-x

Aragão, D., Mitchell, E. P., Frazão, C. F., Carrondo, M. A., and Lindley, P. F. (2008). Structural and functional relationships in the hybrid cluster protein family: structure of the anaerobically purified hybrid cluster protein from *Desulfovibrio vulgaris* at 1.35 Å resolution. *Acta Crystallogr. Sect. D Biol. Crystallogr.* 64, 665–674. doi: 10.1107/S0907444908009165

Bar-Even, A., Flamholz, A., Noor, E., and Milo, R. (2012a). Thermodynamic constraints shape the structure of carbon fixation pathways. *Biochim. Biophys. Acta – Bioenerg.* 1817, 1646–1659. doi: 10.1016/j.bbabio.2012.05.002

Bar-Even, A., Noor, E., and Milo, R. (2012b). A survey of carbon fixation pathways through a quantitative lens. *J. Exp. Bot.* 63, 2325–2342. doi: 10.1093/jxb/err417

Berg, I. A. (2011). Ecological aspects of the distribution of different autotrophic CO2 fixation pathways. *Appl. Environ. Microbiol.* 77, 1925–1936. doi: 10.1128/AEM.02473-10

Biegel, E., and Müller, V. (2010). Bacterial Na^+-translocating ferredoxin: NAD^+ oxidoreductase. *Proc. Natl. Acad. Sci. U.S.A.* 107, 18138–18142. doi: 10.1073/pnas.1010318107

Boetzer, M., and Pirovano, W. (2012).). Toward almost closed genomes with GapFiller. *Genome Biol.* 13:R56. doi: 10.1186/gb-2012-13-6-r56

Boetzer, M., and Pirovano, W. (2014). SSPACE-LongRead: scaffolding bacterial draft genomes using long read sequence information. *BMC Bioinformatics* 15:211. doi: 10.1186/1471-2105-15-211

Bonam, D., Lehman, L., Roberts, G. P., and Ludden, P. W. (1989). Regulation of carbon monoxide dehydrogenase and hydrogenase in *Rhodospirillum rubrum*: effects of CO and oxygen on synthesis and activity. *J. Bacteriol.* 171, 3102–3107. doi: 10.1128/jb.171.6.3102-3107.1989

Bonams, D., and Luddent, P. W. (1987). Purification and characterization of carbon monoxide. *J. Biol. Chem.* 262, 2980–2987.

Caspi, R., Foerster, H., Fulcher, C. A., Kaipa, P., Krummenacker, M., Latendresse, M., et al. (2008). The MetaCyc database of metabolic pathways and enzymes and the BioCyc collection of pathway/genome databases. *Nucleic Acids Res.* 36, 623–631. doi: 10.1093/nar/gkm900

Daims, H., Brühl, A., Amann, R., Schleifer, K.-H., and Wagner, M. (1999). The domain-specific probe EUB338 is insufficient for the detection of all bacteria: development and evaluation of a more comprehensive probe set. *Syst. Appl. Microbiol.* 22, 434–444. doi: 10.1016/s0723-2020(99)80053-8

Daims, H., Lücker, S., and Wagner, M. (2006). Daime, a novel image analysis program for microbial ecology and biofilm research. *Environ. Microbiol.* 8, 200–213. doi: 10.1111/j.1462-2920.2005.00880.x

Daims, H., Stoecker, K., and Wagner, M. (2005). "Fluorescence in situ hybridization for the detection of prokaryotes," in *Molecular Microbial Ecology*, eds A. M. Osborn, and C. J. Smith, (New York, NY: Taylor & Francis), 213–239.

Darnault, C., Volbeda, A., Kim, E. J., Legrand, P., Vernède, X., Lindahl, P. A., et al. (2003). Ni-Zn-[Fe4-S4] and Ni-Ni-[Fe4-S4] clusters in closed and open α subunits of acetyl-CoA synthase/carbon monoxide dehydrogenase. *Nat. Struct. Biol.* 10, 271–279. doi: 10.1038/nsb912

De Kok, S., Meijer, J., van Loosdrecht, M. C. M., and Kleerebezem, R. (2013). Impact of dissolved hydrogen partial pressure on mixed culture fermentations. *Appl. Microbiol. Biotechnol.* 97, 2617–2625. doi: 10.1007/s00253-012-4400-x

Deamer, D., Akeson, M., and Branton, D. (2016). Three decades of nanopore sequencing. *Nat. Biotechnol.* 34, 518–524. doi: 10.1038/nbt.3423

Diender, M., Pereira, R., Wessels, H. J. C. T., Stams, A. J. M., and Sousa, D. Z. (2016). Proteomic analysis of the hydrogen and carbon monoxide metabolism of *Methanothermobacter marburgensis*. *Front. Microbiol.* 7:1049. doi: 10.3389/fmicb.2016.01049

Dobbek, H., Gremer, L., Meyer, O., and Huber, R. (1999). Crystal structure and mechanism of CO dehydrogenase, a molybdo iron-sulfur flavoprotein containing S-selanylcysteine. *Proc. Natl. Acad. Sci. U.S.A.* 96, 8884–8889. doi: 10.1073/pnas.96.16.8884

Doukov, T. I., Iverson, T. M., Seravalli, J., Ragsdale, S. W., and Drennan, C. L. (2002). A Ni-Fe-Cu center in a bifunctional carbon monoxide dehydrogenase/acetyl-CoA synthase. *Science* 298, 567–573. doi: 10.1126/science.1075843

Drake, H. L., Gößner, A. S., and Daniel, S. L. (2008). Old acetogens, new light. *Ann. N. Y. Acad. Sci.* 1125, 100–128. doi: 10.1196/annals.1419.016

Drake, H. L., Hu, S. I., and Wood, H. G. (1981). Purification of five components from *Clostridium thermoaceticum* which catalyze synthesis of acetate from pyruvate and methyltetrahydrofolate. *J. Biol. Chem.* 256, 11137–11144.

Eggen, R. I. L., Geerling, A. C. M., Jetten, M. S. M., and De Vos, W. M. (1991). Cloning, expression, and sequence analysis of the genes for carbon monoxide dehydrogenase of *Methanothrix soehngenii*. *J. Biol. Chem.* 266, 6883–6887.

Eggen, R. I. L., van Kranenburg, R., Vriesema, A. J. M., Geerling, A. C. M., Verhagen, M. F. J. M., Hagen, W. R., et al. (1996). Carbon monoxide dehydrogenase from *Methanosarcina frisia* Gö1. *J. Biol. Chem.* 271, 14256–14263. doi: 10.1074/jbc.271.24.14256

El-Gebali, S., Mistry, J., Bateman, A., Eddy, S. R., Luciani, A., Potter, S. C., et al. (2018). The Pfam protein families database in 2019. *Nucleic Acids Res.* 47, 427–432. doi: 10.1093/nar/gky995

Ensign, S. A., Campbell, M. J., and Ludden, P. W. (1990). Activation of the nickel-deficient carbon monoxide dehydrogenase from *Rhodospirillum rubrum*: kinetic Characterization and reductant requirement. *Biochemistry* 29, 2162–2168. doi: 10.1021/bi00460a029

Ensign, S. A., and Ludden, P. W. (1991). Characterization of the CO oxidation/H2 evolution system of *Rhodospirillum rubrum*: role of a 22-kDa iron-sulfur protein in mediating electron transfer between carbon monoxide dehydrogenase and hydrogenase. *J. Biol. Chem.* 266, 18395–18403.

Figueroa, I. A., Barnum, T. P., Somasekhar, P. Y., Carlström, C. I., Engelbrektson, A. L., and Coates, J. D. (2018). Metagenomics-guided analysis of microbial chemolithoautotrophic phosphite oxidation yields evidence of a seventh natural CO_2 fixation pathway. *Proc. Natl. Acad. Sci.* U.S.A. 115, E92–E101. doi: 10.1073/pnas.1715549114

Fuchs, G. (2011). Alternative pathways of carbon dioxide fixation: insights into the early evolution of life? *Annu. Rev. Microbiol.* 65, 631–658. doi: 10.1146/annurev-micro-090110-102801

Heo, J., Wolfe, M. T., Staples, C. R., and Ludden, P. W. (2002). Converting the NiFeS carbon monoxide dehydrogenase to a hydrogenase and a hydroxylamine reductase. *J. Bacteriol.* 184, 5894–5897. doi: 10.1128/JB.184.21.5894-5897.2002

Ho, J. C. H., Pawar, S. V., Hallam, S. J., and Yadav, V. G. (2018). An improved whole-cell biosensor for the discovery of lignin-transforming enzymes in functional metagenomic screens. *ACS Synth. Biol.* 7, 392–398. doi: 10.1021/acssynbio.7b00412

Jain, M., Olsen, H. E., Paten, B., and Akeson, M. (2016). The oxford nanopore MinION: delivery of nanopore sequencing to the genomics community. *Genome Biol.* 17:239.

Jeoung, J.-H., and Dobbek, H. (2011). Ni, Fe-Containing Carbon Monoxide Dehydrogenases. *Encycl. Inorg. Bioinorg. Chem.* 179, 1–11. doi: 10.1002/9781119951438.eibc0640

Kanehisa, M., Goto, S., Sato, Y., Kawashima, M., Furumichi, M., and Tanabe, M. (2014). Data, information, knowledge and principle: back to metabolism in KEGG. *Nucleic Acids Res.* 42, D199–D205. doi: 10.1093/nar/gkt1076

Kempf, V. A. J., Trebesius, K., and Autenrieth, I. B. (2000). Fluorescent in situ hybridization allows rapid identification of microorganisms in blood cultures. *J. Clin. Microbiol.* 38, 830–838. doi: 10.1128/jcm.38.2.830-838.2000

Kerby, R. L., Ludden, P. W., and Roberts, G. P. (1997). In vivo nickel insertion into the carbon monoxide dehydrogenase of *Rhodospirillum rubrum*: molecular and physiological characterization of cooCTJ. *J. Bacteriol.* 179, 2259–2266. doi: 10.1128/jb.179.7.2259-2266.1997

King, G. M., and Weber, C. F. (2007). Distribution, diversity and ecology of aerobic CO-oxidizing bacteria. *Nat. Rev. Microbiol.* 5, 107–118. doi: 10.1038/nrmicro1595

Kuivanen, J., Biz, A., and Richard, P. (2019). Microbial hexuronate catabolism in biotechnology. *AMB Express* 9, 1–11. doi: 10.1186/s13568-019-0737-1

Markowitz, V. M., Chen, I. M. A., Palaniappan, K., Chu, K., Szeto, E., Grechkin, Y., et al. (2012). IMG: the integrated microbial genomes database and comparative analysis system. *Nucleic Acids Res.* 40, 115–122. doi: 10.1093/nar/gkr1044

Maupin-Furlow, J. A., and Ferry, J. G. (1996). Analysis of the CO dehydrogenase/acetyl-coenzyme A synthase operon of *Methanosarcina thermophila*. *J. Bacteriol.* 178, 6849–6856. doi: 10.1128/jb.178.23.6849-6856.1996

Menon, S., and Ragsdale, S. W. (1996a). Evidence that carbon monoxide is an obligatory intermediate in anaerobic acetyl-CoA synthesis. *Biochemistry* 35, 12119–12125. doi: 10.1021/bi961014d

Menon, S., and Ragsdale, S. W. (1996b). Unleashing hydrogenase activity in carbon monoxide dehydrogenase/acetyl-CoA synthase and pyruvate: ferredoxin oxidoreductase. *Biochemistry* 35, 15814–15821. doi: 10.1021/bi9615598

O'Brien, W. E., and Ljungdahl, L. G. (1972). Fermentation of fructose and synthesis of acetate from carbon dioxide by *Clostridium formicoaceticum*. *J. Bacteriol.* 109, 626–632. doi: 10.1128/jb.109.2.626-632.1972

Parks, D. H., Imelfort, M., Skennerton, C. T., Hugenholtz, P., and Tyson, G. W. (2015). CheckM: assessing the quality of microbial genomes recovered from isolates, single cells, and metagenomes. *Genome Res.* 25, 1043–1055. doi: 10.1101/gr.186072.114

Ragsdale, S. W. (2008). Enzymology of the Woods-Ljundahl pathway of acetogenesis. *Ann. N. Y. Acad. Sci.* 1125, 129–136. doi: 10.1196/annals.1419.015. Enzymology

Ragsdale, S. W., and Kumar, M. (1996). Nickel-containing carbon monoxide dehydrogenase/Acetyl-CoA synthase. *Chem. Rev.* 96, 2515–2539.

Ragsdale, S. W., and Pierce, E. (2008). Acetogenesis and the Wood-Ljungdahl pathway of CO2 fixation. *Biochim. Biophys. Acta* 1784, 1873–1898. doi: 10.1016/j.bbapap.2008.08.012

Roels, J. (1983). *Energetics and Kinetics in Biotechnology*. Amsterdam: Biomedical Press.

Rumble, J. R., Linde, D. R., and Bruno, T. J. (2017). *CRC Handbook of Chemistry and Physics*, 98th Edn. Boca Raton, FL: CRC Press LLC.

Schübel, U., Kraut, M., Mörsdorf, G., and Meyer, O. (1995). Molecular characterization of the gene cluster coxMSL encoding the molybdenum-containing carbon monoxide dehydrogenase of *Oligotropha carboxidovorans*. *J. Bacteriol.* 177, 2197–2203. doi: 10.1128/jb.177.8.2197-2203.1995

Schuchmann, K., and Muller, V. (2013). Direct and reversible hydrogenation of CO_2 to formate by a bacterial carbon dioxide reductase. *Science* 342, 1382–1386. doi: 10.1126/science.1244758

Schuchmann, K., and Müller, V. (2014). Autotrophy at the thermodynamic limit of life: a model for energy conservation in acetogenic bacteria. *Nat. Rev. Microbiol.* 12, 809–821. doi: 10.1038/nrmicro3365

Schuchmann, K., and Müller, V. (2016). Energetics and application of heterotrophy in acetogenic bacteria. *Appl. Environ. Microbiol.* 82, 4056–4069. doi: 10.1128/AEM.00882-16

Schulman, M., Donald Parker, Ljungdahl, L. G., and Wood, H. G. (1972). Total synthesis of acetate from CO_2 V. Determination by mass analysis of the different types of acetate formed from $^{13}CO_2$ by heterotrophic bacteria.*J. Bacteriol.* 109, 633–644. doi: 10.1146/annurev.mi.23.100169.002503

Shimizu, R., Dempo, Y., Nazkayama, Y., Nakamura, S., Bamba, T., Fukusaki, E., et al. (2015). New insight into the role of the Calvin cycle: reutilization of CO_2 emitted through sugar degradation. *Sci. Rep.* 5:11617. doi: 10.1038/srep11617

Shizuya, H., Birren, B., Kim, U.-J., Mancino, V., Slepak, T., Tachiiri, Y., et al. (1992). Cloning and stable maintenance of 300-kilobase-pair fragments of human DNA in *Escherichia coli* using an F-factor-based vector. *Proc. Natl. Acad. Sci.* U.S.A. 89, 8794–8797. doi: 10.1073/pnas.89.18.8794

Techtmann, S. M., Lebedinsky, A. V., Colman, A. S., Sokolova, T. G., Woyke, T., Goodwin, L., et al. (2012). Evidence for horizontal gene transfer of anaerobic carbon monoxide dehydrogenases. *Front. Microbiol.* 3:132. doi: 10.3389/fmicb.2012.00132

Valk, L. C., Frank, J., de la Torre-Cortes, P., van 't Hof, M., van Maris, A. J. A., and Pronk, J. T. (2018). Galacturonate metabolism in anaerobic chemostat enrichment cultures: combined fermentation and acetogenesis by the dominant sp. nov. "*Candidatus* Galacturonibacter soehngenii." *Appl. Environ. Microbiol.* 84:e01370-18. doi: 10.1128/AEM.01370-18

Vallenet, D., Calteau, A., Cruveiller, S., Gachet, M., Lajus, A., Josso, A., et al. (2017). MicroScope in 2017: an expanding and evolving integrated resource for community expertise of microbial genomes. *Nucleic Acids Res.* 45, D517–D528. doi: 10.1093/nar/gkw1101

Vallenet, D., Labarre, L., Rouy, Z., Barbe, V., Bocs, S., Cruveiller, S., et al. (2006). MaGe: a microbial genome annotation system supported by synteny results. *Nucleic Acids Res.* 34, 53–65. doi: 10.1093/nar/gkj406

van den Berg, W. A. M., Hagen, W. R., and van Dongen, W. M. A. M. (2000). The hybrid-cluster protein ('prismane protein') from *Escherichia coli*. *Eur. J. Biochem.* 267, 666–676. doi: 10.1046/j.1432-1327.2000.01032.x

van Maris, A. J. A., Abbott, D. A., Bellissimi, E., van den Brink, J., Kuyper, M., Luttik, M. A. H., et al. (2006). Alcoholic fermentation of carbon sources in biomass hydrolysates by *Saccharomyces cerevisiae*: current status. *Antonie van Leeuwenhoek* 90, 391–418. doi: 10.1007/s10482-006-9085-7

Weghoff, M. C., and Müller, V. (2016). CO metabolism in the thermophilic acetogen *Thermoanaerobacter kivui*. *Appl. Environ. Microbiol.* 82, 2312–2319. doi: 10.1128/AEM.00122-16

Wolfe, M. T., Heo, J., Garavelli, J. S., and Ludden, P. W. (2002). Hydroxylamine reductase activity of the hybrid cluster protein from *Escherichia coli*. *J. Bacteriol.* 184, 5898–5902. doi: 10.1128/JB.184.21.5898-5902.2002

Wood, H. G., and Harris, D. L. (1952). A study of carbon dioxide fixation by mass determination of the types of C13-acetate. *J. Biol. Chem.* 194, 905–931.

Zhuang, W., Yi, S., Bill, M., Brisson, V. L., Feng, X., Men, Y., et al. (2014). Incomplete Wood–Ljungdahl pathway facilitates one-carbon metabolism in organohalide-respiring *Dehalococcoides mccartyi*. *Proc. Natl. Acad. Sci. U.S.A.* 111, 6419–6424. doi: 10.1073/pnas.1321542111

Conflict of Interest: The authors declare that the research was conducted in the absence of any commercial or financial relationships that could be construed as a potential conflict of interest.

frontiers in Microbiology

ORIGINAL RESEARCH
published: 31 January 2020
doi: 10.3389/fmicb.2020.00059

Formate Is Required for Growth of the Thermophilic Acetogenic Bacterium *Thermoanaerobacter kivui* Lacking Hydrogen-Dependent Carbon Dioxide Reductase (HDCR)

Surbhi Jain, Helge M. Dietrich, Volker Müller and Mirko Basen†*

Department of Molecular Microbiology and Bioenergetics, Institute of Molecular Biosciences, Goethe University Frankfurt, Frankfurt am Main, Germany

OPEN ACCESS

Edited by:
Inês A. Cardoso Pereira, New University of Lisbon, Portugal

Reviewed by:
Constanze Pinske, Martin Luther University of Halle-Wittenberg, Germany
Rudolf Kurt Thauer, Max Planck Institute for Terrestrial Microbiology, Germany

***Correspondence:**
Mirko Basen
mirko.basen@uni-rostock.de

†Present address:
Mirko Basen, Institute of Biological Science, University of Rostock, Rostock, Germany

Specialty section:
This article was submitted to Microbial Physiology and Metabolism, a section of the journal Frontiers in Microbiology

Received: *23 August 2019*
Accepted: *13 January 2020*
Published: *31 January 2020*

Citation:
Jain S, Dietrich HM, Müller V and Basen M (2020) Formate Is Required for Growth of the Thermophilic Acetogenic Bacterium Thermoanaerobacter kivui Lacking Hydrogen-Dependent Carbon Dioxide Reductase (HDCR). Front. Microbiol. 11:59. doi: 10.3389/fmicb.2020.00059

The hydrogen-dependent carbon dioxide reductase is a soluble enzyme complex that directly utilizes hydrogen (H_2) for the reduction of carbon dioxide (CO_2) to formate in the first step of the acetyl-coenzyme A- or Wood-Ljungdahl pathway (WLP). HDCR consists of 2 catalytic subunits, a hydrogenase and a formate dehydrogenase (FDH) and two small subunits carrying iron-sulfur clusters. The enzyme complex has been purified and characterized from two acetogenic bacteria, from the mesophile *Acetobacterium woodii* and, recently, from the thermophile *Thermoanaerobacter kivui*. Physiological studies toward the importance of the HDCR for growth and formate metabolism in acetogens have not been carried out yet, due to the lack of genetic tools. Here, we deleted the genes encoding HDCR in *T. kivui* taking advantage of the recently developed genetic system. As expected, the deletion mutant (strain TKV_MB013) did not grow with formate as single substrate or under autotrophic conditions with H_2 + CO_2. Surprisingly, the strain did also not grow on any other substrate (sugars, mannitol or pyruvate), except for when formate was added. Concentrated cell suspensions quickly consumed formate in the presence of glucose only. In conclusion, HDCR provides formate which was essential for growth of the *T. kivui* mutant. Alternatively, extracellularly added formate served as terminal electron acceptor in addition to CO_2, complementing the growth deficiency. The results show a tight coupling of multi-carbon substrate oxidation to the WLP. The metabolism in the mutant can be viewed as a coupled formate + CO_2 respiration, which may be an ancient metabolic trait.

Keywords: hydrogen oxidation, carbon dioxide reduction, hydrogen-dependent carbon dioxide reductase, acetogens, thermophiles, *Thermoanaerobacter kivui*, Wood-Ljungdahl pathway

INTRODUCTION

Acetogenic bacteria thrive on the production of acetic acid from H_2 + CO_2. As such, they are abundant in the environment (Drake et al., 2008), since they link primary fermenters and aceticlastic methanogens in the anoxic food chain (Schink and Stams, 2006). The metabolism of acetogens can be separated into three parts: substrate oxidation (oxidative branch), disposal of

reducing equivalents (reductive branch) and redox balancing by electron-bifurcating hydrogenase and/or ferredoxin (Fd)-oxidizing, partly energy-conserving enzyme complexes (Schuchmann and Müller, 2016). H_2 as electron donor in chemolithotrophic metabolism is primarily oxidized by an electron-bifurcating hydrogenase (Schuchmann and Müller, 2012) providing NADH and reduced ferredoxin (Fd_{red}) for CO_2 reduction. The terminal electron accepting pathway is the presumably ancient Wood-Ljungdahl pathway (WLP; Ljungdahl, 1986; Wood et al., 1986), which is also important in anabolism, since a fraction of its product, acetyl-coenzyme A, is provided for growth. Energy conservation is tightly coupled to redox balancing, since a part of the Fd_{red} is oxidized by energy-conserving membrane-bound enzyme complexes (Schuchmann and Müller, 2014), by the Rnf complex, as present in e.g., *Acetobacterium woodii* (Biegel and Müller, 2010), or by energy-converting hydrogenases Ech encoded in the genome of *Moorella thermoacetica* (Pierce et al., 2008) or as present in *Thermoanaerobacter kivui* (Hess et al., 2014; Schoelmerich and Müller, 2019).

The first step in the methyl-branch of the WLP is the reduction of CO_2 to formate, which is catalyzed by a formate dehydrogenase (FDH). In some acetogenic microorganisms, FDH occurs in a complex with a hydrogenase and two small subunits to form a hydrogen-dependent carbon dioxide reductase (HDCR) (Schuchmann and Müller, 2013). A distinct property of the soluble enzyme complex is the direct use of H_2 as electron donor. Therefore, HDCR is the second H_2-oxidizing hydrogenase in acetogenic catabolism besides the electron-bifurcating hydrogenase. The enzyme complex has been purified from two acetogenic bacteria, the mesophile *Acetobacterium woodii* (Schuchmann and Müller, 2013) and the thermophile *Thermoanaerobacter kivui* (Schwarz et al., 2018). HDCR contained four subunits, a hydrogenase, a formate dehydrogenase and two small subunits bearing iron-sulfur clusters, which are likely to be involved in electron transfer from the hydrogenase to the formate dehydrogenase. HDCR catalyzes formate-dependent hydrogen formation, as determined by the concentrations of H_2, CO_2 and formate. The reduction of CO_2 to formate with hydrogen as electron donor is close to the thermodynamic equilibrium (E_0' [CO_2/formate] = –432 mV; E_0' [2 H^+/H_2] = –414 mV), and HDCR catalyzed formate oxidation to CO_2 at comparable rates. Moreover, the reactions were catalyzed with high turnover frequencies (TOF) of up to 101,600 h^{-1} in *A. woodii* and 10,000,000 h^{-1} in *T. kivui*, making HDCRs promising candidate enzymes for biotechnological applications such as H_2 storage or H_2 release from stored formate (Pereira, 2013; Schuchmann and Müller, 2013; Müller, 2019).

Many acetogens are metabolically versatile, and able to utilize electron donors other than H_2, such as sugars, products of primary fermentations such as alcohols or C1 compounds (methanol, formate, CO), or methylated nitrogen compounds such as glycine betaine, in addition to H_2 (Diekert and Wohlfarth, 1994; Schuchmann and Müller, 2016). Here, we studied the function of the HDCR complex *in vivo* using genetic tools (Basen et al., 2018), with focus on its role in the catabolic conversion of multi-carbon substrates. Our hypotheses were that (i) HDCR is essential in formate oxidation during growth on formate as sole substrate, since it is the only FDH annotated in the genome (Hess et al., 2014), and (ii) in heterotrophic metabolism, HDCR, its product formate and the Wood-Ljungdahl pathway are essential unless electrons are disposed elsewhere, e.g., as H_2 through the reaction of the electron-bifurcating hydrogenase (**Figure 1**). Interestingly, the generation of a mutant, strain TKV_MB013, that lacked the genes predicted to encode for the subunits of HDCR, was only possible if formate was supplied in addition to sugars, and the phenotype of the strain was characterized in detail.

RESULTS

Generation of a HDCR Genes Deletion Mutant

As HDCR likely fulfills an essential function during growth on formate or on H_2 + CO_2, but potentially not during growth on sugars (**Figure 1**), we aimed to delete the genes encoding the four subunits forming the active enzyme, *fdhF* (TKV_c19990), *hycB3* (TKV_c19980), *hycB4* (TKV_c19970), and *hydA2* (TKV_c19960) in *T. kivui* (Schwarz et al., 2018). These consecutive HDCR genes are part of a gene cluster that also contains a fifth gene, *fdhD* (TKV_c19950), presumably encoding a formate dehydrogenase maturation protein (Schwarz et al., 2018). *FdhD* was not deleted, since it was not identified as part of the enzyme complex in *T. kivui*. For ease of understanding, we refer to the four targeted genes *fdhF, hycB3, hycB4*, and *hydA2* as the HDCR genes in the following. In order to create the HDCR genes deletion in *T. kivui*, plasmid pMBTkv012 was designed (**Supplementary Figure S1**), carrying approximately 1000 bp regions flanking the HDCR genes. Apart from these upstream (5′) and downstream (3′) flanking regions (UFR and DFR, respectively), the plasmid also contained the *pyrE* cassette as selectable marker, to be introduced into the *pyrE*-deficient uracil-auxotrophic strain TKV_MB002. The genetic system has been described in detail recently (Basen et al., 2018). In brief, we selected for uracil-prototrophs in the first selection round, and for the loss of the plasmid including *pyrE* with 5-fluoroorotic acid (5-FOA) in the second round of selection (**Figure 2A**), as described previously (Basen et al., 2018). Initially, we used glucose as only substrate, but after screening >50 colonies, we did not obtain any mutant lacking the HDCR gene cluster. In a second approach, we added formate (50 mM) in addition to glucose during the selection as it is the product of HDCR (**Figure 1**). We then obtained five genotypically "clean" HDCR deletion mutants out of 6 screened colonies/isolates as verified by PCR analysis after the second round of selection (**Figure 2B**), while the gene locus in the 6th picked colony likely reverted to the wild type gene locus. The markerless deletion of the genes encoding HDCR in mutant 5 was verified by sequencing and immunoblotting (**Figure 2C**), and the mutant was designated *T. kivui* strain TKV_MB013 (Δ*pyrE*, Δ*fdhF hycB3 hycB4 hydA2*). Unlike cell-free extracts of the wild type, cell-free extracts of strain TKV_MB013 neither carried out H_2-dependent formate production nor formate-dependent H_2 production (**Figure 2D**), an activity specific to the HDCR from

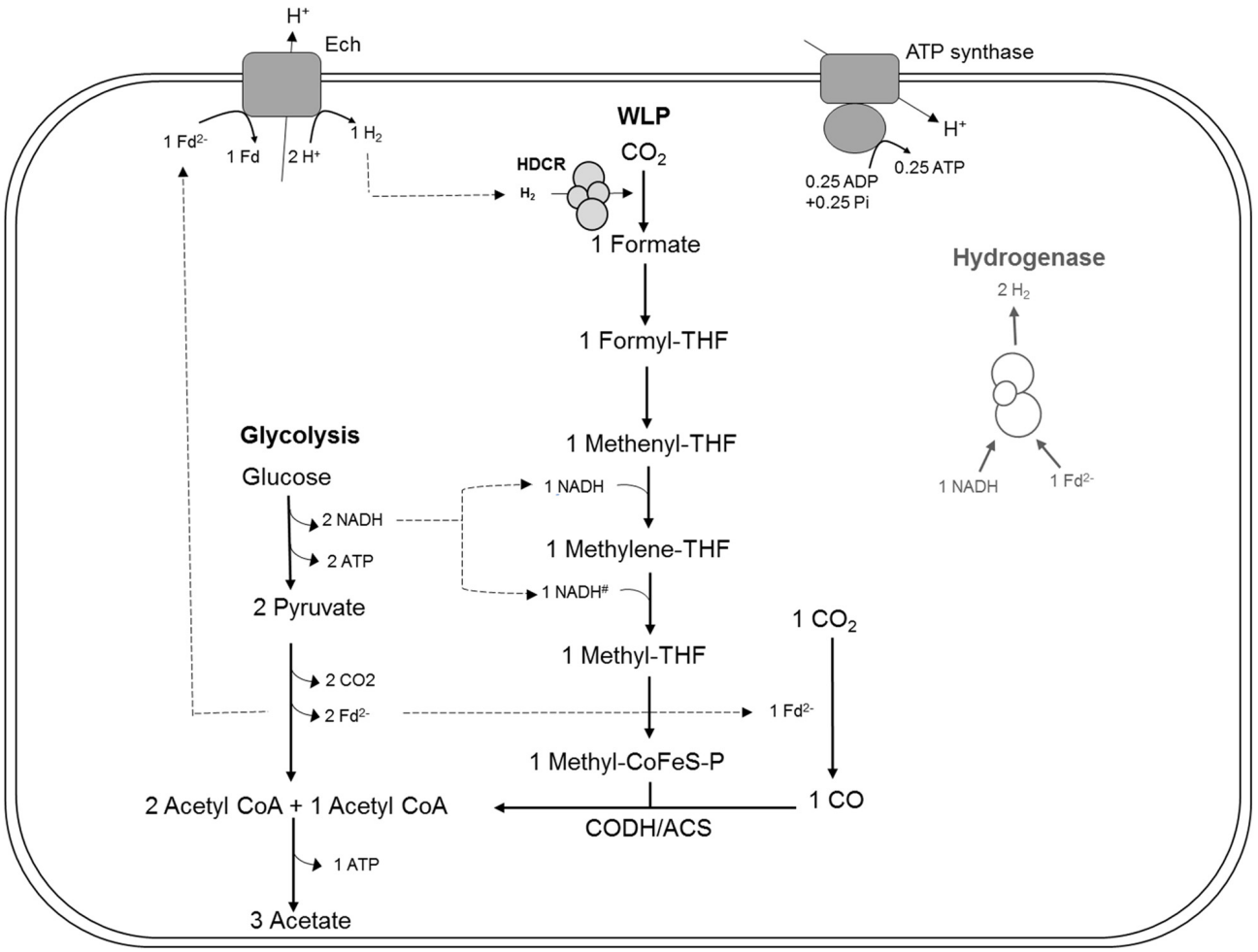

FIGURE 1 | Bioenergetic model of glucose metabolism in *T. kivui,* modified after Hess et al. (2014), highlighting the assumed role of the hydrogen-dependent carbon dioxide reductase (HDCR) in heterotrophic growth. Re-oxidation of ferredoxin (Fd_{red}) may be catalyzed by the electron-converting hydrogenase (Ech) complex, and evolved hydrogen (H_2) may be re-oxidized by HDCR. Alternatively, it may be catalyzed in conjunction with NADH re-oxidation by electron-bifurcating hydrogenase HydABC (transparent, on the right), putatively making HDCR dispensable during heterotrophic growth of *T. kivui*. The stoichiometry of Ech and ATP synthase have been assumed to be 1 proton translocated per one H_2 evolved in the methanogen *Methanosarcina mazei* (Welte et al., 2010), in the thermophilic archaeon *Pyrococcus furiosus* (Sapra et al., 2003) and in *T. kivui* (Schoelmerich and Müller, 2019). The ATP synthase of *T. kivui* is proton-dependent (Hess et al., 2014), and the ratio of 0.25 ATP per proton translocated is supported by thermodynamic calculations in acetogens (Schuchmann and Müller, 2014). #, The NADH-dependence of methylene-THF reductase has been assumed, based on the model of *A. woodii* and no biochemical evidence for electron-bifurcation. CoFeS-P, Corrinoid iron-sulfur protein.

T. kivui or *A. woodii* (Schuchmann and Müller, 2013; Schwarz et al., 2018). Taken together, all genetic and biochemical evidence suggest that *T. kivui* strain TKV_MB013 was devoid of the genes encoding HDCR.

Formate Is Essential for Growth of the HDCR Deletion Mutant

After deletion of the HDCR gene cluster and the absence of the protein in strain TKV_MB013 was confirmed, we analyzed the growth phenotype of the strain on all different substrates with and without formate as electron acceptor in addition to CO_2. Initially, we tested its ability to utilize formate as sole electron donor. As expected, the strain did not grow when 300 mM formate was supplied as sole electron donor (**Table 1**) due to the absence of HDCR, the sole formate oxidizing enzyme encoded in the genome. The wild type grew to an optical density (OD_{600}) of 0.22 ± 0.017. Second, we tested the ability of strain TKV_MB013 to grow chemolithoautotrophically with H_2 + CO_2, and this was also not observed (**Figure 3A**), due to the absence of HDCR as essential formate providing enzyme. In contrast, the wild type grew to an OD_{600} of 0.57 ± 0.02. To indisputably assign this growth deficiency to the loss of the HDCR genes, an ectopic insertion of the wild type genes *fdhF*, *hycB3*, *hycB4*, and *hydA2* into the genome of the mutant strain TKV_MB013 was performed, resulting in strain TKV_MB019. The genes were inserted in between the convergent genes TKV_c24500

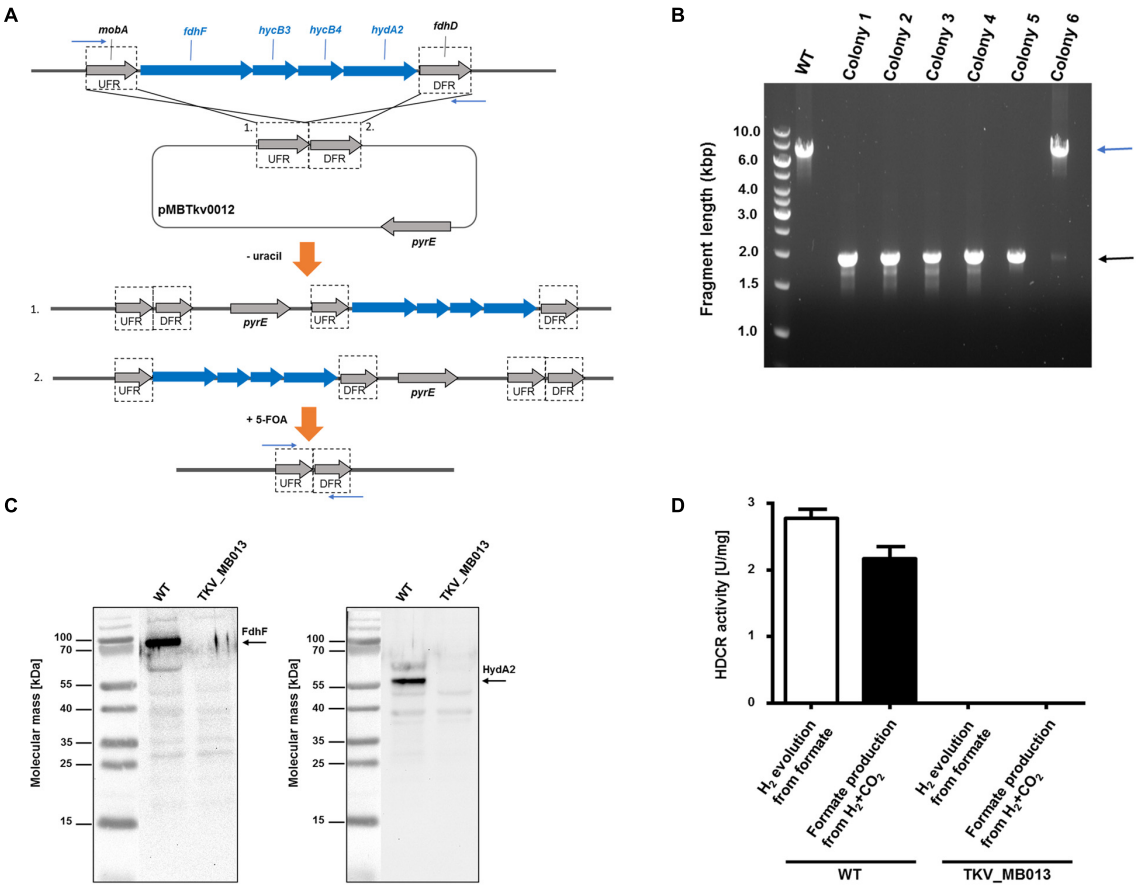

FIGURE 2 | Deletion of the genes encoding HDCR, *fdhF* (TKV_c19990), *hycB3* (TKV_c19980), *hycB4* (TKV_c19970) and *hydA2* (TKV_c19960). **(A)** Strategy for deletion using plasmid pMBTkv0012. 1. and 2. refer to insertion of the plasmid in the first round of selection on uracil prototrophy at the upstream flanking region (UFR) or at the downstream flanking region (DFR), respectively. **(B)** DNA fragments separated by agarose gel electrophoresis after PCR amplification of the HDCR gene locus, using primers outside the flanking regions (indicated as blue arrows). wild type, WT; colonies 1–6). **(C)** Detection of the HDCR subunits FdhF (left side) and HydA2 (right side) in cell free extracts of *T. kivui* DSM2030 (wild type, WT) or of *T. kivui* TKV_MB013. Cells were grown in complex medium (Leigh et al., 1981) with 28 mM glucose and 50 mM formate. 40 μg of cytoplasmic fractions were separated *via* denaturing gel electrophoresis, and then transferred to a nitrocellulose membrane. The presence of FdhF and HydA2 was determined immunologically with antibodies raised against corresponding His-tagged proteins, purified by affinity chromatography. For comparison of the molecular masses, the PageRuler® Prestained Protein Ladder (Thermo Scientific, Dreieich, Germany; left side of both images) was loaded onto the same gel, a picture of the membrane with and without chemiluminescence was taken (ChemoStar, INTAS, Göttingen, Germany), and both images were assembled using the ChemoStar TS software (INTAS, Göttingen, Germany). **(D)** Hydrogen evolution from formate (white bars) and formate formation from $H_2 + CO_2$ (black bars) of cytoplasmic fractions from *T. kivui* wild type (WT) and the HDCR deletion strain (*T. kivui* TKV_MB013). Cells were grown in complex medium with 28 mM glucose and 50 mM formate, and harvested in the late exponential growth phase. 0.3 mg of cytoplasmic protein was incubated in the reaction buffer (100 mM HEPES, 20 mM $MgSO_4$, 0.0001% resazurin, 0.5 mM DTE, pH 7.0) at 64°C, and formate (150 mM) or $H_2 + CO_2$ (80:20 [v:v], 1.1 × 10^5 Pa) were added as substrate. H_2 production from formate was measured in the gas phase, and formate production from $H_2 + CO_2$ was measured in the liquid phase (n = 3).

and TKV_c24520. The addition of the HDCR genes, controlled by the presumably strong promoter of the S-layer protein of *T. kivui*, complemented the growth effect, therefore we conclude that formate, provided by HDCR activity, is essential for chemolithoautotrophic growth of *T. kivui* on $H_2 + CO_2$. This was expected since formate is an intermediate in the methyl branch of the WLP. To prove this hypothesis, we added formate in addition to $H_2 + CO_2$. In that experiment, formate represented the electron acceptor in the methyl branch of the WLP, and indeed, it supported growth of strain TKV_MB013 on $H_2 + CO_2$ (**Figure 3B**), with a similar growth rate and final OD_{600} as the wild type.

Interestingly, heterotrophic growth on glucose also depended on the presence of the HDCR genes. *T. kivui* strain TKV_MB013 only grew to an OD_{600} of 0.2 (**Figure 3C**), which was only slightly higher than growth without any substrate added (0.04 ± 0.01). In contrast, the wild type grew to an OD_{600} of 2.64 ± 0.01, which is comparable to what has been observed before (Basen et al., 2018). Again, the ectopic insertion of the HDCR genes into the genome of strain TKV_MB013 complemented the growth deficiency. While the addition of formate did not influence the wild type, formate again stimulated growth of *T. kivui* strain TKV_MB013 (**Figure 3D**), with a similar OD_{600} of 3.2 reached after 13 h. Interestingly, the addition of formate did not completely restore

TABLE 1 | Average maximal optical densities (OD_{600}) from stationary phase cultures of *T. kivui* DSM2030, the mutant *T. kivui* TKV_MB013 lacking the genes encoding HDCR, and its daughter strain *T. kivui* TKV_MB019, with the HDCR encoding genes re-introduced into the genome.

Substrate used	DSM2030	TKV_MB013	TKV_MB019
No substrate	n.d.	0.04 ± 0.01	n.d.
25 mM Glucose	2.64 ± 0.11	0.2 ± 0.017	2.4 ± 0.09
25 mM Glucose + 50 mM Formate	2.86 ± 0.14	3.3 ± 0.1	2.34 ± 0.20
$H_2 + CO_2$ (1 bar)	0.57 ± 0.02	0.02 ± 0.002	0.48 ± 0.004
$H_2 + CO_2$ (1 bar) + 50 mM Formate	0.8 ± 0.02	0.49 ± 0.01	0.39 ± 0.02
25 mM Mannitol	2.46 ± 0	0.02 ± 0.01	1.08 ± 0.02
25 mM Mannitol + 50 mM Formate	2.45 ± 0	1.99 ± 0.3	2.4 ± 0.01
300 mM Formate	0.22 ± 0.017	0.01 ± 0	0.16 ± 0.02
50 mM Pyruvate	0.15 ± 0.01	0.03 ± 0	0.15 ± 0.001

Growth studies were performed in complex media at 65°C until no further increase in OD_{600} was observed. The cells were grown under an atmosphere of N_2:CO_2 (80:20 [v:v], 1.1 × 10^5 Pa), unless $H_2 + CO_2$ were provided as growth substrates (n = 2; except for DSM2030 and TKV_MB013 grown on mannitol or on glucose, n = 3; n.d., not determined).

the growth behavior in strain TKV_MB013, since only a lower growth rate of 0.38 h^{-1} was reached (vs. 0.56 h^{-1} in the wild type). We then tested whether formate addition was essential for growth with all known electron donors for strain TKV_MB013, and this was indeed the case (**Table 1**). Unlike the wild type, *T. kivui* strain TKV_MB013 neither grew on fructose, mannose (data not shown), pyruvate nor on the recently identified novel substrate mannitol (Moon et al., 2019), to higher optical densities than 0.06, unless formate was added as electron acceptor (**Table 1**). This unambiguously showed that formate, produced by HDCR, and likely the complete WLP as terminal electron accepting pathway, is essential to growth of the acetogen *T. kivui*.

Formate Serves as Additional Electron Acceptor in the HDCR Deletion Mutant

To study substrate consumption and product formation of *T. kivui* strain TKV_MB013, experiments with concentrated suspensions of resting cells were performed. The cells were concentrated to 10× in defined medium and subjected to a short-termed incubation at 65°C. As expected, when glucose was omitted from the medium and when formate was the sole electron donor, the latter was not consumed, due to the absence of HDCR, and no acetate was produced. When formate was provided as electron acceptor in addition to CO_2, glucose was completely consumed (22.7 ± 1.9 mM), while the formate concentration decreased from 40.1 ± 2.9 to 19 ± 0.8 mM. Acetate (76.4 ± 3.2 mM) was the sole product (**Figure 4A**), while only a low concentration of H_2 was detected in the headspace, corresponding to 0.3 mM, if all H_2 was dissolved in the medium. Therefore, the results of the cell suspension experiments with the HDCR mutant strain TKV_MB013 reflected the ones from growth experiments. Formate strongly stimulated glucose consumption in the HDCR deficient *T. kivui* strain TKV_MB013, and formate consumption was strictly coupled to glucose consumption. The theoretically assumed stoichiometry based on glucose oxidation to acetate and CO_2 and concomitant formate and CO_2 reduction to acetate in the mutant strain, TKV_MB013 is depicted in eq. 1.

$$1\ C_6H_{12}O_6 + 1.33\ HCOOH \rightarrow 3.33\ CH_3COOH + 0.66\ CO_2 + 0.66\ H_2O \quad (1)$$

Carbon from glucose and formate was stoichiometrically recovered in acetate carbon, under the assumption that one CO_2 was consumed for each formate consumed (109 ± 14%, n = 3). The electron balance, based on oxidation of glucose and reduction of formate and CO_2 to acetate was nearly closed as well (99 ± 13%, n = 3). Therefore, we assume that no other products were present in high concentrations. The measured average acetate to glucose ratio was slightly higher than three (3.2 ± 0.3; n = 3), as expected. In conclusion, the observed conversion of glucose and formate to acetate by the HDCR mutant, *T. kivui* strain TKV_MB013 is nearly reflected by theoretically assumed stoichiometry (eq. 1), which reveals that formate served as electron acceptor for the oxidation of H_2 and organic electron donors (**Figure 5**).

Since acetogens may dispose electrons from glucose oxidation onto H^+ to form H_2, we tested the effect of omitting formate from the cell suspension experiments with *T. kivui* strain TKV_MB013. Glucose was consumed, but only from 23.2 ± 3.4 to 17 ± 0.8 mM, and acetate production stopped at a concentration of 11.9 ± 1.45 mM (**Figure 4B**). More H_2 was produced (7.8 ± 0.3 mM, if all hydrogen was dissolved) than in the corresponding experiments with formate. This indicates some reducing equivalents (10.5%) from glucose oxidation were indeed channeled toward H_2 when formate was omitted. Growth to higher OD_{600} than 0.2 (**Figure 3C**), however, was not observed.

DISCUSSION

Acetogens utilize C1-compounds of intermediate redox state such as formate or the methyl groups of methanol, methylamines or methoxylated compounds via the WLP (Kerby et al., 1983; Schuchmann and Müller, 2016). Formate-H_2 interconversion, catalyzed by formate:H_2 lyase (FHL), has been studied well in the facultative anaerobe *Escherichia coli* (Mcdowall et al., 2014; Trchounian and Sawers, 2014; Pinske and Sargent, 2016). In contrast to *E. coli*, acetogens utilize formate as sole source of energy and carbon. In principle, acetogens may utilize formate as electron acceptor and electron donor at the same time. Three mols of formate must be oxidized to provide sufficient (6) mols of reductant for the reduction of formate and of CO_2 to one mol of acetate through the Wood-Ljungdahl pathway (Bertsch and Müller, 2015), according to:

$$4\ HCOOH \rightarrow 1\ CH_3COOH + 1\ H_2O + 2\ CO_2 \quad (2)$$

Formate oxidation to CO_2 is catalyzed by formate dehydrogenase (FDH). The *T. kivui* genome only contains one *fdh* copy, *fdhF* (TKV_c19990). Therefore, the deletion of

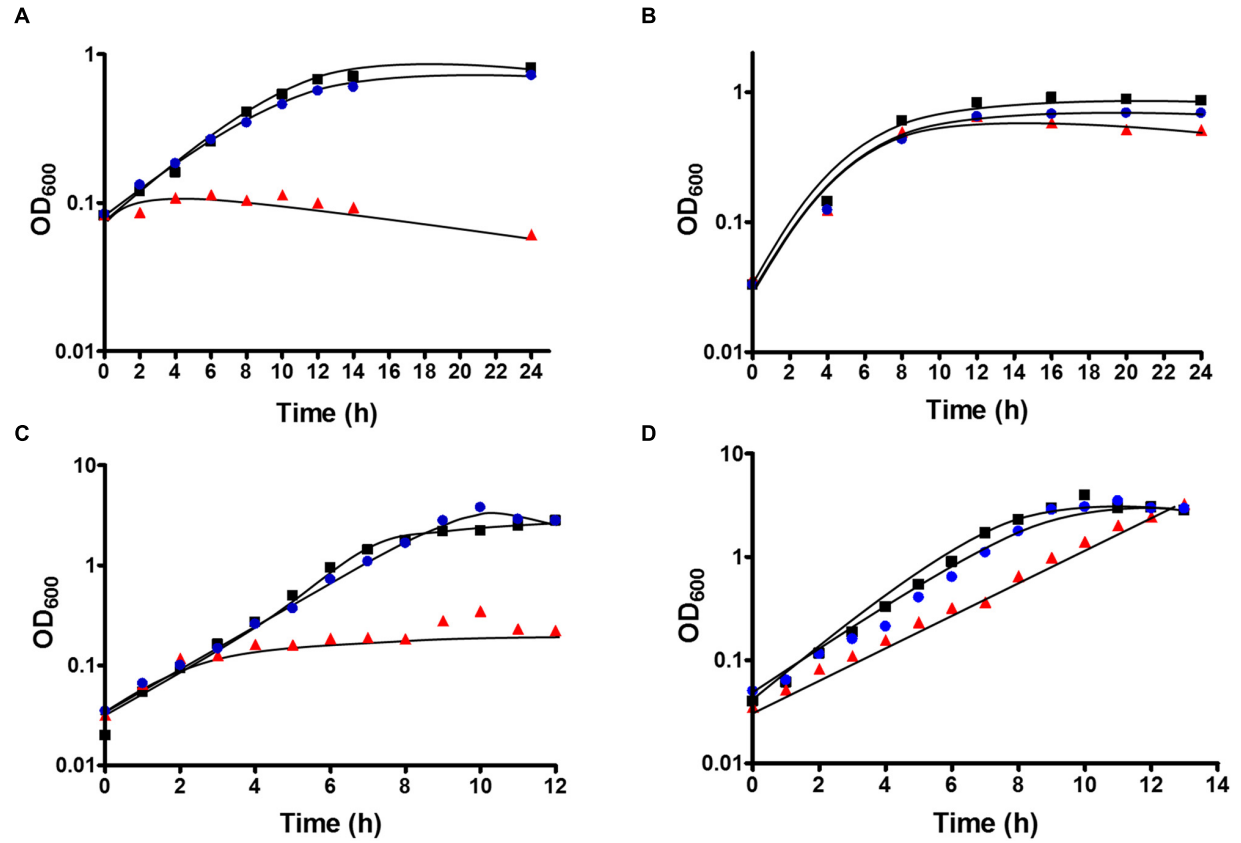

FIGURE 3 | Growth of *T. kivui* strain TKV_MB013 on **(A)** $H_2 + CO_2$ (80:20 [v:v], 2×10^5 Pa), **(B)** $H_2 + CO_2$ (80:20 [v:v], 2×10^5 Pa) + 50 mM formate **(C)** 25 mM glucose or **(D)** 25 mM glucose + 50 mM formate. The cells were grown at 65°C in 100 ml serum bottles containing 25 ml of complex media under an atmosphere of N_2:CO_2 (80:20 [v:v], 1.1×10^5 Pa), unless $H_2 + CO_2$ were provided as growth substrates. TKV_MB013, red triangles; TKV_MB013 plus re-introduced HDCR genes in a different genome location, blue circles; or wild type, black squares. The growth experiments were performed in biological triplicates, and a representative growth curve is shown.

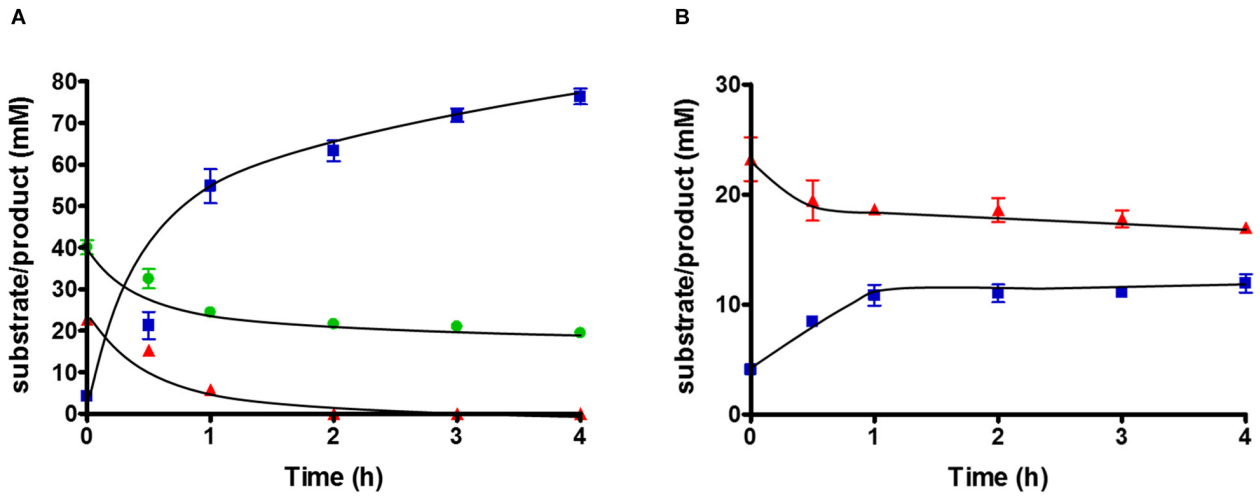

FIGURE 4 | Substrate conversion by 10 ml of 10-fold concentrated cell suspensions of *T. kivui* strain TKV_MB013 (1 mg ml^{-1} protein), pre-grown with glucose and formate, with **(A)** glucose + formate or **(B)** glucose only. Glucose, red triangles; acetate, blue squares; formate, green circles. Experiments were performed in triplicate at 65°C in defined medium, under an atmosphere of N_2:CO_2 (80:20 [v:v], 1.1×10^5 Pa).

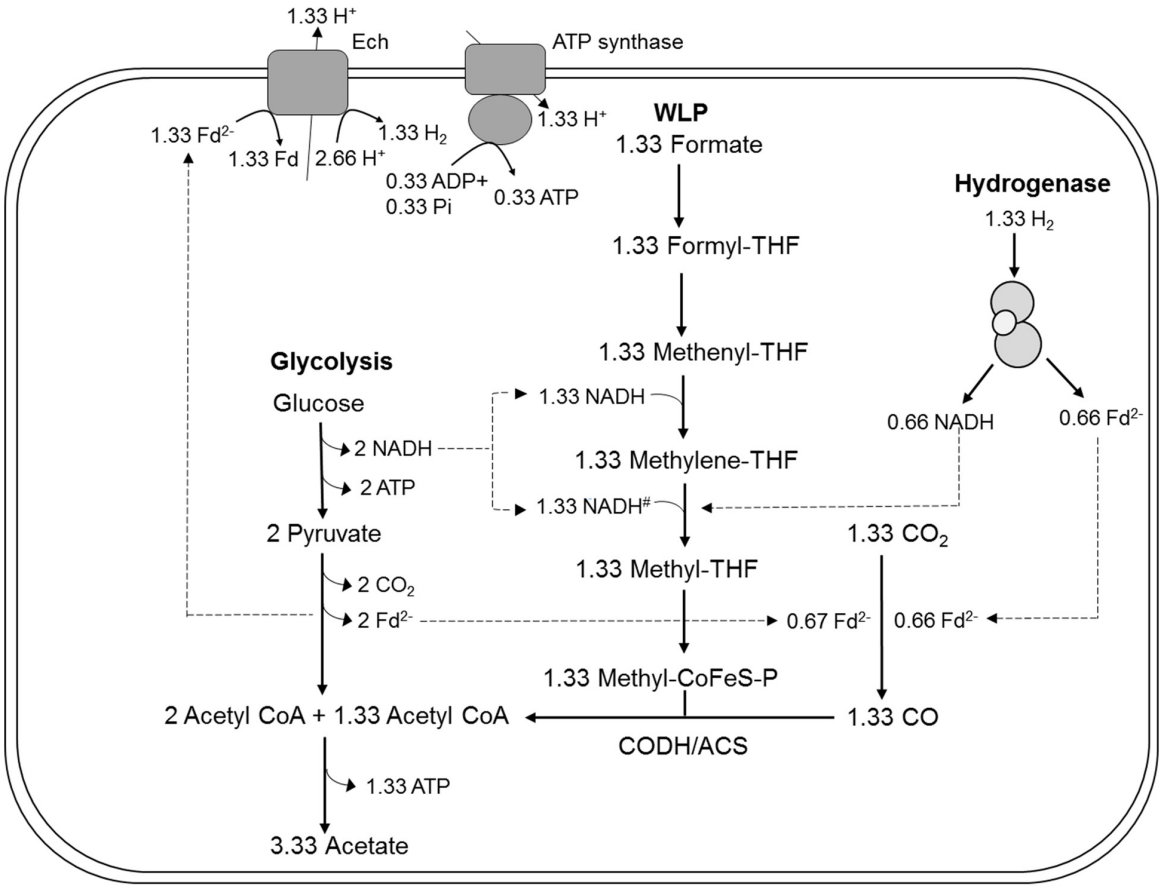

FIGURE 5 | Model for acetogenesis from glucose with formate + CO_2 as electron acceptors in *T. kivui* TKV_MB013 lacking the genes encoding HDCR. WLP, Wood-Ljungdahl-pathway; HDCR, hydrogen-dependent carbon dioxide reductase; Fd^{2-}, reduced ferredoxin; Ech, electron-converting hydrogenase; CoFeS-P, corronoid iron-sulfur protein. For explanations the redox cofactor specificities and of the proposed stoichiometries, please see **Figure 1**.

the HDCR gene cluster including *fdhF* completely abolished its ability to thrive on formate as sole substrate and electron donor (**Table 1**), which may be different in other acetogens such as *A. woodii* or *Treponema primitia* (Matson et al., 2010) that contain several *fdh* copies, or genes encoding FHLs in addition to *fdh* genes (Poehlein et al., 2015).

Acetogens catalyze formate reduction in the methyl branch of the WLP. Formate is provided by FDH, which is bound to hydrogenase in the HDCR complex in at least two acetogens, *A. woodii* and *T. kivui*. So, in contrast to the membrane-bound FHL that primarily oxidizes formate to CO_2 in mixed acid fermentation (Pinske and Sargent, 2016), the metabolic function of HDCR is not only formate oxidation but also catabolic CO_2 reduction to formate in the WLP. Therefore, the ability to use CO_2 as sole electron acceptor through the WLP was abolished by the HDCR genes deletion. The *T. kivui* mutant lacking the HDCR genes, strain TKV_MB013, depended on the complementation with formate as additional electron acceptor for growth (**Figure 3C**) and for complete and efficient glucose oxidation (**Figure 4A**). While our observation has been made - somewhat artificially - with a mutant strain, a similar kind of formate metabolism in native acetogens has been described before, e.g., in *Butyribacterium methylotrophicum*. This bacterium has been reported to utilize CO or H_2 + CO_2 and formate simultaneously (Kerby et al., 1983; Kerby and Zeikus, 1987). The acetogen *Acetobacterium woodii* has also been reported to co-utilize formate with CO (Bertsch and Müller, 2015), however, the study had a different focus, since the authors report that CO is only used in the presence of formate. The determined stoichiometries of 1:1.8:1 (formate:CO:acetate) suggest that formate was mainly used as electron acceptor, while CO was used as electron donor (**Figure 5**). In that scenario, HDCR may be dispensable in the metabolism of *A. woodii*.

The utilization of formate as electron acceptor may indeed be an ancient metabolic trait. Acetogenesis itself supposedly is one of the oldest types of metabolism (Weiss et al., 2016). The first organisms may have thrived on the oxidation of molecular H_2 with CO_2, and there are only two groups of organisms that thrive on the conversion of these compounds – methanogenic archaea and acetogenic bacteria. Interestingly, many genes of the WLP essential for CO_2 fixation in both groups, and the genes essential to acetogenesis, were described as part of the genome of the Last Universal Common Ancestor (Weiss et al., 2016). The role of formate in Early Life, however, is not clear.

Strikingly, in acetogens the genes of the WLP are clustered (Poehlein et al., 2015), also in *T. kivui* (Hess et al., 2014), however, e.g., in *A. woodii* (Poehlein et al., 2012) and *Clostridium aceticum* the genes encoding the formate dehydrogenase/HDCR are separate from this cluster. One may speculate that the WLP may have evolved as three independent parts - CO_2 reduction to formate, formate reduction to a methyl group and the CODH/ACS reaction. In the present study, one of the parts, CO_2 reduction to formate was removed, which could be complemented by the addition of formate. In an Early Earth environment, organic acids have been reported as prevalent forms of carbon (Amend et al., 2013). Formate has been reported to be thermodynamically more stable than CO_2 under alkaline conditions, and significant concentrations of formate were found at the alkaline Lost City hydrothermal field (Lang et al., 2010), an environment discussed to have supported the Evolution of Life (Weiss et al., 2016). Thus, formate may have been present as electron acceptor in Early Earth, and a coupled formate + CO_2 respiration, as described in here, may have allowed the conservation of energy in a primordial environment.

The results also indicate a tight coupling of CO_2 reduction in the WLP to the oxidation of multi-carbon substrates during heterotrophic growth in *T. kivui*. We initially considered that the HDCR reaction may not be essential for growth on sugars, despite many acetogens have been described as "homoacetogens" such as *Moorella thermoacetica* (Fontaine et al., 1942). The term "homoacetogenesis" refers to the conversion of 1 mol of glucose to 3 mols of acetate (eq. 3), in analogy to homolactate fermentation (Drake et al., 2008). The oxidative part of homoacetate fermentation yields only two mols of acetate, 2 mols of CO_2 and 8 reducing equivalents (eq. 4), while in the reductive part, catalyzed by the WLP, two mols of CO_2 are reduced to the third mol of acetate (eq. 5), depleting the reducing equivalents produced in glucose oxidation. This metabolism has been observed during heterotrophic growth of wild type *T. kivui*, with 2.3–3 mols of acetate formed from 1 mol of glucose (Leigh et al., 1981).

$$1\ C_6H_{12}O_6 \rightarrow 3\ CH_3COOH \quad (3)$$

$$1\ C_6H_{12}O_6 + 2\ H_2O \rightarrow 2\ CH_3COOH + 2\ CO_2 + 8\ [H] \quad (4)$$

$$2\ CO_2 + 8\ [H] \rightarrow 1\ CH_3COOH + 2\ H_2O \quad (5)$$

In theory, reducing equivalents may take an alternative route, especially, in case that the electron-accepting WLP is impaired. For example, the Fd_{red} and NADH produced in *T. kivui* sugar oxidation may be oxidized by an electron-confurcating hydrogenase (Schut and Adams, 2009). In result, 4 H_2 were produced per glucose oxidized, in addition to two acetate and two CO_2 (**Figure 1A**). That type of metabolism was originally described for the thermophilic bacterium *Thermotoga maritima* (Schut and Adams, 2009), but it is widespread especially among other thermophilic microorganisms. Indeed, in cell suspension experiments with the *T. kivui* HDCR mutant, 7–8 mM of H_2 (if all headspace H_2 was dissolved) formed from glucose in the absence of formate (**Figure 4B**). However, the reducing equivalents present in H_2 represented only a minor fraction of the total reducing equivalents (10.5%), and the rate of glucose oxidation was much lower than in the experiments with formate present. In growth experiments, cells only reached a low cell density (**Figure 3C**), even after prolonged incubation times of 1 week (data not shown). Cultures did also not reach higher cell densities when grown with a proportionally larger gaseous headspace (data not shown), indicating that the headspace hydrogen concentration itself was not inhibitory. Therefore, we assume that, while electron-channeling toward H_2 production was possible in principle, it may not be fast enough to support growth to high cell densities. For example, the electron-bifurcating hydrogenase HydABC of *T. kivui* may be prone to H_2 oxidation rather than to H_2 formation, as described for membrane-bound hydrogenases of the hyperthermophilic archaeon *Pyrococcus furiosus* (Mcternan et al., 2014). Alternatively, growth on glucose without a functional WLP or HDCR may be impaired by a non-functional C1-metabolism (since the WLP provides C1-units for anabolic reactions) or by a modified ratio of reduced redox carriers. The latter was observed for *A. woodii*, where a functional Rnf complex was essential for providing Fd_{red} during growth on low-energy heterotrophic substrates such as lactate or ethanol (Westphal et al., 2018).

MATERIALS AND METHODS

Growth Experiments

Thermoanaerobacter kivui strain LKT-1 (DSM2030), referred to as wild type, strain TKV_MB002 *(ΔpyrE*, previous name strain TKV002) and strain TKV_MB013 (ΔpyrE ΔTKV_c19960-TKV_c19990) were cultivated under strict anoxic condition at 65°C in complex or defined media as described previously (Weghoff and Müller, 2016; Basen et al., 2018). Complex media contained $Na_2HPO_4 \times 2H_2O$, 50 mM; $NaH_2PO_4 \times 2H_2O$, 50 mM; K_2HPO_4, 1.2 mM; KH_2PO_4, 1.2 mM; NH_4Cl, 4.7 mM; $(NH_4)_2SO_4$, 1.7 mM; NaCl, 7.5 mM; $MgSO_4 \times 7\ H_2O$, 0.37 mM; $CaCl_2 \times 2\ H_2O$, 42 μM; $Fe(II)SO_4 \times 7\ H_2O$, 7.2 μM; $KHCO_3$, 54 mM; cysteine-HCl × H_2O, 3 mM; resazurin, 4.4 μM; 0.2% (w/v) yeast extract, 10 ml/l trace element solution DSM141 and 10 ml/l vitamin solution DSM141. Defined media was prepared similarly, as complex media without addition of yeast extract. The medium was flushed with N_2:CO_2 (80:20 [v:v], 1.1×10^5 Pa) before autoclaving. The pH of the medium was 7.5 after flushing. All gases were purchased from Praxair Deutschland GmbH (Düsseldorf, Germany).

Growth experiments were carried out in 20 ml Hungate glass tubes or serum bottles sealed with butyl rubber stoppers under an atmosphere of N_2:CO_2 (80:20 [v:v], 1.1×10^5 Pa), unless denoted otherwise (Basen et al., 2018). Usually, a concentration of 25 mM of different organic electron donors such as glucose or mannitol was chosen, and 50 mM formate as electron acceptor. Non-gaseous substrates were added from sterile anoxic solutions. If H_2 + CO_2 were used as substrates, tubes were only filled with medium to 1/4 of the volume, and the remaining headspace was replaced with H_2:CO_2 (80:20 [v:v], 2×10^5 Pa). To determine the growth behavior, all cultures were inoculated to an optical density of 0.03–0.08 from a pre-culture grown to the exponential growth phase with the same substrate, and then incubated at 65°C under

slow shaking. The determination of the cell density was carried out in three biological replicates. Growth in liquid medium was monitored by measuring the optical density at 600 nm. Plating and cultivation on solid media was carried out according to Basen et al. (2018).

Deletion of HDCR Gene Cluster

Plasmid pMBTkv0012 (**Supplementary Figure S1**) was used for the deletion of HDCR gene cluster consisting of *fdhF, hycB3, hycB4*, and *hydA2* (TKV_c19960-TKV_c19990). The plasmid was generated by inserting 899 and 1001 bp regions adjacent to the four genes of the cluster (upstream flanking region, UFR, and downstream flanking region, DFR, respectively) into the plasmid pMBTkv005 (Basen et al., 2018). The UFR and DFR were amplified by using the primers NP001 (5′- GCTCG GTACC CGGGG ATCCT AAAGT TTAGT GCATT ACCCC TAAAA TAATG G) and NP002 (5′- CCACT ACCAA CAAAA TTTAA CAAAA CCTCC TCTTA TAACA AAGCA GAAAG G) for UFR, and NP003 (5′- GGAGG TTTTG TTAAA TTTTG TTGGT AGTGG GTTGT AAACA ATCC) and NP004 (5′- GCCGC ATGCC TGCAG GTCGA CTCTA GAGTT ATGTT TAATT TTCTT CCAAC CTCAA CGG) for DFR, followed by the fusion of the PCR products, restriction digest with *Xba*I and *Bam*HI, and by ligation into plasmid pMBTkv005.

Thermoanaerobacter kivui Δ*pyrE* was transformed with the plasmid pMBTkv0012, taking advantage of its natural competence for DNA uptake (Basen et al., 2018). The first round of selection was performed in defined media without uracil in the presence of 25 mM glucose + 50mM formate, to select for transformants with the plasmid integrated into the genome. To verify the integration of plasmid pMBTkv012, genomic DNA was extracted and the HDCR gene region was amplified by PCR with the oligonucleotides, NP005 (5′- GATAG GTGAT ACAAT TGAAG TGC) and NP006 (5′- CGCCT CTTGC AAAAC CCG), both binding outside the HDCR gene cluster. Mutants containing the plasmid and growing in the absence of uracil were subjected to a second round of selection as described previously (Basen et al., 2018). Cells were plated on agar with a defined medium containing 50 μM uracil and 5 mM 5-fluoroorotic acid (5-FOA), selecting against the *pyrE* gene. The substrates used were 25 mM glucose + 50mM formate. The genotype of the cells was again checked by using primer pairs NP005/NP006 binding outside and amplifying the complete HDCR gene locus as well as the primer pairs NP001/SJ003 (5′- AGC CGC ATG CCT GCA GGT CGA CTC TAG ATT CAT ATT GAG GCA ATA GTT CAA TAG CC), P9fw (5′- AAA GAT GGT AAA CAG GAA AAG G)/NP007 (5′- CAG GTG TTA AAT CTC CCA AAT), and PBseq10 (5′- GCT CCG GCT ATT AGA GTT TC)/P18brev (5′- GCG TTA TGC CTA CCT ATA TCT TC) each pair leading to the amplification of part of the HDCR gene cluster. The loss of the HDCR gene cluster in the selected *T. kivui* Δ*hdcr* mutant, strain TKV_MB013, was additionally verified by sequencing.

Plasmid pSJ002 (**Supplementary Figure S2**) was constructed to reintroduce the HDCR gene cluster back into the TKV_MB013 genome, between the convergent genes TKV_c24500 (annoted as AAA family ATPase) and TKV_c24520 (annoted as hydroxylamine reductase), therefore likely not causing polar effects (Basen et al., 2018).

Plasmid pJM006 was used as backbone. Plasmid pJM006 was derived from plasmid pMBTkv007 (Basen et al., 2018), with *pyrE* under control of the promoter controlling gyrase from *Thermoanaerobacter* sp. strain X514, and directly adjacent to the 3′-end, gene Teth514_0627 from *Thermoanaerobacter* sp. strain X514 under control of the promoter of the S-layer protein from *T. kivui*. pJM006 except for *adhE* from *Thermoanaerobacter* sp. strain X514 was amplified by PCR using primers SJ0012 (5′- GAG AAA AAA AGT ATA AAA TTT AAT TTA AAA ATT TCA CAG CAA) and SJ0013 (5′- TTT ACC ATC TTT CAT ACA GTC AAT CCT CCT CCT TG). The HDCR gene cluster of *T. kivui* was amplified by using SJ0010 (5′′- GAG GAG GAT TGA CTG TAT GAA AGA TGG TAA ACA GGA AAA) and SJ0011 (5′- TTT TAA ATT AAA TTT TAT ACT TTT TTT CTC GGT GTA TAT TTA G). The PCR products were then fused to generate the plasmid pSJ002, using Gibson Assembly Mastermix (NEB, Frankfurt/Main, Germany). TKV_MB013 was transformed with plasmid pSJ002. Selection for the transformants was performed by using defined media without uracil in the presence of the substrate 25 mM glucose and 50 mM formate.

Biochemical Verification of the Absence of HDCR

Immunological detection of the presence or absence of HDCR subunits in cell-free extracts of *T. kivui* strains was performed using antisera containing antibodies specific for the formate dehydrogenase (FdhF, encoded by TKV_c19990) and the hydrogenase subunit HydA2 of HDCR (encoded by TKV_c19960). First, genes encoding both subunits were cloned into plasmids pRT001 (*fdhF*) and pRT002 (*hydA2*). For pRT001, primers PRT1d (5′- TTT GTT TAA CTT TAA GAA GGA GAT ATA CAT ATG AAA GAT GGT AAA CAG G) and PRT2b (5′- CAA GCT TGT CGA CTC AAT GGT GAT GGT GAT GGT GTT TTC CTC CCT TTT CCT TTG C) were used to amplify the *fdhF* fragment, followed by digestion with restriction enzymes *Nde*I and *Sal*I. For pRT002, *hydA*2 fragment was amplified using primers PRT3 (5′- TTT GTT TAA CTT TAA GAA GGA GAT ATA CAT ATG TCT GCA AAT AAA GCT ATA ATT AAT ATA G) and PRT4 (5′- GTG GTG GTG CTC GAG TGC GGC CGC AAG CTT GTC GAC TTA ATG GTG ATG GTG ATG GTG TAC TTT TTT TCT CGG TGT ATA TTT AG), again followed by digestion with *Nde*I and *Sal*I. Fragments were cloned into vector pET21a, which was digested using the same restriction enzymes according to manufacturer's guidelines (NEB, Frankfurt/Main, Germany). The recombinant, His-tagged versions of FDH or HydA2 were produced in *E. coli* BL21(DE3), purified by affinity chromatography according to standard procedures (Sambrook and Russell, 2001), and sent for rabbit immunization (Davids Biotechnologie, Regensburg, Germany). For Western Blot analysis, 40 μg of *T. kivui* wild type (WT) or TKV_MB013 cell extract was separated *via* denaturing polyacrylamide gel electrophoresis (12%), and immunoblotting onto a nitrocellulose membrane (Protran BA 83; GE Healthcare, United Kingdom) was performed according to standard procedures (Sambrook and Russell, 2001) with goat-anti-rabbit IG, conjugated to horseradish peroxidase (dilution of 1:10,000; Bio-Rad, München, Germany). Rabbit antisera were diluted 1:15,000 (FdhF) and

1:10,000 (HydA2), respectively. The chemiluminescence signal was detected using a chemiluminescence detector (ChemoStar, INTAS, Göttingen, Germany). For comparison of the molecular masses of the detected proteins, two images were recorded of the same membrane, one with and one without chemiluminescence detection; and both images were assembled using the ChemoStar TS software (INTAS, Göttingen, Germany).

Specific HDCR activity in the cell-free extract of *T. kivui* was determined as formate-dependent H_2 production or as H_2- dependent formate production from CO_2 as reported in Schwarz et al. (2018), but at 64°C. Cells for cytoplasmic fraction preparations were harvested in late exponential growth phase and 0.3 mg of cytoplasmic fraction was used for measuring enzymatic activity, respectively. Experiments were conducted in serum bottles and samples for H_2 or formate measurement were taken about every 2 min. H_2 evolution from formate was measured in 950 µl reaction buffer (100 mM HEPES, 20 mM MgSO4, 0.0001% Resazurin, 0.5 mM DTE, pH 7.0, N_2 atmosphere) with 150 mM formate as a substrate. Formate production from H_2/CO_2 (80:20 [v:v] 1.1×10^5 Pa) was measured in 5 ml reaction buffer (100 mM HEPES, 20 mM MgSO4, 0.0001% Resazurin, 0.5 mM DTE, pH 7.0) in a two-step enzyme assay. After starting the assay, samples were taken from the liquid phase every 2 min and stored on ice. Determination of formate concentration was then performed using a commercially available formic acid-kit (Boehringer Mannheim/R-Biopharm AG, Mannheim/Darmstadt, Germany). Concentrations of purified proteins or proteins in the cell-free extract were determined as described previously (Bradford, 1976).

Experiments With Resting Cells

The stoichiometry of metabolite conversion was determined using concentrated suspensions of resting *T. kivui* cells. Initially, 500 ml cultures of *T. kivui* TKV_MB013 (Δ*pyrE*, Δ*fdhF hycB3 hycB4 hydA2*; HDCR deletion mutant) were grown in defined media, in the presence of formate, to the mid exponential phase (OD_{600} of 0.97 to 1.01), and then harvested by centrifugation (Avanti^{TM}J-25 and JA-10 Fixed-Angle Rotor; Beckman Coulter, Brea, CA, United States) at 12,700 × *g*, 4°C for 10 min. The supernatant was discarded and cells were re-suspended in 50 ml of defined media. The centrifugation step was repeated, and then, cells were re-suspended again in 50 ml of defined media, and distributed to 10 ml into Hungate tubes. All steps were performed in an anoxic glove box (Coy Laboratory Products, Grass Lake, United States) with an atmosphere of N_2:CO_2 (80:20 [v:v], 1.1×10^5 Pa) plus approximately 2% H_2. The Hungate tubes were closed with butyl rubber stoppers inside the chamber, taken out, and then H_2 was removed by exchange of the gaseous headspace against N_2:CO_2 (80:20 [v:v], 1.1×10^5 Pa). As substrates, 25 mM glucose + 50 mM formate, 25 mM glucose or 50 mM formate were added to the Hungate tubes. The experiment was started by incubation of the concentrated resting cells in a water bath set to 65°C, under slow shaking. 1 ml of subsamples were taken for protein, substrate and product measurements. The protein concentration was determined according to Schmidt et al. (1963).

Product Analysis

Organic acid and H_2 production were measured by gas chromatography, in accordance with Weghoff and Müller (2016). Consumption of the substrates glucose and formate was determined by high performance liquid chromatography (HPLC, P680 HPLC Pump, ASI-100 Automated Sample Injector and thermostatted Column Compartment TCC-100, Dionex, Sunnyvale, CA, United States). For the sample preparation, cells were spun down by centrifugation at 13,000 rpm for 5 min and 200 µl of supernatant was filled into 2 ml vials containing 400 µl flat bottom glass insert (Agilent Technologies). A HyperREZ XP Carbohydrate H^+ ion exchange column (Thermo Fisher Scientific, Waltham, MA, United States) was used for separation. For elution, degassed 5 mM sulfuric acid was used at a flow rate of 0.6 ml/min. The temperature of the oven was set at 65°C. 10 µl of sample was injected by auto-sampler and analyzed with a refractive index detector (RefractoMax 520; Dionex, Sunnyvale, CA, United States) set at 55°C.

DATA AVAILABILITY STATEMENT

The datasets generated for this study are available on request to the corresponding author.

AUTHOR CONTRIBUTIONS

VM and MB designed the study. SJ and HD performed the experiments and prepared the figures. All authors analyzed the data and wrote the manuscript.

FUNDING

VM and MB are grateful to Deutsche Forschungsgemeinschaft (DFG) for funding. VM was also supported by an Advanced Grant of the European Research Council under the European Union's Horizon 2020 Research and Innovation Program (grant agreement no. 741791). SJ was funded by a fellowship from Deutscher Akademischer Austauschdienst (DAAD). HD was supported by the Deutsche Bundesstiftung Umwelt (DBU) (Ph.D. grant no. 20016/446). We acknowledge financial support by the Deutsche Forschungsgemeinschaft and Universität Rostock/Universitätsmedizin Rostock within the funding programme Open Access Publishing.

ACKNOWLEDGMENTS

The authors gratefully acknowledge Nils Peiter for his help to obtain plasmid pMBTkv012.

SUPPLEMENTARY MATERIAL

The Supplementary Material for this article can be found online at: https://www.frontiersin.org/articles/10.3389/fmicb.2020.00059/full#supplementary-material

REFERENCES

Amend, J. P., Larowe, D. E., Mccollom, T. M., and Shock, E. L. (2013). The energetics of organic synthesis inside and outside the cell. *Philos. Trans. R. Soc. B* 368:20120255. doi: 10.1098/rstb.2012.0255

Basen, M., Geiger, I., Henke, L., and Müller, V. (2018). A genetic system for the thermophilic acetogenic bacterium *Thermoanaerobacter kivui*. *Appl. Environ. Microbiol.* 84:e02210-17. doi: 10.1128/AEM.02210-17

Bertsch, J., and Müller, V. (2015). CO metabolism in the acetogen *Acetobacterium woodii*. *Appl. Environ. Microbiol.* 81, 5949–5956. doi: 10.1128/AEM.01772-15

Biegel, E., and Müller, V. (2010). Bacterial Na+-translocating ferredoxin: NAD+ oxidoreductase. *Proc. Natl. Acad. Sci. U.S.A.* 107, 18138–18142. doi: 10.1073/pnas.1010318107

Bradford, M. M. (1976). Rapid and sensitive method for quantitation of microgram quantities of protein utilizing principle of protein-dye binding. *Anal. Biochem.* 72, 248–254. doi: 10.1016/0003-2697(76)90527-3

Diekert, G., and Wohlfarth, G. (1994). Metabolism of homoacetogens. *Antonie Van Leeuwenhoek* 66, 209–221. doi: 10.1007/bf00871640

Drake, H. L., Gössner, A. S., and Daniel, S. L. (2008). Old acetogens, new light. *Ann. N. Y. Acad. Sci.* 1125, 100–128. doi: 10.1196/annals.1419.016

Fontaine, F. E., Peterson, W. H., Mccoy, E., Johnson, M. J., and Ritter, G. J. (1942). A new type of glucose fermentation by *Clostridium thermoaceticum*. *J. Bacteriol.* 43, 701–715. doi: 10.1128/jb.43.6.701-715.1942

Hess, V., Poehlein, A., Weghoff, M. C., Daniel, R., and Müller, V. (2014). A genome-guided analysis of energy conservation in the thermophilic, cytochrome-free acetogenic bacterium *Thermoanaerobacter kivui*. *BMC Genomics* 15:1139. doi: 10.1186/1471-2164-15-1139

Kerby, R., Niemczura, W., and Zeikus, J. G. (1983). Single-carbon catabolism in acetogens: analysis of carbon flow in *Acetobacterium woodii* and *Butyribacterium methylotrophicum* by fermentation and 13C nuclear magnetic resonance measurement. *J. Bacteriol.* 155, 1208–1218. doi: 10.1128/jb.155.3.1208-1218.1983

Kerby, R., and Zeikus, J. G. (1987). Anaerobic catabolism of formate to acetate and CO2 by *Butyribacterium methylotrophicum*. *J. Bacteriol.* 169, 2063–2068. doi: 10.1128/jb.169.5.2063-2068.1987

Lang, S. Q., Butterfield, D. A., Schulte, M., Kelley, D. S., and Lilley, M. D. (2010). Elevated concentrations of formate, acetate and dissolved organic carbon found at the Lost City hydrothermal field. *Geochim. Cosmochim. Acta* 74, 941–952. doi: 10.1016/j.gca.2009.10.045

Leigh, J. A., Mayer, F., and Wolfe, R. S. (1981). *Acetogenium kivui*, a new thermophilic hydrogen-oxidizing, acetogenic bacterium. *Arch. Microbiol.* 129, 275–280. doi: 10.1007/bf00414697

Ljungdahl, L. G. (1986). The autotrophic pathway of acetate synthesis in acetogenic bacteria. *Annu. Rev. Microbiol.* 40, 415–450. doi: 10.1146/annurev.mi.40.100186.002215

Matson, E. G., Zhang, X. N., and Leadbetter, J. R. (2010). Selenium controls transcription of paralogous formate dehydrogenase genes in the termite gut acetogen, *Treponema primitia*. *Environ. Microbiol.* 12, 2245–2258. doi: 10.1111/j.1462-2920.2010.02188.x

Mcdowall, J. S., Murphy, B. J., Haumann, M., Palmer, T., Armstrong, F. A., and Sargent, F. (2014). Bacterial formate hydrogenlyase complex. *Proc. Natl. Acad. Sci. U.S.A.* 111, E3948–E3956.

Mcternan, P. M., Chandrayan, S. K., Wu, C. H., Vaccaro, B. J., Lancaster, W. A., Yang, Q. Y., et al. (2014). Intact functional fourteen-subunit respiratory membrane-bound [NiFe]-hydrogenase complex of the hyperthermophilic archaeon *Pyrococcus furiosus*. *J. Biol. Chem.* 289, 19364–19372. doi: 10.1074/jbc.M114.567255

Moon, J., Henke, L., Merz, N., and Basen, M. (2019). A thermostable mannitol-1-phosphate dehydrogenase is required in mannitol metabolism of the thermophilic acetogenic bacterium *Thermoanaerobacter kivui*. *Environ. Microbiol.* 21, 3728–3736. doi: 10.1111/1462-2920.14720

Müller, V. (2019). New horizons in acetogenic conversion of one-carbon substrates and biological hydrogen storage. *Trends Biotechnol.* 37, 1344–1354. doi: 10.1016/j.tibtech.2019.05.008

Pereira, I. A. C. (2013). An enzymatic route to H2 storage. *Science* 342, 1329–1330. doi: 10.1126/science.1247698

Pierce, E., Xie, G., Barabote, R. D., Saunders, E., Han, C. S., Detter, J. C., et al. (2008). The complete genome sequence of *Moorella thermoacetica* (f. *Clostridium thermoaceticum*). *Environ. Microbiol.* 10, 2550–2573. doi: 10.1111/j.1462-2920.2008.01679.x

Pinske, C., and Sargent, F. (2016). Exploring the directionality of *Escherichia coli* formate hydrogenlyase: a membrane-bound enzyme capable of fixing carbon dioxide to organic acid. *Microbiologyopen* 5, 721–737. doi: 10.1002/mbo3.365

Poehlein, A., Cebulla, M., Ilg, M. M., Bengelsdorf, F. R., Schiel-Bengelsdorf, B., Whited, G., et al. (2015). The complete genome sequence of *Clostridium aceticum*: a missing link between Rnf- and cytochrome-containing autotrophic acetogens. *mBio* 6:e1168-15. doi: 10.1128/mBio.01168-15

Poehlein, A., Schmidt, S., Kaster, A. K., Goenrich, M., Vollmers, J., Thurmer, A., et al. (2012). An ancient pathway combining carbon dioxide fixation with the generation and utilization of a sodium ion gradient for ATP synthesis. *PLoS One* 7:e33439. doi: 10.1371/journal.pone.0033439

Sambrook, J., and Russell, D. W. (eds) (2001). *Molecular Cloning: A Laboratory Manual*. Cold Spring Harbor, NY: Cold Spring Harbor Laboratory Press.

Sapra, R., Bagramyan, K., and Adams, M. W. W. (2003). A simple energy-conserving system: proton reduction coupled to proton translocation. *Proc. Natl. Acad. Sci. U.S.A.* 100, 7545–7550. doi: 10.1073/pnas.1331436100

Schink, B., and Stams, A. (2006). "Syntrophism among prokaryotes," in *The Prokaryotes – A Handbook on the Biology of Bacteria*, 3rd Edn, eds M. Dworkin, S. Falkow, E. Rosenberg, K. H. Schleifer, and E. Stackebrandt, (New York, NY: Springer Science+Business Media, LLC), 309–336.

Schmidt, K., Jensen, S. L., and Schlegel, H. (1963). Die Carotinoide der *Thiorhodaceae*. *Arch. Mikrobiol.* 46, 117–126. doi: 10.1007/bf00408204

Schoelmerich, M. C., and Müller, V. (2019). Energy conservation by a hydrogenase-dependent chemiosmotic mechanism in an ancient metabolic pathway. *Proc. Natl. Acad. Sci. U.S.A.* 116, 6329–6334. doi: 10.1073/pnas.1818580116

Schuchmann, K., and Müller, V. (2012). A bacterial electron-bifurcating hydrogenase. *J. Biol. Chem.* 287, 31165–31171. doi: 10.1074/jbc.M112.395038

Schuchmann, K., and Müller, V. (2013). Direct and reversible hydrogenation of CO2 to formate by a bacterial carbon dioxide reductase. *Science* 342, 1382–1385. doi: 10.1126/science.1244758

Schuchmann, K., and Müller, V. (2014). Autotrophy at the thermodynamic limit of life: a model for energy conservation in acetogenic bacteria. *Nat. Rev. Microbiol.* 12, 809–821. doi: 10.1038/nrmicro3365

Schuchmann, K., and Müller, V. (2016). Energetics and application of heterotrophy in acetogenic bacteria. *Appl. Environ. Microbiol.* 82, 4056–4069. doi: 10.1128/AEM.00882-16

Schut, G. J., and Adams, M. W. W. (2009). The iron-hydrogenase of *Thermotoga maritima* utilizes ferredoxin and NADH synergistically: a new perspective on anaerobic hydrogen production. *J. Bacteriol.* 191, 4451–4457. doi: 10.1128/JB.01582-08

Schwarz, F. M., Schuchmann, K., and Müller, V. (2018). Hydrogenation of CO2 at ambient pressure catalyzed by a highly active thermostable biocatalyst. *Biotechnol. Biofuels* 11:237. doi: 10.1186/s13068-018-1236-3

Trchounian, A., and Sawers, G. R. (2014). Novel insights into the bioenergetics of mixed-acid fermentation: can hydrogen and proton cycles combine to help maintain a proton motive force? *IUBMB Life* 66, 1–7. doi: 10.1002/iub.1236

Weghoff, M. C., and Müller, V. (2016). CO metabolism in the thermophilic acetogen *Thermoanaerobacter kivui*. *Appl. Environ. Microbiol.* 82, 2312–2319. doi: 10.1128/AEM.00122-16

Weiss, M. C., Sousa, F. L., Mrnjavac, N., Neukirchen, S., Roettger, M., Nelson-Sathi, S., et al. (2016). The physiology and habitat of the last universal common ancestor. *Nat. Microbiol.* 1:16116. doi: 10.1038/nmicrobiol.2016.116

Welte, C., Kallnik, V., Grapp, M., Bender, G., Ragsdale, S., and Deppenmeier, U. (2010). Function of Ech hydrogenase in ferredoxin-dependent,

membrane-bound electron transport in *Methanosarcina mazei*. *J. Bacteriol.* 192, 674–678. doi: 10.1128/JB.01307-09

Westphal, L., Wiechmann, A., Baker, J., Minton, N. P., and Müller, V. (2018). The Rnf complex is an energy-coupled transhydrogenase essential to reversibly link cellular NADH and ferredoxin pools in the acetogen *Acetobacterium woodii*. *J. Bacteriol.* 200:e00357-18. doi: 10.1128/JB.00357-18

Wood, H. G., Ragsdale, S. W., and Pezacka, E. (1986). The acetyl-CoA pathway of autotrophic growth. *FEMS Microbiol. Lett.* 39, 345–362. doi: 10.1111/j.1574-6968.1986.tb01865.x

Conflict of Interest: The authors declare that the research was conducted in the absence of any commercial or financial relationships that could be construed as a potential conflict of interest.

frontiers in Microbiology

ORIGINAL RESEARCH
published: 31 January 2020
doi: 10.3389/fmicb.2020.00058

Enrichment of Anaerobic Syngas-Converting Communities and Isolation of a Novel Carboxydotrophic *Acetobacterium wieringae* Strain JM

Ana L. Arantes[1,2†], João P. C. Moreira[1,2†], Martijn Diender[1], Sofiya N. Parshina[1,3], Alfons J. M. Stams[1,2], M. Madalena Alves[2], Joana I. Alves[2] and Diana Z. Sousa[1]*

[1] Laboratory of Microbiology, Wageningen University & Research, Wageningen, Netherlands, [2] Centre of Biological Engineering, University of Minho, Braga, Portugal, [3] Laboratory of Microbiology of Anthropogenic Habitats of Winogradsky Institute of Microbiology, Federal State Institution (Fundamentals of Biotechnology) of the Russian Academy of Sciences, Moscow, Russia

OPEN ACCESS

Edited by:
Mirko Basen,
University of Rostock, Germany

Reviewed by:
Michael Pester,
German Collection of Microorganisms and Cell Cultures GmbH (DSMZ), Germany
Isao Yumoto,
National Institute of Advanced Industrial Science and Technology (AIST), Japan

***Correspondence:**
Diana Z. Sousa
diana.sousa@wur.nl

[†] These authors have contributed equally to this work

Specialty section:
This article was submitted to Microbial Physiology and Metabolism, a section of the journal Frontiers in Microbiology

Received: 30 September 2019
Accepted: 13 January 2020
Published: 31 January 2020

Citation:
Arantes AL, Moreira JPC, Diender M, Parshina SN, Stams AJM, Alves MM, Alves JI and Sousa DZ (2020) Enrichment of Anaerobic Syngas-Converting Communities and Isolation of a Novel Carboxydotrophic Acetobacterium wieringae Strain JM. Front. Microbiol. 11:58. doi: 10.3389/fmicb.2020.00058

Syngas is a substrate for the anaerobic bioproduction of fuels and valuable chemicals. In this study, anaerobic sludge was used for microbial enrichments with synthetic syngas and acetate as main substrates. The objectives of this study were to identify microbial networks (in enrichment cultures) for the conversion of syngas to added-value products, and to isolate robust, non-fastidious carboxydotrophs. Enrichment cultures produced methane and propionate, this last one an unusual product from syngas fermentation. A bacterium closely related to *Acetobacterium wieringae* was identified as most prevalent (87% relative abundance) in the enrichments. *Methanospirillum* sp. and propionate-producing bacteria clustering within the genera *Anaerotignum* and *Pelobacter* were also found. Further on, strain JM, was isolated and was found to be 99% identical (16S rRNA gene) to *A. wieringae* DSM 1911^T. Digital DNA-DNA hybridization (dDDH) value between the genomes of strain JM and *A. wieringae* was 77.1%, indicating that strain JM is a new strain of *A. wieringae*. Strain JM can grow on carbon monoxide (100% CO, total pressure 170 kPa) without yeast extract or formate, producing mainly acetate. Remarkably, conversion of CO by strain JM showed shorter lag phase than in cultures of *A. wieringae* DSM 1911^T, and about four times higher amount of CO was consumed in 7 days. Genome analysis suggests that strain JM uses the Wood-Ljungdahl pathway for the conversion of one carbon compounds (CO, formate, CO_2/H_2). Genes encoding bifurcational enzyme complexes with similarity to the bifurcational formate dehydrogenase (Fdh) of *Clostridium autoethanogenum* are present, and possibly relate to the higher tolerance to CO of strain JM compared to other *Acetobacterium* species. *A. wieringae* DSM 1911^T grew on CO in medium containing 1 mM formate.

Keywords: carbon monoxide, syngas, carboxydotrophs, acetogens, *Acetobacterium*

INTRODUCTION

In the frame of a circular bio-economy, it is essential to develop technologies for the sustainable conversion of waste materials to fuels and chemicals. Solutions combining the gasification of low-biodegradable wastes, such as lignocellulosic materials, plastic-based wastes, or municipal solid waste, with the biological conversion of the generated syngas have been subject of growing interest and show excellent perspectives (Bengelsdorf et al., 2018; Yasin et al., 2019). Some microbes can grow on carbon monoxide (CO) and/or CO_2/H_2, which are the main components in syngas. Acetogenic organisms are used in commercial syngas fermentation, such as the LanzaTech® process, to produce ethanol from CO-rich streams (Dürre and Eikmanns, 2015; Molitor et al., 2016; De Tissera et al., 2017; Redl et al., 2017). Carboxydotrophic acetogens are phylogenetically diverse and have been isolated from a variety of habitats including soil, sediments, intestinal tracts of animals and humans (Diender et al., 2015). Acetogens utilize the Wood-Ljungdahl pathway (WL pathway), also known as reductive acetyl-CoA pathway, to conserve energy for growth and perform CO_2 fixation (Ragsdale and Pierce, 2008). The most studied acetogenic bacteria include *Acetobacterium woodii*, *Clostridium ljungdahlii*, *Clostridium autoethanogenum*, *Clostridium carboxidivorans*, *Eubacterium limosum*, *Moorella thermoacetica*, and *Moorella thermoautotrophica* (Bengelsdorf et al., 2018; Müller, 2019). With C1-compounds, some acetogens mainly produce acetate, while others also produce alcohols, such as butanol and hexanol (Diender et al., 2015; Phillips et al., 2015; Abubackar et al., 2016, 2018; Bengelsdorf et al., 2018).

In this work, anaerobic sludge, previously acclimatized to syngas in a continuous bioreactor (Pereira, 2014), was used to start the enrichment of microorganisms capable of converting CO/syngas. Analysis of microbial communities in enrichment cultures allowed the identification of a predominant acetogen closely related to *Acetobacterium wieringae*, together with bacteria clustering within *Anaerotignum* and *Pelobacter* genera. A novel carboxydotrophic acetogen, *A. wieringae* strain JM, was isolated. Growth of strain JM on CO was compared with that of *A. wieringae* DSM 1911^T and *A. woodii* DSM 1030^T.

MATERIALS AND METHODS

Media and Microorganisms

The basal medium for the cultivation of the microbial cultures contained the following (l^{-1}): $Na_2HPO_4.2H_2O$, 0.53 g; KH_2PO_4, 0.41 g; NH_4Cl, 0.3 g; $CaCl_2.2H_20$, 0.11 g; $MgCl_2.6H_20$, 0.10 g; NaCl, 0.3 g; $NaHCO_3$, 4.0 g; and $Na_2S.\ 9H_20$, 0.48 g [as well as acid and alkaline trace elements (each, 1 ml/liter) and vitamins (0.2 ml/liter) prepared as described by Stams et al. (1993)]. For incubations with 100% CO, phosphate buffer medium was used and prepared as described previously by Alves et al. (2013). The headspace of the bottles was pressurized to 170 kPa with 100% (v/v) CO, syngas mixture [CO, H_2, and CO_2 (60:30:10%, v/v)] or H_2-free syngas [CO, N_2, and CO_2 (60:30:10%, v/v)]. The final pH of the media was 7.0–7.2. Medium was autoclaved and before inoculation supplemented with vitamins and reduced with 0.8 mM sodium sulfide ($Na_2S{\cdot}7\text{-}9H_2O$; Stams et al., 1993).

Anaerobic granular sludge from a multi-orifice baffled bioreactor (MOBB) (temperature: 35–37°C; pH: 5.8–6.7) fed with a syngas mixture (60% CO, 30% H_2, and 10% CO_2 (v/v); Pereira, 2014) was used as inoculum for enrichment. *Acetobacterium wieringae* (DSM 1911^T) and *A. woodii* (DSM 1030^T) were purchased from DSMZ (German Collection of Microorganisms and Cell Culture, Braunschweig, Germany).

Enrichment Cultures and Isolation of Strain JM

Enrichment cultures were coded as culture JM(x), where x represents the number of successive transfers (in a total of 18 transfers). Enrichments were started by inoculation of anaerobic sludge (5%, v/v) in anaerobic basal medium (described above). First incubations were done with 170 kPa of syngas [CO, H_2 and CO_2 (60:30:10%, v/v)]; acetate (20 mM) was added to the medium as a trial to promote solventogenic metabolism and divert acetogenesis; no yeast extract or formate were supplemented. Cultivation of enrichments was done under non-shaking conditions at 37°C and pH 7.0.

Growth of the highly enriched culture JM(16) was tested using a syngas mixture [60% CO, 30% H_2, and 10% CO_2 (v/v)] (total pressure 170 kPa) with or without acetate (20 mM). The microbial communities of cultures JM(7) and JM(16) were accessed by 16S rRNA gene analysis (cloning and sequencing, and Illumina® sequencing).

Culture JM(16) was used for the isolation of *Acetobacterium wieringae* strain JM (the most dominant bacterium in that enrichment). Strain JM was further enriched by using dilution technique (up to 10^{-10}), using medium described above and supplemented with 1 mM of formate and under a headspace of 60% CO and 40% N_2 (v/v) (total pressure 170 kPa). The resulting culture was inoculated in roll tubes with 1.5% low melting point agarose (using the same medium and headspace composition) and incubated at 37°C. Colonies were picked and inoculated in fresh liquid phosphate-buffered basal medium supplemented with 1 mM of formate and 0.1 g/l of yeast extract and under a headspace of 60% CO and 40% N_2 (v/v) (total pressure 170 kPa), and incubated at 37°C statically. Purity was checked by phase contrast microscopy using a Leica DM2000 microscope (Leica, Microsystems, Weltzar, Germany) and by direct sequencing of the 16S rRNA gene (GATC Biotech, Konstanz, Germany).

Characterization of Strain JM

The optimum and range of temperature for growth, and ability of growth with different soluble (final concentration of 20 mM) and gaseous (total pressure 170 kPa) substrates were tested. Substrates tested included: D-fructose, D-glucose, sucrose, xylose, lactate, formate, glycerol, ethanol, methanol, pyruvate, fumarate, citrate, glycine, malate, mannitol, galactose, melibiose, glutamate, galactitol, sorbitol, lactose, maltose, serine, H_2/CO_2 [80:20% (v/v)], CO [100% (v/v)], CO [50% (v/v)], CO [50% (v/v)] plus acetate, and mixture of CO + H_2/CO_2 [Syngas: 60% CO, 30% H_2, and 10% CO_2 (v/v)]. Substrate tests were done at the optimum temperature (30°C) and shaken at 130

rpm. Additionally, comparison tests of strain JM and type strains *A. wieringae* DSM 1911^T and *A. woodii* DSM 1030^T were also done at 30°C and at 130 rpm shaking using CO (50%, 170 kPa); medium was supplemented with 20 mM acetate and 1 mM formate. In these experiments CO was refilled as it was consumed.

DNA Isolation, PCR, Sequencing, and Phylogenetic Analysis

Twenty milliliter of enrichment cultures JM(7) and JM(16) were used for DNA extraction using the FastDNA SPIN kit for soil (MP Biomedicals, Solon, OH), according to the manufacturer's instructions. Bacterial and archaeal 16S rRNA gene fragments were amplified by PCR, using respectively the primer sets 27F/1492R (Nübel et al., 1996) and A109F/1386R (Gagliano et al., 2015). PCR programs and reaction mixtures used were as described elsewhere (Sousa et al., 2007). The PCR products were purified and cloned in *Escherichia coli* XL-blue competent cells (Agilent Technologies, Santa Clara, CA) as previously described by Sousa et al. (2007). Plasmid amplification and sanger sequencing was done by GATC biotech (Konstanz, Germany). For bacterial isolates, colony PCR was performed using the same primer set and programme described above, and PCR products were sent to GATC biotech (Konstanz, Germany) for sequencing. 16S rRNA gene sequences were assembled with DNA baser software version 4.36.0 (Heracle BioSoft S.R.L, http://www.dnabaser.com) and further compared with the GenBank database (Altschul et al., 1990) using the NCBI BLAST search tool. Illumina Miseq platform sequencing was performed at the research and testing laboratory—RTL Genomics (Lubbock, TX). The MiSeq method used was the Illumina two-step using universal primers for bacteria and archaea, 515f and 806r developed by Caporaso et al. (2011). After sequencing, the data were processed using the data analysis pipeline from RTL, which consists in two major steps, the denoising and chimera detection step and the microbial diversity analysis step, as described in the company procedures.

The 16S rRNA gene sequence of strain JM was submitted to the European Nucleotide Database (ENA) and is available under the accession number LR655884. All the other 16S rRNA gene sequences obtained were submitted to ENA, under the following accession numbers: clones sequences (Sanger sequencing)—from LR657299 to LR657303; sequences from Illumina MiSeq platform—project PRJEB33623.

Genome Sequencing, Assembling, and Annotation

DNA was extracted from 50 mL of a grown culture of strain JM using MasterPure^{TM} Gram positive DNA purification Kit (Epicenter, Madison, WI). DNA quality was checked by electrophoresis in a 0.8% (w/v) agarose gel, using a mass standard (lambda phage DNA) and a size marker (Hind III digested lambda phage DNA). The genome of strain JM was sequenced using Illumina HiSeq X Ten platform (Illumina Inc., San Diego, CA) at Novogene (Beijing, China). Genome was assembled using a pipeline comprising: Ray (Boisvert et al., 2012) to generate an initial assembly, followed by Opera (Gao et al., 2011) for genome scaffolding, and CAP3 (Huang and Madan, 1999) for assembling optimization. For Ray assembler, the optimal kmer size was calculated with KmerGenie (Chikhi and Medvedev, 2014). Automated annotation was performed using the RAST annotation server (Aziz et al., 2008), followed by manual curation. Digital DNA-DNA hybridization value (dDDH) of strain JM and *A. wieringae* DSM 1911^T were obtained using the Genome-to-Genome Distance Calculator 2.1 (GGDC; https://ggdc.dsmz.de; Meier-Kolthoff et al., 2013, 2014).

The Whole Genome Shotgun project of *Acetobacterium wieringae* strain JM has been deposited at DDBJ/ENA/GenBank under the accession VSLA00000000.

Analytical Techniques

Organic acids and alcohols were analyzed via high pressure liquid chromatography (HPLC) equipped with a MetaCarb 67H column (Agilent Technologies, Santa Clara, CA). The column was operated at a temperature of 45°C with a flow rate of 0.8 ml min^{-1}. Detection was done via a RI and UV detector. 0.01 N H_2SO_4 was used as eluent. Samples of 1.0 ml were taken and immediately centrifuged at 13,000 *g*. Subsequently, vials for HPLC analysis were prepared with the supernatant and 30 mM of arabinose solution with the ratio of 8:2 (v/v). Gas analysis was done by gas chromatography (GC). Gas samples of 0.2 ml were taken using a 1 ml syringe and analyzed in a Compact GC 4.0 (Global Analyser Solutions, Breda, The Netherlands). CO, CH_4, and H_2 were measured using a molsieve 5A column operated at 100°C coupled to a Carboxen 1010 pre-column. CO_2 was measured using a Rt-Q-BOND column operated at 80°C. Detection was done via a thermal conductivity detector.

RESULTS

Physiological and Microbial Characterization of Enrichment Culture JM

Incubation and several transfers of anaerobic sludge with syngas and acetate as substrates, resulted in an enriched culture (culture JM), producing methane and propionate. Substrate consumption and product formation by culture JM(7) are shown in **Figure 1**: syngas (43 mmol L_{medium}^{-1} of CO and 20 mmol L_{medium}^{-1} of H_2) and acetate (17 mM) were completely converted and resulted in 16 mmol L_{medium}^{-1} of methane and 2.4 mM of propionate (**Figure 1A**). In subsequent transfers, acetate consumption by the enrichment cultures stopped as shown for culture JM(16) (**Figure 1B**). When only syngas was added to the culture as substrate, acetogenic activity could be observed (**Figure 1C**).

The microbial diversity of the enriched culture JM(7) consisted for about 50% of bacteria affiliated with the genus *Acetobacterium*, while the most abundant methanogen was closely related to *Methanospirilum hungatei* (24%) (**Table 1A**). In culture JM(16), an organism closely related to *A. wieringae* DSM 1911^T (99% of 16S rRNA gene identity) was highly prevalent (87%) (**Table 1B**). A small fraction of organisms (3%) was related to known propionate producers, namely *Anaerotignum neopropionicum* strain DSM 3847^T (former *Clostridium neopropionicum*) (97% of 16S rRNA gene identity)

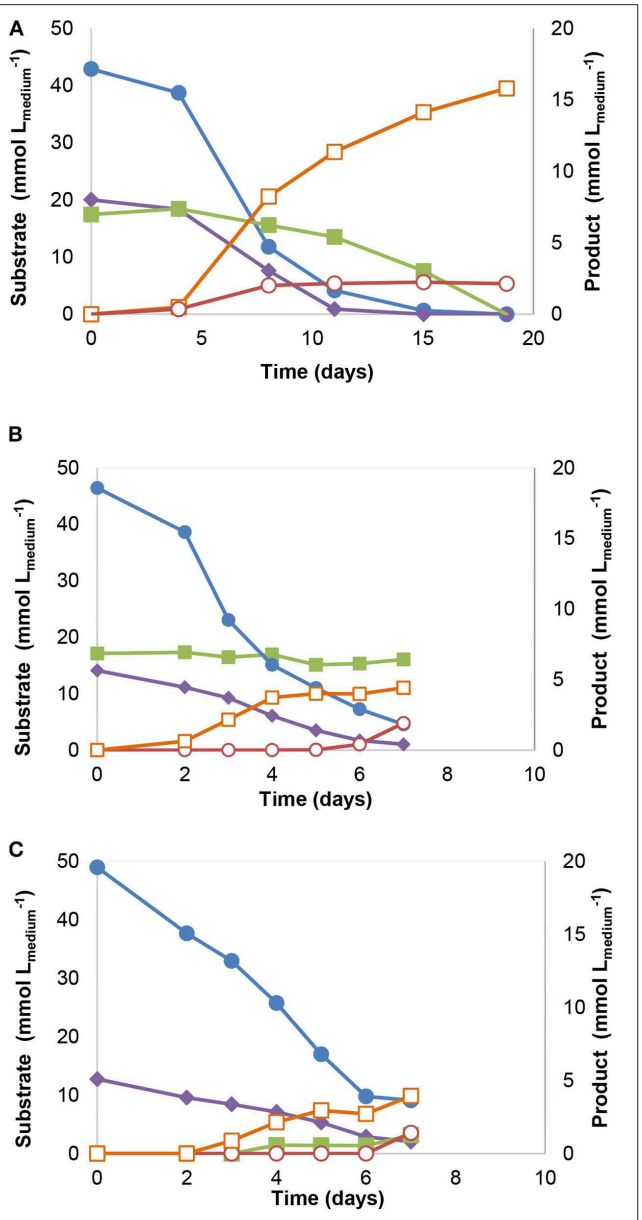

FIGURE 1 | Substrate consumption and product formation by stable enrichment JM cultures with different substrates: **(A)** Syngas and acetate [JM(7)], **(B)** Syngas and acetate [JM(16)] and **(C)** Syngas [JM(16)]. Symbols: (●) carbon monoxide, (◆) hydrogen, (■) acetate, (□) methane, and (○) propionate.

and *Pelobacter propionicus* DSM 2379 ^{T} (92% of 16S rRNA gene identity). From the archaeal domain, *Methanospirillum hungatei* was most dominant (94% of the archaeal clones; **Table 1B**).

Isolation and Physiological Characterization of *Acetobacterium wieringae* Strain JM

Isolation of strain JM was done by 10-fold dilution series (up to 10^{-10}) of culture JM(16), using CO as sole carbon and energy source. After several rounds of dilution series in liquid and solid media, a pure culture (strain JM) was obtained. The 16S rRNA gene sequence was 99% identical to that of *A. wieringae* DSM 1911^{T}. Digital DNA-DNA hybridization (dDDH) between strain JM and *A. wieringae* DSM 1911^{T} was 77.1%, which is above the 70% cut-off value generally recommended for species differentiation (Meier-Kolthoff et al., 2013). These results indicate that strain JM is a novel *A. wieringae* strain.

Strain JM is a rod-shaped bacterium with an optimal temperature for growth at 30°C (growth between 20 and 37°C). Strain JM can utilize and grow on CO, without the need of supplementation with yeast extract or formate. Growth on syngas (60% CO, 30% H_2, and 10% CO_2, 170 kPa), CO (50% CO and 50% N_2, 170 kPa), CO (50% CO and 50% N_2, 170 kPa) plus acetate, and CO (100%, 170 kPa) yielded acetate and CO_2 (**Figure 2**). Growth on syngas (**Figure 2A**) led to the production of higher amounts of acetate (25.3 ± 0.8 mM) and lower CO_2 accumulation (22.9 ± 0.9 mM) than growth on 50% CO (13.7 ± 0.1 mM acetate, 56.1 ± 2.9 mM CO_2; **Figure 2B**). When acetate was added as co-substrate (**Figure 2C**), lower acetate concentrations were reached (11.5 ± 0.9 mM acetate), though no different fermentation products were detected. On the other hand, growth of strain JM with 100% CO in the headspace (55.6 ± 0.8 mmol L_{medium}^{-1}), yielded ethanol (1.8 ± 0.2 mM) in addition to acetate and CO_2 (**Figure 2D**).

The following substrates were tested and utilized by strain JM: H_2/CO_2, CO, H_2/CO_2 + CO, D-fructose, D-glucose, sucrose, xylose, lactate, formate, glycerol, ethanol, methanol, pyruvate, fumarate, citrate, glycine, malate, mannitol, galactose, melibiose, glutamate, galactitol, and sorbitol. Substrates tested that could not be utilized were: lactose, maltose, and serine.

Parallel growth experiments with CO-acetate as substrates (supplemented with 1 mM formate) were performed for strain JM (**Figure 3A**), and its closest relatives *A. wieringae* DSM 1911^{T} (**Figure 3B**) and *A. woodii* DSM 1030^{T} (**Figure 3C**). CO was refilled to 170 kPa once it was consumed. Strain JM consumed 107.9 mmol L_{medium}^{-1} of CO in 7 days (**Figure 3A**). Performance of *A. wieringae* and *A. woodii* during CO conversion was lower: *A. wieringae* consumed 43.1 mmol L_{medium}^{-1} of CO in 11 days on CO-acetate (**Figure 3B**), while *A. woodii* was able to convert 78.5 mmol L_{medium}^{-1} of CO in 7 days on CO-acetate (**Figure 3C**).

Genome Analysis

Genome assembly of strain JM produced 44 contigs with an N50 size of 195,031 bp. The draft genome sequence consists of 3.61 Mbp and a G+C content of 44.3 mol%. The genome has 3,240 protein-coding genes, 46 tRNA genes, and 12 rRNA genes. All enzymes of the WL pathway are encoded for in the genome of strain JM (**Figure 4**), supporting its ability to grow on H_2/CO_2 and/or CO. One formate dehydrogenase (Fdh) (TYC86388) was annotated in the genome, showing similarity to the formate dehydrogenase subunit H (FdhH) of the hydrogen-dependent carbon dioxide reductase (HDCR) complex found in *A. woodii* (Bertsch and Müller, 2015). The genes of the HDCR associated hydrogenase were not found in the vicinity of this Fdh. As the Fdh was located at the end of a contig, it is possible that associated hydrogenase subunits were missed. Genes of the rest of the methyl-branch of the WL pathway are located adjacent to each other, including formyl-THF ligase (TYC83982-83), a bifunctional 5,10-methylenetetrahydrofolate

TABLE 1 | Microbial community analysis of cultures JM(7) and JM(16).

(A) Microbial community analysis of culture JM(7) – Illumina MiSeq

	Closest relatives	Number (%) [a]	Query Coverage (%)	Identity (%)
Bacteria	*Acetobacterium* sp. (*Acetobacterium* sp. strain SVCO-15 16S ribosomal RNA gene, partial sequence) [b]	50	100	99
	Desulfovibrio sp. (*Desulfovibrio* sp. S10 gene for 16S ribosomal RNA, partial sequence) [b]	8	100	100
Archaea	*Methanospirillum* sp. (*Methanospirillum hungatei* strain JF-1 16S ribosomal RNA gene, complete sequence) [b]	24	93	99

(B) Microbial community analysis of culture JM(16) – Cloning and Sanger Sequencing

	Closest relatives	Relative abundance (%) [c]	Query coverage (%)	Identity (%)
Bacteria	*Acetobacterium wieringae* (*Acetobacterium wieringae* strain DP9 16S ribosomal RNA gene, partial sequence) [d]	87	98	99
	Anaerotignum neopropionicum (*Anaerotignum neopropionicum* strain DSM 3847 16S ribossomal RNA, partial sequence) [d]	2	94	97
	Pelobacter propionicus (*Pelobacter propionicus* strain DSM 2379 16S ribossomal RNA, partial sequence) [d]	1	94	92
Archaea	*Methanospririllum hungatei* (*Methanospirillum hungatei* JF-1, complete genome) [d]	94	95	99
	Methanothrix soehngenii (*Methanothrix soehngenii* GP6, complete genome) [d]	4	94	99

[a] *Percentage calculated based on the number of sequence counts obtained for the total community by Illumina sequencing, 27817.*
[b] *Results of sequence alignment by using BLAST toward the NCBI nucleotide database of partial 16S rRNA gene sequences (~291 bp; results obtained from amplicon Illumina sequencing).*
[c] *Percentage calculated based on the total number of clones obtained for each domain: 96 clones for Bacteria and 96 clones for Archaea.*
[d] *Results of sequence alignment by using BLAST toward the NCBI nucleotide database of partial 16S rRNA gene sequences (~1,000 bp; results obtained from cloning and sequencing).*

dehydrogenase/5,10-methenyltetrahydrofolate cyclohydrolase (TYC83959-60) and a methylene-THF reductase (TYC83962-63). Two carbon monoxide dehydrogenases (*codh*) encoding genes (TYC86630, TYC87911-12) were identified. TYC87911-12 is located in close vicinity to a gene sequence encoding for a acetyl-CoA synthase (*acs*) complex (TYC87909-87910) and thus likely serves a dual function: CO-oxidation and acetyl-CoA formation. TYC 86630 appears to have a CODH catalytic subunit (CooS) motive and is next to an iron-sulfur cluster domain protein, suggesting it encodes for a monofunctional CODH. Several genes in the genome (e.g., TYC85757-59, TYC86583-84) show similarity to bifurcating complexes such as the NADH-dependent reduced ferredoxin:$NADP^+$ oxidoreductase (Nfn) complex, or the bifurcating Fdh/[Fe-Fe] hydrogenase complex (Wang et al., 2013). Additionally, two blocks of genes encode for a Ferredoxin:NAD^+ oxidoreductase (Rnf) complex (TYC 88316-21, TYC84275-84280), typically involved in the build-up of a cation gradient.

Genes encoding for acetate and ethanol formation pathways are present. This includes an acetate kinase (*ack*) (TYC88392) and several alcohol/acetaldehyde dehydrogenase genes (**Figure 4**). Additionally, the genome contains two acetaldehyde:ferredoxin oxidoreductase genes (TYC88292, TYC84206), of which the latter is located next to a gene coding for an alcohol dehydrogenase. Pyruvate:ferredoxin oxidoreductase (TYC86008) is present for the formation of pyruvate from acetyl-CoA, allowing for assimilation metabolism.

General propionate formation pathways (e.g., methylmalonyl-pathway), are not annotated or not complete in strain JM. Nevertheless, pathways for conversion of propanoyl-CoA to propionate are present, so indirect formation of propionate from e.g., amino acid metabolism is potentially possible.

DISCUSSION

A novel carboxydotrophic *A. wieringae* (strain JM) was isolated from a syngas-converting enrichment culture, producing mainly acetate and small amounts of ethanol from CO. The fact that *Acetobacterium* species were the most predominant bacteria in the enrichment cultures (**Table 1**), and acetate one of the main products detected in the enrichments, suggests that this bacterium was the main CO-utilizer in the enrichment cultures. Microorganisms closely related to *A. neopropionicum* (2% of total sequences) and *P. propionicus* (1% of total sequences) were present in the enrichment cultures JM(16) (**Table 1**), and were likely responsible for propionate production (**Figures 1B,C**). *A. neopropionicum* and *P. propionicus* are known for their capability to convert ethanol to propionate (Schink et al.,

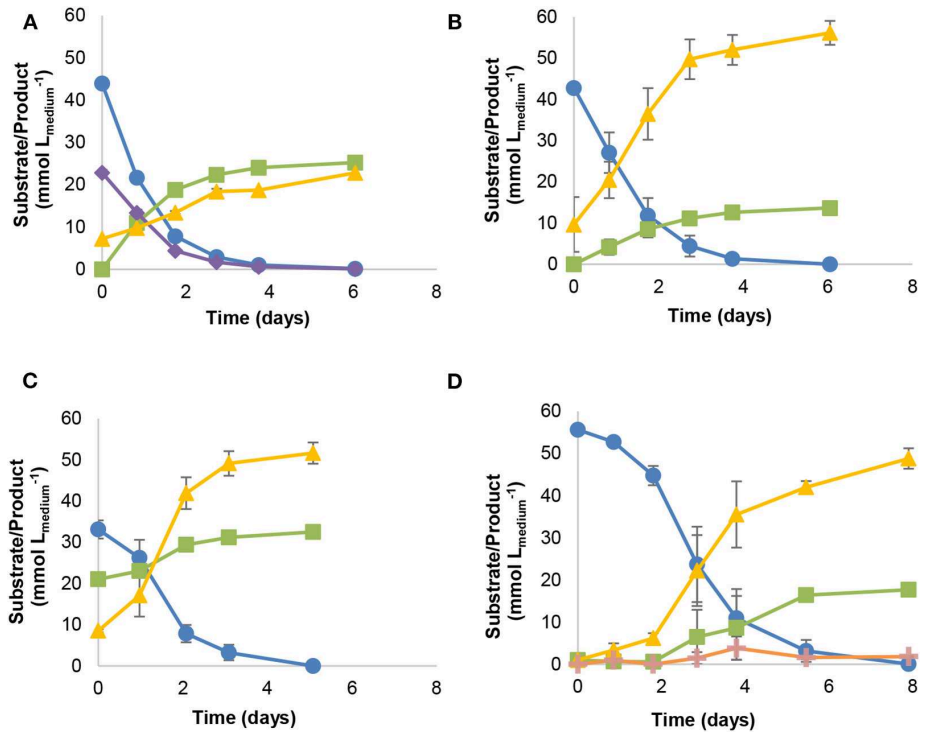

FIGURE 2 | Batch growth of strain JM with different substrate combinations: **(A)** syngas, **(B)** 50% CO, **(C)** 50% CO and acetate (20 mM), **(D)** 100% CO. Symbols: (●) carbon monoxide, (■) acetate, (◆) hydrogen, (▲) carbon dioxide, (+) ethanol. All cultures grown using basal medium, without supplementation with yeast extract or formate.

1987; Tholozan et al., 1992; Ueki et al., 2017). These results suggest that a synergistic interaction between *Acetobacterium* species and propionate-forming bacteria was taking place in the enrichments, where *Acetobacterium* is consuming CO to produce acetate and ethanol, and ethanol further used by close relatives to *A. neopropionicum* and *P. propionicus* to form propionate. Such interactions can be relevant for the overall fitness of microbial communities as they influence thermodynamics of the system. Diender et al. (2019) have recently shown a similar synergistic relation in synthetic co-cultures of *Clostridium autoethanogenum* and *Clostridium kluyveri*. In that study, it was shown that the presence of the ethanol-consuming bacterium *C. kluyveri* induced a higher degree of solventogenesis by the carboxydotrophic organism (compared with monocultures of *C. autoethanogenum*). In the present work, we could derive possibly the same type of interaction by natural enrichment of anaerobic sludge, which points out to a possible significance of this process in natural ecosystems too. Methanogens persisted in the enrichments, despite the reported toxicity of CO toward methanogens (Klasson et al., 1991); species closely related to *Methanospirillum hungatei* JF-1 and *Methanothrix soehngenii* GP6 were present in the enriched cultures (**Table 1B**). There are few methanogens capable of metabolizing CO to methane, belonging to *Methanobrevibacter*, *Methanosarcina*, *Methanothermobacter* genera (Diender et al., 2015). However, *Methanospirillum* is only reported to produce methane from H_2/CO_2 or formate (Iino et al., 2010), indicating that these microorganisms might be responsible for methane production, using H_2 and not CO. We previously tested CO utilization by *Methanospirilum hungatei* JF-1 (DSM 864) but no growth was observed (unpublished data).

Strain JM can grow on CO alone (without supplementation of yeast extract, formate or H_2/CO_2) (**Figure 2**). The type strain of *A. wieringae* (DSM 1911) was described by Braun and Gottschalk (1982), but its capability to use CO has not been tested before. Here we show that *A. wieringae* type strain can grow on CO in the presence of formate. The related *A. woodii* can also grow on CO, but only with H_2/CO_2 or formate as a co-substrate (Bertsch and Müller, 2015). In *A. woodii*, a hydrogen-dependent carbon dioxide reductase (HDCR) complex has been found responsible for the production of formate from CO_2, coupling CO_2 reduction directly to H_2 oxidation (Bertsch and Müller, 2015). A similar HDCR complex is present in the genome of *A. wieringae* (OFV70223 - OFV70228). Fe-Fe hydrogenases in the HDCR complex were thought to be sensitive to high CO concentrations (Bertsch and Müller, 2015), which could explain the need for formate when *A. woodii* was grown on CO. However, later it was shown that CO inhibition of the HDCR is fully reversible (Ceccaldi et al., 2017). Also, the thermophilic *Thermoanaerobacter kivui* employs a similar HDCR complex and, after prolonged adaptation to CO, was able to grow on 100% CO without formate (Weghoff and Müller, 2016). This suggests that hydrogenases in HDCR complex can adapt to CO. Strain JM was isolated from a long-term enrichment

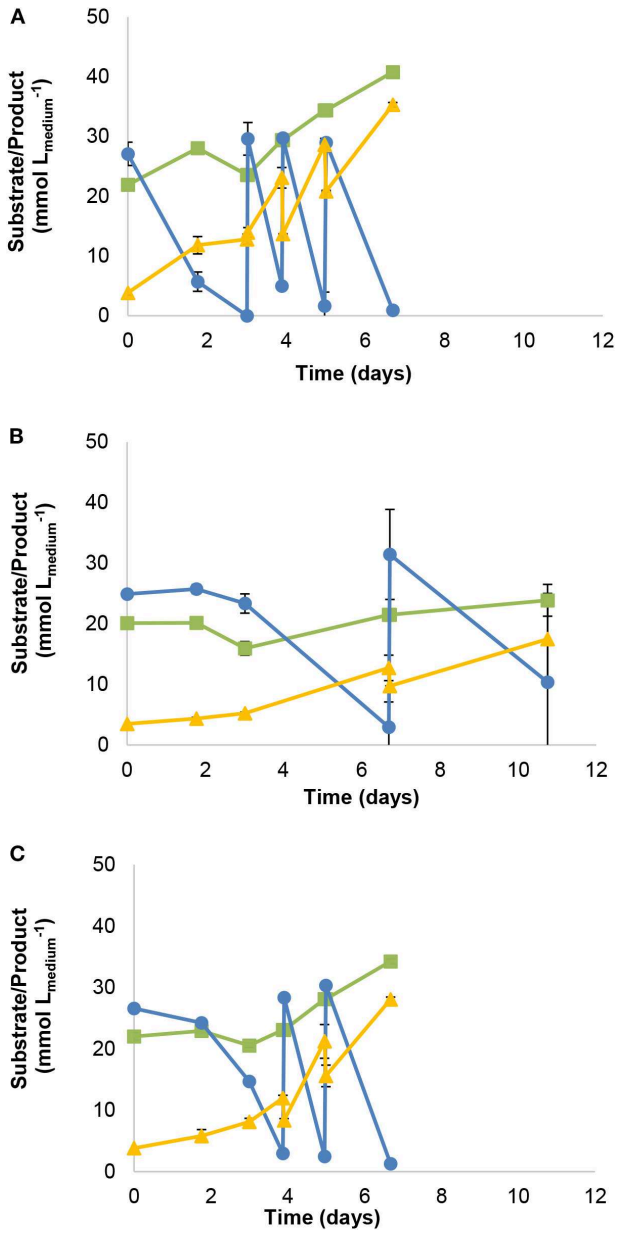

FIGURE 3 | Gas fed-batch growth with CO-acetate of **(A)** strain JM **(B)** *A. wieringae* DSM 1911^T and **(C)** *A. woodii* DSM 1030^T. Symbols: (●) carbon monoxide, (▲) carbon dioxide, (■) acetate. All cultures grown in basal medium supplemented with 1 mM of formate (without yeast extract).

growing on syngas, and this could have resulted in a better adaptation to CO. The genome of strain JM encodes for a formate dehydrogenase with high similarity to the HDCR of *A. woodii*, but the associated hydrogenases were not found. The *fdh* gene of strain JM was located at the end of a contig, and therefore we cannot exclude the possibility of missing part of the sequence of the HDCR. It thus remains unclear if strain JM employs a HDCR, but formate formation does not seem to be a limiting step in its metabolism. Besides adaptation of hydrogenases to CO, a link between the abundance of the monofunctional CODH CooS and the bifunctional CODH/ACS and the efficiency in CO utilization was proposed (Weghoff and Müller, 2016). The genome of strain JM encodes for both, a bifunctional CODH/ACS complex (TYC87911-TYC87912), and an apparent monofunctional CODH (TYC86630). However, as the genomes of both *A. woodii* and *A. wieringae* also appear to carry genes of mono- as well as bi-functional CODH this appears not to make a difference here.

Comparison of CO conversion by strain JM and by the type strains of *A. wieringae* and *A. woodii* shows that strain JM can convert a higher amount of CO during the 7 days of incubation (up to 4- and 2.5-fold higher, respectively) (**Figure 3**), which again could result from metabolic adaptation to CO during enrichment and isolation of strain JM. Adaptation to CO has been previously shown to play a role to increase the growth rate of *A. woodii* up to 3 fold compared to non-adapted cultures (with maximum 75% CO and 100 mM formate) (Bertsch and Müller, 2015). Duplication times in mesophilic carboxydotrophs range from 4 to 14 hours, with the lowest being achieved by *Clostridium* species (namely *C. ljungdahlii*, *C. autoethanogenum* and *C. ragsdalei*); *A. woodii* has reported (or calculated) duplication times between 5.5 and 13 hours (Diender et al., 2015).

Strain JM encodes for both the carbonyl and methyl branches of the WL pathway as found in *A. woodii* (Sharak Genthner and Bryant, 1987; Poehlein et al., 2016). Additionally, the genome analysis of *A. wieringae* strain JM revealed the presence of two CODH encoding sequences, explaining its CO utilizing properties. Strain JM could grow in the presence of different initial partial pressures of CO or CO/H_2, producing acetate and CO_2; to note, though, that incubation of strain JM with 100% CO (170 kPa) led to the production of ethanol as well (**Figure 2D**). Both, aldehyde:ferredoxin oxidoreductase (*aor*) (TYC84206, TYC88292) and alcohol dehydrogenase (*adh*) (TYC84204) encoding genes are present in the genome of strain JM, and are potentially linked to ethanol production by this strain. Conversion of carboxylic acids to alcohols via the AOR-ADH pathway has been previously observed in several carboxydotrophs (Simon et al., 1987; Perez et al., 2013), and further genetic evidence for the pathway reported by Basen et al. (2014). The presence of the AOR may contribute for the efficient growth of strain JM on CO, as redox equivalents can be shuttled into ethanol, without interfering with energy conservation (Köpke et al., 2010). Earlier reports on *A. wieringae* type strain show ethanol formation from fructose and H_2/CO_2 conversion (Buschhorn et al., 1989; Groher and Weuster-Botz, 2016) and on *A. woodii* from glucose fermentation (Buschhorn et al., 1989), though not with CO. The same authors also reported that *A. woodii* and *A. wieringae* could use ethanol as substrate as well (Buschhorn et al., 1989), which is also the case for strain JM. This can also explain ethanol consumption by strain JM in later phase of CO fermentation (**Figure 2D**).

CONCLUSIONS

Enrichment cultures mainly composed of strain JM and close relatives to *A. neopropionicum* and *P. propionicus* were able

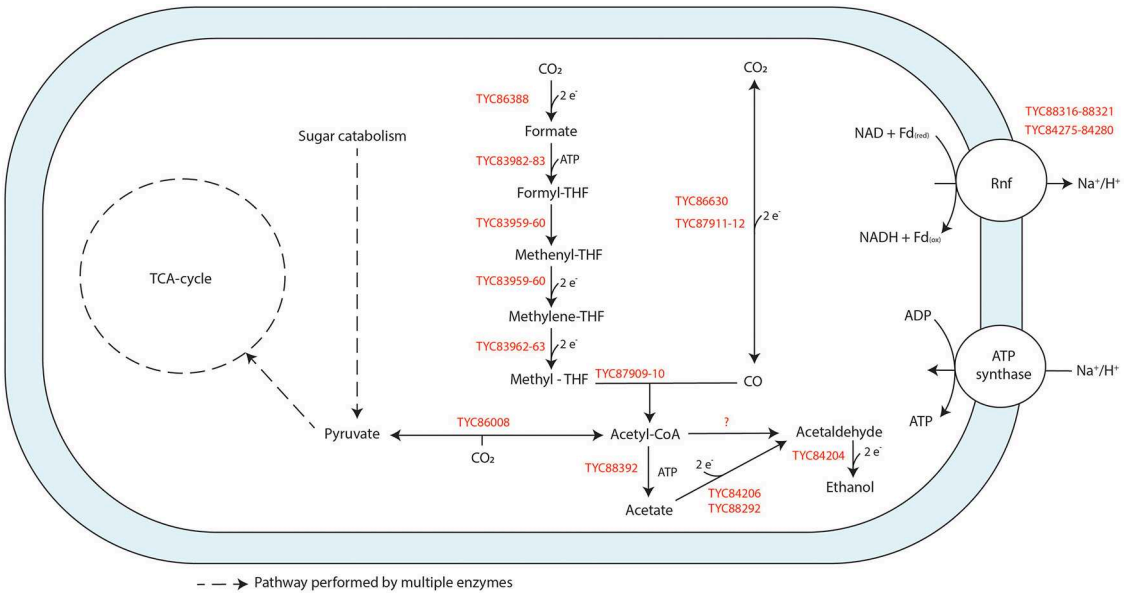

FIGURE 4 | Schematic representation of the physiology of strain JM when grown on CO. Genes found in the genome that are annotated to perform specific reactions are indicated in red. Reactions are not displayed stoichiometrically.

to produce propionate from syngas, which is an uncommon product from syngas fermentation. A novel carboxydotrophic *A. wieringae* strain JM was isolated from the syngas enriched culture. Strain JM could efficiently convert CO to acetate (and CO_2) and small amounts of ethanol. This is the first report of an *A. wieringae* strain able to use CO, and proof that type strain (DSM 1911^T) can also utilize CO, but only in the presence of formate. It is also the first report of isolation of an *Acetobacterium* species from a CO-fed enrichment.

DATA AVAILABILITY STATEMENT

The datasets generated for this study can be found in the 16S rRNA gene sequences submitted to the European Nucleotide Database (ENA) accession numbers LR655884, LR657299 to LR657303, PRJEB33623. The Whole Genome Shotgun project of *Acetobacterium wieringae* strain JM has been deposited at DDBJ/ENA/GenBank under the accession VSLA00000000.

AUTHOR CONTRIBUTIONS

DS, AS, and MA proposed and designed the study. DS and JA provided guidance to AA and JM and streamlined communication between the two labs. Research was performed by AA (initial enrichments), JM (characterization of enrichments and isolation of strain JM), SP and AA (physiological characterization of strain JM), and MD (genomic analysis of strain JM). AA drafted the manuscript with support of JA and DS, and revisions by all the authors.

FUNDING

The involved research was financially supported by Project NWO-GK-07 from the Netherlands Science Foundation (NWO), a Gravitation Grant (Project 024.002.002) of the Netherlands Ministry of Education, Culture and Science, and by the Portuguese Foundation for Science and Technology (FCT) under the scope of the strategic funding of UIDB/04469/2020 unit and BioTecNorte operation (NORTE-01-0145-FEDER-000004) funded by the European Regional Development Fund under the scope of Norte2020–Programa Operacional Regional do Norte. The financial support from FCT and European Social Fund (POPH-QREN) through the grant PD/BD/128030/2016 given to AA, and through the project INNOVsyn – Innovative strategies for syngas fermentation (POCI-01-0145-FEDER-031377), are gratefully acknowledged.

REFERENCES

Abubackar, H. N., Fernández-Naveira, Á., Veiga, M. C., and Kennes, C. (2016). Impact of cyclic pH shifts on carbon monoxide fermentation to ethanol by *Clostridium autoethanogenum*. *Fuel* 178, 56–62. doi: 10.1016/j.fuel.2016.03.048

Abubackar, H. N., Veiga, M. C., and Kennes, C. (2018). Production of acids and alcohols from syngas in a two-stage continuous fermentation process. *Bioresour. Technol.* 253, 227–234. doi: 10.1016/j.biortech.2018.01.026

Altschul, S. F., Gish, W., Miller, W., Myers, E. W., and Lipman, D. J. (1990). Basic local alignment search tool. *J. Mol. Biol.* 215, 403–410. doi: 10.1016/S0022-2836(05)80360-2

Alves, J. I., van Gelder, A. H., Alves, M. M., Sousa, D. Z., and Plugge, C. M. (2013). *Moorella stamsii* sp. nov., a new anaerobic thermophilic hydrogenogenic carboxydotroph isolated from digester sludge. *Int. J. Syst. Evol. Microbiol.* 63, 4072–4076. doi: 10.1099/ijs.0.050369-0

Aziz, R. K., Bartels, D., Best, A. A., DeJongh, M., Disz, T., Edwards, R. A., et al. (2008). The RAST Server: rapid annotations using subsystems technology. *BMC Genomics* 9:75. doi: 10.1186/1471-2164-9-75

Basen, M., Schut, G. J., Nguyen, D. M., Lipscomb, G. L., Benn, R. A., Prybol, C. J., et al. (2014). Single gene insertion drives bioalcohol production by a thermophilic archaeon. *Proc. Natl. Acad. Sci. U.S.A.* 111, 17618–17623. doi: 10.1073/pnas.1413789111

Bengelsdorf, F. R., Beck, M. H., Erz, C., Hoffmeister, S., Karl, M. M., Riegler, P., et al. (2018). Bacterial anaerobic synthesis gas (syngas) and $CO_2 + H_2$ fermentation. *Adv. Appl. Microbiol.* 103, 143–221. doi: 10.1016/bs.aambs.2018.01.002

Bertsch, J., and Müller, V. (2015). CO metabolism in the acetogen *Acetobacterium woodii*. *Appl. Environ. Microbiol.* 81, 5949–5956. doi: 10.1128/AEM.01772-15

Boisvert, F. M., Ahmad, Y., Gierlinski, M., Charrière, F., Lamont, D., Scott, M., et al. (2012). A quantitative spatial proteomics analysis of proteome turnover in human cells. *Mol. Cell Proteomics*. 11:M111.011429. doi: 10.1074/mcp.M111.011429

Braun, M., and Gottschalk, G. (1982). *Acetobacterium wieringae* sp. nov., a new species producing acetic acid from molecular hydrogen and carbon dioxide. *Zentralblatt fur Bakteriol. Angew. und Okol. Microbiol. Abt.1 Orig.C Hyg.* 3, 368–376. doi: 10.1016/S0721-9571(82)80017-3

Buschhorn, H., Dürre, P., and Gottschalk, G. (1989). Production and utilization of ethanol by the homoacetogen *Acetobacterium woodii*. *Appl. Environ. Microbiol.* 55, 1835–1840. doi: 10.1128/AEM.55.7.1835-1840.1989

Caporaso, J. G., Lauber, C. L., Walters, W. A, Berg-Lyons, D., Lozupone, C. A, Turnbaugh, P. J., et al. (2011). Global patterns of 16S rRNA diversity at a depth of millions of sequences per sample. *Proc. Natl. Acad. Sci. U.S.A.* 108(Suppl), 4516–4522. doi: 10.1073/pnas.1000080107

Ceccaldi, P., Schuchmann, K., Müller, V., and Elliott, S. J. (2017). The hydrogen dependent CO_2 reductase: the first completely CO tolerant FeFe-hydrogenase. *Energy Environ. Sci.* 10, 503–508. doi: 10.1039/C6EE02494G

Chikhi, R., and Medvedev, P. (2014). Informed and automated k-mer size selection for genome assembly. *Bioinformatics* 30, 31–37. doi: 10.1093/bioinformatics/btt310

De Tissera, S., Köpke, M., Simpson, S. D., Humphreys, C., Minton, N. P., and Dürre, P. (2017). "Syngas biorefinery and syngas utilization," in *Biorefineries. Advances in Biochemical Engineering/Biotechnology,* Vol. 166, eds K. Wagemann and N. Tippkötter (Cham: Springer), 247–280. doi: 10.1007/10_2017_5

Diender, M., Parera Olm, I., Gelderloos, M., Koehorst, J. J., Schaap, P. J., Stams, A. J. M., et al. (2019). Metabolic shift induced by synthetic co-cultivation promotes high yield of chain elongated acids from syngas. *Sci. Rep.* 9:18081. doi: 10.1038/s41598-019-54445-y

Diender, M., Stams, A. J. M., and Sousa, D. Z. (2015). Pathways and bioenergetics of anaerobic carbon monoxide fermentation. *Front. Microbiol.* 6:1275. doi: 10.3389/fmicb.2015.01275

Dürre, P., and Eikmanns, B. J. (2015). C1-carbon sources for chemical and fuel production by microbial gas fermentation. *Curr. Opin. Biotechnol.* 35, 63–72. doi: 10.1016/j.copbio.2015.03.008

Gagliano, M. C., Braguglia, C. M., Gianico, A., Mininni, G., Nakamura, K., and Rossetti, S. (2015). Thermophilic anaerobic digestion of thermal pretreated sludge: role of microbial community structure and correlation with process performances. *Water Res.* 68, 498–509. doi: 10.1016/j.watres.2014.10.031

Gao, S., Sung, W. K., and Nagarajan, N. (2011). Opera: reconstructing optimal genomic scaffolds with high-throughput paired-end sequences. *J. Comput. Biol.* 18, 1681–1691. doi: 10.1089/cmb.2011.0170

Groher, A., and Weuster-Botz, D. (2016). Comparative reaction engineering analysis of different acetogenic bacteria for gas fermentation. *J. Biotechnol.* 228, 82–94. doi: 10.1016/j.jbiotec.2016.04.032

Huang, X., and Madan, A. (1999). CAP3: a DNA sequence assembly program. *Genome Res.* 9, 868–877. doi: 10.1101/gr.9.9.868

Iino, T., Mori, K., and Suzuki, K. (2010). *Methanospirillum lacunae* sp. nov., a methane-producing archaeon isolated from a puddly soil, and emended descriptions of the genus *Methanospirillum* and *Methanospirillum hungatei*. *Int. J. Syst. Evol. Microbiol.* 60, 2563–2566. doi: 10.1099/ijs.0.020131-0

Klasson, K. T., Ackerson, M. D., Clausen, E. C., and Gaddy, J. L. (1991). Bioreator design for synthesis gas fermentations. *Fuel* 70, 605–614. doi: 10.1016/0016-2361(91)90174-9

Köpke, M., Held, C., Hujer, S., Liesegang, H., Wiezer, A., Wollherr, A., et al. (2010). *Clostridium ljungdahlii* represents a microbial production platform based on syngas. *Proc. Natl. Acad. Sci. U.S.A.* 107, 13087–13092. doi: 10.1073/pnas.1004716107

Meier-Kolthoff, J. P., Auch, A. F., Klenk, H. P., and Göker, M. (2013). Genome sequence-based species delimitation with confidence intervals and improved distance functions. *BMC Bioinformatics* 14:60. doi: 10.1186/1471-2105-14-60

Meier-Kolthoff, J. P., Hahnke, R. L., Petersen, J., Scheuner, C., Michael, V., Fiebig, A., et al. (2014). Complete genome sequence of DSM 30083^T, the type strain (U5/41T) of *Escherichia coli*, and a proposal for delineating subspecies in microbial taxonomy. *Stand. Genomic Sci.* 10:2. doi: 10.1186/1944-3277-9-2

Molitor, B., Richter, H., Martin, M. E., Jensen, R. O., Juminaga, A., Mihalcea, C., et al. (2016). Carbon recovery by fermentation of CO-rich off gases–turning steel mills into biorefineries. *Bioresour. Technol.* 215, 386–396. doi: 10.1016/j.biortech.2016.03.094

Müller, V. (2019). New horizons in acetogenic conversion of one-carbon substrates and biological hydrogen storage. *Trends Biotechnol.* 37, 1344–1354. doi: 10.1016/j.tibtech.2019.05.008

Nübel, U., Engelen, B., Felske, A., Snaidr, J., Wieshuber, A., Amann, R. I., et al. (1996). Sequence heterogeneities of genes encoding 16S rRNAs in *Paenibacillus polymyxa* detected by temperature gradient gel electrophoresis. *J. Bacteriol.* 178, 5636–5643. doi: 10.1128/JB.178.19.5636-5643.1996

Pereira, F. M. (2014). *Intensified bioprocess for the anaerobic conversion of syngas to biofuels* (PhD thesis), University of Minho. Available online at: http://repositorium.sdum.uminho.pt/bitstream/1822/34834/1/Filipa%20Maria%20Rodrigues%20Pereira.pdf (accessed January 21, 2020).

Perez, J. M., Richter, H., Loftus, S. E., and Angenent, L. T. (2013). Biocatalytic reduction of short-chain carboxylic acids into their corresponding alcohols with syngas fermentation. *Biotechnol. Bioeng.* 110, 1066–1077. doi: 10.1002/bit.24786

Phillips, J. R., Atiyeh, H. K., Tanner, R. S., Torres, J. R., Saxena, J., Wilkins, M. R., et al. (2015). Butanol and hexanol production in *Clostridium carboxidivorans* syngas fermentation: medium development and culture techniques. *Bioresour. Technol.* 190, 114–121. doi: 10.1016/j.biortech.2015.04.043

Poehlein, A., Bengelsdorf, F. R., Daniel, R., Dürre, P., and Schiel-Bengelsdorf, B. (2016). Genome sequence of the acetogenic bacterium *Acetobacterium wieringae* DSM 1911^T. *Genome Announc.* 4, 2015–2016. doi: 10.1128/genomeA.01430-16

Ragsdale, S. W., and Pierce, E. (2008). Acetogenesis and the Wood–Ljungdahl pathway of CO_2 fixation. *Biochim. Biophys. Acta* 1784, 1873–1898. doi: 10.1016/j.bbapap.2008.08.012

Redl, S., Diender, M., Jensen, T. Ø., Sousa, D. Z., and Nielsen, A. T. (2017). Exploiting the potential of gas fermentation. *Ind. Crops Prod.* 106, 21–30. doi: 10.1016/j.indcrop.2016.11.015

Schink, B., Kremer, D. R., and Hansen, T. A. (1987). Pathway of propionate formation from ethanol in *Pelobacter propionicus*. *Arch. Microbiol.* 147, 321–327. doi: 10.1007/BF00406127

Sharak Genthner, B. R., and Bryant, M. P. (1987). Additional characteristics of one-carbon-compound utilization by *Eubacterium limosum* and *Acetobacterium woodii*. *Appl. Envir. Microbiol.* 53, 471–476. doi: 10.1128/AEM.53.3.471-476.1987

Simon, H., White, H., Lebertz, H., and Thanos, I. (1987). Reduction of 2-enoates and alkanoates with carbon monoxide or formate, viologens, and *Clostridium thermoaceticum* to saturated acids and unsaturated and saturated alcohols. *Angew. Chem. Int. Ed.* 26, 785–787. doi: 10.1002/anie.198707851

Sousa, D. Z., Alcina Pereira, M., Stams, A. J. M., Alves, M. M., and Smidt, H. (2007). Microbial communities involved in anaerobic degradation of unsaturated or saturated long-chain fatty acids. *Appl. Environ. Microbiol.* 73, 1054–1064. doi: 10.1128/AEM.01723-06

Stams, a,. J. M., Van Dijk, J. B., Dijkema, C., and Plugge, C. M. (1993). Growth of syntrophic propionate-oxidizing bacteria with fumarate in the absence of methanogenic bacteria. *Appl. Environ. Microbiol.* 59, 1114–1119. doi: 10.1128/AEM.59.4.1114-1119.1993

Tholozan, J. L., Touzel, J. P., Samain, E., Grivet, J. P., Prensier, G., and Albagnac, G. (1992). *Clostridium neopropionicum* sp. nov., a strict anaerobic bacterium fermenting ethanol to propionate through acrylate pathway. *Arch. Microbiol.* 157, 249–257. doi: 10.1007/BF00245158

Ueki, A., Goto, K., Ohtaki, Y., Kaku, N., and Ueki, K. (2017). Description of *Anaerotignum aminivorans* gen. nov., sp. nov., a strictly anaerobic, amino-acid-decomposing bacterium isolated from a methanogenic reactor, and reclassification of *Clostridium propionicum*, *Clostridium neopropionicum* and *Clostridium lactatife. Int. J. Syst. Evol. Microbiol.* 67, 4146–4153. doi: 10.1099/ijsem.0.002268

Wang, S., Huang, H., Kahnt, J., Mueller, A. P., Köpke, M., and Thauer, R. K. (2013). NADP-specific electron-bifurcating [FeFe]-hydrogenase in a functional complex with formate dehydrogenase in *Clostridium autoethanogenum* grown on CO. *J. Bacteriol.* 195, 4373–4386. doi: 10.1128/JB.00678-13

Weghoff, M. C., and Müller, V. (2016). CO metabolism in the thermophilic acetogen *Thermoanaerobacter kivui*. *Appl. Environ. Microbiol.* 82 2312–2319. doi: 10.1128/AEM.00122-16

Yasin, M., Jang, N., Lee, M., Kang, H., Aslam, M., Bazmi, A. A., et al. (2019). Bioreactors, gas delivery systems and supporting technologies for microbial synthesis gas conversion process. *Bioresour. Technol. Rep.* 7:100207. doi: 10.1016/j.biteb.2019.100207

Conflict of Interest: The authors declare that the research was conducted in the absence of any commercial or financial relationships that could be construed as a potential conflict of interest.

frontiers in Microbiology

ORIGINAL RESEARCH
published: 11 March 2020
doi: 10.3389/fmicb.2020.00402

Adaptive Laboratory Evolution of *Eubacterium limosum* ATCC 8486 on Carbon Monoxide

*Seulgi Kang[1,2†], Yoseb Song[1,2†], Sangrak Jin[1,2], Jongoh Shin[1,2], Jiyun Bae[1,2], Dong Rip Kim[3], Jung-Kul Lee[4], Sun Chang Kim[1,2,5], Suhyung Cho[1,2] and Byung-Kwan Cho[1,2,5]**

[1] Department of Biological Sciences, Korea Advanced Institute of Science and Technology, Daejeon, South Korea, [2] KAIST Institute for the BioCentury, Korea Advanced Institute of Science and Technology, Daejeon, South Korea, [3] Department of Mechanical Engineering, Hanyang University, Seoul, South Korea, [4] Department of Chemical Engineering, Konkuk University, Seoul, South Korea, [5] Intelligent Synthetic Biology Center, Daejeon, South Korea

OPEN ACCESS

Edited by:
Mirko Basen,
University of Rostock, Germany

Reviewed by:
Amy Michele Grunden,
North Carolina State University, United States
Shunichi Ishii,
Japan Agency for Marine-Earth Science and Technology, Japan

***Correspondence:**
Byung-Kwan Cho
bcho@kaist.ac.kr

[†] These authors have contributed equally to this work

Specialty section:
This article was submitted to Microbial Physiology and Metabolism, a section of the journal Frontiers in Microbiology

Received: 29 September 2019
Accepted: 26 February 2020
Published: 11 March 2020

Citation:
Kang S, Song Y, Jin S, Shin J, Bae J, Kim DR, Lee J-K, Kim SC, Cho S and Cho B-K (2020) Adaptive Laboratory Evolution of Eubacterium limosum ATCC 8486 on Carbon Monoxide. Front. Microbiol. 11:402. doi: 10.3389/fmicb.2020.00402

Acetogens are naturally capable of metabolizing carbon monoxide (CO), a component of synthesis gas (syngas), for autotrophic growth in order to produce biomass and metabolites such as acetyl-CoA via the Wood–Ljungdahl pathway. However, the autotrophic growth of acetogens is often inhibited by the presence of high CO concentrations because of CO toxicity, thus limiting their biosynthetic potential for industrial applications. Herein, we implemented adaptive laboratory evolution (ALE) for growth improvement of *Eubacterium limosum* ATCC 8486 under high CO conditions. The strain evolved under syngas conditions with 44% CO over 150 generations, resulting in a significant increased optical density (600 nm) and growth rate by 2.14 and 1.44 folds, respectively. In addition, the evolved populations were capable of proliferating under CO concentrations as high as 80%. These results suggest that cell growth is enhanced as beneficial mutations are selected and accumulated, and the metabolism is altered to facilitate the enhanced phenotype. To identify the causal mutations related to growth improvement under high CO concentrations, we performed whole genome resequencing of each population at 50-generation intervals. Interestingly, we found key mutations in CO dehydrogenase/acetyl-CoA synthase (CODH/ACS) complex coding genes, *acsA* and *cooC*. To characterize the mutational effects on growth under CO, we isolated single clones and confirmed that the growth rate and CO tolerance level of the single clone were comparable to those of the evolved populations and wild type strain under CO conditions. Furthermore, the evolved strain produced 1.34 folds target metabolite acetoin when compared to the parental strain while introducing the biosynthetic pathway coding genes to the strains. Consequently, this study demonstrates that the mutations in the CODH/ACS complex affect autotrophic growth enhancement in the presence of CO as well as the CO tolerance of *E. limosum* ATCC 8486.

Keywords: acetogens, carbon monoxide, adaptive laboratory evolution, CODH/ACS, *acsA*, *cooC*

INTRODUCTION

Carbon monoxide (CO), generated due to incomplete combustion of organic materials, is a toxic gas that hampers the growth of various organisms. Presently, CO is emitted in large quantities in the form of synthesis gas (syngas) comprising CO, carbon dioxide (CO_2), and hydrogen (H_2). The syngas is produced as a byproduct of fossil fuel combustion for industrial development, specifically by gasification of coal, biomass, and natural gas. The syngas composition depends on the gasifier type and resource, which increases the CO amount up to 67% of the total volume (Subramani and Gangwal, 2008; Munasinghe and Khanal, 2010). Being derived from fossil fuel, syngas needs to be purified in order to prevent air pollution and the greenhouse gas effect, which is conventionally managed via thermochemical processes that convert syngas into liquid hydrocarbons. Unfortunately, the conventional method requires greater operation cost and high temperature and pressure conditions, thus requiring a more efficient method to convert syngas into other chemicals (Bredwell et al., 1999; Munasinghe and Khanal, 2010). As an alternative method, gas fermentation using microorganisms has been suggested to produce industrial commodities with lower operation cost and higher catalyst specificity compared to the thermochemical processes. In addition, the biological process is capable of producing various organic compounds using syngas as feedstock, such as acetate, butyrate, ethanol, butanol, 2,3-butanediol, and other compounds via genetic manipulation (Köpke et al., 2010, 2011; Abubackar et al., 2015; Park et al., 2017). Among the promising biocatalysts for syngas fermentation, with an ability to convert CO into biomass and various biochemicals, acetogenic bacteria (acetogens) have received immense attention and are considered as a novel platform to replace the conventional processes (Henstra et al., 2007; Bengelsdorf et al., 2013; Latif et al., 2014).

Acetogens are anaerobic bacteria that utilize CO and CO_2 as a carbon building block and, initially, synthesize acetyl-CoA as an important metabolic intermediate, by using the Wood–Ljungdahl pathway (WLP) (Drake et al., 2008). The linear WLP comprises two branches, methyl and carbonyl branches, which convert CO into CO_2 and then to acetyl-CoA (Drake et al., 2006). The methyl branch reduces CO_2 converted from CO into formate, catalyzed by formate dehydrogenase (*fdh*) (Ragsdale, 1997). Following the initial reaction, formyl-tetrahydrofolate (THF) is formed using formate and THF, which requires the hydrolysis of ATP (Schuchmann and Müller, 2014). Subsequently, the formyl-THF is converted by methenyl-THF cyclohydrolase into methenyl-THF, and further into methylene-THF via methylene-THF dehydrogenase. Eventually, the methyl branch reduces methylene-THF to methyl-THF by methylene-THF reductase (Ragsdale and Pierce, 2008). For the carbonyl branch, the methyl group of methyl-THF is transferred by methyltransferase to corrinoid Fe-S protein, and then to CO dehydrogenase/acetyl-CoA synthase (CODH/ACS), which carries CO generated by using CODH/ACS from CO_2 (Ljungdahl, 1986). The condensation of methyl group and CO from the methyl and carbonyl branches, respectively, generates acetyl-CoA, which then converts into acetate by generating ATP (Ragsdale and Pierce, 2008). Of all the enzymes associated with the WLP, CODH/ACS plays a pivotal role in autotrophic growth of acetogens by reversibly interconverting CO/CO_2 and synthesizing acetyl-CoA (Doukov et al., 2002).

In acetogens, the CODH/ACS complex is formed by the assembly of ACS and CODH, as $(\alpha\beta)_2$ complex in the presence of [3Fe-4S] cluster (C-cluster), [4Fe-4S] cluster (A-cluster), and metal clusters as the active sites (Darnault et al., 2003; Ragsdale, 2008; Appel et al., 2013; Can et al., 2014). The C-cluster encoded by *acsA* is the active site of CODH subunit for reversible oxidation of CO to CO_2 (Doukov et al., 2002). The A-cluster encoded *acsB* is the active site of ACS subunit, which generates acetyl-CoA from CO, CoA, and methyl group that is transferred from the corrinoid protein (Seravalli et al., 1997; Darnault et al., 2003; Drennan et al., 2004). For CO fixation of *Moorella thermoacetica*, for example, CO catalytic reaction is indicated as "ping-pong" reaction involving two steps, ping and pong step (Diekert and Thauer, 1978). In the ping step, CO binds to the metal center of the C-cluster, which is nickel, and thus reduces the C-cluster; thereafter, in the pong step, the electrons from the C-cluster are transferred to the external electron acceptors, such as ferredoxin, via the B- and D-clusters, and CO_2 is generated by CO oxidation (Can et al., 2014). To activate this complex, specific accessory proteins, such as *cooC*, *cooJ,* or *cooT*, are required, which are responsible for binding the metal and forming metal binding site for the complex interface (Bender et al., 2011; Alfano et al., 2019). In addition, the proteins support maturation of CODH by assembling C-cluster in the CODH/ACS complex and transfer electrons obtained from CO oxidation to the electron carriers (Loke and Lindahl, 2003).

Using the WLP and the associated enzymes, acetogens utilize CO as a carbon substrate for producing biomass building blocks; however, they are inhibited by the high concentration of CO (Daniel et al., 1990). CO competitively binds to the active site of metalloenzyme, such as hydrogenase, and depletes the transition metal that leads to insufficient ligation of the original substrate, and the absence of metals causes low growth rate and eventually leads to mortality of the organism (Bertsch and Müller, 2015). For example, in *Acetobacterium woodii*, one of the well-known model acetogens, the growth rates under autotrophic growth conditions decreased with increasing CO concentrations, which also affected the heterotrophic growth conditions (Bertsch and Müller, 2015). CO inhibited hydrogen-dependent CO_2 reductase of *A. woodii*, which is responsible for CO_2 reduction and hydrogen storage (Bertsch and Müller, 2015). Although acetogens utilize CO as the carbon source, the inhibitory effect of high CO concentration on the growth and lethality of the organisms need to be enhanced for efficient CO fixation.

In the present study, we applied adaptive laboratory evolution (ALE) method to enhance CO tolerance and growth fitness of *Eubacterium limosum* ATCC 8486 under CO presence, by serially transferring the strain on syngas containing 44% CO for 150 generations. ALE is widely utilized, thus allowing self-optimization of the organism to acquire the desired phenotype (Elena and Lenski, 2003; Dragosits and Mattanovich, 2013;

Choe et al., 2019). Genome sequencing of the evolved strains at 50-generation intervals revealed several causal mutations, which were identified in the genes encoding CODH/ACS. Subsequently, via the growth profiling of single isolated clone under syngas growth conditions, we validated that the key mutation altered the tolerance and the growth of the strain. The results provide insights on CO fixation for strain designing.

MATERIALS AND METHODS

Bacterial Strains and Culture Conditions

Eubacterium limosum ATCC 8486 was obtained from the Leibniz Institute DSMZ-German Collection of Microorganisms and Cell Cultures (DSMZ, Braunschweig, Germany). The strain was grown strictly under anaerobic conditions at 37°C in 100 mL of modified DSMZ 135 medium (pH 7.0), which comprised 1 g/L ammonium chloride, 2 g/L yeast extract, 10 g/L sodium bicarbonate, 0.1 g/L magnesium sulfate heptahydrate, 0.3 g/L cysteine-HCl, 10 mL vitamin solution (4 mg/L biotin, 4 mg/L folic acid, 20 mg/L pyridoxine-HCl, 10 mg/L thiamine-HCl, 10 mg/L riboflavin, 10 mg/L nicotinic acid, 10 mg/L pantothenate, 0.2 mg/L vitamin B12, 10 mg/L *p*-aminobenzoic acid, and 10 mg/L lipoic acid), 5.36 mM K_2HPO_4, 4.64 mM KH_2PO_4, 4 μM resazurin, and 20 mL trace element solution (1.0 g/L nitrilotriacetic acid, 3.0 g/L $MgSO_4.7H_2O$, 0.5 g/L $MnSO_4.H_2O$, 1.0 g/L NaCl, 0.1 g/L $FeSO_4.7H_2O$, 180 mg/L $CoSO_4.7H_2O$, 0.1 g/L $CaCl_2.2H_2O$, 180 mg/L $ZnSO_4.7H_2O$, 10 mg/L $CuSO_4.5H_2O$, 20 mg/L $KAI(SO_4)_2.12H_2O$, 10 mg/L H_3BO_3, 10 mg/L $Na_2MO_4.2H_2O$, 30 mg/L $NiCl_2.6H_2O$, 0.3 mg/L $Na_2SeO_3.5\ H_2O$, 0.4 mg/L $Na_2WO_4.2H_2O$), at a pressure of 200 kPa and 50 mL of headspace filled with 0%, 20%, 40%, 60%, 80%, and 100% CO that is balanced using 100%, 80%, 60%, 40%, 20%, and 0% N_2, respectively, for autotrophic growth conditions. To enhance the autotrophic growth rate during adaptation, 40 mM NaCl was supplemented to the media, which couples with sodium dependent ATP synthase (Jeong et al., 2015; Song et al., 2017).

Adaptive Laboratory Evolution

Adaptive laboratory evolution experiment was conducted with a syngas (44% CO, 22% CO_2, 2% H_2, and 32% N_2) described in Section "Bacterial Strains and Culture Conditions." Before the ALE, the strain underwent preadaptation step by passing thrice through the syngas condition at mid-exponential phase. During the ALE experiment with four independent populations, the culture was transferred to a fresh medium at mid-exponential phase.

Whole Genome Resequencing

To construct whole genome resequencing libraries, the genomic DNA samples were extracted from the evolved populations and isolated single clone. Cell stocks were cultured in modified DSMZ 135 medium (pH 7.0) supplemented with glucose (5 g/L) and were incubated for 12 h at 37°C. The harvested cells were resuspended with 500 μL of lysis buffer containing Tris–HCl (pH 7.5), 5 M NaCl, 1 M $MgCl_2$, and 20% triton × 100. Thereafter, the cells were frozen using liquid nitrogen and ground using a mortar and pestle. The powder was resuspended with 600 μL of nuclei lysis solution (Promega, Madison, WI, United States), incubated at 80°C, and then cooled at 4°C. RNAs were removed from the cell lysate using RNase A solution. Proteins in the solution were precipitated using protein precipitation buffer (Promega). Following the protein precipitation, the samples were cooled at 4°C for 10 min, and were then centrifuged at 16,000 *g* for 10 min. The supernatant was transferred to a new tube, and 1 × volume of isopropanol was added. After centrifugation at 16,000 *g* for 5 min, the DNA pellet was obtained, which was then washed with 80% ethanol twice. The obtained DNA quality was determined by the A260/A280 ratio (>1.9) and inspected by gel electrophoresis, and the concentration was quantified via a Qubit 2.0 Fluorometer (Invitrogen, Carlsbad, CA, United States) with a Qubit dsDNA HS Assay kit (Invitrogen). The sequencing libraries were constructed using a TruSeq Nano DNA library prep kit (Illumina, La Jolla, CA, United States). The constructed libraries of evolved populations were sequenced with Illumina HiSeq2500 (rapid-run mode as 50 cycle-ended reaction) and the constructed libraries of isolated clone were sequenced with Illumina MiSeq (a 150 cycle-ended reaction).

Mutation Screening

All process for mutation screening were performed using a CLC genomics Workbench v6.5.1 (CLC bio, Aarhus, Denmark). Adapter sequences of the sequencing reads were removed by using a trimming tool with the default parameters (quality limit and ambiguous nucleotides residues 2). The resulting reads were mapped to the *E. limosum* ATCC 8486 reference genome (NCBI accession NZ_CP019962.1) with mapping parameters (mismatch cost: 2, indel cost: 3, deletion cost: 3, length fraction: 0.9, and similarity fraction: 0.9). Variants were detected from the mapped reads using a Quality-based variant detection tool with the parameters (neighborhood radius: 5, maximum gap and mismatch count: 5, minimum neighborhood quality: 30, minimum central quality: 30, minimum coverage: 10, minimum variant frequency: 10%, maximum expected alleles: 4, non-specific matches: ignore and genetic code: bacterial and plant plastid).

Isolation of Single Clones From the Evolved Populations

The single clones were isolated from the evolved populations by streaking the culture onto RCM agar medium. To confirm the sequence of each mutation site, the genomic regions were amplified by PCR using primer pairs and sequenced by Sanger sequencing (**Supplementary Table S1**). The selected single clones with the mutations were cultured in DSMZ 135 medium supplemented with CO in the headspace to measure the growth rate and metabolite production.

Plasmid Construction for Acetoin Biosynthesis

All primers used to construct plasmid in this study are listed in **Supplementary Table S2**. Initially, the pJIR750ai

plasmid was used as a shuttle vector, and the chemically competent *Escherichia coli* DH5α (Enzynomics, Inc., South Korea) was used for cloning the plasmid. Acetolactate synthase (*alsS*) and acetolactate decarboxylase (*alsD*) were obtained via gene synthesis from *Bacillus subtilis* and *Aeromonas hydrophila*, respectively (Oliver et al., 2013). The synthesized *alsS* and *alsD* were amplified using primer sets alsS_F-alsS_R and alsD_F-alsD_R, respectively. The pJIR750ai reduced by *Pvu*I (named as pJIR750_*Pvu*I_cut) was digested by *Bam*HI and *Sal*I, and was then assembled with the amplified *alsD* by using In-Fusion HD cloning Kit (TaKaRa, Japan). Subsequently, the assembled plasmid (pJIR750_alsD) was linearized by *Sac*I and *Bam*HI, and was then assembled with the amplified *alsS* by In-Fusion cloning Kit, generating the pJIR750_alsS_alsD plasmid. To control the gene expressions, promoters of ELIM_c2885 (pyruvate:ferredoxin oxidoreductase) and ELIM_c1121 ([Fe] hydrogenase) were selected as the two genes were constitutively expressed with high expression levels in *E. limosum* (Song et al., 2018). The native promoters were amplified from genomic DNA of *E. limosum* and inserted in the pJIR750_alsS_alsD plasmid, resulting in the construction of pJIR750_alsS_U_1121_P1121_P2885_U1121_alsD plasmid.

Transformation

To prepare the electrocompetent strains, a previously modified protocol was used (Shin et al., 2019). The cells were cultured in 100 mL of DSM 135 medium supplemented with 5 g/L glucose. At the early exponential phase (OD_{600} 0.3 $\sim$ 0.5), the cells were harvested by centrifuging at 10,000 rpm for 10 min at 4°C. The harvested cells were washed with 50 mL of 270 mM sucrose buffer (pH 6) and resuspended to achieve a final concentration of 10^{11} cells/mL. About 1.5 $\sim$ 2 μg plasmid was added to the electrocompetent cells and then the solution was transferred to a 0.1-cm-gap Gene Pulser cuvette (Bio-Rad, Hercules, CA, United States). Thereafter, the cells were pulsed at 2.0 kV and immediately resuspended with 0.9 mL of reinforced clostridial medium (RCM). The cells were recovered on ice for 5 min, and incubated at 37°C for 16 h. The recovered cells were plated on an RCM plate (1.5% agar) containing 15 μg/mL thiamphenicol. A single colony was selected and cultured in DSM 135 medium supplemented with 5 g/L glucose.

Metabolite Measurement

Primary metabolites were measured via high performance liquid chromatography (Waters, Milford, MA, United States) equipped with refractive index detector and MetaCarb 87 H 300 × 7.8 mm column (Agilent, Santa Clara, CA, United States). The mobile phase used was 0.007 N sulfuric acid solution with 0.6 mL/min flow rate. The oven temperature was set at 37°C for acetate, lactate and butyrate and 50°C for acetoin.

Gas Measurement

CO and CO_2 concentrations were measured via gas chromatography (Shimadzu, Japan) equipped with thermal conductivity detector and ShinCarbon ST Micropacked column (1 mm × 2 m, 1/16″, 100/120 mesh; Restek, Bellefonte, PA, United States). Helium was used as the carrier gas at a flow rate of 30 mL/min. The initial oven temperature was 30°C for 1 min, programmed with a ratio 5°C/min until it reached 100°C. The temperature for injector and detector was 100°C.

RESULTS

Growth of *E. limosum* ATCC 8486 Under CO Culture Conditions

To confirm the CO tolerance of *E. limosum* ATCC 8486, the cell growth was determined by culturing the strain in 100 mL of the modified DSMZ 135 medium with 0%, 20%, 40%, 60%, 80%, and 100% CO concentrations (**Figure 1A**). In the absence of CO, *E. limosum* proliferated to a maximum optical density at 600 nm of 0.062 ± 0.003, which likely due to the presence of sodium bicarbonate and yeast extract in the medium served as the carbon source for the *E. limosum* (**Figure 1B**). Under 20% CO growth condition, the cell reached a growth rate of 0.063 ± 0.011 h^{-1}; whereas, a growth rate of 40% CO growth condition was 0.035 ± 0.002 h^{-1}, which increased by 1.80 folds. In contrast, maximum optical densities (600 nm) of 20% CO and 40% CO culture conditions were 0.193 and 0.438, respectively, which decreased by 2.27 folds (**Figure 1B**). The cell cultivated under CO concentrations exceeding 60% demonstrated insignificant proliferation under the conditions, indicating that cell growth was inhibited with increasing CO concentrations in the growth medium. We performed an additional experiment to confirm the effect of CO on the cell growth. Initially, the cells were cultured in the DSMZ 135 medium containing 5 g/L glucose, then incubated until reaching the mid-exponential phase, optical density (600 nm) of 1.320. When the cell reached the mid-exponential phase, 0% (100% N_2, as control), 20%, 40%, 60%, 80%, or 100% CO was purged to each sample with the same pressure, then measured the optical density (600 nm) of the cells (**Supplementary Figure S1**). Two hours after the CO injection, the optical densities (600 nm) were measured, which decreased compared to the control at all CO concentrations (**Supplementary Figure S1**).

To further understand the phenotypical effect of CO, metabolites produced by *E. limosum* were investigated (**Figure 1C**). Among the identified metabolites, acetate was the dominant metabolic product, which is known as a key end product for acetogens under autotrophic growth conditions. In general, acetate production is well correlated with the cell growth, because acetate synthesis generates ATP that is required for cellular function of acetogens. Under 20% and 40% CO conditions, the acetate production was increased compared to the other CO conditions; moreover, the acetate production patterns revealed growth-dependent profiles. Under high CO conditions, acetate production decreased as the concentrations of CO increased, and insignificant changes were determined (P-value > 0.05) compared to the control experiment. Based on these results, the acetate productions were correlated with the growth pattern, which was influenced by the amount of CO concentration in the culture medium, suggesting that the

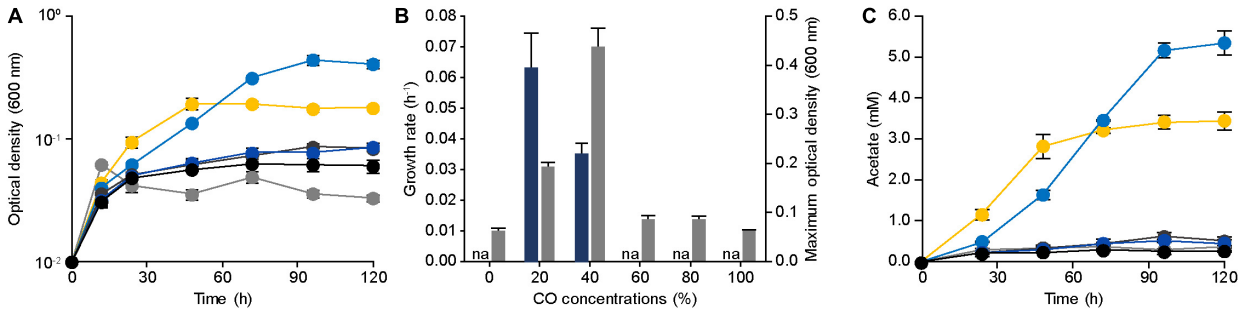

FIGURE 1 | Physiology of *Eubacterium limosum* ATCC 8486 with different amounts of CO as sole substrate and source of energy. **(A)** The growth profiles of the parental strain under 0% (gray circle), 20% (yellow circle), 40% (light blue circle), 60% (dark gray circle), 80% (blue circle), and 100% (black circle) CO conditions that are balanced by N_2 were measured using optical density at 600 nm. **(B)** The growth rates (navy) and the maximum optical density (600 nm) (gray) of the parental strain under 0%, 20%, 40%, 60%, 80%, and 100% CO that is balanced by N_2. "na" is not available. **(C)** Acetate productions by the parental strain under 0% (gray circle), 20% (yellow circle), 40% (light blue circle), 60% (dark gray circle), 80% (blue circle), and 100% (black circle) CO conditions that are balanced by N_2 were measured using HPLC, respectively. The cells were anaerobically cultivated at 37°C in 150 mL anaerobic bottle containing 100 mL of the modified DSMZ 135 medium with 50 mL of headspace purged at a pressure of 200 kPa. Error bars indicate standard deviation of biological triplicates.

increase of CO tolerance potentially enhances *E. limosum* acetate production.

Adaptive Laboratory Evolution of *E. limosum* ATCC 8486 Under CO Culture Conditions

To improve the CO tolerance of *E. limosum*, we applied the robust ALE method to the organism, which is used as a tool to engineer organism for overcoming target stress conditions. For designing the ALE experiment, establishing an appropriate stress condition is an essential factor for an organism to reach the desired phenotype. In this study, syngas was selected for the ALE experiment. Syngas is generated from gasification, and the composition of the gas is determined by a source of gasifier type or biomass, which typically comprises CO and H_2 with 14% ∼ 67% and 5% ∼ 32%, respectively (Munasinghe and Khanal, 2010). To decide the precise composition of syngas for ALE, previous studies on syngas fermentations of acetogens were investigated, and a syngas composition of 44% CO, 22% CO_2, 2% H_2, and balanced N_2 was selected, which was widely observed in the syngas generated by industries (Köpke et al., 2011). Using the syngas composition, *E. limosum* was cultivated in the same basal media, which was utilized for determining the CO tolerance, to determine the transfer point for ALE (**Figure 2A**). The growth rate under the condition was 0.070 ± 0.002 h^{-1} with a maximum optical density (600 nm) of 0.486 ± 0.021, which slightly differs compared to the growth rate (0.058 ± 0.000 h^{-1}) obtained from the 40% CO condition, because a presence of H_2 with CO in the environment enhances the autotrophic growth of acetogens (Bertsch and Müller, 2015; Valgepea et al., 2018). According to the growth profile, the mid-exponential phase is between 42 and 54 h after the initial inoculation; thus, we selected 48 h for the transfer point for ALE. For ALE, four separate populations of *E. limosum* were adapted to confirm the reproducibility, labeling as ALE1, 2, 3, and 4. Initially, at the 40th generation, the growth rates of all populations were increased to 0.085 h^{-1}, which then maintained the enhanced growth rate up to 120th generation (**Figure 2B**). After 120 generations of adaptation, slight variations in the growth rates were observed in the entire population, with growth rate around 0.086 h^{-1}; however, no growth rate changes were observed after 150 generations (**Figure 2B**); thus, the ALE was stopped at 150th generation.

To further investigate the changes in cell growth at the population level, we selected the evolved population (ECO), ALE4, which demonstrated the highest growth rate with 0.089 h^{-1} at the 150th generation. Moreover, the other growth rates were comparable to that of the ECO, which were 0.086, 0.087, and 0.088 h^{-1} for the ALE1, ALE2, and ALE3, respectively. Growth and CO consumption profiles of the ECO and the parental strain were compared under the syngas growth conditions (**Figure 2C**). The two strains completely consumed CO presented in the headspace by 84 and 60 h, respectively, resulting in CO consumption rates of 0.043 ± 0.019 and 0.058 ± 0.003 mmol h^{-1}, respectively, which increased the carbon consumption rate of the adapted strain by 1.35 folds (**Figure 2C**). In addition, the stationary phases of the parental strain and the ECO were attained at 72 and 48 h, respectively, and the maximum optical densities (600 nm) were 0.498 ± 0.028 and 0.639 ± 0.016, respectively, which increased by 1.28 folds (**Figure 2C**).

Following the investigation of its phenotypical changes under the syngas condition, CO tolerance of the ECO was measured by cultivating the strain under different CO concentrations ranging from 0% to 100% CO (**Figure 2D**). Under 20% and 40% CO conditions, the growth rates were 0.076 ± 0.001 and 0.089 ± 0.001 h^{-1}, respectively. Compared to the parental strain, the growth rates of the ECO under 20% and 40% CO conditions were enhanced by 1.21 and 1.65 folds higher. In addition, the growth rates of the inhibitory CO conditions were 0.069 ± 0.001, 0.056 ± 0.001, and 0.048 ± 0.001 h^{-1} under 60%, 80%, and 100% CO conditions, respectively (**Figure 2D**). In addition, the maximum optical density at 600 nm of the ECO were higher than that of the parental strain by 7.49 folds under 60% CO condition (**Figure 2E**). Acetate productions of the ECO were identified under the given conditions, resulting

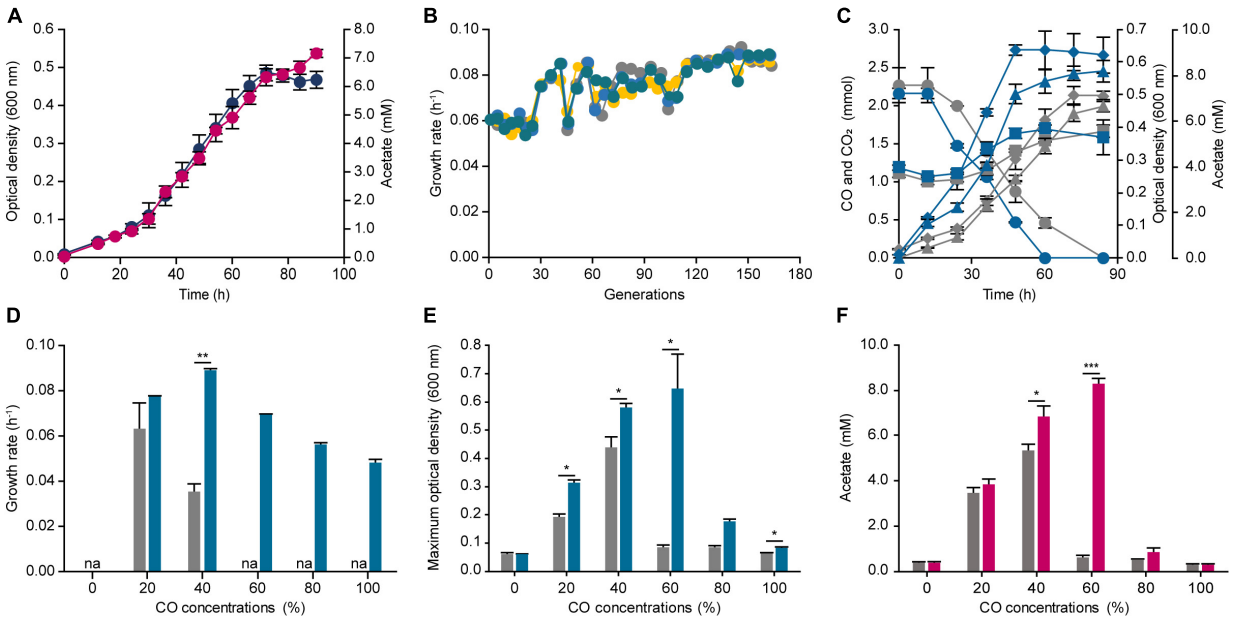

FIGURE 2 | Adaptive laboratory evolution of *Eubacterium limosum* ATCC 8486 under 44% CO syngas condition. **(A)** Optical density (600 nm) (navy circle) and acetate production (pink circle) of *E. limosum* under 44% CO syngas condition were measured over 90 h. **(B)** Changes of four independent population growth rates, ALE1 (gray circle), ALE2 (yellow circle), ALE3 (blue circle), and ALE4 (bluish green circle), during ALE under 44% CO syngas condition. Each circle indicates passage points during ALE. **(C)** The profile of CO consumptions (circle), CO_2 (square), acetate generation (triangle), and optical densities (600 nm) (diamond) of the evolved populations (bluish green lines) compared to the parental strain (gray lines) under 44% CO syngas condition. **(D)** The growth rates of ECO (bluish green bar) compared to the parental strain (gray bar) under 0%, 20%, 40%, 60%, 80%, and 100% CO that is balanced by N_2. "na" is not available. **(E)** The maximum optical densities (600 nm) of the parental strain (gray bar) and ECO (bluish green bar) under 0%, 20%, 40%, 60%, 80%, and 100% CO, which balanced by N_2. **(F)** Acetate production of ECO (pink bar) compared to the parental strain (gray bar) under 0%, 20%, 40%, 60%, 80%, and 100% CO that is balanced by N_2. The cells were anaerobically cultivated at 37°C in 150 mL anaerobic bottle containing 100 mL of the modified DSMZ 135 medium with 50 mL of headspace purged at a pressure of 200 kPa. Error bars indicate standard deviation of biological triplicates. Asterisks indicates as following: *: *P*-value ≤ 0.05, **: *P*-value ≤ 0.01, ***: *P*-value ≤ 0.001.

that 0.274 ± 0.060, 3.835 ± 0.215, 6.819 ± 0.457, 8.311 ± 0.254, 0.866 ± 0.217, and 0.264 ± 0.043 mM of acetate were produced under 0%, 20%, 40%, 60%, 80%, and 100% CO conditions (**Figure 2F**). In general, the acetate productions of the ECO were growth dependent, similar to those of the parental strain; however, they were increased compared to the production by the parental strain. Such results indicate that the adaptively evolved *E. limosum* enhanced CO consumption, growth, and tolerance under the autotrophic conditions, thus questioning about genetic mutations causing the phenotypic changes.

Mutation Profiles by Whole Genome Resequencing

Adaptive laboratory evolution allows a target organism to adapt to the desired condition by modifying the genotype, rewiring and changing the metabolic pathways, and altering enzyme kinetics in the organism. Identification of mutations in the genome throughout the ALE is important to understand the fitness landscape of the organism under the growth condition. Although the ALE revealed that the fitness, tolerance, and acetate production were increased under the 44% CO condition, the causal genotypic changes and their collateral effects on the phenotype remain unclear. To address this, the four evolved populations at initial, 50th, 100th, and 150th generation were proceeded for whole genome resequencing. We identified 39 mutations in all adapted strains, locating 33 and 6 mutations in the genic and intergenic regions, respectively (**Supplementary Table S3**).

Among these, five common mutations were identified across the populations, resulting in five key mutations with top 15% mutation frequency in the evolved populations. The five mutations were located in ELIM_c1038, ELIM_c1073, and ELIM_c1653 as single nucleotide variations (SNVs) and ELIM_c1031 and ELIM_c1654 as nucleotide insertion mutations (**Table 1**). For SNVs, $E^{48}K$ in ELIM_c1038, $Y^{136}X$ in ELIM_c1073, and $A^{97}E$ in ELIM_c1653 were identified, which are responsible for putative ATPase, DNA methylase (*dam*), and CODH catalytic subunit (*acsA*), respectively. For the insertional mutations, $N^{119}KfsX133$ in ELIM_c1031 encoding integrase protein and $A^{72}AfsX92$ in ELIM_c1654 encoding CODH accessory protein (*cooC2*) were observed. Of the five mutated genes, two mutations were located in the putative genes, and interestingly the other three mutations were located in the genes with certain functional roles, of which two mutations occurred in CODH/ACS complex coding genes, *acsA* and *cooC2,* that were reported to play a pivotal role for the active site and maturity of the complex (Morton et al., 1991; Kerby et al., 1997; Bender et al., 2011). The mutation in *acsA* was not located at the activate sites of the enzyme; however, substituting a small non-polar

TABLE 1 | Key mutations in the evolved populations.

Locus tag	Gene	Mutation (Type)	AA change	Description
ELIM_c1031	–	−356T (insertion)	$Asn^{119}LysfsX133$	Integrase family protein
ELIM_c1038	–	G133A (SNV)	$Glu^{48}Lys$	Putative ATPase, transposase-like protein
ELIM_c1073	*dam*	T408G (SNV)	$Tyr^{136}X$	N6 adenine-specific DNA methylase D12 class
ELIM_c1653	*acsA*	C290A (SNV)	$Ala^{97}Glu$	CODH catalytic subunit
ELIM_c1654	*cooC2*	−216A (insertion)	$Ala^{72}AlafsX92$	CODH nickel insertion accessory protein

amino acid into a large polar amino acid potentially altered the protein structure that affects the enzymatic activity. The other mutation, which occurred in *cooC2*, introduced an early stop codon at 20th amino acid downstream of the mutation site, which revealed synonymous substitution at the mutation site. The early termination often leads to a loss of function, suggesting that, despite the importance of *cooC* under the autotrophic growth condition, the functional role of the gene in the evolved strain may be ineffective. Collectively, the five mutations were the dominant variants, and three mutations were located in the genes with functional roles, of which *acsA* was hypothesized to be the driving mutation for the altered phenotype in adapted strain under autotrophic condition.

Effect of the Mutation in *acsA* on CO Fixation

In order to validate the hypothesis, obtaining a strain from ECO with the mutation on *acsA* is essential. For obtaining a single clone with the *acsA* mutation from the evolved populations, 20 colonies were isolated, which then confirmed the presence of *acsA* mutation in 17 of 20 colonies. Of the obtained 17 colonies, a single clone with the *acsA* mutation and without the other key mutations was selected, labeling as ECO_acsA strain (**Supplementary Figure S2**). The obtained strain, ECO_acsA, underwent genome resequencing to identify the mutations embedded in the genome, resulting in six mutations with four in the genic regions and two in the intergenic regions (**Supplementary Table S4**). The four mutations were associated with ELIM_c0006, ELIM_c1653, ELIM_c2214, and ELIM_c2227. Of the four mutations, only ELIM_c1653, which encodes *acsA*, is associated with the autotrophic growth condition.

Initially, growth profile of the strain under syngas condition with 44% CO was measured and compared to the parental strain, resulting in a growth rate of 0.095 ± 0.000 h^{-1} and 0.050 ± 0.001 h^{-1} and a maximum optical density (600 nm) of 0.703 ± 0.023 and 0.498 ± 0.028 for ECO_acsA and parental strain, respectively (**Figure 3A**). These results indicate that ECO_acsA strain proliferates more rapidly by 1.90 folds with higher optical densities (600 nm) by 1.41 folds than the parental strain under CO condition.

To further understand the phenotypic changes, CO consumed and metabolites produced by the ECO_acsA strain were measured under the syngas condition with 44% CO. In accordance to the previous analysis on metabolites, acetate was the dominant end product produced by the ECO_acsA strain, with 6.889 mM. Increase in the acetate production by the strain indicates that the altered C-cluster of the active site of CODH subunit encoded by the mutated *acsA* enhanced CO utilization (**Figure 3A**). Consistent with acetate production, the CO consumption rates by ECO_acsA and parental strain were 0.059 ± 0.002 and 0.043 ± 0.019 mmol h^{-1}, respectively, which differed by 1.37 folds (**Figure 3A**).

Although the growth rate under CO condition was enhanced, the increase in CO tolerance of ECO_acsA strain compared to the parental strain remains unclear. To measure the CO tolerance, the strain was cultured under different CO concentrations. The growth rates of ECO_acsA strain under 20% and 40% CO conditions were 0.070 ± 0.001 and 0.079 ± 0.001 h^{-1}, and these decreased for the strains cultured under high CO conditions with 0.059 ± 0.001, 0.043 ± 0.002, and 0.040 ± 0.001 h^{-1} for 60%, 80%, and 100% CO, respectively (**Figure 3B**). Although the growth rates decreased with increasing CO concentrations, compared to the parental strain, the growth rates of the ECO_acsA strain were increased by 2.25 folds under 40% CO, and the maximum optical density (600 nm) under all CO concentrations (**Supplementary Figure S3**), representing CO tolerance of the strain was greatly enhanced. Based on these results, our hypothesis, in which the mutation on *acsA* affects phenotype of the *E. limosum* under CO growth conditions, was tested through growth profiling and metabolite measurement experiments. We conclude that, indeed, the speculation was correct with enhanced growth rate, CO consumption rate, acetate production, and CO tolerance under CO growth conditions, suggesting that mutation on *acsA* is essential to engineer the strain for CO utilization.

Acetoin Production by ECO_acsA Strain

The ECO_acsA strain demonstrated the enhanced CO consumption and growth rates, thereby querying whether the evolved strain is a better platform to produce biochemical than the parental strain. To investigate the strain capacity to produce biochemicals, acetoin was selected as a target chemical, which is widely utilized in various industries from cosmetics, food flavoring, and pharmaceuticals (Werpy and Petersen, 2004; Bao et al., 2015). Interestingly, in *E. limosum*, the acetoin biosynthetic pathway coding genes are located, but the production was not detected under CO and other conditions, such as glucose and H_2/CO_2 conditions (Song et al., 2017, 2018). In the presence of the genes, *E. limosum* is capable of synthesizing acetoin; however, the insignificant transcriptional and translational expressions under the heterotrophic and autotrophic conditions prevent the production, according to a previous study (Song et al., 2018). Thus, activation of the biosynthetic pathway coding genes using novel bio-parts potentially produce acetoin in *E. limosum*, and

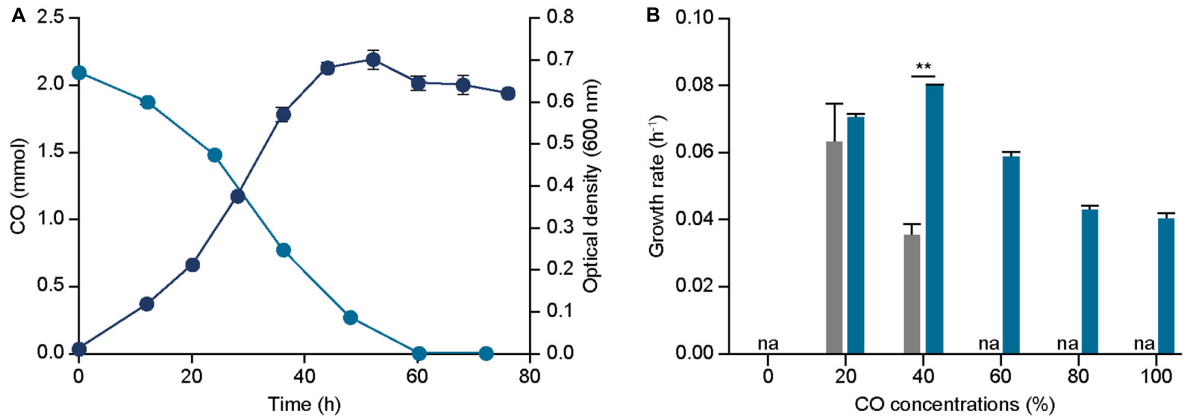

FIGURE 3 | Effect of *acsA* mutation on growth and CO tolerance. **(A)** The profile of CO consumptions (bluish green circle), and optical densities (600 nm) (navy circle) of ECO_acsA under 44% CO syngas. **(B)** The growth rates of ECO_acsA (bluish green bar) and parental strain (gray bar) under 0%, 20%, 40%, 60%, 80%, and 100% CO conditions that are balanced by N_2. The cells were anaerobically cultivated at 37°C in 150 mL anaerobic bottle containing 100 mL of the modified DSMZ 135 medium with 50 mL of headspace purged at a pressure of 200 kPa. "na" is not available. Error bars indicate standard deviation of three biological replicates. Asterisks indicates as following: **: *P*-value ≤ 0.01.

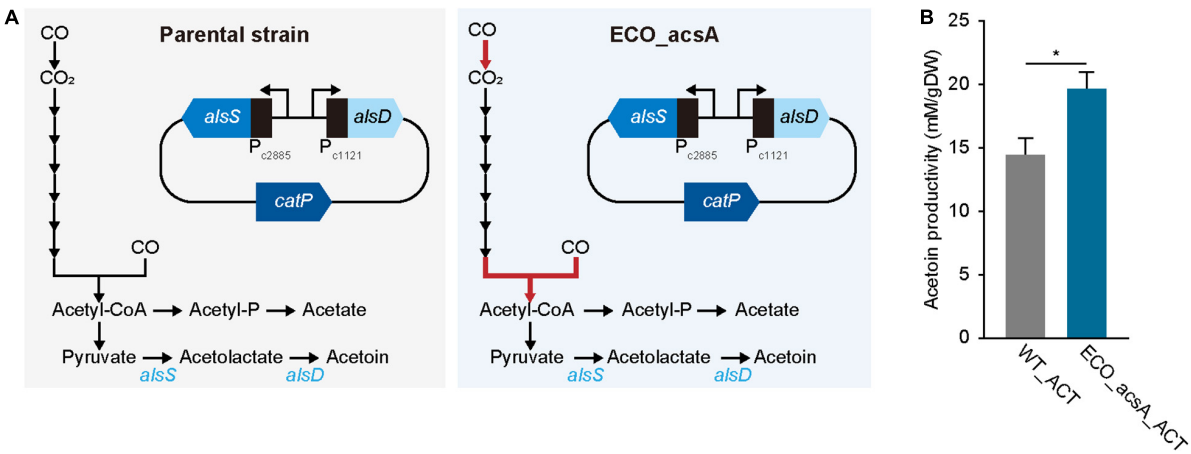

FIGURE 4 | Acetoin production by *Eubacterium limosum*. **(A)** Metabolic pathway from CO to acetoin, in presence of the acetoin biosynthesis carrying plasmid. The constructed plasmid was transformed to ECO_acsA and the parental strain, which was named ECO_acsA_ACT and WT_ACT, respectively. The red arrow indicates CODH/ACS reaction encoded by *acsA*. **(B)** The production of acetoin by ECO_acsA_ACT (bluish green bar) and the WT_ACT (gray bar). The cells were anaerobically cultivated at 37°C in 150 mL anaerobic bottle containing 100 mL of the modified DSMZ 135 medium with 50 mL of headspace purged at a pressure of 200 kPa. Error bars indicate standard deviation of biological triplicates. Asterisks indicates as following: *: *P*-value ≤ 0.05.

then determine whether ECO_acsA is a superior platform to produce the biochemical compounds.

To produce acetoin, a plasmid with *alsS*, which encodes α-acetolactate synthase that condenses two molecules of pyruvate to one acetolactate, and *alsD*, which encodes acetolactate decarboxylase that converts acetolactate to acetoin, was constructed (**Figure 4A** and see "Materials and methods" for more details). For activating the biosynthesis, bio-parts associated with highly expressed genes that are functionally related to CO metabolism were selected, locating promoters of ELIM_c2885 encoding pyruvate:ferredoxin oxidoreductase and ELIM_c1121 encoding hydrogenase subunit for *alsS* and *alsD*, respectively, with 5′ untranslated region that was obtained from ELIM_c1121 (**Figure 4A**; Song et al., 2018). Following the construction, the plasmid was transformed into the parental strain, which was then cultured for biological triplicates under the syngas condition with 44% CO, proliferating with cell density of 0.053 ± 0.002 gDW and producing acetoin of 14.6 ± 0.8 mM/gDW, along with 23.3 ± 1.5 mM/gDW acetate, 4.0 ± 0.0 mM/gDW butyrate, and 6.2 ± 1.7 mM/gDW lactate, which recovered 96.2% of carbons (**Figure 4B**). After confirming acetoin production, the same plasmid was introduced into ECO_acsA strain, and was then cultured under similar CO condition; thereafter, the acetoin production was measured, resulting in 19.6 ± 1.3 mM/gDW, which significantly increased by 1.34 folds (*P*-value ≤ 0.015). In addition, ECO_acsA strain with cell density of 0.034 ± 0.001 gDW produced 23.6 ± 1.1 mM/gDW acetate, 6.4 ± 0.2 mM/gDW butyrate,

TABLE 2 | Comparison of the growth rates of acetogens.

Strain	Gas condition	Growth rate	References
Acetobacterium woodii	5% CO/16% CO_2/64% H_2 (100 kPa)	0.028 h^{-1}	Bertsch and Müller, 2015
	10% CO/16% CO_2/64% H_2 (100 kPa)	~ 0.022 h^{-1}	
	15% CO/16% CO_2/64% H_2 (100 kPa)	~ 0.011 h^{-1}	
	25% CO/15% CO_2 (100 kPa)	No growth	
Butyribacterium methylotrophicum	100% CO (100 kPa)	0.050 h^{-1}	Lynd et al., 1982
Clostridium autoethanogenum	45% CO/20% CO_2/2% H_2 (200 kPa)*	0.057 ± 0.04 h^{-1}	Marcellin et al., 2016
	100% CO (200 kPa)	0.019 h^{-1}	Liew et al., 2016
Clostridium carboxidivorans	100% CO (120 kPa)	0.084 ± 0.004 h^{-1}	Fernandez-Naveira et al., 2016
Clostridium ljungdahlii	80% CO/20% CO_2 (200 kPa)	0.060 h^{-1}	Phillips et al., 1994
Eubacterium limosum	44% CO/22% CO_2/2% H_2 (200 kPa)*	0.095 ± 0.000 h^{-1}	This study
Moorella thermoacetica	30% CO/30% CO_2 (240 kPa)	0.069 h^{-1}	Daniel et al., 1990
Thermoanaerobacter kivui	CO 20% (200 kPa) Makeup gas (80% N_2/20% CO_2)	0.037 h^{-1}	Weghoff and Müller, 2016
	CO 50% (200 kPa) Makeup gas (80% N_2/20% CO_2)	0.045 h^{-1}	
	CO 70% (200 kPa) Makeup gas (80% N_2/20% CO_2)	0.068 h^{-1}	
	CO 90% (200 kPa) Makeup gas (80% N_2/20% CO_2)	0.020 h^{-1}	
	CO 100% (200 kPa)	0.021 h^{-1}	

**Industrial syngas composition.*

and 0.7 ± 0.5 mM/gDW lactate, which recovering 86.7% of carbons. Regarding CO consumption, the WT_ACT strain consumed with 429.8 ± 131.6 mM/gDW and ECO_acsA_ACT strain consumed 642.7 ± 317.8 mM/gDW, indicating higher CO consumption value by ECO_acsA_ACT strain compared to that by WT_ACT strain. Less consumption of CO leads to needing for the reduced ferredoxin, which is essential for *E. limosum* under autotrophic growth condition by generating a chemiosmosis gradient that synthesizes ATP. Depletion of reduced ferredoxin can be replenished by producing lactate from pyruvate via lactate dehydrogenase reaction, which oxidizes NADH and reduces ferredoxin. Based on the assumption, compared to ECO_acsA_ACT strain, the WT_ACT strain consumed less CO that caused less available reduced ferredoxin. To overcome the needs, the WT_ACT strain produced more lactate by catalyzing lactate dehydrogenase that produces reduced ferredoxin. Whereas, with the increased CO consumption capacity and more reduced ferredoxin available, ECO_acsA_ACT strain does not need to catalyze lactate dehydrogenase and alter the carbon flux to produce acetoin. Therefore, the authors hypothesize that the ECO_acsA strain produced significantly enhanced the amount of acetoin, using increased capacity with increased CO consumption and CO tolerance. Further studies on metabolic engineering are needed to verify the effects of the mutations on the change of the production by the acetogens.

DISCUSSION

Converting CO into biofuels and biochemicals provides several advantages such as low feedstock cost, utilization of harmful gas, and reduction of climate-changing substrate. Despite the advantages, CO has been a challenging feedstock due to lack of suitable microorganisms that tolerate and utilize CO as a substrate. Among the candidate organisms, acetogens have been suggested as a crucial platform to convert CO into various biochemicals using the WLP that oxidizes CO into CO_2, and then into an important major metabolite, acetyl-CoA. All acetogens carry the unique pathway to synthesize acetyl-CoA under autotrophic growth conditions; however, the growth is inhibited under high CO concentrations, indicating that CO utilizing acetogens are intolerant toward CO. According to the previous studies, growth of *A. woodii*, a model acetogen that is phylogenetically related to *E. limosum*, is completely inhibited by the presence of CO with higher than 25% in the culture headspace (Bertsch and Müller, 2015). In this study, using ALE, the growth rate and CO tolerance of *E. limosum* were enhanced, which is highly related with the previous studies on *Thermoanaerobacter kivui* and *Butyribacterium methylotrophicum*. The studies reported that passaging the strains under CO conditions few times enhanced the utilization of CO as a feedstock, suggesting that wild type acetogens under CO conditions are not optimal and further enhancement is possible via ALE (Lynd et al., 1982; Weghoff and Müller, 2016). The enhanced growth rate of *E. limosum* was higher than that of other acetogens under CO conditions, including the growth rates of the adjusted acetogens (**Table 2**). Prior to this study, the highest growth rate under CO growth condition was that of *Clostridium carboxidivorans* (0.084 h^{-1}), followed by *T. kivui* (0.068 h^{-1}) and *C. ljungdahlii* (0.060 h^{-1}), which are known as CO utilizing organisms (Phillips et al., 1994; Fernandez-Naveira et al., 2016; Weghoff and Müller, 2016). The growth rates of *E. limosum* under CO condition changed from 0.058 to 0.089 h^{-1} and increased by 1.53 folds through the ALE, and the growth rate under 100% CO condition was 0.048 h^{-1}, thus indicating that *E. limosum* is one of the fastest growing acetogen strains under the autotrophic growth condition.

Understanding the genomes of phenotypically altered organisms reveals a relationship between the genotype and phenotype. Genome resequencing of the evolved *E. limosum*

identified five key mutations sites in the genome. Specifically, mutations on *acsA* and *cooC2* were in accordance with the previous understanding on CO oxidization mechanism that CODH/ACS complex plays a vital role under the CO fixing condition. However, the mutation on *cooC2*, which is crucial for CO oxidation by activating CODH/ACS protein complex by binding to the essential metals, contradicts our hypothesis by introducing an early stop codon at 20 sequences downstream of the mutation site, thus reducing the protein comprising 261 amino acids to 92 amino acids. The insertion of early stop codon prevents translation of the *cooC2* active site that is located at Cys116 and Cys118, which are the conserved sites for metal binding, leading to loss of function. In the previous study (Merrouch et al., 2018), increase in the *cooC* expression elevated CODH activity only in media without nickel supplementation; however, in the present study, nickel was supplemented in the media, making *cooC2* unessential under the condition that led to an introduction of a stop codon for the loss of function; whereas, a mutation on *acsA*, which is responsible for C-cluster of CODH/ACS complex, potentially altered the protein structure.

In the evolved strain, ECO, metabolite production pattern changed compared to the wild type *E. limosum*. In the wild type, acetate was majorly produced, which was similar for the ECO. Interestingly, the ECO, with higher growth rate compared to wild type, produced butyrate under CO condition, with acetate as the major metabolite. Despite the similarity at the genomic level between the *E. limosum* strains (ATCC 8486 and KIST612), butyrate production was not observed for wild type *E. limosum* ATCC 8486 under the CO condition, thus contradicting the previous report on *E. limosum* KIST612 (Chang et al., 1998). *E. limosum* KIST612 produced acetate and butyrate under CO condition (Jeong et al., 2015). For butyrate production, three additional reduction powers are required that recycle the excessive reducing equivalents, with potential ATP production (Kerby et al., 1997). CO oxidation generates reducing equivalent that needs to be oxidized, often utilized for reducing WLP enzymes to convert carbons and pumping ions across the membrane to create a chemiosmotic gradient for ATP synthesis. Based on the phenotypic results, the ECO altered the metabolite pathway to produce butyrate for oxidizing excessive reduction power and generating ATP, which potentially oxidizes CO faster with more available oxidized electron carriers that needs to be further validated (**Supplementary Figure S4**). Overall, we developed *E. limosum* strain that tolerates and efficiently utilizes CO as feedstock via ALE, then identified a key mutation on *acsA* encoding a subunit of CODH/ACS complex that caused phenotypic traits, and thereafter validated the hypothesis through phenotypic assays. Eventually, we utilized the ECO_acsA strain to construct an engineered strain to produce biochemical using CO as carbon source. The results will serve as an important resource for optimizing CO fermentation and strain designing for better biochemical production.

DATA AVAILABILITY STATEMENT

The whole genome resequencing data analyzed by this study are available in the EMBL European Nucleotide Archive (ENA) with Primary accession number PRJEB34640.

AUTHOR CONTRIBUTIONS

B-KC conceived and supervised the study. SK, SJ, JS, and B-KC designed the experiments. SK, SJ, and JB performed the experiments. SK, YS, SJ, SC, J-KL, DK, SCK, and B-KC analyzed the data. SK, YS, SC, and B-KC wrote the manuscript. All authors read and approved the final manuscript.

FUNDING

This work was supported by the Intelligent Synthetic Biology Center of the Global Frontier Project (2011-0031957 to B-KC) and the C1 Gas Refinery Program (2018M3D3A1A01055733 to B-KC) through the National Research Foundation of Korea (NRF) funded by the Ministry of Science and ICT (MSIT).

SUPPLEMENTARY MATERIAL

The Supplementary Material for this article can be found online at: https://www.frontiersin.org/articles/10.3389/fmicb.2020.00402/full#supplementary-material

REFERENCES

Abubackar, H. N., Veiga, M. C., and Kennes, C. (2015). Carbon monoxide fermentation to ethanol by *Clostridium autoethanogenum* in a bioreactor with no accumulation of acetic acid. *Bioresour. Technol.* 186, 122–127. doi: 10.1016/j.biortech.2015.02.113

Alfano, M., Perard, J., Carpentier, P., Basset, C., Zambelli, B., Timm, J., et al. (2019). The carbon monoxide dehydrogenase accessory protein CooJ is a histidine-rich multidomain dimer containing an unexpected Ni(II)-binding site. *J. Biol. Chem.* 294, 7601–7614. doi: 10.1074/jbc.RA119.008011

Appel, A. M., Bercaw, J. E., Bocarsly, A. B., Dobbek, H., Dubois, D. L., Dupuis, M., et al. (2013). Frontiers, opportunities, and challenges in biochemical and chemical catalysis of CO_2 fixation. *Chem. Rev.* 113, 6621–6658.

Bao, T., Zhang, X., Zhao, X., Rao, Z., Yang, T., and Yang, S. (2015). Regulation of the NADH pool and NADH/NADPH ratio redistributes acetoin and 2,3-butanediol proportion in *Bacillus subtilis*. *Biotechnol. J.* 10, 1298–1306. doi: 10.1002/biot.201400577

Bender, G., Pierce, E., Hill, J. A., Darty, J. E., and Ragsdale, S. W. (2011). Metal centers in the anaerobic microbial metabolism of CO and CO_2. *Metallomics* 3, 797–815. doi: 10.1039/c1mt00042j

Bengelsdorf, F. R., Straub, M., and Durre, P. (2013). Bacterial synthesis gas (syngas) fermentation. *Environ. Technol.* 34, 1639–1651. doi: 10.1080/09593330.2013.827747

Bertsch, J., and Müller, V. (2015). CO Metabolism in the acetogen *Acetobacterium woodii*. *Appl. Environ. Microbiol.* 81, 5949–5956. doi: 10.1128/AEM.01772-15

Bredwell, M. D., Srivastava, P., and Worden, R. M. (1999). Reactor design issues for synthesis-gas fermentations. *Biotechnol. Prog.* 15, 834–844. doi: 10.1021/bp990108m

Can, M., Armstrong, F. A., and Ragsdale, S. W. (2014). Structure, function, and mechanism of the nickel metalloenzymes, CO dehydrogenase, and acetyl-CoA synthase. *Chem. Rev.* 114, 4149–4174. doi: 10.1021/cr400461p

Chang, I. S., Kim, D. H., Kim, B. H., Shin, P. K., Sung, H. C., and Lovitt, R. W. (1998). CO fermentation of *Eubacterium limosum* KIST612. *J. Microbiol. Biotechnol.* 8, 134–140.

Choe, D., Lee, J. H., Yoo, M., Hwang, S., Sung, B. H., Cho, S., et al. (2019). Adaptive laboratory evolution of a genome-reduced *Escherichia coli*. *Nat. Commun.* 10:935. doi: 10.1038/s41467-019-08888-6

Daniel, S. L., Hsu, T., Dean, S. I., and Drake, H. L. (1990). Characterization of the H2- and CO-dependent chemolithotrophic potentials of the acetogens *Clostridium thermoaceticum* and *Acetogenium kivui*. *J. Bacteriol.* 172, 4464–4471. doi: 10.1128/jb.172.8.4464-4471.1990

Darnault, C., Volbeda, A., Kim, E. J., Legrand, P., Vernede, X., Lindahl, P. A., et al. (2003). Ni-Zn-[Fe4-S4] and Ni-Ni-[Fe4-S4] clusters in closed and open subunits of acetyl-CoA synthase/carbon monoxide dehydrogenase. *Nat. Struct. Biol.* 10, 271–279. doi: 10.1038/nsb912

Diekert, G. B., and Thauer, R. K. (1978). Carbon monoxide oxidation by *Clostridium thermoaceticum* and *Clostridium formicoaceticum*. *J. Bacteriol.* 136, 597–606. doi: 10.1128/jb.136.2.597-606.1978

Doukov, T. I., Iverson, T. M., Seravalli, J., Ragsdale, S. W., and Drennan, C. L. (2002). A Ni-Fe-Cu center in a bifunctional carbon monoxide dehydrogenase/acetyl-CoA synthase. *Science* 298, 567–572. doi: 10.1126/science.1075843

Dragosits, M., and Mattanovich, D. (2013). Adaptive laboratory evolution - principles and applications for biotechnology. *Microb. Cell. Fact.* 12:64. doi: 10.1186/1475-2859-12-64

Drake, H. L., Gossner, A. S., and Daniel, S. L. (2008). Old acetogens, new light. *Ann. N. Y. Acad. Sci.* 1125, 100–128. doi: 10.1196/annals.1419.016

Drake, H. L., Küsel, K., and Matthies, C. (2006). "Acetogenic prokaryotes," in *The Prokaryotes - Prokaryotic Physiology and Biochemistry*, eds E. Rosenberg, E. F. DeLong, S. Lory, E. Stackebrandt, and F. Thompson (New York, NY: Springer), 354–420. doi: 10.1007/0-387-30742-7_13

Drennan, C. L., Doukov, T. I., and Ragsdale, S. W. (2004). The metalloclusters of carbon monoxide dehydrogenase/acetyl-CoA synthase: a story in pictures. *J. Biol. Inorg. Chem.* 9, 511–515. doi: 10.1007/s00775-004-0563-y

Elena, S. F., and Lenski, R. E. (2003). Evolution experiments with microorganisms: the dynamics and genetic bases of adaptation. *Nat. Rev. Genet.* 4, 457–469. doi: 10.1038/nrg1088

Fernandez-Naveira, A., Abubackar, H. N., Veiga, M. C., and Kennes, C. (2016). Carbon monoxide bioconversion to butanol-ethanol by *Clostridium carboxidivorans*: kinetics and toxicity of alcohols. *Appl. Microbiol. Biotechnol.* 100, 4231–4240. doi: 10.1007/s00253-016-7389-8

Henstra, A. M., Sipma, J., Rinzema, A., and Stams, A. J. (2007). Microbiology of synthesis gas fermentation for biofuel production. *Curr. Opin. Biotechnol.* 18, 200–206. doi: 10.1016/j.copbio.2007.03.008

Jeong, J., Bertsch, J., Hess, V., Choi, S., Choi, I. G., Chang, I. S., et al. (2015). Energy conservation model based on genomic and experimental analyses of a carbon monoxide-utilizing, butyrate-forming acetogen, *Eubacterium limosum* KIST612. *Appl. Environ. Microbiol.* 81, 4782–4790. doi: 10.1128/AEM.00675-15

Kerby, R. L., Ludden, P. W., and Roberts, G. P. (1997). In vivo nickel insertion into the carbon monoxide dehydrogenase of *Rhodospirillum rubrum*: molecular and physiological characterization of cooCTJ. *J. Bacteriol.* 179, 2259–2266. doi: 10.1128/jb.179.7.2259-2266.1997

Köpke, M., Held, C., Hujer, S., Liesegang, H., Wiezer, A., Wollherr, A., et al. (2010). *Clostridium ljungdahlii* represents a microbial production platform based on syngas. *Proc. Natl. Acad. Sci. U.S.A.* 107, 13087–13092. doi: 10.1073/pnas.1004716107

Köpke, M., Mihalcea, C., Liew, F., Tizard, J. H., Ali, M. S., Conolly, J. J., et al. (2011). 2,3-butanediol production by acetogenic bacteria, an alternative route to chemical synthesis, using industrial waste gas. *Appl. Environ. Microbiol.* 77, 5467–5475. doi: 10.1128/AEM.00355-11

Latif, H., Zeidan, A. A., Nielsen, A. T., and Zengler, K. (2014). Trash to treasure: production of biofuels and commodity chemicals via syngas fermenting microorganisms. *Curr. Opin. Biotechnol.* 27, 79–87. doi: 10.1016/j.copbio.2013.12.001

Liew, F., Henstra, A. M., Winzer, K., Kopke, M., Simpson, S. D., and Minton, N. P. (2016). Insights into CO_2 fixation pathway of *Clostridium autoethanogenum* by targeted mutagenesis. *MBio* 7:e00427-16. doi: 10.1128/mBio.00427-16

Ljungdahl, L. G. (1986). The autotrophic pathway of acetate synthesis in acetogenic bacteria. *Annu. Rev. Microbiol.* 40, 415–450. doi: 10.1146/annurev.mi.40.100186.002215

Loke, H. K., and Lindahl, P. A. (2003). Identification and preliminary characterization of AcsF, a putative Ni-insertase used in the biosynthesis of acetyl-CoA synthase from *Clostridium thermoaceticum*. *J. Inorg. Biochem.* 93, 33–40. doi: 10.1016/s0162-0134(02)00457-9

Lynd, L., Kerby, R., and Zeikus, J. G. (1982). Carbon monoxide metabolism of the methylotrophic acidogen *Butyribacterium methylotrophicum*. *J. Bacteriol.* 149, 255–263. doi: 10.1128/jb.149.1.255-263.1982

Marcellin, E., Behrendorff, J. B., Nagaraju, S., DeTissera, S., Segovia, S., Palfreyman, R. W., et al. (2016). Low carbon fuels and commodity chemicals from waste gases – systematic approach to understand energy metabolism in a model acetogen. *Green Chem.* 18, 3020–3028. doi: 10.1039/c5gc02708j

Merrouch, M., Benvenuti, M., Lorenzi, M., Leger, C., Fourmond, V., and Dementin, S. (2018). Maturation of the [Ni-4Fe-4S] active site of carbon monoxide dehydrogenases. *J. Biol. Inorg. Chem.* 23, 613–620. doi: 10.1007/s00775-018-1541-0

Morton, T. A., Runquist, J. A., Ragsdale, S. W., Shanmugasundaram, T., Wood, H. G., and Ljungdahl, L. G. (1991). The primary structure of the subunits of carbon-monoxide dehydrogenase/acetyl-coa synthase from *Clostridium-Thermoaceticum*. *J. Biol. Chem.* 266, 23824–23828.

Munasinghe, P. C., and Khanal, S. K. (2010). Biomass-derived syngas fermentation into biofuels: opportunities and challenges. *Bioresour. Technol.* 101, 5013–5022. doi: 10.1016/j.biortech.2009.12.098

Oliver, J. W., Machado, I. M., Yoneda, H., and Atsumi, S. (2013). Cyanobacterial conversion of carbon dioxide to 2,3-butanediol. *Proc. Natl. Acad. Sci. U. S.A.* 110, 1249–1254. doi: 10.1073/pnas.1213024110

Park, S., Yasin, M., Jeong, J., Cha, M., Kang, H., Jang, N., et al. (2017). Acetate-assisted increase of butyrate production by *Eubacterium limosum* KIST612 during carbon monoxide fermentation. *Bioresour. Technol.* 245, 560–566. doi: 10.1016/j.biortech.2017.08.132

Phillips, J. R., Clausen, E. C., and Gaddy, J. L. (1994). Synthesis Gas as Substrate for the Biological Production of Fuels and Chemicals. *Appl. Biochem. Biotechnol.* 4, 145–157. doi: 10.1007/bf02941794

Ragsdale, S. W. (1997). The eastern and western branches of the Wood/Ljungdahl pathway: how the east and west were won. *Biofactors* 6, 3–11. doi: 10.1002/biof.5520060102

Ragsdale, S. W. (2008). Enzymology of the wood-ljungdahl pathway of acetogenesis. *Ann. N.Y. Acad. Sci.* 1125, 129–136. doi: 10.1196/annals.1419.015

Ragsdale, S. W., and Pierce, E. (2008). Acetogenesis and the Wood-Ljungdahl pathway of CO_2 fixation. *Biochim. Biophys. Acta.* 1784, 1873–1898. doi: 10.1016/j.bbapap.2008.08.012

Schuchmann, K., and Müller, V. (2014). Autotrophy at the thermodynamic limit of life: a model for energy conservation in acetogenic bacteria. *Nat. Rev. Microbiol.* 12, 809–821. doi: 10.1038/nrmicro3365

Seravalli, J., Kumar, M., Lu, W. P., and Ragsdale, S. W. (1997). Mechanism of carbon monoxide oxidation by the carbon monoxide dehydrogenase/acetyl-CoA synthase from *Clostridium thermoaceticum*: kinetic characterization of the intermediates. *Biochemistry* 36, 11241–11251. doi: 10.1021/bi970590m

Shin, J., Kang, S., Song, Y., Jin, S., Lee, J. S., Lee, J. K., et al. (2019). Genome engineering of *Eubacterium limosum* using expanded genetic tools and the CRISPR-Cas9 system. *ACS. Synth. Biol.* 8, 2059–2068. doi: 10.1021/acssynbio.9b00150

Song, Y., Shin, J., Jeong, Y., Jin, S., Lee, J. K., Kim, D. R., et al. (2017). Determination of the genome and primary transcriptome of syngas fermenting *Eubacterium limosum* ATCC 8486. *Sci. Rep.* 7:13694. doi: 10.1038/s41598-017-14123-3

Song, Y., Shin, J., Jin, S., Lee, J. K., Kim, D. R., Kim, S. C., et al. (2018). Genome-scale analysis of syngas fermenting acetogenic bacteria reveals the translational regulation for its autotrophic growth. *BMC Genomics* 19:837. doi: 10.1186/s12864-018-5238-0

Subramani, V., and Gangwal, S. K. (2008). A review of recent literature to search for an efficient catalytic process for the conversion of syngas to ethanol. *Energy. Fuels.* 22, 814–839. doi: 10.1021/ef700411x

Valgepea, K., De Souza Pinto Lemgruber, R., Abdalla, T., Binos, S., Takemori, N., Takemori, A., et al. (2018). H_2 drives metabolic rearrangements in gas-fermenting *Clostridium autoethanogenum*. *Biotechnol. Biofuels.* 11, 55. doi: 10.1186/s13068-018-1052-9

Weghoff, M. C., and Müller, V. (2016). CO metabolism in the thermophilic acetogen *Thermoanaerobacter kivui*. *Appl. Environ. Microbiol.* 82, 2312–2319. doi: 10.1128/AEM.00122-16

Werpy, T., and Petersen, G. (2004). *Top Value Added Chemicals From Biomass: Volume I-Results of Screening for Potential Candidates From Sugars and Synthesis Gas*. Golden, CO: National Renewable Energy Lab.

Conflict of Interest: The authors declare that the research was conducted in the absence of any commercial or financial relationships that could be construed as a potential conflict of interest.

frontiers in Microbiology

ORIGINAL RESEARCH
published: 17 March 2020
doi: 10.3389/fmicb.2020.00416

Energy Conservation and Carbon Flux Distribution During Fermentation of CO or H_2/CO_2 by *Clostridium ljungdahlii*

Hai-Feng Zhu[1†], Zi-Yong Liu[2†], Xia Zhou[3], Ji-Hong Yi[4], Zeng-Min Lun[3], Shu-Ning Wang[4], Wen-Zhu Tang[1] and Fu-Li Li[2*]*

[1] School of Biological Engineering, Dalian Polytechnic University, Dalian, China, [2] Shandong Provincial Key Laboratory of Synthetic Biology, Key Laboratory of Biofuels, Qingdao Institute of Bioenergy and Bioprocess Technology, Chinese Academy of Sciences, Qingdao, China, [3] State Key Laboratory of Shale Oil and Gas Enrichment Mechanisms and Effective Development, SINOPEC Exploration and Production Research Institute, Beijing, China, [4] State Key Laboratory of Microbial Technology, Shandong University, Qingdao, China

OPEN ACCESS

Edited by:
Mirko Basen,
University of Rostock, Germany

Reviewed by:
Largus Angenent,
University of Tübingen, Germany
Nicolai Müller,
University of Konstanz, Germany

***Correspondence:**
Wen-Zhu Tang
tangwenzhu2000@163.com
Fu-Li Li
lifl@qibebt.ac.cn

[†] These authors have contributed equally to this work

Specialty section:
This article was submitted to Microbiotechnology, a section of the journal Frontiers in Microbiology

Received: 11 September 2019
Accepted: 27 February 2020
Published: 17 March 2020

Citation:
Zhu H-F, Liu Z-Y, Zhou X, Yi J-H, Lun Z-M, Wang S-N, Tang W-Z and Li F-L (2020) Energy Conservation and Carbon Flux Distribution During Fermentation of CO or H_2/CO_2 by Clostridium ljungdahlii. Front. Microbiol. 11:416. doi: 10.3389/fmicb.2020.00416

Both CO and H_2 can be utilized as energy sources during the autotrophic growth of *Clostridium ljungdahlii*. In principle, CO is a more energetically and thermodynamically favorable energy source for gas fermentation in comparison to H_2. Therefore, metabolism may vary during growth under different energy sources. In this study, *C. ljungdahlii* was fed with CO and/or CO_2/H_2 at pH 6.0 with a gas pressure of 0.1 MPa. *C. ljungdahlii* primarily produced acetate in the presence of H_2 as an energy source, but produced alcohols with CO as an energy source under the same fermentation conditions. A key enzyme activity assay, metabolic flux analysis, and comparative transcriptomics were performed for investigating the response mechanism of *C. ljungdahlii* under different energy sources. A CO dehydrogenase and an aldehyde:ferredoxin oxidoreductase were found to play important roles in CO utilization and alcohol production. Based on these findings, novel metabolic schemes are proposed for *C. ljungdahlii* growing on CO and/or CO_2/H_2. These schemes indicate that more ATP is produced during CO-fermentation than during H_2-fermentation, leading to increased alcohol production.

Keywords: gas fermentation, *Clostridium ljungdahlii*, acetogen, biofuel, ethanol, energy conservation

INTRODUCTION

Clostridium ljungdahlii, a close relative of "*Clostridium autoethanogenum*," is used as a model organism for studying the production of ethanol and acetate from syngas, which is a gas mixture mainly composed of carbon monoxide (CO), carbon dioxide (CO_2), and hydrogen (H_2) (Köpke et al., 2010, 2011a; Adamberg et al., 2015; Dürre and Eikmanns, 2015; Liew et al., 2016a). Both CO and H_2 can act as energy sources for growth and metabolism of *C. ljungdahlii* during gas fermentation. Notably, CO and H_2 have different patterns of providing energy equivalents during metabolism. In CO-fermentation, reduced ferredoxin (Fd_{red}), which is formed during CO oxidization by CO dehydrogenase, is the sole redox carrier that could allow the generation of a proton gradient across the membrane for energy conservation. On the other hand, Fd_{red} and

NADPH are generated by an electron bifurcation reaction in the H_2-fermentation by the NADP-specific [FeFe]-hydrogenase complex (Wang et al., 2013; Schuchmann and Müller, 2014; Mock et al., 2015). In addition, the free standard enthalpy changes are different for the conversion of CO or H_2/CO_2 to acetate and ethanol synthesis (**Table 1**; Wang et al., 2013; Mock et al., 2015; Esquivel-Elizondo et al., 2017). Therefore, the basic differences of energy conservation between CO and H_2 as energy sources reveal that fermentation profiles and products are distinct in gas fermentation of *C. ljungdahlii* (Bertsch and Müller, 2015; Valgepea et al., 2018).

Regardless of whether CO or H_2 is used as an energy source, *C. ljungdahlii* must gain ATP during autotrophic growth. Moreover, *C. ljungdahlii* grows better in CO than in H_2/CO_2, indicating that different energy sources result in different ATP formation rates. However, the metabolic schemes of ATP generation and redox balance for cell growth and products formation by *C. ljungdahlii* growing on CO or H_2/CO_2 are not well understood (Schuchmann and Müller, 2014; Jones et al., 2016; Liew et al., 2016b; Valgepea et al., 2017). It has been reported that ATP formation in *C. ljungdahlii* gas fermentation relies on a Rnf-ATPase system, which can establish a proton (H^+)-dependent transmembrane ion gradient during the Fd_{red} oxidation reaction (**Figure 1**; Fast and Papoutsakis, 2012; Schuchmann and Müller, 2014). It is clear that this energy conservation system is affected by the pH of the broth. The optimal pH for the growth of *C. ljungdahlii* is pH 6, which indicates that the optimal pH of the Rnf-ATPase system for ATP formation is also pH 6 (Köpke et al., 2010; Tremblay et al., 2013). Thus, the pH of the whole fermentation process was controlled at the optimal pH during the investigation of metabolic differences in CO- and H_2-fermentation in this study.

The composition of syngas can affect the titers and ratios of acetate and ethanol, which are the major products of gas fermentation (Mohammadi et al., 2012; Aklujkar et al., 2017; Liew et al., 2017). Furthermore, 2,3-butanediol is not detected in broth during continuous fermentation by "*C. autoethanogenum*" grown on H_2/CO_2, but it is produced when CO is utilized as the energy source under the same growth conditions (Wang et al., 2013; Mock et al., 2015). Analysis of the metabolic pathways of ethanol and acetate indicates that acetate formation can produce ATP, whereas ethanol formation requires NADPH as a cofactor (**Figure 1**) during gas fermentation of *C. ljungdahlii* (Wang et al., 2013; Mock et al., 2015; Xie et al., 2015). Furthermore, acetate can be converted to ethanol through the aldehyde:ferredoxin oxidoreductase (AOR) pathway, in which ferredoxin is the essential cofactor (Liew et al., 2017). This indicates that acetate and ethanol production and their ratios in the broth are regulated by energy metabolic balance. However, the response of *C. ljungdahlii* toward different energy sources (CO or H_2) and regulation of product formation (ethanol/acetate ratios) to maintain redox balance during autotrophic growth is still not completely understood (Richter et al., 2016; Valgepea et al., 2017).

In this study, *C. ljungdahlii* was cultured with $CO:CO_2$ (80:20) or $H_2:CO_2$ (60:40) to investigate the effects of different energy sources on carbon flux distribution during autotrophic growth. The pH was controlled at pH 6 to provide constant optimal conditions for the Rnf-ATPase system. The gas pressure was controlled at 0.1 MPa to enhance gas (CO and H_2) availability in gas-liquid fermentation bioreactor. We compared growth, product profiles, transcriptomes, and key enzyme activities of cells grown with these energy sources. We investigated the metabolic redox balance and propose metabolic schemes.

TABLE 1 | Stoichiometries and free standard enthalpies of acetate and ethanol formation from CO and H_2/CO_2.

	Reactions	$\Delta G^{\circ\prime}$(kJ)[a]
1	$4\ CO + 2\ H_2O \rightarrow CH_3COO^- + H^+ + 2\ CO_2$	−175
2	$4\ H_2 + 2\ CO_2 \rightarrow CH_3COO^- + H^+ + 2\ H_2O$	−95
3	$6\ CO + 3\ H_2O \rightarrow CH_3CH_2OH + 4\ CO_2$	−224
4	$6\ H_2 + 2\ CO_2 \rightarrow CH_3CH_2OH + 3\ H_2O$	−105
5	$11\ CO + 5\ H_2O \rightarrow CH_3CHOHCHOHCH_3 + 7\ CO_2$	−388
6	$1\ CO + 1\ Fd_{ox} + 1\ H_2O \rightarrow 2\ H^+ + 1\ CO_2 + 1\ Fd_{red}$	−14
7	$2\ H^+ + 1\ Fd_{red} \rightarrow 1\ H_2 + 1\ Fd_{ox}$	−7

[a]*Calculated from free energies of formation in reaction equations 1–7.*

MATERIALS AND METHODS

Bacterial Strains and Media

Escherichia coli strains were cultivated at 37°C in LB medium in the presence of appropriate antibiotic for general plasmid propagation and cultivation. *C. ljungdahlii* DSM 13528 was purchased from the Deutsche Sammlung von Mikroorganismen und Zellkulturen GmbH, Braunschweig, Germany and conserved by freezing mid-exponential phase cultures at −80°C with 30% glycerol. *C. ljungdahlii* was cultivated at 37°C under anaerobic conditions. A modified DSMZ 879 medium with a headspace of gas mixture ($CO: CO_2$, 80:20 or $H_2: CO_2$, 60:40) as the carbon and energy source was used in gas fermentation (Xie et al., 2015). The modified DSMZ 879 medium with the following composition (per liter): 1.0 g NH_4Cl, 0.1 g KCl, 0.2 g $MgSO_4 \times 7\ H_2O$, 0.8 g NaCl, 0.02 g $CaCl_2 \times 2\ H_2O$, 0.1 g KH_2PO_4, 2.5 mg $Na_2WO_4 \times 2\ H_2O$, 1.0 g $NaHCO_3$, 1.0 g cysteine-HCl × H_2O, 1 g yeast extract, 0.5 g cysteine, 0.5 mg resazurin, 10 ml trace element solution and 10 ml vitamin solution. Trace element solution contains 2.0 g nitrilotriacetic acid, 1.3 g $MnCl_2 \times H_2O$, 0.4 g $FeSO_4 \times 7\ H_2O$, 0.2 g $CoCl_2 \times 7\ H_2O$, 0.2 g $ZnSO_4 \times 7\ H_2O$, 0.2 g $Na_2MoO_4 \times 2\ H_2O$, 0.02 g $NiCl_2 \times 6\ H_2O$ and 0.1 g $Na_2SeO_3 \times 5\ H_2O$ in 1 L distilled water. Vitamin solution involves 2 mg biotin, 2 mg folic acid, 10 mg pyridoxine–HCl, 25 mg thiamine-HCl × $2\ H_2O$, 5 mg riboflavin, 5 mg Nicotinic acid, 5 mg D-Ca-pantothenate, 0.1 mg vitamin B12, 5 mg ρ-aminobenzoic acid and 5 mg lipoic acid in 1 L distilled water. Analytical grade chemicals used in the medium were purchased from Sinopharm Chemical Reagent Co., Ltd. (Shanghai, China). All antibiotics were purchased from Sangon Co., Ltd. (Shanghai, China).

Fed-Batch Fermentation With Syngas

Batch fermentation was performed in a 250-ml screw-cap bottle with a 50-ml working volume of modified DSMZ 879 medium as

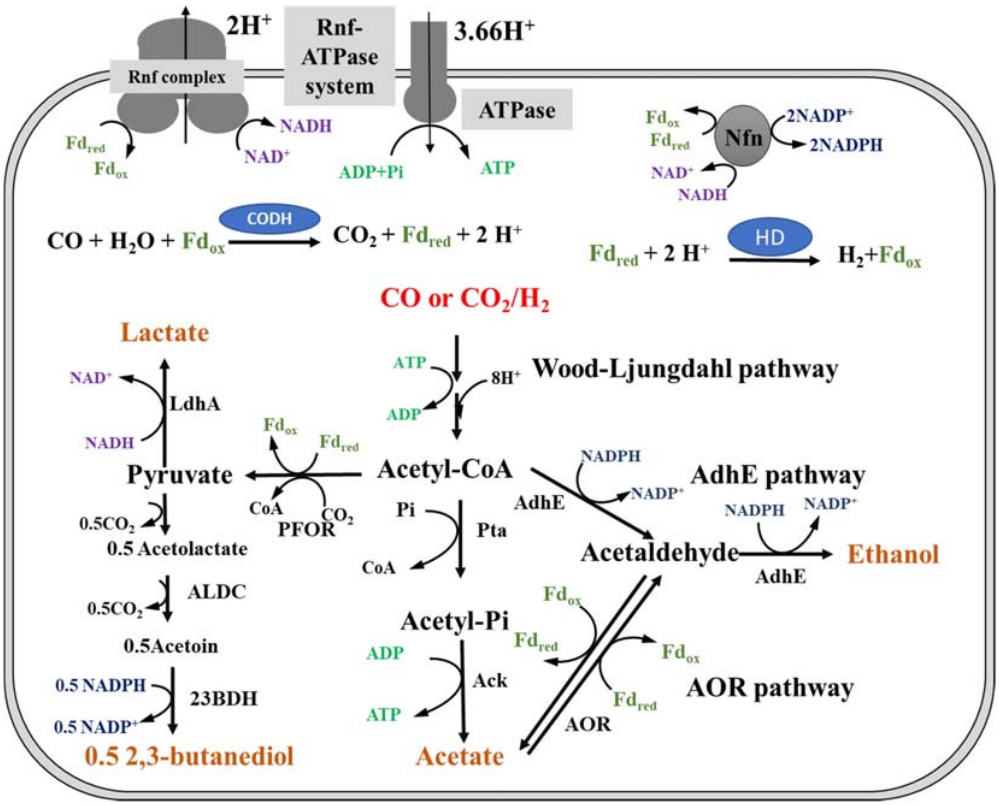

FIGURE 1 | Metabolic pathway of ethanol biosynthesis in *Clostridium ljungdahlii*. Pta, phosphotransacetylase; Ack, acetate kinase; AdhE, aldehyde/alcohol dehydrogenase; AOR, acetaldehyde:ferredoxin oxidoreductase; PFOR, pyruvate:ferredoxin oxidoreductase; LdhA, lactate dehydrogenase; ALDC, acetolactate decarboxylase; 23BDH, 2,3-butanediol dehydrogenase; CODH, carbon monoxide dehydrogenase; HD, hydrogenase; Fd_{red}, reduced ferredoxin; Fd_{ox}, oxidized ferredoxin; Nfn, electron-bifurcating and ferredoxin-dependent transhydrogenase; Rnf complex, membrane-associated and energy-conserving reduced ferredoxin:NAD^+ oxidoreductase; Rnf-ATPase system: a system of two enzyme complexes in which Rnf complex generates a proton gradient across the membrane by the oxidation of Fd_{red} with NAD^+; ATPase complex, consumes the proton gradient and phosphorylates ADP to ATP in the cytoplasm; AdhE pathway, ethanol formation by AdhE catalysis; AOR pathway, AOR participates in acetate and ethanol formation.

pre-culture. The medium was assembled in anaerobic chamber (COY Laboratory Products, Grass Lake, MI, United States). After autoclaving, $FeSO_4$, vitamins, cysteine-HCl and $NaHCO_3$ were added using syringe with 0.2 μm filter. Then gas in the headspace was substituted by syngas as required with a pressure of 0.2 MPa. Fed-batch fermentation with pH control was carried out in a FUS-5L bioreactor in duplicate (Guoqiang Biotech Co. Ltd., Shanghai, China) containing 2.5 L of modified DSM 897 medium. The supplied gas pressure was controlled at 0.1 MPa and the gas flow rate was 30 ml/min during the whole fermentation process in the bioreactor. Bioreactor pH was controlled at 6 automatically by adding 4 M KOH. 300 mL pre-culture of *C. ljungdahlii* was inoculated into the bioreactor and 5 mL samples were withdrawn every 12 h for cell density monitoring and products analysis.

Gene Expression Analysis by RNA-Seq

Comparative transcriptomics of cells grown on CO and H_2/CO_2 was performed to investigate gene expression profiles based on three biological replicates. Cell pellets from cultures in the bioreactor were collected by centrifugation at 10000 × *g* under −4°C for 10 min at exponential phase and frozen in liquid nitrogen immediately and stored at −80°C. The RNA isolation and high-through RNA sequencing (RNA-Seq) were accomplished by Allwegenetech Corp (Beijing, China). Total RNA was extracted using the mirVana miRNA Isolation Kit (Ambion, Santa Clara, CA, United States) following the manufacturer's protocol. RNA integrity was evaluated using the Agilent 2100 Bio-analyzer (Agilent Technologies, Santa Clara, CA, United States). The samples with RNA Integrity Number (RIN) ≥ 7 were subjected to subsequent analysis. The libraries were constructed using TruSeq Stranded mRNA LTSample Prep Kit (Illumina, San Diego, CA, United States) according to the manufacturer's instructions. Then these libraries were sequenced on the Illumina sequencing platform (HiSeqTM 2500) and 150 bp/125bp paired-end reads were generated. Based on reads per kilobase of transcript per million mapped reads (RPKM) normalization, the genes expression profiles were analyzed. The processed RNA-Seq data were submitted to the ArrayExpress database[1] under the accession number E-MEAB-8260.

[1]www.ebi.ac.uk/arrayexpress

Preparation of Cell Extracts and Enzyme Activity Analysis

500 mL exponential cells growing on CO or H_2/CO_2 were collected by centrifugation at 10000 × *g* under 4°C under strictly anoxic condition. The pellets were suspended in 20 mL of anoxic 50 mM potassium phosphate (pH 7.4), containing 2 mM DTT. Lysozyme was added to the cell suspension before incubation at 37°C for 30 min. Then the mixture was moved to anaerobic chamber for ultrasonication. Finally, cells debris was removed by centrifugation at 35000 × *g* and 4°C for 1 h. The supernatant was transferred to a new tube for enzyme assay and protein concentration determination using Bio-Rad protein assay with bovine serum albumin as the standard (Wang et al., 2013).

Acetaldehyde:ferredoxin oxidoreductase (AOR) activities were determined under strictly anoxic condition at 37°C in 1.5-mL anaerobic cuvettes sealed with rubber stopper (Hellma GmbH, Müllheim, Germany). The cuvettes were filled with pure N_2 at 1.2 × 10^5 Pa as the gas phase before use to maintain anaerobic condition during enzyme catalysis. The reactions were monitored photometrically at the specified wavelength. Ferredoxin reduction was monitored at 430 nm ($\Delta\varepsilon_{ox-red}\approx$13.1 $mM^{-1}cm^{-1}$). One unit (1 U) was defined as the transfer of 2 μmol electrons min^{-1}. The assay mixture contained 50 mM Tris–HCl (pH 7.4), 2 mM DTT, 1.5 mM acetaldehyde, and 30 μM ferredoxin in the AOR activity assay (Wang et al., 2013).

Ferredoxin of "*C. autoethanogenum*" (WP_013236834.1) was obtained by heterologous expression in *E. coli*. Gene amplification was performed by PCR with genomic DNA of "*C. autoethanogenum*" as the template. The following primers were used: 5′-CATGCCATGGCATATAAAATTACAGAGGAT-3′ (reverse primer, the *Nco*I restriction site is underlined); 5′-CCGCTCGAGGCTTTCTTCAACTGGTGCTC-3′ (forward primer, the *Xho*I restriction site is underlined). The PCR fragment was digested by restriction endonucleases and subsequently ligated into expression vector *p*ET28b, which had been digested by the same restriction endonucleases. Finally, the constructed plasmid was transformed into *E. coli* C41 (DE3), which already harbored plasmids *p*RKISC and *p*CodonPlus for production of iron-sulfur proteins. The cell cultivation and ferredoxin purification steps were performed according to the previous description (Demmer et al., 2015). Ferredoxin was stored at −20°C in an N_2 atmosphere until use.

Analytical Methods

The concentrations of ethanol, acetic acid, lactate, and 2,3-butanediol were determined using an Agilent 1100 high-performance liquid chromatography (HPLC) system with an Agilent Hi-Plex H column (Agilent Technologies, Santa Clara, CA, United States) equipped with a refractive index detector operated at 35°C. Column temperature was maintained at 55°C. Slightly acidified (5 mM H_2SO_4) water was used as the mobile phase at a flow rate of 0.7 ml/min.

The cells growing on gas under controlled pH and gas pressure were withdrawn from the bioreactor at 12 h interval. The growth of *C. ljungdahlii* was monitored by using a 2600 spectrophotometer (Unico instrument company, China) to measure the optical densities at 600 nm in a quartz-type cuvette (Hellma GmbH, Müllheim, Germany).

RESULTS AND DISCUSSION

Fed-Batch Fermentation in the Case of pH and Gas Pressure Control

Clostridium ljungdahlii grew well in the case of gas fermentation with CO/CO_2 as carbon and energy source and the optical density (OD, 600 nm) reached 8.4 ± 0.4 after 120 h. In contrast, the strain grew poorly in the presence of H_2/CO_2 as carbon and energy source with peak cell density of 1.6 ± 0.3 after 168 h (**Figure 2**). These results indicate that *C. ljungdahlii* can more easily gain energy from CO than from H_2 for autotrophic growth under the same fermentation conditions.

Regarding the products, *C. ljungdahlii* mainly produced ethanol (713 ± 21 mM) in the presence of CO as energy source in the end-products. Furthermore, the concentrations of 2,3-butanediol and acetate were 188 ± 4 mM and 185 ± 7 mM, respectively (**Figure 3A**). On the other hand, acetate was found to be dominant among the end-products in the presence of H_2 as energy source, achieving 512 ± 6 mM at the end of the experiment (**Figure 3B**). These results clearly show that different energy sources affect not only biomass accumulation but also product titers in fed-batch fermentation of *C. ljungdahlii*.

ATP formation is highly susceptible to pH changes in *C. ljungdahlii* gas fermentation (**Figure 1**; Schuchmann and Müller, 2014). Furthermore, gas-liquid mass transfer limitation results in the inefficient utilization of CO or H_2/CO_2 (Ungerman and Heindel, 2007; Xu et al., 2017). As a result, *C. ljungdahlii* produces low biomass and low ethanol and acetate titers in the traditional batch gas fermentation

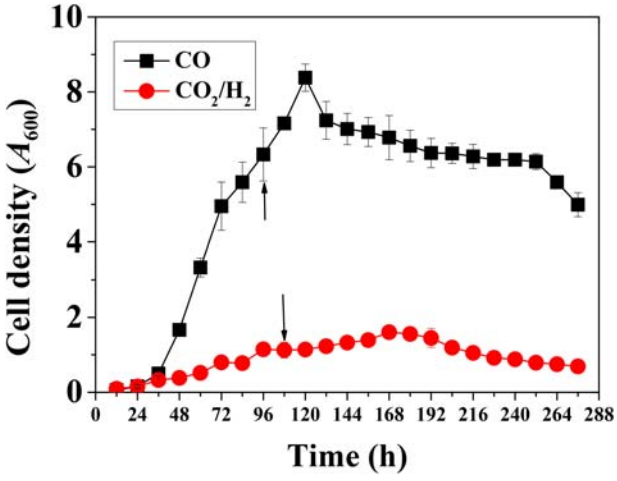

FIGURE 2 | Cell growth of *Clostridium ljungdahlii* with CO or H_2/CO_2. Arrows: These two time points represent exponential growth phases, respectively. Samples were withdrawn from fermenter at these time points for RNA-Seq analysis.

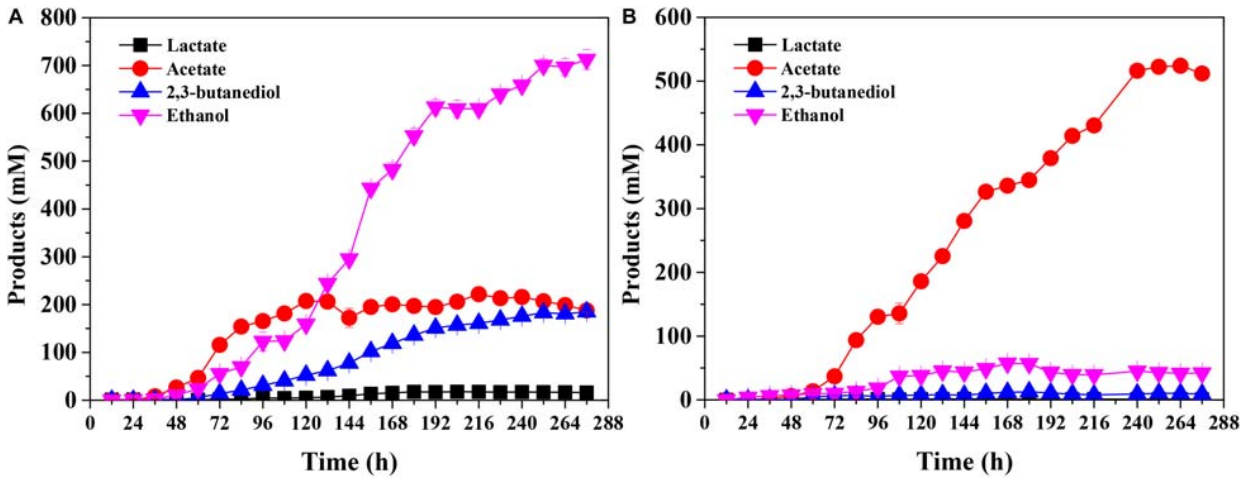

FIGURE 3 | Product concentration of *Clostridium ljungdahlii* grown on CO **(A)** and H_2/CO_2 **(B)** at pH 6.0 and gas pressure of 0.1 MPa.

(Ungerman and Heindel, 2007; Köpke et al., 2011b; Xie et al., 2015; Xu et al., 2017). In this study, we improved the fermentation conditions and provided ideal growth conditions for *C. ljungdahlii* via pH and gas pressure control during autotrophic growth (**Figure 3**). *C. ljungdahlii* exhibited distinct differences in fermentation profiles when grown on CO and/or H_2/CO_2. This information is useful for studying differences in energy metabolism when acetogenic bacteria grown on different energy sources.

Genome-Wide Transcriptional Analysis With CO or H_2 as Energy Source

Comparative transcriptomics was conducted by RNA-Seq technology for the investigation of the intracellular flux patterns at the transcriptional levels. The original and processed RNA-Seq data were submitted to the ArrayExpress database[1] under accession number E-MEAB-8260. **Supplementary Table S1** shows the expression profiles of 62 genes located in the central carbon and energy metabolic pathways (Köpke et al., 2010, 2011b). Among these, we particularly focused on the genes with transcriptional reads per kilobase of transcript per million mapped reads (RPKM) greater than 50 and change folds greater than 2 ($\log_2$ value greater than 1 or less than −1).

The energy supply modes are different for *C. ljungdahlii* during autotrophic growth on CO or H_2. Fd_{red}, formed during CO oxidation to CO_2 by CO dehydrogenase (CODH, *cooS*), is the initial energy source in CO fermentation. Both Fd_{red} and NADPH, formed simultaneously by electron bifurcation via hydrogenase, are the initial energy sources in H_2 fermentation (Wang et al., 2013; Mock et al., 2015). Therefore, we investigated the transcriptional levels of the CODH and hydrogenase genes. There are four putative genes/gene clusters, i.e., CLJU_c01650, CLJU_c09110, CLJU_c37560 and CLJU_c37660-70 encoding CODH, among which only the transcriptional level of CLJU_c09110 was induced during CO fermentation, in comparison with H_2 fermentation (**Supplementary Table S1**; Köpke et al., 2010). Furthermore, there are four putative hydrogenases in *C. ljungdahlii*, based on genome sequence analysis. The genes CLJU_c28660-70 and CLJU_c23060-90 showed few changes in gene expression under both CO fermentation and H_2 fermentation (Köpke et al., 2010). The gene expression level of CLJU_c37220 encoding an Fe-only hydrogenase was higher in H_2 fermentation than in CO fermentation (**Supplementary Table S1**). The role of Fe-only hydrogenase is oxidation of reduced ferredoxin, and we speculate its expression was inhibited in presence of CO to some extent (Goldet et al., 2009). The fourth hydrogenase gene is located in a large gene cluster (CLJU_c06990-07080), and its expression level was higher under H_2 fermentation than under CO fermentation (**Supplementary Table S1**). The function of this gene cluster has been clarified in "*C. autoethanogenum,*" which encodes a NADP-specific electron bifurcating hydrogenase in complex with formate dehydrogenase (Wang et al., 2013). Therefore, this hydrogenase plays a critical role in providing reducing equivalents in H_2 fermentation.

The product concentrations were remarkably different for CO fermentation and H_2 fermentation (**Figure 3**). The related genes for product biosynthesis were also analyzed (**Figure 1**; Köpke et al., 2010). Comparative transcriptomics data showed that the expression level of 2,3-butanediol dehydrogenase, which was encoded by CLJU_c01650, was higher in the CO fermentation than that in the H_2 fermentation (**Supplementary Table S1**; Tan et al., 2015), and these transcriptome results were consistent with those of the 2,3-butanediol fermentation titer (**Figure 3**). However, the expression levels of genes involved in acetate and ethanol formation were lower under CO fermentation (**Figure 1**; Köpke et al., 2010). Of note, the RPKM values of an AOR gene encoded by CLJU_c20210 and a pyruvate:ferredoxin oxidoreductase (PFOR) gene encoded by CLJU_c09340 were high in both the CO and H_2 fermentation. This indicates these two functional enzymes play crucial roles during gas fermentation. It has been reported that ethanol formation is mainly dependent on the AOR pathway during gas fermentation (Mock et al., 2015; Liew et al., 2017). Our results are consistent with the finding that the *aor2* gene is strongly

expressed during autotrophic growth in CO in previous studies. Interestingly, *aor2* was also transcribed at a high level when grown with H_2/CO_2, suggesting that AOR is also active in H_2 fermentation (**Supplementary Table S1**). The specific activity of acetaldehyde:ferredoxin oxidoreductase was determined in the cell extracts growing on CO (6.7 U/mg) and H_2/CO_2 (2.5 U/mg). This result also shows that AOR is functional during H_2/CO_2 fermentation. However, the ethanol titer (42 ± 1 mM) was very low under these fermentation conditions (**Figure 3B**). This can be elucidated by the fact that partial acetate in the broth comes from the oxidation of acetaldehyde (**Figures 1**, **4**). This result indicates that AOR (CLJU_c20210) catalyzed the reaction from acetate to acetaldehyde in CO fermentation, but catalyzed the inverse reaction in H_2 fermentation. We suggest that this flexible mechanism aids in maintaining redox balance in response to different fermentation conditions.

The low biomass accumulation indicated that ATP supply was low during growth with H_2. Thus, the genes associated with ATP formation, including Rnf–ATPase genes and *nfn*, had higher transcriptional levels (**Supplementary Table S1**). It is clear that low levels of ATP not only reduced biomass but also decreased alcohol production in this study and previous reports (Valgepea et al., 2018).

Calculation of ATP Gains During CO and H_2 Fermentation

Mock et al. (2015) completed a metabolic scheme for "*C. autoethanogenum*" in H_2/CO_2 fermentation. We fully agree with the principles of metabolic pathways and energy conservation in this scheme, but modified the pathway of acetate synthesis. The deletion of the acetate formation pathway through the inactivation of phosphate acetyltransferase, encoded by *pta* (CLJU_c12770), leads to lethal in gas fermentation (Huang et al., 2016). Therefore, the acetate biosynthesis pathway from acetyl-CoA is necessary in the scheme. Meanwhile, acetate formation from acetaldehyde should also be included, based on AOR specific activity (2.5 U/mg) verified in this study and transcriptomics data (**Supplementary Table S1**). Furthermore, we cannot rule out the possibility, that H_2 was produced during the fermentation process, yet H_2 concentrations were not monitored in this study. The scheme of energy metabolism of *C. ljungdahlii* is given in **Figure 4**, under the assumption that only acetate is formed in H_2/CO_2 fermentation (**Figure 3B**). Our metabolic scheme indicates that 0.75 mole ATP is produced during 1 mole of acetate formed from H_2/CO_2 (**Figure 4**).

Clostridium ljungdahlii exhibited a significant difference in alcohol production in CO fermentation as compared with that in H_2/CO_2 fermentation. Ethanol was the main product in CO fermentation (**Figure 3A**), suggesting a key role of AOR, converting acetate to acetaldehyde for further reduction to ethanol by AdhE in the metabolism of CO (**Figure 1**). Gene knockout studies in "*C. autoethanogenum*" demonstrated AOR is critical to ethanol formation (Liew et al., 2017). Based on these findings and equations in the **Table 1**, three schemes of the energy metabolism of *C. ljungdahlii* are exhibited under three assumptions: (i) only acetate formation (**Supplementary Figure S1**); (ii) acetate and 2,3-butanediol formed (**Supplementary Figure S2**); and (iii) acetate, ethanol, and 2,3-butanediol formed (**Figure 5**). Among these three schemes, **Figure 5** most closely reflects the actual metabolic process in CO fermentation found in this study. This scheme indicates that 10 moles ATPs are

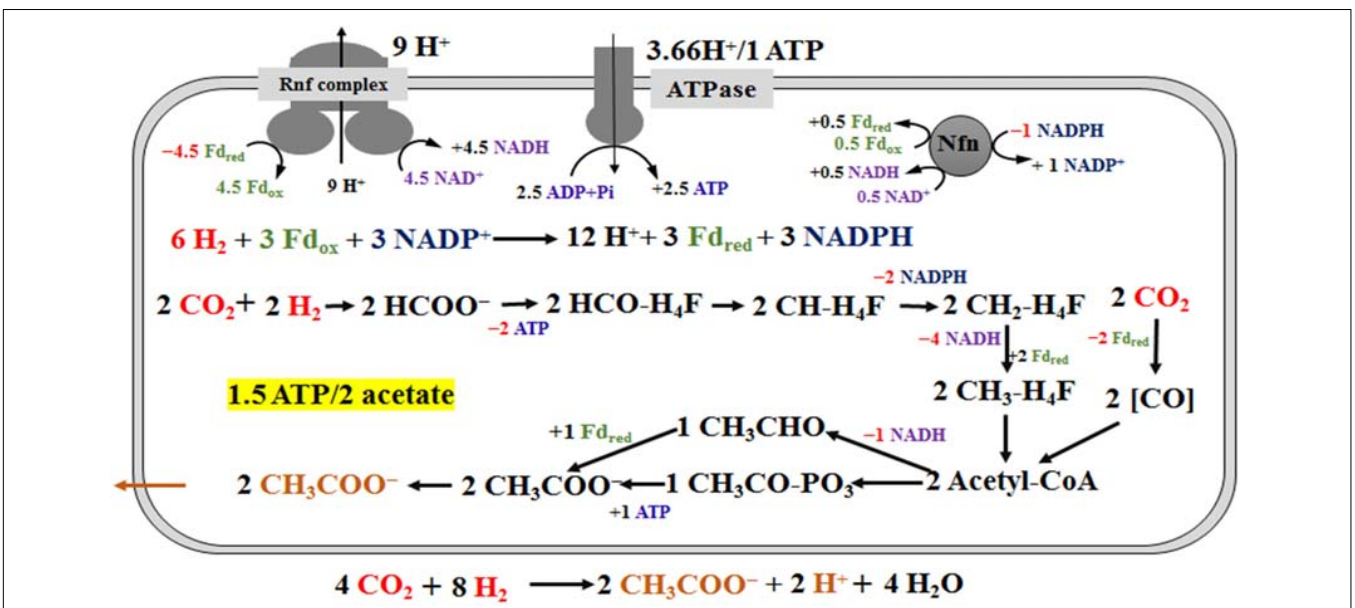

FIGURE 4 | Schemes of the metabolism of *Clostridium ljungdahlii* grown on H_2/CO_2 at pH 6.0 and gas pressure of 0.1 MPa. For simplification, an electron-bifurcating methylene-THF reductase is assumed here, and protons in the individual reactions are omitted. The energy source (H_2) and carbon source (CO_2) are in red and the product (acetate) is in orange. "+ ×" indicates ATP and reduced electron carriers (Fd_{red}, NADH and NADPH), which are in different color in the scheme, are produced. On the contrary, "− ×" indicates ATP and reduced electron carriers are consumed in redox reactions.

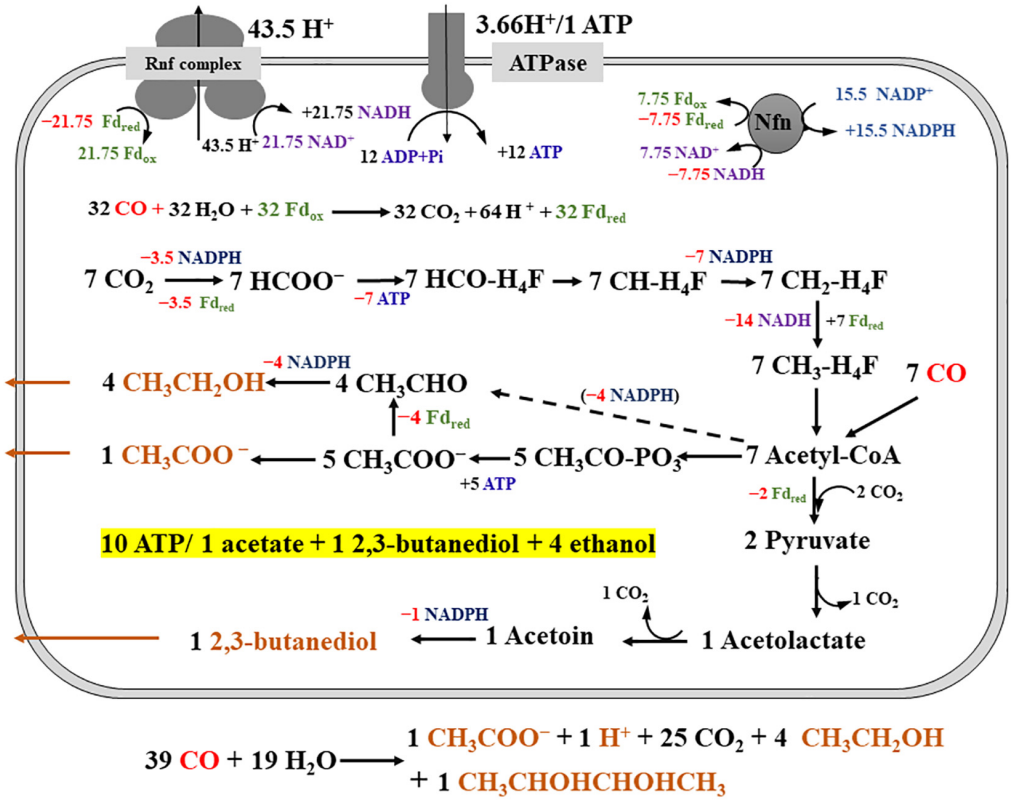

FIGURE 5 | Schemes of the metabolism of *Clostridium ljungdahlii* grown on CO at pH 6.0 and gas pressure 0.1 MPa. For simplification, an electron-bifurcating methylene-THF reductase is assumed, ethanol is produced via acetic reduction to acetaldehyde, and protons in the individual reactions are omitted. The energy and carbon source (CO) is in red and the products (acetate, ethanol, and 2,3-butanediol) are in orange. "+ ×" indicates ATP and reduced electron carriers (Fd_{red}, NADH and NADPH), which are in different color in the scheme, are produced. On the contrary, "− ×" indicates ATP and reduced electron carriers are consumed in redox reactions. The dashed arrow means the redox reaction is also a possible pathway for ethanol production.

produced during formation of 1 mole of acetate, 1 mole of 2,3-butanediol, and 4 moles of ethanol from CO. The mole ratio of dominant end-products (acetate, 2,3-butanediol, and ethanol) is very close to 1:1:4 (**Figure 3A**).

All of the acetogenic bacteria are able to produce acetate via Wood-Ljungdahl pathway during CO and/or H_2/CO_2 fermentation (Schuchmann and Müller, 2014). However, only some acetogenic bacteria, including *C. ljungdahlii*, can grow in the presence of CO to produce ethanol (Köpke et al., 2011b). This indicates that *C. ljungdahlii* has a unique mechanism to achieve CO fixation and energy conservation (Buckel and Thauer, 2018; Peters et al., 2018). Based on findings in this work, we speculate that an independent and specific CODH is necessary for *C. ljungdahlii* fermentation on CO. This enzyme is used to convert CO to CO_2 for formation of Fd_{red}, which provides reducing equivalents in the fermentation (**Supplementary Table S1**; Köpke et al., 2010). Furthermore, the AOR pathway plays an important role in *C. ljungdahlii* gas fermentation. AOR, together with the bi-functional aldehyde/alcohol dehydrogenase (AdhE), can achieve flexible conversion between two C2-compounds, ethanol and acetate (Liew et al., 2017). Ethanol formation by the AOR pathway requires sufficient energy equivalents (NADPH and Fd_{red}); on the contrary, this reaction can provide energy equivalents to support cell metabolism via ethanol oxidation (**Figure 1**). Therefore, the ratio between ethanol and acetate is closely associated with redox balance but not with carbon flux balance. Owing to these characteristics, *C. ljungdahlii* and "*C. autoethanogenum*" grow better, and produce more ATP and ethanol in CO than that in H_2/CO_2 (Mock et al., 2015; Liew et al., 2017).

The low yields of 2,3-butanediol and lactate result in poor understanding of the metabolic mechanism of these two products (Köpke et al., 2011b; Wang et al., 2013; Mock et al., 2015; Valgepea et al., 2018). Our fermentation technology increased the titer of 2,3-butanediol to 188 ± 4 mM (**Figure 3**). Based on our knowledge, this is the highest titer of 2,3-butanediol in gas fermentation among the published reports. Importantly, these results provide a platform to study the biosynthesis and metabolism of 2,3-butanediol in the future.

CONCLUSION

Clostridium ljungdahlii is able to produce ethanol and acetate with CO as the carbon and energy source, unlike other acetogenic

bacteria with acetate as the main product. To elucidate this unique metabolism, we cultivated *C. ljungdahlii* with CO or H_2/CO_2 using a fed-batch fermentation technology with pH and gas pressure control. The results show that *C. ljungdahlii* mainly produced alcohols (ethanol and 2,3-butanediol) under CO fermentation and mainly produced acetate under H_2/CO_2 fermentation. The comparative transcriptomics analysis and AOR activities suggest that a CODH (encoded by CLJU_09110) and an AOR (encoded by CLJU_20210) play important roles in CO metabolism. This CODH can provide an energy equivalent (Fd_{red}), as required, by oxidizing CO to CO_2 for metabolism in CO fermentation. Additionally, the AOR pathway can provide a flexible regulation mechanism for energy balance by the conversion of acetate and ethanol. According to these results and previous reports, we propose metabolic schemes for *C. ljungdahlii* growing on CO and/or H_2/CO_2. Stoichiometric analysis of ATP gains estimated that ATP yield is 0.75 ATP with 1 mole of acetate formed during autotrophic growth on H_2/CO_2, in contrast to 10 moles of ATPs with 1 mole of acetate, 1 mole of 2,3-butanediol, and 4 moles of ethanol formed in *C. ljungdahlii* fermentation on CO at pH 6.0.

DATA AVAILABILITY STATEMENT

The datasets generated for this study can be found in the ArrayExpress database (www.ebi.ac.uk/arrayexpress) under the accession number E-MEAB-8260.

AUTHOR CONTRIBUTIONS

F-LL and W-ZT conceived and designed the study. H-FZ, Z-YL, and J-HY performed the experiments. S-NW analyzed the enzyme activities data. Z-YL completed metabolic schemes guided by F-LL. Z-YL and F-LL wrote the manuscript with input from all authors.

FUNDING

This study was supported by grants from the National Natural Science Foundation of China (31800026), Key Laboratory of Biofuel, Chinese Academy of Sciences (CASKLB2018X), the QIBEBT Funding (QIBEBT I201805), State Key Laboratory of Microbial Technology Open Projects Fund (M2019-2), Basic Research Projects of Liaoning Higher Education Institutions (2017J030), Dalian High-level Talent Innovation Support Program (2018RQ24), and the China Petrochemical Corporation (Sinopec).

SUPPLEMENTARY MATERIAL

The Supplementary Material for this article can be found online at: https://www.frontiersin.org/articles/10.3389/fmicb.2020.00416/full#supplementary-material

REFERENCES

Adamberg, K., Valgepea, K., and Vilu, R. (2015). Advanced continuous cultivation methods for systems microbiology. *Microbiology* 161, 1707–1719. doi: 10.1099/mic.0.000146

Aklujkar, M., Leang, C., Shrestha, P. M., Shrestha, M., and Lovley, D. R. (2017). Transcriptomic profiles of *Clostridium ljungdahlii* during lithotrophic growth with syngas or H2 and CO2 compared to organotrophic growth with fructose. *Sci. Rep.* 7;13135.

Bertsch, J., and Müller, V. (2015). Bioenergetic constraints for conversion of syngas to biofuels in acetogenic bacteria. *Biotechnol. Biofuels* 8;210. doi: 10.1186/s13068-015-0393-x

Buckel, W., and Thauer, R. K. (2018). Flavin-based electron bifurcation, ferredoxin, flavodoxin, and anaerobic respiration with protons (Ech) or NAD+ (Rnf) as electron acceptors: a historical review. *Front. Microbiol.* 9:410. doi: 10.3389/fmicb.2018.00401

Demmer, J. K., Huang, H., Wang, S., Demmer, U., Thauer, R. K., and Ermler, U. (2015). Insights into flavin-based electron bifurcation via the NADH-dependent reduced ferredoxin:NADP oxidoreductase structure. *J. Biol. Chem.* 290, 21985–21995. doi: 10.1074/jbc.M115.656520

Dürre, P., and Eikmanns, B. J. (2015). C1-carbon sources for chemical and fuel production by microbial gas fermentation. *Curr. Opin. Biotechnol.* 35, 63–72. doi: 10.1016/j.copbio.2015.03.008

Esquivel-Elizondo, S., Delgado, A. G., Rittmann, B. E., and Krajmalnik-Brown, R. (2017). The effects of CO2 and H2 on CO metabolism by pure and mixed microbial cultures. *Biotechnol. Biofuels* 10;220. doi: 10.1186/s13068-017-0910-1

Fast, A. G., and Papoutsakis, E. T. (2012). Stoichiometric and energetic analyses of non-photosynthetic CO2-fixation pathways to support synthetic biology strategies for production of fuels and chemicals. *Curr. Opin. Chem. Eng.* 1, 380–395. doi: 10.1016/j.coche.2012.07.005

Goldet, G., Brandmayr, C., Stripp, S. T., Happe, T., Cavazza, C., Fontecilla-Camps, J. C., et al. (2009). Electrochemical kinetic investigations of the reactions of [FeFe]-hydrogenases with carbon monoxide and oxygen: comparing the importance of gas tunnels and active-site electronic/redox effects. *J. Am. Chem. Soc.* 131, 14979–14989. doi: 10.1021/ja905388j

Huang, H., Chai, C., Li, N., Rowe, P., Minton, N. P., Yang, S., et al. (2016). CRISPR/Cas9-based efficient genome editing in *Clostridium ljungdahlii*, an autotrophic gas-fermenting bacterium. *ACS Synth Biol.* 5, 1355–1361. doi: 10.1021/acssynbio.6b00044

Jones, S. W., Fast, A. G., Carlson, E. D., Wiedel, C. A., Au, J., Antoniewicz, M. R., et al. (2016). CO2 fixation by anaerobic non-photosynthetic mixotrophy for improved carbon conversion. *Nat. Commun.* 7;12800. doi: 10.1038/ncomms12800

Köpke, M., Held, C., Hujer, S., Liesegang, H., Wiezer, A., Wollherr, A., et al. (2010). *Clostridium ljungdahlii* represents a microbial production platform based on syngas. *Proc. Natl. Acad. Sci. U.S.A.* 107, 13087–13092. doi: 10.1073/pnas.1004716107

Köpke, M., Mihalcea, C., Bromley, J. C., and Simpson, S. D. (2011a). Fermentative production of ethanol from carbon monoxide. *Curr. Opin. Biotechnol.* 22, 320–325. doi: 10.1016/j.copbio.2011.01.005

Köpke, M., Mihalcea, C., Liew, F., Tizard, J. H., Ali, M. S., Conolly, J. J., et al. (2011b). 2,3-butanediol production by acetogenic bacteria, an alternative route to chemical synthesis, using industrial waste gas. *Appl. Environ. Microbiol.* 77, 5467–5475. doi: 10.1128/AEM.00355-11

Liew, F., Henstra, A. M., Köpke, M., Winzer, K., Simpson, S. D., and Minton, N. P. (2017). Metabolic engineering of *Clostridium autoethanogenum* for selective alcohol production. *Metab. Eng.* 40, 104–114. doi: 10.1016/j.ymben.2017.01.007

Liew, F., Henstra, A. M., Winzer, K., Köpke, M., Simpson, S. D., and Minton, N. P. (2016a). Insights into CO2 Fixation Pathway of *Clostridium autoethanogenum* by targeted mutagenesis. *mBio* 7:e00427-16.. doi: 10.1128/mBio.00427-16

Liew, F., Martin, M. E., Tappel, R. C., Heijstra, B. D., Mihalcea, C., and Köpke, M. (2016b). Gas fermentation-a flexible platform for commercial scale production of low-carbon-fuels and chemicals from waste and renewable feedstocks. *Front. Microbiol.* 7:694. doi: 10.3389/fmicb.2016.00694

Mock, J., Zheng, Y. N., Müller, A. P., Ly, S., Tran, L., Segovia, S., et al. (2015). energy conservation associated with ethanol formation from H2 and CO2 in *Clostridium autoethanogenum* involving electron bifurcation. *J. Bacteriol.* 197, 2965–2980. doi: 10.1128/JB.00399-15

Mohammadi, M., Younesi, H., Najafpour, G., and Mohamed, A. R. (2012). Sustainable ethanol fermentation from synthesis gas by *Clostridium ljungdahlii* in a continuous stirred tank bioreactor. *J. Chem. Technol. Biotechnol.* 87, 837–843. doi: 10.1002/jctb.3712

Peters, J. W., Beratan, D. N., Bothner, B., Dyer, R. B., Harwood, C. S., Heiden, Z. M., et al. (2018). A new era for electron bifurcation. *Curr. Opin. Chem. Biol.* 47, 32–38. doi: 10.1016/j.cbpa.2018.07.026

Richter, H., Molitor, B., Wei, H., Chen, W., Aristilde, L., and Angenent, L. T. (2016). Ethanol production in syngas-fermenting *Clostridium ljungdahlii* is controlled by thermodynamics rather than by enzyme expression. *Energ .Environ. Sci.* 9, 2392–2399. doi: 10.1039/c6ee01108j

Schuchmann, K., and Müller, V. (2014). Autotrophy at the thermodynamic limit of life: a model for energy conservation in acetogenic bacteria. *Nat. Rev. Microbiol.* 12, 809–821. doi: 10.1038/nrmicro3365

Tan, Y., Liu, Z. Y., Liu, Z., and Li, F. L. (2015). Characterization of an acetoin reductase/2,3-butanediol dehydrogenase from *Clostridium ljungdahlii* DSM 13528. *Enzyme Microb. Technol.* 7, 1–7. doi: 10.1016/j.enzmictec.2015.06.011

Tremblay, P. L., Zhang, T., Dar, S. A., Leang, C., and Lovley, D. R. (2013). The Rnf complex of *Clostridium ljungdahlii* is a proton-translocating ferredoxin:NAD(+) oxidoreductase essential for autotrophic growth. *mBio* 4:00406-12. doi: 10.1128/mBio.00406-12

Ungerman, A. J., and Heindel, T. J. (2007). Carbon monoxide mass transfer for syngas fermentation in a stirred tank reactor with dual impeller configurations. *Biotechnol. Prog.* 23, 613–620. doi: 10.1021/bp060311z

Valgepea, K., de Souza Pinto Lemgruber, R., Abdalla, T., Binos, S., Takemori, N., Takemori, A., et al. (2018). H2 drives metabolic rearrangements in gas-fermenting *Clostridium autoethanogenum*. *Biotechnol. Biofuels.* 11;55. doi: 10.1186/s13068-018-1052-9

Valgepea, K., de Souza Pinto Lemgruber, R., Meaghan, K., Palfreyman, R. W., Abdalla, T., Heijstra, B. D., et al. (2017). Maintenance of ATP homeostasis triggers metabolic shifts in gas-fermenting acetogens. *Cell Syst.* 4;e5. doi: 10.1016/j.cels.2017.04.008

Wang, S., Huang, H., Kahnt, J., Müller, A. P., Köpke, M., and Thauer, R. K. (2013). NADP-specific electron-bifurcating [FeFe]-hydrogenase in a functional complex with formate dehydrogenase in *Clostridium autoethanogenum* grown on CO. *J. Bacteriol.* 195, 4373–4386. doi: 10.1128/jb.00678-13

Xie, B. T., Liu, Z. Y., Tian, L., Li, F. L., and Chen, X. H. (2015). Physiological response of *Clostridium ljungdahlii* DSM 13528 of ethanol production under different fermentation conditions. *Bioresour. Technol.* 177, 302–307. doi: 10.1016/j.biortech.2014.11.101

Xu, H., Liang, C., Yuan, Z., Xu, J., Hua, Q., and Guo, Y. (2017). A study of CO/syngas bioconversion by *Clostridium autoethanogenum* with a flexible gas-cultivation system. *Enzyme Microb. Technol.* 101, 24–29. doi: 10.1016/j.enzmictec.2017.03.002

Conflict of Interest: The authors declare that the research was conducted in the absence of any commercial or financial relationships that could be construed as a potential conflict of interest.

frontiers in Microbiology

MINI REVIEW
published: 03 April 2020
doi: 10.3389/fmicb.2020.00486

CO_2-Fixation Strategies in Energy Extremophiles: What Can We Learn From Acetogens?

*Olivier N. Lemaire, Marion Jespersen and Tristan Wagner**

Microbial Metabolism Group, Max Planck Institute for Marine Microbiology, Bremen, Germany

Domestication of CO_2-fixation became a worldwide priority enhanced by the will to convert this greenhouse gas into fuels and valuable chemicals. Because of its high stability, CO_2-activation/fixation represents a true challenge for chemists. Autotrophic microbial communities, however, perform these reactions under standard temperature and pressure. Recent discoveries shine light on autotrophic acetogenic bacteria and hydrogenotrophic methanogens, as these anaerobes use a particularly efficient CO_2-capture system to fulfill their carbon and energy needs. While other autotrophs assimilate CO_2 via carboxylation followed by a reduction, acetogens and methanogens do the opposite. They first generate formate and CO by CO_2-reduction, which are subsequently fixed to funnel the carbon toward their central metabolism. Yet their CO_2-reduction pathways, with acetate or methane as end-products, constrain them to thrive at the "thermodynamic limits of Life". Despite this energy restriction acetogens and methanogens are growing at unexpected fast rates. To overcome the thermodynamic barrier of CO_2-reduction they apply different ingenious chemical tricks such as the use of flavin-based electron-bifurcation or coupled reactions. This mini-review summarizes the current knowledge gathered on the CO_2-fixation strategies among acetogens. While extensive biochemical characterization of the acetogenic formate-generating machineries has been done, there is no structural data available. Based on their shared mechanistic similarities, we apply the structural information obtained from hydrogenotrophic methanogens to highlight common features, as well as the specific differences of their CO_2-fixation systems. We discuss the consequences of their CO_2-reduction strategies on the evolution of Life, their wide distribution and their impact in biotechnological applications.

Keywords: acetogenic bacteria, hydrogenotrophic methanogens, CO_2-fixation, formate dehydrogenase, evolution, biotechnology, coupled reaction

OPEN ACCESS

Edited by:
Mirko Basen,
University of Rostock, Germany

Reviewed by:
Kathleen Scott,
University of South Florida, United States
Wolfgang Buckel,
University of Marburg, Germany
Volker Müller,
Goethe University Frankfurt, Germany

***Correspondence:**
Tristan Wagner
twagner@mpi-bremen.de

Specialty section:
This article was submitted to Microbial Physiology and Metabolism, a section of the journal Frontiers in Microbiology

Received: *15 December 2019*
Accepted: *05 March 2020*
Published: *03 April 2020*

Citation:
Lemaire ON, Jespersen M and Wagner T (2020) CO_2-Fixation Strategies in Energy Extremophiles: What Can We Learn From Acetogens? Front. Microbiol. 11:486. doi: 10.3389/fmicb.2020.00486

INTRODUCTION

CO_2, the most oxidized state of carbon, has become a major concern to society due to its greenhouse gas properties and its increasing accumulation in our atmosphere since the 20th-century. Efficient CO_2-sequestration techniques, as well as concomitant applications in biochemical synthesis and alternative energy source storage, being developed to reduce its impact on global warming (Schuchmann and Müller, 2013). Yet CO_2 is a stable, inert molecule. The few applicable

chemical processes allowing its unfavorable fixation (like the Monsanto and Cativa processes) require high temperatures and pressures as well as expensive and polluting catalysts while only exhibiting moderate catalytic rates (Appel et al., 2013; Fujita et al., 2013; Schuchmann and Müller, 2013). New alternative chemistry based on metal-organic framework (Hou et al., 2019) or transition metal-free catalysis (Cherubini-Celli et al., 2018) are upcoming and might be applied in the near future. Nevertheless, none of these artificial processes matches the efficiency of their biological counterpart.

At least six different autotrophic carbon fixation pathways exist among the domains of Life (Berg et al., 2010; Fuchs, 2011; Appel et al., 2013). The most common scenario is a two-step process where CO_2 is branched on a reactive group (carboxylation) and then reduced (e.g., Calvin–Benson–Bassham or the 3-hydroxypropionate 4-hydroxybutyrate cycle). To date, there is only one exception that uses the reverse way, CO_2-reduction before carboxylation: the reductive acetyl-CoA pathway. This pathway constitutes the "cheapest" option to fix CO_2 in term of energy-consumption and is thought to be the most ancient one (Berg et al., 2010; Martin and Thauer, 2017).

The reductive acetyl-CoA pathway has two CO_2 entry points: the methyl-branch, where a reductive cascade turns CO_2 in a methyl-group (**Figure 1A**, reaction from the CO_2-activation to the methyl-H_4F for acetogens or methyl-H_4MPT for methanogens) and the carbonyl-branch. In the latter, CO_2 is converted into carbon monoxide (CO; **Figure 1A**), further combined with the methyl group and Coenzyme A (CoA) to ultimately produce acetyl-CoA, the "turntable" of the central carbon metabolism (Ragsdale and Pierce, 2008; Thauer et al., 2008; Berg et al., 2010; Sousa et al., 2013; Fuchs and Berg, 2014).

Hydrogenotrophic methanogens (Euryarchaea, simplified as methanogens below) and autotrophic acetogens (Bacteria, simplified as acetogens below) use the reductive acetyl-CoA pathway to derive their cellular carbon and energy by growing on H_2 plus CO_2. The final product for methanogens and acetogens are methane and acetate, respectively. Under physiological conditions, such metabolism provides less than half a molecule of ATP per acetate/methane, constraining these organisms to live at the "thermodynamic limits of Life" (Buckel and Thauer, 2013; Schuchmann and Müller, 2014). Nevertheless, methanogens and acetogens are found in various ecological niches, ranging from rumen to deep-sea volcanoes and they are crucial actors in organic matter conversion and element cycling (e.g., carbon assimilation and nitrogen fixation). Despite drastically low energy yields, their doubling time is surprisingly short: ranging from only one to a few hours under laboratory conditions (Thauer et al., 2008; Basen et al., 2018).

The energy metabolism of acetogens and methanogens was puzzling for a long time until the discovery of energy conserving enzymes (i.e., Rnf and Ech membrane complexes), which use low-potential electrons from ferredoxins, reduced by H_2 oxidation via flavin-based electron bifurcation (**Figure 1D**). The use of low-potential electrons provided a rational explanation as to how these organisms derive enough energy to survive and grow under such stringent metabolic conditions (Buckel and Thauer, 2013, 2018; Schuchmann and Müller, 2014; Peters et al., 2018). Considered to be among the first metabolic processes, methanogenesis and acetogenesis might have been crucial for shaping ecosystems since the first Lifeforms arose.

This review summarizes our current understanding of the CO_2-activation steps orchestrated by these fantastic machineries, which evolved to fulfill the physiological needs for carbon-assimilation and energy-conservation. The structural knowledge gathered from hydrogenotrophic methanogens provides insights in the shared and distinct features between the acetogenic and methanogenic CO_2-conversion systems, due to both metabolic adaptation and ecological specialization.

THE CO_2-REDUCTION/FIXATION COMPLEX IN METHANOGENS

The entire energy metabolism of methanogens relies on highly efficient CO_2-capture. This challenging task is overcome by the formyl-methanofuran dehydrogenase (Fwd) complex catalyzing both the reduction of CO_2 and the conversion of formate ($HCOO^-$) into a formyl group (**Figures 1A**, **2**). So far, two isoforms of this enzyme are described, containing either a molybdenum- or tungsten-dependent formate dehydrogenase (Fdh) subunit (Bertram et al., 1994; Thauer et al., 2008; Leimkühler and Iobbi-Nivol, 2016; Wagner et al., 2018). Depending on the organism, the molybdo/tungstopterin cofactor can be coordinated by a cysteine or seleno-cysteine. Unlike nearly all described Fdh that perform formate oxidation releasing CO_2, methanogenic and acetogenic Fdh physiologically run toward CO_2-fixation. Until now, only a few enzymes found in the *Synthrophobacter* genus share this feature (de Bok et al., 2003).

The reaction remained a mystery for a long time: how can the enzyme couple formate to the C1-carrier methanofuran (MFR) without any ATP investment (Bertram et al., 1994)? The secret was eventually unraveled by its crystal structure (Wagner et al., 2016). The overall complex is constituted of an unprecedented electron transfer apparatus containing a total of 46-[Fe_4S_4] clusters flanked by two catalytic modules, a tungstopterin-dependent Fdh and a binuclear metallo-hydrolase. Based on the molecular details, a scenario of the reaction has been proposed where; (1) CO_2 is funneled to the active site of Fdh by a selective, hydrophobic channel; (2) CO_2 is reduced to formate (**Figures 1A,B**, **2A,B**; Wagner et al., 2016); (3) a second hydrophilic tunnel channels and accumulates formate at the active site of the metallo-hydrolase; and (4) formate is condensed on the amino-group of MFR as a formyl-group. The accumulation of formate is predicted to thrive the conversion of formate to a formyl group on MFR without the investment of ATP, an endergonic reaction under standard conditions. However, since Fdh are reversible, the driver of the overall reaction is the electron donor.

From MFR the formyl group is transferred to the second C1-carrier tetrahydromethanopterin (H_4MPT), successively dehydrated and fully reduced (i.e., by the F_{420} cofactor or alternatively with H_2 by the [Fe]-hydrogenase) to a methyl group (dashed line, **Figure 1A**). The methyl-H_4MPT represents the crossroad between carbon-assimilation and energy conservation

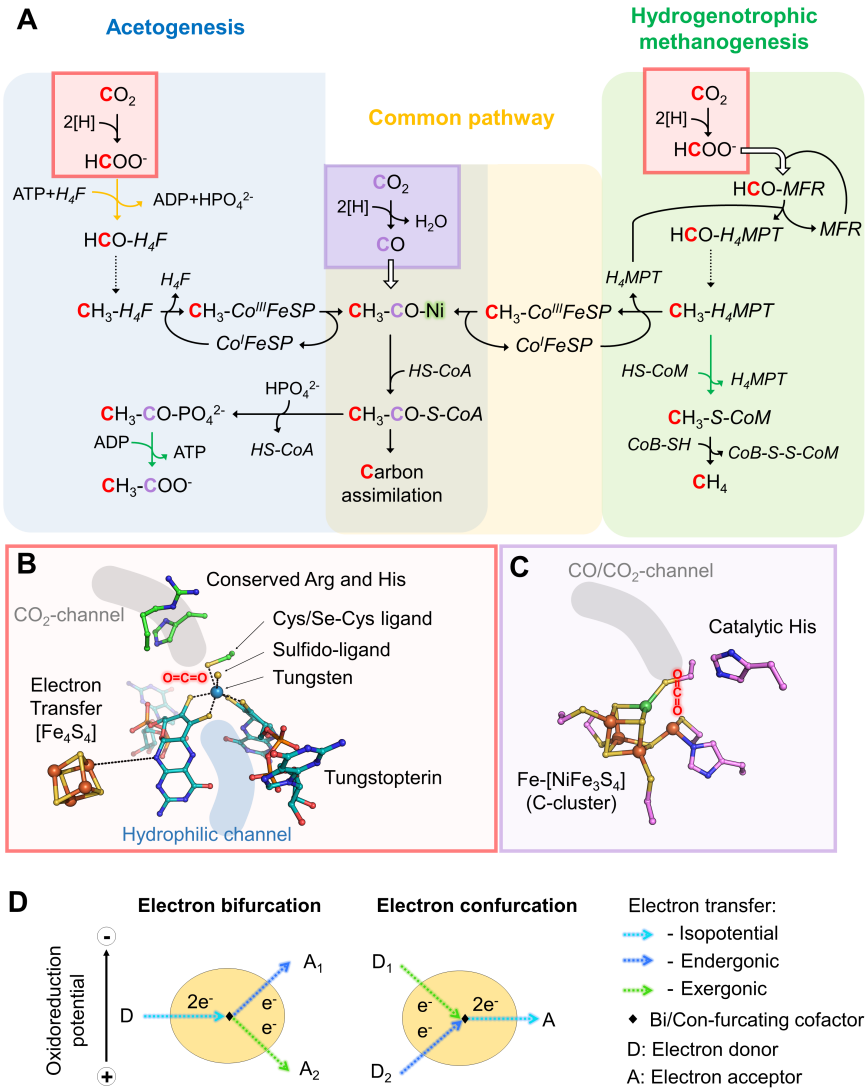

FIGURE 1 | Variations in the reductive acetyl-CoA pathway between acetogenic bacteria and hydrogenotrophic methanogens, implicated active sites and mechanisms. **(A)** Differences in the reductive acetyl-CoA pathway between acetogenic bacteria (left and middle) and methanogenic archaea (right and middle). Acetogens and methanogens share a conserved "carbonyl" branch (common pathway) used to build biomass for both and to conserve energy for acetogens. The green arrows correspond to reactions coupled to energy-conservation (ATP or electrochemical ion gradient generation across the membrane) and the orange one to ATP hydrolysis-coupled reaction. Dashed arrows correspond to three successive reactions: dehydration and two reduction steps. White arrows indicate the usage of an internal channeling system between two active sites. Red and purple squares highlight CO_2-reduction events, in red Fdh reaction and in purple the CODH reaction. The ACS contains the A-cluster harboring the binuclear Nickel center highlighted by a green glow. The cofactors involved in these processes are: tetrahydrofolate (H_4F), tetrahydromethanopterin (H_4MPT), coenzyme A (CoA-SH), methanofuran (MFR), reduced/oxidized corrinoid FeS containing protein (Co^I/CH_3-Co^{III}-FeSP), coenzyme B (CoB-SH), coenzyme M (CoM-SH). **(B)** Close up of a Fdh catalytic site (PDB code 5T5I) containing the tungstopterin, which could be replaced by molybdopterin for other Fdh. Carbons are colored in green for the residues involved in the catalysis and dark cyan for the tungstopterin. Dashed line between the $[Fe_4S_4]$-cluster and the pterin represents the hypothetic electron transfer from the cluster to the tungstopterin. **(C)** Close up of the catalytic site of CODH from *Moorella thermoacetica* (PDB code 1MJG) containing the C-cluster. Carbons from protein residues are colored in light pink. For both panels, **B** and **C**, nitrogen, oxygen, phosphorous, sulfur, iron, tungsten, and nickel are colored as dark blue, red, light orange, yellow, orange, metallic blue, and green, respectively. A molecule highlights the putative CO_2 position in both panels. **(D)** Scheme of electron bifurcation/confurcation mechanism. During electron bifurcation, a two-electron transfer from an electron donor (D) is bifurcated by a specific cofactor to both endergonic and exergonic one-electron transfers to two different acceptors (A_1 and A_2). The overall reaction is slightly exergonic. The opposite reaction occurs during electron confurcation.

(Thauer, 2012). The latter is formed during the methyl group transfer from nitrogen-bound methyl-H_4MPT to the thiol group of the coenzyme-M acceptor. The methyl-transfer is coupled to a sodium translocation across the membrane, used to feed the ATP-synthase, which is generating only half an ATP per processed C1-unit (Schäfer et al., 1999). Finally, methylated coenzyme-M becomes oxidized to a heterodisulfide with coenzyme-B (CoB-S-S-CoM), releasing methane by using the F_{430}-cofactor (Thauer et al., 2008; Thauer, 2012; Sousa et al., 2013).

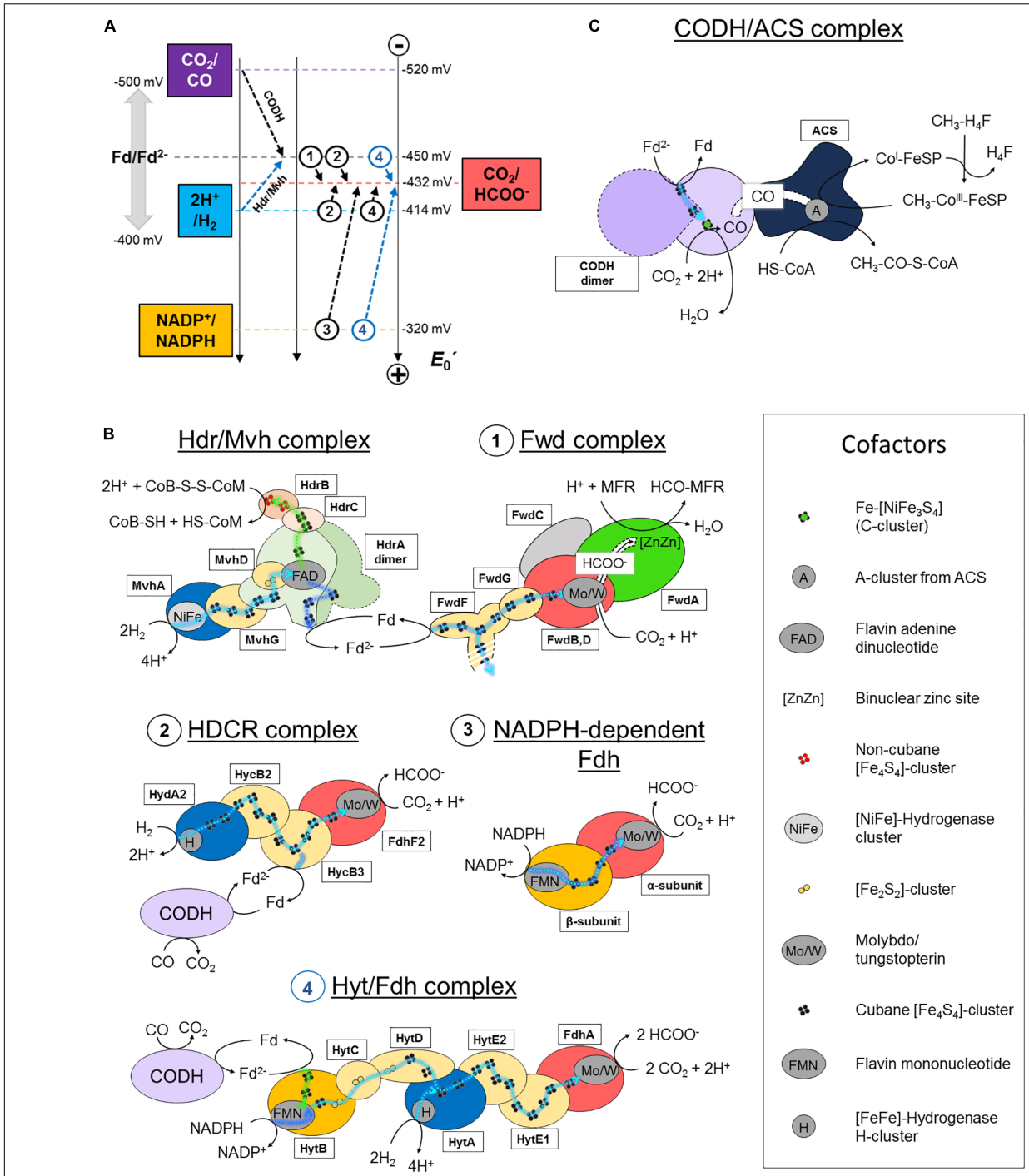

FIGURE 2 | CO_2-activation strategies in hydrogenotrophic methanogens and acetogens. **(A)** Standard redox potential (E_0') of redox couples implicated in CO_2-activation in methanogenic and acetogenic processes. Dashed arrows schematize the reactions performed by the enzymes listed in panel **B**. A name or circled number indicates which complex is implicated. The blue arrows correspond to a coupled electron confurcating reaction. To simplify the scheme, the endergonic reaction of the Hdr/Mvh complex (CoB-S-S-CoM/CoB-SH + CoM-SH = −140 mV) has been omitted. Standard redox potentials were taken from Schuchmann and Müller (2014). Ferredoxin can exhibit potentials ranging from −400 to −500 mV, depending on the organism. An averaged potential of −450 mV is thus used in the figure. **(B,C)** Schemes of the characterized and putative organizations of the enzymes involved in CO_2-reduction in hydrogenotrophic methanogens and acetogens. Catalytic subunits are colored according to their substrate as in panel **A**. All electron transfers except for con/bifurcation events are shown as cyan dashed lines. For con/bifurcation events, the endergonic reactions are colored in dark blue and exergonic in light green, as illustrated in **Figure 1D**. Due to the absence of acetogenic structural data, hypothetic architectures are represented based on their original publications, biochemical data and homologies (Yamamoto et al., 1983; Schuchmann and Müller, 2013; Wang et al., 2013). Monomeric forms are schematized. The localization of the electron confurcation event in the Hyt complex is purely hypothetic. The [NiFe]-hydrogenase module from the Hdr/Mvh complex can be replaced by a Fdh. All known cofactors involved in the different reactions of panels **B** and **C** are listed. Fd stands for oxidized ferredoxin and Fd^{2-} for reduced ferredoxin.

ELECTRON-BIFURCATION FUELS METHANOGENIC CO_2 FIXATION

The electron donor for the Fwd complex is predicted to be reduced ferredoxin or a direct electron transfer by the heterodisulfide reductase (Costa et al., 2010; Kaster et al., 2011; Milton et al., 2018). Two versions of this enzyme have been described in hydrogenotrophic methanogens depending on the coupled electron donor: a [NiFe]-hydrogenase or a Fdh (the structurally characterized hydrogenase-dependent one called the Hdr/Mvh complex is shown in **Figures 1**, **2B**).

The overall process starts with the transfer of two electrons from the donor (H_2 or formate) to a flavin. Flavin-based electron bifurcation then splits the two electrons at different potentials (**Figures 1D**, **2B**). The high-potential electron is used for the exergonic reduction of the heterodisulfide. The low-potential electron reduces ferredoxin or might even be directly delivered to the 46-[Fe_4S_4] relay of the formyl-methanofuran dehydrogenase to allow CO_2-capture. The whole reaction is performed in two rounds (Wagner et al., 2017).

DIVERSITY OF CO_2-ACTIVATION SYSTEMS IN ACETOGENS

Like methanogens, acetogenic bacteria perform initial CO_2-reduction via molybdo/tungstopterin-dependent Fdh. However, in contrast to methanogens, all described acetogenic CO_2-reducing systems produce detectable formate, indicating that CO_2-reduction and formate condensation are uncoupled (Yamamoto et al., 1983; Schuchmann and Müller, 2013, 2014; Wang et al., 2013). Formate conversion into a formyl group on a C1-carrier (i.e., tetrahydrofolate, H_4F) is thermodynamically unfavorable and acetogens must therefore invest one ATP. Then, the successive dehydration and reduction into methenyl, methylene and finally methyl group can occur, similar to the methanogenic process but involving different systems, reductants and cofactors (Mock et al., 2014; Schuchmann and Müller, 2014). The methyl group is further fused to CO and CoA by the CO dehydrogenase/acetyl-CoA synthase complex (CODH/ACS) to form acetyl-CoA (see below, **Figures 1**, **2C**; Ragsdale, 2008; Can et al., 2014).

Despite a common Fdh module, acetogens evolved their CO_2-fixation system in many variations, a real example of "mix and match" from the redox module toolbox, as already shown for sulfate-reducing organisms (Grein et al., 2013). Some of them have been reported to be molybdopterin dependent (e.g., *Acetobacterium woodii*) while others require tungstopterin (e.g., *Moorella thermoacetica*, *Clostridium autoethanogenum*, etc.). There are selenium-dependent or selenium-free formate dehydrogenases and some organisms encode both (Yamamoto et al., 1983; Schuchmann and Müller, 2013; Wang et al., 2013). This diversity allows the use of different electron donors (Schuchmann and Müller, 2014).

Acetobacterium woodii uses a hydrogen-dependent CO_2-reductase (HDCR) which couples the oxidation of H_2 to the reduction of CO_2 (Schuchmann and Müller, 2013). The enzyme is composed of a selenocysteine–molybdopterin dependent Fdh linked to a [FeFe]-hydrogenase via an electron bridge (**Figure 2B**, 2). The genome also encodes a cysteine-dependent Fdh isoform, supposedly expressed under selenium deprivation. The reduction of CO_2 to formate with H_2 is slightly endergonic at standard conditions (**Figure 2A**). However, at the relatively important threshold concentration of H_2, necessary for acetogenesis in *A. woodii* (measured at 0.0025 Bar, around thirty times superior to the threshold of hydrogenotrophic methanogens; Thauer et al., 2008), the equilibrium concentration of generated formate becomes sufficient to fuel the methyl branch of the pathway (Schuchmann and Müller, 2014). The enzyme can also perform carbon fixation by ferredoxin oxidation, albeit exhibiting a 1000-times lower reaction rate (**Figure 2B**, 2). This ability is thought to be crucial in presence of CO, a strong inhibitor of hydrogenases. The coupling of HDCR with CODH is an efficient way to regenerate reduced ferredoxin.

Moorella thermoacetica contains a two subunit NADPH-dependent Fdh containing selenocysteine and tungstopterin cofactor, which catalyzes the reversible formate generation through NADPH oxidation (**Figure 2B**, 3; Thauer, 1972; Yamamoto et al., 1983). Despite being thermodynamically highly unfavorable under standard conditions, it appears that the NADPH-dependent Fdh is the only formate generating enzyme in *M. thermoacetica*. High NADPH/$NADP^+$ and CO_2/formate ratios are necessary to push the reaction toward carbon reduction.

Clostridium autoethanogenum exploits a seven subunit complex (Hyt/Fdh), the so far most complicated formate-generating system in acetogens (**Figure 2B**, 4; Wang et al., 2013; Schuchmann and Müller, 2014). The selenium-dependent tungstopterin-containing Fdh module performs CO_2-reduction by receiving electrons from H_2-oxidation via a [FeFe]-hydrogenase subunit (similar to HDCR) or by concomitant oxidation of NADPH and ferredoxin through an internal confurcation event (**Figures 1D**, **2B**, 4). Like in HDCR, the reduced ferredoxin could directly come from CO-oxidation by the CODH. Where and how the electron confurcation is carried out is still unresolved, as the only known flavin cofactor present in the complex (in HytB) is thought to be not involved (Wang et al., 2013). A novel type of electron bifurcation is thus suspected, one that is similar to the related electron-bifurcating hydrogenase. The structural features of this bifurcation mechanism have to be deciphered and as said by Buckel and Thauer (2018): "A crystal structure is urgently needed to solve this problem."

A COMMON CO_2-FIXATION SYSTEM: THE CO-DEHYDROGENASE/ACETYL-COA SYNTHASE

While methanogens and acetogens employ different strategies to reduce CO_2 for the methyl-branch, the activation step of the carbonyl-branch, catalyzed by Ni,Fe-containing CODH, is remarkably conserved (Lindahl, 2002; Jeoung et al., 2019).

The initial CO_2-reduction to CO, powered by low-potential electrons from ferredoxins or flavodoxins (Ragsdale et al., 1983;

Can et al., 2014; Schuchmann and Müller, 2014), occurs at the C-cluster composed of a Fe-[$NiFe_3S_4$] (**Figure 1C**). CO is transferred to the ACS by a long internal hydrophobic channel (**Figure 2C**; Doukov et al., 2002; Can et al., 2014). Here, it is fixed on the A-cluster, which is composed of a Ni-[Fe_4S_4] cluster bridged to another Ni atom (Ragsdale and Pierce, 2008). Ultimately, the ACS forms acetyl-CoA by associating the CO-ligand, CoA and the methyl-ligand from the methyl-branch. A cobalamin-containing FeS protein (CoFeSP) serves as a shuttle for the methyl group between the Methyl-H_4F and the ACS. The transfer mechanism from the CoFeSP to the ACS is so far unknown. The enzyme thus performs the biological equivalent of the Monsanto and Cativa processes, where CO and methanol are converted to acetate by metal-based catalysts (Appel et al., 2013).

Even if the overall reaction is the same between methanogens and acetogens some subtleties concerning the CODH/ACS composition exist. According to the classification of Lindahl (2002), archaea and predominantly methanogens use preferentially Ni,Fe-CODH of Class I and II (also called acetyl-CoA decarbonylases/synthases), which consist of five different subunits that form oligomeric complexes of approximately 2-MDa. This super-complex contains the CODH/ACS (Doukov et al., 2002; Can et al., 2014), the CoFeSP and the enzyme responsible for methyl-transfer from methyl-H_4F to cobalamin. These three sub-complexes are separated in acetogenic systems. The CODH subunit in methanogens contains two extra [Fe_4S_4]-clusters, putatively implicated in the rerouting of electrons. Acetogenic complexes have been extensively studied (Ragsdale and Kumar, 1996; Ragsdale and Pierce, 2008) thanks to a few available crystal structures of the whole CODH/ACS complex from *M. thermoacetica* (Doukov et al., 2002; Darnault et al., 2003; Kung et al., 2009) and the knowledge gathered on this enzyme has already been reviewed (Can et al., 2014).

Beside these slight differences, all classes of the CODH/ACS complex are thought to be homologous and thus may have been acquired from a common ancestor (Sousa et al., 2013).

CONCLUSION AND PERSPECTIVES

As previously depicted, the Fdh subunit and CODH/ACS complex are conserved in methanogens and acetogens. These elementary modules are therefore thought to have evolved before the divergence of acetogens and methanogens, thus in the Last Universal Common Ancestor (LUCA) (Sousa et al., 2013; Martin and Thauer, 2017). Because they harbor "ancestral" cofactors like Fe-S clusters or tungstopterin and since the substrates H_2 and CO_2 should have been abundant in Early Earth, these pathways are considered to be among the first, if not the first, biological energetic processes (Fuchs, 2011; Sousa et al., 2013; Martin and Thauer, 2017). Understanding the mechanisms and limitations of methanogenesis and acetogenesis will help to unravel the fundamental questions of how Life arose from the pre-existing inorganic world and could provide information about its first evolutionary steps in the new organic one.

While the carbonyl-branch of the reductive acetyl-CoA pathway might be an early and highly conserved invention in LUCA, the methyl-branch is not. Here, methanogens and acetogens use non-homologous enzymes to perform similar reactions. This parallel evolution gave birth to a variety of formate-generating, CO_2-reducing enzymes, albeit using similar modules (Sousa et al., 2013) and invented different strategies for C1-reduction and formate condensation by the use of different C1-carriers. The evolutionary plasticity of the methyl-branch compared to the strict conservation of the carbonyl-branch might derive from its requirement for low-potential electrons. Because of the low-potential of the CO_2/CO couple, the CODH could not adapt to a partner other than ferredoxin for CO generation, while the CO_2-reduction to formate can accommodate different electron donors, allowing variability of enzymes according to the metabolic needs for physiological requirements.

Furthermore, the functional modules coupled to Fdh systems might be the foundation for other "modern" enzymes, from the formate-hydrogen lyase complex to the respiratory complex I (Marreiros et al., 2016). Elucidating methanogenic and acetogenic enzymes has therefore the potential to provide hints to how the ancestral energetic pathways diversified, thereby creating new processes and gradually giving birth to the plethora of bio-energetically important complexes.

A striking difference between formate generating enzymes from acetogens and methanogens is the energy investment. While methanogens bypass the latter (**Figure 1A**), acetogens need to sacrifice one ATP to allow formate fixation. They counterbalance this energy loss via substrate level phosphorylation of acetyl-phosphate in the last step of acetogenesis. In comparison, no ATP is generated through methanogenesis (**Figure 1A**). Nevertheless, ATP sparing is critical for energy-limited extremophiles and one could ask why acetogens did not develop an equivalent of the Hdr/Mvh/Fwd coupling system. The explanation could come from the use of low-potential ferredoxins. The last step of methanogenesis releases CoB-S-S-CoM, which is recycled by the heterodisulfide reductase (downhill reaction) with the concomitant generation of low-potential electrons (uphill reaction). Most of these low-potential electrons generated in the cell are assumed to be dedicated for the CO_2-fixation (**Figure 2B**, 1; Thauer, 2012).

Acetogenic bacteria are restricted to ecological niches with higher H_2 pressure than methanogens. The main reason is that electron bifurcating [FeFe]-hydrogenases are necessary for ferredoxin reduction (Schuchmann and Müller, 2012, 2014), the electron acceptor for the downhill reaction being $NAD(P)^+$. According to the current knowledge, the uphill electron generated during the flavin-based electron bifurcation could have a lower potential if the electron downhill is the heterodisulfide ($E_0' \approx -140$ mV) compared to $NAD(P)^+$ ($E_0' = -320$ mV). Therefore, the ferredoxins reduced via electron bifurcation in methanogens are expected to have higher reducing power compared to acetogens. Thus, in the latter the potential could not be low enough to allow both, formate generation and conversion to formyl group, unlike in methanogens. Thus, despite sparing one ATP, coupling formate generation and fixation may be not favorable for acetogenic bacteria and will not sustain a metabolic high-flow toward acetyl-CoA synthesis.

A way to bypass H_2 is CO-oxidation. To handle CO, acetogens use different strategies. *A. woodii* thrives episodically on weak CO concentrations, possible due to the reversibility of the CO inhibition of the HDCR system and the ability to oxidize ferredoxin, albeit with a weak turnover (**Figure 2B**, 2; Schuchmann and Müller, 2013; Bertsch and Müller, 2015; Ceccaldi et al., 2017). Acetogenic bacteria, which use CO as substrate, like *M. thermoacetica* and *C. autoethanogenum*, exhibit metabolic adaptations. For instance, albeit it has not been tested so far, the NADPH-dependent Fdh system from *M. thermoacetica* should be insensitive to CO as it is not directly using the CO-sensitive hydrogenase, like the HDCR. However, the enzyme depends on a high $NADPH/NADP^+$ ratio or high pressure of CO_2. The Hyt/Fdh system from *C. autoethanogenum*, a chimera between HDCR and the electron bifurcating/confurcating hydrogenase (**Figure 2B**, 4), shows a reactional plasticity by switching from the CO-sensitive hydrogenase to NADPH plus ferredoxin oxidation to drive CO_2-reduction despite inhibition (Wang et al., 2013). Interestingly, to date, a formyl group generation directly driven by CO-oxidation has never been found in any CO fermenting acetogen. Still, the low redox potential of the CO_2/CO couple could allow an Fwd-like coupled mechanism, sparing a molecule of ATP, crucial for such energetic extremophiles.

The diversity of the electron-donating Fdh systems reflects and allowed the widespread distribution of these microbes, from H_2 rich to CO saturated niches. However, their dependence on oxygen-sensitive cofactors constrains them to strictly anaerobic but also metal-rich environments, since such carbon fixation pathways require more metallic cofactors than the others. Studying the diversity of these systems provides modern snapshots of the evolution of such "ancestral" organisms to accommodate various ecological niches.

Because syngas ($H_2/CO_2/CO$) is the main source of carbon and energy for hydrogenotrophic methanogens and acetogens, they are excellent "bio-converters." For instance, acetogens turn industrial waste gases, rich in H_2, CO and CO_2, to butanediol, ethanol or acetate, potential biofuels or starting points for new chemical synthesis (Wang et al., 2013; Mock et al., 2015; Liew et al., 2016). With the discovery of genetically tractable acetogens (Liew et al., 2016; Basen et al., 2018) the possibilities for bio-compound synthesis, and bioremediation are expanding.

Moreover, acetogenic CO_2-activation systems as HDCR and Hyt/Fdh are a treasure trove to realize the Holy Grail reaction of our century: the reversible hydrogenation of CO_2 to formate, offering a stable way to store energy with the concomitant advantage of trapping the greenhouse gas (Schuchmann and Müller, 2013; Müller, 2019).

Studies of acetogenic physiology and carbon fixation pathways are still an ongoing growing field. More work has to be conducted to truly understand their enzymes, metabolic fluxes, the molecular juggling of their reactions and their limitations. It is crucial to ensure the success of biotechnological applications, including synthetic biology, that will – let's hope – bring a brighter future.

AUTHOR CONTRIBUTIONS

All authors participated to the manuscript writing.

FUNDING

This work was funded by the Max-Planck-Gesellschaft and the Deutsche Forschungsgemeinschaft priority program 1927, "Iron-Sulfur for Life" WA 4053/1-1.

ACKNOWLEDGMENTS

We would like to acknowledge the Max Planck Institute for Marine Microbiology for continuous support.

REFERENCES

Appel, A. M., Bercaw, J. E., Bocarsly, A. B., Dobbek, H., DuBois, D. L., Dupuis, M., et al. (2013). Frontiers, opportunities, and challenges in biochemical and chemical catalysis of CO2 fixation. *Chem. Rev.* 113, 6621–6658. doi: 10.1021/cr300463y

Basen, M., Geiger, I., Henke, L., and Müller, V. (2018). A genetic system for the thermophilic acetogenic bacterium *Thermoanaerobacter kivui*. *Appl. Environ. Microbiol.* 84, e2210–e2217. doi: 10.1128/AEM.02210-17

Berg, I. A., Kockelkorn, D., Ramos-Vera, W. H., Say, R. F., Zarzycki, J., Hügler, M., et al. (2010). Autotrophic carbon fixation in archaea. *Nat. Rev. Microbiol.* 8, 447–460. doi: 10.1038/nrmicro2365

Bertram, P. A., Karrasch, M., Schmitz, R. A., Böcher, R., Albracht, S. P., and Thauer, R. K. (1994). Formylmethanofuran dehydrogenases from methanogenic archaea. Substrate specificity, EPR properties and reversible inactivation by cyanide of the molybdenum or tungsten iron-sulfur proteins. *Eur. J. Biochem.* 220, 477–484. doi: 10.1111/j.1432-1033.1994.tb18646.x

Bertsch, J., and Müller, V. (2015). CO metabolism in the acetogen *Acetobacterium woodii*. *Appl. Environ. Microbiol.* 81, 5949–5956. doi: 10.1128/AEM.01772-15

Buckel, W., and Thauer, R. K. (2013). Energy conservation via electron bifurcating ferredoxin reduction and proton/Na+ translocating ferredoxin oxidation. *Biochim. Biophys. Acta* 1827, 94–113. doi: 10.1016/j.bbabio.2012.07.002

Buckel, W., and Thauer, R. K. (2018). Flavin-based electron bifurcation, a new mechanism of biological energy coupling. *Chem. Rev.* 118, 3862–3886. doi: 10.1021/acs.chemrev.7b00707

Can, M., Armstrong, F. A., and Ragsdale, S. W. (2014). Structure, function, and mechanism of the nickel metalloenzymes, CO dehydrogenase, and acetyl-CoA synthase. *Chem. Rev.* 114, 4149–4174. doi: 10.1021/cr400461p

Ceccaldi, P., Schuchmann, K., Müller, V., and Elliott, S. J. (2017). The hydrogen dependent CO2 reductase: the first completely CO tolerant FeFe-hydrogenase. *Energy Environ. Sci.* 10, 503–508. doi: 10.1039/C6EE02494G

Cherubini-Celli, A., Mateos, J., Bonchio, M., Dell'Amico, L., and Companyó, X. (2018). Transition metal-free CO2 fixation into new carbon-carbon bonds. *ChemSusChem* 11, 3056–3070. doi: 10.1002/cssc.201801063

Costa, K. C., Wong, P. M., Wang, T., Lie, T. J., Dodsworth, J. A., Swanson, I., et al. (2010). Protein complexing in a methanogen suggests electron bifurcation and electron delivery from formate to heterodisulfide reductase. *Proc. Natl. Acad. Sci. U.S.A.* 107, 11050–11055. doi: 10.1073/pnas.1003653107

Darnault, C., Volbeda, A., Kim, E. J., Legrand, P., Vernède, X., Lindahl, P. A., et al. (2003). Ni-Zn-[Fe4-S4] and Ni-Ni-[Fe4-S4] clusters in closed and open α subunits of acetyl-CoA synthase/carbon monoxide dehydrogenase. *Nat. Struct. Biol.* 10, 271–279. doi: 10.1038/nsb912

de Bok, F. A., Hagedoorn, P. L., Silva, P. J., Hagen, W. R., Schiltz, E., Fritsche, K., et al. (2003). Two W-containing formate dehydrogenases (CO2-reductases) involved in syntrophic propionate oxidation by *Syntrophobacter fumaroxidans*. *Eur. J. Biochem.* 270, 2476–2485. doi: 10.1046/j.1432-1033.2003.03619.x

Doukov, T. I., Iverson, T. M., Seravalli, J., Ragsdale, S. W., and Drennan, C. L. (2002). A Ni-Fe-Cu center in a bifunctional carbon monoxide dehydrogenase/acetyl-CoA synthase. *Science* 298, 567–572. doi: 10.1126/science.1075843

Fuchs, G. (2011). Alternative pathways of carbon dioxide fixation: insights into the early evolution of life? *Annu. Rev. Microbiol.* 65, 631–658. doi: 10.1146/annurev-micro-090110-102801

Fuchs, G., and Berg, I. A. (2014). Unfamiliar metabolic links in the central carbon metabolism. *J. Biotechnol.* 192(Pt B), 314–322. doi: 10.1016/j.jbiotec.2014.02.015

Fujita, E., Muckerman, J. T., and Himeda, Y. (2013). Interconversion of CO2 and formic acid by bio-inspired Ir complexes with pendent bases. *Biochim. Biophys. Acta* 1827, 1031–1038. doi: 10.1016/j.bbabio.2012.11.004

Grein, F., Ramos, A. R., Venceslau, S. S., and Pereira, I. A. (2013). Unifying concepts in anaerobic respiration: insights from dissimilatory sulfur metabolism. *Biochim. Biophys. Acta* 1827, 145–160. doi: 10.1016/j.bbabio.2012.09.001

Hou, S. L., Dong, J., and Zhao, B. (2019). Formation of C-X bonds in CO2 chemical fixation catalyzed by metal-organic frameworks. *Adv. Mater.* 32:e1806163. doi: 10.1002/adma.201806163

Jeoung, J. H., Martins, B. M., and Dobbek, H. (2019). Carbon monoxide dehydrogenases. *Methods Mol. Biol.* 1876, 37–54. doi: 10.1007/978-1-4939-8864-8_3

Kaster, A. K., Moll, J., Parey, K., and Thauer, R. K. (2011). Coupling of ferredoxin and heterodisulfide reduction via electron bifurcation in hydrogenotrophic methanogenic archaea. *Proc. Natl. Acad. Sci. U.S.A.* 108, 2981–2986. doi: 10.1073/pnas.1016761108

Kung, Y., Doukov, T. I., Seravalli, J., Ragsdale, S. W., and Drennan, C. L. (2009). Crystallographic snapshots of cyanide- and water-bound C-clusters from bifunctional carbon monoxide dehydrogenase/acetyl-CoA synthase. *Biochemistry* 48, 7432–7440. doi: 10.1021/bi900574h

Leimkühler, S., and Iobbi-Nivol, C. (2016). Bacterial molybdoenzymes: old enzymes for new purposes. *FEMS Microbiol. Rev.* 40, 1–18. doi: 10.1093/femsre/fuv043

Liew, F., Henstra, A. M., Winzer, K., Köpke, M., Simpson, S. D., and Minton, N. P. (2016). Insights into CO2 fixation pathway of *Clostridium autoethanogenum* by targeted mutagenesis. *mBio* 7:e00427-16. doi: 10.1128/mBio.00427-16

Lindahl, P. A. (2002). The Ni-containing carbon monoxide dehydrogenase family: light at the end of the tunnel? *Biochemistry* 41, 2097–2105. doi: 10.1021/bi015932%2B

Marreiros, B. C., Calisto, F., Castro, P. J., Duarte, A. M., Sena, F. V., Silva, A. F., et al. (2016). Exploring membrane respiratory chains. *Biochim. Biophys. Acta* 1857, 1039–1067. doi: 10.1016/j.bbabio.2016.03.028

Martin, W. F., and Thauer, R. K. (2017). Energy in ancient metabolism. *Cell* 168, 953–955. doi: 10.1016/j.cell.2017.02.032

Milton, R. D., Ruth, J. C., Deutzmann, J. S., and Spormann, A. M. (2018). *Methanococcus maripaludis* employs three functional heterodisulfide reductase complexes for flavin-based electron bifurcation using hydrogen and formate. *Biochemistry* 57, 4848–4857. doi: 10.1021/acs.biochem.8b00662

Mock, J., Wang, S., Huang, H., Kahnt, J., and Thauer, R. K. (2014). Evidence for a hexaheteromeric methylenetetrahydrofolate reductase in *Moorella thermoacetica*. *J. Bacteriol.* 196, 3303–3314. doi: 10.1128/JB.01839-14

Mock, J., Zheng, Y., Mueller, A. P., Ly, S., Tran, L., Segovia, S., et al. (2015). Energy conservation associated with ethanol formation from H2 and CO2 in *Clostridium autoethanogenum* involving electron bifurcation. *J. Bacteriol.* 197, 2965–2980. doi: 10.1128/JB.00399-15

Müller, V. (2019). New horizons in acetogenic conversion of one-carbon substrates and biological hydrogen storage. *Trends Biotechnol.* 37, 1344–1354. doi: 10.1016/j.tibtech.2019.05.008

Peters, J. W., Beratan, D. N., Bothner, B., Dyer, R. B., Harwood, C. S., Heiden, Z. M., et al. (2018). A new era for electron bifurcation. *Curr. Opin. Chem. Biol.* 47, 32–38. doi: 10.1016/j.cbpa.2018.07.026

Ragsdale, S. W. (2008). Enzymology of the Wood-Ljungdahl pathway of acetogenesis. *Ann. N. Y. Acad. Sci.* 1125, 129–136. doi: 10.1196/annals.1419.015

Ragsdale, S. W., and Kumar, M. (1996). Nickel-containing carbon monoxide dehydrogenase/acetyl-CoA synthase. *Chem. Rev.* 96, 2515–2540. doi: 10.1021/cr950058%2B

Ragsdale, S. W., Ljungdahl, L. G., and DerVartanian, D. V. (1983). Isolation of carbon monoxide dehydrogenase from *Acetobacterium woodii* and comparison of its properties with those of the *Clostridium thermoaceticum* enzyme. *J. Bacteriol.* 155, 1224–1237. doi: 10.1128/jb.155.3.1224-1237.1983

Ragsdale, S. W., and Pierce, E. (2008). Acetogenesis and the Wood-Ljungdahl pathway of CO2 fixation. *Biochim. Biophys. Acta* 1784, 1873–1898. doi: 10.1016/j.bbapap.2008.08.012

Schäfer, G., Engelhard, M., and Müller, V. (1999). Bioenergetics of the archaea. *Microbiol. Mol. Biol. Rev.* 63, 570–620.

Schuchmann, K., and Müller, V. (2012). A bacterial electron-bifurcating hydrogenase. *J. Biol. Chem.* 287, 31165–31171. doi: 10.1074/jbc.M112.395038

Schuchmann, K., and Müller, V. (2013). Direct and reversible hydrogenation of CO2 to formate by a bacterial carbon dioxide reductase. *Science* 342, 1382–1385. doi: 10.1126/science.1244758

Schuchmann, K., and Müller, V. (2014). Autotrophy at the thermodynamic limit of life: a model for energy conservation in acetogenic bacteria. *Nat. Rev. Microbiol.* 12, 809–821. doi: 10.1038/nrmicro3365

Sousa, F. L., Thiergart, T., Landan, G., Nelson-Sathi, S., Pereira, I. A., Allen, J. F., et al. (2013). Early bioenergetic evolution. *Phil. Trans. R. Soc. B* 368:20130088. doi: 10.1098/rstb.2013.0088

Thauer, R. K. (1972). CO2-reduction to formate by NADPH. The initial step in the total synthesis of acetate from CO2 in *Clostridium thermoaceticum*. *FEBS Lett.* 27, 111–115. doi: 10.1016/0014-5793(72)80421-6

Thauer, R. K. (2012). The Wolfe cycle comes full circle. *Proc. Natl. Acad. Sci. U.S.A.* 109, 15084–15085. doi: 10.1073/pnas.1213193109

Thauer, R. K., Kaster, A. K., Seedorf, H., Buckel, W., and Hedderich, R. (2008). Methanogenic archaea: ecologically relevant differences in energy conservation. *Nat. Rev. Microbiol.* 6, 579–591. doi: 10.1038/nrmicro1931

Wagner, T., Ermler, U., and Shima, S. (2016). The methanogenic CO2 reducing-and-fixing enzyme is bifunctional and contains 46 [4Fe-4S] clusters. *Science* 354, 114–117. doi: 10.1126/science.aaf9284

Wagner, T., Ermler, U., and Shima, S. (2018). "Tungsten-containing formylmethanofuran dehydrogenase," in *Encyclopedia of Inorganic and Bioinorganic Chemistry (online)*, ed. A. Messerschmidt (Hoboken: John Wiley and Sons, Inc).

Wagner, T., Koch, J., Ermler, U., and Shima, S. (2017). Methanogenic heterodisulfide reductase (HdrABC-MvhAGD) uses two noncubane [4Fe-4S] clusters for reduction. *Science* 357, 699–703. doi: 10.1126/science.aan0425

Wang, S., Huang, H., Kahnt, J., Mueller, A. P., Köpke, M., and Thauer, R. K. (2013). NADP-specific electron-bifurcating [FeFe]-hydrogenase in a functional complex with formate dehydrogenase in *Clostridium autoethanogenum* grown on CO. *J. Bacteriol.* 195, 4373–4386. doi: 10.1128/JB.00678-13

Yamamoto, I., Saiki, T., Liu, S. M., and Ljungdahl, L. G. (1983). Purification and properties of NADP-dependent formate dehydrogenase from *Clostridium thermoaceticum*, a tungsten-selenium-iron protein. *J. Biol. Chem.* 258, 1826–1832.

Conflict of Interest: The authors declare that the research was conducted in the absence of any commercial or financial relationships that could be construed as a potential conflict of interest.

frontiers in Microbiology

ORIGINAL RESEARCH
published: 06 May 2020
doi: 10.3389/fmicb.2020.00724

Nitrate Feed Improves Growth and Ethanol Production of *Clostridium ljungdahlii* With CO_2 and H_2, but Results in Stochastic Inhibition Events

*Christian-Marco Klask[1], Nicolai Kliem-Kuster[1], Bastian Molitor[1] and Largus T. Angenent[1,2]**

[1] Environmental Biotechnology Group, Center for Applied Geoscience, University of Tübingen, Tübingen, Germany, [2] Max Planck Fellow Groups, Max Planck Institute for Developmental Biology, Tübingen, Germany

The pH-value in fermentation broth is a critical factor for the metabolic flux and growth behavior of acetogens. A decreasing pH level throughout time due to undissociated acetic acid accumulation is anticipated under uncontrolled pH conditions such as in bottle experiments. As a result, the impact of changes in the metabolism (e.g., due to a genetic modification) might remain unclear or even unrevealed. In contrast, pH-controlled conditions can be achieved in bioreactors. Here, we present a self-built, comparatively cheap, and user-friendly multiple-bioreactor system (MBS) consisting of six pH-controlled bioreactors at a 1-L scale. We tested the functionality of the MBS by cultivating the acetogen *Clostridium ljungdahlii* with CO_2 and H_2 at steady-state conditions (=chemostat). The experiments (total of 10 bioreactors) were addressing the two questions: (1) does the MBS provide replicable data for gas-fermentation experiments?; and (2) does feeding nitrate influence the product spectrum under controlled pH conditions with CO_2 and H_2? We applied four different periods in each experiment ranging from pH 6.0 to pH 4.5. On the one hand, our data showed high reproducibility for gas-fermentation experiments with *C. ljungdahlii* under standard cultivation conditions using the MBS. On the other hand, feeding nitrate as sole N-source improved growth by up to 62% and ethanol production by 2–3-fold. However, we observed differences in growth, and acetate and ethanol production rates between all nitrate bioreactors. We explained the different performances with a pH-buffering effect that resulted from the interplay between undissociated acetic acid production and ammonium production and because of stochastic inhibition events, which led to complete crashes at different operating times.

Keywords: gas fermentation, *Clostridium ljungdahlii*, acetogenic bacteria, bioreactor system, pH-regulation, nitrate

OPEN ACCESS

Edited by:
Hari S. Misra, Bhabha Atomic Research Centre (BARC), India

Reviewed by:
Denys Kristalia Villa Gomez, The University of Queensland, Australia
Baris Çalli, Marmara University, Turkey

***Correspondence:**
Largus T. Angenent
l.angenent@uni-tuebingen.de

Specialty section:
This article was submitted to Microbial Physiology and Metabolism, a section of the journal Frontiers in Microbiology

Received: *15 December 2019*
Accepted: *27 March 2020*
Published: *06 May 2020*

Citation:
Klask C-M, Kliem-Kuster N, Molitor B and Angenent LT (2020) Nitrate Feed Improves Growth and Ethanol Production of Clostridium ljungdahlii With CO_2 and H_2, but Results in Stochastic Inhibition Events. Front. Microbiol. 11:724. doi: 10.3389/fmicb.2020.00724

INTRODUCTION

An increasing world population will likely lead to growing energy demands. To meet these demands in a sustainable way, we need to rethink the *status quo* of a fossil-based economy and transition into a renewable-based and circular economy. Furthermore, we have to mitigate the apparent climate effects of anthropogenic greenhouse gas emissions, such as carbon dioxide (CO_2),

which are caused preliminary by industry, agriculture, and transportation. Biotechnology offers potential to contribute to climate-friendly and economically feasible solutions. One promising solution is synthesis gas (syngas) fermentation with microbes (Mohammadi et al., 2011). For syngas fermentation, mixtures of the gases CO_2, hydrogen (H_2), and carbon monoxide (CO) are converted into products, such as acetate and ethanol, by acetogenic bacteria (Dürre, 2017). This process provides a promising way to produce chemicals and biofuels with a reduced CO_2-footprint (Latif et al., 2014; Molitor et al., 2017; Phillips et al., 2017).

In recent years, the company LanzaTech (Skokie, IL, United States) demonstrated that ethanol production from syngas with the acetogen *Clostridium autoethanogenum* is possible at commercial scale, which further indicates the potential of this platform. While the LanzaTech technology is based on proprietary strains of *C. autoethanogenum*, in academic research the most frequently studied acetogen is the closely related microbe *Clostridium ljungdahlii*. Both microbes produce acetic acid, ethanol, and some 2,3-butanediol from gaseous substrates (Tanner et al., 1993; Abrini et al., 1994; Köpke et al., 2010; Brown et al., 2014).

Different strategies are employed to optimize *C. autoethanogenum* and *C. ljungdahlii* for biotechnology. On the one hand, genetic engineering is used to generate modified strains that produce butyrate (Köpke et al., 2010), butanol (Köpke and Liew, 2012; Ueki et al., 2014), acetone, and isopropanol (Bengelsdorf et al., 2016; Köpke et al., 2016). In academic research, the physiological characterization of these genetically engineered strains is typically performed in batch experiments with serum bottles, which does not allow to control important process parameters such as the pH-value. On the other hand, bioprocess engineering is used to investigate and optimize the production of naturally occurring products, such as ethanol, in optimized bioreactor systems (Younesi et al., 2005; Mohammadi et al., 2012; Richter et al., 2013; Abubackar et al., 2015). While the impact of cultivation parameters can be investigated within one study, these studies often are difficult to compare with each other, because very different bioreactor architectures and process parameters are used (Asimakopoulos et al., 2018). Furthermore, because of the complexity, these setups are not suitable to perform preliminary experiments with genetically engineered strains. These issues can be partly overcome by utilizing commercially available bioreactor (chemostat) systems. However, these systems are costly, and therefore often not available to laboratories that do not focus on bioprocess engineering. Consequently, genetically engineered strains are typically not studied in fermentations beyond the serum bottle size, which leaves a gap between the construction of these strains and the investigation under controlled fermentation conditions.

To close this gap, we developed a cost-efficient, multiple-bioreactor system (MBS) that can be built from off-the-shelf components for a considerably smaller investment compared to the cost of commercial bioreactor systems. We give all information on purchasing the required parts, the assembly of the MBS, the process control elements (e.g., stirring, pH, temperature), and further improvement ideas. We tested our MBS with *C. ljungdahlii* and CO_2 and H_2 as substrate under controlled pH conditions by addressing the two questions: (1) does the MBS provide replicable data for gas-fermentation experiments?; and (2) does feeding nitrate influence the product spectrum under controlled pH conditions with CO_2 and H_2? In a recent study, nitrate was used as an alternative electron acceptor for *C. ljungdahlii*, while it also served as sole nitrogen source (N-source) in batch cultivations (Emerson et al., 2019). To our knowledge, this was the first study which investigated nitrate reduction by any known acetogen in detail. The co-utilization of CO_2 and nitrate enhanced the autotrophic biomass formation with CO_2 and H_2 compared to standard cultivation conditions with ammonium as the sole N-source. Contrarily, ethanol production was strongly reduced under nitrate conditions with CO_2 and H_2. The authors discussed that nitrate reduction consumes electrons, which would be no longer available for the reduction of acetate into ethanol. At the same time, nitrate reduction led to an accumulation of ammonium. This resulted in a continuous increase of the pH from 6.0 to 8.0 during the batch cultivations in serum bottles (Emerson et al., 2019), which would intrinsically prevent ethanol production, because ethanol production is most likely triggered by a low pH (Mock et al., 2015; Richter et al., 2016). It is well-known that growth of acetogens, such as *C. ljungdahlii*, is highly dependent on the pH (Drake et al., 2008). Since their main fermentation product is acetate, which acts (in the form of the undissociated acetic acid) as a weak acid, a missing pH control, such as in serum bottles, intrinsically lowers the pH of the medium during growth. In contrast, the pH can be controlled in bioreactors such as in our MBS.

MATERIALS AND METHODS

Microbial Strains and Medium Composition

Wild type *C. ljungdahlii* PETC (DSM 13528) was obtained from the DSMZ (Braunschweig, Germany). Generally, pre-cultures were grown heterotrophically at 37°C (IN260 stand incubator, Memmert, Germany) in 100 mL serum bottles with 50 mL of standard PETC medium containing (per liter): 0.5 g yeast extract; 1.0 g NH_4Cl; 0.1 g KCl; 0.2 g $MgSO_4 \cdot 7\ H_2O$; 0.8 g NaCl; 0.1 g KH_2PO_4; 0.02 g $CaCl_2 \cdot 2\ H_2O$; 4 mL resazurin-solution (0.025 vol%); 10 ml trace element solution (TE, 100×); 10 mL Wolfe's vitamin solution (100×); 10 mL reducing agent (100×); and 20 mL of fructose/2-(*N*-morpholino)ethanesulfonic acid (MES) solution (50×). Vitamins, reducing agent, and fructose/MES solution were added after autoclaving under sterile conditions. TE was prepared as 100x stock solution containing (per liter): 2 g nitrilotriacetic acid (NTA); 1 g $MnSO_4 \cdot H_2O$; 0.8 g $Fe(SO_4)_2(NH_4Cl)_2 \cdot 6\ H_2O$; 0.2 g $CoCl_2 \cdot 6\ H_2O$; 0.0002 g $ZnSO_4 \cdot 7\ H_2O$; 0.2 g $CuCl_2 \cdot 2\ H_2O$; 0.02 g $NiCl_2 \cdot 6\ H_2O$; 0.02 g $Na_2MoO_4 \cdot 2\ H_2O$; 0.02 g Na_2SeO_4; and 0.02 g Na_2WO_4. The pH of the TE was adjusted to 6.0 after adding NTA. The solution was autoclaved and stored at 4°C. Wolfe's vitamin

solution was prepared aerobically containing (per liter): 2 mg biotin; 2 mg folic acid; 10 mg pyridoxine-hydrochloride; 5 mg thiamin-HCl; 5 mg riboflavin; 5 mg nicotinic acid; 5 mg calcium pantothenate; 5 mg *p*-aminobenzoic acid; 5 mg lipoic acid; and 0.1 mg cobalamin. The vitamin solution was sterilized using a sterile filter (0.2 μm), sparged with N_2 through a sterile filter, and stored at 4°C. The 50x fructose/MES solution contained (per 100 mL): 25 g fructose; and 10 g MES. The pH was adjusted to 6.0 by adding KOH. The solution was sterilized, sparged with N_2 through a sterile filter, and stored at room temperature. The reducing agent was prepared under 100% N_2 in a glove box (UniLab Pro Eco, MBraun, Germany) and contained (per 100 mL): 0.9 g NaOH; 4 g cysteine-HCl; and 2.17 g/L Na_2S (60 weight%). Anaerobic water was used for the preparation of the reducing agent. The reducing agent was autoclaved and stored at 4°C.

For all bioreactor experiments, the standard PETC medium for the initial batch phase was supplemented with 0.5 g L^{-1} yeast extract and autoclaved inside the bioreactor vessel with an open off-gas line to enable pressure balance. The autoclaved bioreactors were slowly cooled down at room temperature overnight with an attached sterile filter at the off-gas line. After transferring each bioreactor to the MBS frame, the medium was continuously sparged with a sterile gas mixture of CO_2 and H_2 (20:80 vol%). After 1 h, vitamins and reducing agent were added through the sampling port. N_2 gas was applied through a sterile filter to flush the sampling port after each addition of media components. Subsequently, each bioreactor was inoculated with 5 mL of an exponential heterotrophically grown PETC culture (OD_{600} 0.5–0.8). All feed bottles for continuous mode containing 4 L of PETC medium with additions, as described below, were autoclaved and stored overnight with an attached sterile filter on the off-gas line. The bottles were sparged with N_2 for 2 h through a sterile filter. Vitamins and reducing agents were added under sterile conditions. A gas bag with N_2 gas was attached with a sterile filter to balance the pressure in the feed bottle during the bioreactor run. Standard PETC medium for continuous mode did not contain yeast extract and was adjusted to the respective pH of the period. One feed bottle was simultaneously used to provide medium for three bioreactors of the same triplicate. For all nitrate experiments we replaced NH_4Cl, with the equivalent amount of nitrogen as $NaNO_3$ (18.7 mM) in the feed medium.

Bioreactor Setup and Standard Operating Conditions

Six 1 L self-built bioreactors (**Figure 1**, **Supplementary Data Sheet S1**, **Supplementary Figures S1–S3**, **Supplementary Results S1**, and **Supplementary Table S1** in **Supplementary Data Sheet S2**) with a working volume of 0.5 L (1-L double walled jacketed GLS 80 bottle, Duran, Germany) were operated simultaneously for two experimental bioreactor runs, while four of these bioreactors were operated simultaneously for two additional experimental bioreactor runs, with a total of 10 bioreactors (**Figures 2–5**). The cultivation temperature was 37°C and the agitation was set to 300 rpm. The gas flow rate was adjusted to 30 mL min^{-1} *prior* to inoculation. To establish microbial growth in the MBS after one inoculation event for each bioreactor, we operated the MBS in batch mode for 3–4 days before switching to continuous mode. The pH was set to 6.0 during the batch mode and the first 6 days (Period I) in continuous mode. Subsequently, the pH setting was lowered stepwise in 6 days to a pH of 5.5, 5.0, and 4.5 (Period II-IV). The pH of the feed medium was adjusted to the anticipated pH of each period. In our preliminary experiment (bioreactor 1/2/3) and the first nitrate experiment (bioreactor 4/5/6) (**Figures 2**, **3**), we did not use the acid feed to actively adjust the pH within the bioreactor. Instead, we let the pH decrease to the set value by the microbial production of undissociated acetic acid to avoid a pH shock. This took approximately one to 2 days of each 6-day period. For the preliminary experiment and the first nitrate experiment we chose a medium feed rate of 0.10 mL min^{-1}, which resulted in a 3.5-day hydraulic retention time (HRT), and which represents 1.7 HRT periods within each period of 6 days. In our second and third nitrate experiment, the medium feed rate was 0.19 mL min^{-1}. This was equal to a 2-day HRT and resulted in 3.2 HRT periods within each pH period. We only used base feed to maintain the pH in the second nitrate experiment (bioreactor 7 and 8) (**Figure 4**), while base and acid feed was actively applied for the third nitrate experiment (bioreactor 9 and 10) (**Figure 5**) to immediately adjust the pH of the bioreactor to the anticipated pH-value of each period. We used 2 M KOH and 2 M HCl in our experiments.

Sampling and Analyses

Bioreactors were sampled once or twice per day. A pre-sample of 3 mL of cell suspension was discarded, before taking a 2 mL sample (main sample) during batch mode. For sampling in continuous mode, the multi-channel pump (Masterflex L/S pump equipped with a Multichannel Cartridge Pump Head and twelve catridges, Cole Parmer, Germany) was switched off during the sampling procedure. Cell growth was monitored by measuring the optical density at 600 nm (OD_{600}) (Nanophotometer NP80, Implen, Germany). For OD_{600}-values larger than 0.5, dilutions with 100 mM phosphate-buffered saline (PBS) at pH 7.4 were prepared. Nitrate and nitrite concentrations were qualitatively monitored using test stripes (Quantofix nitrate/nitrite, Macherey-Nagel, Germany). A correlation between cellular dry weight (CDW) and OD_{600} was calculated by harvesting 50 mL of culture sample from every bioreactor, centrifugation of the samples at 3428 relative centrifugal force (rcf) (Eppendorf centrifuge 5920R) for 12 min at room temperature (RT) and, subsequently, drying the pellet at 65°C for 3 days. The CDW for an OD_{600} of 1 was determined to be 0.24 g L^{-1} for cultures grown in PETC medium with ammonium and 0.29 g L^{-1} for cultures grown in PETC medium with nitrate as sole nitrogen source, respectively.

Acetate and ethanol concentrations were analyzed *via* a high-pressure liquid chromatography (HPLC) (LC20, Shimadzu, Japan) system that was equipped with an Aminex HPX-87H

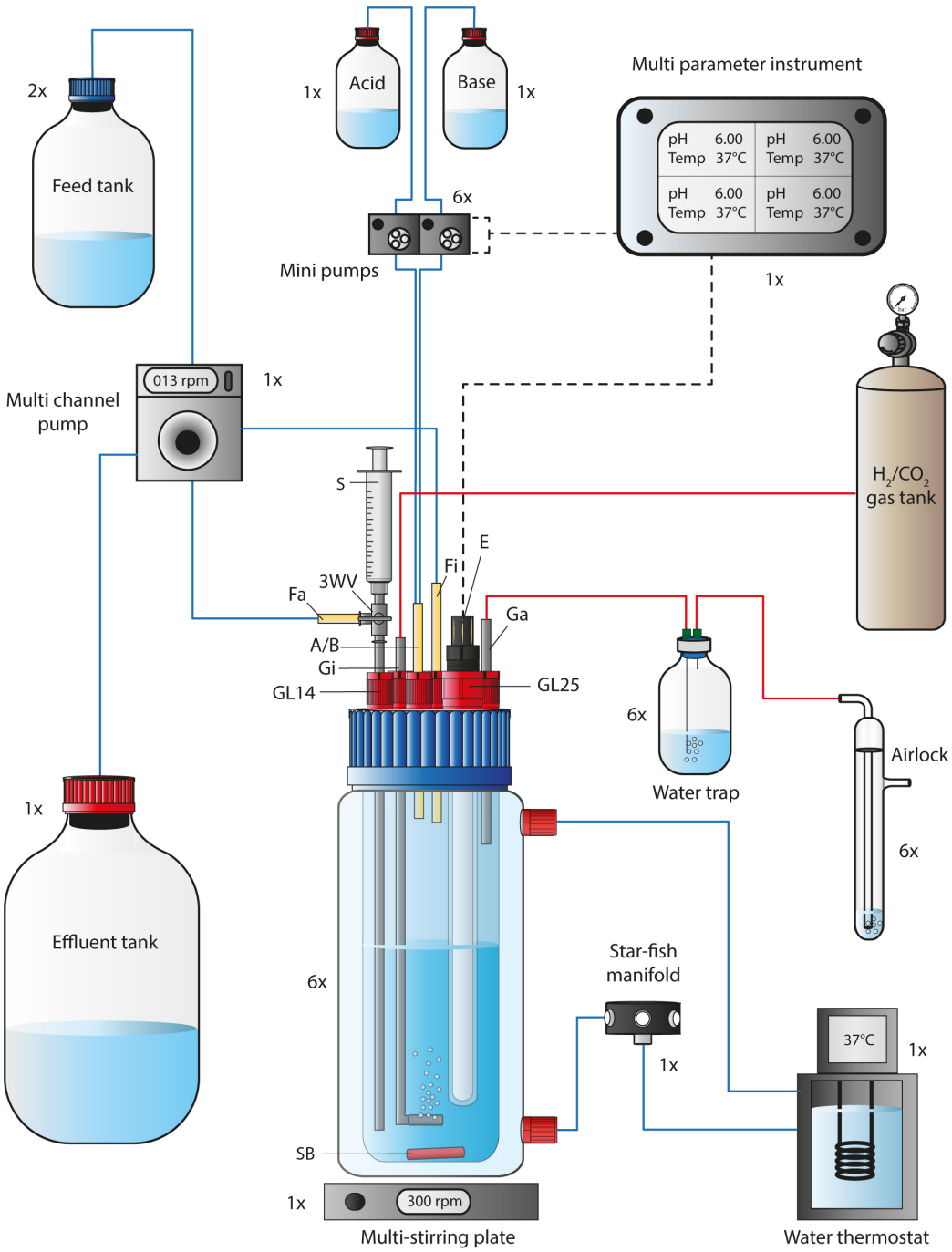

FIGURE 1 | Flow chart of a single bioreactor operated in the MBS. The 1-L bioreactor vessel consisted of a double-walled glass vessel and a customized lid, while it was placed on a multi-stirring plate with up to six bioreactors. The bioreactor temperature was maintained through a water circulation unit at 37°C. The autoclavable lid offered connections for 5x GL14 and 1x GL25. A set of stainless-steel tubing was used for the gas-in/-out lines and for the medium feed-out line. The three-way valve at the medium feed-out line was required for sampling using a 5-mL syringe. The pH and bioreactor medium temperature was tracked *via* a pH/pt1000-electrode that was connected to a multi-parameter instrument. The multi-parameter instrument controlled and triggered two mini pumps (for base and acid) at programmable conditions. For continuous mode, the feed medium to each bioreactor was pumped *via* a single multi-channel pump from the feed tank into the bioreactor. The same pump was used to transfer the effluent from each bioreactor into the effluent tank. Sterile CO_2 and H_2 gas (20:80 vol-%) was sparged into the system through stainless-steel tubing with an attached sparger. The gas-out line was connected to a 100-mL serum bottle to serve as a water trap before the outgoing gas passed an airlock. The 1×, 2×, and 6× next to each unit in the figure describe the quantity, which is required to operate six bioreactors simultaneously. A/B, Acid and/or base feed line; E, pH/pt1000 electrode; Fa, medium feed-out line; Fi, medium feed-in line; Ga, gas-out line; Gi, gas-in line; GL14, screw joint connection size 14; GL25, screw joint connection size 25; rpm, revolutions per minute; SB, stirring bar; 3WV, three-way valve. Blue lines indicate liquid transfer, red lines contain gas, and dotted black lines provide electric power or signals.

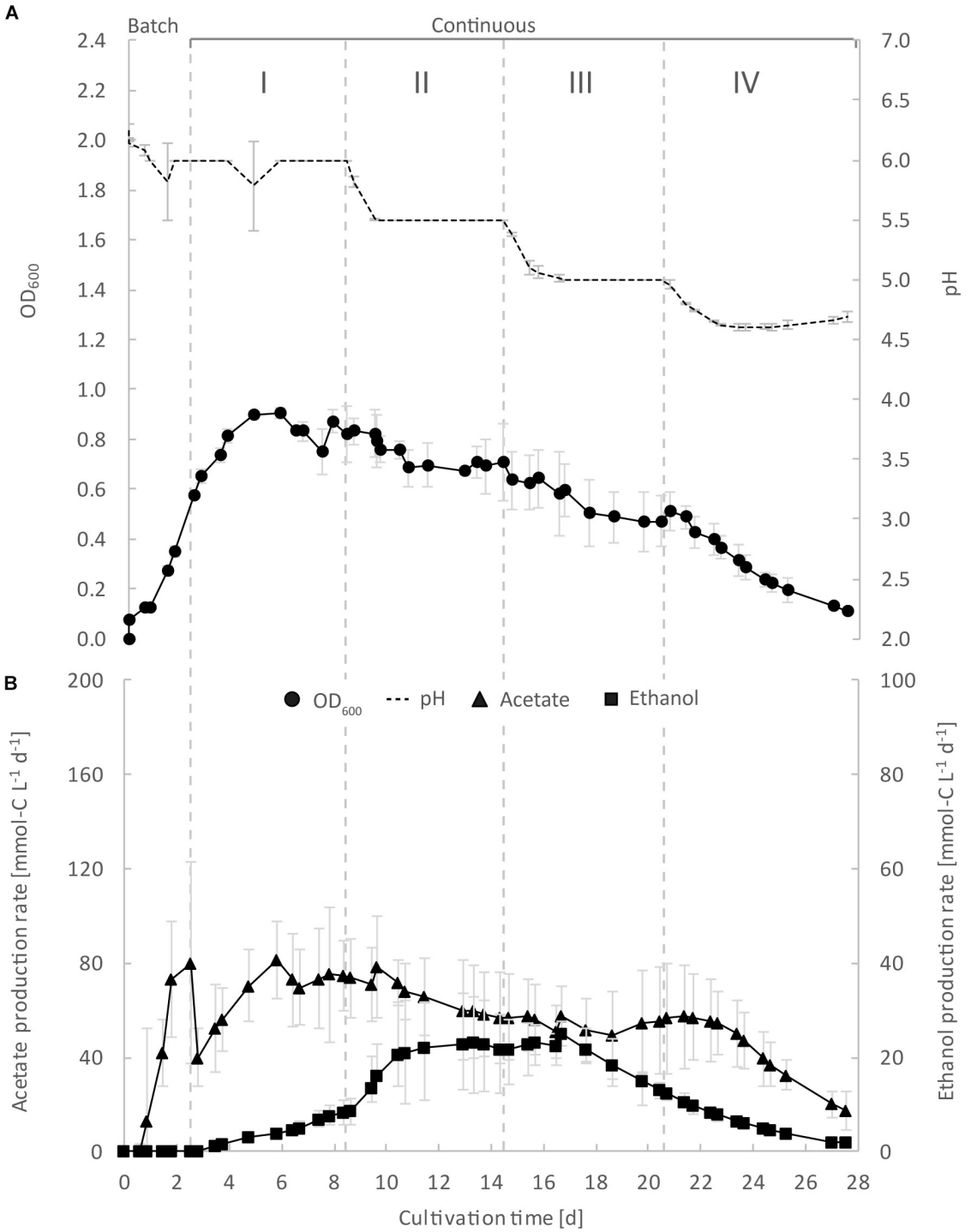

FIGURE 2 | Continuous gas fermentation of *C. ljungdahlii* with CO_2 and H_2 in standard PETC medium at different periods in a priliminary experiment (bioreactor 1/2/3). Mean values of triplicates with standard deviation (n = 3) for pH and OD_{600} **(A)**, and for acetate and ethanol production rates in mmol-C L^{-1} d^{-1} **(B)**. Standard PETC medium containing 18.7 mM ammonium chloride as sole N-source was used. The horizontal dotted lines indicate the continuous process in which medium of different pH was fed to each bioreactor. Period: I, pH = 6.0; II, pH = 5.5, III, pH = 5.0; and IV, pH = 4.5.

column and operated with 5 mM sulfuric acid as eluent. The flow was 0.6 mL min^{-1} (LC-20AD). The oven temperature was 65°C (CTO-20AC). The sample rack of the HPLC was constantly cooled to 15°C in the autosampler unit (SIL-20AC_{HT}). For HPLC sample preparation, all culture samples were centrifuged for 3 min at 15871 rcf (Centrifuge 5424, Eppendorf, Germany) in

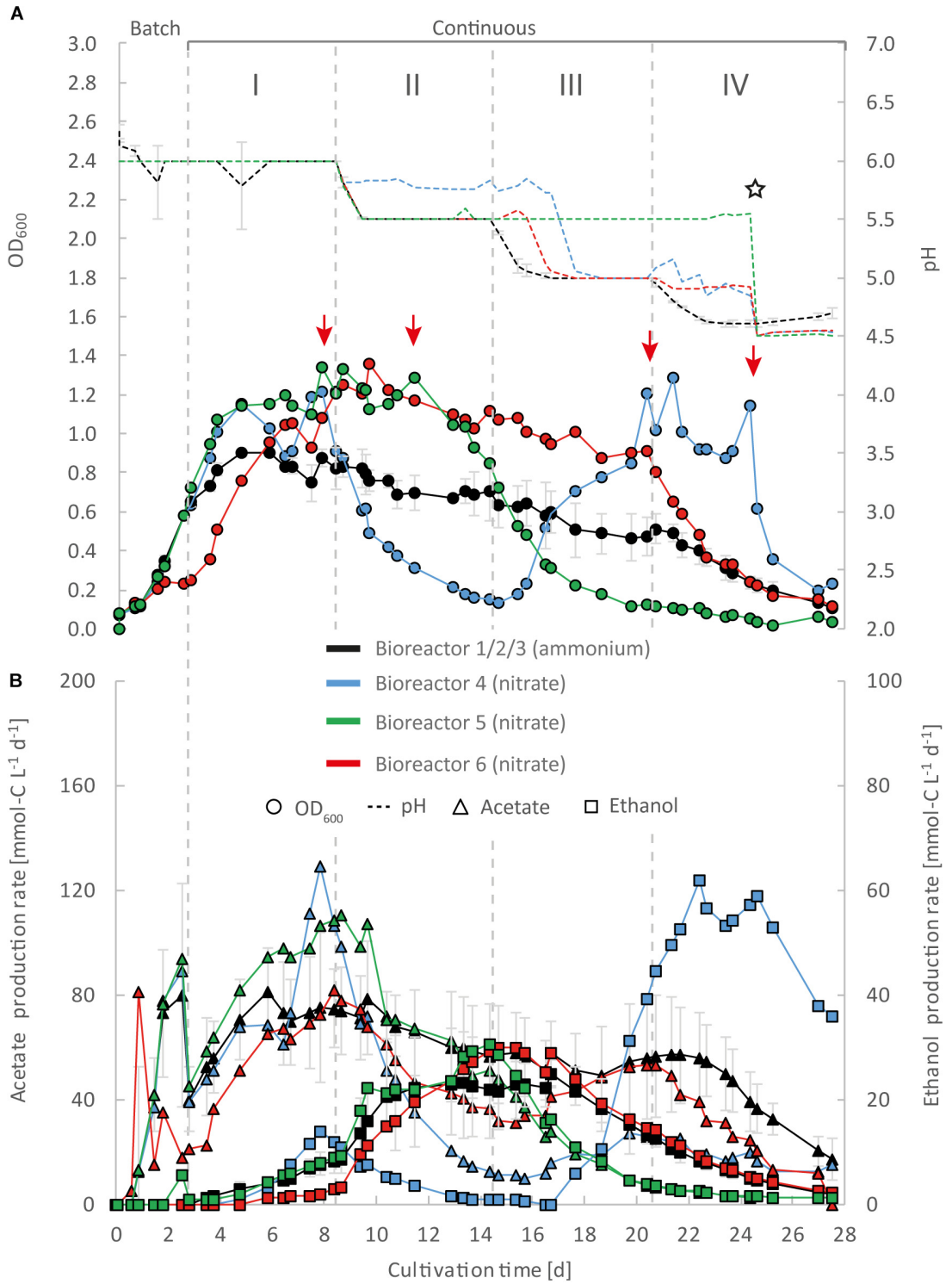

FIGURE 3 | Impact of nitrate as an alternative N-source on continuous gas fermentation of *C. ljungdahlii* using CO_2 and H_2 at different periods with a medium feed rate of 0.10 mL min^{-1} (experiment 1). Single values for pH and OD_{600} **(A)**, and for acetate and ethanol production rates in mmol-C L^{-1} d^{-1} **(B)**. The bioreactors with nitrate feed were grown in ammonium-free PETC medium supplemented with 18.7 mM Na-nitrate. The horizontal dotted lines indicate the continuous process in which medium of different pH was fed to each bioreactor. The red arrows indicate the crash in OD_{600} of each bioreactor with nitrate feed at different time points. The star symbol describes the time point were the pH was lowered manually by adding HCl to the system until a pH of 4.5 was reached. Period: I, pH = 6.0; II, pH = 5.5, III, pH = 5.0; and IV, pH = 4.5.

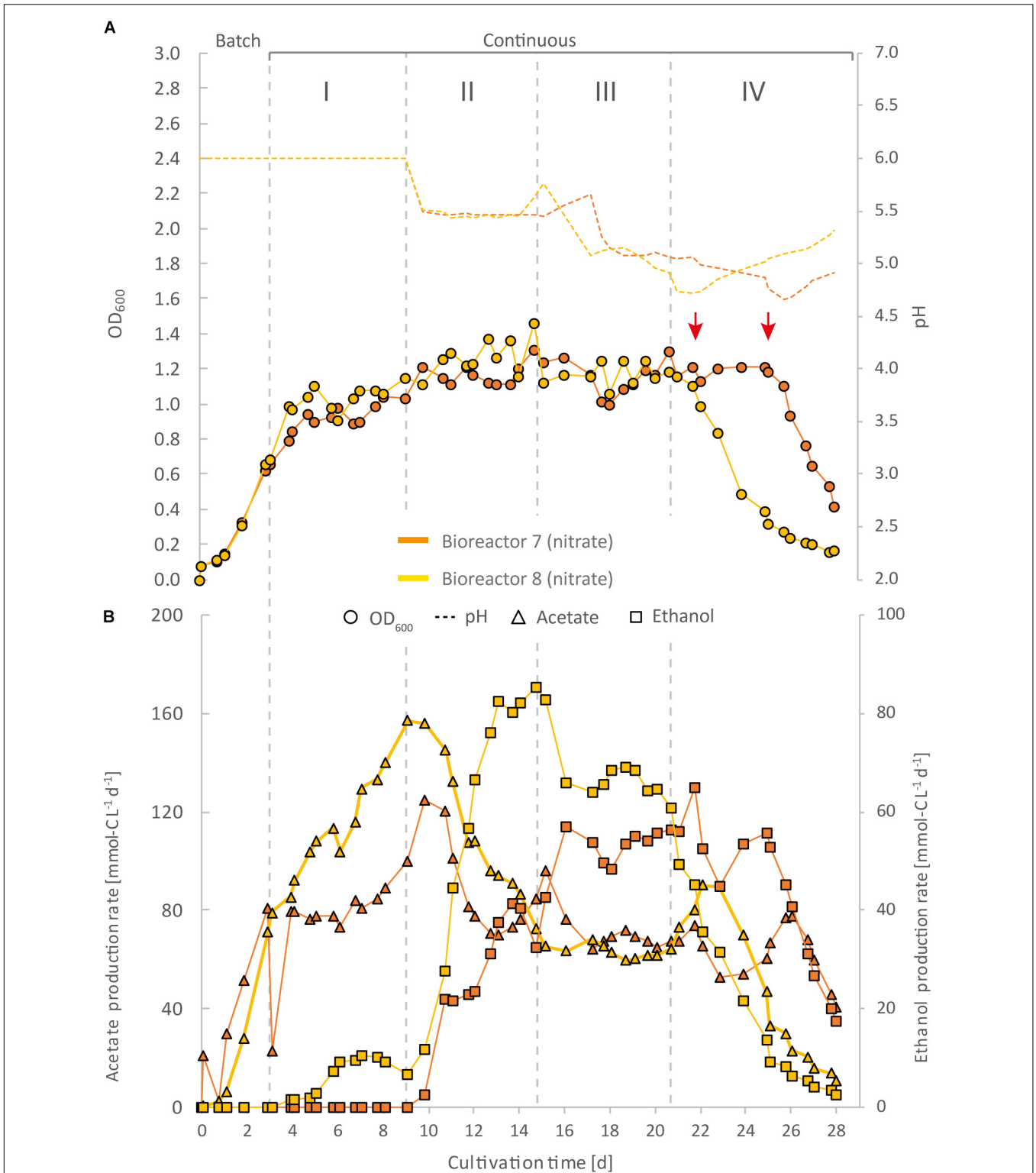

FIGURE 4 | Impact of nitrate as an alternative N-source on continuous gas fermentation of *C. ljungdahlii* using CO_2 and H_2 at different periods with a medium feed rate of 0.19 mL min^{-1} (experiment 2). Single values for pH and OD_{600} **(A)**, and for acetate and ethanol production rates in mmol-C L^{-1} d^{-1} **(B)**. The bioreactors were grown in ammonium-free PETC medium supplemented with 18.7 mM Na-nitrate. The horizontal dotted lines indicate the continuous process in which medium of different pH was fed to each bioreactor. The red arrows indicate the crash in OD_{600} of each bioreactor at different time points. Period: I, pH = 6.0; II, pH = 5.5, III, pH = 5.0; and IV, pH = 4.5.

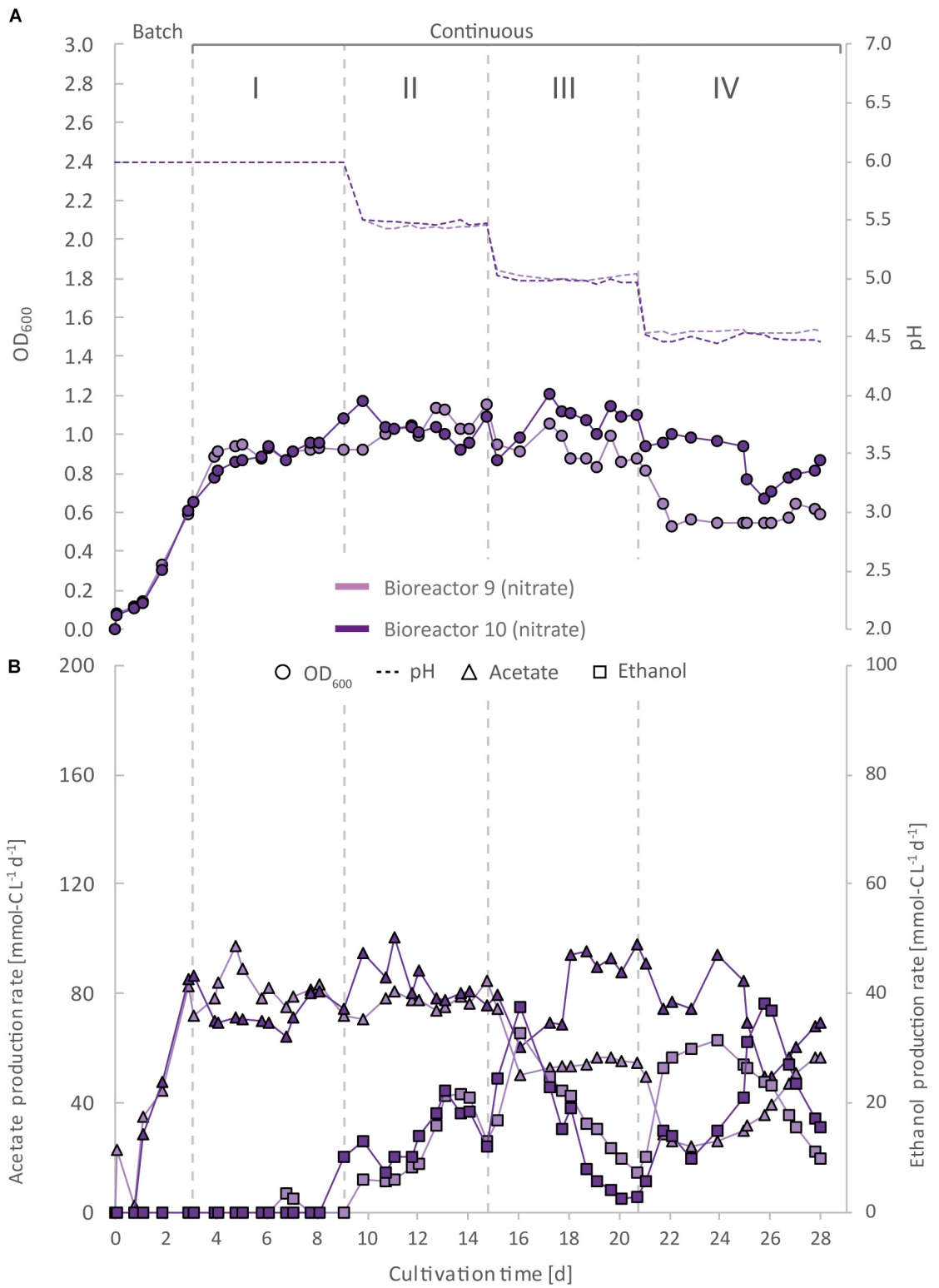

FIGURE 5 | Impact of nitrate as an alternative N-source on continuous gas fermentation of *C. ljungdahlii* using CO_2 and H_2 at different periods with a medium feed rate of 0.19 mL min^{-1} (experiment 3). Single values for pH and OD_{600} **(A)**, and for acetate and ethanol production rates in mmol-C L^{-1} d^{-1} **(B)**. The bioreactors were grown in ammonium-free PETC medium supplemented with 18.7 mM Na-nitrate. The horizontal dotted lines indicate the continuous process in which medium of different pH was fed to each bioreactor. Period: I, pH = 6.0; II, pH = 5.5, III, pH = 5.0; and IV, pH = 4.5.

1.5 mL reaction tubes. 750 µl of the supernatant was transferred into clean reaction tubes and stored at −20°C until use. Frozen samples were thawed at 30°C and 250 revolutions per minute (rpm) for 10 min (Thermomixer C, Eppendorf, Germany). The samples were centrifuged again and 500 µl of the supernatant was transferred into short thread HPLC/GC vials (glass vial ND9, VWR, Germany) and sealed with short screw caps, which contained rubber septa (6 mm for ND9, VWR, Germany). New standards for acetate and ethanol were prepared for every analysis. All HPLC samples were randomized.

RESULTS

Operating the MBS for Replicable Gas Fermentation Experiments

We based our experiments in this study on a versatile self-built multiple-bioreactor system (MBS). The MBS (**Figure 1**, **Supplementary Data Sheet S1**, **Supplementary Figures S1–S3**, **Supplementary Table S1**, and **Supplementary Results S1** in **Supplementary Data Sheet S2**) was designed to either perform heterotrophic or autotrophic cultivation experiments in batch or continuous mode. The MBS can be used to operate up to six bioreactors simultaneously, each individually at different pH conditions or, if necessary, with different feed medium. The MBS platform might be especially interesting for cost-effective research in academia.

To show high comparability and reproducibility of our MBS, as a preliminary experiment (control), we grew *C. ljungdahlii* simultaneously as triplicates in standard PETC medium with CO_2 and H_2 (ammonium, bioreactors 1/2/3) (**Figure 2** and **Supplementary Figure S4** in **Supplementary Data Sheet S2**). We observed that growth was similar in the triplicate bioreactors during the cultivation of 27.5 days. During the initial batch mode, the average OD_{600} increased to 0.58 ± 0.01 (**Figure 2A**). After switching to continuous mode, the average OD_{600} increased further to values of 0.82 ± 0.04 during Period I. For Periods II, III, and IV, the average OD_{600} for the bioreactors constantly decreased to values of 0.69 ± 0.01, 0.51 ± 0.05, and 0.18 ± 0.06 (**Figure 2A** and **Table 1**). As expected, the pH of each bioreactor was decreasing during all periods by microbial acetate production. The simultaneous and constant decrease of OD_{600} indicated reduced growth rates of *C. ljungdahlii* at a lower pH level in our system. In batch mode, the acetate production rates increased with increasing OD_{600}, but then considerably dropped after switching to continuous mode (**Figure 2A**). The acetate production rates increased again to the highest measured average value of 73.1 ± 2.1 mmol-C L^{-1} d^{-1} for Period I (**Figure 2B**). The acetate production rates decreased to average values of 60.1 ± 3.4 mmol-C L^{-1} d^{-1}, and 53.7 ± 3.3 mmol-C L^{-1} d^{-1} for Periods II and III, respectively. For Period IV, the acetate production rate had only an average value of 29.2 ± 10.0 mmol-C L^{-1} d^{-1} (**Figure 2B**). Ethanol production rates were negligible during batch mode, but slowly increased after switching to continuous mode. The highest ethanol production rates were observed for Period II with average values of 22.5 ± 0.5 mmol-C L^{-1} d^{-1}. During the Periods III and IV, the ethanol production rates kept decreasing to average values of 18.7 ± 4.8 mmol-C L^{-1} d^{-1} and 3.4 ± 1.4 mmol-C L^{-1} d^{-1}, respectively (**Figure 2B**). The results of our preliminary experiment showed high reproducibility with small standard deviations for all tested parameters using the MBS, which creates an environment to investigate the impact of different cultivation parameters simultaneously in a single system providing statistically relevant fermentation data.

TABLE 1 | Average values for OD_{600} and acetate/ethanol production rates during the continuous fermentation of *C. ljungdahlii* with CO_2 and H_2 at four different pH conditions in standard PETC medium using the MBS (priliminary experiment, control).

Operating conditions	OD_{600}[1]	Acetate production rate [mmol-C L^{-1} d^{-1}][1]	Ethanol production rate [mmol-C L^{-1} d^{-1}][1]	$Ratio_{Et/Ac}$[2]
Period I (pH 6.0)	0.82 ± 0.04	73.1 ± 2.1	6.4 ± 1.6	0.1
Period II (pH 5.5)	0.69 ± 0.01	60.1 ± 3.4	22.5 ± 0.5	0.4
Period III (pH 5.0)	0.51 ± 0.05	53.7 ± 3.3	18.7 ± 4.8	0.3
Period IV (pH 4.5)	0.18 ± 0.06	29.2 ± 10.0	3.4 ± 1.4	0.1

[1]*Values for the bioreactors with ammonium feed (n = 3) are given as the average (±standard deviation) from three bioreactors for the last 5 data points of every period.* [2]*Et, Ethanol; Ac, Acetate.*

Feeding Nitrate to *C. ljungdahlii* in Continuous Operating Bioreactors With H_2 and CO_2

For three main experiments with operating periods of 27.5 days (experiment 1), and 28 days (experiments 2 and 3), we investigated the impact of nitrate as an alternative N-source on growth and the production of ethanol from CO_2 and H_2 (**Figures 3–5**). For these experiments, the bioreactors (experiment 1, bioreactor 4/5/6; experiment 2, bioreactor 7/8; experiment 3, bioreactor 9/10) were fed with PETC medium containing nitrate instead of ammonium at an equivalent molar amount of nitrogen (=18.7 mM). We found an increasing pH due to ammonium production in preliminary bottle experiments in nitrate-containing PETC medium (**Supplementary Figure S5** in **Supplementary Data Sheet S2**). A pH increase was also observed in the nitrate bottle experiments of Emerson et al. (2019). Despite the pH-control in our experiments, all bioreactors with nitrate feed showed remarkable differences in growth, pH, acetate production, and ethanol production rates. Therefore, we report individual data for each bioreactor and highlight lowest and highest values (**Tables 2**, **3**). We use the data of the preliminary experiment (ammonium, bioreactor 1/2/3) as the control in which ammonium served as the sole N-source (**Figure 3**). Unexpectedly, we observed a pH-buffering effect for experiment 1 (bioreactor 4/5/6) and experiment 2 (bioreactor 7/8) with nitrate feed during the fermentation (**Figures 3A**, **4A**). This was most likely due to an interplay between the produced acetate and ammonium by the microbes. Overall, the

pH was slowly decreasing in these bioreactors with nitrate feed (**Figures 3–5**), and we did not measure increasing pH values. To study this effect further, we actively reduced the pH in every pH period to the anticipated pH-value by feeding acid for experiment 3 (bioreactor 9/10).

During the initial batch mode of all performed bioreactor experiments, growth was similar in each bioreactor and reached highest OD_{600}-values between 0.5 and 0.7 after 2–3 days (**Figures 2A–5A**). In the first nitrate experiment, bioreactor 6 stagnated after 2 days of cultivation in batch with an OD_{600} of 0.23 (**Figure 3A**). However, after switching to continuous mode, all three nitrate bioreactors of experiment 1 (bioreactor 4/5/6) reached similar OD_{600}-values of ∼1.2 during the end of Period I, which were 48% higher compared to the mean OD_{600}-value of the control bioreactors with ammonium feed and the same medium feed rate during Period I (**Figures 2A**, **3A** and **Table 1**). The highest observed OD_{600} was 1.29 on day 21 during Period IV for bioreactor 4, 1.36 on day 10 during Period II for bioreactor 5, and 1.34 on day 8 during Period I for bioreactor 6 (**Figure 3** and **Table 2**). In comparison, the bioreactors with ammonium feed had the highest average OD_{600}-value of 0.90 ± 0.02 on day 4 for Period I (**Figure 2** and **Table 1**). The increase of biomass was also observed in our second and third nitrate experiment (**Figures 4A**, **5A** and **Table 3**). When applying higher medium feed rates in these experiments, the highest OD_{600}-values were increased by 29–62% compared to the ammonium bioreactors (**Figures 4A**, **5A** and **Tables 2**, **3**). This indicated that the increased dilution rate did not exceed the growth rate of the microbes under our conditions. The highest OD_{600}-values for the bioreactors of experiments 2 and 3 were 1.31 for bioreactor 7 on day 15 during Period II, 1.46 for bioreactor 8 on day 15 during Period II, 1.16 for bioreactor 9 on day 15 during Period II, and 1.21 for bioreactor 10 on day 17 during Period III.

A noticeable difference was that the OD_{600}-values were unstable for all bioreactors with nitrate feed (**Figures 3A–5A**). Each nitrate bioreactor showed fluctuating OD_{600}-values of ±0.1 to ±0.3 during the experiment. This effect was not observed for the control bioreactors with ammonium feed, which showed continuously decreasing OD_{600}-values (**Figure 2A**). However, the fluctuating growth of the nitrate bioreactors was interrupted, when crash events occurred at different time points during the first and second nitrate experiment (**Figures 3A**, **4A**, red arrow). We observed these crash events in OD_{600} for bioreactor 4 on day 8 during Period I and again on day 24 during Period IV, for bioreactor 5 on day 20 during Period III, and for bioreactor 6 on day 11 at the end of Period III. The second crash event of bioreactor 4 was observed after a previous phase of recovery during Period III in which the cells grew again to an OD_{600} of 1.2 on day 20 (**Figure 3A**). The recovery of growth was only observed for bioreactor 4. Crash events also occurred at the higher medium feed rates in our second nitrate experiment, but at later time points of the cultivation (**Figure 4A**). Bioreactor 7 underwent a crash event on day 26 during Period IV, while bioreactor 8 crashed on day 21 during Period IV. It is noteworthy, that we detected nitrate and nitrite in culture samples of all nitrate bioreactors undergoing a crash event, while neither nitrate nor nitrite were detectable in actively growing or recovering bioreactors with nitrate feed (see **Supplementary Data Sheet S3**). This indicates a high uptake rate for nitrate by the microbes from the feed medium, and an immediate conversion of the nitrate to ammonium *via* nitrite as an intermediate. During our third nitrate experiment (bioreactor 9 and 10) (**Figure 5**), we neither observed crash events nor the accumulation of nitrate or nitrite in any culture sample. Nevertheless, both bioreactors 9 and 10 showed a short duration of decreasing OD_{600}-values during Period IV, but their growth remained stable afterward. Despite the occurrence of crash events, we found that all nitrate bioreactors showed high OD_{600}-values even at lower pH (Period II-IV (**Figures 3A–5A** and **Tables 2**, **3**). In contrast, the control bioreactors, growing with ammonium feed, showed high OD_{600}-values only at pH 6.0, while the OD_{600} kept constantly decreasing at lower pH (**Figure 2A**, **Supplementary Figure S4** in **Supplementary Data Sheet S2**, and **Table 1**).

The acetate production rates of all bioreactors with nitrate feed somewhat followed the OD_{600} profile, and reached the highest values that we observed in all our experiments with a maximum value of 139 mmol-C L^{-1} d^{-1} for bioreactor 8 of experiment 2 during Period II (**Figure 4B** and **Table 3**). Overall, the acetate production rates were more stable during experiment 3, when the pH was actively decreased with an acid feed (**Figure 5B**). The acetate production rate considerably decreased at the time point of the OD_{600} crashes for the three bioreactors for experiment 1 and the two bioreactors for experiment 2 (**Figures 3B**, **4B**).

Ethanol production rates were negligible during batch mode for all bioreactors with nitrate feed, and increased with decreasing pH during the different periods. After switching to continuous mode, and considerably dropped for each bioreactor that crashed (**Figures 2B–5B**). For our first nitrate experiment with a medium feed rate of 0.10 mL min^{-1}, we observed similar ethanol production rates for bioreactor 5 and 6 compared to the control experiment with ammonium feed (**Figure 4B**). The highest ethanol production rates were 30 mmol-C L^{-1} d^{-1} for bioreactor 5 on day 15 during Period III and 31 mmol-C L^{-1} d^{-1} for bioreactor 6 on day 14 during Period II. While for bioreactors 5 and 6 the ethanol production rates did not recover after the crashes, for bioreactor 4 the ethanol production rate increased with increasing OD_{600} after the crash, and reached a maximum of 62 mmol-C L^{-1} d^{-1} on day 22 during Period IV. This value is ∼2.5-fold higher compared to the highest ethanol production rate observed for *C. ljungdahlii* growing with ammonium (**Figure 2B** and **Table 2**) with the same medium feed rate of 0.10 mL min^{-1}. When we applied a higher medium feed rate of 0.19 ml min^{-1}, we found that ethanol production was strongly enhanced for bioreactor 7 and bioreactor 8 for experiment 2 (**Figure 4B** and **Table 3**). Highest ethanol production rates were 65 mmol-C L^{-1} d^{-1} for bioreactor 7 on day 22 during Period IV and 85 mmol-C L^{-1} d^{-1} for bioreactor 8 on day 15 during Period II. On the contrary, the ethanol production rates of bioreactor 9 and bioreactor 10 for experiment 3 that operated with the same medium feed rate but with acid feed to control the pH, were lower with highest rates of 33 mmol-C L^{-1} d^{-1} for bioreactor 9 and 38 mmol-C L^{-1} d^{-1} for bioreactor 10, both on day 16 during Period III (**Figure 5B** and **Table 3**). It should be noted that acetate production rates of bioreactor 4 remained low after the recovery,

which led to the highest measured ethanol/acetate ratio of ∼4.2 with CO_2 and H_2 in this study (**Table 2**). To our knowledge it is also the highest ethanol/acetate ratio for published studies with acetogens and CO_2 and H_2, because Mock et al. (2015) achieved a ratio of ∼1:1. In contrast, the acetate production rates of bioreactor 7, 8, 9, and 10 for experiment 2 and 3 were similar, even when we observed the high ethanol production rates in bioreactor 7 and 8 (**Table 3**).

We found in our first nitrate experiment with a medium feed rate of 0.10 mL min^{-1} that each bioreactor behaved differently and underwent stochastic crashes in the OD_{600} at different time points that were most likely connected to a simultaneous accumulation of nitrite (**Figure 3A**). One bioreactor recovered from this crash and showed increased ethanol production rates after the crash (**Figure 3B**). When we increased the medium feed rate to 0.19 mL min^{-1} for experiment 2, we observed again crash events at different time points (**Figure 4A**). Interestingly. before these crashes, these bioreactors already showed increased ethanol production rates compared to experiment 1. Furthermore, we found that crash events did not occur for experiment 3 during which we actively and immediately decreased the pH to the anticipated pH-value (**Figure 5A**). However, overall ethanol production rates were lower then. It is likely that the simultaneous production of acetate from acetogenesis and ammonium from nitrate reduction creates a sensitive environment for *C. ljungdahlii*, which supports growth and production rates of ethanol through a self-buffering pH effect of the cell, but with a high instability of the system, as discussed in detail below.

DISCUSSION

Our MBS Resulted in Reproducible Gas-Fermentation Experiments With *C. ljungdahlii*

The MBS was successfully tested to cultivate *C. ljungdahlii* with CO_2 and H_2 under various pH conditions during four experiments (total of 10 bioreactors). The highly comparable growth behavior of the triplicate bioreactors under batch and continuous conditions in the preliminary experiment, using standard medium with ammonium as the N-source (control), confirm a high stability of our MBS (**Figure 2A** and **Supplementary Figure S4A** in **Supplementary Data Sheet S2**). We did observe minor differences for the preliminary experiment in the ethanol and acetate production rates between replicates, which were connected to the same medium feed bottle under continuous conditions (**Figure 2B** and **Supplementary Figure S4B** in **Supplementary Data Sheet S2**). These differences in single replicates may lead to different production rates, even in controlled bioreactors, and may result from slightly varying gassing or medium feed rates, variations in the pH control, or small but varying diffusion of oxygen into individual bioreactors. This finding clearly indicates the need for replicates during strain characterization and pre-selection in lab-scale bioreactor experiments before scaling up to larger fermentations. With our MBS, we can combine experiments at steady-state conditions for replicates, which saves time in generating statistically relevant data sets. Our future work to further optimize the MBS will target the additional integration of analytic equipment to calculate gas

TABLE 2 | Highest observed values for OD_{600} and acetate/ethanol production rates at specific pH during continuous fermentation of *C. ljungdahlii* with CO_2 and H_2 in nitrate-containing medium with a feed rate of 0.10 mL min^{-1}.

Highest value for	Control[1,2]	Experiment 1[2]		
	Bioreactor 1-3 (ammonium)	Bioreactor 4 (nitrate)	Bioreactor 5 (nitrate)	Bioreactor 6 (nitrate)
OD_{600}	0.90 ± 0.02 (pH 6.0)	1.29 (pH 5.2)	1.36 (pH 5.5)	1.34 (pH 6.0)
Acetate production rate [mmol-C L^{-1} d^{-1}]	81.4 ± 3.0 (pH 6.0)	128.8 (pH 6.0)	81.5 (pH 6.0)	110.6 (pH 5.8)
Ethanol production rate [mmol-C L^{1} d^{-1}]	25.0 ± 2.7 (pH 5.0)	62.0 (pH 5.0)	29.9 (pH 5.0)	30.6 (pH 5.5)
$Ratio_{Et/Ac}$[3]	0.4 (pH 5.5)	4.2 (pH 4.5)	1.0 (pH 5.6)	0.6 (pH 5.5)

[1]Values for the bioreactors with ammonium feed (n = 3) are given as the average (±standard deviation) from three bioreactors for the last 5 data points. [2] Only base was fed to maintain the pH, while a pH decrease was caused by microbial acetic acid production. [3]Et, Ethanol; Ac, Acetate.

TABLE 3 | Highest observed values for OD_{600} and acetate/ethanol production rates at specific pH during continuous fermentation of *C. ljungdahlii* with CO_2 and H_2 in nitrate-containing medium with a feed rate of 0.19 mL min^{-1}.

Highest value for	Experiment 2[1]		Experiment 3[2]	
	Bioreactor 7 (nitrate)	Bioreactor 8 (nitrate)	Bioreactor 9 (nitrate)	Bioreactor 10 (nitrate)
OD_{600}	1.31 (pH 5.5)	1.46 (pH 5.6)	1.16 (pH 5.5)	1.21 (pH 5.0)
Acetate production rate [mmol-C L^{-1} d^{-1}]	124.8 (pH 5.5)	139.2 (pH 5.5)	97.4 (pH 6.0)	100.7 (pH 5.5)
Ethanol production rate [mmol-C L^{-1} d^{-1}]	65.1 (pH 5.1)	85.4 (pH 5.6)	32.6 (pH 5.0)	38.1 (pH 4.5)
$Ratio_{Et/Ac}$[3]	1.0 (pH 4.9)	1.4 (pH 5.8)	1.2 (pH 4.6)	0.8 (pH 4.5)

[1]Only base was fed to maintain the pH of the bioreactor, while a pH decrease was caused by microbial acetic acid production. [2]Base and acid were fed to maintain the pH of the bioreactor. The pH was actively decreased to the feed medium pH when entering a new pH period. [3]Et, Ethanol; Ac, Acetate.

consumption and carbon uptake rates. We had sampled the inlet and outlet gases during all experiments, but our current setup was not adequate to obtain reliable results. Additional equipment, such as mass-flow controllers, will fill this gap and further increase the data quality during future experiments.

Feeding Nitrate as Sole N-Source Led to Enhanced Cell Growth Even at Low pH

For our three main experiments (**Figures 3–5**), we tested the impact of nitrate as sole N-source on the growth and production rates of acetate and ethanol under pH-controlled conditions. It was recently demonstrated that *C. ljungdahlii* can use nitrate simultaneously for the generation of ammonium (assimilatory nitrate reduction) (Nagarajan et al., 2013), and as an alternative electron acceptor (dissimilatory nitrate reduction) (Emerson et al., 2019). This resulted in enhanced cell growth with sugars or CO_2 and H_2 in bottle experiments (Emerson et al., 2019). From these findings and our own preliminary batch experiments (**Supplementary Figure S5** in **Supplementary Data Sheet S2**), we also expected enhanced cell growth in our bioreactor experiment. Our data confirmed that the use of nitrate as sole N-source is enhancing CO_2 and H_2-dependent growth of *C. ljungdahlii* by up to 62% (based on OD_{600}) in continuous mode (**Figure 3** and **Table 2**). Emerson et al. (2019) observed 42% increased growth rates for bottle experiments with CO_2 and H_2, while the pH increased from 6.0 to 8.0. We observed a similar increase in the pH-value and a ∼200% increased OD_{600} in our preliminary bottle experiments (**Supplementary Figure S5** in **Supplementary Data Sheet S2**). All our bioreactors with nitrate feed had high OD_{600}-values even at low pH values, whereas the ammonium bioreactors showed a correlation between low pH and low OD_{600} (**Tables 1–3**). We had not anticipated this uncoupling of pH and OD_{600}, because biomass production is becoming limited at lower pH (Richter et al., 2016). Consequently, less acetate is produced from acetyl-CoA and, in turn, less ATP is available for the Wood-Ljungdahl pathway (Schuchmann and Müller, 2014). One possible explanation for this observation is that the depleting pool of ATP at a low pH is refilled with ATP generated through the reduction of nitrate and concomitant redirection of reducing equivalents. This ATP can then be used for biomass formation.

Our data show that the highest OD_{600} in our bioreactors with nitrate feed ranged between an OD_{600} of 1.29 and 1.36 at a medium feed rate of 0.10 mL min^{-1} (**Table 2**), and an OD_{600} of 1.21 and 1.49 at a medium feed rate of 0.19 mL min^{-1} during different periods (**Table 3**). This indicates that ATP was not the limiting factor for growth for the bioreactors with nitrate feed. Thus, nitrate reduction, on the one hand, was sufficient to regenerate redox cofactors, and on the other hand, provided more ATP for biomass formation. Ethanol formation was neither observed in our bottle experiments nor in the experiments by Emerson et al. (2019). This led to the hypothesis by Emerson et al. (2019) that *C. ljungdahlii* predominantly shifts electrons into nitrate reduction rather than toward ethanol formation. Noteworthy, however, is that the generated ammonium was responsible for an increasing pH-value. Here, we demonstrated for all bioreactors with nitrate feed that ethanol production was still possible when the pH was controlled to lower values, which rejects the hypothesis by Emerson et al. (2019) (**Figures 3B–5B**). We theorize here that ethanol formation was absent in the bottle experiments due to the increasing pH-value from ammonium production, which we were able to prevent with the bioreactors (**Supplementary Figure S5**). Again, this shows that observations with bottles should be followed up with pH-controlled bioreactors.

Nitrite Accumulation Indicated a Metabolic Crash of *C. ljungdahlii*

All bioreactors with nitrate feed showed different performance behavior during continuous mode (**Figures 3–5**). We observed crash events for nitrate bioreactors in which we did not force a decrease of the pH by feeding acid, but let the pH decrease by means of microbial acetate production (experiments 1 and 2) (**Figure 3**, **4**). These crashes were stochastic, because they occurred at different time points of the cultivation. This was independent of the bioreactors, because we had already observed the reproducible nature of our MBS in our preliminary experiment with ammonium feed (**Figure 2**). For each nitrate bioreactor that crashed, we measured an accumulation of nitrite and nitrate at the time point when the crash occurred and afterward (see **Supplementary Data Sheet S3**). Before the crashes, we were not able to detect nitrate in any sample. Therefore, we assume that the applied nitrate feed rates of 0.11 mmol h^{-1} (18.7 mM × 0.10 mL min^{-1}) for the first nitrate experiment (bioreactor 4/5/6) and 0.21 mmol h^{-1} (18.7 mM × 0.19 mL mnvalues, whereas the ammonium bioreactors showed a correlationi[1]) for the second and third nitrate experiment (bioreactor 7/8/9/10) was lower than the metabolic uptake rate for nitrate of *C. ljungdahlii*. However, our results indicate that an accumulation of nitrite and nitrate above a certain threshold is harmful to the microbes and leads to an abrupt halt of the metabolism for yet unknown reasons. A complete physiological characterization of the nitrate metabolism of *C. ljungdahlii,* or any other acetogen, is still missing in literature. Emerson et al. (2019) described that once the applied nitrate was depleted, the culture halted acetate production and crashed (as measured by the OD_{600}). The authors explained the crash with an abrupt end of the ATP supply, which is critical to maintain high cell densities for *C. autoethanogenum* (Valgepea et al., 2017). However, the bottle cultures of Emerson et al. (2019) did not crash completely. The OD_{600} decreased by 50% but recovered after a short lag phase, indicating that the remaining CO_2 and H_2 was further consumed. An accumulation of nitrite was neither observed during the crash in these experiments nor in our own preliminary bottle experiments (**Supplementary Figure S5** in **Supplementary Data Sheet S2**). One explanation might be that the metabolic crash was triggered by an insufficient regeneration of NADH. *C. ljungdahlii* possesses two putative hydroxylamine reductases (CLJU_c22260 and CLJU_c07730), which could catalyze the reduction of nitrite to ammonium with electrons from NADH (Köpke et al., 2010; Nagarajan et al., 2013). Since we observed simultaneous nitrite and nitrate accumulation in crashing cultures, a metabolic bottleneck at this catalytic step is possible. Another explanation

might be that nitrite and/or nitrate inhibit one or several enzymes in *C. ljungdahlii*. Then, as soon as some nitrite and/or nitrate accumulated and inhibited the metabolism, a feedback loop was triggered that quickly led to a complete crash of the metabolism.

For recovering the culture, we assume that the inhibiting compounds have to be washed out of the system to a certain critical threshold. In addition, some removal of the inhibiting compounds due to the recovering activity of the culture would also contribute. For bioreactor 4, we observed a constant decrease of the OD_{600} and acetate and ethanol production rates after the crash in Period I (**Figure 3**). However, on day 13–14 the decrease started to reach a valley, which indicates that the microbial growth was able to catch up with the dilution of our continuous process. For this bioreactor, the pH in Period II was still high enough to support sufficient growth, and after ∼2 HRT periods the growth rate of the microbes exceeded the dilution rate and the OD_{600} increased again (**Figure 3A**). The recovery of this bioreactor 4 in growth as well as in acetate and ethanol production rates indicates that: (1) the nitrate reduction pathway is not *per se* inhibited at low pH; and (2) the reduction of nitrate and the production of ethanol is possible simultaneously, and that most likely the low pH triggers a thermodynamic shift toward ethanol production (Richter et al., 2016). However, it remains elusive why the ethanol/acetate ratio in bioreactor 4 reached a nearly 10-fold higher value after recovering from the crash in the presence of nitrate compared to the bioreactors with ammonium feed (**Figure 3B** and **Table 2**). Importantly, applying a higher feed rate and similar cultivation conditions with another set of bioreactors for experiment 2 reached only a maximum ethanol/acetate ratio of 1.4 (**Table 3**). In contrast, the crash occurred for bioreactor 5 in Period II. While the OD_{600} immediately decreased after the crash, the acetate and ethanol production rates remained somewhat constant until the switch to Period III. However, this bioreactor 5 never recovered from the crash in terms of OD_{600}. We believe that the lower pH levels during Period III for bioreactor 5 prevented the growth recovery, which for bioreactor 4 took place at the higher pH level of Period II. We had found reduced growth conditions for bioreactors with ammonium at the lower pH levels, indicating that the growth rate is constantly decreasing while decreasing the medium pH (**Figure 2**, **Supplementary Figure S4** in **Supplementary Data Sheet S2**, and **Table 2**). The same findings hold true for bioreactor 6 for which the crash occurred even later in the cultivation. When we applied the 90% higher medium feed rate but kept the same pH maintenance conditions for bioreactor 7 and bioreactor 8 for experiment 2, single crash events still occurred, but at later time points (**Figure 4**).

What could be the reason for the stochastic crashes? Valgepea et al. (2017) discussed occurring "crash and recover cycles" during syngas fermentation with *C. autoethanogenum*. They hypothesized that the Wood-Ljungdahl pathway becomes the limiting factor during a period of ample supply of acetyl-CoA at higher biomass and acetate concentration. This can result in an insufficient supply of reducing equivalents due to a loss of H_2 uptake when the Wood-Ljungdahl pathway cannot keep up anymore. Consequently, the cells are not able to deliver the ATP demand, resulting in a crash. The cells recovered once the extracellular acetate concentration went below a certain threshold but crashed again after exceeding the threshold. Unfortunately, these threshold acetate concentrations were not given.

We observed higher acetate production rates for bioreactor 4 and 6 before the crash, compared to those of the bioreactors with ammonium feed (**Figures 2B**, **3B**). Bioreactor 5 did not reach a similarly high acetate concentration, but the crash occurred at the beginning of Period IV at the lower pH of 4.5. Intrinsically, the extracellular acetate concentration would be higher as a key to trigger the crash event. We assume a similar correlation of high acetate concentration and low pH for bioreactor 7 and bioreactor 8, which had a similar acetate production rate compared to bioreactor 5 at the time point of the crash event (**Figure 4**).

A Sensitive pH-Environment Based on an Interplay Between Undissociated Acetic Acid and Ammonium Increased Growth and Ethanol Production Rates

To further tackle the question of why we observed the crash events, we applied active pH maintenance with base and acid feed in our third experiment (bioreactor 9 and 10) (**Figure 5**). This immediate adjustment of the pH environment influenced growth, and acetate and ethanol production rates. At a pH of 5.5 (Period II), it caused stagnation of growth and acetate production rates, while simultaneously ethanol production started to increase. In contrast, the slow decrease of the pH in Period II due to microbial acetic acid production in bioreactor 7 and 8 accelerated ethanol production by 2–4-fold and biomass production by 11–28% compared to bioreactor 9 and 10, while acetate production first increased, but then quickly decreased (**Figure 4**). We believe that nitrate-reducing cells of *C. ljungdahlii* generate a sensitive pH-environment based on the buffering effect of the interplay between undissociated acetic acid production and ammonium production. This enables a more efficient pH balance and electron flow toward biomass production, and more reduced fermentation products, such as ethanol, but at the cost of a highly unstable environment. Small perturbations to the system seem to lead to a severe disbalance and immediate crash of the microbial growth. By feeding acid to actively lower the pH, this highly unstable environment can be controlled better, but at the cost of lower biomass and ethanol production rates. Without actively decreasing the pH with acid feed, the pH-environment remains sensitive to external influences. This could also explain the partly increasing pH-values during periods of higher (unbalanced) ammonium production with respect to acetate production. By a detailed look into literature and to the best of our knowledge there is no study that describes a similar pH effect for an acetogen. Our experiments showed highest ethanol production rates for nitrate-reducing cultures of *C. ljungdahlii* at pH 5.6 under fully controlled pH conditions. This indicates that optimum production conditions exist, and it will be of particular interest to maintain the bioreactors at this pH for longer cultivation times in future experiments (**Tables 2**, **3**).

In conclusion, nitrate reduction offers a great potential to further optimize gas fermentation of *C. ljungdahlii*. Because ATP limitation is one of the highest burdens to overcome for acetogens

(Schuchmann and Müller, 2014; Molitor et al., 2017), the surplus of ATP derived from nitrate reduction could be used to extent the product portfolio toward energy-intense products (Emerson et al., 2019). However, our work clearly demonstrates that nitrate metabolism of *C. ljungdahlii* needs further investigation on both a physiological and a bioprocessing level. The stochastic metabolic crashes demonstrate the importance of replicated bioreactor experiments in the field of acetogen research.

DATA AVAILABILITY STATEMENT

The datasets generated for this study are available in the **Supplementary Tables S2–S6** in **Supplementary Data Sheet S3**.

AUTHOR CONTRIBUTIONS

C-MK and LA designed the MBS. LA, C-MK, and BM planned the experiments. C-MK and NK-K built, maintained, and sampled the bioreactors. LA and BM supervised the project. C-MK analyzed the raw data and drafted the manuscript. All authors edited the manuscript and approved the final version.

FUNDING

This work was funded through the Alexander von Humboldt Foundation in the framework of the Alexander von Humboldt Professorship, which was awarded to LA. We are also thankful for additional funding to LA and BM from the Deutsche Forschungsgemeinschaft (DFG, German Research Foundation) under Germany's Excellence Strategy – EXC 2124 – 390838134. Finally, we acknowledge support by the DFG and Open Access Publishing Fund of University of Tübingen.

SUPPLEMENTARY MATERIAL

The Supplementary Material for this article can be found online at: https://www.frontiersin.org/articles/10.3389/fmicb.2020.00724/full#supplementary-material

REFERENCES

Abrini, J., Naveau, H., and Nyns, E. J. (1994). *Clostridium autoethanogenum*, Sp-Nov, an anaerobic bacterium that produces ethanol from carbon monoxide. *Arch. Microbiol.* 161, 345–351. doi: 10.1007/Bf00303591

Abubackar, H. N., Veiga, M. C., and Kennes, C. (2015). Carbon monoxide fermentation to ethanol by *Clostridium autoethanogenum* in a bioreactor with no accumulation of acetic acid. *Bioresour. Technol.* 186, 122–127. doi: 10.1016/j.biortech.2015.02.113

Asimakopoulos, K., Gavala, H. N., and Skiadas, I. V. (2018). Reactor systems for syngas fermentation processes: a review. *Chem. Eng. J.* 348, 732–744. doi: 10.1016/j.cej.2018.05.003

Bengelsdorf, F. R., Poehlein, A., Linder, S., Erz, C., Hummel, T., Hoffmeister, S., et al. (2016). Industrial acetogenic biocatalysts: a comparative metabolic and genomic analysis. *Front. Microbiol.* 7:1036. doi: 10.3389/fmicb.2016.01036

Brown, S. D., Nagaraju, S., Utturkar, S., De Tissera, S., Segovia, S., Mitchell, W., et al. (2014). Comparison of single-molecule sequencing and hybrid approaches for finishing the genome of *Clostridium autoethanogenum* and analysis of CRISPR systems in industrial relevant Clostridia. *Biotechnol. Biofuels* 7, 1–18. doi: 10.1186/1754-6834-7-40

Drake, H. L., Gossner, A. S., and Daniel, S. L. (2008). Old acetogens, new light. *Ann. N. Y. Acad. Sci.* 1125, 100–128. doi: 10.1196/annals.1419.016

Dürre, P. (2017). Gas fermentation - a biotechnological solution for today's challenges. *Microb. Biotechnol.* 10, 14–16. doi: 10.1111/1751-7915.12431

Emerson, D. F., Woolston, B. M., Liu, N., Donnelly, M., Currie, D. H., and Stephanopoulos, G. (2019). Enhancing hydrogen-dependent growth of and carbon dioxide fixation by *Clostridium ljungdahlii* through nitrate supplementation. *Biotechnol. Bioeng.* 116, 294–306. doi: 10.1002/bit.26847

Köpke, M., Held, C., Hujer, S., Liesegang, H., Wiezer, A., Wollherr, A., et al. (2010). *Clostridium ljungdahlii* represents a microbial production platform based on syngas. *Proc. Natl. Acad. Sci. U.S.A.* 107, 13087–13092. doi: 10.1073/pnas.1004716107

Köpke, M., and Liew, F. (2012). *Production of Butanol from Carbon Monoxide by a Recombinant Microorganism*. Patent No. WO2012053905A1. New Zealand: World Intellectual Property Organization.

Köpke, M., Simpson, S. D., Liew, F., and Chen, W. (2016). *Fermentation Process for Producing Isopropanol using a Recombinant Microorganism*. U.S. Patent No. US9365868B2. Alexandria, VA: U.S. Patent and Trademark Office.

Latif, H., Zeidan, A. A., Nielsen, A. T., and Zengler, K. (2014). Trash to treasure: production of biofuels and commodity chemicals via syngas fermenting microorganisms. *Curr. Opin. Biotechnol.* 27, 79–87. doi: 10.1016/j.copbio.2013.12.001

Mock, J., Zheng, Y., Müller, A. P., Ly, S., Tran, L., Segovia, S., et al. (2015). Energy conservation associated with ethanol formation from H2 and CO2 in *Clostridium autoethanogenum* involving electron bifurcation. *J. Bacteriol.* 197, 2965–2980. doi: 10.1128/JB.00399-15

Mohammadi, M., Najafpour, G. D., Younesi, H., Lahijani, P., Uzir, M. H., and Mohamed, A. R. (2011). Bioconversion of synthesis gas to second generation biofuels: a review. *Renew. Sust. Energ. Rev.* 15, 4255–4273. doi: 10.1016/j.rser.2011.07.124

Mohammadi, M., Younesi, H., Najafpour, G., and Mohamed, A. R. (2012). Sustainable ethanol fermentation from synthesis gas by *Clostridium ljungdahlii* in a continuous stirred tank bioreactor. *J. Chem. Technol. Biot.* 87, 837–843. doi: 10.1002/jctb.3712

Molitor, B., Marcellin, E., and Angenent, L. T. (2017). Overcoming the energetic limitations of syngas fermentation. *Curr. Opin. Chem. Biol.* 41, 84–92. doi: 10.1016/j.cbpa.2017.10.003

Nagarajan, H., Sahin, M., Nogales, J., Latif, H., Lovley, D. R., Ebrahim, A., et al. (2013). Characterizing acetogenic metabolism using a genome-scale metabolic reconstruction of *Clostridium ljungdahlii*. *Microb Cell Fact.* 12:118. doi: 10.1186/1475-2859-12-118

Phillips, J. R., Huhnke, R. L., and Atiyeh, H. K. (2017). Syngas fermentation: a microbial conversion process of gaseous substrates to various products. *Fermentation* 3, 1–28. doi: 10.3390/fermentation3020028

Richter, H., Martin, M. E., and Angenent, L. T. (2013). A two-stage continuous fermentation system for conversion of syngas into ethanol. *Energies* 6, 3987–4000. doi: 10.3390/en6083987

Richter, H., Molitor, B., Wei, H., Chen, W., Aristilde, L., and Angenent, L. T. (2016). Ethanol production in syngas-fermenting *Clostridium ljungdahlii* is controlled by thermodynamics rather than by enzyme expression. *Energ. Environ. Sci.* 9, 2392–2399. doi: 10.1039/c6ee01108j

Schuchmann, K., and Müller, V. (2014). Autotrophy at the thermodynamic limit of life: a model for energy conservation in acetogenic bacteria. *Nat. Rev. Microbiol.* 12, 809–821. doi: 10.1038/nrmicro3365

Tanner, R. S., Miller, L. M., and Yang, D. (1993). *Clostridium ljungdahlii* sp. nov., an acetogenic species in clostridial rRNA homology group I. *Int. J. Syst. Bacteriol.* 43, 232–236. doi: 10.1099/00207713-43-2-232

Ueki, T., Nevin, K. P., Woodard, T. L., and Lovley, D. R. (2014). Converting carbon dioxide to butyrate with an engineered strain of *Clostridium ljungdahlii*. *mBio* 5:e01636-14. doi: 10.1128/mBio.01636-14

Valgepea, K., de Souza Pinto Lemgruber, R., Meaghan, K., Palfreyman, R. W., Abdalla, T., Heijstra, B. D., et al. (2017). Maintenance of ATP homeostasis triggers metabolic shifts in gas-fermenting acetogens. *Cell Syst.* 4, 505–515. doi: 10.1016/j.cels.2017.04.008

Younesi, H., Najafpour, G., and Mohamed, A. R. (2005). Ethanol and acetate production from synthesis gas via fermentation processes using anaerobic bacterium, *Clostridium ljungdahlii*. *Biochem. Eng. J.* 27, 110–119. doi: 10.1016/j.bej.2005.08.015

Conflict of Interest: The authors declare that the research was conducted in the absence of any commercial or financial relationships that could be construed as a potential conflict of interest.

frontiers in Microbiology

REVIEW
published: 04 June 2020
doi: 10.3389/fmicb.2020.00817

Older Than Genes: The Acetyl CoA Pathway and Origins

*William F. Martin**

Institute for Molecular Evolution, University of Düsseldorf, Düsseldorf, Germany

For decades, microbiologists have viewed the acetyl CoA pathway and organisms that use it for H_2-dependent carbon and energy metabolism, acetogens and methanogens, as ancient. Classical evidence and newer evidence indicating the antiquity of the acetyl CoA pathway are summarized here. The acetyl CoA pathway requires approximately 10 enzymes, roughly as many organic cofactors, and more than 500 kDa of combined subunit molecular mass to catalyze the conversion of H_2 and CO_2 to formate, acetate, and pyruvate in acetogens and methanogens. However, a single hydrothermal vent alloy, awaruite (Ni_3Fe), can convert H_2 and CO_2 to formate, acetate, and pyruvate under mild hydrothermal conditions on its own. The chemical reactions of H_2 and CO_2 to pyruvate thus have a natural tendency to occur without enzymes, given suitable inorganic catalysts. This suggests that the evolution of the enzymatic acetyl CoA pathway was preceded by—and patterned along—a route of naturally occurring exergonic reactions catalyzed by transition metal minerals that could activate H_2 and CO_2 by chemisorption. The principle of forward (autotrophic) pathway evolution from preexisting non-enzymatic reactions is generalized to the concept of patterned evolution of pathways. In acetogens, exergonic reduction of CO_2 by H_2 generates acyl phosphates by highly reactive carbonyl groups undergoing attack by inert inorganic phosphate. In that ancient reaction of biochemical energy conservation, the energy behind formation of the acyl phosphate bond resides in the carbonyl, not in phosphate. The antiquity of the acetyl CoA pathway is usually seen in light of CO_2 fixation; its role in primordial energy coupling via acyl phosphates and substrate-level phosphorylation is emphasized here.

Keywords: origin of life, bioenergetics, hydrothermal vents, autotrophic origins, evolution of pathways

OPEN ACCESS

Edited by:
Mirko Basen,
University of Rostock, Germany

Reviewed by:
Shunichi Ishii,
Japan Agency for Marine-Earth Science and Technology (JAMSTEC), Japan
Ivan A. Berg,
University of Münster, Germany

***Correspondence:**
William F. Martin
bill@hhu.de

Specialty section:
This article was submitted to Microbial Physiology and Metabolism, a section of the journal Frontiers in Microbiology

Received: *16 December 2019*
Accepted: *06 April 2020*
Published: *04 June 2020*

Citation:
Martin WF (2020) Older Than Genes: The Acetyl CoA Pathway and Origins. Front. Microbiol. 11:817. doi: 10.3389/fmicb.2020.00817

INTRODUCTION

It is part of our human condition to want to know about the past, where things come from and ultimately how life began. Indeed, most human cultures have an origins narrative of some sort. Scientists are also a form of human culture, in the broad sense, and as such scientists also have origins narratives. However, just like the origins narratives of different cultures tend to differ, so do the origins narratives of different groups of scientists. Mathematicians tend to prefer stochastic or probabilistic models; physicists tend to prefer complicated models that gravitate toward problems of self-organization, whereas chemists tend to prefer models that focus on the synthesis and polymerization of RNA bases. Biologists, on the other hand, tend to find deficiencies with all such models, probably because biologists recognize that life is a very complicated action involving all of the above and more. Life is a set of chemical reactions that are set in motion by energy metabolism. Given a source of electrons, energy metabolism, carbon metabolism, and sufficient nutrients, life reacts to generate cells that produce more cells until one of the educts becomes limiting. Cells

deposit protein as the main substance, RNA as peptide-condensing agents, and DNA as memory; they self-organize, and they generate populations as side products of energy metabolism, the main chemical reaction that runs all of the above. The self-organization property of cells is not obvious. Hansen et al. (2009, p. 1843) reviewed studies of entropy change measurements during growth; the entropy change in cells is always zero or close to zero because, as they succinctly explained, "cells are assembled in a spontaneous process." That is, if a cell has what it needs to grow, it organizes environmentally available components into more of itself as an effortless byproduct of the exergonic growth process. Growth means energy conversion, placing energy metabolism and changes in Gibbs free energy (Thauer, 2015) at the center of the origins question, from the perspective of physiology.

WHAT IS ANCIENT?

What do acetogens have to do with origins, and why include a chapter on the origin of life in a special issue about acetogens? The simplest answer is perhaps that biologists have always had an intuition that anaerobic bacteria capable of reducing CO_2 are ancient. The idea that the first cells on earth were anaerobes and met their carbon needs from CO_2 alone without the help of chlorophyll goes back 110 years. In 1902, Haeckel expressed the view that the first step in the origin of life (*Archigonie* he called it, from Greek *archae* ancient, *gone* seed) was the formation of an inorganic formative fluid ("*anorganische Bildungs-Flüssigkeit*") containing the essential components, namely, carbonic acid, ammonia, and binary salts ("*Kohlensäure, Ammoniak, binäre Salze*") (Haeckel, 1902, p. 361). As shown in **Figure 1**, Haeckel also saw the very first organisms as synthesizing their cell plasma reductively ("*Bilden Plasma unter Reduction*"), which today we would call autotrophy. Famous for his classifications, Haeckel placed these first organisms at the top of his system in the class Probiontes, represented by the first order Archibiontes, which contained only hypothetical types named *Primordia vitae hypothetica!* (**Figure 1**). Haeckel did not discuss the matter of origins much further in that book, although the exclamation point in *Primordia vitae hypothetica!*, possibly a punctuational singularity in the history of taxonomy, seems to underscore the importance of the issue.

In 1910, Mereschkowsky took the issue of origins in the same direction but several explicit steps further. Mereschkowsky divided Earth's early history into four phases, Epochs I–IV, as it pertained to origins. In the first epoch, the Earth had a fiery glowing surface; in the second, the fire had subsided, but the surface was still very hot, $\geq$100°C, and therefore dry; in the third Epoch, the surface was covered with boiling water (50–100°C); in the fourth, the water had cooled to less than 50°C (Mereschkowsky, 1910; p. 359). Based on observations of cells that grow at high temperatures, he then concluded that the first forms of life arose in Epoch III, as the Earth was covered in boiling water. Those first life forms furthermore had the following properties (translation by the author, the original German is in **Figure 2**): (1) a minimal size, inaccessible to the microscope; (2) a lack of organization; (3) the ability to survive temperatures close to the boiling point; (4) the ability to live without oxygen; (5) the ability to synthesize proteins and carbohydrates (the latter without the help of chlorophyll) from inorganic substances. [*Fähigkeit, Eiweiße und Kohlenhydrate (letzteres ohne Vermittlung des Chlorophylls) aus unorganischen Stoffen zu bilden.*]; and (6) resilience against alkaline solutions, concentrated salt solutions, sulfur compounds, and diverse toxins (Mereschkowsky, 1910; p. 359). Those six properties, taken together, are very close to what proponents of autotrophic origins at alkaline hydrothermal vents are saying today. This fifth criterion, autotrophy without chlorophyll, means chemolithoautotrophy in modern terms. Chemolithoautotrophic origins at H_2-rich hydrothermal vents are concepts that tend to appeal to microbiologists because we can observe chemolithoautotrophs growing at hydrothermal vents today, and those modern environments are probably not much different than they were four billion years ago.

The idea that the first forms of life might have been phenotypically simple and chemically robust, arising in and inhabiting geochemically active environments, is intuitive conjecture. A similar conjecture shared by many biologists is that clues about the origin and early history of life are preserved in the biology of cells themselves and that some lineages of modern cells might be physiologically unchanged relative to the first life forms, which had to have been anaerobes, as Mereschkowsky (1910) and later Haldane (1929) were aware. Lipmann, who pioneered the concept of ATP- and energy-rich phosphate bonds as chemical currencies of energy in cells, was explicit about inferences from physiology when he wrote "Projecting backward makes it necessary to make assumptions which may seem difficult or perhaps impossible to verify. I think it might be possible to find links by looking more attentively for primitive evolutionary stages within the metabolic picture in the hope to apprehend there surviving metabolic fossils" (Lipmann, 1965, p. 273). The idea expressed there is not trivial. Biologists tend to hold that there are life forms still in existence today that have preserved aspects of physiology that were present in the first forms of life. This stands in contrast to much of the origins literature, where it is widely assumed and sometimes actively argued chemistry at origins is solely a process of generating RNA and has no connection at all to modern physiology (Orgel, 2008). Lipmann's 1965 chapter is good reading; it makes a case for the greater antiquity of substrate-level phosphorylation over ion gradient coupled phosphorylation, the antiquity of ferredoxin, and, as a side note, the antiquity of RNA over DNA.

What were ancient life forms doing from the standpoint of energy metabolism? Electromagnetic radiation from the sun was long assumed to be energy source for energy at origins: Miller and Urey (1959, p. 247) stated that "At the present time the direct or indirect source of free energy for all living organisms is the sunlight utilized by photosynthetic organisms," as expressed by Miller and Urey (1959, p. 247) as did Morowitz (1968, p. 79): "All biological processes depend on the absorption of solar photons and the transfer of heat to celestial sinks." Of course, today we know that life in the crust and within hydrothermal vents proceeds in complete darkness, fueled exclusively by

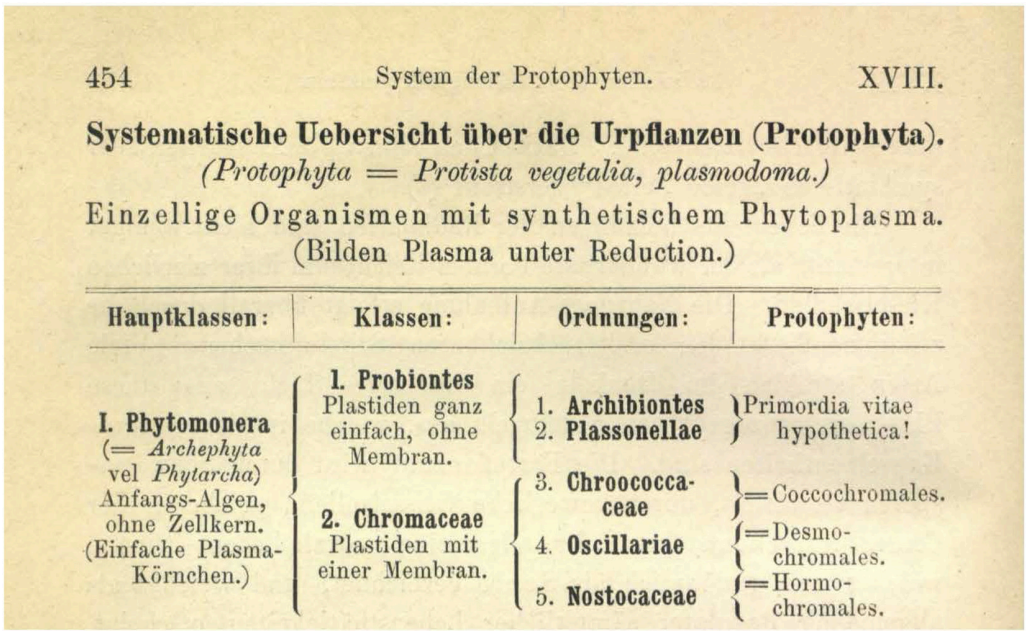

454 System der Protophyten. XVIII.

Systematische Uebersicht über die Urpflanzen (Protophyta).

(Protophyta = Protista vegetalia, plasmodoma.)

Einzellige Organismen mit synthetischem Phytoplasma.
(Bilden Plasma unter Reduction.)

Hauptklassen:	Klassen:	Ordnungen:	Protophyten:
I. Phytomonera (= *Archephyta* vel *Phytarcha*) Anfangs-Algen, ohne Zellkern. (Einfache Plasma-Körnchen.)	**1. Probiontes** Plastiden ganz einfach, ohne Membran.	1. **Archibiontes**	Primordia vitae hypothetica!
		2. **Plassonellae**	
	2. Chromaceae Plastiden mit einer Membran.	3. **Chroococcaceae**	= Coccochromales.
		4. **Oscillariae**	= Desmochromales.
		5. **Nostocaceae**	= Hormochromales.

FIGURE 1 | Haeckel's proposal for Probiontes and Archibiontes. In my view, Probiontes would correspond to LUCA, whereas Archibiontes would correspond to the first free-living cells, which could have been cytochrome-lacking acetogens and methanogens that use the acetyl CoA pathway for H_2-dependent carbon and energy metabolism (a grade not a clade). Note the term "Reduction" that Haeckel used to designate the growth of autotrophs (for heterotrophs, he used Oxidation). *Bilden Plasma unter Reduction:* Synthesize plasma reductively.

chemical energy provided by purely geochemical processes, without any need for sunlight whatsoever (Corliss et al., 1981; Baross and Hoffmann, 1985). That kind of harsh geochemical environment is much more in line with what Haeckel and Mereschkowsky had in mind. It is also the kind of environment where organisms that live from the reduction of CO_2 with electrons from H_2, acetogens, and methanogens have what they need for growth.

Acetogens and methanogens growing from geochemical H_2 are not dependent on solar radiation. Following the lead of Decker et al. (1970) and advice from microbiologists knowledgeable of acetogen and methanogen physiology, I have made a case in recent years that acetogens and methanogens lacking cytochromes could have arisen from reactions of H_2 and CO_2 at hydrothermal vents ca. four billion years ago and have preserved to this day the founding physiology of the first free-living cells in the bacteria and archaeal lineages (Martin and Russell, 2007; Martin, 2008, 2012). Genomic reconstructions of the last universal common ancestor (LUCA) (Weiss et al., 2016) point very much in the same direction as to chemical experiments in the laboratory (Preiner et al., 2020). Microbiologists tend to understand that case; in textbooks, the theory is present (Madigan et al., 2019). In a hydrothermal origins scenario in which LUCA, confined to the site of the synthesis of its chemical constituents, had not yet progressed to the stage of a free-living cell, LUCA would correspond to Haeckel's Probiontes (which in that case would possibly have priority over LUCA as a name). The first membrane-bounded cells to escape the vent, domain-founding acetogens and methanogens, would correspond to a grade comprising the first free-living cells, equivalent to Archibiontes. In that view, the differences that distinguish archaea from bacteria, including lipid and cell wall chemistry, would reflect their divergence from LUCA before the transition to the free-living state (Martin and Russell, 2003). That would correspond to a progenote organization of LUCA, something simpler than a free-living cell (Di Giulio, 2011; Weiss et al., 2016). Other views have it that LUCA was a fully fledged bacterium (Valas and Bourne, 2011), requiring complex evolutionary processes to account for the change in lipid and cell wall chemistry at the origin of archaea from bacterial roots (for a discussion see Sojo et al., 2014). There are a number of suggestions that LUCA was eukaryotic in organization, but from the standpoint of physiology, that possibility seems unlikely enough that we need not discuss it here. There might be suggestions out there that LUCA was an archaeon from which the bacteria would be derived, but this author is unaware of them. Haeckel's designation of Archibiontes (**Figure 1**; from Greek *arkhaios* primitive) is an interesting ancient name for an ancient grade, the first free-living cells, which could have been acetogens and methanogens, based on their physiology (Decker et al., 1970).

ACETOGENS ARE ANCIENT

How far back can we trace the idea that acetogens might be living fossils from the origin of life? Lipmann (1965; p. 265) opined: "...the chlorophylls could scarcely be early in

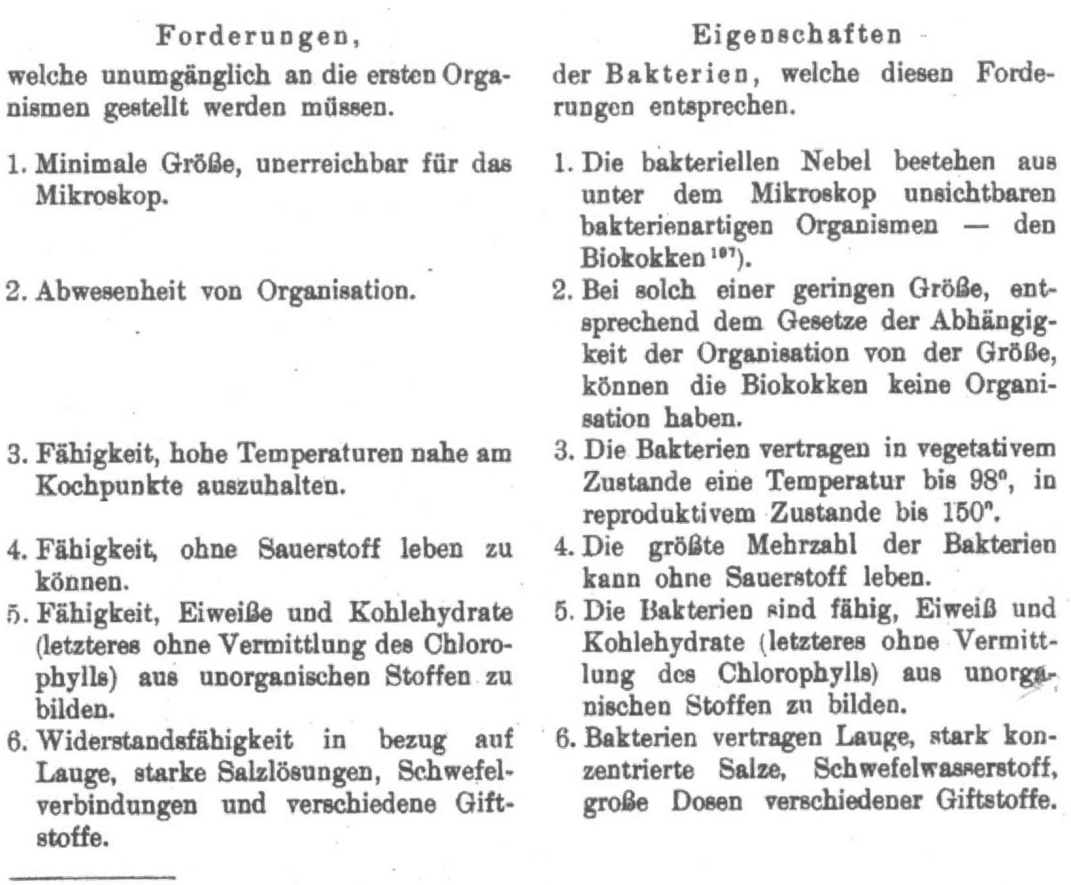

Forderungen, welche unumgänglich an die ersten Organismen gestellt werden müssen.	Eigenschaften der Bakterien, welche diesen Forderungen entsprechen.
1. Minimale Größe, unerreichbar für das Mikroskop.	1. Die bakteriellen Nebel bestehen aus unter dem Mikroskop unsichtbaren bakterienartigen Organismen — den Biokokken[107]).
2. Abwesenheit von Organisation.	2. Bei solch einer geringen Größe, entsprechend dem Gesetze der Abhängigkeit der Organisation von der Größe, können die Biokokken keine Organisation haben.
3. Fähigkeit, hohe Temperaturen nahe am Kochpunkte auszuhalten.	3. Die Bakterien vertragen in vegetativem Zustande eine Temperatur bis 98°, in reproduktivem Zustande bis 150°.
4. Fähigkeit, ohne Sauerstoff leben zu können.	4. Die größte Mehrzahl der Bakterien kann ohne Sauerstoff leben.
5. Fähigkeit, Eiweiße und Kohlehydrate (letzteres ohne Vermittlung des Chlorophylls) aus unorganischen Stoffen zu bilden.	5. Die Bakterien sind fähig, Eiweiß und Kohlehydrate (letzteres ohne Vermittlung des Chlorophylls) aus unorganischen Stoffen zu bilden.
6. Widerstandsfähigkeit in bezug auf Lauge, starke Salzlösungen, Schwefelverbindungen und verschiedene Giftstoffe.	6. Bakterien vertragen Lauge, stark konzentrierte Salze, Schwefelwasserstoff, große Dosen verschiedener Giftstoffe.

FIGURE 2 | Mereschkowsky's 1910 list of "Demands that inevitably must apply to the first organisms" (*Forderungen welche umumgänglich an die ersten Organismen gestellt wereden können*) and "Properties of bacteria that meet these demands" (*Eigenschaften der Bakterien, welche diese Forderungen entsprechen*). See text for translation of Demands 1–6. The demands are derived from his inference that life arose at a time when water on the young Earth's surface was still hot, close to the boiling point (see text).

chemical evolution; if not for other reasons, this suggests that photosynthesis came relatively late, preceded by chemosynthesis already highly developed in anaerobic clostridia." In a survey of energy conservation among anaerobes, and with keen attention to the evolutionary progression from cobalamin (ancestral) to chlorophyll via heme, Decker, Jungermann, and Thauer surmised that "From this point of view the methane-forming bacteria and the clostridia described in this article are closest to the primordial anaerobes" (Decker et al., 1970; p. 157) at a time before the recognition that methanogens are archae(bacteri)a. There might or might not be statements conjoining the evolutionary antiquity of acetogens and methanogens in earlier literature. Although Decker et al. (1970) were not talking about clostridia that grow from H_2 and CO_2, they were talking about methanogens that do, and they reported the thermodynamic values for both the acetogenic and the methanogenic reaction from H_2 and CO_2. The idea that acetogens and methanogens could harbor ancestral forms of prokaryotic energy metabolism has remained current in thoughts about ancient physiology because the more details that emerged from the investigation of enzymes, structures, and cofactors underpinning the pathway(s), the more ancient they appeared.

Chemists and biologists working on the acetyl CoA pathway agree that it is ancient, as a few quotes attest. Wood wrote "Perhaps we are uncovering some reactions used by primitive forms of life before the use of ATP was developed and before CO_2 was used by the Calvin cycle" (Wood, 1991, p. 161). Ljungdahl surmised: "The autotrophic fixation of CO_2 forming acetate is the most direct pathway for forming acetyl CoA, which may be the primary building block of life" (Ljungdahl, 2009, p. 20). For more than three decades, Fuchs has maintained that the acetyl CoA pathway is ancient: "The total synthesis of acetyl CoA fulfills most of the criteria postulated for an ancient pathway. Its distribution in only distantly related anaerobes (Archaebacteria and Eubacteria) [. . .] and its unusual biochemistry are noteworthy. It requires the lowest amount of ATP. It is a versatile one-carbon and two-carbon assimilation path" (Fuchs and Stupperich, 1985, p. 245–246) or "The common ancestor of life was probably a chemolithoautotrophic thermophilic anaerobe. . . [. . .] one attractive idea is that minerals

catalyzed a primitive acetyl CoA pathway" (Berg et al., 2010, p. 11). Drake et al. concur: "The acetyl-CoA pathway and variants thereof appear to be important to primary production in certain habitats and may have been the first autotrophic process on earth and important to the evolution of life" (Drake et al., 2008). Ragsdale sees the situation similarly: "The isotopic fractionation pattern of anaerobic organisms using the Wood-Ljungdahl pathway suggests that they may have been the first autotrophs, using inorganic compounds like CO and H_2 as an energy source and CO_2 as an electron acceptor approximately one billion years before O_2 appeared" (Ragsdale and Pierce, 2008. p. 1877). The editors of this volume do not dissent: "Acetogenic microorganisms may also have been among the first microorganisms" (Basen and Müller, 2017, p. 15) or, more recently, "The pioneer organism in a primordial world was probably a chemolithoautotrophic thermophilic anaerobe that employed the reductive acetyl CoA pathway" (Schoelmerich and Müller, 2019). Physiology tends to put acetogens at Square one of bacterial evolution.

Carbon isotope evidence consistent with the operation of the acetyl CoA pathway is found in rocks that are 3.8 billion years old (Ueno et al., 2006) and even 3.95 billion years old (Tashiro et al., 2017). The evidence for biological origin is founded in light carbon, an enrichment of ^{12}C versus ^{13}C. The alternative interpretation that those ancient carbon isotope signatures might reflect abiotic processes would suggest the existence of abiotic CO_2 fixation prior to the origin of life, which would be compatible with theories for autotrophic origins. By about 3.5 billion years ago, stromatolites were present, suggesting the existence of photosynthetic communities, and many modern biochemical pathways had evolved (Nisbet and Sleep, 2001; Arndt and Nisbet, 2012). Nearly four billion years later, the acetyl CoA pathway is still the backbone of acetogen physiology (Wood, 1991; Ragsdale, 2008; Ljungdahl, 2009; Fuchs, 2011; Basen and Müller, 2017). The first organisms could have lived from H_2 and CO_2 in the geochemical setting of hydrothermal vents, fueled by the redox potential that exists between H_2 from serpentinization and CO_2 from the ancient oceans, the same redox potential that fuels growth of modern acetogens and methanogens (Preiner et al., 2018). The same reactions still fuel life for acetogens and methanogens in the deep crust today (Magnabosco et al., 2018). That kind of continuity from the first forms of metabolism into the physiology of modern cells is undoubtedly what Lipmann (1965) meant with the term "metabolic fossils."

SQUARE TWO

The first cells were likely autotrophs. What's next? Comparative physiology of the six known CO_2 fixation pathways among prokaryotes indicates that the acetyl CoA pathway is the most ancient, mainly because (i) it is linear rather than cyclic, (ii) it is the only exergonic CO_2 fixing pathway, (iii) it is the only CO_2 fixing pathway that occurs in archaea and bacteria (Berg et al., 2010; Fuchs, 2011; Hügler and Sievert, 2011), and (iv) it is a strictly anaerobic pathway, and it is replete with transition metal clusters (Ragsdale and Pierce, 2008). It is the only CO_2 fixing pathway that operates via CO as an intermediate (Ragsdale, 2004), generating carboxyl groups from carbonyl, rather than reducing carboxyl groups, which is the key to its exergonic nature, as the other pathways expend energy to reduce carboxyl groups (Xavier et al., 2018). Furthermore, it is a pathway of both carbon and energy metabolism, which is an excellent starting point from which to undergo evolutionary specialized into distinct, dedicated pathways of independent carbon and energy metabolism (Martin and Russell, 2007). The linear nature of the pathway to acetate speaks for its antiquity over the other five cyclic pathways because they entail numerous stereochemically defined intermediates, whereas the condensation of a methyl group and CO generate no chiral centers in the CO_2 fixation intermediates. The other five pathways are more restricted in distribution, the dicarboxylate/4-hydroxybutyrate cycle and the hydroxypropionate/4-hydroxybutyrate cycle occurring in archaea, the reductive citric acid cycle, the 3-hydroxypropionate bi-cycle, and the Calvin cycle occurring in bacteria (Berg et al., 2010; Fuchs, 2011).

Starting from the acetyl CoA pathway for carbon and energy, gluconeogenic carbohydrate pathways could have arisen (Say and Fuchs, 2010), accompanied by specialization of the pathway toward carbon assimilation supported by an energy metabolism that does not reduce CO_2, as in sulfur reducers that oxidize H_2, cell mass, or end products such as acetate or lactate (Liu et al., 2012; Schut et al., 2013; Sousa et al., 2013; Rabus et al., 2015). The invention of heme from corrin precursors (Decker et al., 1970) could have occurred in clostridial sulfate–reducing lineages (Martin and Sousa, 2015), where cytochromes are abundant. The closure of the horseshoe citric acid cycle into the reverse citric acid cycle in bacteria (Mall et al., 2018; Nunoura et al., 2018) likely marked the origin of the second CO_2 fixation pathway. The first cells would have been dependent on H_2 for carbon and/or energy metabolism, but in the absence of H_2, only incremental physiological innovations were required for adaptation. The acetyl CoA pathway is reversible, as demonstrated in a sulfate reducer (Schauder et al., 1988), such that in the presence of low H_2 partial pressures the pathway can support growth in the acetate oxidizing direction (Zinder, 1994; Hattori et al., 2005). Operation in the acetate oxidizing direction is likely an ancient property of the pathway, although the mechanism of coupling appears to be still unresolved.

The first specialized heterotrophs could have arisen using amino acid, nucleoside, and ribose fermentations of the cell mass left behind by H_2-dependent autotrophs when their local geochemical supply of H_2 subsided (Schönheit et al., 2016) because in the absence of H_2 the fermentations become thermodynamically favorable. These innovations would have occurred in a world where primary production was dependent on geochemical H_2 provided by serpentinization. Even the origin of photosynthesis is likely to have occurred at hydrothermal vents, taking root in mild thermal radiation rather than from harsh sunlight at the surface (Nisbet et al., 1995). Anoxygenic photosynthesis using a type I reaction center (linear electron flow) was likely key in that process, providing a means of primary production (ferredoxin reduction) that was no longer

H_2-dependent (Martin et al., 2018) and possibly involving zinc cytochromes as functional precursors of chlorophyll, the last of the tetrapyrroles to evolve (Decker et al., 1970). Chlorophyll-dependent light harnessing enabled the colonization of new niches and the establishment of new, ocean surface ecosystems by primary producers, paving the way to oxygenic photosynthesis (Allen, 2005; Fischer et al., 2016). In the archaea, metabolic innovations seem to often entail gene transfer from bacteria for physiological evolution (Nelson-Sathi et al., 2012, 2015; Martin and Sousa, 2016; Wagner et al., 2017).

THREE PROBLEMS: THEY BIFURCATE, PUMP, AND DIFFER

The idea that acetogenesis and methanogenesis are ancient (Decker et al., 1970) is appealing. But is it robust, is it *belastbar* (German: able to bear weight)? One has to think things through in full, whereby the details can harbor demons. Three problems stand out.

One problem concerns the noteworthy aspect of acetogen and methanogen physiology that they require chemiosmotic coupling—ion gradient formation and ATP synthesis via a gradient-harnessing rotor–stator ATPase—for growth because there is not enough energy in the H_2–CO_2 couple to simultaneously support carbon assimilation and ATP synthesis via substrate-level phosphorylation. Their mechanisms of ion gradient formation entail flavin-based electron bifurcation (Herrmann et al., 2008; Buckel and Thauer, 2013). Electron bifurcation is, among other things, a very ancient mechanism to generate reduced ferredoxin from H_2 (Müller et al., 2018). Ferredoxin is, in turn, the source of reducing power that acetogens and methanogens use for CO_2 reduction because under standard physiological conditions the midpoint potential of the H_2/H^+ couple is not sufficiently negative to reduce CO_2 (Herrmann et al., 2008; Buckel and Thauer, 2018; Müller et al., 2018; Peters et al., 2018). Electron bifurcation involves enzymes and cofactors. That would appear to complicate the idea that H_2–CO_2-dependent growth via acetogenesis and methanogenesis can be traced all the way back to exergonic reactions of CO_2 in hydrothermal vents (Martin, 2012). Vents, however, offer a solution to this problem (see following section).

Moreover, the primitive forms of acetogens and methanogens that grow on H_2 and CO_2 for carbon and energy lack cytochromes and quinones (Thauer et al., 2008; Hess et al., 2014). For pumping, the acetogens that lack cytochromes and quinones use either an energy-converting hydrogenase (Ech) (Schoelmerich and Müller, 2019) or a ferredoxin-NAD^+ oxidoreductase (Rnf) (Schuchmann and Müller, 2014). The methanogens that lack cytochromes and quinones pump via a methyl transferase that harnesses the energy in the transfer of a methyl group from a sulfur atom in a thiol to a nitrogen atom in a pterin to pump Na^+ ions (Thauer et al., 2008). At first sight, this also appears to run counter to the idea that acetogens and methanogens (and their acetyl CoA pathway) are ancient. The fact that acetogens and methanogens growing on H_2 and CO_2 have to pump ions and use a rotor–stator ATPase in order to conserve energy would appear to squelch the idea. But that is not the case, because all prokaryotes (or their clades) use chemiosmotic coupling, and the rotor–stator ATP synthase is not only structurally conserved across bacteria and archaea (Grüber et al., 2014), it is as universal among prokaryotes and the genetic code itself (Sousa et al., 2013). The ATP synthase furthermore traces to LUCA in genomic reconstructions (Weiss et al., 2016). The problem that ensues is this: the principle and the enzyme of ion gradient harnessing, the ATP synthase, are conserved across acetogens and methanogens, but the mechanism of pumping is not. Vents also offer a solution to this problem (see following section).

Adding more complication to what seemed at the outset to be a fairly straightforward idea (carbon and energy metabolism via the acetyl CoA pathway in acetogens and methanogens is as ancient as rocks) is the circumstance that acetyl CoA pathway has two segments: one of which is conserved across acetogens and methanogens; the other is not. The two segments are CO-dependent acetyl CoA synthesis at carbon monoxide dehydrogenase/acetyl CoA synthase (CODH/ACS) (Ragsdale, 2008; Fuchs, 2011) and methyl synthesis from CO_2 and H_2. CODH/ACS is conserved; methyl synthesis is not (Sousa and Martin, 2014). Using electrons from H_2 via ferredoxin, CODH/ACS reduces CO_2 to CO at an FeNiS cluster and directs the CO through a tunnel in the enzyme to a second FeNiS cluster where it binds to a Ni atom as nickel carbonyl (Dobbek et al., 2001; Drennan et al., 2004; Doukov et al., 2008). The methyl synthesis branch is very different in acetogens and methanogens: the pathways use different cofactors (Maden, 2000), and the enzymes of the acetogen and methanogen pathways are not homologous (Sousa and Martin, 2014). To me, the methyl synthesis problem, or "the early formyl pterin problem," has appeared to be the most severe (Martin and Russell, 2007; Martin, 2012), until recently. There is now a solution to this problem as well. All three solutions entail natural chemical properties of serpentinizing hydrothermal vents.

THREE SOLUTIONS, ONE ENVIRONMENT, AND CATALYST

If acetogenesis and the acetyl CoA pathway are genuinely ancient (as in originating from rocks, water, and CO_2), robust geochemical (prebiotic) solutions to the three problems outlined in the foregoing section—electron bifurcation, ion gradient formation, and methyl synthesis—are required. In **Figure 3A**, the acetyl CoA pathway is represented as a series of chemical conversions showing the oxidation state of carbon as it is reduced to a methyl group, to CO, to an enzyme-bound and cofactor-bound acetyl moiety and ultimately converted to acetate or methane in energy metabolism of acetogens and methanogens, or pyruvate in their carbon metabolism (Fuchs, 2011). The only difference in this depiction relative to Fuchs (2011) is the recent finding that free formate is generated in the methanogen pathway as revealed by the structure of the methanofuran dehydrogenase complex (Wagner et al., 2016), rendering the state of substrate carbon (although not its covalent ligands, generically represented

A **Acetyl-CoA pathway**

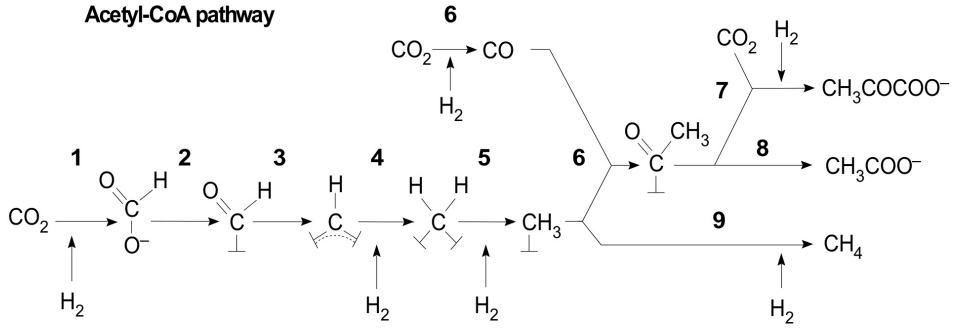

B

Step	Reaction		Cofactor	Subunit size kDa
Moorella thermoacetica				
1	Formate dehydrogenase		MoCo; NADPH	177
1'	Hydrogen dependent CO_2 reductase		MoCo	169
2	10-Formyl H_4 folate synthetase		H_4F, ATP	61
3	5,10-Methenyl H_4 folate cyclohydrolase			
4	5,10-Methylene H_4 folate dehydrogenase		NADPH	31
5	5,10-Methylene H_4 folate reductase		Fd	34
6	CoFeS, Methyltransferase, CODH/ACS		Cobamide; CoA	193
7	Pyruvate synthase		Thiamine; Fd	129
8	Phosphotransacetylase, acetate kinase		P_i, ADP	66
1-6, 7	$H_2 + CO_2$ to pyruvate	~5300 amino acids, 7 cofactors		~580 kDa
1-6, 8	$H_2 + CO_2$ to acetate	~5900 amino acids, 9 cofactors		~510 kDa
Methanothermobacter marburgensis				
1	Formylmethanofuran dehydrogenase		MoCo; MF	200
2	Formyl transferase			32
3	5,10-Methenyl H_4 methanopterin cyclohydrolase		H_4MPT	35
4	5,10-Methylene H_4 methanopterin dehydrogenase		F_{420}	30
4'	[Fe]-hydrogenase (under Ni limitation)		FeGP	43
5	5,10-Methylene H_4 methanopterin reductase		F_{420}	35
6	CoFeS, Methyltransferase, CODH/ACS		Cobamide; CoA	357
7	Pyruvate synthase		Thiamine; Fd	92
9	Heterodisulfide reductase, MtrA-H methyltransferase		CoM, CoB	302
1-6, 7	$H_2 + CO_2$ to pyruvate	~7100 amino acids, 8 cofactors		~781 kDa
1-6, 9	$H_2 + CO_2$ to methane	~9800 amino acids, 10 cofactors		~980 kDa
Awaruite (Ni_3Fe) in H_2O				
1-7	$H_2 + CO_2$ to pyruvate	0 amino acids, 0 cofactors		0
1-6, 8	$H_2 + CO_2$ to acetate	0 amino acids, 0 cofactors		0
1-6, 9	$H_2 + CO_2$ to methane	0 amino acids, 0 cofactors		0

FIGURE 3 | Chemical conversions in the acetyl CoA pathway. **(A)** The pathway as drawn by Fuchs (2011) but including the finding that in the methanogen pathway free formate is formed (Wagner et al., 2016). Modified from Preiner et al. (2020). The ligands of carbon represented as "⊥" are nitrogen atoms of pterin cofactors in the case of formyl, methenyl, methylene, and methyl groups in Reactions 3–5, cobalt and nickel atoms in the case of methyl group at Reaction 6, nickel atoms for the acetyl group at Reaction 6, or sulfur atoms in Reactions 8 (CoA) and 9 (CoM) (see Maden, 2000; Svetlitchnaia et al., 2006; Ragsdale and Pierce, 2008; Thauer et al., 2008; Ragsdale, 2009). **(B)** Cofactor requirements and the monomeric subunit size of the enzymes involved in the pathway in the acetogen *Morella* and the methanogen *Methanothermobacter* as summarized in the legend of Figure 1 of Fuchs (2011). Methyl syntheses in the bacterial pathway (also termed the Wood-Ljungdahl pathway) and the archaeal pathway differ in terms of their enzymology and cofactor requirements (Fuchs, 2011). The alternative [Fe]-hydrogenase (Huang et al., 2020), Reaction 4 of the methanogen, which is expressed under Ni limitation, is indicated. At the bottom of **(B)**, the end products of reactions catalyzed by awaruite (Preiner et al., 2020) are shown.

as "⊥") in the acetogen and methanogen pathways identical. Also, the pathway presented by Fuchs (2011) indicates the classical route of formate formation via NADPH-dependent formate dehydrogenase, whereby recently an alternative enzyme of formate synthesis in acetogens was reported, an H_2-dependent CO_2 reductase (Schuchmann and Müller, 2013) present in *Acetobacterium woodii* and *Thermoanaerobacter kivui*. It is conspicuous that, with the exception of CO and formate, substrate carbon is covalently bound either to cofactors or to active site atoms of the enzymes until released as acetate or methane (energy metabolism) or pyruvate (carbon metabolism).

Although not shown in **Figure 3A**, both pathways can assimilate environmentally available methyl groups via methyl transferases proximal to ACS or heterodisulfide reductase (Ragsdale, 2008; Thauer et al., 2008; Berg, 2011; Fuchs, 2011; Mayumi et al., 2016). Reductants in the pathway are indicated as H_2, which is the environmental source of electrons during growth on H_2 and CO_2, although the reduced cosubstrates of the reactions are either NAD(P)H, reduced ferredoxin, or F_{420} (Fuchs, 2011). **Figure 3B** summarizes the names and molecular mass of the subunits of the enzymes of the acetyl CoA pathway from the acetogen *Morrella thermoacetica* and the methanogen *Methanothermobacter marburgensis*, compiled from the information in the legend of Figure 1 from Fuchs (2011). For the acetogen pathway, 10 enzymes with a subunit mass of more than 500 kDa and seven or nine cofactors are involved in the synthesis of pyruvate or acetate. Each of the cofactors (NADH, MoCo, thiamine, tetrahydrofolate, cobamide, CoA, ADP) has its own biosynthetic pathway of similar enzymatic demand. For the methanogen pathway, the situation is similar (>700 kDa), but perhaps more demanding because of the participation of additional cofactors including methanofuran, coenzyme B, coenzyme M, and F_{420}, all of which have their own demanding biosynthetic routes (White, 2001; Graham and White, 2002).

Considering the intense enzymatic effort acetogens and methanogens invest into making pyruvate, acetate, and methane out of H_2 and CO_2 (**Figure 3B**), what initially looked simple starts looking like an insurmountable hurdle for prebiotic chemistry. We were therefore very surprised to find that formate, acetate, pyruvate, and methane are synthesized from H_2 and CO_2 under mild alkaline hydrothermal conditions (100°C, 24 bar, 16 h) using only one very simple and naturally occurring iron nickel compound, awaruite (Ni_3Fe, both metals in the elemental zero valent state), as the catalyst (Preiner et al., 2020). That is, the entire function of the acetyl CoA pathway in carbon metabolism can be replaced by a piece of metal.

The findings of Preiner et al. (2020) fall very much in line with the old biochemical axiom that transition metal biocatalysis and transition metal sulfide clusters are ancient relicts from the early phases of chemical evolution (Eck and Dayhoff, 1966; Hall et al., 1971; Wächtershäuser, 1992; Volbeda and Fontecilla-Camps, 2006). The conversions of H_2 and CO_2 to formate, acetate, pyruvate, and methane shown in **Figure 3A** all involve transition metals. The hydrogenases of archaea and bacteria that channel electrons into CO_2 reduction all have either Fe or Fe and Ni at their active sites (Thauer, 2011). Most, but not all, of those hydrogenase reactions reduce FeS clusters and then soluble redox cofactors or ferredoxins as the initial product of the hydrogenase reaction. The exception is the [Fe] hydrogenase (Hmd) of methanogens that lack cytochromes. Hmd transfers the electrons directly from H_2, which is bound by the active site iron-guanylylpridinol (FeGP) cofactor, to an organic substrate, methenyl H_4MPT, generating methylene H_4MPT (Huang et al., 2020). This property of direct organic substrate reduction is so far unique among H_2-activating enzymes (Huang et al., 2020). In **Figure 3B**, the biological reactions of the pathway involve catalysis requiring transition metals (Drennan et al., 2004; Dobbek, 2018), usually coordinated by sulfur (Sousa et al., 2018), sometimes coordinated by carbon (Martin, 2019), sometimes coordinated by nitrogen (Wongnate et al., 2016), or in the case of the Fe atom in Hmd, all three plus oxygen (the resting state VI of the mechanism; Huang et al., 2020). Catalysis and redox chemistry via transition metals and transition metal clusters, traditionally viewed as ancient, are the underlying theme of the acetyl CoA pathway.

That a single alloy, awaruite (Ni_3Fe), can substitute for the entire enzymatic pathway (**Figure 3**) is either surprising or expected, depending on one's standpoint. Awaruite is a typical constituent of serpentinizing systems. It is formed there by reduction of the divalent metals in host rocks by H_2 from serpentinization (Krishnaro, 1964). A very similar spectrum of small organic products, but without methane detection, was obtained without H_2, using native iron alone as both the catalyst and the reductant (Varma et al., 2018). Taken together, those findings indicate two things. First, the backbone of carbon and energy metabolism in acetogens and methanogens unfolds naturally from H_2 and CO_2 with a catalyst, Ni_3Fe, which consists only of metal atoms and hence could not be simpler. Second, the findings provide concrete chemical evidence to support the view that the acetyl CoA pathway is not only ancient, as those who have worked on it always suspected, but it is older than the enzymes that catalyze it, either today or in the very first cells. The acetyl CoA pathway is older than the genes that encode its enzymes.

Given those observations, what are the solutions to the three problems? For bifurcation (generating low-potential reduced ferredoxin from H_2), the solution is that serpentinization generates alkaline and H_2-rich hydrothermal fluid. The midpoint potential of the low potential ferredoxins in acetogens and methanogens is on the order of −500 mV (Buckel and Thauer, 2013). The midpoint potential of H_2 at pH 7 and 1 atm H_2 is −414 mV. Flavin-based electron bifurcation provides a mechanism to generate low-potential ferredoxins for CO_2 reduction (Buckel and Thauer, 2013; Müller et al., 2018). The midpoint potential of hydrothermal effluents stemming from serpentinizing systems can reach −900 mV (Suzuki et al., 2018). This introduces the possibility that organisms living in such environments might not need bifurcation for reduced ferredoxin synthesis (Sousa et al., 2018; Boyd et al., 2019). At origins, similar considerations apply. Using the Nernst equation for the dissociation of H_2 into protons and electrons, the H_2 partial pressures (1–10 atm), temperatures (100°C), and pH (8–10) used in the H_2-dependent CO_2-reducing reactions reported by Preiner et al. (2020) correspond to midpoint potentials in the range of −592 to −777 mV, sufficient for conversion of CO_2 to organics or ferredoxin reduction if suitable catalysts are provided. The

reducing power of serpentinizing systems in the Earth can, in principle, functionally substitute for electron bifurcation in cells by providing conditions sufficiently reducing to generate reduced ferredoxin (Sousa et al., 2018; Boyd et al., 2019), but whether this occurs in modern metabolism is so far unknown. In an origins context, however, it is now clearly demonstrated that methyl groups can be generated from H_2 and CO_2 under hydrothermal conditions using iron minerals without cofactors or enzymes (Preiner et al., 2020).

For the methyl synthesis problem, the solution is that in the presence of awaruite, or magnetite (Fe_3O_4) or greigite (Fe_3S_4), methyl synthesis from H_2 and CO_2 under hydrothermal conditions is facile (Preiner et al., 2020). Acetogens and methanogens have to invest energy in the form of ATP or reduced ferredoxin to generate methyl groups in the acetyl CoA pathway. That is the crux of the early formyl pterin problem. Modern serpentinizing systems emit methane in their effluent (Proskurowski et al., 2008; Etiope and Schoell, 2014), and methyl groups, as well as methanol itself, arise readily from H_2 and CO_2 in the presence of hydrothermal minerals as catalysts (Preiner et al., 2020). That indicates that the pathway could have gotten started with CODH/ACS as the first enzyme, operating with a geochemical supply of methyl groups, followed by independent origins (Sousa and Martin, 2014) of the unrelated methyl synthesis pathways of the bacteria and archaea. That would solve the energetic aspect of the early formyl pterin problem and explain why the chemistry of the pathway is so similar in bacteria and archaea (**Figure 3A**), but the enzymes and cofactors involved are so different. Enzymes do not shift equilibria; they just accelerate reactions that tend to occur anyway. The reactions were there first; the enzymes increased the reaction rates (Wolfenden, 2011).

For ion gradient formation, the solution is that the serpentinization process generates magnesium hydroxides from magnesium silicates (Bach et al., 2006; Russell et al., 2010; Sleep et al., 2011) with the result that the effluent of serpentinizing systems is generally alkaline, on the order of pH 9–11. This creates an ion gradient relative to the modern ocean, ca. pH 8 on the outside of the vent and ca. pH 9–11 on the inside. On the early Earth, the global ocean was more acidic, however, on the order of pH 6, because vast amounts of CO_2 dissolved in it. Thus, in serpentinizing hydrothermal vents of the Hadean, alkalinity generated by serpentinization created a pH gradient, a proton (H^+ ion) gradient, between the emerging effluent of the serpentinizing system and the ocean bottom water at the vent ocean interface of roughly three to four orders of magnitude. The polarity of the gradient is the same as that in modern cells: more alkaline on the inside than on the outside, generating a proton motive force from outside to in Martin and Russell (2007), Lane et al. (2010), Lane and Martin (2012)). That is about the same ΔpH range that biological systems generate in the process of ion pumping for the purpose of ATP synthesis. Such a geochemically generated ion gradient could have been harnessed by an ATPase at the origin of biochemistry, once genes and proteins had evolved (Martin and Russell, 2007; Martin, 2012). This solves the problem of how ion gradients arose before there were specific biochemical mechanisms to generate them: the first biochemical systems arose in environments where geochemical ion gradients were naturally existing (Russell and Hall, 1997; Martin and Russell, 2007; Lane et al., 2010; Sojo et al., 2014). Again, the polarity of ion gradients at alkaline hydrothermal vents (more alkaline on the inside than on the outside) is exactly the same as in cells (Martin and Russell, 2007; Lane and Martin, 2012). The evolutionary relationship of substrate-level phosphorylation (SLP) to chemiosmotic coupling is traditionally viewed as SLP coming first with chemiosmotic coupling coming later (Lipmann, 1965; Decker et al., 1970; de Duve, 1991; Ferry and House, 2006; Martin and Russell, 2007). Chemiosmosis enables energy conservation with substrates that provide less energy than necessary for SLP (Schuchmann and Müller, 2014).

PHOSPHATE AND ENERGY

Although serpentinizing systems solve several problems in early physiological evolution, they present another: How, in terms of energetics, could genes and proteins (protein synthesis is ATP and GTP dependent) have evolved before a universal mechanism of ATP synthesis, ion gradient harnessing via a rotor–stator ATP synthase, which is a protein encoded by genes, had come to be? This question touches many facets of the origins problem, because it concerns the relationship between nucleic acids as molecular memory, peptides as catalysts, and the coupling of environmental energy to the polymerization reactions that generate both classes of biopolymers from their monomers. This harkens to the genetics-first versus metabolism-first discussion, which is widely thought to stem from the clash in the origins literature of the 1990s between Wächtershäuser's ideas about pyrite-based metabolism contra efforts by proponents of an RNA world to quash them. As with most debates, the debate is older, as summarized yet again by Lipmann (1965; his opening statement on p. 259): "My motivation for entering into this discussion is an uneasy feeling about the tenet that a genetic information transfer system is essential at the very start of life. All efforts seem to be fixed exclusively on using presumably available energy sources, for example, electric discharges, for synthesizing nucleotides and amino acids and, therefrom, polynucleotides and polypeptides from various carbon–nitrogen sources. As I interpret it, the fascination with the two classes of compounds indicates the assumption that they are essential at the very outset. Being dissatisfied with this fixation on starting with the hen rather than with the egg, I have attempted to find alternatives. I am afraid that what I have to say will be just as much natural philosophy as necessarily most discussion on the origin of life need be at present. But try we must." The concern from physiology that origins research is too focused on nucleic acids has tradition. In brief digression, note that Lipmann's essay also discusses H_2, H_2S, and iron ions as sources of energy, in addition to a statement (p. 265) that will ring true to those interested in acetogens and methanogens: "I find it possibly of relevance that hydrogen activation, which would be involved here, is mediated by one of the more primitive catalysts, the recently discovered ferredoxin."

Living cells are approximately 80–90% water by fresh weight. Nonetheless, a common criticism of hydrothermal systems as

sites for biochemical origins is that they are full of water. This criticism typically comes from the genetics first camp and is based on the argument that, in aqueous solution, peptide bonds and the phosphoester bonds linking nucleotides will hydrolyze, leading to an inference that systems containing genetic material could not have evolved in a permanently aqueous environment (Bada and Lazcano, 2002; Orgel, 2008). Rather than prompt a conclusion that life must have evolved where there was no water (Benner and Kim, 2015), the thought about polymer hydrolysis should prompt the question: How does life deal with this problem? The answer is that life harnesses environmentally available energy and couples it to the synthesis of peptides and nucleic acids such that their polymerization is much faster than their hydrolysis. Let us assume for the sake of argument that it has always been this way. The hen to which Lipmann alluded was biopolymers; the egg was energy harnessing.

In biological systems, energy is mainly saved and spent in the currency of high-energy phosphate bonds: acyl phosphates, phosphoanhydrides, phosphoamides, carbamoyl phosphate, and phosphoenolate, all of which were known in 1941 (Lipmann, 1941). Phosphorus forms long covalent bonds with oxygen (Wald, 1962). This invites nucleophilic attack by water. The P–O and P–N bonds in the organophosphates of energy metabolism have high free energies of hydrolysis. In terms of Gibbs free energy under standard conditions at pH 7 ($\Delta G_0'$), hydrolysis of these high-energy phosphate bonds in metabolism releases on the order of −60 to −30 kJ/mol (**Table 1**). This release of free energy, if coupled to a slightly endergonic reaction, can make the reaction go forward. Coupled to many reactions, the hydrolysis of high-energy bonds makes the metabolism of a whole cell (life) go forward. That means that the high-energy bonds must constantly be resynthesized; otherwise, life comes to a halt. An *Escherichia coli* cell synthesizes roughly of 30 billion ATP (30 pg) or approximately 30 times its bodyweight (1 pg) per cell division (Akashi and Gojobori, 2002), a human synthesizes about a bodyweight of ATP per day.

As Lipmann (1965) pointed out, there are two mechanisms to make ATP. There is substrate-level phosphorylation (Lipmann called it fermentative phosphorylation or extract phosphorylation) in which a phosphate-containing carbon compound (**Table 1**) with a sufficiently high-energy bond phosphorylates ADP in a stoichiometric reaction. The other way to make ATP is the chemiosmotic mechanism of Mitchell (1961) with ion pumping plus ion gradient harnessing, which Lipmann called oxidation-chain phosphorylation because the mechanism of electron transfer to coupling via the ATP synthase had not yet been worked out. Lipmann concluded that substrate-level phosphorylation entailed a far simpler machinery; hence, it was the more ancient form of making high-energy phosphate bonds. From today's perspective, that still seems correct (Martin and Thauer, 2017).

TABLE 1 | Free energy of hydrolysis for some biological compounds.

Phosphoenolpyruvate[a]	$\Delta G^{o\prime} = -62$ kJ·mol^{-1}
1,3-Bisphosphoglycerate[b]	$\Delta G^{o\prime} = -52$ kJ·mol^{-1}
Acetyl phosphate[a]	$\Delta G^{o\prime} = -43$ kJ·mol^{-1}
Creatine phosphate[a]	$\Delta G^{o\prime} = -43$ kJ·mol^{-1}
Carbamoyl phosphate[b]	$\Delta G^{o\prime} = -39$ kJ ol^{-1}
Acetyl CoA[c]	$\Delta G^{o\prime} = -32$ kJ·mol^{-1}
ATP (to ADP)[a]	$\Delta G^{o\prime} = -31$ kJ·mol^{-1}
Glucose-1-phosphate[a]	$\Delta G^{o\prime} = -21$ kJ·mol^{-1}
Inorganic pyrophosphate[d]	$\Delta G^{o\prime} = -20$ kJ·mol^{-1}
Glucose-6-phosphate[a]	$\Delta G^{o\prime} = -14$ kJ·mol^{-1}

Values from Berg et al. (2015)[a], Thauer et al. (1977)[b], Buckel and Eggerer (1965)[c], and Frey and Arabshahi (1995)[d].

But Lipmann (1965) blazed a too seldom questioned trail in origins literature by suggesting that the participation of high-energy phosphate bonds in metabolism started with inorganic pyrophosphate (PP_i) as the first chemical energy currency, coupled with his notion that SLP is more ancient than the ion gradient phosphorylation, which led to the idea that the entry of high-energy phosphate bonds into primitive metabolism came from high-energy phosphate bonds in phosphorus minerals in the environment. Although Lipmann's idea of obtaining metabolic energy from pyrophosphate or polyphosphate minerals in the environment has a long tradition of acceptance in origins literature (Morowitz, 1992; Russell, 2006; Deamer and Weber, 2010; Pasek et al., 2017), the idea does not withstand inspection (see following paragraph). It furthermore distracts from the main issue at hand—the coupling of exergonic reactions of carbon reduction to early energy conservation (see following section).

One problem with PP_i or other environmental sources of preformed "high-energy" phosphorous bonds as the starting point for high-energy organophosphate bonds in metabolism is that it has no homolog in biology. That is not to say that there are no PP_i-dependent reactions in metabolism—there are many. The point is that no biological systems are known to this author that access environmental PP_i or environmental polyphosphates as a source of energy. Stated another way, what cell will grow chemotrophically from PP_i or polyphosphate without the involvement of redox chemistry? None is probably the answer. The only examples from biology in which environmentally available phosphorous compounds play a role in energy metabolism involve phosphite as an electron donor in ion-pumping electron transport chains (Schink and Friedrich, 2000). The phosphite oxidizers are fascinating and important; they also clearly show that there is enough phosphite in the environment to support the existence of phosphite-reducing electron transport chains. However, that circumstance has nothing to do with Lipmann's suggestion that environmental PP_i was a primordial energy source or an ancient energy currency. Another problem with PP_i that is equally pressing, if not more so, is that PP_i has a lower free energy of hydrolysis than glucose-1-phosphate (**Table 1**); it has low group transfer potential and is thus fighting a steeply uphill energetic battle in any effort to phosphorylate ADP for SLP or to activate any metabolic compound via formation of phosphoanhydride, phosphoester, or similar bonds. With the advantage of 50 years of hindsight following Lipmann's 1965 suggestion, we now know that the most common function of PP_i in metabolism is not in energy metabolism, but immediate hydrolysis following reactions in which ATP is cleaved to AMP and PP_i so as to make the

reaction irreversible under physiological conditions, such as in the activation of amino acids for translation (Berg et al., 2015).

ACYL PHOSPHATES THROUGH CO_2 REDUCTION

In SLP, ATP is usually synthesized during the oxidation of a reduced carbon compound (Lipmann, 1941; Decker et al., 1970; Martin and Thauer, 2017). When de Duve (1991) suggested that phosphorolysis of a thioester bond to form an acyl phosphate, as it occurs in the reaction mechanism of glyceraldehyde-3-phosphate dehydrogenase (**Figure 4A**), might mark the entry of phosphate into metabolism, he might have had the right kind of reaction mechanism, although it appears, from my perspective, that he put it in the context of the wrong upstream and downstream reactions. Leaning on the GAPDH reaction (**Figure 4A**), de Duve (1991) was suggesting that the oxidation of reduced carbon compounds present in the environment provided the source of energy. That is exactly what Wald (1964) had said 27 years prior about the origin of metabolism: life started from glucose fermentations (see Table 1 of Wald, 1964). Whatever happened to Mereschkowsky and autotrophic origins? Wald (1964) was suggesting that life started from glucose disproportionation (glycolysis and ethanol fermentation, where acetyl CoA is ultimately the electron acceptor), whereas de Duve (1991) was suggesting that sugars were oxidized with Fe^{3+} in the oceans being his preferred electron acceptor. The idea that there were enough free sugars lying around in the environment to provide an energy source

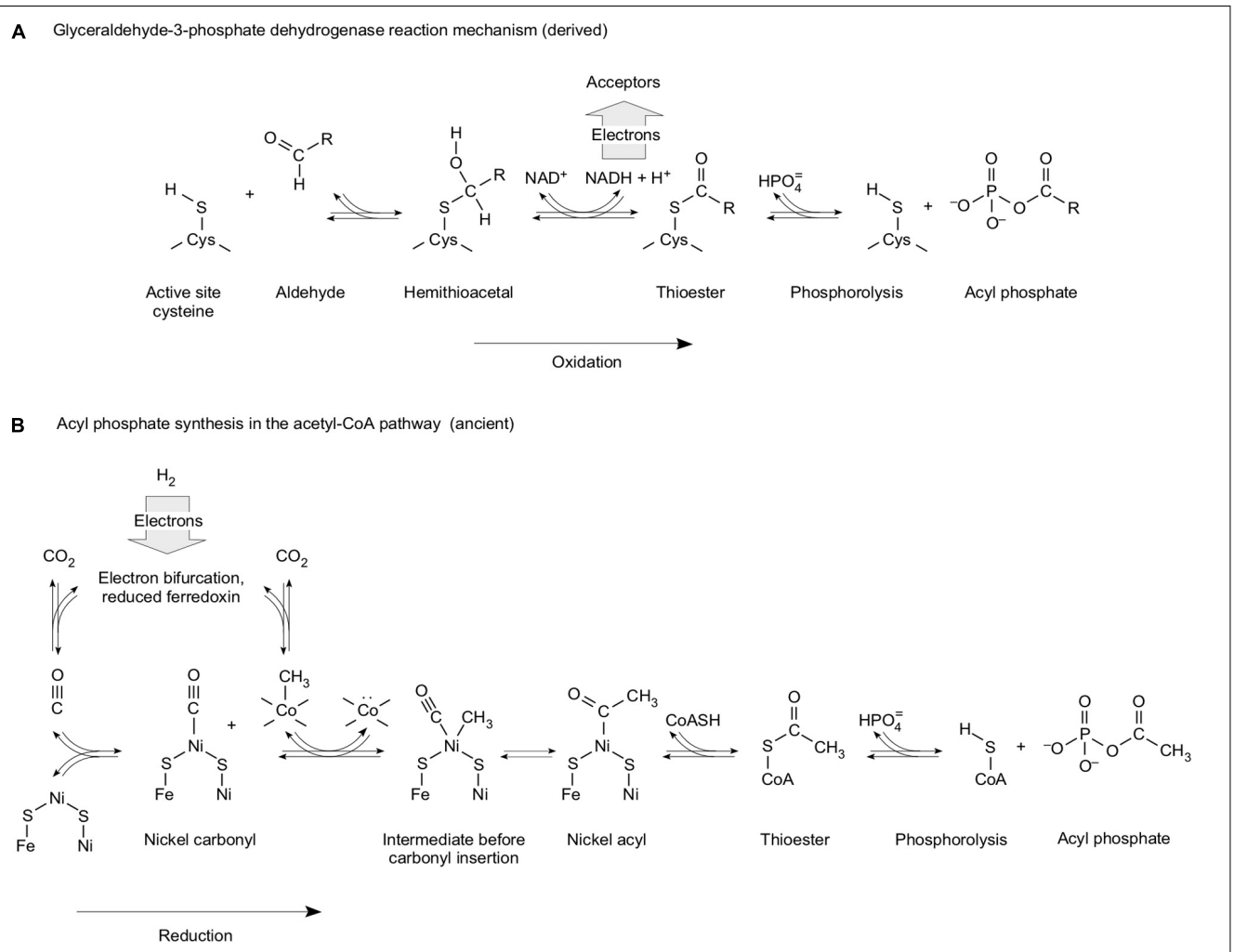

FIGURE 4 | Energy conservation as high-energy phosphate bonds from carbon oxidation and carbon reduction [modified from Martin and Cerff (2017)]. **(A)** Mechanism of the D-glyceraldehyde-3-phosphate dehydrogenase reaction in the glycolytic (oxidative) direction to generate the mixed anhydride bond in 1,3-bisphospho-D-glycerate. *R* = $CH(OH)CH_2OPO_3^{2-}$. The vertical arrow underscores the oxidative nature of the reaction in the energy-conserving direction. **(B)** Synthesis of acyl phosphate from H_2 and CO_2 as it occurs in the acetyl CoA pathway. Modified from Martin and Cerff (2017) and Martin and Thauer (2017). The reactions are drawn from data compiled in Svetlitchnaia et al. (2006), in Ragsdale (2009), in Fuchs (2011), and in Schuchmann and Müller (2014). Some methanogens can generate reduced ferredoxin via an energy-conserving hydrogenase, Ech, which does not entail bifurcation, but operates at the expense of an ion gradient, the generation of which demands bifurcation at the Mvh–Hdr complex (Thauer et al., 2008) in methanogens without cytochromes.

for first life is still current in modern literature (Keller et al., 2014). More likely is the idea (**Figure 2**) that free sugars are made by cells from CO_2 (Say and Fuchs, 2010; Fuchs, 2011). At any rate, following Lipmann's lead, de Duve (1991) suggested that the acyl phosphate could be used to form PP_i as an ancestral metabolic energy currency, whereby PP_i will not work as an energy currency, as we saw above. The oxidation of preexisting reduced carbon compounds as a source of energy is couched in the outdated (Maden, 1995) concept of an organic soup, 100 year-old notion tracing to Oparin and Haldane concerning the origin of organic compounds in the first place. Soup was once popular (Garrison et al., 1951), but that was at a time before much was known about energy conservation in anaerobic autotrophs. That is, de Duve (1991) was deriving thioesters via analogy to heterotrophic metabolism.

In heterotrophic metabolism, SLP is always coupled to oxidation of reduced carbon substrates (Decker et al., 1970) except at the glycine reductase reaction of Stickland reactions, which generates acetyl phosphate (Andreesen, 2004). A carbon-oxidizing start to metabolism will not work, because a soup of substrates will be too complex to support energy metabolism (Schönheit et al., 2016), and because if strong oxidants are invoked, the accumulation of reduced organic compounds is thermodynamically unfavorable in the first place (Sousa et al., 2013). In autotrophy, carbon backbones unfold in a very natural and orderly manner that specifically generates the compounds of the acetyl CoA pathway (**Figure 3**).

Here, a point cannot be overemphasized. In SLP, the high-energy organophosphate bonds that are used to make ATP are formed by reactions of reactive carbon backbones with phosphate. It is not the reaction of reactive phosphorus compounds with unreactive organic substrates. It is the reaction of unreactive phosphate with reactive carbon compounds. The energy in the high-energy organophosphate bonds that are used for SLP (acyl phosphates, phosphoenolate) resides in carbon, not in phosphorus.

In autotrophic metabolism, acetyl phosphate can be synthesized for SLP during the process of CO_2 reduction. SLP powered by CO_2 reduction appears to be restricted to the acetyl CoA pathway. In that sense, **Figure 3A** (CO_2 reduction) and **Figure 4B** (energy conservation) overlap well. In metabolism, phosphate is a cofactor, not a source of energy. It is an innocent bystander that forms a high-energy bond by its ability to perform nucleophilic attack of a reactive carbonyl. Does **Figure 4B** recapitulate a primordial reaction sequence coupling of CO_2 reduction and energy metabolism? It well could be. Does that energy coupling work without enzymes? Almost.

The phosphorylation of ADP with acetyl phosphate is facile in the presence of Fe^{3+} (Kitani et al., 1991, 1995); acetyl phosphate can be readily generated from thioacetate and phosphate (Whicher et al., 2018). So far, no synthesis of acyl phosphates from CO_2 and P_i has been reported. Would acyl phosphates from scratch be a big advance? It clearly depends on one's point of view. It would help to explain how early energetic coupling was possible.

Findings from various disciplines tend to home in on the acetyl CoA pathway when it comes to origins. Investigations into ancient metabolism from the standpoint of modern metabolic networks are uncovering clues that converge on the acetyl CoA pathway (Goldford et al., 2017, 2019). Autocatalytic cycles can be identified within the metabolism of methanogens and acetogens (Xavier et al., 2020). Reactive chemical networks based on thioesters have been reported (Semenov et al., 2016). Starting from products of the acetyl CoA pathway, reactions of the reverse citric acid cycle take place in the absence of enzymes (Muchowska et al., 2017, 2019). Tryptophan is synthesized deep in geochemical systems (Ménez et al., 2018), which supports to the idea that reductive reactions at hydrothermal vents could have fostered life (Baross, 2018). Genomic reconstructions of LUCA indicate that it lived from gasses, using reactions and enzymes germane to the acetyl CoA pathway (Weiss et al., 2016). The enzymes of the acetyl CoA pathway are not only replete with transition metal sulfide centers (Russell and Martin, 2004), but they also contain half of all the carbon–metal bonds currently known in biology (Martin, 2019). Carbon–metal bonds are extremely rare in metabolism, and they are ancient. They occur only in enzymes that form the interface between metabolism and the gasses from which LUCA lived (H_2, CO_2, N_2), or in enzymes and cofactors that transfer methyl groups, as shown in **Figure 4B**, or in cofactors that initiate radical reactions (Martin, 2019). They appear, to me at least, to be relicts of the catalysts that gave rise to primordial physiology.

AMINO ACYL PHOSPHATES

And what good are acyl phosphates? They are energy currency, better than ATP. A look at Katchalsky and Paecht (1954, p. 6042) reveals that "In aqueous solution at room temperature, the phosphate anhydride of leucine polymerizes spontaneously to produce polypeptides of 3–20 amino acids." Significant? Clearly, an energetic coupling of CO_2 reduction to acyl or amino acyl phosphate synthesis would enable a great many biologically relevant reactions, such as peptide synthesis. One thinks of small molecule chemical networks of the kind that Kauffman had in mind (Xavier et al., 2020), and the words of Shapiro, who like Kauffman and many others was unconvinced that genetic material (the "hen" in Lipmann's 1965 quote) came before the exergonic synthesis of the chemical components of which its monomers are comprised (the "egg"): "A more likely alternative for the origin of life is one in which a collection of small organic molecules multiply their numbers through catalyzed reaction cycles, driven by a flow of available free energy. Although a number of possible systems of this type have been discussed, no experimental demonstration has been made. The inclusion of a 'driver' reaction, directly coupled to the energy source, may lead to a solution" (Shapiro, 2006, p. 105). Spontaneous reactions that couple a biological driver reaction to synthesis of a biological energy currency cannot be far away. The overall reaction will probably look very much like acetogen energy metabolism, but with metals in place of enzymes. If carbon-based energy metabolism came first, carbon metabolism and, given a natural source of activated

nitrogen (Preiner et al., 2018), the rest of metabolism would naturally follow.

PATTERNED EVOLUTION OF PATHWAYS, NOT RETROGRADE EVOLUTION

Prior to the publication of this article, a reader lamented that I seemed to be assuming retrograde evolution of pathways without saying so. This article is not about retrograde evolution of pathways; it is about the antiquity of a CO_2 fixing pathway in the context autotrophic origins, which posit the outward evolution of pathways emanating from CO_2, which is the opposite of retrograde evolution. Hence, there is clearly a gap in understanding between this author's text and one reader's subjective interpretation of same concerning the evolution of metabolism. Other readers might encounter the same problem, so it is worthwhile to briefly recapitulate retrograde pathway evolution and contrast it to the ideas in the present article.

The term "retrograde" comes from *retro* (Latin, backward) and *gradus* (Latin, step), or stepping backward. The concept of retrograde evolution of pathways traces to an article by Horowitz (1945), who argued that in the beginning there was a rich organic soup of the components from which cells are composed, amino acids bases and the like, in line with ideas of Oparin. These components, the products of modern pathways, became depleted through biological activity, creating pressure to synthesize them from their immediate biosynthetic precursors, which are presumed to exist in the soup as well. Notably, Horowitz assumes the existence of heterotrophic cells as the starting point of retrograde pathway evolution. Depletion of a given product Z creates pressure for the terminal enzyme in the pathway to be fixed so as to supply Z from precursor Y in a one-step pathway. In this way, the last enzyme in the pathway evolves first, catalyzing the reaction Y → Z. Subsequent depletion of Y generated, in turn, the pressure to supply Y from its preexisting precursor X, leading to evolution of the next to last enzyme in the pathway, catalyzing the reaction X → Y, yielding a pathway X → Y → Z, and so forth. In this way, pathways and metabolism as a whole evolved from the distal tips, the products, inward to the proximal core of central intermediates from which all products (amino acids and bases) are synthesized.

From tips to root means backward steps in evolution along the pathway relative to the biosynthetic direction, hence retrograde, although Horowitz did not use that word. Horowitz required the pathway evolving species to be heterotrophic for the compound in question, or in modern terms auxotrophic for all pathway products, taken across all pathways. Note that Horowitz's model starts with organisms, species that already are alive, such that the retrograde model describes a process of inward biochemical pathway growth in a world where genes and organisms already exist in an organic soup having all intermediates and end products of a modern metabolic map in ample supply. A related concept is that of Ycas (1974), who suggested that gene duplications for an initially small number of enzymes of relaxed substrate specificity gave rise to toward a larger collection of enzymes each having higher substrate specificity. The theories of Horowitz and Ycas concern the vector of gene and enzyme evolution after the origin of organisms. The retrograde model of Horowitz explicitly posits that the first organisms were heterotrophs.

Autotrophic theories assume that the first organisms were autotrophs that obtained carbon from CO_2. They differ from heterotrophic theories in that they assume that the organic molecules from which life arose were synthesized from CO_2 and that the evolution of biochemical pathways to complex organics (amino acids and bases) thus recapitulates a vector of biochemical evolution that starts from CO_2 and moves outward toward the tips, or products, of metabolism. In that regard, the main products that we see in metabolism today (amino acids and nucleic acids, together approximately 80% of the cell by weight) were not selected from a soup; rather, they were synthesized in a sequence of reactions such that they were the endpoints, not the starting points of biochemical evolution. In other words, heterotrophic origin theories operate via consumption of preformed products, whereas autotrophic origin theories operate via synthesis of products from CO_2. In contrast to Horowitz (1945), autotrophic theories do not start with organisms. In contrast to Ycas (1974), they do not start with genes. Rather autotrophic theories entail the concept of chemical or physiological evolution before genes, starting from CO_2. That is true for autotrophic theories of Mereschkowsky (1910), of Wächtershäuser (1992), of Shapiro (2006), and for autotrophic theories that are based on the acetyl CoA pathway (Martin and Russell, 2007).

Autotrophic theories have in common that they assume that life and metabolism started from CO_2, hence that biochemical synthesis evolved from C_1 compounds to C_2 compounds to C_3 and larger, such that the origin of metabolic networks was a process of growth from simpler to more complex (Wächtershäuser, 1992; Martin and Russell, 2007). Investigations of metabolic maps to uncover ancient cores and structures in metabolism are much in line with that view, as they uncover conservation surrounding an autotrophic core (Goldford et al., 2017; Xavier et al., 2020). The same core is uncovered in gene evolution studies that trace ancient genes to LUCA (Weiss et al., 2016, 2018). The most highly conserved core of that network, $C_1 \rightarrow C_2 \rightarrow C_3$, or formate → acetate → pyruvate (**Figure 3A**), unfolds in simple laboratory reactors overnight from H_2 and CO_2 using hydrothermal minerals as catalysts (Preiner et al., 2020).

That said, what do autotrophic theories say about the evolution of genetically encoded biochemical pathways? Autotrophic theories assume that there was a process of chemical "evolution" before genes came into existence, whereby the term "evolutionary" in this context designates increases in complexity, not mutation or selection (processes connoting genes). Genes require the existence of the code; this article is not about the origin of the code. Once genes had arisen (we all have to agree that they did arise somewhere at some point), it is eminently reasonable to posit that the first genes to arise and evolve, in general, were those that anchored the genetic code in place, namely, aminoacyl tRNA synthetases (Carter and Wills, 2019). In terms of physiology, the first genes to arise and evolve were

likely those that channeled a necessarily exergonic preexisting flux of carbon and nitrogen into components that reinforced the synthesis of genes and proteins (Martin and Russell, 2007). A survey of genes that trace to LUCA found precisely, namely, eight genes for aminoacyl tRNA synthetases and several enzymes involved in the acetyl CoA pathway, in nitrogen metabolism, in H_2 assimilation, in cofactor biosynthesis, and in the synthesis of amino acids, bases, and modified bases (Weiss et al., 2016), which are essential for the code to operate (Becker et al., 2018; Weiss et al., 2018).

Of the autotrophic pathways known, only the acetyl CoA pathway occurs in both bacteria and archaea and enables ATP synthesis during CO_2 fixation (Berg et al., 2010; Fuchs, 2011). The reverse oxidative citric acid cycle employing citrate synthase, the roTCA cycle, requires very little ATP input (Mall et al., 2018; Nunoura et al., 2018), but it does require the hydrolysis of one ATP per acetyl CoA generated, as opposed to supporting ATP synthesis while generating acetyl CoA. The interested reader is directed to Table S10 of Mall et al. (2018) for an excellent comparison of the overall energetics and ATP demand of CO_2 fixing pathways in bacteria and archaea. In line with its favorable thermodynamics, the acetyl CoA pathway is also the only one of the autotrophic pathways known that has been shown so far to operate *in toto* without enzymes, as acetate and pyruvate are generated from H_2 and CO_2 by mineral catalysts alone (Preiner et al., 2020). Thus, from the standpoint of thermodynamics, it is the one from which to start (**Figure 3**). That would provide formate, acetate, and pyruvate, which in acetogens and methanogens spill over into the incomplete reverse citric acid cycle as the main source of carbon skeletons for biosynthesis (Martin and Russell, 2007; Fuchs, 2011; Goldford et al., 2017; Muchowska et al., 2019). The central proposition of autotrophic origins is that first biochemical pathways evolved outward from such a central core in a way that brought forth central intermediary metabolism from inorganically catalyzed non-enzymatic reactions. Inorganically catalyzed reactions came to be accelerated and channeled into metabolism-like conversions by accrual of organic catalysts (organic cofactors or their abiotic precursors) and then finally enzymes. In that sequence of events, the cofactors themselves could have been products of inorganic catalysis, with enzymes, however, being the products of genes.

This sequence of pathway evolution, namely, a sequence of CO_2 assimilating reactions starting from inorganic catalysts, progressing to organic catalysts (cofactors), and on to enzymatic (gene encoded) catalysts, entails the very broad premise that the reactions of central metabolism leading to products (amino acids and bases) tend to take place naturally. Catalysts merely accelerate chemical reactions that tend to take place anyway, or the catalysts can alter the immediate products in the case kinetically controlled reactions. In that sense, the evolution of pathways under such a set of premises for autotrophic origins is prepatterned (Ger. *vorgezeichnet*; predrawn, sketched for the purpose of subsequent bolder drawing), or simply *patterned* by the natural reactions of carbon. Some readers will ask why not use the word palimpsestic instead of patterned. Palimpsestic, in addition to lacking all prosody, emphasizes the process of overbuilding or overwriting a prior state. Patterned, and more specifically *vorgezeichnet*, places the emphasis on the process of putting the original pattern, the ancestral state, in place. Patterned evolution of pathways emphasizes the process of generating the original pattern, namely, the natural reactions of organic compounds.

Thus, the concept of patterned evolution of pathways is the autotrophic counterpart of retrograde pathway evolution inherent to heterotrophic theories. Patterned pathway evolution has it that the reactions that comprise biochemical pathways were etched into the space of all possible chemical reactions according to kinetic and thermodynamic constraints, with environmentally available and novel synthesized catalysts bearing upon the relative rates of competing reactions. As pathways evolved forward, the spontaneous chemical reactions of preceding products determined the vector of evolutionary progression. The connections between products of different pathways, sometimes connecting pathway intermediates to generate new routes and products (widespread in cofactor biosynthesis) as one moves distal to the core, emerge as a natural result of patterned pathway evolution, as does the noteworthy thermodynamic stability of the main pathway end products, amino acids, and bases. Patterned evolution of pathways would readily explain why so many reactions in metabolism work well without enzymes (Martin and Russell, 2007; Keller et al., 2015; Muchowska et al., 2019; Preiner et al., 2020; Xavier et al., 2020).

LIFE IS A CHEMICAL REACTION

The same reader who was interested in retrograde evolution also suggested that I discuss an alternative theory that life evolved from large amounts of abiotically formed acetate. As it stands, there is no such theory out there in the literature to discuss, nor is there currently clear evidence for accumulation of abiotic acetate in large amounts, in contrast to clear evidence for abiotic accumulation of formate (Lang et al., 2018) and methane (Etiope and Schoell, 2014). Furthermore, if life started from acetate, the extraction of energy would be problematic. Acetate disproportionation to H_2 and CO_2 for energy metabolism generally requires a syntrophic partner that can scavenge the H_2 so that the H_2-producing reaction is exergonic (Hattori et al., 2005), meaning that for acetate disproportionation to work as the very first metabolism, the methanogen already has to be there, such that that acetate oxidation can hardly be the first metabolism, coming in second at best. Acetate disproportionation might, however, have arisen very early after acetogenesis (Martin and Russell, 2007). The alternative energy extraction route, acetate oxidation using high-potential terminal acceptors, is not an option at origins for the same reason that methane oxidation is not an option at origins: In the presence of high-potential acceptors, the reduced carbon compounds that need to accumulate for metabolism and life to arise in the first place are converted to CO_2 (Sousa et al., 2013). The synthesis of acetate from H_2 and CO_2 is exergonic all by itself, as long as there is sufficient H_2 and as long as there are no strong oxidants around. Acetate synthesis from H_2 and CO_2 is hence

a good starting point for metabolic origins. Let's take the idea one step further.

Figure 5 summarizes metabolism in an ancient cell; an earlier and more preliminary version of the figure is found in Martin and Russell (2007). It conveys an approximation of the life process as a chemical reaction using the example of an acetogen. The starting point of **Figure 5** is a study by Drake and colleagues (Daniel et al., 1990) in which they quantified the carbon flux through the cell as acetate and into cell mass for two acetogens. For *Clostridium thermoaceticum*, they found that during growth on H_2 and CO_2 approximately 0.1 mol of carbon accumulates as cell mass for each 2.4 mol of CO_2 consumed. That is shown with the large gray arrow at the left of **Figure 5**. Thus, if we start with 2,500 atoms of carbon in CO_2, approximately 2,400 of them are converted to acetate for energy metabolism, and approximately 100 of them go to cell mass. The fate of those 100 carbons in metabolism is given by Fuchs (2011), who provided a summary of carbon distribution in an idealized primordial metabolism based on the acetyl CoA pathway. The numbers next to the arrows in **Figure 5** indicate the percent of acetyl moieties going toward C_2 metabolism or being extended by further CO_2 incorporation as given in Figure 6 of Fuchs (2011). Fuchs' 2011 figure does not extend to amino acids but includes, probably by design, exactly the compounds from which the amino acid biosynthetic families (Berg et al., 2015) are derived—pyruvate, phosphoenolpyruvate, 3-phosphoglycerate, oxaloacetate, 2-oxoglutarate, and sugars. The amino acids are used to make protein, which comprises 50% to 60% of the cell's mass.

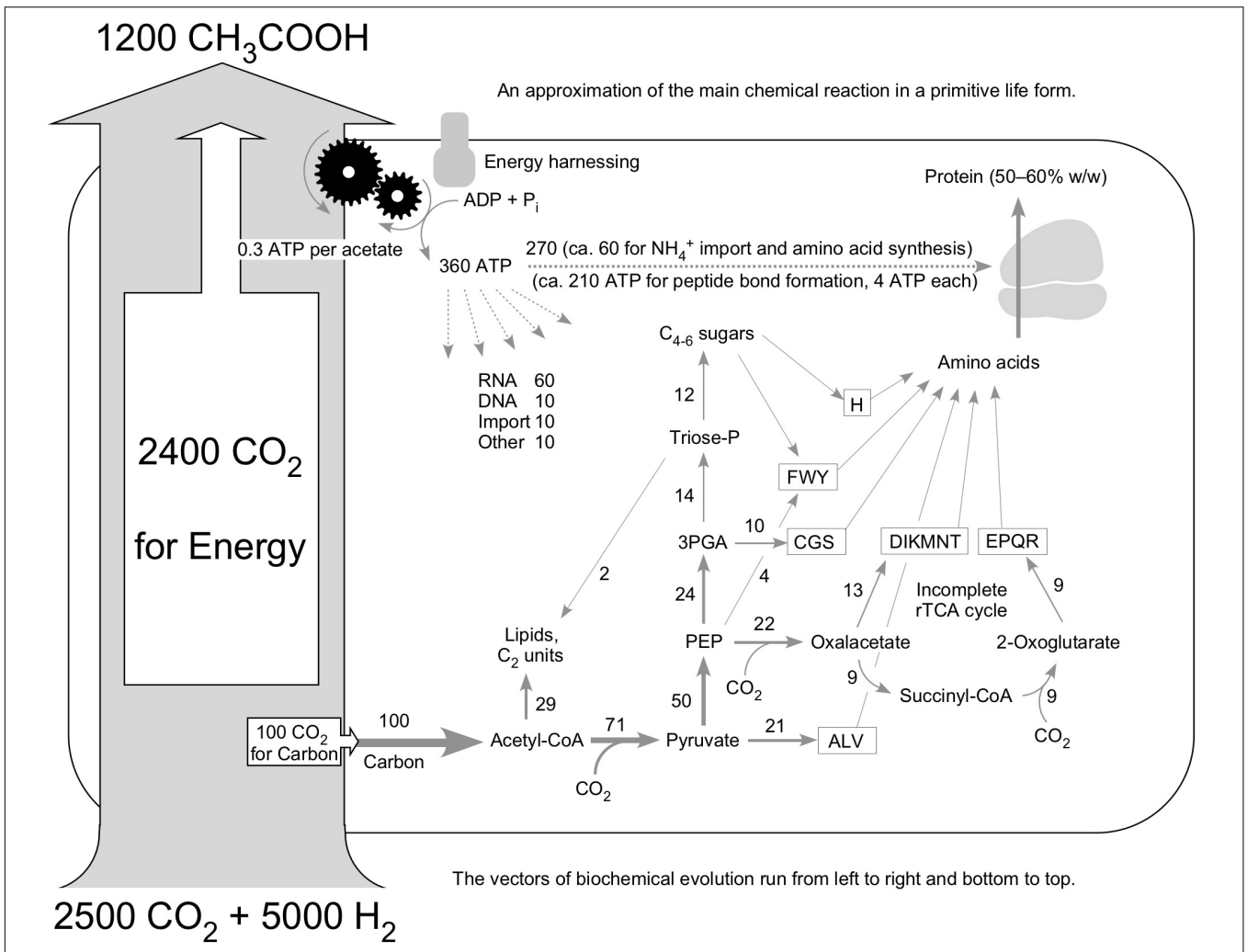

FIGURE 5 | Idealized primordial metabolism for a hydrogenotrophic acetogen (see text). The carbon pathways are taken from Figure 6 of Fuchs (2011); the amino acid biosynthetic families are taken from Berg et al. (2015); the energy investment (dotted arrows at top) is taken from Stouthamer (1978); the 24:1 carbon ratio for energy metabolism versus cell mass accumulation is taken from Daniel et al. (1990); the ATP per acetate is taken from Müller et al., 2018). For fairness, Daniel et al. (1990) also reported that 0.3 mol of the carbon was unrecovered, which is neglected here. Numbers next to arrows in carbon pathways are from Fuchs (2011) and indicate the approximate percentage of flux. Relative width of carbon flux arrows is drawn roughly to scale, including the large gray arrow at left, to underscore the relative flux of material through the cell (large) versus the residue that remains (small). The acetyl CoA pathway roughly as indicated in **Figure 4B** resides within the large gray arrow and is not shown in detail.

The "additional" CO_2 incorporations at pyruvate, oxaloacetate, and 2-oxoglutarate add up. Ten amino acids contain one additional carbon beyond the C_2 starting unit, six amino acids have two additional carbons, and four amino acids have three additional carbons that are added from CO_2. Had we started with 100 acetyl units (200 carbon atoms), pyruvate synthesis adds 71 more carbon atoms, oxaloacetate synthesis adds 22 more carbon atoms, and 2-oxoglutarate synthesis adds nine more (Fuchs, 2011), yielding 102 additional carbon atoms. Thus, per 100 carbon atoms from acetyl CoA, approximately 50 more are incorporated after acetyl CoA synthesis. The acetyl CoA pathway provides approximately two-thirds of the carbon, roughly one-third coming from subsequent incorporations.

To make protein, the amino acids have to be activated as aminoacyl tRNA, which hydrolyzes ATP to release PP_i at synthesis of the amino adenylate intermediate, requiring two ATP as input and then two steps of GTP-dependent ribosome movement, or four ATP per peptide bond (Berg et al., 2015). The energy for that comes from acetogenesis, which delivers approximately 0.27 or, rounded, 0.3 ATP per acetate, as Müller et al. (2018) worked out. For the 1,200 acetate produced, that yields approximately 360 ATP, which, if we consult Stouthamer (1978) regarding the rough distribution of energy costs across the cell, is enough to make approximately 52 peptide bonds. A smaller amount of ATP is required for RNA, DNA, and other things (**Figure 5**).

Keeping in mind that approximately only 60% of cell carbon goes to protein (cells are 50% carbon and 30% carbon in protein by weight), **Figure 5** has it that 60% of the 150 carbon atoms assimilated per 1,200 acetate, or 90 carbon atoms can be directed toward peptide synthesis. But an average amino acid has five carbons, so that there is enough energy to make 52 peptide bonds but only enough carbon to make 18 amino acids. The available energy for peptide synthesis exceeds the available carbon for peptide synthesis by approximately a factor of three. Can that be right?

A three-fold excess of energy relative to protein cell mass seems odd at first sight, but in **Figure 5**, we have not considered maintenance energy or ATP spilling, which can be substantial. Stouthamer (1973) showed that the theoretical maximum yield for cell mass for *E. coli* (on the order of 28 g per mol ATP synthesized) is approximately three times the measured value (approximately 10 g per mol ATP synthesized). *Escherichia coli* cells synthesize approximately three times more ATP than they require for biomass synthesis, similar to the situation in **Figure 5**. The efficiency of ATP utilization in living cells is often approximately three-fold lower than would be predicted from standard biosynthetic costs. This is because of the existence of processes such as maintenance energy, futile cycling, ATP spilling, and uncoupling that consume ATP (or diminish synthesis) with no yield in terms of growth or cell mass (Russell and Cook, 1995; Russell, 2007; Hoehler and Jörgensen, 2013). The theoretical maximum yield in terms of net cell mass increase per ATP is always lower than the observed value in studies of modern cells (Stouthamer, 1978); it is also lower in **Figure 5**.

Primordial carbon metabolism involves successive incorporation of CO_2 into acetyl CoA, pyruvate, oxaloacetate, and 2-oxoglutarate via the acetyl CoA pathway and incomplete reverse citric acid cycle. This conserved core provides the carbon backbones for the synthesis of amino acids, whereby amino acids (glycine, aspartate, glutamine) plus CO_2 and C_1 intermediates of the acetyl CoA pathway provide in turn the carbon backbones and nitrogen for the synthesis of purines and pyrimidines (Lipmann, 1965; Martin and Russell, 2007). Note that amino acid, sugar (for example, ribose), and nucleobase synthesis in microbial metabolism does not start from the successive incorporation of formaldehyde units (Ricardo et al., 2004), cyanide units (Canavelli et al., 2019), oxidized methane units (Nitschke and Russell, 2013), or acetate units, as one reader suggested. Rather, it starts with the successive incorporation of CO_2 units (**Figure 5**), and is energetically financed in acetogens and methanogens by exergonic reactions of CO_2 with H_2.

If we step back for a moment, we recognize that the CO_2-based design of central intermediary metabolism is a very, very strong argument in favor of autotrophic origins (carbon from CO_2). Theories based in polymerization of formaldehyde, cyanide, activated methane, or acetate do not intersect at all with central metabolism of real cells, whereas theories based in the sequential condensation of CO_2 do—seamlessly (**Figure 5**) and without corollary assumptions.

Figure 5 also underscores that synthesis of protein (the main substance of life) is a side reaction of a main exergonic reaction. It furthermore underscores the point that there is a kind of natural order in metabolism, as Morowitz (1968) suggested. Note that the line widths of gray arrows indicating carbon flux in **Figure 5**, also the large vertical one at left, are drawn roughly to scale relative to one another. The main reaction in the cell is bioenergetic. Cell mass is a byproduct.

If we keep thermodynamic constraints on metabolism in mind, it is evident that the vectors of evolutionary progression across the reactions in **Figure 5** cannot start with ribosomes at the top right, because the energy-releasing reactions required for their synthesis start at the lower left, from H_2 and CO_2. For thermodynamic reasons, the vector of evolutionary progression in **Figure 5** has to start at the bottom left. In autotrophic origins, the evolution of carbon pathways progresses from left to right and bottom to top, from simpler to complex. At the very beginning of evolution, small pathways had to start without enzymes and had to be exergonic (Preiner et al., 2020), autocatalytic reaction sets probably played a role as intermediates (Kauffman, 1986; Hordijk and Steel, 2004; Xavier et al., 2020), and, once genes arose, more specific biochemical pathways could evolve, probably in a patterned fashion, with naturally occurring chemical reactions paving the way of the evolution of the first metabolic pathways. But for all of that to occur, there had to be a continuous, uninterrupted energy-releasing reaction driving it all. H_2-dependent CO_2 reduction as it occurs at hydrothermal vents is the proposition.

The complex reactions moving left to right and bottom to top in **Figure 5** are in many cases not sufficiently exergonic to go forward by themselves and hence require come kind of chemical connection, or coupling, to the main exergonic acetate-generating reaction. In this article, I have argued that energetic coupling first involved SLP (abiotic) to generate acyl phosphates in the course of continuous acetate synthesis from H_2 and CO_2

and later involved the harnessing of naturally preexisting proton gradients by the ATP synthase subsequent to the origin of genes. I made a similar case previously (Martin and Russell, 2007; Lane and Martin, 2012), but the case is now better backed by evidence. At origins, there had to be energy harnessing from the very start, because most of the reactions in metabolism are not strongly exergonic, and some are endergonic, requiring coupling to ATP (or similar) hydrolysis to move forward. Thus, evolution at the level of genes and pathways depends, from the very start of biochemical evolution, upon exergonic redox reactions of carbon (Martin and Thauer, 2017) during H_2-dependent CO_2 reduction to acetyl CoA and pyruvate. In **Figure 5**, as in the experiments of Preiner et al. (2020), acetate is synthesized via the intermediates of the acetyl CoA pathway.

CONCLUSION

Autotrophic theories have a long tradition. Hydrogen-dependent acetogens figure centrally in modern autotrophic theory because the backbone of their metabolism, the acetyl CoA pathway, provides both carbon and energy from the H_2-dependent synthesis of acetate from CO_2. Of the six CO_2 fixing pathways known, only the acetyl CoA pathway generates ATP; the other five require ATP input. Because primordial biochemical reactions had to be exergonic, this is a strong argument for antiquity of the acetyl CoA pathway. The unique involvement of CO as an intermediate in the pathway has the consequence that it generates carboxyls (acetate) from carbonyls (acetyl), whereas the other five pathways incorporate CO_2 as carboxyls that have to be reduced to carbonyls at the cost of energy input. As with almost all forms of SLP, SLP in the acetogen pathway entails the nucleophilic attack of a carbonyl carbon in a thioester by an otherwise inert inorganic phosphate ion to generate an acyl phosphate that can phosphorylate ADP (Weiße et al., 2016). The energy in SLP thus stems from activated carbon atoms reacting with phosphate, not from compounds such as pyrophosphate, polyphosphates, phosphites, or phosphides reacting with unreactive carbon species. Because the reaction of H_2 and CO_2 continuously generates reactive carbonyl intermediates *en route* to free organic acids, the source of energy behind phosphate-based energy conservation at origins was most likely H_2-dependent CO_2 reduction, not reactive phosphorous minerals, counter to many traditional concepts about prebiotic chemistry. Primordial carbon metabolism consists of the sequential addition of CO_2 molecules to form acetyl moieties, pyruvate, oxaloacetate, 2-oxoglutarate, and sugars, from which all 20 amino acids are ultimately derived. This strongly suggests that metabolism arose from CO_2 in accordance with theories for autotrophic origins, as opposed to origins from other carbon species such as formaldehyde condensations, cyanide condensations, or methane oxidation. The central reactions of the acetyl CoA pathway to form formate, acetate, and pyruvate from H_2 and CO_2 take place overnight at 100°C without enzymes under hydrothermal vent conditions using only hydrothermal vent minerals as catalysts. This suggests that biochemical pathways evolved from CO_2 outward via a process of patterned pathway evolution, in which naturally occurring anabolic chemical reactions paved the way for reactions that later came to be catalyzed by enzymes. Patterned evolution of pathways is the autotrophic counterpart and converse of retrograde pathway evolution in heterotrophic theories. Carbon and energy metabolism as they are manifest in the metabolism of acetogens (and methanogens) that lack cytochromes growing on H_2 and CO_2 likely reflects an ancestral state of microbial physiology from which the evolution of more complex pathways involving fermentations and cytochrome-dependent electron transport chains emerged.

AUTHOR CONTRIBUTIONS

WM wrote the manuscript and prepared the figures.

FUNDING

The author thanks the ERC (666053), the VW Foundation (93046 and 96742), and the DFG (Ma 1426/21-1) for funding.

ACKNOWLEDGMENTS

The author is grateful to Verena Zimorski and Jessica Wimmer for help with preparing the paper. This paper is dedicated to the memory of Rüdiger Cerff, lifelong friend and mentor.

REFERENCES

Akashi, H., and Gojobori, T. (2002). Metabolic efficiency and amino acid composition in the proteomes of *Escherichia coli* and *Bacillus subtilis*. *Proc. Natl. Acad. Sci. U.S.A.* 99, 3695–3700.

Allen, J. F. (2005). A redox switch hypothesis for the origin of two light reactions in photosynthesis. *FEBS Lett.* 579, 963–968. doi: 10.1016/J.Febslet.2005.01.015

Andreesen, J. R. (2004). Glycine reductase mechanism. *Curr. Opin. Chem. Biol.* 8, 454–461.

Arndt, N. T., and Nisbet, E. G. (2012). Processes on the young Earth and the habitats of early life. *Annu. Rev. Earth. Planet. Sci.* 40, 521–549.

Bach, W., Paulick, H., Garrido, C. J., Ildefonse, B., Meurer, W. P., and Humphris, S. (2006). Unraveling the sequence of serpentinization reactions: petrography, mineral chemistry, and petrophysics of serpentinites from MAR 15°N (ODP Leg 209, Site 1274). *Geophys. Res. Lett.* 33:L13306. doi: 10.1029/2006GL025681

Bada, J. L., and Lazcano, A. (2002). Some like it hot, but not the first biomolecules. *Science* 296, 1982–1983. doi: 10.1126/science.1069487

Baross, J. A. (2018). The rocky road to biomolecules. *Nature* 564, 42–43. doi: 10.1038/d41586-018-07262-8

Baross, J. A., and Hoffmann, S. E. (1985). Submarine hydrothermal vents and associated gradient environments as sites for the origin and evolution of life. *Orig. Life Evol. Biosph.* 15, 327–345. doi: 10.1007/BF01808177

Basen, M., and Müller, V. (2017). Hot" acetogenesis. *Extremophiles* 21, 15–26. doi: 10.1007/s00792-016-0873-3

Becker, S., Schneider, C., Crisp, A., and Carell, T. (2018). Non-canonical nucleosides and chemistry of the emergence of life. *Nat. Comm.* 9:5174. doi: 10.1038/s41467-018-07222-w

Benner, S. A., and Kim, H.-J. (2015). "The case for a martian origin for earth life," in *Proceedings of the SPIE 9606, Instruments, Methods, and Missions for Astrobiology XVII, 96060C*, eds R. B. Hoover, G. V. Levin, A. Y. Rozanov, and N. C. Wickramasinghe (Bellingham, WA: SPIE), doi: 10.1117/12.2192890

Berg, I. A. (2011). Ecological aspects of the distribution of different autotrophic CO_2 fixation pathways. *Appl. Environ. Microbiol.* 77, 1925–1936.

Berg, I. A., Kockelkorn, D., Ramos-Vera, W. H., Say, R. F., Zarzycki, J., Hügler, M., et al. (2010). Autotrophic carbon fixation in archaea. *Nat. Rev. Microbiol.* 8, 447–460. doi: 10.1038/nrmicro2365

Berg, J. M., Tymoczko, J. L., Gatto, G. J., and Stryer, L. (2015). *Biochemistry*, 8th Edn. New York, NY: W. W. Freemann.

Boyd, E. S., Amenabar, M. J., Poudel, S., and Templeton, A. S. (2019). Bioenergetic constraints on the origin of autotrophic metabolism. *Philos. Trans. R. Soc. A* 378:20190151. doi: 10.1098/rsta.2019.0151

Buckel, W., and Eggerer, H. (1965). On the optical determination of citrate synthase and acetyl-coenzyme A. *Biochem. Z.* 343, 29–43.

Buckel, W., and Thauer, R. K. (2013). Energy conservation via electron bifurcating ferredoxin reduction and proton/Na^+ translocating ferredoxin oxidation. *Biochim. Biophys. Acta Bioenergy* 1827, 94–113. doi: 10.1016/j.bbabio.2012.07.002

Buckel, W., and Thauer, R. K. (2018). Flavin-based electron bifurcation, ferredoxin, flavodoxin, and anaerobic respiration with protons (Ech) or NAD^+ (Rnf) as electron acceptors: a historical review. *Front. Microbiol.* 9:401. doi: 10.3389/fmicb.2018.00401

Canavelli, P., Islam, S., and Powner, M. W. (2019). Peptide ligation by chemoselective aminonitrile coupling in water. *Nature* 571, 546–549.

Carter, C. W., and Wills, P. R. (2019). Class I and II aminoacyl-tRNA synthetase tRNA groove discrimination created the first synthetase–tRNA cognate pairs and was therefore essential to the origin of genetic coding. *IUBMB Life* 71, 1088–1098. doi: 10.1002/iub.2094

Corliss, J. B., Baross, J. A., and Hoffmann, S. E. (1981). An hypothesis concerning the relationship between submarine hot springs and the origin of life on Earth. *Oceanol. Acta* 4(Suppl.), 59–69.

Daniel, S. L., Hsu, T., Dean, S. I., and Drake, H. L. (1990). Characterization of the H_2^- and CO-dependent chemolithotrophic potentials of the acetogens *Clostridium thermoaceticum* and *Acetogenium kivui*. *J. Bacteriol.* 172, 4464–4471.

Deamer, D., and Weber, A. L. (2010). Bioenergetics and life's origins. *Cold Spring Harb. Perspect. Biol.* 2:a004929. doi: 10.1101/cshperspect.a004929

Decker, K., Jungermann, K., and Thauer, R. K. (1970). Energy production in anaerobic organisms. *Angew. Chem. Int. Ed.* 9, 138–158. doi: 10.1002/anie.197001381

de Duve, C. (1991). *Blueprint for a Cell: The Nature and Origin of Life*. Burlington, NC: Neil Patterson Publishers.

Di Giulio, M. (2011). The last universal common ancestor (LUCA) and the ancestors of archaea and bacteria were progenotes. *J. Mol. Evol.* 72, 119–126. doi: 10.1007/s00239-010-9407-2

Dobbek, H. (2018). "Metallocofactors that activate small molecules," in *Structure and Bonding*, Vol. 179, ed. M. W. Ribbe (Cham: Springer International Publishing), 153. doi: 10.1007/430_2018_27

Dobbek, H., Svetlitchnyi, V., Gremer, L., Huber, R., and Meyer, O. (2001). Crystal structure of a carbon monoxide dehydrogenase reveals a [Ni-4Fe-5S] cluster. *Science* 293, 1281–1285. doi: 10.1126/science.1061500

Doukov, T. I., Blasiak, L. C., Seravalli, J., Ragsdale, S. W., and Drennan, C. L. (2008). Xenon in and at the end of the tunnel of bifunctional carbon monoxide dehydrogenase/acetyl-CoA synthase. *Biochemistry* 47, 3474–3483. doi: 10.1021/bi702386t

Drake, H. L., Gößner, A. S., and Daniel, S. L. (2008). Old acetogens, new Light. *Ann. N. Y. Acad. Sci.* 1125, 100–128. doi: 10.1196/annals.1419.016

Drennan, C. L., Doukov, T. I., and Ragsdale, S. W. (2004). The metalloclusters of carbon monoxide dehydrogenase/acetyl-CoA synthase: a story in pictures. *J. Biol. Inorg. Chem.* 9, 511–515. doi: 10.1007/s00775-004-0563-y

Eck, R. V., and Dayhoff, M. O. (1966). Evolution of the structure of ferredoxin based on living relics of primitive amino acid sequences. *Science* 152, 363–366.

Etiope, G., and Schoell, M. (2014). Abiotic gas: atypical, but not rare. *Elements* 10, 291–296. doi: 10.2113/gselements.10.4.291

Ferry, J. G., and House, C. H. (2006). The stepwise evolution of early life driven by energy conservation. *Mol. Biol. Evol.* 23, 1286–1292.

Fischer, W. W., Hemp, J., and Johnson, J. E. (2016). Evolution of oxygenic photosynthesis. *Ann. Rev. Earth Planet Sci.* 44, 647–683.

Frey, P. A., and Arabshahi, A. (1995). Standard free energy change for the hydrolysis of the alpha, beta-phosphoanhydride bridge in ATP. *Biochemistry* 34, 11307–11310.

Fuchs, G. (2011). Alternative pathways of carbon dioxide fixation: insights into the early evolution of life? *Annu. Rev. Microbiol.* 65, 631–658. doi: 10.1146/annurev-micro-090110-102801

Fuchs, G., and Stupperich, E. (1985). "Evolution of autotrophic CO2 fixation," in *Evolution of Prokaryotes*, eds K. H. Schleifer and E. Stackebrandt (London: Academic Press), 235–225.

Garrison, W. M., Morrison, D. C., Hamilton, J. G., Benson, A. A., and Calvin, M. (1951). Reduction of carbon dioxide in aqueous solutions by ionizing radiation. *Science* 114, 416–418. doi: 10.1126/science.114.2964.416

Goldford, J. E., Hartman, H., Marsland, R., and Segrè, D. (2019). Environmental boundary conditions for the origin of life converge to an organo-sulfur metabolism. *Nat. Ecol. Evol.* 3, 1715–1724. doi: 10.1038/s41559-019-1018-8

Goldford, J. E., Hartman, H., Smith, T. F., and Segre, D. (2017). Remnants of an ancient metabolism without phosphate. *Cell* 168, 1126–1134.

Graham, D. E., and White, R. H. (2002). Elucidation of methanogenic coenzyme biosyntheses: from spectroscopy to genomics. *Nat. Prod. Rep.* 19, 133–147. doi: 10.1039/b103714p

Grüber, G., Manimekalai, M. S. S., Mayer, F., and Müller, V. (2014). ATP synthases from archaea: the beauty of a molecular motor. *Biochim. Biophys. Acta Bioenergy* 1837, 940–952. doi: 10.1016/j.bbabio.2014.03.004

Haeckel, E. (1902). *Natürliche Schöpfungs-Geschichte. Gemeinverständliche Wissenschaftliche Vorträge über die Entwickelungslehre Zehnte verbesserte Auflage. Zweiter Theil: Allgemeine Stammesgeschichte* (Berlin: Georg Reimer Verlag).

Haldane, J. B. S. (1929). The origin of life. *Ration. Annu.* 148, 3–10.

Hall, D. O., Cammack, R., and Rao, K. K. (1971). Role of ferredoxins in the origin of life and biological evolution. *Nature* 233, 136–138.

Hansen, L. D., Criddle, R. S., and Battley, E. H. (2009). Biological calorimetry and the thermodynamics of the origination and evolution of life. *Pure Appl. Chem.* 81, 1843–1855. doi: 10.1351/PAC-CON-08-09-09

Hattori, S., Galushko, A. S., Kamagata, Y., and Schink, B. (2005). Operation of the CO dehydrogenase/acetyl coenzyme A pathway in both acetate oxidation and acetate formation by the syntrophically acetate-oxidizing bacterium *Thermacetogenium phaeum*. *J. Bacteriol.* 187, 3471–3476.

Herrmann, G., Jayamani, E., Mai, G., and Buckel, W. (2008). Energy conservation via electron-transferring flavoprotein in anaerobic bacteria. *J. Bacteriol.* 190, 784–791. doi: 10.1128/JB.01422-07

Hess, V., Poehlein, A., Weghoff, M. C., Daniel, R., and Müller, V. (2014). A genome-guided analysis of energy conservation in the thermophilic, cytochrome-free acetogenic bacterium *Thermoanaerobacter kivui*. *BMC Genomics* 15:1139. doi: 10.1186/1471-2164-15-1139

Hoehler, T. M., and Jörgensen, B. B. (2013). Microbial life under extreme energy limitation. *Nat. Rev. Microbiol.* 2013, 83–94.

Hordijk, W., and Steel, M. (2004). Detecting autocatalyctic, self-sustaining sets in chemical reaction systems. *J. Theor. Biol.* 227, 451–461.

Horowitz, N. H. (1945). On the evolution of biochemical syntheses. *Proc. Natl. Acad. Sci U.S.A.* 31, 153–157.

Huang, G., Wagner, T., Ermler, U., and Shima, S. (2020). Methanogenesis involves direct hydride transfer from H_2 to an organic substrate. *Nat. Rev. Chem.* 4, 213–221.

Hügler, M., and Sievert, S. M. (2011). Beyond the calvin cycle: autotrophic carbon fixation in the ocean. *Annu. Rev. Mar. Sci.* 3, 261–289. doi: 10.1146/annurev-marine-120709-142712

Katchalsky, A., and Paecht, M. (1954). Phosphate anhydrides of amino Acids. *J. Biol Chem.* 76, 6042–6044.

Kauffman, S. A. (1986). Autocatalytic sets of proteins. *J. Theor. Biol.* 19, 1–24.

Keller, M. A., Piedrafita, G., and Ralser, M. (2015). The widespread role of non-enzymatic reactions in cellular metabolism. *Curr. Opin. Biotechnol.* 34, 153–161. doi: 10.1016/j.copbio.2014.12.020

Keller, M. A., Turchyn, A. V., and Ralser, M. (2014). Non-enzymatic glycolysis and pentose phosphate pathway-like reactions in a plausible Archean ocean. *Mol. Syst. Biol.* 10:725. doi: 10.1002/msb.20145228

Kitani, A., Tsunetsugu, S., and Sasaki, K. (1991). FeIII-ion-catalyzed nonenzymatic transformation of ADP into ATP. *J. Chem. Soc. Perkin Trans.* 2, 329–331.

Kitani, A., Tsunetsugu, S., Suzuki, A., Ito, S., and Sasaki, K. (1995). Fe(III)-ion-catalyzed nonenzymatic transformation of adenosine-diphosphate into adenosine-triphosphate. 2. Evidence of catalytic nature of Fe ions. *Bioelectrochem. Bioenerget.* 36, 47–51.

Krishnaro, J. S. R. (1964). Native nickel-iron alloy, its mode of occurrence, distribution and origin. *Econ. Geol.* 59, 443–448.

Lane, N., Allen, J. F., and Martin, W. F. (2010). How did LUCA make a living? Chemiosmosis in the origin of life. *BioEssays* 32, 271–280. doi: 10.1002/bies.200900131

Lane, N., and Martin, W. F. (2012). The origin of membrane bioenergetics. *Cell* 151, 1406–1416. doi: 10.1016/j.cell.2012.11.050

Lang, S. Q., Fruh-Green, G. L., Bernasconi, S. M., Brazelton, W. J., Schrenk, M. O., McGonigle, J. M., et al. (2018). Deeply-sourced formate fuels sulfate reducers but not methanogens at Lost City hydrothermal field. *Sci. Rep.* 8:755.

Lipmann, F. (1941). Metabolic generation and utilization of phosphate bond energy. *Adv. Enzymol.* 1, 99–162. doi: 10.1002/9780470122464.ch4

Lipmann, F. (1965). "Projecting backward from the present stage of evolution of biosynthesis," in *The Origin of Prebiological Systems and of their Molecular Matrices*, ed. S. W. Fox (New York, NY: Academic Press), 259–280.

Liu, Y. C., Beer, L. L., and Whitman, W. B. (2012). Methanogens: a window into ancient sulfur metabolism. *Trends. Microbiol.* 20, 251–258.

Ljungdahl, L. G. (2009). A life with acetogens, thermophiles, and cellulolytic anaerobes. *Annu. Rev. Microbiol.* 63, 1–25. doi: 10.1146/annurev.micro.091208.073617

Maden, B. E. (1995). No soup for starters? Autotrophy and the origins of metabolism. *Trends Biochem. Sci.* 20, 337–341. doi: 10.1016/s0968-0004(00)89069-6

Maden, B. E. H. (2000). Tetrahydrofolate and tetrahydromethanopterin compared: functionally distinct carriers in C1 metabolism. *Biochem. J.* 350, 609–629. doi: 10.1042/bj3520935u

Madigan, M. T., Martinko, J. M., Bender, K. S., Buckley, D. H., and Stahl, D. A. (2019). *Brock Biology of Microorganisms*, 15th Edn. Harlow: Pearson Education.

Magnabosco, C., Lin, L.-H., Dong, H., Bomberg, M., Ghiorse, W., Stan-Lotter, H., et al. (2018). The biomass and biodiversity of the continental subsurface. *Nat. Geosci.* 11, 707–717. doi: 10.1038/s41561-018-0221-6

Mall, A., Sobotta, J., Huber, C., Tschirner, C., Kowarschik, S., Bačnik, K., et al. (2018). Reversibility of citrate synthase allows autotrophic growth of a thermophilic bacterium. *Science* 359, 563–567. doi: 10.1126/science.aao2410

Martin, W. (2008). On the ancestral state of microbial physiology. In Amann R, Goebel W, Schink B, Widdel F (Ed) life strategies of microorganisms in the environment and in host organisms. *Nova Acta Leopoldina* 96, 53–60.

Martin, W., and Russell, M. J. (2003). On the origins of cells: a hypothesis for the evolutionary transitions from abiotic geochemistry to chemoautotrophic prokaryotes, and from prokaryotes to nucleated cells. *Philos. Trans. R. Soc. Lond. B Biol. Sci.* 358, 59–83.

Martin, W. F. (2012). Hydrogen, metals, bifurcating electrons, and proton gradients: the early evolution of biological energy conservation. *FEBS Lett.* 586, 485–493. doi: 10.1016/j.febslet.2011.09.031

Martin, W. F. (2019). Carbon metal bonds, rare and primordial in metabolism. *Trends Biochem. Sci.* 44, 807–818.

Martin, W. F., Bryant, D. A., and Beatty, J. T. (2018). A physiological perspective on the origin and evolution of photosynthesis. *FEMS Microbiol. Rev.* 42, 201–231.

Martin, W. F., and Cerff, R. (2017). Physiology, phylogeny, early evolution, and GAPDH. *Protoplasma* 254, 1823–1834. doi: 10.1007/s00709-017-1095-y

Martin, W. F., and Russell, M. J. (2007). On the origin of biochemistry at an alkaline hydrothermal vent. *Philos. Trans. R. Soc. B* 362, 1887–1925. doi: 10.1098/rstb.2006.1881

Martin, W. F., and Sousa, F. L. (2015). Early microbial evolution: the age of anaerobes. *Cold Spring Harb. Perspect. Biol.* 8:a018127. doi: 10.1101/cshperspect.a018127

Martin, W. F., and Sousa, F. L. (2016). Early microbial evolution: the age of anaerobes. *Cold Spring Harb. Perspect. Biol.* 8:a018127. doi: 10.1101/cshperspect.a018127

Martin, W. F., and Thauer, R. K. (2017). Energy in ancient metabolism. *Cell* 168, 953–955. doi: 10.1016/j.cell.2017.02.032

Mayumi, D., Mochimaru, H., Tamaki, H., Yamamoto, K., Yoshioka, H., Suzuki, Y., et al. (2016). Methane production from coal by a single methanogen. *Science* 354, 222–225. doi: 10.1126/science.aaf8821

Ménez, B., Pisapia, C., Andreani, M., Jamme, F., Vanbellingen, Q. P., Brunelle, A., et al. (2018). Abiotic synthesis of amino acids in the recesses of the oceanic lithosphere. *Nature* 564, 59–63.

Mereschkowsky, C. (1910). Theorie der zwei Plasmaarten als Grundlage der Symbiogenesis, einer neuen Lehre von der Entstehung der Organismen. *Biol. Centralbl.* 30, 278–288, 289–303, 353–367.

Miller, S. L., and Urey, H. (1959). Organic compound synthesis on the primitive Earth. *Science* 130, 245–251. doi: 10.1126/science.130.3370.245

Mitchell, P. (1961). Coupling of phosphorylation to electron and hydrogen transfer by a chemi-osmotic type of mechanism. *Nature* 191, 144–148. doi: 10.1038/191144a0

Morowitz, H. J. (1968). *Energy Flow in Biology*. New York, NY: Academic Press.

Morowitz, H. J. (1992). *Beginnings of Cellular Life: Metabolism Recapitulates Biogenesis*. New Haven, CT: Yale University Press.

Muchowska, K. B., Varma, S. J., Chevallot-Berou, E., Lethuillier-Karl, L., Li, G., and Moran, J. (2017). Metals promote sequences of the reverse Krebs cycle. *Nature Ecol. Evol.* 1, 1716–1721.

Muchowska, K. B., Varma, S. J., and Moran, J. (2019). Synthesis and breakdown of universal metabolic precursors promoted by iron. *Nature* 569, 104–107.

Müller, V., Chowdhury, N. P., and Basen, M. (2018). Electron bifurcation: a long-hidden energy-coupling mechanism. *Annu. Rev. Microbiol.* 72, 331–353. doi: 10.1146/annurev-micro-090816-093440

Nelson-Sathi, S., Dagan, T., Landan, G., Janssen, A., Steel, M., McInerney, J. O., et al. (2012). Acquisition of 1,000 eubacterial genes physiologically transformed a methanogen at the origin of Haloarchaea. *Proc. Natl. Acad. Sci. U.S.A.* 109, 20537–20542.

Nelson-Sathi, S., Sousa, F. L., Roettger, M., Lozada-Chávez, N., Thiergart, T., Janssen, A., et al. (2015). Origins of major archaeal clades correspond to gene acquisitions from bacteria. *Nature* 517, 77–80.

Nisbet, E. G., Cann, J. R., and Van Dover, C. L. (1995). Origins of photosynthesis. *Nature* 373, 479–480.

Nisbet, E. G., and Sleep, N. H. (2001). The habitat and nature of early life. *Nature* 409, 1083–1091.

Nitschke, W., and Russell, M. J. (2013). Beating the acetyl coenzyme A-pathway to the origin of life. *Philos Trans. R. Soc. Lond. B* 368:20120258.

Nunoura, T., Chikaraishi, Y., Izaki, R., Suwa, T., Sato, T., Harada, T., et al. (2018). A primordial and reversible TCA cycle in a facultatively chemolithoautotrophic thermophile. *Science* 359, 559–563. doi: 10.1126/science.aao3407

Orgel, L. E. (2008). The implausibility of metabolic cycles on the prebiotic earth. *PLoS Biol.* 6:e18. doi: 10.1371/journal.pbio.0060018

Pasek, M. A., Gull, M., and Herschy, B. (2017). Phosphorylation on the early earth. *Chem. Geol.* 475, 149–170. doi: 10.1016/j.chemgeo.2017.11.008

Peters, J. W., Beratan, D. N., Bothner, B., Dyer, R. B., Harwood, C. S., Heiden, Z. M., et al. (2018). A new era for electron bifurcation. *Curr. Opin. Chem. Biol.* 47, 32–38. doi: 10.1016/j.cbpa.2018.07.026

Preiner, M., Igarashi, K., Muchowska, K. B., Yu, M., Varma, S. J., Kleinermanns, K., et al. (2020). A hydrogen dependent geochemical analogue of primordial carbon and energy metabolism. *Nat. Ecol. Evol.* 4, 534–542.

Preiner, M., Xavier, J., Sousa, F., Zimorski, V., Neubeck, A., Lang, S. Q., et al. (2018). Serpentinization: connecting geochemistry, ancient metabolism and industrial hydrogenation. *Life* 8:41.

Proskurowski, G., Lilley, M. D., Seewald, J. S., Früh-Green, G. L., Olson, E. J., Lupton, J. E., et al. (2008). Abiogenic hydrocarbon production at lost city hydrothermal field. *Science* 319, 604–607. doi: 10.1126/science.1151194

Rabus, R., Venceslau, S. S., Wohlbrand, L., Voordouw, G., Wall, J. D., and Pereira, I. A. C. (2015). "A post-genomic view of the ecophysiology, catabolism and biotechnological relevance of sulphate-reducing prokaryotes," in *Advances in Microbial Physiology*, Vol. 66, ed. R. K. Poole (Oxford: Academic Press), 55–321.

Ragsdale, S. W. (2004). Life with carbon monoxide. *Crit. Rev. Biochem. Mol. Biol.* 39, 165–195. doi: 10.1080/10409230490496577

Ragsdale, S. W. (2008). Enzymology of the Wood-Ljungdahl pathway of acetogenesis. *Ann. N. Y. Acad. Sci.* 1125, 129–136. doi: 10.1196/annals.1419.015

Ragsdale, S. W. (2009). Nickel-based enzyme systems. *J. Biol. Chem.* 284, 18571–18575.

Ragsdale, S. W., and Pierce, E. (2008). Acetogenesis and the Wood-Ljungdahl pathway of CO_2 fixation. *Biochim. Biophys. Acta* 1784, 1873–1898. doi: 10.1016/j.bbapap.2008.08.012

Ricardo, A., Carrigan, M. A., Olcott, A. N., and Benner, S. A. (2004). Borate minerals stabilize ribose. *Science* 303, 196.

Russell, J. B. (2007). The energy spilling reactions of bacteria and other organisms. *J. Mol. Microbiol. Biotechnol.* 13, 1–11. doi: 10.1159/000103591

Russell, J. B., and Cook, G. M. (1995). Energetics of bacterial growth: balance of anabolic and catabolic reactions. *Microbiol. Rev.* 59, 48–62.

Russell, M. J. (2006). First life. *Am. Sci.* 94, 32–39. doi: 10.1511/2006.57.32

Russell, M. J., and Hall, A. J. (1997). The emergence of life from iron monosulphide bubbles at a submarine hydrothermal redox and pH front. *J. Geol. Soc. Lond.* 154, 377–402.

Russell, M. J., and Martin, W. (2004). The rocky roots of the acetyl-CoA pathway. *Trends Biochem. Sci.* 29, 358–363.

Russell, M. J., Hall, A. J., and Martin, W. (2010). Serpentinization as a source of energy at the origin of life. *Geobiology* 8, 355–371. doi: 10.1111/j.1472-4669.2010.00249.x

Say, R. F., and Fuchs, G. (2010). Fructose 1,6-bisphosphate aldolase/phosphatase may be an ancestral gluconeogenic enzyme. *Nature* 464, 1077–1081. doi: 10.1038/nature08884

Schauder, R., Preuß, A., Jetten, M., and Fuchs, G. (1988). Oxidative and reductive acetyl CoA/carbon monoxide dehydrogenase pathway in *Desulfobacterium autotrophicum*. 2. Demonstration of the enzymes of the pathway and comparison of CO dehydrogenase. *Arch. Microbiol.* 151, 84–89.

Schink, B., and Friedrich, M. (2000). Phosphite oxidation by sulphate reduction. *Nature* 406:37. doi: 10.1038/35017644

Schoelmerich, M. C., and Müller, V. (2019). Energy conservation by a hydrogenase-dependent chemiosmotic mechanism in an ancient metabolic pathway. *Proc. Natl. Acad. Sci. U.S.A.* 116, 6329–6334. doi: 10.1073/pnas.1818580116

Schönheit, P., Buckel, W., and Martin, W. (2016). On the origin of heterotrophy. *Trends Microbiol.* 24, 12–25. doi: 10.1016/j.tim.2015.10.003

Schuchmann, K., and Müller, V. (2014). Autotrophy at the thermodynamic limit of life: a model for energy conservation in acetogenic bacteria. *Nat. Rev. Microbiol.* 12, 809–821.

Schuchmann, K., and Müller, V. (2013). Direct and reversible hydrogenation of CO_2 to formate by a bacterial carbon dioxide reductase. *Science* 342, 1382–1385. doi: 10.1126/science.1244758

Schut, G. J., Boyd, E. S., Peters, J. W., and Adams, M. W. W. (2013). The modular respiratory complexes involved in hydrogen and sulfur metabolism by heterotrophic hyperthermophilic archaea and their evolutionary implications. *FEMS Microbiol. Rev.* 37, 182–203. doi: 10.1111/j.1574-6976.2012.00346.x

Semenov, S. N., Kraft, L. J., Ainla, A., Zhao, M., Baghbanzadeh, M., Campbell, V. E., et al. (2016). Autocatalytic, bistable, oscillatory networks of biologically relevant organic reactions. *Nature* 537, 656–660.

Shapiro, R. (2006). Small molecule interactions were central to the origin of life. *Q. Rev. Biol.* 81, 105–126. doi: 10.1086/506024

Sleep, N. H., Bird, D. K., and Pope, E. C. (2011). Serpentinite and the dawn of life. *Philos. Trans. R. Soc. B* 366, 2857–2869. doi: 10.1098/rstb.2011.0129

Sojo, V., Pomiankowski, A., and Lane, N. (2014). A bioenergetic basis for membrane divergence in archaea and bacteria. *PLoS Biol.* 12:e1001926. doi: 10.1371/journal.pbio.1001926

Sousa, F., and Martin, W. F. (2014). Biochemical fossils of the ancient transition from geoenergetics to bioenergetics in prokaryotic one carbon compound metabolism. *Biochim. Biophys. Acta* 1837, 964–981. doi: 10.1016/j.bbabio.2014.02.001

Sousa, F. L., Hordijk, W., Steel, M., and Martin, W. F. (2015). Autocatalytic sets in *E. coli* metabolism. *J. Systems Chem.* 6:4.

Sousa, F. L., Preiner, M., and Martin, W. F. (2018). Native metals, electron bifurcation and CO_2 reduction in early biochemical evolution. *Curr. Opin. Microbiol.* 43, 77–83. doi: 10.1016/j.mib.2017.12.010

Sousa, F. L., Thiergart, T., Landan, G., Nelson-Sathi, S., Pereira, I. A. C., Allen, J. F., et al. (2013). Early bioenergetic evolution. *Philos. Trans. R. Soc. B* 368:20130088. doi: 10.1098/rstb.2013.0088

Stouthamer, A. H. (1973). A theoretical study on the amount of ATP required for synthesis of microbial cell material. *Antonie Leeuwenhoek* 39, 545–565.

Stouthamer, A. H. (1978). "Energy-yielding pathways," in *The Bacteria Vol VI: Bacterial Diversity*, ed. I. C. Gunsalus (New York, NY: Academic Press).

Suzuki, S., Nealson, K. H., and Ishii, S. (2018). Genomic and in-situ transcriptomic characterization of the candidate phylum NPL-UPL2 from highly alkaline highly reducing serpentinized groundwater. *Front. Microbiol.* 9:3141. doi: 10.3389/fmicb.2018.03141

Svetlitchnaia, T., Svetlitchnyi, V., Meyer, O., and Dobbek, H. (2006). Structural insights into methyltransfer reactions of a corrinoid iron-sulfur protein involved in acetyl-CoA synthesis. *Proc. Natl. Acad. Sci. U.S.A.* 103, 14331–14336.

Tashiro, T., Ishida, A., Hori, M., Igisu, M., Koike, M., Méjean, P., et al. (2017). Early trace of life from 3.95 Ga sedimentary rocks in Labrador, Canada. *Nature* 549, 516–518. doi: 10.1038/nature24019

Thauer, R. K. (2011). Hydrogenases and the global H_2 cycle. *Eur. J. Inorg. Chem.* 2011, 919–921.

Thauer, R. K. (2015). My lifelong passion for biochemistry and anaerobic microorganisms. *Annu. Rev. Microbiol.* 69, 1–30. doi: 10.1146/annurev-micro-091014-104344

Thauer, R. K., Jungermann, K., and Decker, K. (1977). Energy conservation in chemotrophic anaerobic bacteria. *Bacteriol. Rev.* 41, 100–180.

Thauer, R. K., Kaster, A.-K., Seedorf, H., Buckel, W., and Hedderich, R. (2008). Methanogenic archaea: ecologically relevant differences in energy conservation. *Nat. Rev. Microbiol.* 6, 579–591. doi: 10.1038/nrmicro1931

Ueno, Y., Yamada, K., Yoshida, N., Maruyama, S., and Isozaki, Y. (2006). Evidence from fluid inclusions for microbial methanogenesis in the early Archaean era. *Nature* 440, 516–519. doi: 10.1038/nature04584

Valas, R. E., and Bourne, P. E. (2011). The origin of a derived superkingdom: how a gram-positive bacterium crossed the desert to become an archaeon. *Biol. Direct.* 6:16. doi: 10.1186/1745-6150-6-16

Varma, S. J., Muchowska, K. B., Chatelain, P., and Moran, J. (2018). Native iron reduces CO_2 to intermediates and endproducts of the acetyl-CoA pathway. *Nat. Ecol. Evol.* 2, 1019–1024. doi: 10.1038/s41559-018-0542-2

Volbeda, A., and Fontecilla-Camps, J. C. (2006). Catalytic nickel–iron–sulfur clusters: from minerals to enzymes. *Top. Organomet. Chem.* 17, 57–82. doi: 10.1007/3418_003

Wächtershäuser, G. (1992). Groundworks for an evolutionary biochemistry: the iron-sulphur world. *Prog. Biophys. Mol. Biol.* 58, 85–201.

Wagner, A., Whitaker, R. J., Krause, D. J., Heilers, J. H., van Wolferen, M., van der Does, C., et al. (2017). Mechanisms of gene flow in archaea. *Nat. Rev. Microbiol.* 2017, 492–501.

Wagner, T., Ermler, U., and Shima, S. (2016). The methanogenic CO_2 reducing-and-fixing enzyme is bifunctional and contains 46 [4Fe-4S] clusters. *Science* 354, 114–117. doi: 10.1126/science.aaf9284

Wald, G. (1962). "Life in the second and third periods; or why phosphorus and sulfur for high-energy bonds?," in *Horizons in Biochemistry*, eds M. Kasha and B. Pullman (New York, NY: Academic Press), 127–142.

Wald, G. (1964). The origins of life. *Proc. Natl. Acad. Sci. U.S.A.* 52, 595–611. doi: 10.1073/pnas.52.2.595

Weiss, M., Preiner, M., Xavier, J. C., Zimorski, V., and Martin, W. F. (2018). The last universal common ancestor between ancient Earth chemistry and the onset of genetics. *PLoS Genet.* 14:e1007518. doi: 10.1371/journal.pgen.1007518

Weiss, M. C., Sousa, F. L., Mrnjavac, N., Neukirchen, S., Roettger, M., Nelson-Sathi, S., et al. (2016). The physiology and habitat of the last universal common ancestor. *Nat. Microbiol.* 1:16116. doi: 10.1038/nmicrobiol.2016.116

Weiße, R. H., Faust, A., Schmidt, M., Schönheit, P., and Scheidig, A. J. (2016). Structure of NDP-forming Acetyl-CoA synthetase ACD1 reveals a large rearrangement for phosphoryl transfer. *Proc. Natl. Acad. Sci. U.S.A.* 113, E519–E528. doi: 10.1073/pnas.1518614113

Whicher, A., Camprubi, E., Pinna, S., Herschy, B., and Lane, N. (2018). Acetyl phosphate as a primordial energy currency at the origin of life. *Orig. Life Evol. Biosph.* 48, 159–179.

White, R. H. (2001). Biosynthesis of the methanogenic cofactors. *Vitam. Horm.* 61, 299–337. doi: 10.1016/s0083-6729(01)61010-0

Wolfenden, R. (2011). Benchmark reaction rates, the stability of biological molecules in water, and the evolution of catalytic power in enzymes. *Annu. Rev. Biochem.* 80, 645–667.

Wongnate, T., Sliwa, D., Ginovska, B., Smith, D., Wolf, M. W., Lehnert, N., et al. (2016). The radical mechanism of biological methane synthesis by methyl-coenzyme M reductase. *Science* 352, 953–958.

Wood, H. G. (1991). Life with CO or CO_2 and H_2 as a source of carbon and energy. *FASEB J.* 5, 165–163. doi: 10.1096/fasebj.5.2.1900793

Xavier, J. C., Hordijk, W., Kauffman, S., Steel, M., and Martin, W. F. (2020). Autocatalytic chemical networks preceded proteins and RNA in evolution. *Proc. R. Soc. Lond. B* 287.

Xavier, J. C., Preiner, M., and Martin, W. F. (2018). Something special about CO-dependent CO_2 fixation. *FEBS J.* 285, 4181–4195. doi: 10.1111/febs.14664

Ycas, M. (1974). On earlier states of the biochemical system. *J. Theor. Biol.* 44, 145–160.

Zinder, S. H. (1994). "Syntrophic acetate oxidation and "reversible acetogenesis"," in *Acetogenesis*, ed. H. L. Drake (New York, NY: Chapman and Hall), 386–415.

Conflict of Interest: The author declares that the research was conducted in the absence of any commercial or financial relationships that could be construed as a potential conflict of interest.

frontiers in Microbiology

ORIGINAL RESEARCH
published: 09 June 2020
doi: 10.3389/fmicb.2020.01031

Single-Cell Genomics of Novel Actinobacteria With the Wood–Ljungdahl Pathway Discovered in a Serpentinizing System

Nancy Merino[1,2,3], Mikihiko Kawai[4,5], Eric S. Boyd[6], Daniel R. Colman[6], Shawn E. McGlynn[1,7,8], Kenneth H. Nealson[2], Ken Kurokawa[1,9] and Yuichi Hongoh[1,4]**

[1] Earth-Life Science Institute, Tokyo Institute of Technology, Tokyo, Japan, [2] Department of Earth Sciences, University of Southern California, Los Angeles, CA, United States, [3] Biosciences and Biotechnology Division, Lawrence Livermore National Laboratory, Livermore, CA, United States, [4] School of Life Sciences and Technology, Tokyo Institute of Technology, Tokyo, Japan, [5] Graduate School of Human and Environmental Studies, Kyoto University, Kyoto, Japan, [6] Department of Microbiology and Immunology, Montana State University, Bozeman, MT, United States, [7] Biofunctional Catalyst Research Team, RIKEN Center for Sustainable Resource Science, Saitama, Japan, [8] Blue Marble Space Institute of Science, Seattle, WA, United States, [9] Department of Informatics, National Institute of Genetics, Shizuoka, Japan

OPEN ACCESS

Edited by:
Mirko Basen, University of Rostock, Germany

Reviewed by:
Daan R. Speth, California Institute of Technology, United States
Donald A. Bryant, The Pennsylvania State University, United States

***Correspondence:**
Nancy Merino
nmerino@elsi.jp
Yuichi Hongoh
yhongo@bio.titech.ac.jp

Specialty section:
This article was submitted to Extreme Microbiology, a section of the journal Frontiers in Microbiology

Received: *16 December 2019*
Accepted: *27 April 2020*
Published: *09 June 2020*

Citation:
Merino N, Kawai M, Boyd ES, Colman DR, McGlynn SE, Nealson KH, Kurokawa K and Hongoh Y (2020) Single-Cell Genomics of Novel Actinobacteria With the Wood–Ljungdahl Pathway Discovered in a Serpentinizing System. Front. Microbiol. 11:1031. doi: 10.3389/fmicb.2020.01031

Serpentinite-hosted systems represent modern-day analogs of early Earth environments. In these systems, water-rock interactions generate highly alkaline and reducing fluids that can contain hydrogen, methane, and low-molecular-weight hydrocarbons-potent reductants capable of fueling microbial metabolism. In this study, we investigated the microbiota of Hakuba Happo hot springs (~50°C; pH~10.5–11), located in Nagano (Japan), which are impacted by the serpentinization process. Analysis of the 16S rRNA gene amplicon sequences revealed that the bacterial community comprises *Nitrospirae* (47%), "Parcubacteria" (19%), *Deinococcus-Thermus* (16%), and *Actinobacteria* (9%), among others. Notably, only 57 amplicon sequence variants (ASV) were detected, and fifteen of these accounted for 90% of the amplicons. Among the abundant ASVs, an early-branching, uncultivated actinobacterial clade identified as RBG-16-55-12 in the SILVA database was detected. Ten single-cell genomes (average pairwise nucleotide identity: 0.98–1.00; estimated completeness: 33–93%; estimated genome size: ~2.3 Mb) that affiliated with this clade were obtained. Taxonomic classification using single copy genes indicates that the genomes belong to the actinobacterial class-level clade UBA1414 in the Genome Taxonomy Database. Based on metabolic pathway predictions, these actinobacteria are anaerobes, capable of glycolysis, dissimilatory nitrate reduction and CO_2 fixation *via* the Wood–Ljungdahl (WL) pathway. Several other genomes within UBA1414 and two related class-level clades also encode the WL pathway, which has not yet been reported for the *Actinobacteria* phylum. For the Hakuba actinobacterium, the energy metabolism related to the WL pathway is likely supported by a combination of the Rnf complex, group 3b and 3d [NiFe]-hydrogenases, [FeFe]-hydrogenases, and V-type (H^+/Na^+ pump) ATPase. The genomes also harbor a form IV ribulose 1,5-bisphosphate carboxylase/oxygenase

(RubisCO) complex, also known as a RubisCO-like protein, and contain signatures of interactions with viruses, including clustered regularly interspaced short palindromic repeat (CRISPR) regions and several phage integrases. This is the first report and detailed genome analysis of a bacterium within the *Actinobacteria* phylum capable of utilizing the WL pathway. The Hakuba actinobacterium is a member of the clade UBA1414/RBG-16-55-12, formerly within the group "OPB41." We propose to name this bacterium '*Candidatus* Hakubanella thermoalkaliphilus.'

Keywords: serpentinization, single-cell genomics, *Actinobacteria*, subsurface, alkaliphile, hydrogenase

INTRODUCTION

The serpentinization reaction is fundamental to one of the leading hypotheses regarding the emergence of life on Earth, known as the submarine alkaline hydrothermal vent model (Russell et al., 2010; Branscomb and Russell, 2018). It follows that contemporary serpentinite-hosted systems might provide a window into early life. This model is based on the formation of highly reduced products (e.g., H_2, CH_4, and formate) from the hydration of ferromagnesian minerals in mafic and ultramafic rocks (e.g., olivine), which are subsequently mixed with solutes in comparatively more oxidized early Earth ocean waters. The resulting geochemical disequilibria could have been an energy source for the formation of early life. Importantly, this combination of alkaline pH and elevated H_2 concentrations of systems undergoing active serpentinization has been suggested to help overcome key biochemical bottlenecks in autotrophic metabolism, including that of acetogens and methanogens (Boyd et al., 2020), two groups of organisms commonly argued to be among the earliest evolving (Martin and Russell, 2006).

The modern-day analog of this system includes terrestrial serpentinite-hosted ecosystems, or ophiolites, created by the obduction of the oceanic lithosphere thrust onto the continental plate (Nicolas, 2012). Ophiolites are markers for the early oceanic crust, with ages ranging from 2 to 0.6 Ga (Condie, 2016). Moreover, ophiolitic terranes can be several kilometers thick (Condie, 2016), providing access to subsurface life that can persist in these reducing and alkaline (pH > 10) environments. Several studies have examined the microbial communities present in serpentinite-influenced environments, including in the Samail ophiolite (Rempfert et al., 2017; Fones et al., 2019), the Cedars (Suzuki et al., 2013), the Cabeço de Vide Aquifer (Tiago and Veríssimo, 2013), the Coast Range Ophiolite Microbial Observatory (Crespo-Medina et al., 2014; Twing et al., 2017), the Voltri Massif (Quéméneur et al., 2015; Brazelton et al., 2017), and the Zambales ophiolite (Meyer-Dombard et al., 2018). Although these can be distant locations from each other, Meyer-Dombard et al. (2018) identified a 'principal community' amongst serpentinizing environments, consisting of key members in the phyla *Firmicutes* (e.g., *Dethiobacter* sp.) and *Proteobacteria* (e.g., *Serpentinomonas* sp.).

The microbial communities of the Hakuba Happo hot spring (36°42′N, 137°48′E) ophiolite located along the Itoigawa–Shizuoka Tectonic Line in central Honshu, Japan have yet to be investigated. This region consists of an ultramafic rock body that is ∼580 Ma old (Sato et al., 2019) and has ongoing serpentinization activity (Suda et al., 2014, 2017). The geochemistry of the site is characteristic of a serpentinite-hosted system, with highly alkaline waters (pH > 10.6) and high concentrations of dissolved H_2 (201–664 μM) and CH_4 (124–201 μM) (Suda et al., 2014). The source of H_2 is likely derived from 'low' temperature serpentinization reactions occurring at ∼50°C (Mayhew et al., 2013) while CH_4 could be from abiotic or biotic origins (Suda et al., 2014). Two wells (well #1 and #3) have been drilled into the Hakuba Happo ophiolite that permit acquisition of subsurface fluids for geochemical and microbiological analyses.

In the present study, we obtained single-cell genomes of an early-branching, uncultivated actinobacterial lineage from Hakuba Happo well #3 (abbreviated hereafter Happo #3), which were among the dominant taxa found in the bacterial community based on 16S rRNA gene amplicon sequences. This actinobacterial lineage was previously designated as RBG-16-55-12 in the SILVA database (Quast et al., 2012; Yilmaz et al., 2014) and approximately corresponds to the UBA1414/RBG-13-55-18/UBA9087 clade in the Genome Taxonomy Database (GTDB) (Parks et al., 2018). Herein, we predict the metabolic properties and provide the first detailed genome analysis of a bacterium in the clade UBA1414/RBG-13-55-18/UBA9087. This comes two decades after the discovery of its presence by 16S rRNA gene sequencing analysis from samples collected at Obsidian Pool in Yellowstone National Park where it acquired the name "OPB41" (Hugenholtz et al., 1998).

MATERIALS AND METHODS

Sample Collection and Geochemical Measurements

Samples were collected from Happo #3 (36°42'48.6″N 137°48'26.3″E) in October 2016. Detailed geochemical analysis of Happo #3 was previously described in Suda et al. (2014), including isotope compositions and ion concentrations. Happo #3 is a drilling well that extends to about 700 m depth and water is pumped to the surface for the hot spring facilities provided in Happo Town, Japan (Suda et al., 2014). In the field, water temperature (water resistant thermometer CT-430WP, CUSTOM, Japan), pH (pH meter model D-51 with electrode 9625-10D and B-712, HORIBA, Japan), oxidation-reduction potential (ORP; ORP meter model RM-30P with electrode

PST-2739C, TOA-DKK, Japan), dissolved oxygen (DO; DO meter model DO-31P with electrode OE-270AA, Japan), electrical conductivity (EC; EC meter model CM-31P with electrode CT-27112B, Japan), salinity (B-721 meter, HORIBA, Japan), calcium (B-751 meter, HORIBA, Japan), sodium (B-722 meter, HORIBA, Japan), and potassium (B-731 meter, HORIBA, Japan) ion concentrations were measured. Analysis of ions and organic acids are described in the **Supplementary Information**.

Happo #3 water was filtered using two different methods ("Total" and "Sequential") at a flow rate of about 15 mL per min for 22 h (total water filtered ∼ 19.8 L). For the "Total" method, a 0.1 μm Omnipore membrane (25 mm diameter, Millipore, United States) was used, while the "Sequential" method used in-series filtration consisting of a 0.22 μm Sterivex-GP (polyethersulfone, Millipore, United States), followed by a 0.1 μm Omnipore membrane. The Omnipore membrane was housed in a PerFluoroAlkoxy filter holder (Advantec, United States). Filtered samples were aseptically placed in 100 μL of fresh glycerol-Tris-EDTA buffer (Rinke et al., 2014) for single-cell genomics. Glycerol-Tris-EDTA consisted of 20 mL TE buffer (100×, pH 8) and 100 mL glycerol per 180 mL, which was sterilized by passing through a 0.1 μm filter. Samples were immediately shipped at −20°C overnight and stored at −80°C.

16S rRNA Gene Amplicon Sequencing

For 16S rRNA gene amplicon sequencing, another set of filters was collected as described above. DNA was extracted from the "Total" and "Sequential" samples, using the ZymoBIOMICS DNA/RNA Miniprep Kit (Zymo Research, United States). The V3–V4 region of the 16S rRNA genes was amplified by PCR with primers 341F (5'-CCTACGGGNGGCWGCAG) and 785R (5'-GACTACHVGGGTATCTAATCC) according to the Illumina MiSeq Protocol "16S Metagenomic Sequencing Library Preparation," and the amplicons were used for preparation of sequencing libraries with the KOD FX Neo Kit (Toyobo Life Science, Japan). Sequencing was performed using the Illumina MiSeq platform with the V3 reagent kit (600 cycles). A total of 17,058 ("Total") and 10,390 ("Sequential") reads were obtained after quality filtering and trimming via DADA2 (Callahan et al., 2016). The reads were sorted to amplicon sequence variants (ASV), or unique sequences, using DADA2 and taxonomically identified (Callahan et al., 2016, 2017). Afterward, phyloseq v1.26.1 (McMurdie and Holmes, 2013) was used to prune the samples of ASVs observed in a negative control of filtered air collected during field sampling. For the remaining ASVs, a prevalence threshold of 0.1 was determined by phyloseq.

Single-Cell Sorting, Whole Genome Amplification, and Library Preparation

A fluorescence-activated cell sorter (FACS; BD FACS Aria IIU, BD Biosciences, United States) with a 70 μm nozzle orifice was used to sort single cells into 96-well plates. Filters stored in glycerol-Tris-EDTA stock were thawed on ice and briefly shaken to re-suspend cells from the filter, and 0.65 μL of 1 g/L FM™ 1-43FX (Thermo Fisher Scientific, United States) was then added to an aliquot (350 μL) to stain the cell membrane. The sample was incubated for at least 15 min on ice and was not pre-screened through a 70 μm mesh-size cell strainer (BD Biosciences, United States) to prevent the loss of microbial cells since the Happo #3 water did not contain large particles or microorganisms > 70 μm. The FACS sorting operating condition was checked by calibrating against the BD CS&T Beads (BD Biosciences, United States). A total of 5 plates were sorted for "Total" filters and 8 plates for "Sequential" filters. FACS parameters are further described in **Supplementary Information**. Targeted cells were sorted into 96-well plates with 2 wells reserved for whole genome amplification (WGA) positive controls (with added template DNA) and 8 wells were reserved for the negative control (without droplet deposition). Each plate was immediately placed at −80°C until processed. Several single-cell lysis methods were tested and described in the **Supplementary Information**. For WGA, the Qiagen REPLI-g Single Cell Kit (Qiagen, Germany) was used with a modified protocol, as described in the **Supplementary Information**.

The WGA products were diluted (5 μL WGA product, 95 μL UV-sterilized H_2O), mixed by pipetting 15 times, and 1 μL was used in a qPCR reaction (SsoAdvanced™ Universal SYBR® Green Supermix, Bio-Rad Laboratories, United States) to amplify the 16S rRNA gene V6–V8 hypervariable regions with primers 926wF and 1392R (Rinke et al., 2014). The qPCR reaction contained 5 μL SsoAdvanced™ Supermix, 0.2 μL forward primer (10 μM stock), 0.2 μL reverse primer (10 μM stock), 3.6 μL UV-sterilized H_2O, and 1 μL of the diluted WGA product. The qPCR reaction cycle comprised 98°C for 3 min, 35 cycles of 98°C for 15 s and 60°C for 1 min, a melt curve of 95°C for 15 s, 60°C for 1 min, with ramp of +0.3°C to 95°C for 15 s, followed by a 4°C hold. Amplification of 16S rRNA genes was confirmed by gel electrophoresis, and 5 μL of qPCR products were treated with 2 μL ExoSAP-IT Express (ThermoFisher Scientific, United States). The cleaned qPCR products were then sent for Sanger sequencing with primer 1392R to enable cell selection for sequence library preparation. **Supplementary Table S1** describes the cells selected for sequencing, including FACS conditions, lysis and WGA reaction conditions, and single-cell genome statistics referenced against the minimum information of single amplified genome (MISAG) criteria (Bowers et al., 2017). Libraries were prepared using the TruSeq DNA PCR-Free Library Preparation Kit (Illumina, United States) and a Covaris M220 to obtain 550 bp sheared DNA.

Sequencing, Assembly, Binning, and Annotation

All single-cell amplified genome (SAG) libraries were sequenced on the Illumina MiSeq platform using 2 × 300 bp paired-end sequencing (MiSeq v3 Reagent Kit). Raw reads were evaluated using FastQC v0.11.5[1] and trimmed and quality filtered by Trim_galore! v0.4.1[2], which uses the

[1]https://www.bioinformatics.babraham.ac.uk/projects/fastqc/

[2]https://www.bioinformatics.babraham.ac.uk/projects/trim_galore/

cutadapt v1.9.1 program (Martin, 2011). Trim_galore! parameters were set for paired-end files and included a stringency of 5, e 0.1 (error rate), q 20,20 (quality), with the option to retain unpaired reads. Reads were then assembled with SPAdes v3.10.1 (Bankevich et al., 2012) for single-cell samples with the "careful" option and default parameters (k-mers: 21, 33, and 55). Scaffold names were simplified for the Anvi'o v5.3 workflow (Eren et al., 2015), followed by read-mapping with Bowtie2 v2.3.2 (Langmead and Salzberg, 2012) (parameters very-sensitive-local and dovetail) with the samtools depth function to determine coverage values by searching the trimmed reads against the assembled scaffolds. The Anvi'o workflow was then used to cluster and profile the scaffolds greater than 1,000 bp and potential contaminants were removed. The ACDC program (Lux et al., 2016) was also used for contamination screening. Subsequently, gene identification was conducted using Prodigal v2.6.2 (Hyatt et al., 2010) and HMMER v3.1b2[3]. Functional classification was conducted using InterProScan v5.28-67.0 (with databases: TIGRFAMs, SFLD, HAMAP, ProSiteProfiles, ProSitePatterns, PANTHER, Pfam, CDD) (Jones et al., 2014) and imported into Anvi'o. Secondary metabolite biosynthetic gene clusters were identified using antiSMASH v4.1.0 with the options –clusterblast –subclusterblast –knownclusterblast –smcogs –inclusive –borderpredict –full-hmmer –asf –tta (Blin et al., 2017). MAPLE was used to obtain KEGG orthologous (KO) group assignments (Takami, 2014; Arai et al., 2018). Gas vesicle genes were annotated by using a manually curated gas vesicle hidden Markov model database, which is described in the **Supplementary Information**.

Taxonomic classification was conducted with Kaiju v1.5.0 (Menzel et al., 2016) against the NCBI non-redundant (nr) database (nr + euk database) and imported into Anvi'o. Prophage regions were detected on contigs > 2,000 bp in PHASTER (Zhou et al., 2011; Arndt et al., 2016), and clustered regularly interspaced short palindromic repeat (CRISPR) and its associated gene (Cas) regions were annotated using CRISPRCasFinder (Couvin et al., 2018). SAG sequences were manually refined through Anvi'o (anvi-interactive). CheckM v1.0.7 (Parks et al., 2015) was also used to estimate completeness, degree of contamination, and strain heterogeneity. The number of rRNA genes was determined by the Anvi'o v5.3 method (Eren et al., 2015) and Barrnap v0.6[4].

Co-assembly of SAGs

Ten SAGs (**Supplementary Table S1**) were subsequently co-assembled using SPAdes v3.10.1 with k-mers that were normalized to achieve a flat coverage distribution (target normalization depth = 100 for k-mers with at least 5 depth coverage) via BBNorm v37.95[5] using default parameters. A range of k-mers were tested (21, 33, 55, 77, 99, and 127) and scaffolds produced when using k-mers 21 and 33 achieved the highest N50 of 7,442 bp based on Quast v4.5 (Gurevich et al., 2013). The generated scaffolds were subsequently placed into the Anvi'o v5.3 workflow with Bowtie2 v2.3.2 read-mapping, as described above, and after removal of contigs < 1,000 bp and potential contaminants (based on sequence composition clustering), the N50 was 8,580 bp. Functional and taxonomic classification were also conducted as described above. The number of tRNA and rRNA genes were determined using tRNAscan-SE v2.0 (Lowe and Eddy, 1997) and Anvi'o v5.3 or Barrnap v0.6, respectively. Effective DB (Eichinger et al., 2016) was used to predict the fully functional bacterial secretion systems Type III, IV, and VI.

Phylogenetic and Comparative Genomic Analyses

The co-assembly was then placed into phylogenetic trees with reference genomes from the NCBI RefSeq and GenBank databases (O'Leary et al., 2016). The trees included *Actinobacteria* genomes from Rifle, CO (United States) (Anantharaman et al., 2016), a CO_2-driven geyser (Colorado Plateau, Utah, United States) (Probst et al., 2018), the Sanford Underground Research Facility (SURF) (Momper et al., 2017), and Baltic Sea sediments (Bird et al., 2019; cleaned assemblies provided by Dr. Karen Lloyd). These genomes were the most closely related to the Hakuba SAGs, as determined by classification using the Genome Taxonomy Database Toolkit v0.2.2 (GTDB-Tk), which is a database of quality-controlled genomes that aims to standardize microbial taxonomy through genome phylogeny (Parks et al., 2018). Pyani v0.2.8[6] and the enveomics collection toolbox were used to calculate the pairwise average nucleotide identity (ANI) and the pairwise average amino acid identity (AAI) between the genomes, respectively (Konstantinidis and Tiedje, 2005a,b; Rodriguez-R and Konstantinidis, 2014, 2016). The occurrence of split genes was analyzed as described in **Supplementary Information**. Two phylogenetic reconstructions were conducted to evaluate the phylogenetic placement of the Hakuba *Actinobacteria* genome:

(1) A maximum likelihood (ML) tree was created using the GToTree v1.1.6 (Lee, 2019) pipeline based on 138 *Actinobacteria*-specific single copy genes[7]. Reference genomes from *Actinobacteria* were used, and the outgroups consisted of several genomes from each family of *Firmicutes* and *Proteobacteria* (**Supplementary Table S2**). The concatenated multiple sequence alignment of deduced amino acids was then uploaded to the CIPRES Science Gateway (Miller et al., 2010) to create a ML tree using RAxML-HPC2 on XSEDE (Stamatakis et al., 2008; Stamatakis, 2014) with options WAG PROTGAMMA model and autoMRE bootstrapping.

(2) A Bayesian phylogenetic reconstruction was conducted in Beast2 v2.5.2 (Bouckaert and Vaughan, 2019) with a subset of reference genomes used for the ML tree reconstruction (**Supplementary Table S3**). After generating a multiple sequence alignment using GToTree, a Bayesian tree was constructed using the WAG substitution model that assumed a gamma distribution with 4 categories and a relaxed clock log normal distribution with

[3]http://hmmer.org

[4]https://github.com/tseemann/barrnap/blob/master/README.md

[5]https://jgi.doe.gov/data-and-tools/bbtools/bb-tools-user-guide/bbnorm-guide/

[6]https://github.com/widdowquinn/pyani

[7]https://github.com/AstrobioMike/GToTree/tree/master/hmm_sets

Markov chain Monte Carlo simulations (Drummond et al., 2002) set to 50,000,000 (logging every 5,000). This substitution model was selected with PartitionFinder v2.1.1 (Lanfear et al., 2016). A burn-in of 70 percent was set to combine two converging trees of Beast2, as viewed using Tracer v1.7.1 (Rambaut et al., 2018), resulting in 13,501 samples and an effective sample size of 1,278 for tree likelihood and 529 for posterior.

The phylogenetic placement of the Hakuba *Actinobacteria* co-assembled genome amongst all the genomes available in the NCBI RefSeq and Genbank database was confirmed using GTDB-Tk v0.2.2 (reference database version r86 v3). Taxonomic classification was confirmed with the classify workflow (classify_wf), which utilizes the third-party dependencies pplacer (Matsen et al., 2010), FastANI (Jain et al., 2018), Prodigal (Hyatt et al., 2010), FastTree (Price et al., 2010), and HMMR (Eddy, 2011). The classify workflow will first identify bacterial and archaeal marker genes, followed by creating and concatenating multiple sequence alignments. After filtering the alignment to 5,000 amino acids, the workflow will then classify each genome using the GTDB-Tk reference tree and determine the relative evolutionary divergence and ANI.

Selected Protein Sequences [Carbon Monoxide Dehydrogenase / Acetyl-CoA Synthase (CODH/ACS), formylmethanofuran dehydrogenase (Fwd), V-type ATPase, adenosine-5′-phosphosulfate (APS), 3′-phosphoadenosine 5′-phosphosulfate (PAPS) reductase, nitrate reductase alpha subunit NarG, and RubisCO] were aligned using MAFFT (Katoh et al., 2002) with options –maxiterate 1000 and default parameters. For the proteins CODH/ACS, APS, PAPS, NarG, and RubisCO, phylogenetic trees were created. Briefly, gaps were removed with trimAI v1.4.rev15 (Capella-Gutierrez et al., 2009) using option automated1. Manual curation was also done before creating a ML tree using either FastTree v2 (Price et al., 2010) or RAxML on the CIPRES Science Gateway (Miller et al., 2010). All phylogenetic trees were checked using Archaeopteryx (Han and Zmasek, 2009) and FigTree[8].

Genes coding for [NiFe]- and [FeFe]-hydrogenases were identified by comparison against a curated in-house database (E.S. Boyd, unpublished data). Resulting catalytic subunits were checked for characteristic N- and C-terminal cysteine motifs associated with [NiFe]-hydrogenase variants and the L1, L2, and L3 motifs for [FeFe]-hydrogenase variants (Vignais and Billoud, 2007). The large catalytic subunits of the [NiFe]-hydrogenases were subjected to phylogenetic analysis, as described above, but using the IQtree ML algorithm with the LG+G amino acid substitution model and 1,000 bootstraps to evaluate node support. The phylogenetic analysis included representatives of the primary [NiFe]-hydrogenase groups (Greening et al., 2016) in addition to close representatives of the query sequences that were present in the NCBI database. Gene neighborhood analysis was conducted by surveying the co-assembly and individual SAGs for representatives associated with either Group 3 [NiFe]-hydrogenases (Peters et al., 2015) or those associated with [FeFe]-hydrogenases (Poudel et al., 2016).

[8]http://tree.bio.ed.ac.uk/software/figtree/

RESULTS AND DISCUSSION

Bacterial Community Structure of the Hakuba Happo #3 Well

The geochemistry of Happo #3 waters from 2011 to 2016 is summarized in **Table 1**. The taxonomic composition of the bacterial community based on 16S rRNA gene amplicon sequencing is depicted in **Supplementary Figure S1** and summarized in **Supplementary Table S4**. The dominant bacterial phyla were *Nitrospirae* (47%), "Parcubacteria" (19%), *Deinococcus-Thermus* (16%), and *Actinobacteria* (9%), followed by *Firmicutes* (5%), *Bacteroidetes* (2%), among others (<1%). Only 57 ASVs were detected from both the "Total" (17,058 total reads) and "Sequential" (10,390 total reads) samples, and the majority (90%) were represented by 15 ASVs. Such low bacterial diversity is consistent among serpentinite-hosted systems. For example, at The Cedars, 16 phylotypes (>99% sequence similarity cutoff) represented 84% of the 16S rRNA amplicon sequences recovered from the shallow-sourced spring

TABLE 1 | Geochemistry of Happo #3 from 2011 to 2016.

	2011[a]	2016
Temperature	48°C	47.5°C[b]
pH	10.7	10.95[b]
ORP	n.m.	−435 mV[b]
EC	48.3 mS/m	47.7 mS/m[b]
DO	0.59 mg/L	0.10 mg/L[b]
Salinity	0.02%	n.d.[b] (detection limit 0.1%)
H_2	201 μM	n.m.
CH_4	124 μM	n.m.
C_2H_6	0.2 μM	n.m.
N_2	1298 μM	n.m.
Ca^{2+}	130 μM	220 μM
K^+	70 μM	125 μM
Na^+	1160 μM	1565 μM
NH_3	n.m.	7 μM
Al_3^+	10 μM	n.m.
Li^+	10 μM	n.m.
Cl^-	180 μM	155 μM
SO_4^{2-}	10 μM	8 μM
F^-	4 μM	n.m.
Formate	n.m.	80 μM
Acetate	n.m.	<40 μM
Not detected[c]		Pyruvate, lactate propionate, NO_2^-, NO_3^-, HCO_3^-, Mg^{2+}, PO_4^{2-}, total Fe, nucleobases, nucleosides, and amino acids

[a]Published in Suda et al. (2014). [b]Nobu et al., unpublished data. [c]No peak detected; Detection limits: Pyruvate (40 μM), lactate (40 μM), propionate (40 μM), NO_2^- (2.2 μM), NO_3^- (1.6 μM), HCO_3^- (0.02 μM), Mg^{2+} (20.6 μM), PO_4^{2-} (0.01 μM). CO_2 and total Fe not detected as described in Suda et al. (2014). Nucleobases and nucleosides include cytosine (179 nM), uracil (659 nM), adenine (740 nM), guanine (1.3 μM), C-ribonucleosides (47 nM), U-ribonucleosides (340 nM), A deoxyribonucleosides (71 nM), G deoxyribonucleosides 64 nM), C-deoxyribonucleosides (470 nM), T-deoxyribonucleosides (133 nM), A-deoxyribonucleosides (400 nM), and CH1 amino acids (50 μM). n.m. = not measured. n.d. = not detected.

and 98% of those from the deep-sourced spring (Suzuki et al., 2013). In the Cabeço de Vide Aquifer, 45 phylotypes (≥97% similarity cutoff) were identified, dominated by four major taxonomic classes (Tiago and Veríssimo, 2013). Other serpentinite-hosted systems with comparatively few phylotypes include the Samail ophiolite (Rempfert et al., 2017; Fones et al., 2019), the Coast Range Ophiolite Microbial Observatory (Crespo-Medina et al., 2014; Twing et al., 2017), the Voltri Massif (Quéméneur et al., 2015; Brazelton et al., 2017), and the Zambales ophiolite (Meyer-Dombard et al., 2018). The microbial diversity and abundance of cells were previously shown to be pH-dependent within the Samail ophiolite (Rempfert et al., 2017; Fones et al., 2019). Compared to the 'principal community' amongst several serpentinite-hosted systems identified by Meyer-Dombard et al. (2018), Happo #3 contained few *Proteobacteria*, whereas *Nitrospirae* and "Parcubacteria" predominated.

The Happo #3 community included three ASVs affiliated with an early-branching, uncultivated *Actinobacteria* lineage that has not been previously observed in terrestrial serpentinite-hosted systems. These *Actinobacteria* ASVs shared 98% sequence identity and clustered with the clade RBG-16-55-12 in the SILVA v132 database (Quast et al., 2012; Yilmaz et al., 2014), previously classified within the clade OPB41 in the SILVA v128 database. The RBG-16-55-12 members are located in a variety of environments, including subsurface environments (Anantharaman et al., 2016), mine tailing ponds (Ramos-Padrón et al., 2011), mud volcanoes (Chang et al., 2012), hot springs (Hugenholtz et al., 1998), and deep sea sediments (Kato et al., 2009).

General Characteristics and Taxonomic Classification of the Hakuba Actinobacteria SAGs

We conducted single-cell genomics of the Happo #3 samples and identified 10 SAGs belonging to the RBG-16-55-12 clade based on their 16S rRNA sequences. The general characteristics of these 10 SAGs are listed in **Supplementary Table S1**. "Low" (n = 6), "Medium" (n = 3), and "High" (n = 1) quality SAGs were identified according to the MISAG standard for *Bacteria* and *Archaea* (Bowers et al., 2017). The range of completeness was between 33.1 and 92.8% with 0.7% and 6.5% contamination (median = 1.4% contamination), as estimated by the Anvi'o marker gene-based approach (Eren et al., 2015; **Supplementary Table S5**). Based on ANI (**Supplementary Table S6**) and AAI (**Supplementary Table S7**), these 10 SAGs represent the same species (≥98% pairwise ANI for all 10 SAGs; ≥ 90% pairwise AAI for SAGs with > 50% completeness) with GC content ranging from 48.5 to 49.2%. It has been suggested that species boundary is approximately 95% (ANI) and 90% (AAI) (Konstantinidis and Tiedje, 2005a; Richter and Rosselló-Móra, 2009).

The genomes were subsequently co-assembled into one composite genome assembly ("Hakuba co-assembly") of all 10 SAGs combined, resulting in 93.5% completeness and 6.5% contamination (**Table 2**). The co-assembly was generated to guide genome analysis of the SAGs to supplement the inherent biases of single-cell genomics caused during WGA (e.g., chimeric DNA, uneven genome coverage, low completeness) (Xu and Zhao, 2018). Sequence similarity analysis of the 588 co-assembled contigs using the Kaiju taxonomic classifier (Menzel et al., 2016) with the NCBI nr database did not provide confident placement of the taxonomic position of this genome. The taxonomic affiliation of the contigs was not consistent (**Supplementary Table S8**): the contigs were affiliated with "unclassified" (43%), *Firmicutes* (11%), *Proteobacteria* (9%), *Actinobacteria* (5%), *Chloroflexi* (4%), *Nitrospirae* (4%), *Euryarchaeota* (2%), "Omnitrophica" (2%), and others (<1%). The contigs not taxonomically identified as *Actinobacteria* were not removed for two reasons: (1) the SAG and co-assembled genome redundancy (Anvi'o) and contamination (CheckM) were < 6.5% (median = 1.4% contamination) (**Supplementary Table S1**) and (2) contig clustering by sequence composition on Anvi'o and ACDC did not reveal that these taxa contributed to contamination (**Supplementary Figure S2**). Similar inconsistent results of taxonomic affiliation were reported for genomes of *Bacteria* belonging to deeply branching lineages with limited reference sequences, such as members within the candidate bacterial phylum OP9 (Dodsworth et al., 2013).

Based on taxonomic analysis using GTDB-Tk (**Supplementary Table S9**), the Hakuba co-assembly and the 10 SAGs were classified to the uncultured, class-level clade "UBA1414" in the *Actinobacteria* phylum. This clade includes four Baltic Sea SAGs and one metagenome-assembled genome (MAG) from the Rifle aquifer (GCA_001767735). GTDB-Tk was also used to estimate the novelty of the Hakuba *Actinobacteria* genomes by calculating a relative evolutionary divergence metric and comparing against the GTDB rank normalized taxonomy. This metric is more robust than pairwise AAI to assign taxonomic rank as it considers the variation in the evolutionary tempos amongst different lineages (Hugenholtz et al., 2016; Parks et al., 2018). Based on this metric, the Hakuba SAGs and co-assembly could represent a new order within the UBA1414 class while the Baltic Sea SAGs and Rifle MAG represent new species within the genus currently named "20-14-0-20-35-9" in GTDB. According to the classification of GTDB, two closely related class-level clades to UBA1414 are "UBA9087" and "RBG-13-55-18," which consist of several MAGs from the Rifle aquifer, one MAG from Crystal Geyser, and one MAG from SURF (**Table 3**). These three clades (UBA1414, UBA9087, and RBG-13-55-18) correspond to two 16S rRNA-based clades in the SILVA v132 database: WCHB1-81 and the above-mentioned clade, RBG-16-55-12.

The relationship of the clades UBA1414, UBA9087, and RBG-13-55-18 was further examined by ML and Bayesian phylogenetic analyses of a concatenated protein sequence (**Figure 1** and **Supplementary Figure S3**). The monophyly of the three clades was confirmed by both methods, which generated identical topologies with a high confidence level for the clades. The Hakuba co-assembly formed a clade with the Baltic Sea SAGs and one Rifle MAG (GCA_001767735), similar to the analysis using GTDB-Tk (**Supplementary Table S9**).

TABLE 2 | Basic information for the co-assembled Hakuba genome and SAG S34.

Analysis project type	Co-assembled genome	SAG ID: S34
DDBJ BioProject	PRJDB8357	PRJDB8357
DDBJ Accession Number Co-assembly	BLSE01000001–BLSE01000587	
DDBJ Accession Number SAGs	BLRU01000000–BLRZ01000000, BLSA01000000–BLSD01000000	BLRZ01000001–BLRZ01000510
Co-assembly/SAG information		
Cell isolation approach	FACS	
Single cell lysis approach	Chemical and enzymatic	
Single cell kit	Qiagen REPLI-g Single Cell Kit (multiple displacement amplification)	
Assembly software	SPAdes v3.10.1	
Estimation of completeness	Anvi'o v5.3 (marker gene-based approach)	
Assembly quality[a]	Medium quality	High quality
Estimated completeness	93.5%	92.8%
Contamination	6.5%	1.4%
Genome information		
Genome size	2,947,136 bp	2,120,563 bp
Number of contigs	588	316
N50	8,580	13,695
Max contig length	37,255 bp	55,032 bp
rRNAs	2 (16S), 2 (23S), 1 (5S)	1 (16S), 1 (23S)
tRNAs	45	47
GC Content	48.5%	48.6%

*The genome was co-assembled from 10 single-cell amplified genomes (SAGs) collected from Happo #3 (see **Supplementary Table S1** for individual SAGs). The SAG S34 represents the highest quality SAG obtained. [a]Based on the minimum information of single amplified genome (MISAG) criteria (Bowers et al., 2017).*

TABLE 3 | Information for the metagenome-assembled genomes (MAGs) and single-cell amplified genomes (SAGs) analyzed in this paper.

Clade	ID	NCBI BioProject (BioSample)	Completeness (%)	Contamination (%)	References
UBA1414	Baltic Sea_59E_21H_M23	PRJNA417388[a]	54.7	1.4	Bird et al., 2019
	Baltic Sea_59E_21H_O21	PRJNA417388[a]	52.5	1.4	Bird et al., 2019
	Baltic Sea_60B_13H_A10	PRJNA417388[a]	69.8	2.9	Bird et al., 2019
	Baltic Sea_60B_13H_C09	PRJNA417388[a]	71.9	1.4	Bird et al., 2019
	GCA_001767735_Rifle_CO	PRJNA288027 (SAMN04314056)	63.3	2.9	Anantharaman et al., 2016
	Hakuba_co-assembly[b]	PRJDB8357	93.5	6.5	This study
RBG-13-55-18	GCA_001767755_Rifle_CO	PRJNA288027 (SAMN04313673)	60.4	0.0	Anantharaman et al., 2016
	GCA_001768645_Rifle_CO	PRJNA288027 (SAMN04313996)	97.1	0.7	Anantharaman et al., 2016
	GCA_001767605_Rifle_CO	PRJNA288027 (SAMN04313722)	97.8	0.0	Anantharaman et al., 2016
	SURF_21	PRJNA355136[c]	89.2	0.7	Momper et al., 2017
UBA9087	GCA_001767575_Rifle_CO	PRJNA288027 (SAMN04314195)	78.4	1.4	Anantharaman et al., 2016
	GCA_001871795_Crystal_Geyser	PRJNA297582 (SAMN04328288)	95.7	0.7	Burstein et al., 2016

Completeness and contamination were determined by Anvi'o marker gene-based approach (Eren et al., 2015). [a] The cleaned genome assemblies were provided by Dr. Karen Lloyd. [b]The highest quality Hakuba SAG S34 has 92.8% completeness and 1.4% contamination. [c] The cleaned genome assemblies were obtained from the data depository referenced in Momper et al. (2017).

However, no genomes showed > 45% pairwise AAI and > 76% pairwise ANI to the Hakuba co-assembly and 10 SAGs (**Supplementary Tables S6, S7**). It has been suggested that the genus-level boundary is ≥ 60% for pairwise AAI (Rodriguez-R and Konstantinidis, 2014). This further demonstrates the novelty of the Hakuba SAGs, possibly as a new order

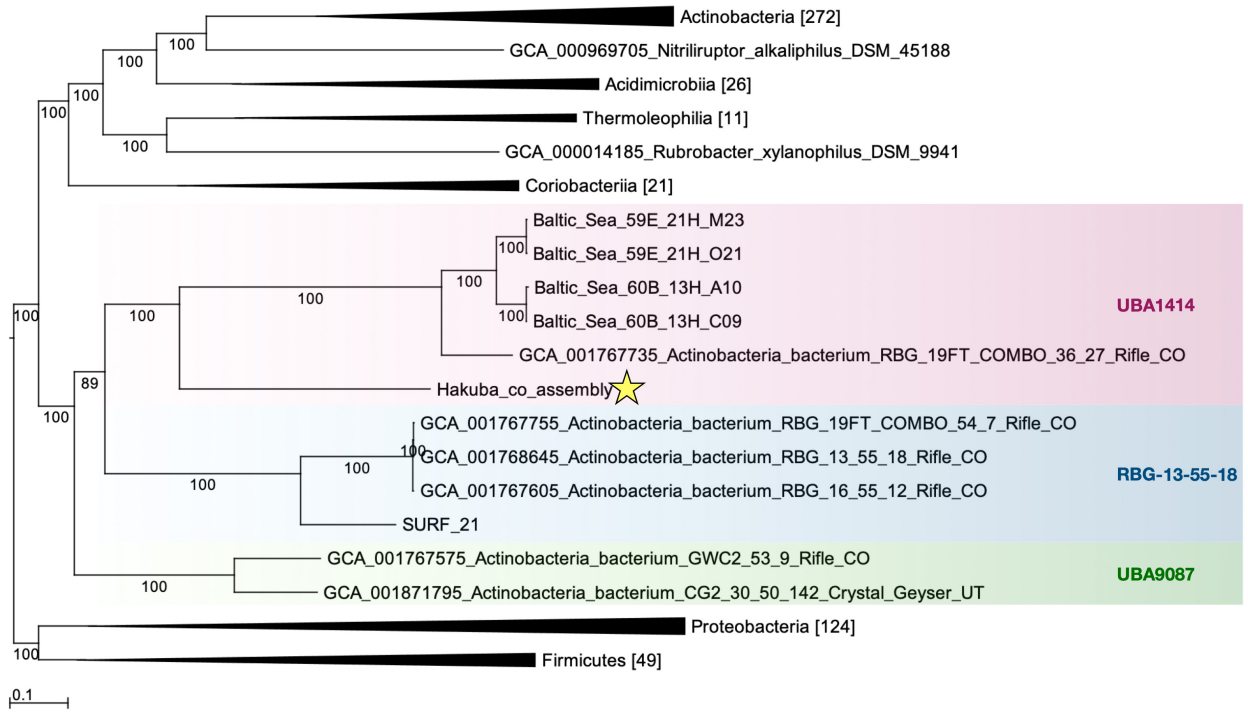

FIGURE 1 | Maximum-likelihood phylogenetic tree of clades UBA1414, RBG-13-55-18, and UBA9087. The Hakuba co-assembly (denoted by a star) formed a clade with the Baltic Sea SAGs and a Rifle MAG. Bootstrap support values are shown on each branch, and the Bayesian posterior probability is depicted in **Supplementary Figure S3**. Representatives of *Proteobacteria* and *Firmicutes* were used as the outgroups. The genomes used in this figure are listed in **Supplementary Table S2** and the number in brackets represents the count of genomes used in the clade. GToTree v1.1.6 (Lee, 2019) and RAxML-HPC2 (Stamatakis et al., 2008; Stamatakis, 2014) on the CIPRES Science Gateway (Miller et al., 2010) were used to create the ML tree, which is based on 138 concatenated *Actinobacteria*-specific single copy genes.

within the UBA1414 class, as suggested by the GTDB-Tk analysis.

The Hakuba Actinobacteria Genomes Encode the Wood–Ljungdahl Pathway

The Hakuba co-assembly contains all key genes for the Wood–Ljungdahl (WL) pathway for CO_2 fixation (Ragsdale, 2008; **Figure 2**). The presence of this pathway has yet to be reported in *Actinobacteria* (Adam et al., 2018); only genes homologous to CODH (*cooS/cdhA/acsB*) in five actinobacterial genomes have been reported (Inoue et al., 2019). The genes for the WL pathway found in the Hakuba co-assembly are: CODH/acetyl-CoA synthase complex (*acs*), formate dehydrogenase (*fdhDF*), formyl-tetrahydrofolate (THF) synthase (*fhs*), bifunctional 5,10-methenyl-THF cyclohydrolase / 5,10-methylene-THF dehydrogenase (*folD*), and methylene-THF reductase (*metF*). These genes, including those for the CODH/ACS complex, are also found in four other genomes within the clades UBA1414 and RBG-13-55-18, including two genomes from the Baltic Sea (60B_13H_A10 and 60B_13H_C09) and two genomes from Rifle (GCA_001768645 and GCA_001767605).

The Hakuba co-assembly harbors the genes *fdhD* and *fdhF* that encode proteins involved in the reduction of CO_2 to formate. The source of inorganic carbon could be from the environment or from pyruvate oxidation by the action of pyruvate ferredoxin oxidoreductase (PorABDG) (Ragsdale, 2003) or pyruvate dehydrogenase (PdhABCD) (de Kok et al., 1998). In serpentinite-hosted environments, there is limited dissolved inorganic carbon, and due to the alkaline pH and presence of high concentrations of divalent cations (e.g., Ca^{2+}), inorganic carbon, such as CO_2, is rapidly sequestered into mineral carbonates (Matter and Kelemen, 2009). Indeed, the total inorganic carbon in Happo #3 was undetectable (Suda et al., 2014). One candidate source of inorganic carbon is carbon monoxide (CO). CO can be synthesized in these types of environments (Seewald et al., 2006; McCollom and Seewald, 2007) and has been detected in other serpentinite-hosted systems, such as the Coast Range Ophiolite Microbial Observatory (Twing et al., 2017). Furthermore, CO can be utilized by the microbial community in these ecosystems (Morrill et al., 2014; Fones et al., 2019). The Hakuba co-assembly contains genes for anaerobic-type CO dehydrogenase (*cooS* and *cooF*), and the CO dehydrogenase maturation protein (*cooC*). Bicarbonate, if present, could also be another source of inorganic carbon as the Hakuba co-assembly encodes two Na^+-dependent bicarbonate transporters, indicating the potential to uptake HCO_3^-, similar to acetogens (Braus-Stromeyer et al., 1997; Smith and Ferry, 2000; Pander et al., 2019). However, homologs of genes coding for carbonic anhydrase that converts HCO_3^- to CO_2 were not detected in the genome assembly.

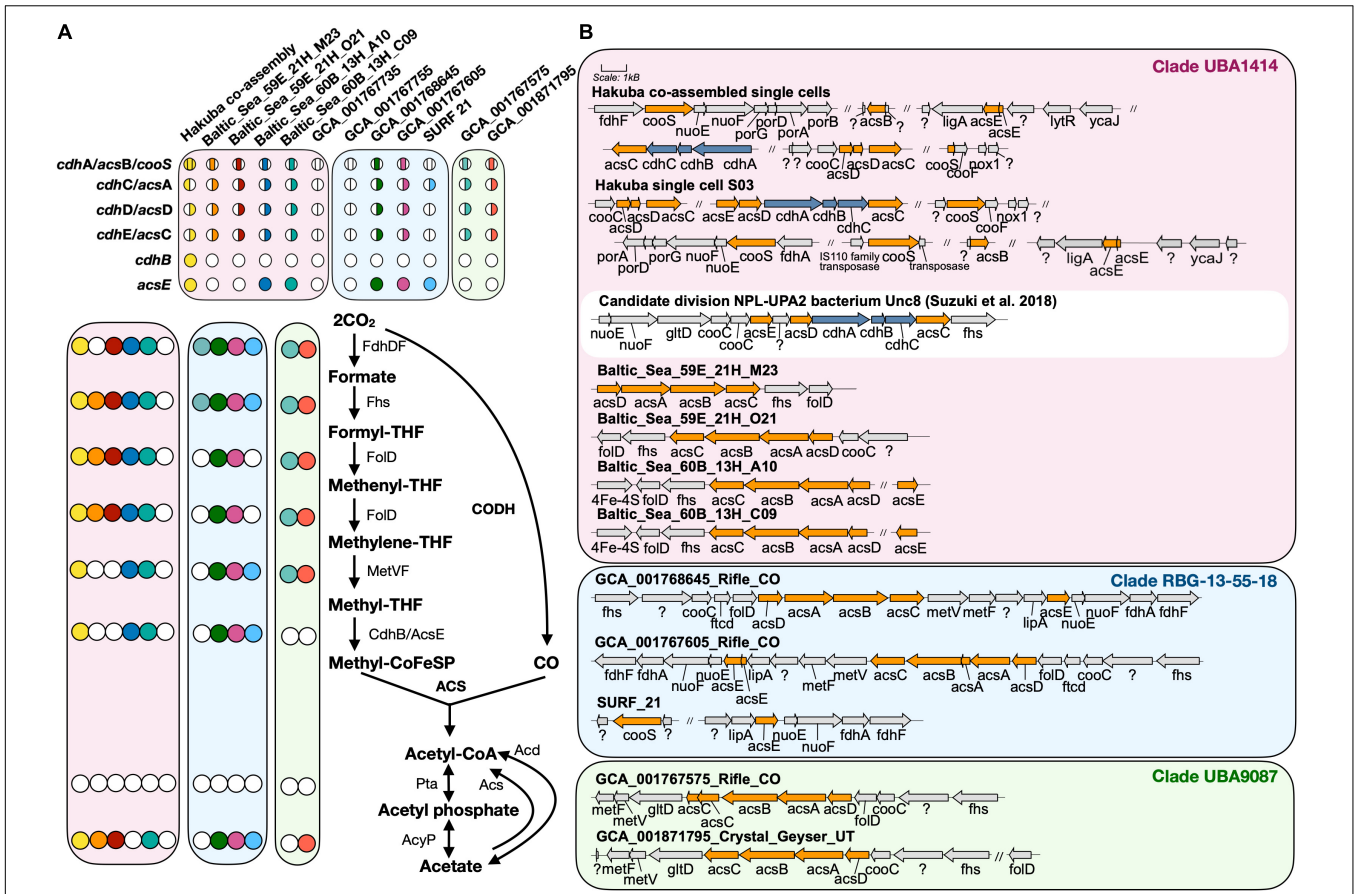

FIGURE 2 | Key enzymes encoded by genomes within clades UBA1414, RBG-13-55-18, and UBA9087 for the Wood–Ljungdahl Pathway. **(A)** The presence of proteins involved in the WL pathway are depicted with a colored circle while the absence is depicted by a white circle. Each color corresponds to a genome used in this study. For CODH/ACS, the colored circle is split by the bacterial- or archaeal-type subunit, and the location of the color indicates whether a gene was present or not within the assembly. The proteins Acs and Acd do not have corresponding circles. **(B)** The gene neighborhood of CODH/ACS is shown for each genome and was designed using Gene Graphics (Harrison et al., 2017). Gene neighborhoods on different contigs are denoted by "//." The three clades are color coded as done in **Figure 1**. The gene neighborhood of Candidate division NPL-UPA2 bacterium Unc8 (Suzuki et al., 2018), a putative acetogen from a serpentinite-hosted system called The Cedars, is depicted in a white box for comparison of hybrid CODH/ACS. Abbreviations: *acyP* (acylphosphatase), *acd* (ADP-forming acetyl-CoA synthetase), *acs* (acetyl-CoA synthase), *cdh* (carbon monoxide dehydrogenase), *cooS* (carbon monoxide dehydrogenase), *fdh* (formate dehydrogenase), *fhs* [formyl-tetrahydrofolate (THF) synthase], *folD* (bifunctional 5,10-methenyl-THF cyclohydrolase/5,10-methylene-THF dehydrogenase), *ftcD* (glutamate formiminotransferase /formiminotetrahydrofolate cyclodeaminase), *gltD* (glutamate synthase), *ligA* (DNA ligase), *lipA* (lipoyl synthase), *lytR* (cell envelope-related function), *met* (Methylene-THF reductase), *nox1* (NADH oxidase), *nuo* (NADH-quinone oxidoreductase), *pta* (phosphotransacetylase), *por* (pyruvate ferredoxin oxidoreductase), *ycaJ* (putative ATPase).

Besides environmental sources of inorganic carbon, CO_2 can be generated *via* the action of PorABDG or PdhABCD, as described above. Pyruvate, as the substrate, is produced in glycolysis in this bacterium. Although there are no reports of the abiotic serpentinization reaction resulting in formation of sugars, such as galactose, the Happo #3 well is located in an alpine, forested ecosystem, and the sugars could be derived from soil organic carbon. The utilization of CO_2 by the WL pathway from pyruvate oxidation *via* glycolysis has been observed in acetogens, such as *Moorella thermoacetica* (Fontaine et al., 1942; Barker and Kamen, 1945; Drake et al., 1981; Menon and Ragsdale, 1996). In such cases, the WL pathway may also work to balance redox and regenerate the electron carriers used during glycolysis or other carbon substrate oxidation (Schuchmann and Müller, 2016).

Genes for the formylmethanofuran dehydrogenase-like complex (*fwdABCD*) are also present within the Hakuba co-assembly or SAGs but without the genes for subunit *fwdE* and the ferredoxin subunits *fwdFG*. The Fwd complex catalyzes the first step in CO_2 reduction for methanogenesis and contains a tungsten active site (within FwdB), as compared to the molybdenum-dependent isoenzyme Fmd (Hochheimer et al., 1995, 1996; Wagner et al., 2016). The full operon is present in SAG S47 (*fwdDBA-ftr-fwdC*) with formylmethanofuran-tetrahydromethanopterin N-formyltransferase (*ftr*). This operon structure is similar to the organization of a homologous complex, formyltransferase/hydrolase complex (Fhc), found in methylotrophs that converts formyl-H_4MPT (tetrahydromethanopterin) to formate

(Pomper et al., 2002; Adam et al., 2019; Hemmann et al., 2019). However, the genes to synthesize methanopterin derivatives, such as dihydromethanopterin reductase and tetrahydromethanopterin:alpha-L-glutamate ligase (Xu et al., 1999; Maden, 2000; Scott and Rasche, 2002), were not observed in the Hakuba actinobacterium genome. In addition, compared to *fhcB* from the methylotroph *Methylorubrum extorquens* (Hemmann et al., 2019), the amino acid sequence of the catalytic subunit *fwdB* from the Hakuba SAGs lacks the sequence motifs for a tungstopterin cofactor and contains two necessary components for a functioning *fwdB*: a N-terminal domain with [4Fe-4S] cluster and a catalytic Cys118 (**Supplementary Figure S4**).

In methanogens, FwdABD comprise the catalytic subcomplex while the function of FwdC remains unknown (Wagner et al., 2016). FwdE is an iron-sulfur protein (Hochheimer et al., 1995) and is hypothesized to function as a DNA-binding protein in acetogens (Shin et al., 2016). The gene cluster *fwdABCD* without *fwdE* was also identified in the methanogen OP bin 54 (*Methanomethyliales*) (Berghuis et al., 2019). In *Methanosarcina acetivorans*, the synthesis of FwdDBAC is likely important for carboxydotrophic growth and is potentially involved in the production of formate (Matschiavelli and Rother, 2015). In comparison, in the genomes of 14 cultivated acetogens, only the subunit *fwdE* is observed (Shin et al., 2016). Similarly, the Rifle MAGs within sub-clades RBG-13-55-18 and UBA9087 harbor *fwdE* but not *fwdABCD*. The presence of the catalytic subunits *fwdABD* in the Hakuba co-assembly or SAGs suggests that the Fwd-like complex could be active, with potential function during growth on CO, as demonstrated for *Methanosarcina acetivorans* (Matschiavelli and Rother, 2015).

CO_2 reduction could be driven by reducing equivalents generated by hydrogen (H_2) oxidation *via* [NiFe]- or [FeFe]-hydrogenases (**Figure 3** and **Supplementary Figures S5**, **S6**). Although known acetogens encode hydrogenase modules in a gene cluster containing a *fdh* gene (Shin et al., 2016), the hydrogenase genes in genomes of clades UBA1414, UBA9087, and RBG-13-55-18 are not clustered with *fdh,* with the exception of the Rifle MAG GCA_001767575. Considering that these are incomplete genomes derived from metagenomic or single-cell genomic assemblies (**Table 3**), it is possible that a gene cluster containing *fdh* and hydrogenases was fragmented. Two [NiFe]-hydrogenase genes were identified in the Hakuba co-assembly and were phylogenetically affiliated with Group 3b and Group 3d [NiFe]-hydrogenases (**Figure 3A**) that are coupled to the bidirectional reduction of $NADP^+$ and NAD^+, respectively, in other organisms (Vignais et al., 2001; Peters et al., 2015). Accordingly, the diaphorase (*hyhG* or *hoxF*) and Fe-S (*hyhB* or *hoxU*) cluster modules associated with these two enzymes were also co-localized with the large (*hyhL* or *hoxL*) and small (*hyhS* or *hoxS*) subunits of the respective [NiFe]-hydrogenase groups (**Figure 3B**; Peters et al., 2015). The other genome assemblies in the three clades also encoded [NiFe]-hydrogenases that were variably affiliated with either group 1, group 3b, group 3c, or group 3d (**Supplementary Figures S5**, **S6**). Amongst all the genome assemblies in the three clades, the Hakuba co-assembly is the only genome to encode a [FeFe]-hydrogenase. The Hakuba co-assembly encoded the catalytic subunit HydA, and the Hakuba SAG S47 also encoded the cluster HydABC along with [FeFe]-hydrogenase accessory proteins, including HydEFG (Posewitz et al., 2004). The HydABC cluster was present within the gene neighborhood of the Group 3b-like [NiFe]-hydrogenase (**Figure 3**). Homologs of HydABC have been suggested to be involved in electron bifurcation (Schut and Adams, 2009; Poudel et al., 2016), a process where reversible H_2 oxidation is coupled to simultaneous reduction of NAD^+ and ferredoxin (Fd) (Buckel and Thauer, 2013). Electron bifurcating hydrogenases are implicated in the energy conservation of model acetogens like *Acetobacterium woodii* (Wiechmann et al., 2020) *via* coupling of Fd (oxidation/reduction) and NAD^+/NADH reduction and oxidation with H_2 (oxidation/reduction). It is possible that such activities are also catalyzed by the Hakuba actinobacterial cells in conjunction with the reduction/oxidation of $NAD(P)^+$/NAD(P)H via the [NiFe]-hydrogenases.

Over the next few steps of the WL pathway, formate is likely converted to methyl-THF. From formyl-THF to methenyl-THF, the bifunctional 5,10-methenyl-THF cyclohydrolase / 5,10-methylene-THF dehydrogenase (FolD) is likely the enzyme used by the Hakuba bacterium and those within clades UBA1414, UBA9087, and RBG-13-55-18. In comparison, pan-genome analysis of 14 cultivated acetogens demonstrated that this conversion mainly occurs with the enzyme formyl-THF cyclohydrolase (Fch) (Shin et al., 2016). However, in the acetogen *Moorella thermoacetica*, FolD is used as a bifunctional protein with cyclohydrolase and dehydrogenase activity for the two-step conversion of formyl-THF to methylene-THF (O'Brien et al., 1973). Given the absence of *fch* and presence of *folD* in the clades UBA1414, UBA9087, and RBG-13-55-18, these genomes likely contain a bifunctional *folD* similar to *Moorella thermoacetica*. Methylene-THF reductase subunits V and F (MetVF) then catalyze the reduction from methylene-THF to methyl-THF (**Figure 4**). Interestingly, *metVF* in the Hakuba co-assembly is located with the F_{420}-non-reducing hydrogenase iron-sulfur subunit D (*mvhD*) and heterodisulfide reductase subunits *hdrA*, *hdrB*, and *hdrC* (*hdrA-mvhD-metVF-hdrCB*). In comparison, genome assemblies within clade RBG-13-55-18 encode a gene cluster with only *mvhD*/*hdrABC* while the other MAGs/SAGs of clades UBA1414, UBA9087, and RBG-13-55-18 do not harbor this gene cluster. The genes *hdrABC* encode a key enzyme in methanogens that is usually complexed with a [NiFe]-hydrogenase (HdrABC-MvhAGD) and functions in electron bifurcation to oxidize H_2 coupled with the reduction of Fd and CoM-S-S-CoB (a final product of methanogenesis; heterodisulfide coenzyme M and coenzyme B) (Kaster et al., 2011; Wagner et al., 2017). The *metVF*/*mvhD*/*hdrABC* gene cluster has been observed in acetogens, such as *Moorella thermoacetica* (Mock et al., 2014) and '*Candidatus* Adiutrix intracellularis' (Ikeda-Ohtsubo et al., 2016). In *Moorella thermoacetica*, this complex can reduce methylene-THF with benzyl viologen, and benzyl viologen can be reduced by NADH (Mock et al., 2014). Although the second electron acceptor remains unknown, it is likely that MetVF/MvhD/HdrABC from *Moorella thermoacetica* is capable of electron bifurcation *via* an electron-bifurcating flavin in the subunit HdrA (Mock et al., 2014). The MvhD

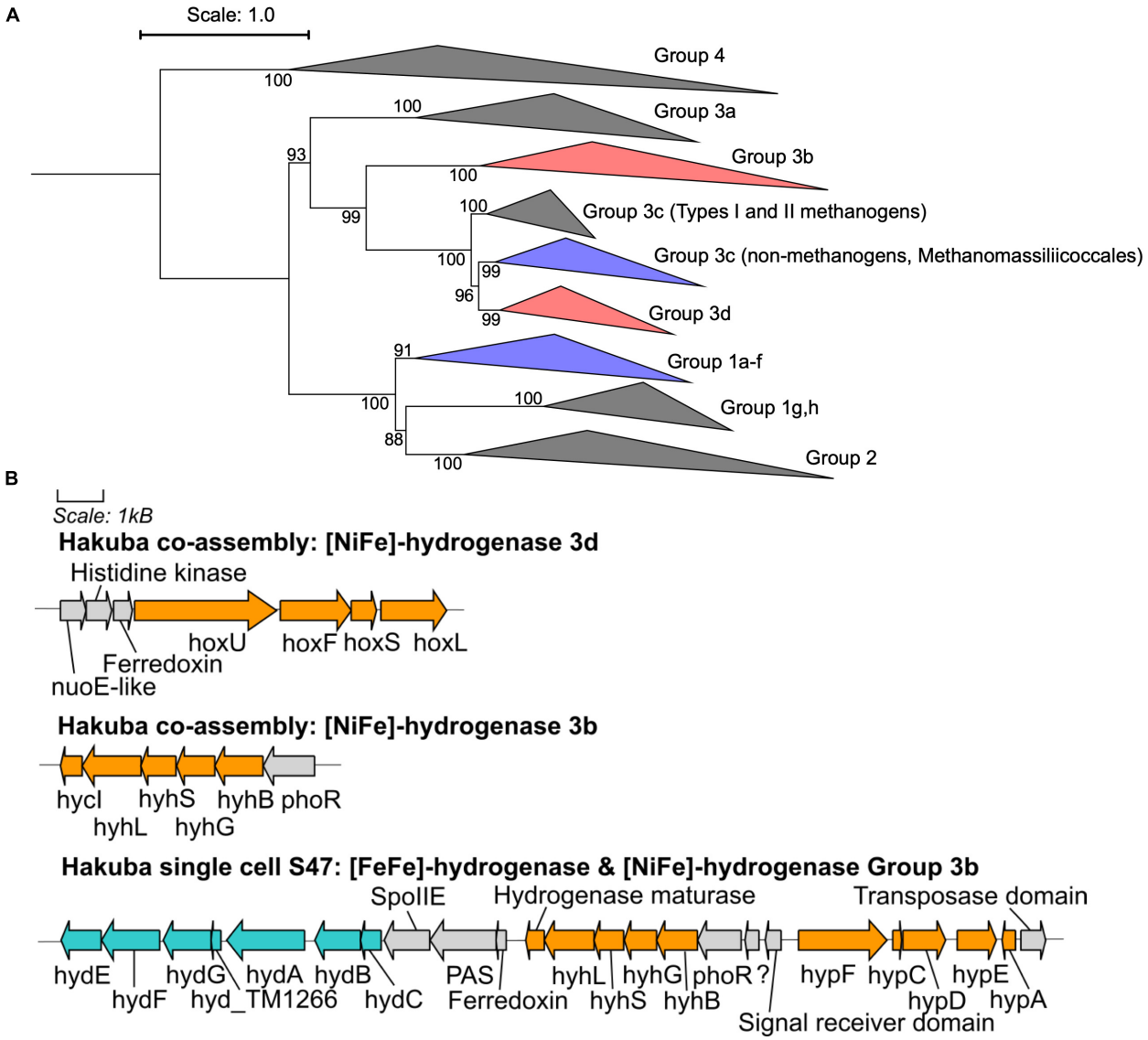

FIGURE 3 | Phylogenetic topology and gene neighborhood of hydrogenases. **(A)** The phylogenetic topology of [NiFe]-hydrogenases for clades UBA1414, RBG-13-55-18, and UBA9087. Groups 3b, 3c, 3d, and 1a-f are further expanded in **Supplementary Figures S5**, **S6**. The Hakuba co-assembly is indicated by red color and the other genomes are indicated in blue color. Bootstraps (out of 1000 replicates) are shown at the nodes. **(B)** The gene neighborhood of [NiFe]- and [FeFe]-hydrogenases in the Hakuba co-assembly and SAG S47, as designed using Gene Graphics (Harrison et al., 2017). The genes related to [NiFe]-hydrogenase and hydrogenase maturation are depicted in orange color. The genes related to [FeFe]-hydrogenase and hydrogenase maturation are depicted in blue color. Abbreviations: *hox* (NAD-Coupled [NiFe]-hydrogenase group 3d), *hycI* (hydrogenase maturase), *hydABC* ([FeFe-hydrogenase], *hydEFG* ([FeFe]-hydrogenase maturation), *hyd_TM1266* (putative iron-only hydrogenase system regulator), *hyh* (NADP-coupled [NiFe]-hydrogenase group 3b), *hyp* (hydrogenase expression/formation), *hypA* (hydrogenase nickel incorporation protein), *hypF* (hydrogenase maturation protein F), *nuoE* (NADH dehydrogenase subunit E-like), *phoR* (two-component system; phosphate regulon sensor histidine kinase P), *spoIIE* (Stage II sporulation protein E).

subunit of MvhAGD contains a [2Fe-2S] cluster (Wagner et al., 2017) and could potentially function to donate electrons to HdrABC. It is possible that this *metVF*/*mvhD*/*hdrABC* cluster is regulated by the same mechanism for the catalysis of methylene-THF to methyl-THF.

The next step in the WL pathway utilizes CODH/ACS to produce acetyl-CoA. A complete or partial gene cluster for the CODH/ACS complex was identified in all genomes in the three clades except for GCA_001767735 (Rifle; clade UBA1414) and GCA_001767755 (Rifle; clade RBG-13-55-18) (**Figure 2A**). The CODH/ACS enzyme complex consists of five subunits, in which four share homology between *Bacteria* and *Archaea* (Adam et al., 2018; Inoue et al., 2019): *cdhA* (*acsB* in *Bacteria*; α-subunit), *cdhC* (*acsA*; β-subunit), *cdhD* (*acsD*; δ-subunit), *cdhE* (*acsC*; γ-subunit). The gene only found in *Archaea* is *cdhB* (ε-subunit) while *acsE* is unique to *Bacteria*.

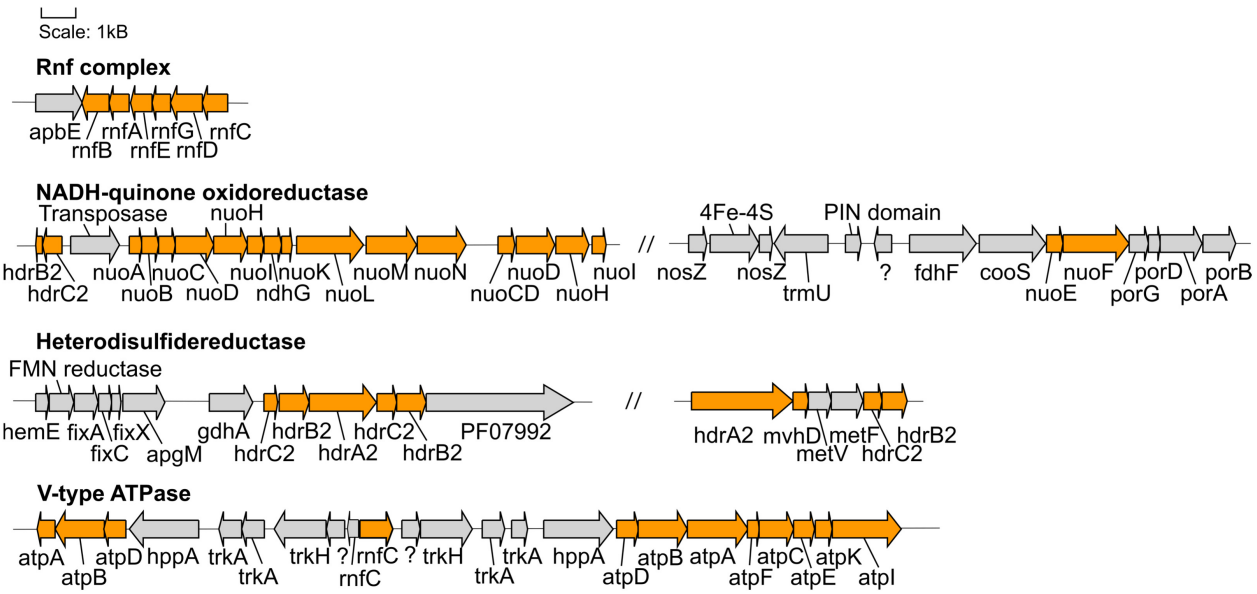

FIGURE 4 | Gene neighborhoods of genes encoding proteins involved in energy conservation found in the Hakuba co-assembly. The genes within the Hakuba co-assembly are colored orange while the other genes are colored gray. Gene neighborhoods on different contigs are denoted by "//." The gene neighborhood was designed using Gene Graphics (Harrison et al., 2017). Abbreviations: *apbE* (Mg^{2+}-dependent flavin transferase), *apgM* (2,3-bisphosphoglycerate-independent phosphoglycerate mutase), *coo* (carbon monoxide dehydrogenase), *fdh* (formate dehydrogenase), *fix* (electron transfer flavoprotein), *gdhA* (glutamate dehydrogenase), *hdr* (heterodisulfide reductase), *hemE* (uroporphyrinogen decarboxylase), *hppA* (K^+-stimulated pyrophosphate-energized sodium pump), *met* (methylenetetrahydrofolate reductase), *mvhD* (F420-non-reducing hydrogenase iron-sulfur subunit), *ndh* (NAD(P)H-quinone oxidoreductase), *nuo* (NADH-quinone oxidoreductase), *nosZ* (nitrous oxide reductase), *rnf* (Na^+-translocating ferredoxin:NAD^+ oxidoreductase), PF07992 (Pyridine nucleotide-disulphide oxidoreductase), *por* (pyruvate ferredoxin oxidoreductase), *trk* (Trk system potassium uptake protein), *trmU* (tRNA-uridine 2-sulfurtransferase).

Notably, the Hakuba co-assembly is the only genome amongst the three clades to harbor a hybrid CODH/ACS consisting of both archaeal- (*cdhABC)* and bacterial-type (*acsCDE*) subunits (**Figure 2** and **Supplementary Figure S7**). Although the Hakuba co-assembly did not contain the entire gene cluster for the CODH/ACS complex on one contig, the Hakuba SAG S03 had the full operon of *acsED-cdhABC-acsC*, in addition to separate gene clusters containing another *acsC*, a split *acsD*, and a split *acsE* (**Figure 2B**). The hybrid CODH/ACS has been observed in some putative acetogens, and several subunits have sequence similarity to subunits identified in a MAG of the candidate phylum NPL-UPA2 from the serpentinizing environment of The Cedars (Suzuki et al., 2018; **Supplementary Figure S7**). The hybrid CODH/ACS could be a result of horizontal transfer from *Archaea* to *Bacteria* (Adam et al., 2018; Suzuki et al., 2018). The biochemical properties of a hybrid CODH/ACS remain unknown and could provide insight into metabolisms present in serpentinizing systems and subsurface environments.

In the final steps of the WL pathway, acetyl-CoA is converted to acetate. Although none of the genomes within clades UBA1414, UBA9087, and RBG-13-55-18 harbor phosphotransacetylase (*pta*; acetyl-CoA to acetyl phosphate) or acetate kinase (*ack*; acetyl phosphate to acetate), several genome assemblies within all three clades contain homologs of acylphosphatase (*acyP*), suggesting the likely conversion of acetyl phosphate to acetate. It remains unclear whether the bacteria in all three clades can convert acetyl-CoA to acetyl phosphate, and potential genes which could replace *pta*, such as phosphotransbutyrylase (*ptb*), butyrate kinase (*buk*), or propanediol utilization protein (*pduL*) (Köpke et al., 2010; Poehlein et al., 2015), were not detected amongst any of the genomes. All genomes, except for three (Hakuba co-assembly/SAGs, BS_59E_21H_M23, and GCA_001767575), have the ADP-forming acetyl-CoA synthetase (*acd*) (**Supplementary Table S10**). The presence of the WL pathway and the absence of *ack* and *acd* in the Hakuba co-assembly/SAGs suggests that this bacterium likely cannot autotrophically fix CO_2, although the genome is incomplete. It is known that autotrophic growth by acetogenesis requires the ATP generated by the action of *ack* or *acd* (Musfeldt et al., 1999; Schuchmann and Müller, 2014).

Several genomes within clades UBA1414, UBA9087, and RBG-13-55-18 harbor genes that can convert acetate to other products, such as acetyl-CoA (acetyl-CoA synthetase, *acs*), acetaldehyde (aldehyde ferredoxin oxidoreductase, *aor*), and ethanol (aldehyde-alcohol dehydrogenase, *adhE;* alcohol dehydrogenase, *adh*) (**Supplementary Table S10**). Acetate may be derived from several sources, including the WL pathway, the L-cysteine synthesis pathway, and the environment *via* a putative acetate transporter. However, it remains unclear whether the Hakuba actinobacterium is a bonafide acetogen as it likely cannot convert acetyl-CoA to the major end products (acetate, acetone, ethanol, and butyrate) of the WL pathway, and several genes are missing for these pathways, as mentioned above, including genes

involved in acetone or butyrate synthesis (e.g., 3-hydroxybutyryl-CoA dehydrogenase and enoyl-CoA hydratase).

Energy Conservation Mechanisms in the Hakuba Co-assembly

The Hakuba co-assembly encodes enzymes involved in energy conservation used by homoacetogens that exploit the WL pathway (**Figures 3**, **4** and **Supplementary Table S11**). In addition to hydrogenases and heterodisulfide reductase, genes coding for several subunits of the Na^+-dependent V-type ATPase (*atpABCDEFIK*) were identified with key amino acid residues within subunit AtpK implicated in Na^+ translocation (Mulkidjanian et al., 2008; **Supplementary Figure S8**). The Na^+-dependent V-type ATPase can also translocate H^+ (Dimroth, 1997; von Ballmoos and Dimroth, 2007). There were no genes encoding the H^+-dependent F-type ATPase and only one subunit for the Ca^{2+}/Mg^{2+}-dependent P-type ATPase was identified. For the Hakuba bacterium, the translocation of Na^+ compared to other ions (H^+, Ca^{2+}, or Mg^{2+}) is likely to occur since there is about 1–1.6 mM Na^+ in Happo #3 (**Table 1**), which is ten times higher than the concentration of Ca^{2+}. Magnesium ions were not detected, and protons in serpentinite-hosted ecosystems are expected to be extremely low in concentration and are consumed during serpentinization, leading to alkaline pH (Okland et al., 2012).

The Hakuba co-assembly also encodes all subunits of the Rnf complex (RnfABCDEG). In model acetogens, such as *A. woodii*, the Rnf complex couples Fd oxidation to NAD^+ reduction and Na^+ translocation across the membrane, creating a sodium ion gradient that is subsequently utilized by the V-type ATPase for ATP synthesis (Biegel and Müller, 2010; Biegel et al., 2011; Schuchmann and Müller, 2014, 2016). The Hakuba bacterium may generate ATP via the combination of the Rnf complex and the V-type ATPase, as described above (Schuchmann and Müller, 2014, 2016). The lack of *ack* or *acd* suggests that the bacterium likely cannot conduct net ATP production *via* only the WL pathway. Thus, the bacterium would require ATP production *via* glycolysis coupled with the H^+-translocating NADH-quinone oxidoreductase (NuoABCDGHIKLMN, NuoE, NuoF and NuoG) and dissimilatory nitrate reduction with nitrate reductase, NarGH. Reduction of nitrate *via* nitrate reductase may be coupled with the oxidation of hydrogen *via* hydrogenases, although *narG* is pseudogenized in some SAGs, as discussed below. The genome assemblies of potential acetogens with the complete WL pathway and *acd* (GCA_001768645_Rifle_CO, and GCA_001767605_Rifle_CO) also encode the V-type ATPase and Rnf complex, but not NarGH and the NADH-quinone oxidoreductase (**Supplementary Table S10**).

The Hakuba Actinobacterium Is a Possible Heterotroph

We further characterized the Hakuba co-assembly to ascertain the metabolic capabilities other than utilizing the WL pathway (**Figure 5**). The Hakuba co-assembly is capable of assimilatory sulfate reduction (see **Supplementary Figure S9** and **Supplementary Information**) and has the complete set of genes for glycolysis (Embden-Meyerhof-Parnas pathway), converting glucose to acetyl-CoA (**Supplementary Table S10**). Sugars can be imported via the ABC transporter GanOPQ-MsmX and subsequently converted to glucose with genes, such as galactokinase (*galK*) and galactose-1-phosphate uridylyltransferase (*galT*). However, the Hakuba co-assembly and all SAGs lack fructose-1,6-bisphosphatase or diphosphate-dependent phosphofructokinase; therefore, it may not complete gluconeogenesis. This suggests that this bacterium cannot grow solely by carbon fixation *via* the WL pathway and is likely a heterotroph. In addition, the bacterium is likely not capable of producing major WL pathway end products from acetyl-CoA, as mentioned above, further supporting its dependence on glycolysis for energy generation. As Happo #3 is nutrient limited and organic carbon may not always be present, the Hakuba bacterium may supplement anabolic processes *via* the WL pathway.

The Hakuba co-assembly harbors all the genes for the non-oxidative pentose-phosphate pathway. The tricarboxylic acid cycle is incomplete, as seen in other known acetogens (Shin et al., 2016). Pyruvate can be reduced to malate using malate dehydrogenase, which is further converted to fumarate using fumarate hydratase. The Hakuba co-assembly contains genes for fumarate reductase catalytic, cytosolic subunits (*frdAB*), but the membrane-bound subunits are missing. The Hakuba co-assembly also contains glutamine synthetase indicating that it can potentially assimilate ammonia as a nitrogen source.

Characterization of Nitrate Reductase and Pseudogenization of narG With Intraspecies-Variations

Nitrate reductase may confer the ability to respire nitrate for the Hakuba bacterium. Its genes, *narGHJ*, were not found in the same operon within the Hakuba co-assembly, but the intact full-length operon was identified in the Hakuba SAGs S03, S09, S34, and S42. Although the co-assembly and SAGs are missing the integral membrane subunit *narI*, which is often observed with *narGHJ* (Philippot, 2002; Cabello et al., 2004), there is at least one known denitrifying microorganism that encodes only the subunits NarGH and NarJ, *Haloarcula marismortui* (Yoshimatsu et al., 2000, 2002). It is also possible that *narI* was not sequenced, or there is a yet to be identified putative *narI*, such as observed in the secretome of *Aeropyrum pernix* K1 (Palmieri et al., 2009) but not in the genome (Kawarabayasi et al., 1999). The subunit NarH is responsible for electron transfer (Blasco et al., 1989) while NarJ is a chaperone protein necessary for assembling an active NarGH complex (Dubourdieu and DeMoss, 1992; Liu and DeMoss, 1997; Blasco et al., 1998). The subunit NarG is the catalytic subunit and can be located in either the cytoplasm or the periplasm (Richardson et al., 2001). The Hakuba co-assembly NarG has a canonical twin-arginine motif, [S/T]RR, at the N-terminal region, which is responsible for protein export to the periplasm (Martinez-Espinosa et al., 2007; Kameya et al., 2017; **Supplementary Figure S10**), and it phylogenetically clustered with NarG from *Hydrogenobacter thermophilus* (**Supplementary Figure S11**). The NarG from *H. thermophilus* was the first known

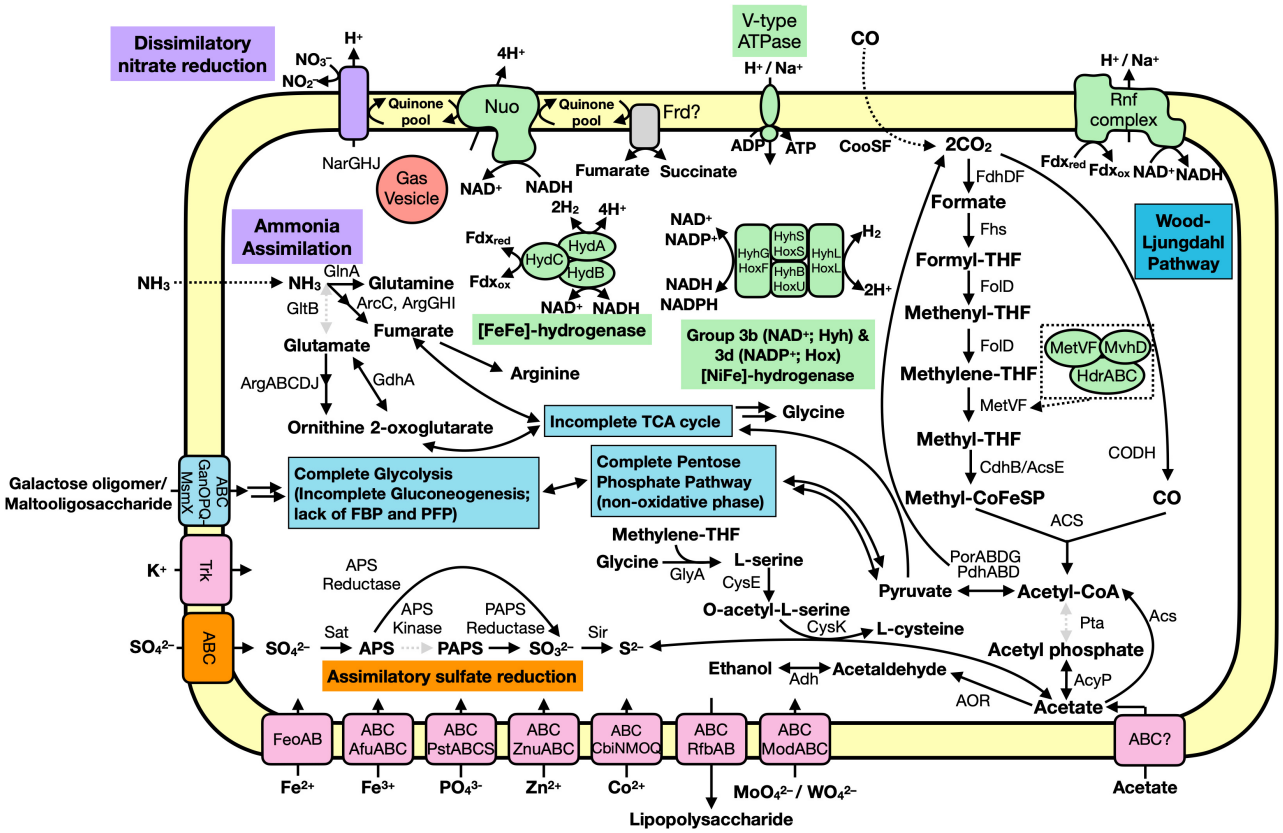

FIGURE 5 | Predicted metabolic functions of the Hakuba co-assembly. Each overall feature is color coded according to metabolic function (assimilatory sulfate reduction, orange; nitrogen cycle, purple; carbon cycle, blue; transporter, pink; or energy conservation, green). Dotted, gray arrows indicate the gene is not present while the dotted box is a zoom-in of the MetVF/MvhD/HdrABC-like complex. Double arrows indicate one or more genes are involved which are not depicted. Abbreviations: ABC (ABC transporter), Acs (acetyl-CoA synthase), AcyP (acylphosphatase), Adh (alcohol dehydrogenase; as YiaY), Afu (iron(III) transport system), Arc (carbamate kinase), Arg (amino-acid N-acetyltransferase), APS (adenosine-5′-phosphosulfate), AOR (aldehyde ferredoxin oxidoreductase), Cbi (cobalt/nickel transport system), Cdh (carbon monoxide dehydrogenase), CooS (carbon monoxide dehydrogenase), CysE (serine O-acetyltransferase), CysK (cysteine synthase), Fd (ferredoxin), Fdh (formate dehydrogenase), Feo (ferrous iron transport system), Fhs [formyl-tetrahydrofolate (THF) synthase], FolD (Methylene-THF dehydrogenase), Frd (succinate dehydrogenase / fumarate reductase), Gan (maltooligosaccharide transport system), GdhA (glutamate dehydrogenase), GlnA (glutamine synthetase), GltB (glutamate synthase), GlyA (glycine hydroxymethyltransferase), Hdr (heterodisulfide reductase), Hyd (hydrogenase), Mod (molybdate transport system), MvhD (F420-non-reducing hydrogenase iron-sulfur subunit), Msm (multiple sugar transport system ATP-binding protein), NADH (nicotinamide adenine dinucleotide), Nar (nitrate reductase), Nuo (NADH-oxidoreductase), PAPS (3′-phosphoadenosine 5′-phosphosulfate reductase), Por (pyruvate ferredoxin oxidoreductase), Pst (phosphate transport system), PTS (phosphotransferase), Rfb (lipopolysaccharide transport system), Rnf (Na^+-translocating ferredoxin:NAD^+ oxidoreductase), Sat (ATP sulfurylase enzyme), SbtA (high affinity Na^+-dependent bicarbonate transporter), Sir (sulfite reductase), Trk (Trk system potassium uptake protein), Znu (zinc transport system).

bacterial NarG to be localized on the periplasmic side of the cell membrane (Kameya et al., 2017). Similar to *H. thermophilus*, the Hakuba co-assembly genome also does not contain genes for any nitrate/nitrite transporters, further supporting the periplasmic localization of NarG. After nitrate reduction, nitrite does not appear to be utilized by the Hakuba organisms. Although the Hakuba co-assembly does not encode nitrite reductase (Nir) and nitric oxide reductase (Nor), the gene neighborhood of *narGHJ* contains several Fe–S cluster-containing proteins, putative ubiquinol oxidases, and two putative *nosZ* genes. These proteins may be involved in preventing toxicity from nitrite and potentially, nitric oxide.

The gene *narG* appears to be pseudogenized by a nonsense mutation ("TGG" to "TAG") in the Hakuba co-assembly and several SAGs (S03, S09, and S34), whereas SAGs S06, S33, and S42 have a complete *narG* sequence (**Supplementary Figure S12**). Examination of raw reads mapped to the region suggest that the pseudogenized *narG* was not derived from sequencing errors because the same mutation occurred at the same position on orthologous contigs among three independent samples. Moreover, this mutation was not within a homopolymeric region, which could have easily resulted in indel errors during sequencing. The potential loss of function for dissimilatory nitrate reduction in SAGs S03, S09, and S34 may arise from either functional heterogeneity amongst the individual strains of this species or an adaptation to the serpentinite-hosted environment, which has no detectable amount of nitrate or nitrite (**Table 1**) and may lead to the

loss of NarGHJ amongst the whole population of this species. Without the utilization of nitrate, the Hakuba actinobacterium may use fumarate as an electron acceptor, although it is unclear whether the putative fumarate reductase is membrane-bound or not.

The split *narG* amongst the 10 SAGs coincide with two intraspecies-level phylotypes observed by ANI (**Supplementary Table S6**) and AAI (**Supplementary Table S7**). Based on the criteria of ANI $\geq$ 99% and AAI $\geq$ 94%, one phylotype consists of SAGs S03, S09, S34, S44, and S47 ("first phylotype") and another phylotype consists of S25, S33, and S43 ("second phylotype"). The SAGs S06 and S42 are closer to the second phylotype, but the similarity is lower (AAI < 94%). Further examination of the genome assemblies identified 12 split genes (**Supplementary Figure S13** and **Supplementary Table S12**), and the two phylotypes coincided with 9 out of the 12 genes. Notably, the bacterial subunit *acsE* of CODH/ACS (**Figure 2B**) was split only in the first phylotype (**Supplementary Figure S13C**). The discovery of split genes coinciding with two phylotypes clarified the strength of our approach to analyze multiple SAGs of the same species, while the co-assembly provided higher completeness and facilitated analysis of potential metabolic traits of the Hakuba actinobacterium as a species.

Transporters, Stress Response, Motility, and RubisCO-Like Protein of the Hakuba Co-assembly

The Hakuba actinobacterium genome encodes several mechanisms that may allow it to survive in the nutrient-limited, serpentinite-hosted ecosystem of Happo #3. Several transporters are encoded by the Hakuba co-assembly, including organic carbon and inorganic ion transporters (K^+, Fe(II/III), SO_4^{2-}, PO_4^{3-}, Zn^{2+}, Co^{2+}, and MoO_4^{2-}/WO_4^{2-}). In addition to the H^+/Na^+-dependent V-type ATPase and Na^+/H^+-translocating Rnf complex, the K^+/H^+- symporter (Trk) is needed to maintain homeostasis in an alkaline environment and to create a Na^+/K^+ gradient, which likely has greater electrochemical storage capacity than a proton gradient (Dibrova et al., 2015). Moreover, the Happo #3 alkaline environment contains high concentrations of K^+ and Na^+ compared to protons (**Table 1**). The genome also encodes several secondary metabolite biosynthetic gene clusters related to putative saccharide and fatty acid biosynthesis with unknown products (**Supplementary Table S13**). Although the function remains unknown for these pathways, secondary metabolites are known to exhibit diverse biological activities and play an important role in community interactions (Cimermancic et al., 2014).

The genome encodes a range of anti-stress and defense mechanisms, including cold and heat shock proteins (YfiA, CspA, HspR) and defense against phage infection (AbiEii toxin-antitoxin Type IV system and CRISPR/Cas system). A Cas Type IIIB operon is located near a short (99 bp) putative CRISPR sequence, which was identified at the end of the contig and could be truncated (**Supplementary Figure S14**). The Type III CRISPR/Cas defense mechanism produces a complex for targeted search and elimination (Wright et al., 2016). However, the corresponding virus remains unknown as the spacer within the CRISPR sequence did not match any known sequences in the CRISPRCasFinder database (Couvin et al., 2018) or the NCBI nr database. There are also three putative tyrosine-type phage integrases in the Hakuba co-assembly. One integrase is located next to a tRNA gene. In general, tRNA genes are the preferred integration site of prophages (Williams, 2002), and accordingly, this integrase region located next to a tRNA gene could be a part of a prophage. Within the gene neighborhood, there was also a Type IIG restriction-modification gene, which is one defense mechanism against 'non-self' DNA (Naito et al., 1995; Kobayashi, 2001).

Flagellar motility for the cells represented by the Hakuba co-assembly is unclear as there are only a few genes for biosynthesis of flagella (*fliAD*) and Type IV pili. On the other hand, the Hakuba actinobacterium may be capable of flotation using gas vesicles. The Hakuba co-assembly contains genes for several gas vesicle proteins (*gvpGK[L/F]MNOVY*) spread across three contigs, and the SAG S33 has the *gvp* genes (*gvpAGHJK*[*L/F*]*MNOV*) located on one contig (**Supplementary Table S14**). Gas vesicles are proteinaceous organelles, generally in the shape of a spindle or cylinder, found in both *Bacteria* and *Archaea*, and impart buoyancy to cells by allowing passive gas diffusion (e.g., O_2, N_2, H_2, CO_2, CO, and CH_4) (Walsby, 1994; Oesterhelt, 1998; Oren et al., 2006; Coker and DasSarma, 2007; Hechler and Pfeifer, 2009; Pfeifer, 2012; Tashiro et al., 2016). The major gas vesicle protein GvpA is known to have an important role in assembling a gas vesicle while the other proteins play minor (e.g., GvpCG), regulatory (e.g., GvpDE), or unknown (e.g., GvpHI) roles (DasSarma and DasSarma, 2015). A single cell can contain several gas vesicles and likely produces gas vesicles in response to stress or environmental stimuli, such as light, oxygen concentrations, and available nutrients (Pfeifer, 2012). The Hakuba actinobacterium may synthesize gas vesicles in response to heat shock since *hsp20* (heat shock protein) is located in the same gene neighborhood as the *gvp* genes (**Supplementary Table S14**).

The Hakuba co-assembly encodes RubisCO (ribulose 1,5-bisphosphate carboxylase/oxygenase) Form IV protein, also known as a RubisCO-like protein (**Supplementary Figure S15**), which was identified in six SAGs S03, S25, S34, S42, S43, and S44. RubisCO is one of the enzymes involved in carbon fixation and is categorized into four forms. However, Form IV is known as a RubisCO-like protein because it lacks the catalytic site residue involved in the carboxylation reaction and is thought to be the ancestral form of RubisCO, arising before the great oxygenation event (Kacar et al., 2017; Erb and Zarzycki, 2018). Some RubisCO-like proteins are known to be involved in the methionine salvage pathway (Ashida, 2003; Erb et al., 2012) and the degradation of four carbon sugar acids (Zhang et al., 2016). The full metabolic range of RubisCO-like proteins remains unknown, although most are likely isomerases and/or epimerases (Erb and Zarzycki, 2018). In the Hakuba actinobacterium, the RubisCO-like protein may function as an epimerase acting on

sugars, as the gene neighborhood of the RubisCO-like protein harbors genes with an epimerase conserved domain (cd09023) and a sugar substrate binding site (DeoR C-terminal sensor domain, PF00455). Closely related RubisCO-like proteins to the Hakuba co-assembly, as determined by BLASTp searches, include those from the Candidate Phyla Radiation, *Spirochaetes*, *Planctomycetes*, and the model acetogen *Moorella thermoacetica*. The functions of RubisCO-like proteins in these genomes are also unknown.

CONCLUSION

Terrestrial serpentinite-hosted ecosystems are important modern-day analogs of early Earth and can also provide insights into processes that may have supported life at that time. Here, we present a genomic characterization of a dominant member in the Hakuba Happo hot spring ecosystem that belongs to the early-branching actinobacterial clade UBA1414. Single-cell genomics revealed that the bacterium utilizes the WL pathway for converting CO_2 to acetyl-CoA and could be represented by two phylotypes within a single species. We also identified related genome assemblies that encode the WL pathway; these bacteria are the first known to encode the WL pathway within the *Actinobacteria* phylum. Within Happo #3, examination of other dominant members, such as "Parcubacteria" and *Nitrospirae,* will further reveal the characteristics of this ecosystem. On the basis of the single-cell genome sequences, we propose a novel order '*Candidatus* Hakubanellales' and novel family '*Candidatus* Hakubanellaceae.' We propose to name this bacterium '*Candidatus* Hakubanella thermoalkaliphilus' as described below.

Description of '*Candidatus* Hakubanella' gen. nov

Hakubanella [ha.ku.ba.nel'la, N.L. fem. dim. n. *Hakubanella* of Hakuba Happo, a serpentinite-hosted environment located in Nagano (Japan) from where the single-cell genome assemblies were obtained. The type species is '*Candidatus* Hakubanella thermoalkaliphilus' with the single-cell genome assemblies as the type material.

Description of '*Candidatus* Hakubanella thermoalkaliphilus' sp. nov

Hakubanella thermoalkaliphilus (ther.mo.al.ka.liphil.us, Gr. adj. *thermos* hot; N.L. n. *alkali* from Arabic *al-qaliy* the ashes of saltwort; Gr. adj. *philos* friend, loving; N.L. adj. *alkaliphilus* liking alkaline environments). The genome of the bacterium was discovered in Hakuba Happo hot springs, where temperatures reach about 50°C and pH∼11. Based on genome analysis, the bacterium is anaerobic and possesses glycolysis for energy harvesting and the WL pathway for anabolic processes. The bacteria can potentially utilize sugars and accommodate two phylotypes: one is capable of dissimilatory nitrate reduction and another has lost the activity. The bacteria probably cannot grow autotrophically. The assignment is based on single-copy taxonomic marker genes.

DATA AVAILABILITY STATEMENT

The 16S rRNA amplicon sequences (DRR198702–DRR198704 under DRA009263), the raw fastq files (DRR198705–DRR198714 under DRA009264), and cleaned assemblies for SAGs (BLRU01000000–BLRZ01000000, BLSA01000000–BLSD01000000) and the co-assembly (BLSE01000000) were deposited into DDBJ under BioProject accession no. PRJDB8357. The gas vesicle hidden Markov model database is available on GitHub at https://github.com/Arkadiy-Garber/MagicCave/tree/master/hmms/gas.

AUTHOR CONTRIBUTIONS

NM, KK, and YH designed the study. NM contributed to the field sampling and the collection, sequencing, and bioinformatics analyses of the single-cell genomes. MK and YH contributed to the sequencing and bioinformatics analyses. EB and DC contributed to analysis of hydrogenases. NM, MK, EB, DC, SM, KN, KK, and YH wrote the manuscript.

FUNDING

NM was supported by the ELSI Origins Network (EON) research fellowship, which is supported by a grant from the John Templeton Foundation. The opinions expressed in this publication are those of the authors and do not necessarily reflect the views of the John Templeton Foundation. NM was also partially supported by the NASA Grant NNA13AA92A and Air Force Office of Scientific Research Grant FA9550-14-1-0114. EB acknowledges support from the NASA Astrobiology Institute (NNA15BB02A). KN was supported in part by the NSF Grant #1638216. Lawrence Livermore National Laboratory is operated by Lawrence Livermore National Security, LLS, for the U.S. Department of Energy, National Nuclear Security Administration under Contract DE-AC52-07NA27344 (LLNL-JRNL-800258).

ACKNOWLEDGMENTS

We thank the members of Yoichi Kamagata's lab (Hideyuki Tamaki, Masaru K. Nobu, Ryosuke Nakai, Satoshi Tamazawa, and Yoichi Kamagata) for field sampling and geochemical measurements, which was supported by the JSPS KAKENHI grant JP26106004, and advice on co-assembly of the single cells. We thank members of Yuichi Hongoh's lab (Hirokazu Kuwahara, Yuniar Devi Utami, Takumi Murakami, and Katsura Igai) for advice and help with collection and sequencing of the single-cells. Sanger sequencing was done at the Biomaterial Analysis Center of the Tokyo Institute of Technology. We thank Yayoi Hongo and Yoko Shibamoto for analyzing the nucleobases, nucleotides, and amino acids. We thank Shino Suzuki and Arkadiy Garber for advice on bioinformatics analyses and John Yu for setup of bioinformatics tools on the University of Southern California server. We thank Karen Lloyd for providing cleaned assemblies

collected from the Baltic Sea. We also thank Tanja Woyke for advice on single cell collection and Philip Hugenholtz for advice on GTDB-Tk. Computational resources were partly provided by the Data Integration and Analysis Facility, National Institute for Basic Biology, Japan.

SUPPLEMENTARY MATERIAL

The Supplementary Material for this article can be found online at: https://www.frontiersin.org/articles/10.3389/fmicb.2020.01031/full#supplementary-material

REFERENCES

Adam, P. S., Borrel, G., and Gribaldo, S. (2018). Evolutionary history of carbon monoxide dehydrogenase/acetyl-CoA synthase, one of the oldest enzymatic complexes. *Proc. Natl. Acad. Sci. U.S.A.* 115, E1166–E1173. doi: 10.1073/pnas.1807540115

Adam, P. S., Borrel, G., and Gribaldo, S. (2019). An archaeal origin of the Wood–Ljungdahl H4MPT branch and the emergence of bacterial methylotrophy. *Nat. Microbiol.* 4, 2155–2163. doi: 10.1038/s41564-019-0534-2

Anantharaman, K., Brown, C. T., Hug, L. A., Sharon, I., Castelle, C. J., Probst, A. J., et al. (2016). Thousands of microbial genomes shed light on interconnected biogeochemical processes in an aquifer system. *Nat. Commun.* 7:13219. doi: 10.1038/ncomms13219

Arai, W., Taniguchi, T., Goto, S., Moriya, Y., Uehara, H., Takemoto, K., et al. (2018). MAPLE 2.3.0: an improved system for evaluating the functionomes of genomes and metagenomes. *Biosci. Biotechnol. Biochem.* 82, 1515–1517. doi: 10.1080/09168451.2018.1476122

Arndt, D., Grant, J. R., Marcu, A., Sajed, T., Pon, A., Liang, Y., et al. (2016). PHASTER: a better, faster version of the PHAST phage search tool. *Nucleic Acids Res.* 44, W16–W21. doi: 10.1093/nar/gkw387

Ashida, H. (2003). A functional link between RuBisCO-like protein of *Bacillus* and photosynthetic RuBisCO. *Science* 302, 286–290. doi: 10.1126/science.1086997

Bankevich, A., Nurk, S., Antipov, D., Gurevich, A. A., Dvorkin, M., Kulikov, A. S., et al. (2012). SPAdes: a new genome assembly algorithm and its applications to single-cell sequencing. *J. Comput. Biol.* 19, 455–477. doi: 10.1089/cmb.2012.0021

Barker, H. A., and Kamen, M. D. (1945). Carbon dioxide utilization in the synthesis of acetic acid by *Clostridium thermoaceticum*. *Proc. Natl. Acad. Sci. U.S.A.* 31, 219–225. doi: 10.1073/pnas.31.8.219

Berghuis, B. A., Yu, F. B., Schulz, F., Blainey, P. C., Woyke, T., and Quake, S. R. (2019). Hydrogenotrophic methanogenesis in archaeal phylum *Verstraetearchaeota* reveals the shared ancestry of all methanogens. *Proc. Natl. Acad. Sci. U.S.A.* 116, 5037–5044. doi: 10.1073/pnas.1815631116

Biegel, E., and Müller, V. (2010). Bacterial Na+-translocating ferredoxin:NAD+ oxidoreductase. *Proc. Natl. Acad. Sci. U.S.A.* 107, 18138–18142. doi: 10.1073/pnas.1010318107

Biegel, E., Schmidt, S., González, J. M., and Müller, V. (2011). Biochemistry, evolution and physiological function of the Rnf complex, a novel ion-motive electron transport complex in prokaryotes. *Cell. Mol. Life Sci.* 68, 613–634. doi: 10.1007/s00018-010-0555-8

Bird, J. T., Tague, E. D., Zinke, L., Schmidt, J. M., Steen, A. D., Reese, B., et al. (2019). Uncultured microbial phyla suggest mechanisms for multi-thousand-year subsistence in Baltic Sea Sediments. *mBio* 10:e02376-18. doi: 10.1128/mBio.02376-18

Blasco, F., Dos Santos, J., Magalon, A., Frixon, C., Guigliarelli, B., Santini, C., et al. (1998). NarJ is a specific chaperone required for molybdenum cofactor assembly in nitrate reductase A of *Escherichia coli*. *Mol. Microbiol.* 28, 435–447. doi: 10.1046/j.1365-2958.1998.00795.x

Blasco, F., Lobbi, C., Giordano, G., Chippaux, M., and Bonnefoy, V. (1989). Nitrate reductase of *Escherichia coli*: completion of the nucleotide sequence of the nar operon and reassessment of the role of the α and β subunits in iron binding and electron transfer. *Mol. Gen. Genet.* 218, 249–256. doi: 10.1007/BF00331275

Blin, K., Wolf, T., Chevrette, M. G., Lu, X., Schwalen, C. J., Kautsar, S. A., et al. (2017). antiSMASH 4.0—improvements in chemistry prediction and gene cluster boundary identification. *Nucleic Acids Res.* 45, W36–W41. doi: 10.1093/nar/gkx319

Bouckaert, R., and Vaughan, T. G. (2019). BEAST 2.5: an advanced software platform for Bayesian evolutionary analysis. *PLoS Comput. Biol.* 15:e1006650. doi: 10.1371/journal.pcbi.1006650

Bowers, R. M., Kyrpides, N. C., Stepanauskas, R., Harmon-Smith, M., Doud, D., Reddy, T. B. K., et al. (2017). Minimum information about a single amplified genome (MISAG) and a metagenome-assembled genome (MIMAG) of bacteria and archaea. *Nat. Biotechnol.* 35, 725–731. doi: 10.1038/nbt.3893

Boyd, E. S., Amenabar, M. J., Poudel, S., and Templeton, A. S. (2020). Bioenergetic constraints on the origin of autotrophic metabolism. *Philos. Trans. R. Soc. A* 1378:2019015. doi: 10.1098/rsta.2019.0151

Branscomb, E., and Russell, M. J. (2018). Frankenstein or a submarine alkaline vent: who is responsible for abiogenesis: Part 2: as life is now, so it must have been in the beginning. *Bioessays* 40:1700182. doi: 10.1002/bies.201700182

Braus-Stromeyer, S. A., Schnappauf, G., Braus, G. H., Gössner, A. S., and Drake, H. L. (1997). Carbonic anhydrase in *Acetobacterium woodii* and other acetogenic bacteria. *J. Bacteriol.* 179, 7197–7200. doi: 10.1128/jb.179.22.7197-7200.1997

Brazelton, W. J., Thornton, C. N., Hyer, A., Twing, K. I., Longino, A. A., Lang, S. Q., et al. (2017). Metagenomic identification of active methanogens and methanotrophs in serpentinite springs of the Voltri Massif, Italy. *PeerJ* 5:e2945. doi: 10.7717/peerj.2945

Buckel, W., and Thauer, R. K. (2013). Energy conservation via electron bifurcating ferredoxin reduction and proton/Na^+ translocating ferredoxin oxidation. *Biochim. Biophys. Acta*. 1827, 94–113. doi: 10.1016/j.bbabio.2012.07.002

Burstein, D., Sun, C. L., Brown, C. T., Sharon, I., Anantharaman, K., Probst, A. J., et al. (2016). Major bacterial lineages are essentially devoid of CRISPR-Cas viral defence systems. *Nat. Commun.* 7:10613. doi: 10.1038/ncomms10613

Cabello, P., Roldán, M. D., and Moreno-Vivián, C. (2004). Nitrate reduction and the nitrogen cycle in *Archaea*. *Microbiology* 150, 3527–3546. doi: 10.1099/mic.0.27303-0

Callahan, B. J., McMurdie, P. J., and Holmes, S. P. (2017). Exact sequence variants should replace operational taxonomic units in marker-gene data analysis. *ISME J.* 11, 2639–2643. doi: 10.1038/ismej.2017.119

Callahan, B. J., McMurdie, P. J., Rosen, M. J., Han, A. W., Johnson, A. J. A., and Holmes, S. P. (2016). DADA2: high-resolution sample inference from Illumina amplicon data. *Nat. Methods* 13, 581–583. doi: 10.1038/nmeth.3869

Capella-Gutierrez, S., Silla-Martinez, J. M., and Gabaldon, T. (2009). trimAl: a tool for automated alignment trimming in large-scale phylogenetic analyses. *Bioinformatics* 25, 1972–1973. doi: 10.1093/bioinformatics/btp348

Chang, Y.-H., Cheng, T.-W., Lai, W.-J., Tsai, W.-Y., Sun, C.-H., Lin, L.-H., et al. (2012). Microbial methane cycling in a terrestrial mud volcano in eastern Taiwan: Microbial methane cycling in mud volcano. *Environ. Microbiol.* 14, 895–908. doi: 10.1111/j.1462-2920.2011.02658.x

Cimermancic, P., Medema, M. H., Claesen, J., Kurita, K., Wieland Brown, L. C., Mavrommatis, K., et al. (2014). Insights into secondary metabolism from a global analysis of prokaryotic biosynthetic gene clusters. *Cell* 158, 412–421. doi: 10.1016/j.cell.2014.06.034

Coker, J. A., and DasSarma, S. (2007). Genetic and transcriptomic analysis of transcription factor genes in the model halophilic Archaeon: coordinate action of TbpD and TfbA. *BMC Genet.* 8:61. doi: 10.1186/1471-2156-8-61

Condie, K. C. (ed.). (2016). "Chapter 3 - Tectonic Settings," in *Earth as an Evolving Planetary System* (Amsterdam: Elsevier), 43–88.

Couvin, D., Bernheim, A., Toffano-Nioche, C., Touchon, M., Michalik, J., Néron, B., et al. (2018). CRISPRCasFinder, an update of CRISRFinder, includes a portable version, enhanced performance and integrates search for Cas proteins. *Nucleic Acids Res.* 46, W246–W251. doi: 10.1093/nar/gky425

Crespo-Medina, M., Twing, K. I., Kubo, M. D. Y., Hoehler, T. M., Cardace, D., McCollom, T., et al. (2014). Insights into environmental controls on microbial communities in a continental serpentinite aquifer using a microcosm-based approach. *Front. Microbiol.* 5:604. doi: 10.3389/fmicb.2014.00604

DasSarma, S., and DasSarma, P. (2015). Gas vesicle nanoparticles for antigen display. *Vaccines* 3, 686–702. doi: 10.3390/vaccines3030686

de Kok, A., Hengeveld, A. F., Martin, A., and Westphal, A. H. (1998). The pyruvate dehydrogenase multi-enzyme complex from Gram-negative bacteria. *Biochim. Biophys. Acta* 1385, 353–366. doi: 10.1016/S0167-4838(98)00079-X

Dibrova, D. V., Galperin, M. Y., Koonin, E. V., and Mulkidjanian, A. Y. (2015). Ancient systems of sodium/potassium homeostasis as predecessors of membrane bioenergetics. *Biochemistry* 80, 495–516. doi: 10.1134/S0006297915050016

Dimroth, P. (1997). Primary sodium ion translocating enzymes. *Biochim. Biophys. Acta* 1318, 11–51. doi: 10.1016/S0005-2728(96)00127-2

Dodsworth, J. A., Blainey, P. C., Murugapiran, S. K., Swingley, W. D., Ross, C. A., Tringe, S. G., et al. (2013). Single-cell and metagenomic analyses indicate a fermentative and saccharolytic lifestyle for members of the OP9 lineage. *Nat. Commun.* 4:1854. doi: 10.1038/ncomms2884

Drake, H. L., Hu, S., and Wood, H. G. (1981). Purification of Five Components from *Clostridium themnoaceticum* Which Catalyze Synthesis of Acetate from Pyruvate and Methyltetrahydrofolate. *J. Biol. Chem.* 256, 11137–11144.

Drummond, A. J., Nicholls, G. K., Rodrigo, A. G., and Solomon, W. (2002). Estimating mutation parameters, population history and genealogy simultaneously from temporally spaced sequence data. *Genetics* 161, 1307–1320.

Dubourdieu, M., and DeMoss, J. A. (1992). The *narJ* gene product is required for biogenesis of respiratory nitrate reductase in *Escherichia coli*. *J. Bacteriol.* 174, 867–872. doi: 10.1128/JB.174.3.867-872.1992

Eddy, S. R. (2011). Accelerated profile HMM searches. *PLoS Comput. Biol.* 7:e1002195. doi: 10.1371/journal.pcbi.1002195

Eichinger, V., Nussbaumer, T., Platzer, A., Jehl, M.-A., Arnold, R., and Rattei, T. (2016). EffectiveDB—updates and novel features for a better annotation of bacterial secreted proteins and Type III, IV, VI secretion systems. *Nucleic Acids Res.* 44, D669–D674. doi: 10.1093/nar/gkv1269

Erb, T. J., Evans, B. S., Cho, K., Warlick, B. P., Sriram, J., Wood, B. M., et al. (2012). A RubisCO-like protein links SAM metabolism with isoprenoid biosynthesis. *Nat. Chem. Biol.* 8, 926–932. doi: 10.1038/nchembio.1087

Erb, T. J., and Zarzycki, J. (2018). A short history of RubisCO: the rise and fall (?) of Nature's predominant CO_2 fixing enzyme. *Curr. Opin. Biotechnol.* 49, 100–107. doi: 10.1016/j.copbio.2017.07.017

Eren, A. M., Esen, Ö. C., Quince, C., Vineis, J. H., Morrison, H. G., Sogin, M. L., et al. (2015). Anvi'o: an advanced analysis and visualization platform for 'omics data. *PeerJ* 3:e1319. doi: 10.7717/peerj.1319

Fones, E. M., Colman, D. R., Kraus, E. A., Nothaft, D. B., Poudel, S., Rempfert, K. R., et al. (2019). Physiological adaptations to serpentinization in the Samail Ophiolite, Oman. *ISME J* 13, 1750–1762. doi: 10.1038/s41396-019-0391-2

Fontaine, F. E., Peterson, W. H., McCoy, E., Johnson, M. J., and Ritter, G. J. (1942). A new type of glucose fermentation by *Clostridium thermoaceticum* n.sp. *J. Bacteriol.* 43, 701–715.

Greening, C., Biswas, A., Carere, C. R., Jackson, C. J., Taylor, M. C., Stott, M. B., et al. (2016). Genomic and metagenomic surveys of hydrogenase distribution indicate H2 is a widely utilised energy source for microbial growth and survival. *ISME J.* 10, 761–777. doi: 10.1038/ismej.2015.153

Gurevich, A., Saveliev, V., Vyahhi, N., and Tesler, G. (2013). QUAST: quality assessment tool for genome assemblies. *Bioinformatics* 29, 1072–1075. doi: 10.1093/bioinformatics/btt086

Han, M. V., and Zmasek, C. M. (2009). phyloXML: XML for evolutionary biology and comparative genomics. *BMC Bioinformatics* 10:356. doi: 10.1186/1471-2105-10-356

Harrison, K. J., de Crecy-Lagard, V., and Zallot, R. (2017). Gene Graphics: a genomic neighborhood data visualization web application. *Bioinformatics* 34, 1406–1408. doi: 10.1093/bioinformatics/btx793

Hechler, T., and Pfeifer, F. (2009). Anaerobiosis inhibits gas vesicle formation in halophilic *Archaea*. *Mol. Microbiol.* 71, 132–145. doi: 10.1111/j.1365-2958.2008.06517.x

Hemmann, J. L., Wagner, T., Shima, S., and Vorholt, J. A. (2019). Methylofuran is a prosthetic group of the formyltransferase/hydrolase complex and shuttles one-carbon units between two active sites. *Proc. Natl. Acad. Sci. U.S.A.* 116, 25583–25590. doi: 10.1073/pnas.1911595116

Hochheimer, A., Linder, D., Thauer, R. K., and Hedderich, R. (1996). The molybdenum formylmethanofuran dehydrogenase operon and the tungsten formylmethanofuran dehydrogenase operon from *Methanobacterium Thermoautotrophicum*. *Eur. J. Biochem.* 242, 156–162. doi: 10.1111/j.1432-1033.1996.0156r.x

Hochheimer, A., Schmitz, R. A., Thauer, R. K., and Hedderich, R. (1995). The tungsten formylmethanofuran dehydrogenase from *Methanobacterium Thermoautotrophicum* contains sequence motifs characteristic for enzymes containing molybdopterin dinucleotide. *Eur. J. Biochem.* 234, 910–920. doi: 10.1111/j.1432-1033.1995.910_a.x

Hugenholtz, P., Pitulle, C., Hershberger, K. L., and Pace, N. R. (1998). Novel division level bacterial diversity in a yellowstone hot spring. *J. Bacteriol.* 180, 366–376.

Hugenholtz, P., Skarshewski, A., and Parks, D. H. (2016). Genome-based microbial taxonomy coming of age. *Cold Spring Harb. Perspect. Biol.* 8:a018085. doi: 10.1101/cshperspect.a018085

Hyatt, D., Chen, G.-L., LoCascio, P. F., Land, M. L., Larimer, F. W., and Hauser, L. J. (2010). Prodigal: prokaryotic gene recognition and translation initiation site identification. *BMC Bioinformatics* 11:119. doi: 10.1186/1471-2105-11-119

Ikeda-Ohtsubo, W., Strassert, J. F. H., Köhler, T., Mikaelyan, A., Gregor, I., McHardy, A. C., et al. (2016). '*Candidatus* Adiutrix intracellularis', an endosymbiont of termite gut flagellates, is the first representative of a deep-branching clade of *Deltaproteobacteria* and a putative homoacetogen: a homoacetogenic deltaproteobacterium from termite guts. *Environ. Microbiol.* 18, 2548–2564. doi: 10.1111/1462-2920.13234

Inoue, M., Nakamoto, I., Omae, K., Oguro, T., Ogata, H., Yoshida, T., et al. (2019). Structural and phylogenetic diversity of anaerobic carbon-monoxide dehydrogenases. *Front. Microbiol.* 9:3353. doi: 10.3389/fmicb.2018.03353

Jain, C., Rodriguez-R, L. M., Phillippy, A. M., Konstantinidis, K. T., and Aluru, S. (2018). High throughput ANI analysis of 90K prokaryotic genomes reveals clear species boundaries. *Nat. Commun.* 9:5114. doi: 10.1038/s41467-018-07641-9

Jones, P., Binns, D., Chang, H.-Y., Fraser, M., Li, W., McAnulla, C., et al. (2014). InterProScan 5: genome-scale protein function classification. *Bioinformatics* 30, 1236–1240. doi: 10.1093/bioinformatics/btu031

Kacar, B., Hanson-Smith, V., Adam, Z. R., and Boekelheide, N. (2017). Constraining the timing of the Great Oxidation Event within the RubisCO phylogenetic tree. *Geobiology* 15, 628–640. doi: 10.1111/gbi.12243

Kameya, M., Kanbe, H., Igarashi, Y., Arai, H., and Ishii, M. (2017). Nitrate reductases in *Hydrogenobacter thermophilus* with evolutionarily ancient features: distinctive localization and electron transfer: nitrate reductases of *Hydrogenobacter thermophilus*. *Mol. Microbiol.* 106, 129–141. doi: 10.1111/mmi.13756

Kaster, A.-K., Moll, J., Parey, K., and Thauer, R. K. (2011). Coupling of ferredoxin and heterodisulfide reduction via electron bifurcation in hydrogenotrophic methanogenic archaea. *Proc. Natl. Acad. Sci. U.S.A.* 108, 2981–2986. doi: 10.1073/pnas.1016761108

Kato, S., Yanagawa, K., Sunamura, M., Takano, Y., Ishibashi, J., Kakegawa, T., et al. (2009). Abundance of *Zetaproteobacteria* within crustal fluids in back-arc hydrothermal fields of the Southern Mariana Trough. *Environ. Microbiol.* 11, 3210–3222. doi: 10.1111/j.1462-2920.2009.02031.x

Katoh, K., Misawa, K., Kuma, K., and Miyata, T. (2002). MAFFT: a novel method for rapid multiple sequence alignment based on fast Fourier transform. *Nucleic Acids Res.* 30, 3059–3066. doi: 10.1093/nar/gkf436

Kawarabayasi, Y., HlNO, Y., Horikawa, H., Yamazaki, S., Haikawa, Y., Jin-No, K., et al. (1999). Complete Genome Sequence of an Aerobic Hyper-thermophilic Crenarchaeon, *Aeropyrum pernix* K1. *DNA Res.* 6, 83–101. doi: 10.1093/dnares/6.2.83

Kobayashi, I. (2001). Behavior of restriction-modification systems as selfish mobile elements and their impact on genome evolution. *Nucleic Acids Res.* 29, 3742–3756. doi: 10.1093/nar/29.18.3742

Konstantinidis, K. T., and Tiedje, J. M. (2005a). Genomic insights that advance the species definition for prokaryotes. *Proc. Natl. Acad. Sci. U.S.A.* 102, 2567–2572. doi: 10.1073/pnas.0409727102

Konstantinidis, K. T., and Tiedje, J. M. (2005b). Towards a genome-based taxonomy for prokaryotes. *J. Bacteriol.* 187, 6258–6264. doi: 10.1128/JB.187.18.6258-6264.2005

Köpke, M., Held, C., Hujer, S., Liesegang, H., Wiezer, A., Wollherr, A., et al. (2010). *Clostridium ljungdahlii* represents a microbial production platform based on syngas. *Proc. Natl. Acad. Sci. U.S.A.* 107, 13087–13092. doi: 10.1073/pnas.1004716107

Lanfear, R., Frandsen, P. B., Wright, A. M., Senfeld, T., and Calcott, B. (2016). PartitionFinder 2: new methods for selecting partitioned models of evolution for molecular and morphological phylogenetic analyses. *Mol. Biol. Evol.* 34, 772–773. doi: 10.1093/molbev/msw260

Langmead, B., and Salzberg, S. L. (2012). Fast gapped-read alignment with Bowtie 2. *Nat. Methods* 9, 357–359. doi: 10.1038/nmeth.1923

Lee, M. D. (2019). GToTree: a user-friendly workflow for phylogenomics. *Bioinformatics* 35, 4162–4164. doi: 10.1093/bioinformatics/btz188

Liu, X., and DeMoss, J. A. (1997). Characterization of NarJ, a system-specific chaperone required for nitrate reductase biogenesis in *Escherichia coli*. *J. Biol. Chem.* 272, 24266–24271. doi: 10.1074/jbc.272.39.24266

Lowe, T. M., and Eddy, S. R. (1997). tRNAscan-SE: a program for improved detection of transfer RNA genes in genomic sequence. *Nucleic Acids Res.* 25, 955–964. doi: 10.1093/nar/25.5.955

Lux, M., Krüger, J., Rinke, C., Maus, I., Schlüter, A., Woyke, T., et al. (2016). acdc – automated contamination detection and confidence estimation for single-cell genome data. *BMC Bioinformatics* 17:543. doi: 10.1186/s12859-016-1397-7

Maden, B. E. H. (2000). Tetrahydrofolate and tetrahydromethanopterin compared: functionally distinct carriers in C1 metabolism. *Biochem. J.* 350, 609–629.

Martin, M. (2011). Cutadapt removes adapter sequences from high-throughput sequencing reads. *EMBnet J.* 17, 10–12. doi: 10.14806/ej.17.1.200

Martin, W., and Russell, M. J. (2006). On the origin of biochemistry at an alkaline hydrothermal vent. *Philos. Trans. R. Soc. B Biol. Sci.* 362, 1887–1926. doi: 10.1098/rstb.2006.1881

Martinez-Espinosa, R. M., Dridge, E. J., Bonete, M. J., Butt, J. N., Butler, C. S., Sargent, F., et al. (2007). Look on the positive side! The orientation, identification and bioenergetics of "Archaeal" membrane-bound nitrate reductases. *FEMS Microbiol. Lett.* 276, 129–139. doi: 10.1111/j.1574-6968.2007.00887.x

Matschiavelli, N., and Rother, M. (2015). Role of a putative tungsten-dependent formylmethanofuran dehydrogenase in *Methanosarcina acetivorans*. *Arch. Microbiol.* 197, 379–388. doi: 10.1007/s00203-014-1070-3

Matsen, F. A., Kodner, R. B., and Armbrust, E. V. (2010). pplacer: linear time maximum-likelihood and Bayesian phylogenetic placement of sequences onto a fixed reference tree. *BMC Bioinformatics* 11:538. doi: 10.1186/1471-2105-11-538

Matter, J. M., and Kelemen, P. B. (2009). Permanent storage of carbon dioxide in geological reservoirs by mineral carbonation. *Nat. Geosci.* 2, 837–841. doi: 10.1038/ngeo683

Mayhew, L. E., Ellison, E. T., McCollom, T. M., Trainor, T. P., and Templeton, A. S. (2013). Hydrogen generation from low-temperature water–rock reactions. *Nat. Geosci.* 6, 478–484. doi: 10.1038/ngeo1825

McCollom, T. M., and Seewald, J. S. (2007). Abiotic synthesis of organic compounds in deep-sea hydrothermal environments. *Chem. Rev.* 107, 382–401. doi: 10.1021/cr0503660

McMurdie, P. J., and Holmes, S. (2013). phyloseq: an R package for reproducible interactive analysis and graphics of microbiome census data. *PLoS One* 8:e61217. doi: 10.1371/journal.pone.0061217

Menon, S., and Ragsdale, S. W. (1996). Evidence that carbon monoxide is an obligatory intermediate in anaerobic Acetyl-CoA synthesis. *Biochemistry* 35, 12119–12125. doi: 10.1021/bi961014d

Menzel, P., Ng, K. L., and Krogh, A. (2016). Fast and sensitive taxonomic classification for metagenomics with Kaiju. *Nat. Commun.* 7:11257. doi: 10.1038/ncomms11257

Meyer-Dombard, D. R., Casar, C. P., Simon, A. G., Cardace, D., Schrenk, M. O., and Arcilla, C. A. (2018). Biofilm formation and potential for iron cycling in serpentinization-influenced groundwater of the Zambales and Coast Range ophiolites. *Extremophiles* 122, 407–431. doi: 10.1007/s00792-018-1005-z

Miller, M. A., Pfeiffer, W., and Schwartz, T. (2010). "Creating the CIPRES Science Gateway for inference of large phylogenetic trees," in *Proceedings of the 2010 Gateway Computing Environments Workshop (GCE)*, (New Orleans, LA: IEEE), 1–8. doi: 10.1109/GCE.2010.5676129

Mock, J., Wang, S., Huang, H., Kahnt, J., and Thauer, R. K. (2014). Evidence for a Hexaheteromeric Methylenetetrahydrofolate Reductase in *Moorella thermoacetica*. *J. Bacteriol.* 196, 3303–3314. doi: 10.1128/JB.01839-14

Momper, L., Jungbluth, S. P., Lee, M. D., and Amend, J. P. (2017). Energy and carbon metabolisms in a deep terrestrial subsurface fluid microbial community. *ISME J.* 11, 2319–2333. doi: 10.1038/ismej.2017.94

Morrill, P. L., Brazelton, W. J., Kohl, L., Rietze, A., Miles, S. M., Kavanagh, H., et al. (2014). Investigations of potential microbial methanogenic and carbon monoxide utilization pathways in ultra-basic reducing springs associated with present-day continental serpentinization: the Tablelands, NL, CAN. *Front. Microbiol.* 5:613. doi: 10.3389/fmicb.2014.00613

Mulkidjanian, A. Y., Galperin, M. Y., Makarova, K. S., Wolf, Y. I., and Koonin, E. V. (2008). Evolutionary primacy of sodium bioenergetics. *Biol. Direct* 3:13. doi: 10.1186/1745-6150-3-13

Musfeldt, M., Selig, M., and Schönheit, P. (1999). Acetyl Coenzyme A Synthetase (ADP Forming) from the Hyperthermophilic Archaeon *Pyrococcus furiosus*: identification, cloning, separate expression of the encoding genes, *acdAI* and *acdBI*, in *Escherichia coli*, and *in vitro* reconstitution of the active heterotetrameric enzyme from its recombinant subunits. *J. Bacteriol.* 181, 5885–5888. doi: 10.1128/JB.181.18.5885-5888.1999

Naito, T., Kusano, K., and Kobayashi, I. (1995). Selfish behavior of restriction-modification systems. *Science* 267, 897–899. doi: 10.1126/science.7846533

Nicolas, A. (2012). "27 - Ophiolites and oceanic lithosphere," in *Regional Geology and Tectonics: Principles of Geologic Analysis*, eds D. G. Roberts, and A.W. Bally (Amsterdam: Elsevier), 820–835.

O'Brien, W. E., Brewer, J. M., and Ljungdahl, L. G. (1973). Purification and characterization of thermostable 5,10-methylenetetrahydrofolate dehydrogenase from *Clostridium thermoaceticum*. *J. Biol. Chem.* 248, 403–408.

Oesterhelt, D. (1998). The structure and mechanism of the family of retinal proteins from halophilic archaea. *Curr. Opin. Struct. Biol.* 8, 489–500. doi: 10.1016/s0959-440x(98)80128-0

Okland, I., Huang, S., Dahle, H., Thorseth, I. H., and Pedersen, R. B. (2012). Low temperature alteration of serpentinized ultramafic rock and implications for microbial life. *Chem. Geol.* 318–319, 75–87. doi: 10.1016/j.chemgeo.2012.05.015

O'Leary, N. A., Wright, M. W., Brister, J. R., Ciufo, S., Haddad, D., McVeigh, R., et al. (2016). Reference sequence (RefSeq) database at NCBI: current status, taxonomic expansion, and functional annotation. *Nucleic Acids Res.* 44, D733–D745. doi: 10.1093/nar/gkv1189

Oren, A., Pri-El, N., Shapiro, O., and Siboni, N. (2006). Buoyancy studies in natural communities of square gas-vacuolate archaea in saltern crystallizer ponds. *Saline Syst.* 2:4. doi: 10.1186/1746-1448-2-4

Palmieri, G., Cannio, R., Fiume, I., Rossi, M., and Pocsfalvi, G. (2009). Outside the unusual cell wall of the hyperthermophilic archaeon *Aeropyrum pernix* K1. *Mol. Cell. Proteomics* 8, 2570–2581. doi: 10.1074/mcp.M900012-MCP200

Pander, B., Harris, G., Scott, D. J., Winzer, K., Köpke, M., Simpson, S. D., et al. (2019). The carbonic anhydrase of *Clostridium autoethanogenum* represents a new subclass of β-carbonic anhydrases. *Appl. Microbiol. Biotechnol.* 103, 7275–7286. doi: 10.1007/s00253-019-10015-w

Parks, D. H., Chuvochina, M., Waite, D. W., Rinke, C., Skarshewski, A., Chaumeil, P.-A., et al. (2018). A standardized bacterial taxonomy based on genome phylogeny substantially revises the tree of life. *Nat. Biotechnol.* 36, 996–1004. doi: 10.1038/nbt.4229

Parks, D. H., Imelfort, M., Skennerton, C. T., Hugenholtz, P., and Tyson, G. W. (2015). CheckM: assessing the quality of microbial genomes recovered from isolates, single cells, and metagenomes. *Genome Res.* 25, 1043–1055. doi: 10.1101/gr.186072.114

Peters, J. W., Schut, G. J., Boyd, E. S., Mulder, D. W., Shepard, E. M., Broderick, J. B., et al. (2015). [FeFe]- and [NiFe]-hydrogenase diversity, mechanism, and maturation. *Biochim. Biophys. Acta* 1853, 1350–1369. doi: 10.1016/j.bbamcr.2014.11.021

Pfeifer, F. (2012). Distribution, formation and regulation of gas vesicles. *Nat. Rev. Microbiol.* 10, 705–715. doi: 10.1038/nrmicro2834

Philippot, L. (2002). Denitrifying genes in bacterial and Archaeal genomes. *Biochim. Biophys. Acta* 1577, 355–376. doi: 10.1016/S0167-4781(02)00420-7

Poehlein, A., Cebulla, M., Ilg, M. M., Bengelsdorf, F. R., Schiel-Bengelsdorf, B., Whited, G., et al. (2015). The Complete Genome Sequence of *Clostridium aceticum*: a Missing Link between Rnf- and Cytochrome-Containing Autotrophic Acetogens. *mBio* 6:e01168-15. doi: 10.1128/mBio.01168-15

Pomper, B. K., Saurel, O., Milon, A., and Vorholt, J. A. (2002). Generation of formate by the formyltransferase/hydrolase complex (Fhc) from *Methylobacterium extorquens* AM1. *FEBS Lett.* 523, 133–137. doi: 10.1016/S0014-5793(02)02962-9

Posewitz, M. C., King, P. W., Smolinski, S. L., Zhang, L., Seibert, M., and Ghirardi, M. L. (2004). Discovery of two novel radical S-Adenosylmethionine proteins required for the assembly of an active [Fe] Hydrogenase. *J. Biol. Chem.* 279, 25711–25720. doi: 10.1074/jbc.M403206200

Poudel, S., Tokmina-Lukaszewska, M., Colman, D. R., Refai, M., Schut, G. J., King, P. W., et al. (2016). Unification of [FeFe]-hydrogenases into three structural and functional groups. *Biochim. Biophys. Acta* 1860, 1910–1921. doi: 10.1016/j.bbagen.2016.05.034

Price, M. N., Dehal, P. S., and Arkin, A. P. (2010). FastTree 2 – approximately maximum-likelihood trees for large alignments. *PLoS One* 5:e9490. doi: 10.1371/journal.pone.0009490

Probst, A. J., Ladd, B., Jarett, J. K., Geller-McGrath, D. E., Sieber, C. M. K., Emerson, J. B., et al. (2018). Differential depth distribution of microbial function and putative symbionts through sediment-hosted aquifers in the deep terrestrial subsurface. *Nat. Microbiol.* 3, 328–336. doi: 10.1038/s41564-017-0098-y

Quast, C., Pruesse, E., Yilmaz, P., Gerken, J., Schweer, T., Yarza, P., et al. (2012). The SILVA ribosomal RNA gene database project: improved data processing and web-based tools. *Nucleic Acids Res.* 41, D590–D596. doi: 10.1093/nar/gks1219

Quéméneur, M., Palvadeau, A., Postec, A., Monnin, C., Chavagnac, V., Ollivier, B., et al. (2015). Endolithic microbial communities in carbonate precipitates from serpentinite-hosted hyperalkaline springs of the Voltri Massif (Ligurian Alps, Northern Italy). *Environ. Sci. Pollut. Res.* 22, 13613–13624. doi: 10.1007/s11356-015-4113-7

Ragsdale, S. W. (2003). Pyruvate ferredoxin oxidoreductase and its radical intermediate. *Chem. Rev.* 103, 2333–2346. doi: 10.1021/cr020423e

Ragsdale, S. W. (2008). Enzymology of the wood–ljungdahl pathway of acetogenesis. *Ann. N. Y. Acad. Sci.* 1125, 129–136. doi: 10.1196/annals.1419.015

Rambaut, A., Drummond, A. J., Xie, D., Baele, G., and Suchard, M. A. (2018). Posterior summarization in bayesian phylogenetics using tracer 1.7. *Syst. Biol.* 67, 901–904. doi: 10.1093/sysbio/syy032

Ramos-Padrón, E., Bordenave, S., Lin, S., Bhaskar, I. M., Dong, X., Sensen, C. W., et al. (2011). Carbon and sulfur cycling by microbial communities in a gypsum-treated oil sands tailings pond. *Environ. Sci. Technol.* 45, 439–446. doi: 10.1021/es1028487

Rempfert, K. R., Miller, H. M., Bompard, N., Nothaft, D., Matter, J. M., Kelemen, P., et al. (2017). Geological and Geochemical Controls on Subsurface Microbial Life in the Samail Ophiolite, Oman. *Front. Microbiol.* 8:56. doi: 10.3389/fmicb.2017.00056

Richardson, D. J., Berks, B. C., Russell, D. A., Spiro, S., and Taylor, C. J. (2001). Functional, biochemical and genetic diversity of prokaryotic nitrate reductases. *Cell. Mol. Life Sci.* 58, 165–178. doi: 10.1007/PL00000845

Richter, M., and Rosselló-Móra, R. (2009). Shifting the genomic gold standard for the prokaryotic species definition. *Proc. Natl. Acad. Sci. U.S.A.* 106, 19126–19131. doi: 10.1073/pnas.0906412106

Rinke, C., Lee, J., Nath, N., Goudeau, D., Thompson, B., Poulton, N., et al. (2014). Obtaining genomes from uncultivated environmental microorganisms using FACS–based single-cell genomics. *Nat. Protoc.* 9, 1038–1048. doi: 10.1038/nprot.2014.067

Rodriguez-R, L. M., and Konstantinidis, K. T. (2014). Bypassing Cultivation To Identify Bacterial Species: culture-independent genomic approaches identify credibly distinct clusters, avoid cultivation bias, and provide true insights into microbial species. *Microbe Mag.* 9, 111–118. doi: 10.1128/microbe.9.111.1

Rodriguez-R, L. M., and Konstantinidis, K. T. (2016). The enveomics collection: a toolbox for specialized analyses of microbial genomes and metagenomes. *PeerJ* 1 4:e1900v1. doi: 10.7287/peerj.preprints.1900v1

Russell, M. J., Hall, A. J., and Martin, W. (2010). Serpentinization as a source of energy at the origin of life. *Geobiology* 8, 355–371. doi: 10.1111/j.1472-4669.2010.00249.x

Sato, T., Yoshiya, K., and Maruyama, S. (2019). History of the Hadean "Living Microfossil" OD1 and Ultra-reducing Environments. *J. Geogr.* 128, 571–596. doi: 10.5026/jgeography.128.571

Schuchmann, K., and Müller, V. (2014). Autotrophy at the thermodynamic limit of life: a model for energy conservation in acetogenic bacteria. *Nat. Rev. Microbiol.* 12, 809–821. doi: 10.1038/nrmicro3365

Schuchmann, K., and Müller, V. (2016). Energetics and application of heterotrophy in Acetogenic Bacteria. *Appl. Environ. Microbiol.* 82, 4056–4069. doi: 10.1128/AEM.00882-16

Schut, G. J., and Adams, M. W. W. (2009). The Iron-Hydrogenase of *Thermotoga maritima* Utilizes Ferredoxin and NADH Synergistically: a New Perspective on Anaerobic Hydrogen Production. *J. Bacteriol.* 191, 4451–4457. doi: 10.1128/JB.01582-08

Scott, J. W., and Rasche, M. E. (2002). Purification, Overproduction, and Partial Characterization of β-RFAP Synthase, a Key Enzyme in the Methanopterin Biosynthesis Pathway. *J. Bacteriol.* 184, 4442–4448. doi: 10.1128/JB.184.16.4442-4448.2002

Seewald, J. S., Zolotov, M. Y., and McCollom, T. (2006). Experimental investigation of single carbon compounds under hydrothermal conditions. *Geochim. Cosmochim. Acta* 70, 446–460. doi: 10.1016/j.gca.2005.09.002

Shin, J., Song, Y., Jeong, Y., and Cho, B.-K. (2016). Analysis of the core genome and pan-genome of autotrophic Acetogenic Bacteria. *Front. Microbiol.* 7:1531. doi: 10.3389/fmicb.2016.01531

Smith, K. S., and Ferry, J. G. (2000). Prokaryotic carbonic anhydrases. *FEMS Microbiol. Rev.* 24, 335–366. doi: 10.1111/j.1574-6976.2000.tb00546.x

Stamatakis, A. (2014). RAxML version 8: a tool for phylogenetic analysis and post-analysis of large phylogenies. *Bioinformatics* 30, 1312–1313. doi: 10.1093/bioinformatics/btu033

Stamatakis, A., Hoover, P., and Rougemont, J. (2008). A rapid bootstrap algorithm for the RAxML web servers. *Syst. Biol.* 57, 758–771. doi: 10.1080/10635150802429642

Suda, K., Gilbert, A., Yamada, K., Yoshida, N., and Ueno, Y. (2017). Compound– and position–specific carbon isotopic signatures of abiogenic hydrocarbons from on–land serpentinite–hosted Hakuba Happo hot spring in Japan. *Geochim Cosmochim Acta* 206, 201–215. doi: 10.1016/j.gca.2017.03.008

Suda, K., Ueno, Y., Yoshizaki, M., Nakamura, H., Kurokawa, K., Nishiyama, E., et al. (2014). Origin of methane in serpentinite-hosted hydrothermal systems: The CH4–H2–H_2O hydrogen isotope systematics of the Hakuba Happo hot spring. *Earth Planet. Sci. Lett.* 386, 112–125. doi: 10.1016/j.epsl.2013.11.001

Suzuki, S., Ishii, S., Wu, A., Cheung, A., Tenney, A., Wanger, G., et al. (2013). Microbial diversity in The Cedars, an ultrabasic, ultrareducing, and low salinity serpentinizing ecosystem. *Proc. Natl. Acad. Sci. U.S.A.* 110, 15336–15341. doi: 10.1073/pnas.1302426110

Suzuki, S., Nealson, K. H., and Ishii, S. (2018). Genomic and in-situ transcriptomic characterization of the candidate phylum NPL-UPL2 from highly alkaline highly reducing serpentinized groundwater. *Front. Microbiol.* 9:3141. doi: 10.3389/fmicb.2018.03141

Takami, H. (2014). "New method for comparative functional genomics and metagenomics using KEGG MODULE," in *Encyclopedia of Metagenomics*, ed. K. E. Nelson (New York, NY: Springer), 1–15. doi: 10.1007/978-1-4614-6418-1_183-3

Tashiro, Y., Monson, R. E., Ramsay, J. P., and Salmond, G. P. C. (2016). Molecular genetic and physical analysis of gas vesicles in buoyant enterobacteria. *Environ. Microbiol.* 18, 1264–1276. doi: 10.1111/1462-2920.13203

Tiago, I., and Veríssimo, A. (2013). Microbial and functional diversity of a subterrestrial high pH groundwater associated to serpentinization: microbial and functional diversity of subsurface aquifer. *Environ. Microbiol.* 15, 1687–1706. doi: 10.1111/1462-2920.12034

Twing, K. I., Brazelton, W. J., Kubo, M. D. Y., Hyer, A. J., Cardace, D., Hoehler, T. M., et al. (2017). Serpentinization-influenced groundwater harbors extremely low diversity microbial communities adapted to high pH. *Front. Microbiol.* 8:308. doi: 10.3389/fmicb.2017.00308

Vignais, P. M., and Billoud, B. (2007). Occurrence, classification, and biological function of hydrogenases: an overview. *Chem. Rev.* 107, 4206–4272. doi: 10.1021/cr050196r

Vignais, P. M., Billoud, B., and Meyer, J. (2001). Classification and phylogeny of hydrogenases. *FEMS Microbiol. Rev.* 25, 455–501. doi: 10.1111/j.1574-6976.2001.tb00587.x

von Ballmoos, C., and Dimroth, P. (2007). Two distinct proton binding sites in the ATP synthase family. *Biochemistry* 46, 11800–11809. doi: 10.1021/bi701083v

Wagner, T., Ermler, U., and Shima, S. (2016). The methanogenic CO_2 reducing-and-fixing enzyme is bifunctional and contains 46 [4Fe-4S] clusters. *Science* 354, 114–117. doi: 10.1126/science.aaf9284

Wagner, T., Koch, J., Ermler, U., and Shima, S. (2017). Methanogenic heterodisulfide reductase (HdrABC-MvhAGD) uses two noncubane [4Fe-4S] clusters for reduction. *Science* 357, 699–703. doi: 10.1126/science.aan0425

Walsby, A. E. (1994). Gas vesicles. *Microbiol. Rev.* 58, 94–144.

Wiechmann, A., Ciurus, S., Oswald, F., Seiler, V. N., and Müller, V. (2020). It does not always take two to tango: "Syntrophy" via hydrogen cycling in one bacterial cell. *ISME J*. doi: 10.1038/s41396-020-0627-1 [Epub ahead of print].

Williams, K. P. (2002). Integration sites for genetic elements in prokaryotic tRNA and tmRNA genes: sublocation preference of integrase subfamilies. *Nucleic Acids Res*. 30, 866–875. doi: 10.1093/nar/30.4.866

Wright, A. V., Nuñez, J. K., and Doudna, J. A. (2016). Biology and applications of CRISPR systems: harnessing nature's toolbox for genome engineering. *Cell* 164, 29–44. doi: 10.1016/j.cell.2015.12.035

Xu, H., Aurora, R., Rose, G. D., and White, R. H. (1999). Identifying two ancient enzymes in Archaea using predicted secondary structure alignment. *Nat. Struct. Biol.* 6, 750–754. doi: 10.1038/11525

Xu, Y., and Zhao, F. (2018). Single-cell metagenomics: challenges and applications. *Protein Cell* 9, 501–510. doi: 10.1007/s13238-018-0544-5

Yilmaz, P., Parfrey, L. W., Yarza, P., Gerken, J., Pruesse, E., Quast, C., et al. (2014). The SILVA and "All-species Living Tree Project (LTP)" taxonomic frameworks. *Nucleic Acids Res*. 42, D643–D648. doi: 10.1093/nar/gkt1209

Yoshimatsu, K., Iwasaki, T., and Fujiwara, T. (2002). Sequence and electron paramagnetic resonance analyses of nitrate reductase NarGH from a denitrifying halophilic euryarchaeote *Haloarcula marismortui*. *FEBS Lett*. 516, 145–150. doi: 10.1016/S0014-5793(02)02524-3

Yoshimatsu, K., Sakurai, T., and Fujiwara, T. (2000). Purification and characterization of dissimilatory nitrate reductase from a denitrifying halophilic archaeon, *Haloarcula marismortui*. *FEBS Lett.* 470, 216–220. doi: 10.1016/s0014-5793(00)01321-1

Zhang, X., Carter, M. S., Vetting, M. W., San Francisco, B., Zhao, S., Al-Obaidi, N. F., et al. (2016). Assignment of function to a domain of unknown function: DUF1537 is a new kinase family in catabolic pathways for acid sugars. *PNAS* 113, E4161–E4169. doi: 10.1073/pnas.1605546113

Zhou, Y., Liang, Y., Lynch, K. H., Dennis, J. J., and Wishart, D. S. (2011). PHAST: a fast phage search tool. *Nucleic Acids Res.* 39, W347–W352. doi: 10.1093/nar/gkr485

Conflict of Interest: The authors declare that the research was conducted in the absence of any commercial or financial relationships that could be construed as a potential conflict of interest.

frontiers in Microbiology

ORIGINAL RESEARCH
published: 15 September 2020
doi: 10.3389/fmicb.2020.571736

Homoacetogenic Conversion of Mannitol by the Thermophilic Acetogenic Bacterium *Thermoanaerobacter kivui* Requires External CO_2

Jimyung Moon, Surbhi Jain, Volker Müller and Mirko Basen†*

Department of Molecular Microbiology and Bioenergetics, Institute of Molecular Biosciences, Johann Wolfgang Goethe University, Frankfurt, Germany

OPEN ACCESS

Edited by:
Hauke Smidt, Wageningen University & Research, Netherlands

Reviewed by:
Bernhard Schink, University of Konstanz, Germany
Shigeyuki Kawai, Ishikawa Prefectural University, Japan

***Correspondence:**
Mirko Basen
mirko.basen@uni-rostock.de

†Present address:
Mirko Basen, Institute of Biological Sciences, University of Rostock, Rostock, Germany

Specialty section:
This article was submitted to Microbial Physiology and Metabolism, a section of the journal Frontiers in Microbiology

Received: *11 June 2020*
Accepted: *24 August 2020*
Published: *15 September 2020*

Citation:
Moon J, Jain S, Müller V and Basen M (2020) Homoacetogenic Conversion of Mannitol by the Thermophilic Acetogenic Bacterium Thermoanaerobacter kivui Requires External CO_2. Front. Microbiol. 11:571736. doi: 10.3389/fmicb.2020.571736

Acetogenic microorganisms utilize organic substrates such as sugars in addition to hydrogen (H_2) + carbon dioxide (CO_2). Recently, we reported that the thermophilic acetogenic microorganism *Thermoanaerobacter kivui* is among the few acetogens that utilize the sugar alcohol mannitol, dependent on a gene cluster encoding mannitol uptake, phosphorylation and oxidation of mannitol-1-phosphate to fructose-6-phosphate. Here, we studied mannitol metabolism with resting cells of *T. kivui*; and found that mannitol was "fermented" in a homoacetogenic manner, i.e., acetate was the sole product if HCO_3^- was present. We found an acetate:mannitol ratio higher than 3, indicating the requirement of external CO_2, and the involvement of the WLP as terminal electron accepting pathway. In the absence of CO_2 (or bicarbonate, HCO_3^-), however, the cells still converted mannitol to acetate, but slowly and with stoichiometric amounts of H_2 formed in addition, resulting in a "mixed" fermentation. This showed that–in addition to the WLP–the cells used an additional electron sink–protons, making up for the "missing" CO_2 as electron sink. Growth was 2.5-fold slower in the absence of external CO_2, while the addition of formate completely restored the growth rate. A model for mannitol metabolism is presented, involving the major three hydrogenases, to explain how [H] make their way from glycolysis into the products acetate or acetate + H_2.

Keywords: carbon dioxide reduction, mannitol, acetogenic, thermophilic, *Thermoanaerobacter kivui*, Wood–Ljungdahl pathway

INTRODUCTION

Acetogens thrive from the formation of acetate from hydrogen (H_2) + carbon dioxide (CO_2). Hence, they are an important part of the anaerobic food web, linking primary fermentation to methanogenesis (Schink and Stams, 2006). In addition to H_2 + CO_2, most acetogens utilize a variety of "heterotrophic substrates" (Diekert and Wohlfarth, 1994; Schuchmann and Müller, 2016). For example, most acetogens also grow heterotrophically with C6 sugars as substrates, as discovered already in 1942 (Fontaine et al., 1942). Since they convert these to three molecules of acetate as sole major product, acetogens have originally been described as "homoacetogens" (Drake et al., 2008).

In "homoacetogenesis," glucose is oxidized to 2 acetate, 2 CO_2, yielding 8 reducing equivalents [H] (eq. 1) and 4 ATP (not shown in the equation; for bioenergetics, please see Schuchmann and Müller, 2014).

$$C_6H_{12}O_6 + 2H_2O \rightarrow 2CH_3COOH + 2CO_2 + 8[H] \quad (1)$$

Importantly and uniquely within the fermentative organisms, homoacetogens then recycle the excess reducing equivalents ("electrons") in form of 2 NADH and 2 molecules ferredoxin (Fd_{red}) by reducing 2 CO_2 in the Wood–Ljungdahl pathway (WLP) (eq. 2), with *n* ATP being formed in the acetogenic respiratory chain (Schuchmann and Müller, 2014).

$$2CO_2 + 8[H] \rightarrow CH_3COOH + 2H_2O \quad (2)$$

In sum, glucose is oxidized to 3 acetates according to eq. 3.

$$C_6H_{12}O_6 \rightarrow 3CH_3COOH \quad (3)$$

The question now arises how molecules are metabolized that are more reduced, such as the C6 sugar alcohol mannitol. Mannitol, an abundant reserve carbohydrate in brown algae (Adams et al., 2011) has been described as a growth substrate for 8 out of the 47 acetogens that have been sequenced (Moon et al., 2019, and references therein). Mannitol oxidation to acetate yields 10 [H], 2 [H] more than glucose (eq. 4 vs. eq. 1).

$$C_6H_{14}O_6 + 2H_2O \rightarrow 2CH_3COOH + 2CO_2 + 10[H] \quad (4)$$

In mannitol conversion by acetogens, consequently, electrons have to be deposited either internally on an intermediate of the sugar oxidation, yielding a more reduced product than acetate, or on an external electron acceptor. The coupling of mannitol oxidation to the WLP, however, has not been studied in detail in any acetogen.

Here, we describe the catabolism of the thermophilic acetogenic bacterium *Thermoanaerobacter kivui* growing on the sugar alcohol mannitol. We recently characterized the uptake of mannitol by a phosphotransferase system (PTS) and the subsequent conversion of mannitol-1-phosphate by a thermostable mannitol-1-phosphate dehydrogenase in *T. kivui* (Moon et al., 2019). By a variety of physiological experiments with growing cells and cell suspension, we now show unambiguously that *T. kivui* utilizes external CO_2 as additional electron acceptor during growth on and conversion of mannitol; the biochemical and eco-physiological consequences are discussed.

RESULTS AND DISCUSSION

Homoacetogenic Conversion of Mannitol Plus CO_2 in Cell Suspensions

While homoacetate fermentation theoretically yields three molecules of acetate as sole product from C6 sugars, experimentally, acetate to C6 (fructose or glucose) ratios of 2.6, 2.7, and 2.3–3 have been observed in growing cultures of the acetogens *Moorella thermoacetica* (Fontaine et al., 1942), *Acetobacterium woodii* (Heise et al., 1989) and *T. kivui* (Leigh et al., 1981), respectively. In our hands, non-growing cells of *T. kivui* in concentrated suspensions (which excludes that carbon and reducing equivalents were channeled into biomass), converted glucose to mainly acetate (**supplementary Figure S1**), with only minor amounts of H_2 (0.2 mM; **Figure 1C**, for comparison calculated as if all H_2 in was dissolved; *n* H_2 in headspace/*vol* medium). The resulting acetate:glucose ratio of 2.6 ± 0.1, clearly indicates the involvement of the WLP in the recycling of reduced redox carriers, since the ratio is >2.0. Omitting HCO_3^- (the hydrated, deprotonated form of CO_2) in the cell suspension experiments did not lead to a significantly different acetate:glucose ratio (**supplementary Figure S1D**) and, again, only little H_2 (1.9 ± 0.5) mM was formed (**supplementary Figure S1C**), showing only a minor fraction of the reductant was removed by proton reduction. As expected from thermodynamic considerations, however, the rates of glucose consumption and acetate production decreased by approximately 60%, from −197 ± 14 nmol min^{-1} mg^{-1} (protein) to −71 ± 4 nmol min^{-1} mg^{-1} and 438 ± 47 nmol min^{-1} mg^{-1} (protein) to 199 ± 13 nmol min^{-1} mg^{-1} (**supplementary Figures S1A,B**). To directly demonstrate the effect of CO_2 on glucose conversion, HCO_3^- was added to a subset of cell suspensions after 3 h. The rate of glucose consumption and acetate production increased, and most obviously, intermediately accumulated H_2 (∼0.5 mM) was re-utilized by the cells.

As mannitol is more reduced than glucose by two electrons, the question arose where the additional electrons go that are transferred to NAD^+ in the MtlD reaction. One option would be an additional reduced product, such as lactate, H_2, ethanol or formate. Metabolite analyses in our recent experiments with *T. kivui* growing on mannitol (Moon et al., 2019), however, revealed no major other products. We are aware of only one other study in which products of mannitol utilization in an acetogen, *Sporomusa termitida*, were quantified; and in that organism, acetate was as well the major product, with a slightly lower ratio (2.6 mol per mol mannitol), and with minor amounts of some other products such as propionate or ethanol detected (Breznak et al., 1988). We performed more experiments, actively searching for such reduced compounds using HPLC and GC analyses; however, maximally trace amounts (<0.5 mM lactate or ethanol) were detected in the supernatant of growing or resting cells. Therefore, we hypothesized that CO_2 present in the medium is the sole major electron acceptor according to eq. 2. Hence, mannitol would be converted to acetate according to eq. 5.

$$4C_6H_{14}O_6 + 2CO_2 \rightarrow 13CH_3COO^- + 13H^+ + 2H_2O \quad (5)$$

To prove the involvement of CO_2, concentrated cell suspensions of *T. kivui* were incubated at 65°C with mannitol in the presence and in the absence of HCO_3^- in the medium. In the control experiment with 54 mM of HCO_3^- present, 23.8 ± 1.5 mM mannitol was rapidly consumed (**Figure 1A**), and acetate (73.2 ± 4.1 mM) was produced (**Figure 1B**). No major other product was detected and, consequently, almost all of the reducing equivalents (92 ± 2%) from mannitol oxidation were recovered in the product acetate, even more than in incubations

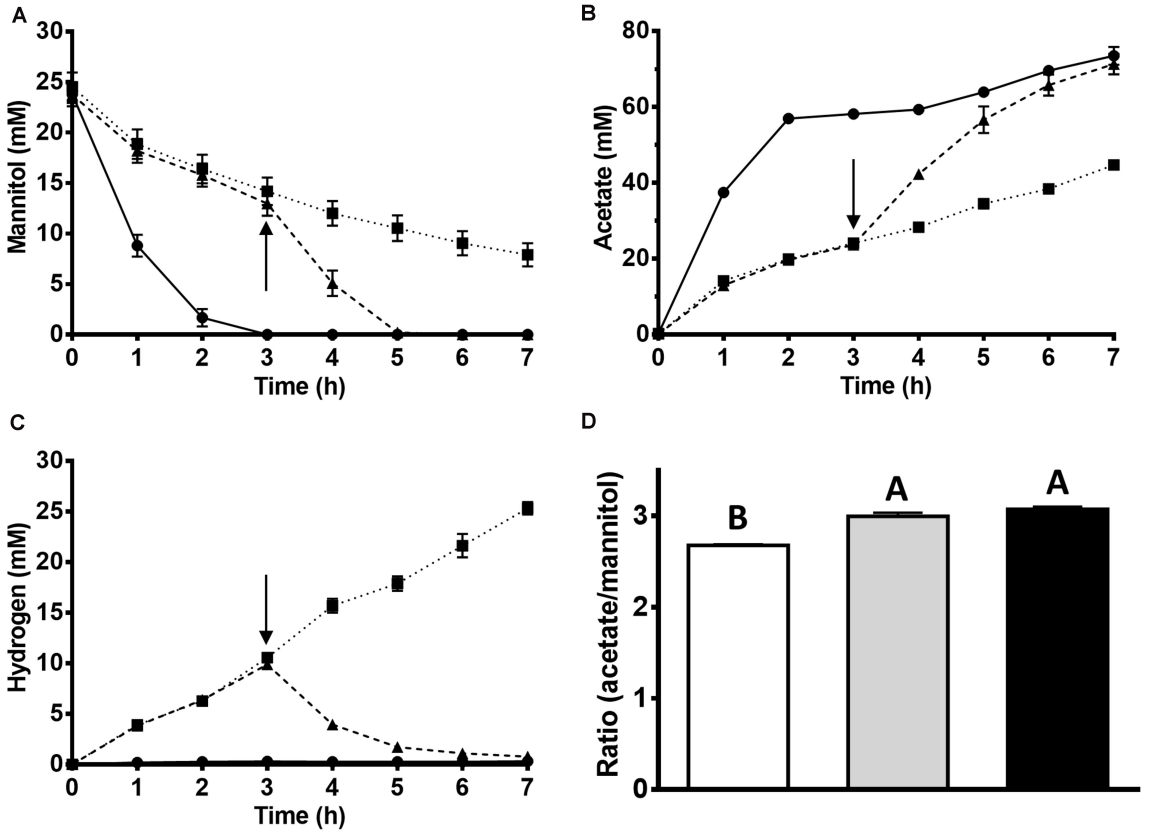

FIGURE 1 | Effect of $KHCO_3$ on acetate and hydrogen formation from mannitol by cell suspensions of *T. kivui*. 10 ml of the resting cells (1.0 mg/ml protein) were incubated at 65°C for 7 h under anoxic conditions (N_2 headspace). 0.8 ml samples were taken for determination of **(A)** mannitol and **(B)** acetate. **(C)** Hydrogen gas was determined by gas chromatography. Cell suspensions were either not supplied with $KHCO_3$ (squares), supplied with 54 mM $KHCO_3$ after 3 h of incubation (triangles) or supplied with 54 mM $KHCO_3$ (circles) from the beginning. The arrow indicates the addition of 54 mM $KHCO_3$. **(D)** Ratio of acetate produced to mannitol consumed after 7 h of incubation. White, without $KHCO_3$; gray, addition of 54 mM $KHCO_3$ at 3 h; black, with 54 mM $KHCO_3$ from the beginning. The experiments were performed in biological triplicates. Bars not sharing the same letter indicate a significant difference ($p \leq 0.05$) according to Tukey's HSD test.

with glucose. Considering mannitol conversion according to eq. 5 and assuming 1/2 molecule of CO_2 reduced per molecule mannitol, all substrate carbon (mannitol and CO_2) was re-found in the product acetate (100 ± 2%). The observed acetate:mannitol ratio of 3.1 ± 0.1 (**Figure 1D**) supports the hypothesis of a homoacetogenic conversion of mannitol, with the need for additional CO_2, putatively according to eq. 5. This is in contrast to glucose metabolism, where the amount of CO_2 released from glucose oxidation equals the amount of CO_2 needed as electron acceptor in the WLP (no net consumption of CO_2 according to eq. 3).

Therefore, mannitol consumption and conversion to acetate should be more affected than glucose conversion if HCO_3^-/CO_2 is omitted from incubations; and that is what we observed. In the incubations without HCO_3^-, less mannitol was consumed (16.6 ± 0.5 mM) and less acetate (44.5 ± 1.4 mM) was produced. The rate of mannitol consumption decreased to a third (from −185 ± 18 nmol min^{-1} mg^{-1} to −58 ± 9 nmol min^{-1} mg^{-1}), as the rate of acetate formation did concomitantly (from 472 ± 34 nmol min^{-1} mg^{-1} to 129 ± 11 μmol min^{-1} mg^{-1}). Accordingly, the ratio of acetate produced per mannitol in the experiment without HCO_3^- was significantly lower, 2.7 ± 0.0, **Figure 1D**). Instead, significantly more H_2 was produced (corresponding to 25.3 ± 1.1 mM if all hydrogen was dissolved, **Figure 1C**) compared to the corresponding incubations with glucose (1.9 mM ± 1.4 mM). This shows that *T. kivui* used protons as electron acceptors in mannitol metabolism in the absence of external CO_2/HCO_3^-. The metabolism can be seen as a mixed fermentation, with part of the reductant going to protons, similar to what has been observed for sugar oxidation e.g., in *Thermotoga maritima* (Schröder et al., 1994). The other part is still channeled to the WLP, since CO_2 is released from mannitol oxidation through the PFOR reaction (eq. 6) In conclusion, mannitol metabolism in *T. kivui* cell suspensions in the absence of CO_2 can be described by eq. 6 (more reductant channeled to protons), eq. 7 (only "extra" reductant from sugar alcohol phosphate oxidation to a sugar phosphate channeled to protons, **supplementary Figure S2**), or a mixture thereof.

$$C_6H_{14}O_6 + 2H_2O \rightarrow 2CH_3COOH + 2CO_2 + 5H_2 \quad (6)$$

$$C_6H_{14}O_6 \rightarrow 3CH_3COOH + H_2 \quad (7)$$

When HCO_3^- was added to the HCO_3^- free incubations after 3 h, mannitol consumption and acetate production accelerated again (**Figures 1A,B**). H_2 that had accumulated intermediately in the absence of HCO_3^- was consumed again after its addition (∼10 mM), leaving only a minor amount (0.8 ± 0.1 mM, **Figure 1C**). No other major products were observed in any of the incubations, and the reducing equivalents were almost stoichiometrically recovered in the products (92–95% recovery).

Growth on Mannitol Is CO_2-Dependent

While the experiments with concentrated cell suspensions directly demonstrated the influence of external HCO_3^-/CO_2 on glucose, but particularly on mannitol conversion (**Figure 1** and **supplementary Figure S1**), it remained to be tested whether and how this affects growth on both substrates. We hypothesized that growth on both substrates was affected due to thermodynamic reasons, and the effect may be stronger during growth on mannitol. To test this hypothesis, we grew *T. kivui* in defined medium with 25 mM glucose or mannitol under a pure N_2 atmosphere in the presence or absence of 54 mM $KHCO_3$.

Growth on glucose was slowed down in HCO_3^- (and CO_2) free defined medium, as the doubling time (t_D) of *T. kivui* increased from 1.7 ± 0.2 h to 2.9 ± 0.1 h (**Figure 2A**). An increase in the doubling time (t_D) was expected for thermodynamic reasons, the concentration of CO_2 was much lower–only the CO_2 released in the PFOR reaction was present. As expected, a more severe effect was observed in the incubations with mannitol, where the t_D increased from 2.0 ± 0.0 to 5.2 ± 0.0 h. The maximum OD_{600} of *T. kivui* cultures grown on mannitol in HCO_3^- -free medium was 0.86 compared to OD_{600} higher than 2.0 in the presence of HCO_3^-. Differences were found in the product concentrations as well (**Figure 2B**). Without HCO_3^-, cells grown on glucose produced slightly less acetate (56.4 ± 1.4 mM) than with HCO_3^- (60.3 ± 1.0 mM), and some H_2 was produced (4.5 ± 0.4 mM). Cells grown on mannitol showed the same tendency, but much bigger differences between incubations were observed with and without HCO_3^-. The amount of acetate produced by cells without HCO_3^- reached 43.3 ± 2.6 mM, which is much less compared to those grown in the presence of HCO_3^- (62.3 ± 0.6 mM). Instead, more H_2 was produced (17.7 ± 1.2 mM vs. 0.4 ± 0.0 mM), as observed in the experiments with the (non-growing) cell suspensions (**Figure 1**).

One major outcome of the growth experiment was that CO_2 released from sugar or sugar alcohol oxidation was sufficient to sustain growth, though at significantly decreased growth rates. CO_2 dependence and fermentation capabilities of acetogens sugar conversion have not been studied much recently. Early evidence for CO_2-dependence of acetogenic conversion of sugars were obtained in a study from Andreesen et al. (1970) who found that the mesophilic carboxydotroph *Clostridium formicoaceticum* grew only with a long lag phase and to much lower optical densities in the absence of $NaHCO_3$. Also, it was shown in the same study that $^{14}CO_2$ was incorporated into ^{14}C-acetate, with both the methyl and the carbonyl group being labeled, consistent with the utilization of the WLP as terminal electron accepting pathway (Wood et al., 1986). Contrarily, a study from 1996 then revealed that the mesophilic acetogen *Blautia producta* still grew on fructose or xylose in the absence of CO_2, with molar growth yields reduced by about 30–35%, and [H] channeled into the reduced carbon products succinate and lactate, instead of into H_2 (Misoph and Drake, 1996). Moreover, the acetate:fructose ratio was below 2, indicating that the WLP was potentially not involved in re-oxidation of reduced electron carriers. Another acetogen, the mesophilic model organism *A. woodii* produces a yet unknown reduced metabolite and less acetate when its Rnf complex is dysfunctional in the absence of Na^+, or deleted (Heise et al., 1989; Westphal et al., 2018). Acetogens utilize other reduced substrates; alcohols such as methanol or ethanol for example, and the basic metabolic "problem" applies here: Growth on these substrates require additional electron removal. Accordingly, electron removal through the WLP with reduced non-sugar substrates has been proposed e.g., for *A. woodii* growing on methanol (Bache and Pfennig, 1981) ethanol (Buschhorn et al., 1989; Bertsch et al., 2016), or *Acetobacterium carbinolicum* on

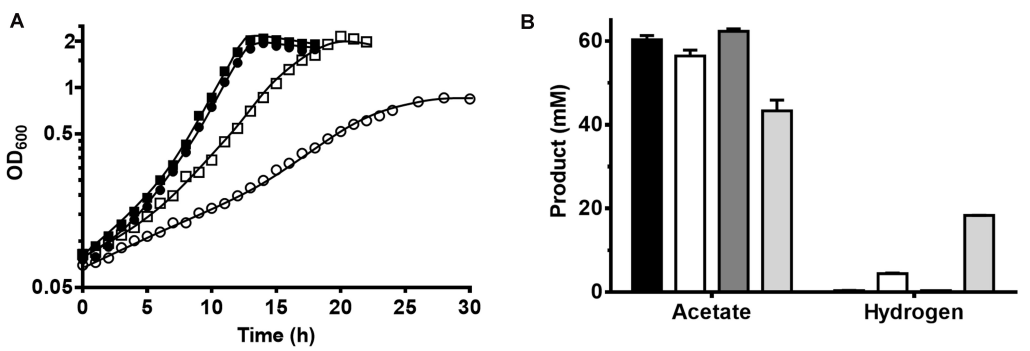

FIGURE 2 | Growth of *T. kivui* on glucose and on mannitol in the presence or absence of carbonate in medium at 65°C. **(A)** Growth of *T. kivui* on 25 mM glucose in carbonate buffered defined medium (black squares), on 25 mM glucose in carbonate free defined medium (white squares), on 25 mM mannitol in carbonate buffered defined medium (black circles), and on 25 mM mannitol in carbonate free defined medium (white circles) at 65°C. The experiments were performed in biological triplicates and one representative growth curve is shown. **(B)** Acetate and hydrogen produced during growth. Black bars, on 25 mM glucose in carbonate buffered defined medium; white bars, on 25 mM glucose in carbonate free defined medium; dark gray bars, on 25 mM mannitol in carbonate buffered defined medium; light gray bars, on 25 mM mannitol in carbonate free defined medium.

a variety of alcohols (Eichler and Schink, 1984), with the closed carbon balances indicating CO_2 utilization in the latter, at least.

So similarly to the cell suspension experiments, *T. kivui* utilized protons as electron acceptors in the absence of CO_2, supposedly, via the electron-bifurcating hydrogenase, working in confurcating direction. This is slightly different (albeit not contradictory) to our recent observations of a strict dependency of *T. kivui* on the WLP in a strain where the WLP was functionally abolished. The *T. kivui* mutant lacked the hydrogen-dependent CO_2 reductase (HDCR), the first enzyme of the methyl branch of the WLP (Jain et al., 2020). Cell suspension of that mutant strain also produced H_2 from glucose in the absence of formate - similar to mannitol conversion in the wild type (**Figure 1**). Growth, however, was not only significantly impaired as observed here (**Figure 2**), but completely inhibited, except for when formate was added as additional electron acceptor (Jain et al., 2020). Therefore, we concluded that the WLP as terminal electron accepting pathway is essential for growth of *T. kivui* on all substrates (Jain et al., 2020). Here, we provide evidence that *T. kivui* utilized additional electron acceptors (protons) during growth if forced to do so; but the WLP was still the major electron sink, and [H] removal through proton reduction is not fast enough to keep up the growth rate.

Formate Stimulates Growth in the Absence of External CO_2

Since in the absence of added HCO_3^- (and therefore CO_2), growth was significantly slowed down, we tested whether external formate could account for the "missing" CO_2 in wild type *T. kivui*, as recently described for the *T. kivui* HDCR deletion strain (Jain et al., 2020). A growth experiment was set up with *T. kivui* wild type inoculated into CO_2 and HCO_3^- free defined medium (**Figure 3**). While in the absence of formate (or CO_2) again a maximal OD_{600} of only 0.7 was observed and a prolonged doubling time of 5.2 ± 0.2 h, the addition of formate as external electron acceptor increased the maximal OD_{600} to 2.34 and decreased the doubling time to 2.0 ± 0.0 (**Figure 3**), which corresponds to the growth behavior observed before during growth on mannitol in the presence of CO_2/HCO_3^- (Moon et al., 2019). Growth on formate as sole substrate contributed only little (**Figure 3**). 19.7 ± 0.8 mM of mannitol was consumed in the presence of 40.3 ± 2.0 mM formate (which was completely consumed), and 66.0 ± 15.5 mM acetate was produced. We therefore conclude that external formate completely replaced external CO_2/HCO_3^- during growth on mannitol, constituting the only added electron acceptor. The ability to utilize an electron acceptor other than CO_2 enhances the metabolic flexibility of acetogens in environments where no or little CO_2 is present, or to changing environmental conditions. Few additional electron acceptors such as nitrate or aromatic compounds are utilized by some acetogens. In the absence of CO_2, *A. woodii* for example grows with caffeate as electron acceptor, forming hydrocaffeate as reduced product (Tschech and Pfennig, 1984), potentially giving the organism a metabolic advantage when no CO_2 is present.

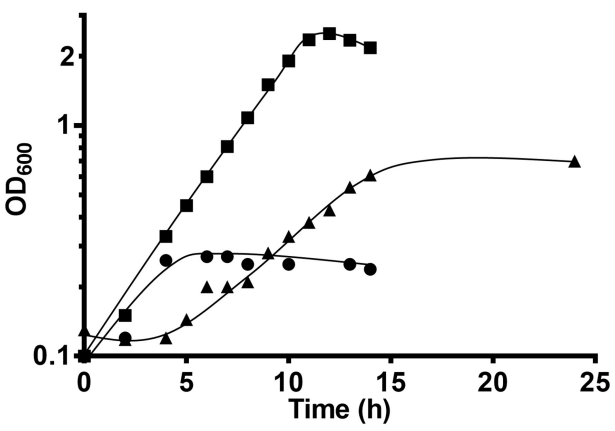

FIGURE 3 | Growth of *T. kivui* on mannitol (25 mM) on defined medium without formate (triangles) or with formate (50 mM, squares) in the absence of HCO_3^-/CO_2, at 65°C. Growth on 50 mM formate (circles) only is shown as a control. Experiments were performed in biological duplicates and a representative growth curve is shown.

Mannitol Metabolism in *T. kivui* Is Supported by Its Mode of Energy Conservation

In conclusion, the experiments with resting and growing cells of *T. kivui* with and without HCO_3^- showed that the additional electrons from mannitol oxidation were channeled into the WLP for CO_2 fixation. In the absence of CO_2 in the medium, additionally protons were reduced to H_2 (approximately according to eq. 8), but growth and mannitol conversion were significantly reduced. Based on these observations and on the genome model, the following model for mannitol metabolism in *T. kivui* in the presence of external CO_2 is postulated (**Figure 4**). Four (molecules of) mannitol are taken up and phosphorylated by a PTS system. Then, four mannitol-1-phosphate are oxidized to four fructose-6-phosphate, yielding 4 NADH. Glycolysis and PFOR yield 8 acetyl-coenzyme A, which is further converted to acetate, 8 CO_2, 8 NADH and 8 Fd_{red}. In the presence of external CO_2, the reductant (in form of 8 NADH and 8 Fd_{red}) is utilized to reduce CO_2 to acetate. We assume the WLP needs 1 H_2 for the HDCR, two NADH and 1 Fd_{red} (Hess et al., 2014; Basen and Müller, 2017). When it is run four times to reduce the 8 CO_2 produced by PFOR, and then another time to reduce 2 additional CO_2, the redox carriers are not balanced, with 2 spare NADH and 3 spare Fd_{red} on the one hand, and 5 H_2 needed on the other hand. Redox balancing could be explained by the involvement of energy-converting hydrogenases (Ech), producing 1 H_2 from 1 Fd_{red}, and the electron-bifurcating hydrogenase, producing 4 H_2 from the remaining 2 NADH and 2 Fd_{red} (**Figure 4**; Hess et al., 2014; Basen and Müller, 2017).

Accordingly, the involvement of two hydrogenases in redox carrier oxidation may also explain the production of H_2 in the absence of CO_2 by *T. kivui* cells, the electron-bifurcating hydrogenase (HydABC) and the membrane-bound Ech, oxidizing the accrued reduced electron carriers, NADH and Fd_{red} or only Fd_{red}, respectively. Fd_{red} may also serve as physiological electron donor for HDCR (containing the

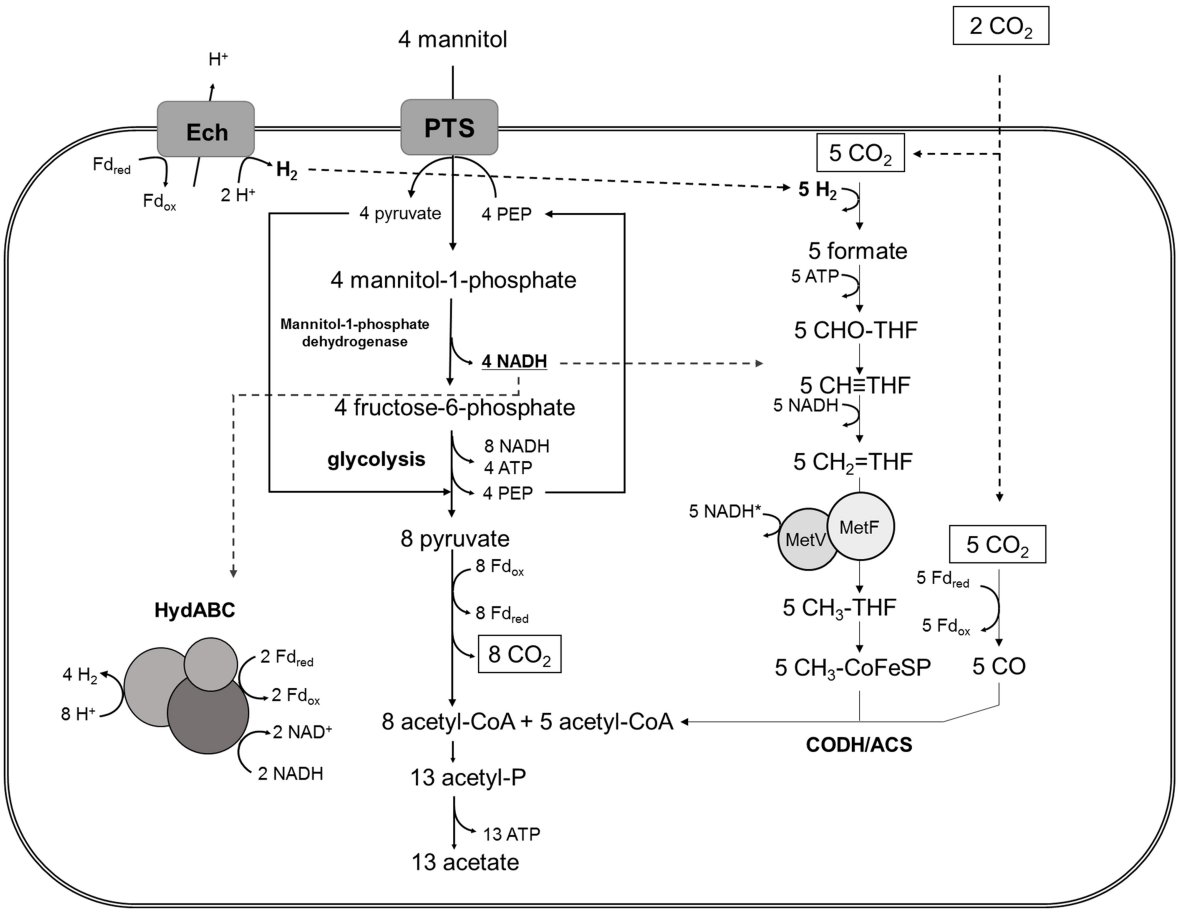

FIGURE 4 | Model for "homoacetogenic" mannitol metabolism in *T. kivui* in the presence of external CO_2, involving its three major hydrogenases. Reduced ferredoxin (Fd_{red}), produced from mannitol oxidation, is oxidized by energy-converting hydrogenase (Ech) and, together with NADH, by electron bifurcating hydrogenase (HydABC) to produce H_2. The latter is subsequently consumed by hydrogen dependent carbon dioxide reductase (HDCR), containing a hydrogenase subunit, to reduce CO_2 to formate. In the absence of external CO_2, a fraction of the reducing equivalents [H] is used to reduce protons to H_2, likely *via* HydABC. THF, tetrahydrofolate; CODH/ACS, carbon monoxide dehydrogenase/acetyl-CoA synthase; MetV/MetF, methylene-THF reductase (unknown cofactor specificity, *).

third hydrogenase involved) as in *A. woodii* (Schuchmann and Müller, 2013). H_2 production from sugar involving an electron-confurcating hydrogenase is likely widespread among fermentative anaerobes (Schut and Adams, 2009; Verbeke et al., 2013; Zheng et al., 2014; Cha et al., 2016). The essential principle here is the involvement an electron-bifurcating hydrogenase operating reverse (confurcating) direction, and concomitantly oxidizing NADH and Fd_{red}, as originally described in the thermophilic fermentative bacterium *T. maritima* (Schut and Adams, 2009). In acetogens, the intermediate accumulation of only small concentrations of H_2 during sugar metabolism has been demonstrated, for the thermophile *M. thermoacetica* (Kellum and Drake, 1984), and more recently in the mesophile *A. woodii* (Wiechmann et al., 2020). In the latter, the electron-bifurcating hydrogenase has been shown to be involved in a variation of H_2 cycling (see below), which had also been proposed for *M. thermoacetica* (Wang et al., 2013). Our genetic experiments with *T. kivui* (Jain et al., 2020) as well as the experiments presented with excess [H] from mannitol presented herein now go in line with the earlier observations with *M. thermoacetica*, suggesting that both organisms may have a similar metabolism during growth on sugars or sugar alcohols. The observed stoichiometric coupling of mannitol oxidation to CO_2 reduction the WLP, with the (proposed) involvement of Ech during heterotrophic growth, indicate that the module of reductant removal (the WLP) and the mode of energy conservation (chemiosmosis *via* Ech) may have been maintained in (the thermophilic) acetogens as conservative traits, enabling the ability to adapt to different electron donors. Indeed both, membrane-bound hydrogenases (Schut et al., 2016) and the WLP (Weiss et al., 2016) have been considered ancient metabolic modules. The interplay of the two hydrogenases (Ech and electron-bifurcating hydrogenase) may enable *T. kivui* the adaptation to substrates at different redox states, since different ratios of NADH and Fd_{red} may be achieved, and this remains subject of future studies.

MATERIALS AND METHODS

Growth Experiments

The wild type *T. kivui* strain LKT-1 (DSM2030) was cultivated under strict anoxic conditions at 65°C in either complex or carbonate buffered defined medium as described previously (Moon et al., 2019). Carbonate free medium was prepared as carbonate buffered defined medium, but no $KHCO_3$ was added and the medium was flushed with 100% N_2. To account for traces of CO_2 in the carbonate free medium, the growth experiments toward the effect of formate (**Figure 3**) were carried out with medium that has been boiled (autoclaved) to remove traces of CO_2, and then flushed with N_2 (CO_2-free medium). For determining the growth behavior, cultures were inoculated to an optical density of ∼0.1 from a pre-culture grown on the same substrate (glucose or mannitol), and then incubated at 65°C under slow shaking. Growth was monitored by measuring the optical density of subsamples at 600 nm in cuvettes with 1 cm light path.

Experiments With Resting Cells

A 500 ml cultures of *T. kivui* were grown in complex or defined medium to late exponential growth phase (OD_{600} of 1.7 to 2.3) and then harvested by centrifugation (Avanti^{TM}J-25 and JA-10 Fixed-Angle Rotor; Beckman Coulter, Brea, CA, United States) at 7,000 × *g* and 4°C for 10 min. The harvested cells were washed with 30 ml of the respective medium by centrifugation at 8,500 rpm (5948 × *g*) and 4°C for 10 min (Avanti^{TM}J-25 and JA-25.50 Fixed-Angle Rotor; Beckman Coulter, Brea, CA, United States). Then, the cells were resuspended in 5 ml of the respective medium and kept in 16 ml Hungate tubes. Resuspended cells were distributed into in Hungate tubes to a final volume of 10 mL and a final protein concentration of 10 mg ml^{-1}. All the steps were performed under strictly oxygen free conditions in an anoxic chamber (Coy Laboratory Products, Grass Lake, MI, United States) filled with N_2/CO_2 (80/20; v/v) for carbonate medium or with 100% N_2 for carbonate free medium. As substrate, 25 mM glucose or 25 mM mannitol was added to the resting cells. The experiment started with incubation at 65°C in water bath with shaking (150 rpm). 0.8 ml subsamples were taken for determination of protein, substrate and product concentration. The total protein concentration in the cell suspension was measured using the method by Schmidt et al. (1963).

Analysis of Substrate Decrease and Product Formation

H_2, alcohol and organic acid concentrations were determined by gas chromatography as described previously (Weghoff and Müller, 2016). The concentrations of glucose and mannitol were determined by high performance liquid as described previously (Moon et al., 2019). Lactic acid and formic acid concentrations were determined using test kits (R-Biopharm AG, Darmstadt, Germany) according to supplier's instruction.

Statistical Analysis

The ratio of acetate/substrate of *T. kivui* in cell suspension experiments was evaluated by comparing the average values of three biological replicates. For comparison of multiple groups, one-way analysis of variance (ANOVA) with Tukey's HSD test was carried out by the XLStat software (Version 2019, Addinsoft, New York, NY, United States).

DATA AVAILABILITY STATEMENT

All datasets presented in this study are included in the article/**Supplementary Material**.

AUTHOR CONTRIBUTIONS

VM and MB designed the study. JM and SJ performed the experiments and prepared the figures. JM, VM, and MB wrote the manuscript. All authors analyzed the data.

FUNDING

VM was supported by an Advanced Grant of the European Research Council under the European Union's Horizon 2020 Research and Innovation Program (grant agreement no. 741791). SJ was funded by a fellowship from Deutscher Akademischer Austauschdienst (DAAD). We acknowledge financial support by the Deutsche Forschungsgemeinschaft and Universität Rostock/Universitätsmedizin Rostock within the funding programme Open Access Publishing.

ACKNOWLEDGMENTS

MB thanks Benjamin Zeldes for proofreading the manuscript. VM and MB are grateful to Deutsche Forschungsgemeinschaft (DFG) for funding.

SUPPLEMENTARY MATERIAL

The Supplementary Material for this article can be found online at: https://www.frontiersin.org/articles/10.3389/fmicb.2020.571736/full#supplementary-material

REFERENCES

Adams, J. M., Ross, A. B., Anastasakis, K., Hodgson, E. M., Gallagher, J. A., Jones, J. M., et al. (2011). Seasonal variation in the chemical composition of the bioenergy feedstock *Laminaria digitata* for thermochemical conversion. *Bioresour. Technol.* 102, 226–234. doi: 10.1016/j.biortech.2010.06.152

Andreesen, J. R., Gottschalk, G., and Schlegel, H. G. (1970). Clostridium formicoaceticum nov. *spec. Isolation, description and distinction from C. aceticum and C. thermoaceticum. Arch. Mikrobiol.* 72, 154–174. doi: 10.1007/bf00409521

Bache, R., and Pfennig, N. (1981). Selective isolation of *Acetobacterium woodii* on methoxylated aromatic acids and determination of

growth yields. *Arch. Microbiol.* 130, 255–261. doi: 10.1007/bf00459530

Basen, M., and Müller, V. (2017). "Hot" acetogenesis. *Extremophiles* 21, 15–26. doi: 10.1007/s00792-016-0873-3

Bertsch, J., Siemund, A. L., Kremp, F., and Müller, V. (2016). A novel route for ethanol oxidation in the acetogenic bacterium *Acetobacterium woodii*: the acetaldehyde/ethanol dehydrogenase pathway. *Environ. Microbiol.* 18, 2913–2922. doi: 10.1111/1462-2920.13082

Breznak, J. A., Switzer, J. M., and Seitz, H. J. (1988). *Sporomusa termitida* sp. *nov., an H2*/CO2-utilizing acetogen isolated from termites. *Arch. Microbiol.* 150, 282–288. doi: 10.1007/bf00407793

Buschhorn, H., Dürre, P., and Gottschalk, G. (1989). Production and utilization of ethanol by the homoacetogen *Acetobacterium woodii*. *Appl. Environ. Microbiol.* 55, 1835–1840. doi: 10.1128/aem.55.7.1835-1840.1989

Cha, M., Chung, D., and Westpheling, J. (2016). Deletion of a gene cluster for [Ni-Fe] hydrogenase maturation in the anaerobic hyperthermophilic bacterium *Caldicellulosiruptor bescii* identifies its role in hydrogen metabolism. *Appl. Microbiol. Biotechnol.* 100, 1823–1831. doi: 10.1007/s00253-015-7025-z

Diekert, G., and Wohlfarth, G. (1994). Metabolism of homoacetogens. *Antonie Van Leeuwenhoek* 66, 209–221. doi: 10.1007/bf00871640

Drake, H. L., Gössner, A. S., and Daniel, S. L. (2008). Old acetogens, new light. *Ann. N.Y. Acad. Sci.* 1125, 100–128. doi: 10.1196/annals.1419.016

Eichler, B., and Schink, B. (1984). Oxidation of primary aliphatic alcohols by *Acetobacterium carbinolicum* sp. nov., a homoacetogenic anaerobe. *Arch. Microbiol.* 140, 147–152. doi: 10.1007/bf00454917

Fontaine, F. E., Peterson, W. H., Mccoy, E., Johnson, M. J., and Ritter, G. J. (1942). A new type of glucose fermentation by *Clostridium thermoaceticum*. *J. Bacteriol.* 43, 701–715. doi: 10.1128/jb.43.6.701-715.1942

Heise, R., Müller, V., and Gottschalk, G. (1989). Sodium dependence of acetate formation by the acetogenic bacterium *Acetobacterium woodii*. *J. Bacteriol.* 171, 5473–5478. doi: 10.1128/jb.171.10.5473-5478.1989

Hess, V., Poehlein, A., Weghoff, M. C., Daniel, R., and Müller, V. (2014). A genome-guided analysis of energy conservation in the thermophilic, cytochrome-free acetogenic bacterium *Thermoanaerobacter kivui*. *BMC Genomics* 15:1139. doi: 10.1186/1471-2164-15-1139

Jain, S., Dietrich, H. M., Müller, V., and Basen, M. (2020). Formate Is required for growth of the thermophilic acetogenic bacterium *Thermoanaerobacter kivui* lacking hydrogen-dependent carbon dioxide reductase (HDCR). *Front. Microbiol.* 11:59. doi: 10.3389/fmicb.2020.00059

Kellum, R., and Drake, H. L. (1984). Effects of cultivation gas phase on hydrogenase of the acetogen *Clostridium thermoaceticum*. *J. Bacteriol.* 160, 466–469. doi: 10.1128/jb.160.1.466-469.1984

Leigh, J. A., Mayer, F., and Wolfe, R. S. (1981). *Acetogenium kivui*, a new thermophilic hydrogen-oxidizing, acetogenic bacterium. *Arch. Microbiol.* 129, 275–280. doi: 10.1007/bf00414697

Misoph, M., and Drake, H. L. (1996). Effect of CO2 on the fermentation capacities of the acetogen *Peptostreptococcus productus* U-1. *J. Bacteriol.* 178:3140. doi: 10.1128/jb.178.11.3140-3145.1996

Moon, J., Henke, L., Merz, N., and Basen, M. (2019). A thermostable mannitol-1-phosphate dehydrogenase is required in mannitol metabolism of the thermophilic acetogenic bacterium *Thermoanaerobacter kivui*. *Environ. Microbiol.* 21, 3728–3736. doi: 10.1111/1462-2920.14720

Schink, B., and Stams, A. (2006). "Syntrophism among prokaryotes," in *The Prokaryotes - A handbook on the biology of bacteria*, 3rd Edn, eds M. Dworkin, S. Falkow, E. Rosenberg, K. H. Schleifer, and E. Stackebrandt (Berlin: Springer Science+Business Media, LLC), 309–336. doi: 10.1007/0-387-30742-7_11

Schmidt, K., Jensen, S. L., and Schlegel, H. (1963). Die Carotinoide der *Thiorhodaceae*. *Arch. Mikrobiol.* 46, 117–126. doi: 10.1007/bf00408204

Schröder, C., Selig, M., and Schönheit, P. (1994). Glucose fermentation to acetate, CO2 and H2 in the anaerobic hyperthermophilic eubacterium *Thermotoga maritima*: involvement of the Embden-Meyerhof pathway. *Arch. Microbiol.* 161, 460–470. doi: 10.1007/bf00307766

Schuchmann, K., and Müller, V. (2013). Direct and reversible hydrogenation of CO2 to formate by a bacterial carbon dioxide reductase. *Science* 342, 1382–1385. doi: 10.1126/science.1244758

Schuchmann, K., and Müller, V. (2014). Autotrophy at the thermodynamic limit of life: a model for energy conservation in acetogenic bacteria. *Nat. Rev. Microbiol.* 12, 809–821. doi: 10.1038/nrmicro3365

Schuchmann, K., and Müller, V. (2016). Energetics and application of heterotrophy in acetogenic bacteria. *Appl. Environ. Microbiol.* 82, 4056–4069. doi: 10.1128/aem.00882-16

Schut, G. J., and Adams, M. W. W. (2009). The iron-hydrogenase of *Thermotoga maritima* utilizes ferredoxin and NADH synergistically: a new perspective on anaerobic hydrogen production. *J. Bacteriol.* 191, 4451–4457. doi: 10.1128/jb.01582-08

Schut, G. J., Zadvornyy, O., Wu, C.-H., Peters, J. W., Boyd, E. S., and Adams, M. W. W. (2016). The role of geochemistry and energetics in the evolution of modern respiratory complexes from a proton-reducing ancestor. *Biochim.Biophys. Acta Bioenerg.* 1857, 958–970. doi: 10.1016/j.bbabio.2016.01.010

Tschech, A., and Pfennig, N. (1984). Growth yield increase linked to caffeate reduction in *Acetobacterium woodii*. *Arch. Microbiol.* 137, 163–167. doi: 10.1007/bf00414460

Verbeke, T. J., Zhang, X., Henrissat, B., Spicer, V., Rydzak, T., Krokhin, O. V., et al. (2013). Genomic evaluation of *Thermoanaerobacter* spp. for the construction of designer co-cultures to improve lignocellulosic biofuel production. *PLoS One* 8:e59362. doi: 10.1371/journal.pone.0059362

Wang, S. N., Huang, H. Y., Kahnt, J., and Thauer, R. K. (2013). A reversible electron-bifurcating ferredoxin- and NAD-dependent [FeFe]-hydrogenase (HydABC) in *Moorella thermoacetica*. *J. Bacteriol.* 195, 1267–1275. doi: 10.1128/jb.02158-12

Weghoff, M. C., and Müller, V. (2016). CO metabolism in the thermophilic acetogen *Thermoanaerobacter kivui*. *Appl. Environ. Microbiol.* 82, 2312–2319. doi: 10.1128/aem.00122-16

Weiss, M. C., Sousa, F. L., Mrnjavac, N., Neukirchen, S., Roettger, M., Nelson-Sathi, S., et al. (2016). The physiology and habitat of the last universal common ancestor. *Nat. Microbiol.* 1, 16116.

Westphal, L., Wiechmann, A., Baker, J., Minton, N. P., and Müller, V. (2018). The Rnf complex Is an energy-coupled transhydrogenase essential to reversibly Link cellular NADH and ferredoxin pools in the acetogen *Acetobacterium woodii*. *J. Bacteriol.* 200:e00357-18.

Wiechmann, A., Ciurus, S., Oswald, F., Seiler, V. N., and Müller, V. (2020). It does not always take two to tango: "Syntrophy" via hydrogen cycling in one bacterial cell. *ISME J.* 14, 1561–1570. doi: 10.1038/s41396-020-0627-1

Wood, H. G., Ragsdale, S. W., and Pezacka, E. (1986). The acetyl-CoA pathway of autotrophic growth. *FEMS Microbiol. Lett.* 39, 345–362. doi: 10.1111/j.1574-6968.1986.tb01865.x

Zheng, Y. N., Kahnt, J., Kwon, I. H., Mackie, R. I., and Thauer, R. K. (2014). Hydrogen formation and its regulation in *Ruminococcus albus*: Involvement of an electron-bifurcating [FeFe]-hydrogenase, of a non-electron-bifurcating [FeFe]-hydrogenase, and of a putative hydrogen-sensing [FeFe]-hydrogenase. *J. Bacteriol.* 196, 3840–3852. doi: 10.1128/jb.02070-14

Conflict of Interest: The authors declare that the research was conducted in the absence of any commercial or financial relationships that could be construed as a potential conflict of interest.

frontiers in Microbiology

ORIGINAL RESEARCH
published: 03 February 2021
doi: 10.3389/fmicb.2020.635786

Metabolic Potential for Reductive Acetogenesis and a Novel Energy-Converting [NiFe] Hydrogenase in *Bathyarchaeia* From Termite Guts – A Genome-Centric Analysis

Hui Qi Loh†, *Vincent Hervé*† *and Andreas Brune**†

Research Group Insect Microbiology and Symbiosis, Max Planck Institute for Terrestrial Microbiology, Marburg, Germany

OPEN ACCESS

Edited by:
Mirko Basen,
Universität Rostock, Germany

Reviewed by:
Michael W. Adams,
University of Georgia, United States
Volker Müller,
Goethe University Frankfurt, Germany

***Correspondence:**
Andreas Brune
brune@mpi-marburg.mpg.de

†ORCID:
Hui Qi Loh
0000-0002-4613-2477
Vincent Hervé
0000-0002-3495-561X
Andreas Brune
0000-0002-2667-4391

Specialty section:
This article was submitted to Microbial Physiology and Metabolism, a section of the journal Frontiers in Microbiology

Received: *30 November 2020*
Accepted: *31 December 2020*
Published: *03 February 2021*

Citation:
Loh HQ, Hervé V and Brune A (2021) Metabolic Potential for Reductive Acetogenesis and a Novel Energy-Converting [NiFe] Hydrogenase in Bathyarchaeia From Termite Guts – A Genome-Centric Analysis. Front. Microbiol. 11:635786. doi: 10.3389/fmicb.2020.635786

Symbiotic digestion of lignocellulose in the hindgut of higher termites is mediated by a diverse assemblage of bacteria and archaea. During a large-scale metagenomic study, we reconstructed 15 metagenome-assembled genomes of *Bathyarchaeia* that represent two distinct lineages in subgroup 6 (formerly MCG-6) unique to termite guts. One lineage (TB2; *Candidatus* Termitimicrobium) encodes all enzymes required for reductive acetogenesis from CO_2 via an archaeal variant of the Wood–Ljungdahl pathway, involving tetrahydromethanopterin as C_1 carrier and an (ADP-forming) acetyl-CoA synthase. This includes a novel 11-subunit hydrogenase, which possesses the genomic architecture of the respiratory Fpo-complex of other archaea but whose catalytic subunit is phylogenetically related to and shares the conserved [NiFe] cofactor-binding motif with [NiFe] hydrogenases of subgroup 4 g. We propose that this novel Fpo-like hydrogenase provides part of the reduced ferredoxin required for CO_2 reduction and is driven by the electrochemical membrane potential generated from the ATP conserved by substrate-level phosphorylation; the other part may require the oxidation of organic electron donors, which would make members of TB2 mixotrophic acetogens. Members of the other lineage (TB1; *Candidatus* Termiticorpusculum) are definitely organotrophic because they consistently lack hydrogenases and/or methylene-tetrahydromethanopterin reductase, a key enzyme of the archaeal Wood–Ljungdahl pathway. Both lineages have the genomic capacity to reduce ferredoxin by oxidizing amino acids and might conduct methylotrophic acetogenesis using unidentified methylated compound(s). Our results indicate that *Bathyarchaeia* of subgroup 6 contribute to acetate formation in the guts of higher termites and substantiate the genomic evidence for reductive acetogenesis from organic substrates, possibly including methylated compounds, in other uncultured representatives of the phylum.

Keywords: *Bathyarchaeota*, Wood-Ljungdahl pathway, termites, gut microbiota, comparative genomics, metagenome-assembled genomes, acetogens

INTRODUCTION

Although *Bathyarchaeia* are widespread in anoxic environments, their physiology is only poorly understood. In the absence of any isolates and with only a few microscopic observations of their cells (Collins et al., 2005; Kubo et al., 2012), our knowledge about this deep-branching lineage is based almost exclusively on amplicon libraries of archaeal 16S rRNA genes and metagenomic studies (reviewed by Zhou et al., 2018).

Ribosomal RNA genes affiliated with the Miscellaneous Crenarchaeotal Group (MCG) had already been recovered in early analyses of archaeal diversity in diverse anoxic habitats (e.g., Schleper et al., 1997; Inagaki et al., 2003; Ochsenreiter et al., 2003), including the intestinal tract of termites (Friedrich et al., 2001). Meanwhile, an enormous diversity of sequences from this group, which comprises numerous deep-branching lineages, has been recovered from a wide range of marine and freshwater habitats and terrestrial environments (e.g., Kubo et al., 2012; Fillol et al., 2016). A few years ago, the MCG was elevated to the phylum level (*Bathyarchaeota*; Meng et al., 2014), but the most recent genome-based taxonomy demoted them again to the class level (*Bathyarchaeia*; Rinke et al., 2020). While the rank of the taxon is not relevant in the current context, we maintained the subgroup numbering used in previous studies (e.g., Kubo et al., 2012; Lazar et al., 2016) but replaced the prefix "MCG–" with the prefix "Bathy–" (Yu T. et al., 2018).

The abundance of *Bathyarchaeia* in many anoxic habitats implies potentially important roles in biogeochemical cycles (Evans et al., 2015; He et al., 2016). Reconstruction of metagenome-assembled genomes (MAGs) provided information concerning the metabolic capacities of *Bathyarchaeia* and inspired predictions of their putative roles in anoxic sediments (reviewed by Zhou et al., 2018). Several studies suggested that *Bathyarchaeia* are organotrophic and utilize a variety of organic substrates (e.g., Meng et al., 2014; He et al., 2016; Lazar et al., 2016). The discovery of genes encoding a methyl-coenzyme M reductase (Mcr) complex and a complete Wood–Ljungdahl pathway in bathyarchaeon BA1 provided the first evidence of methanogenesis outside the Euryarchaeota (Evans et al., 2015). Other studies detected key enzymes of the pathway in bathyarchaeal genomes of several subgroups and proposed that these lineages are involved in reductive acetogenesis from CO_2 (He et al., 2016; Lazar et al., 2016).

Considering the putative roles of *Bathyarchaeia* in methanogenesis and reductive acetogenesis and the evidence for the utilization of lignin-derived methoxy groups (Yu T. et al., 2018), the presence of this group in termite guts is intriguing. Termites efficiently digest wood and other lignocellulosic substrates, either sound or in different stages of humification (Brune, 2014), in symbiosis with a specialized gut microbiota housed in their enlarged hindgut compartments (Brune and Dietrich, 2015). Hydrogen produced in microbial fermentation processes serves as an electron donor for the reduction of CO_2, yielding acetate and methane as major products (Breznak and Switzer, 1986; Brauman et al., 1992). Methanogenesis in termite guts involves a diverse assemblage of hydrogenotrophic and methyl-reducing archaea (Brune, 2018), but reductive acetogenesis, which can contribute up to two-thirds of total acetate production, has so far been considered a bacterial activity.

In lower termites, reductive acetogenesis has been attributed to acetogenic members of the phylum *Spirochaetes*) (e.g., Leadbetter et al., 1999; Ohkuma et al., 2015) and a novel lineage of uncultured *Deltaproteobacteria* (Rosenthal et al., 2013; Ikeda-Ohtsubo et al., 2016). In higher termites (family Termitidae), which diverged from the lower termites about 50 million years ago (Bucek et al., 2019), the situation is more complex. Particularly in the humus-feeding and soil-feeding groups, where the potential rates of reductive acetogenesis decrease in favor of methanogenesis (Brauman et al., 1992; Tholen and Brune, 1999), spirochetes are less abundant than in wood-feeding groups (Mikaelyan et al., 2016). A study based on the formyltetrahydrofolate synthetase (FTHFS) gene, a key enzyme of the Wood–Ljungdahl pathway that has been used as a marker for reductive acetogenesis, indicated that the community of potential acetogens shifts from spirochetes in lower termites to clostridia in higher termites (Ottesen and Leadbetter, 2011).

In a large-scale metagenomic study of the gut microbiota of eight higher termites, we obtained 15 MAGs assigned to *Bathyarchaeia* (Hervé et al., 2020). Preliminary analysis revealed that they fell into a cluster comprising mainly termite gut MAGs, with members of Bathy-1 and Bathy-6 as next relatives. Here, we conducted detailed phylogenomic analyses of these MAGs and investigated their potential capacity for methanogenesis and reductive acetogenesis using a genome-centric approach.

RESULTS AND DISCUSSION

Phylogeny of Termite Gut *Bathyarchaeia*

Bathyarchaeal MAGs were recovered from seven of the eight higher termites investigated, regardless of their feeding group (Hervé et al., 2020; **Table 1**). Their absence from *Microcerotermes parvus* is most likely caused by the low total number of MAGs obtained from the metagenomes of this species. Based on average nucleotide identity (ANI), the MAGs were assigned to nine phylotypes (**Table 1**). MAGs of the same phylotype were always derived from different gut compartments of the same host species, indicating that they most likely represent bathyarchaeal populations distributed along the entire hindgut. Eleven of the 15 MAGs fulfill the criteria for high-quality MAGs (>90% complete and <5% contamination; Bowers et al., 2017). Except for phylotype 5, each phylotype is represented by at least one high-quality MAG, which allows robust inference of metabolic potentials (Nelson et al., 2020).

Phylogenomic analysis placed all phylotypes from termite guts within subgroup Bathy-6, an apical lineage of *Bathyarchaeia* that is well represented mostly in 16S rRNA gene libraries (He et al., 2016) but comprises only a few MAGs from marine or estuarine sediments and the deep subsurface (**Figure 1**). The MAGs from termite guts form two distinct lineages, TB1 (phylotypes 1–7) and TB2 (phylotypes 8 and 9). TB2 is a sister group of bathyarchaeon SZUA-568 (hereafter denoted as Bathy-6-S), a MAG retrieved from marine hydrothermal vent sediments. Other MAGs in the radiation of Bathy-6 are

TABLE 1 | Characteristics of the MAGs of *Bathyarchaeia* from termite guts and other members of Bathy-6 included in the analyses.

Phylotype[a]	MAG[b]	Compartment	Relative abundance (%)[c]	Completeness (%)[d]	Contamination (%)[d]	Assembly size (bp)	Number of contigs	G+C content (mol%)	Coding density (%)	Predicted genes	Accession number[e]
1	Co191P1_bin46	P1	0.36	95.8	5.7	1762101	230	37.8	80.2	1772	WQRU00000000
	Co191P3_bin4	P3	0.09	99.1	4.2	1808297	159	37.8	79.6	1717	WQSY00000000
	Co191P4_bin18	P4	2.46	99.2	4.2	1994150	212	37.9	80.0	1899	WQTO00000000
2	Emb289P3_bin80	P3	0.13	96.3	6.3	2128005	163	39.0	82.5	2062	WQYG00000000
3	Lab288P3_bin115	P3	0.20	91.5	3.3	1167853	190	38.2	86.9	1242	WRCG00000000
	Lab288P4_bin25	P4	0.13	96.3	3.3	1375305	225	38.1	85.1	1455	WREZ00000000
4	Th196P4_bin19	P4	1.76	99.2	3.7	2287482	173	35.6	74. 9	2201	WRNB00000000
5	Cu122P1_bin20	P1	0.07	90.0	8.9	1504932	227	37.4	84.2	1628	WQTR00000000
6	Nc150P3_bin14	P3	0.02	63.8	2.3	656967	123	38.5	84.5	772	WRGI00000000
	Nc150P4_bin1	P4	0.28	98.1	4.7	1587817	173	38.9	82.6	1621	WRGM00000000
7	Nt197P4_bin22	P4	0.76	99.1	4.7	2179374	105	39.3	82.8	2153	WRJX00000000
8	Emb289P1_bin127	P1	0.08	99.1	1.9	2139595	140	43.4	82.9	2055	WQVG00000000
	Emb289P3_bin109	P3	0.23	96.3	2.8	2080780	121	43.4	83.1	2162	WQWQ00000000
9	Lab288P3_bin169	P3	1.20	98.6	2.8	2243011	107	43.3	83.3	2269	WRCX00000000
	Lab288P4_bin61	P4	0.52	99.1	3.7	2504117	128	43.0	83.2	2483	WRFL00000000
S	SZUA-568[f]	NA	NA	90.7	8.4	1641847	207	41.1	86.5	1810	QKIA00000000
B	Be326-BA-RLH[f]	NA	NA	89.8	3.7	2076091	227	44.9	86.1	2394	QYYE00000000
A	AD8-1[f]	NA	NA	95.8	4.2	1583813	83	32.4	84.5	1735	LFWW00000000

[a]*Average nucleotide identity (ANI) = 99%; for details, see* ***Supplementary Figure S1****.*

[b]*The first letters of the MAG names indicate the host species (Co, Cornitermes sp.; Emb, Embiratermes neotenicus; Lab, Labiotermes labralis; Th, Termes hospes; Cu, Cubitermes ugandensis; Nc, Nasutitermes corniger; Nt, Neocapritermes taracua).*

[c]*Relative abundance of the reads assigned to each MAG among the total number of reads in the corresponding metagenome (Hervé et al., 2020).*

[d]*Completeness and contamination were estimated with CheckM using 107 single-copy marker genes (Parks et al., 2015). For detailed results of the CheckM analysis, see* ***Supplementary Table S1****.*

[e]*For NCBI Nucleotide database; IMG genome IDs are given in* ***Supplementary Table S1****.*

[f]*Referred to as phylotypes Bathy-6-S (J. Pan and Z. Zhou, unpublished), Bathy-6-B (Harris et al., 2018), and Bathy-6-A (Lazar et al., 2016).*

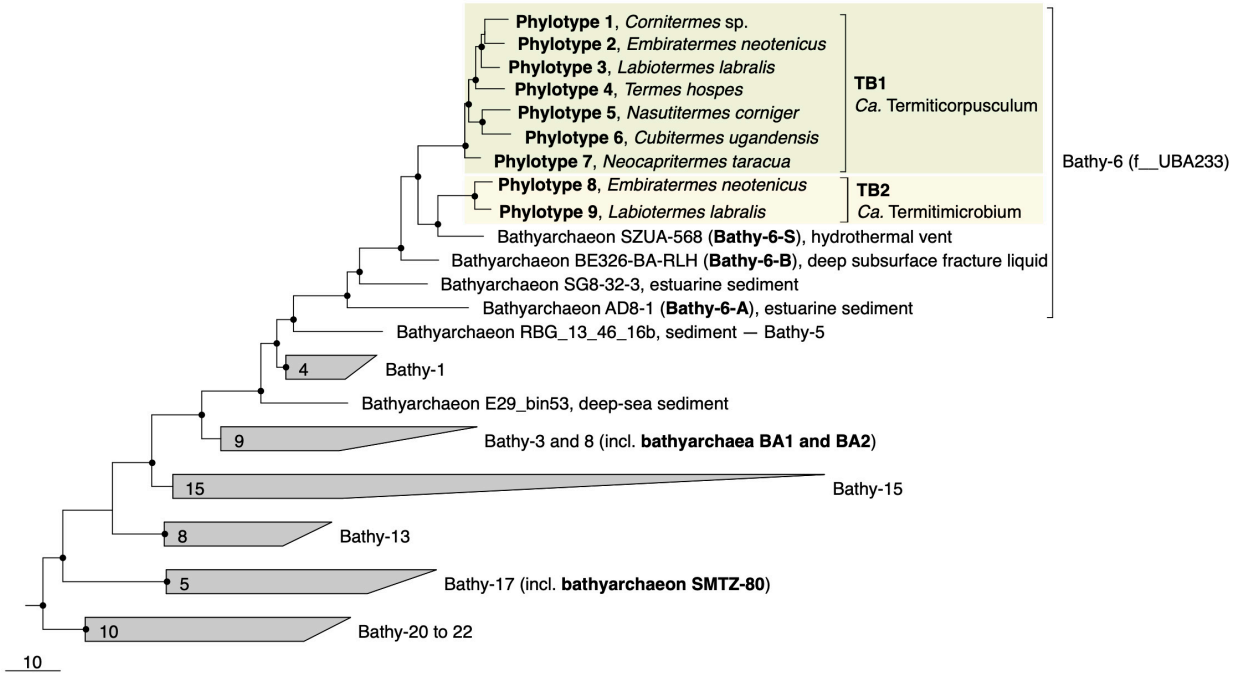

FIGURE 1 | Genome-based phylogeny of termite gut *Bathyarchaeia*, illustrating the relationship of lineages TB1 and TB2 to other MAGs in the Bathy-6 subgroup (f__UBA233 in the GTDB taxonomy). MAGs of other subgroups that are mentioned in the text are marked in bold. The maximum-likelihood tree was inferred from a concatenated alignment of 43 marker genes using the LG+F+I+G4 model and rooted with selected Crenarchaeota and Euryarchaeota as outgroup. A fully expanded tree with the accession numbers for all genomes is shown in the **Supplementary Material** (**Supplementary Figure S2**). The scale bar indicates 10-amino-acid 10% sequence divergence. Highly supported nodes (SH-aLRT, ● ≥ 95%, 1,000 replications) are indicated.

bathyarchaea BE326-BA-RLH (hereafter denoted as Bathy-6-B) and AD8-1 (hereafter denoted as Bathy-6-A). They are all high-quality MAGs and were included in the subsequent analyses (**Table 1**). Only bathyarchaeon SG8-32-3 (previously assigned to Bathy-1) was omitted because the completeness of the assembly (50.4%; based on our CheckM analysis) was too low for a reliable assessment of its metabolic capacity.

Predicted genome sizes (1.0–2.5 Mbp), G++C contents (37.4–43.4 mol%), and coding densities (74.9–86.9%) of the MAGs from termite guts are in the same range as those of the other representatives of this subgroup (**Table 1**). While the ANI values among the phylotypes of TB1 and TB2 range between 78.1 and 81.6%, the ANI values between members of TB1, TB2, and the other phylotypes of Bathy-6 are below the cutoff of the fastANI tool (<75%; **Supplementary Figure S1**), indicating that each lineage represents a separate genus-level taxon. This is confirmed by the results obtained with the Genome Taxonomy Database (GTDB) toolkit, which classified members of TB1 and TB2 as separate, genus-level lineages in the family UBA233 (order B26-1), a family that comprises also other members of Bathy-6. This indicates that TB1 and TB2 represent novel candidate genera in family UBA233, for which the names "*Candidatus* Termiticorpusculum" and "*Candidatus* Termitimicrobium" are proposed.

To identify the closest relatives of termite gut *Bathyarchaeia* and their respective habitats, we analyzed their phylogenetic position in the framework of rRNA genes available in public databases, which provides much better coverage than the small number of MAGs of the Bathy-6 subgroup available to date (**Figure 2**). The 16S rRNA gene sequences encoded by the MAGs form a well-supported monophyletic group with all other sequences of *Bathyarchaeia* that were previously obtained from the hindguts of higher termites (Friedrich et al., 2001; Shi et al., 2015; Grieco et al., 2019). Although each ribotype appears to be specific for a particular host species, the internal topology of the termite clade is not well resolved because of the large number of short sequences and the absence of 16S rRNA genes from many MAGs. The sequences in the termite clade are most closely related to clones obtained from a manure pit (EU662668; J. Ding, unpublished) and an anaerobic digestor fed with vinasses (U81774; Godon et al., 1997) and fall into the radiation of bathyarchaeal lineages in freshwater sediments, salt marshes, and anaerobic wastewater bioreactors (group 1.3 b; Ochsenreiter et al., 2003; Collins et al., 2005).

Capacity for CO_2-Reductive Acetogenesis

We investigated the presence of all genes required for methanogenesis and reductive acetogenesis in all members of Bathy-6 with sufficiently complete genomes (**Figure 3**). All members of TB2 (phylotypes 8 and 9) encode the complete set of genes required for the reduction of CO_2 to acetyl-CoA via the archaeal version of the Wood–Ljungdahl pathway, using

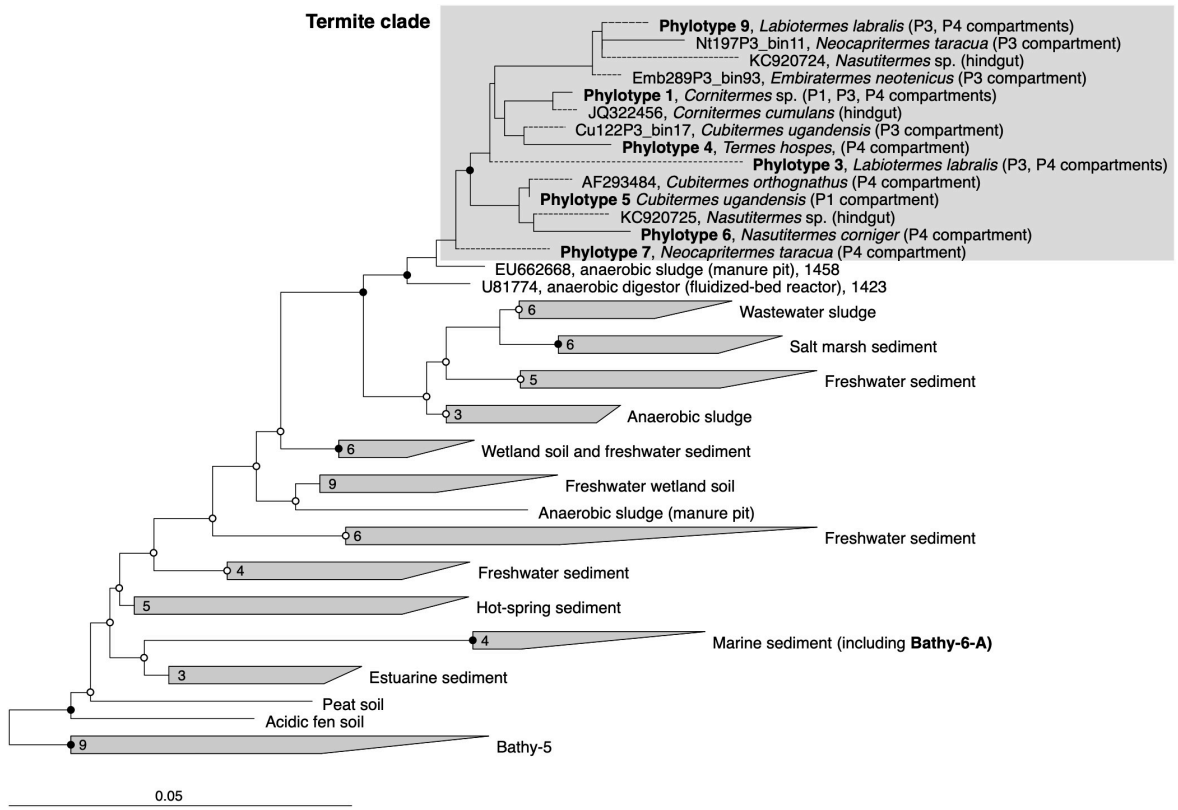

FIGURE 2 | 16S rRNA-based phylogeny of subgroup Bathy-6, indicating the placement of the termite clade among *Bathyarchaeia* from other environments. The maximum-likelihood tree is based on a curated alignment (1,424 positions) of all sequences in the SILVA database and their homologs retrieved from the bathyarchaeal MAGs and the low-quality bins obtained from the termite gut metagenomes (Hervé et al., 2020). The tree was rooted with members of Bathy-5 as outgroup. The scale bars indicate 0.05 nucleotide substitutions per site. SH-aLRT values (● ≥ 95%; ○ ≥ 80%, 1,000 replications) indicate node support. Branches marked with dashed lines indicate shorter sequences that were added using the parsimony tool. A fully expanded tree with the accession numbers of all sequences is shown in the **Supplementary Material** (**Supplementary Figure S3**).

methanofuran (MFR) and tetrahydromethanopterin (H_4MPT) as C_1 carriers (**Figure 4**). Formyl-MFR dehydrogenase is molybdenum-dependent (FmdABCDF; Hochheimer et al., 1996) and not the tungsten-dependent paralog. A homolog of *fmdE*, which occurs in methanogens, was not found in any of the MAGs, which suggests that the absence of subunit E is a characteristic feature of the bathyarchaeal complex. It has been shown that the Fmd complexes of *Methanobacterium thermoautotrophicum* and *Methanosarcina barkeri* are active also without this subunit (Hochheimer et al., 1996; Vorholt et al., 1996). Methylene-H_4MPT dehydrogenase (Mtd) is more closely related to the NADH-dependent homolog of methylotrophic bacteria than to the $F_{420}H_2$-dependent homolog of methanogens. The CO dehydrogenase/acetyl-CoA synthase complex (CdhABCDE) and the (ADP-forming) acetyl-CoA synthetase (Acd; Musfeldt et al., 1999) are typical archaeal enzymes.

Enzymes characteristic for the bacterial Wood–Ljungdahl pathway (FTHFS, methylene-THF cyclohydrolase/dehydrogenase, and methylene-THF reductase), which had been identified in MAGs of Bathy-3, -8, and -17 (Evans et al., 2015; Zhou et al., 2018), were not encoded by any member of Bathy-6. Also, phosphate acetyltransferase and acetate kinase, which are responsible for substrate-level phosphorylation (SLP) in both fermenting and acetogenic bacteria, were absent from all MAGs (**Figure 4**).

The same gene sets as in TB2 are also encoded by the more basal Bathy-6-S and Bathy-6-B (**Figure 3**), which indicates that the capacity to produce acetate from CO_2 might be a plesiomorphic trait of the Bathy-6 subgroup. The consistent absence of a key enzyme of the archaeal Wood–Ljungdahl pathway, methylene-H_4MPT reductase (Mer), from all seven phylotypes (11 MAGs) of the TB1 lineage and from the most basal member of the subgroup, Bathy-6-A, suggests that the capacity to reduce CO_2 to the methyl level was lost at least twice during the evolutionary radiation of Bathy-6.

Homologs of the methyl-coenzyme M reductase (Mcr) complex, which encodes the key enzyme of methanogenesis, were not detected in any of the MAGs (**Figure 4**). Our observation contrasts with the report of Harris et al. (2018), who claimed that Bathy-6-B might represent an anaerobic methane oxidizer. However, their conclusion is based on the recovery of a 265-bp gene fragment classified as an *mcrA* gene in the original metagenome from which Bathy-6-B was assembled, i.e., not from the metagenomic bin. Considering also that the gene fragment

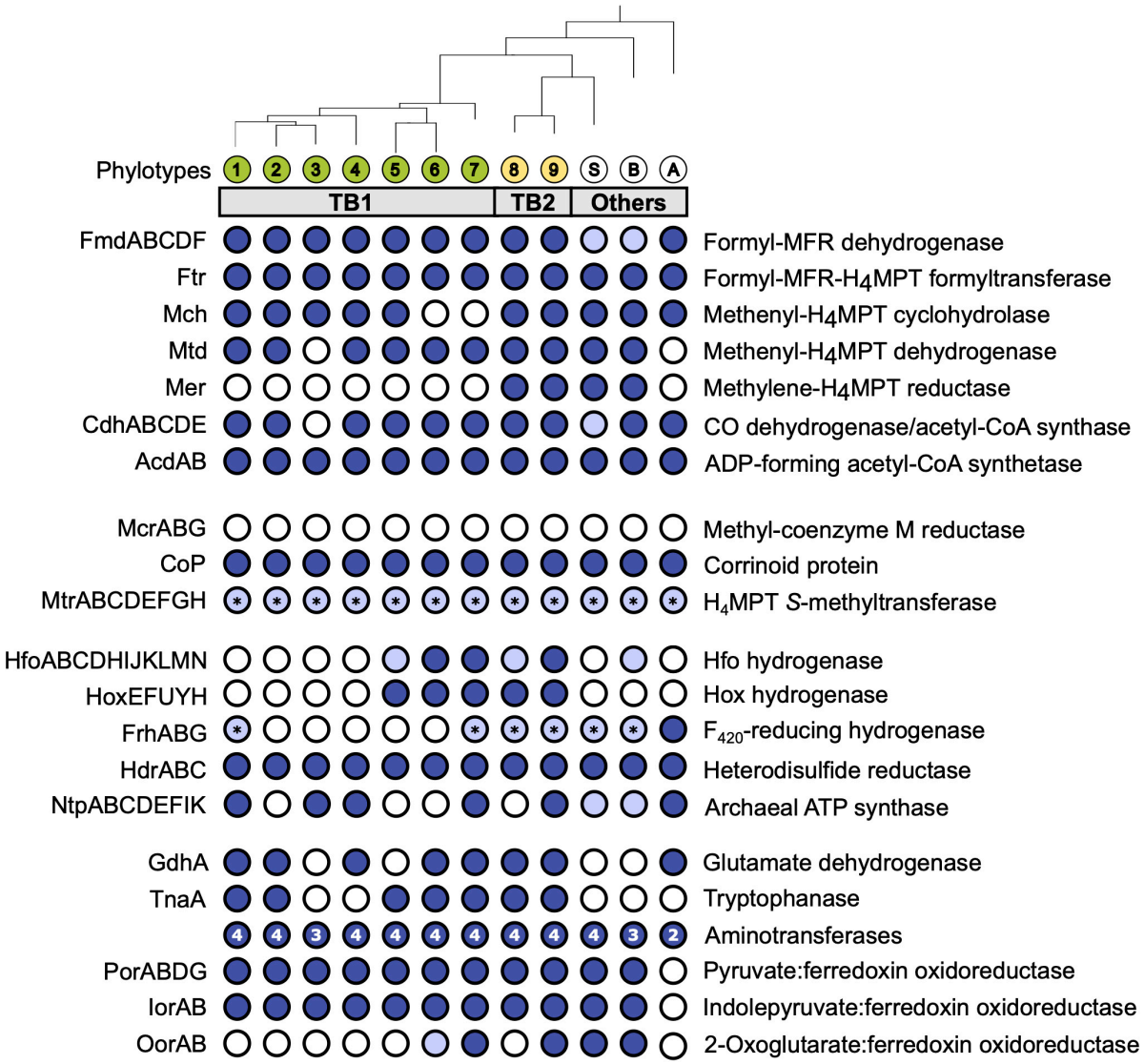

FIGURE 3 | Gene functions encoded by termite gut bathyarchaea (TB1 and TB2) and other representatives of the Bathy-6 subgroup. All phylotypes with sufficiently complete genomes were included; their phylogenetic relationship was taken from **Figure 1** (for strain designations, see **Table 1**). Colored circles indicate presence, and open circles indicate absence of the respective function; light blue indicates that a gene set is incomplete. The asterisks (*) in MtrABCDEFGH and FrhABG indicate that only MtrH or FrhB, respectively, is present. The number of aminotransferases encoded by each phylotype is indicated in the circle. If a phylotype is represented by more than one MAG, the annotation results were combined; details can be found in the **Supplementary Material** (**Supplementary Table S2**). H_4MPT, tetrahydromethanopterin; MFR, methanofuran; Fpo, F_{420}:methanophenazine oxidoreductase.

in question shows the highest similarity to a homolog from an uncultured euryarchaeal methanogen (GenBank: JX907770.1), it seems safe to conclude that members of the Bathy-6 subgroup are not methanogenic.

Although the capacity of *Bathyarchaeia* for reductive acetogenesis from CO_2 has been claimed repeatedly for several subgroups (He et al., 2016; Lazar et al., 2016; Yu T. et al., 2018; Zhou et al., 2018), the evidence was never fully conclusive. Actually, the comprehensive survey of all bathyarchaeal MAGs compiled by Zhou et al. (2018) lists only two MAGs that encode all genes required to operate the entire Wood–Ljungdahl pathway. One is the putatively methanogenic BA1 (Bathy-8) from a deep aquifer (Evans et al., 2015); the other is bathyarchaeon ex4484_135 (Bathy-15) from marine hydrothermal sediment (Dombrowski et al., 2017).

Capacity for Methylotrophic Acetogenesis

As all members of Bathy-6 encode a complete CO dehydrogenase/acetyl-CoA synthase (Cdh) complex (**Figure 3**), they might still synthesize acetyl-CoA using methyl groups derived from external sources. In all acetogenic bacteria and methylotrophic methanogens studied to date, the

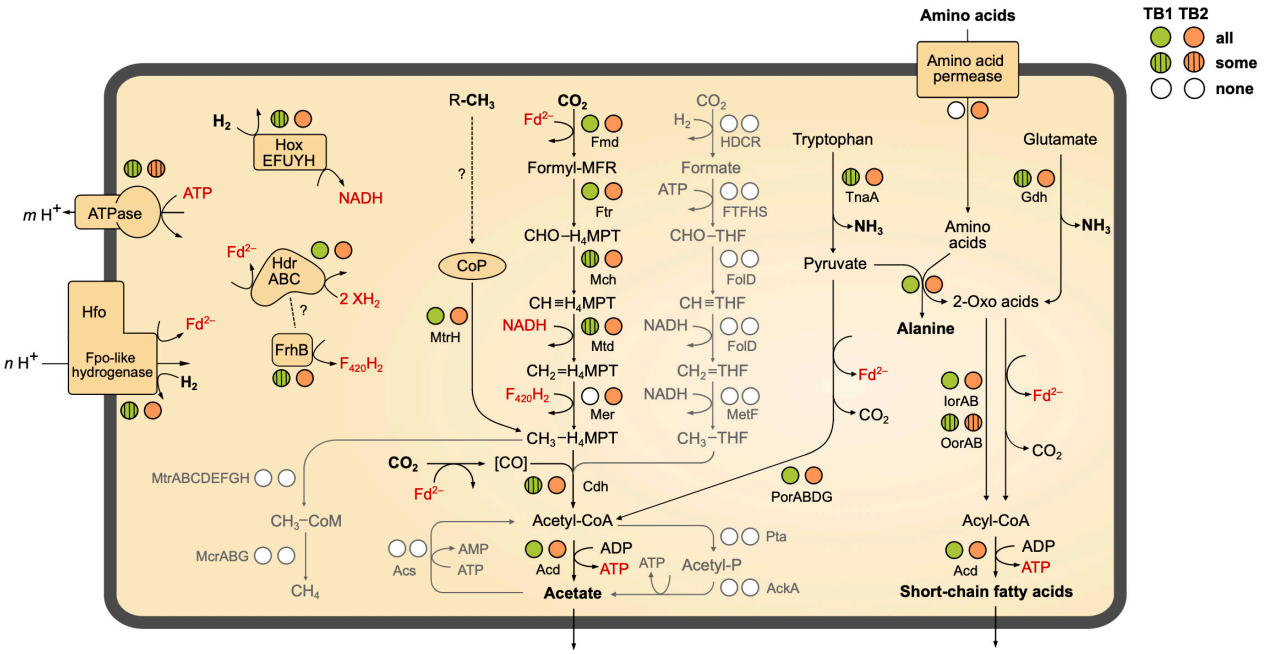

FIGURE 4 | Catabolic pathways encoded by the MAGs of termite gut *Bathyarchaeia*. The circles next to each enzyme indicate the presence of the coding genes in all, some, or none of the phylotypes of TB1 and TB2 (more details in **Figure 3**). Gray shading indicates pathways that are absent from all MAGs. The directionality of Fpo-like hydrogenase (Hfo) and ATP (synth)ase is discussed in the text. Dashed lines with question marks indicate hypothetical interactions. MFR, methanofuran; H_4MPT, tetrahydromethanopterin (archaeal pathway); THF, tetrahydrofolate (bacterial pathway). A detailed list of genes present/absent in the respective MAGs is provided as **Supplementary Material** (**Supplementary Table S2**).

methyltransferase systems consist of three components: (i) a set of substrate-specific methyltransferases (MT-I), (ii) their cognate methyl-accepting corrinoid proteins (CoP), and (iii) a second methyltransferase (MT-II) that transfers the methyl group of methyl-CoPs to THF (bacteria) or coenzyme M (archaea) (van der Meijden et al., 1983; Kreft and Schink, 1994; Kremp and Müller, 2020; **Supplementary Figure S4A**). We found that all MAGs of Bathy-6 encode CoPs that fall into the radiation of homologs assigned to other uncultured Archaea, with the CoPs of the di- and trimethylamine-specific methyltransferase systems (MtbC and MttC) of *Methanomassiliicoccus luminyensis* (Kröninger et al., 2017) and *Acetobacterium woodii* (Kremp et al., 2018) as closest relatives with a reliable functional annotation (**Supplementary Figure S4**). However, unlike the situation in methylotrophic bacteria and euryarchaea, where the CoP gene is colocalized with the gene of the cognate substrate-specific MT-I homologs (MtbB or MttB), the CoP gene of Bathy-6 is flanked by a gene encoding subunit H of tetrahydromethanopterin *S*-methyltransferase (MtrH; **Supplementary Figure S4B**).

In many methanogenic archaea, MtrH is part of the energy-conserving MtrABCDEFGH complex and catalyzes the transfer of the (CO_2-derived) methyl group from methyl-tetrahydromethanopterin to the corrinoid prosthetic group of MtrA (Hippler and Thauer, 1999). However, in obligately methyl-reducing methanogens (Galagan et al., 2002; Borrel et al., 2014; Lang et al., 2015), which methylate CoM via their diverse methyltransferase systems (see above), the Mtr complex is absent. The presence of an isolated *mtrH* gene co-localized with a CoP gene has also been observed in the putatively methanogenic BA1 and BA2 (*Bathyarchaeia*) and several MAGs related to "*Ca.* Methanomethylicus mesodigestum" (*Thermoproteota*). It was proposed that the encoded proteins represent methyltransferase systems, which prompted the hypothesis that these uncultured lineages are methylotrophic methanogens (Evans et al., 2015; Vanwonterghem et al., 2016).

It is tempting to assume that also the CoP–MtrH couple of Bathy-6 is involved in the transfer of methyl groups from so far unidentified, substrate-specific methyltransferases to H_4MPT (**Figure 4**). However, a catabolic role of the CoP–MtrH couple is not the only possible interpretation. In "*Ca.* Methanomethylicus mesodigestum," the genes are co-localized with a homolog of *metE* encoding methionine synthase (**Supplementary Figure S4B**); it is also possible that the CoP–MtrH couple of Bathy-6 is involved in anabolic reactions that transfer methyl groups (provided by the cleavage of acetyl-CoA) from H_4MPT to an unknown acceptor.

Hydrogen as Electron Donor

The operation of the Wood–Ljungdahl pathway requires electron donors in the form of reduced ferredoxin, NADH, and, in the case of archaea, also reduced cofactor F_{420} ($F_{420}H_2$) (Thauer et al., 2008; Schuchmann and Müller, 2014). The reduction of ferredoxin with H_2 is a critical step because it is endergonic at low hydrogen partial pressures and requires either an energy-converting hydrogenase or a flavin-based electron bifurcation system (Schut and Adams, 2009; Schuchmann and Müller, 2012).

Hydrogenases are present only in TB2 and the basal lineages of TB1 (**Figure 3**). One is a cytosolic, bidirectional [NiFe] hydrogenase of subgroup 3d, which uses NAD as electron acceptor (Greening et al., 2016). Phylogenetic analysis of the gene encoding the large subunit (*hoxH*) placed all homologs in a sister position to the Hox hydrogenases of phototrophic bacteria (**Supplementary Figure S5**). The gene order in the *hoxEFUYH* cluster is the same as in the gene clusters of other Hox complexes, which encode a prototypical heterodimeric [NiFe]-hydrogenase moiety (HoxHY) and a diaphorase moiety (HoxEFU); HoxEFU is homologous to the NuoEFG module of complex I and mediates the electron transport to NAD(P) (Eckert et al., 2012). Although members of group 3 are called "bidirectional hydrogenases," hydrogen formation requires reduced ferredoxin or flavodoxin as electron donor (Gutekunst et al., 2014).

All MAGs that encode a Hox hydrogenase also possess a gene cluster that closely resembles those encoding the respiratory F_{420}:methanophenazine oxidoreductases (Fpo) of Euryarchaeota and the homologous NADH:quinone oxidoreductases (Nuo/Nqo) of bacteria (complex I) (**Figure 5**). As in other Fpo-like or Nuo-like complexes, the genes encoding the FpoFO and NuoEFG modules, which provide substrate specificity for $F_{420}H_2$ or NADH, respectively, are absent (Moparthi and Hägerhäll, 2011). However, six of the 11 subunits common to all Fpo and Nuo/Nqo complexes are also homologous to subunits of the energy-converting [NiFe] hydrogenases of group 4, underscoring their ancestral relationship to the respiratory complex I (Friedrich and Scheide, 2000; Schoelmerich and Müller, 2019).

Classification with HydDB placed the D subunit of the 11-subunit complex of the Bathy-6 MAGs among the catalytic subunits of [NiFe] hydrogenases in subgroup 4 g. The hydrogenases in subgroup 4 g are structurally heterogeneous and differ fundamentally both in the number of their subunits and the arrangement of their coding genes (Greening et al., 2016; Schoelmerich and Müller, 2019; **Figure 5**). Their large subunits form several distinct phylogenetic lineages (Subgroups 4g-1 to 4g-6; **Figure 6**), which indicates that they evolved independently from each other. The gene cluster encoding the Fpo-like hydrogenase complex of Bathy-6 (hereafter referred to as Hfo) has an organization almost identical to that of the corresponding clusters of *Ca.* Methanomethylicus mesodigestum (*Thermoproteota*) and *Pyrodictium delaney* (*Crenarchaeota*) (**Figure 5**), whose large subunits represent phylogenetic sister groups of subgroup 4g-6 (**Figure 6**). The coordination sites of the [NiFe] cofactor on the large subunit of all [NiFe] hydrogenases (L1 and L2 motifs; Vignais and Billoud, 2007), which are no longer conserved in NuoD and FpoD, are present in all Bathy-6 homologs (**Figure 7**).

The Hfo hydrogenase of *Bathyarchaeia* is most interesting from an evolutionary perspective, as it represents the first [NiFe] hydrogenase that is composed of the same 11 subunits and shares the same organization of the coding genes as the archaeal Fpo complex and the bacterial Nuo/Nqo complex (**Figure 5**). Both Hfo and the predicted Hfo-like complexes of *Pyrodictium delaneyi* and *Ca.* Methanomethylicus mesodigestum (subgroup 4g-6) lack the Na^+ transport module of the membrane-bound hydrogenase (Mbh) complex of *Pyrococcus furiosus* (subgroup 4d), whose similarity to the respiratory complex I (Nqo) of *Thermus thermophilus* has been well documented (Yu H. et al., 2018). Notably, the Na^+ transport module (MbhABCF) in the Mbh of *P. furiosus* is also present in the gene cluster encoding the [NiFe] hydrogenase of *Thermosphaera aggregans* (subgroup 4g-5) and other members of *Desulfurococcales* (not shown), which encode all subunits of the Mbh complex of *P. furiosus*, albeit in a different gene order. The striking synteny between the gene clusters encoding the Hfo of *Bathyarchaeia* and the Fpo-like complex of *Methanomassiliicoccales*, including the absence of genes encoding the F_{420}-binding module (FpoFO), and the phylogeny of its large subunit suggest that the Hfo complex represent a closer evolutionary link between the energy-converting hydrogenases and the modern respiratory complexes than the Mbh of *Thermococci*.

None of the hydrogenases of subgroup 4 g have been biochemically characterized, but they are presumed to couple

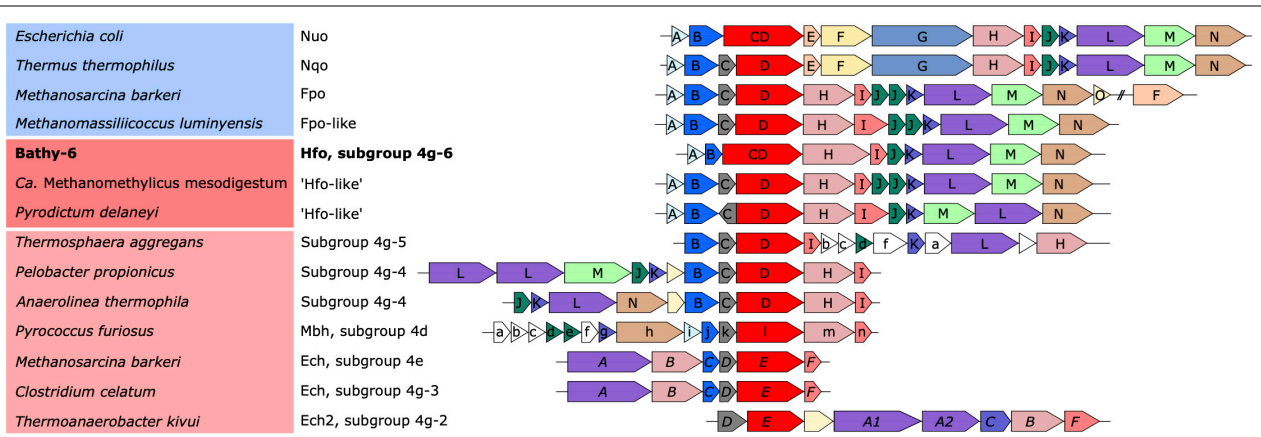

FIGURE 5 | Organization of the gene clusters encoding the respiratory complexes (blue background) and the ancestral [NiFe] hydrogenases in group 4 (red background). Identical colors indicate homologous genes; a phylogenetic analysis of the catalytic subunit of [NiFe] hydrogenases and its homologs (red) is shown in **Figure 6**. The font style of the gene labels indicates differences in the subunit nomenclature of Nuo/Fpo (uppercase), Mbh (lowercase), and Ech (italics).

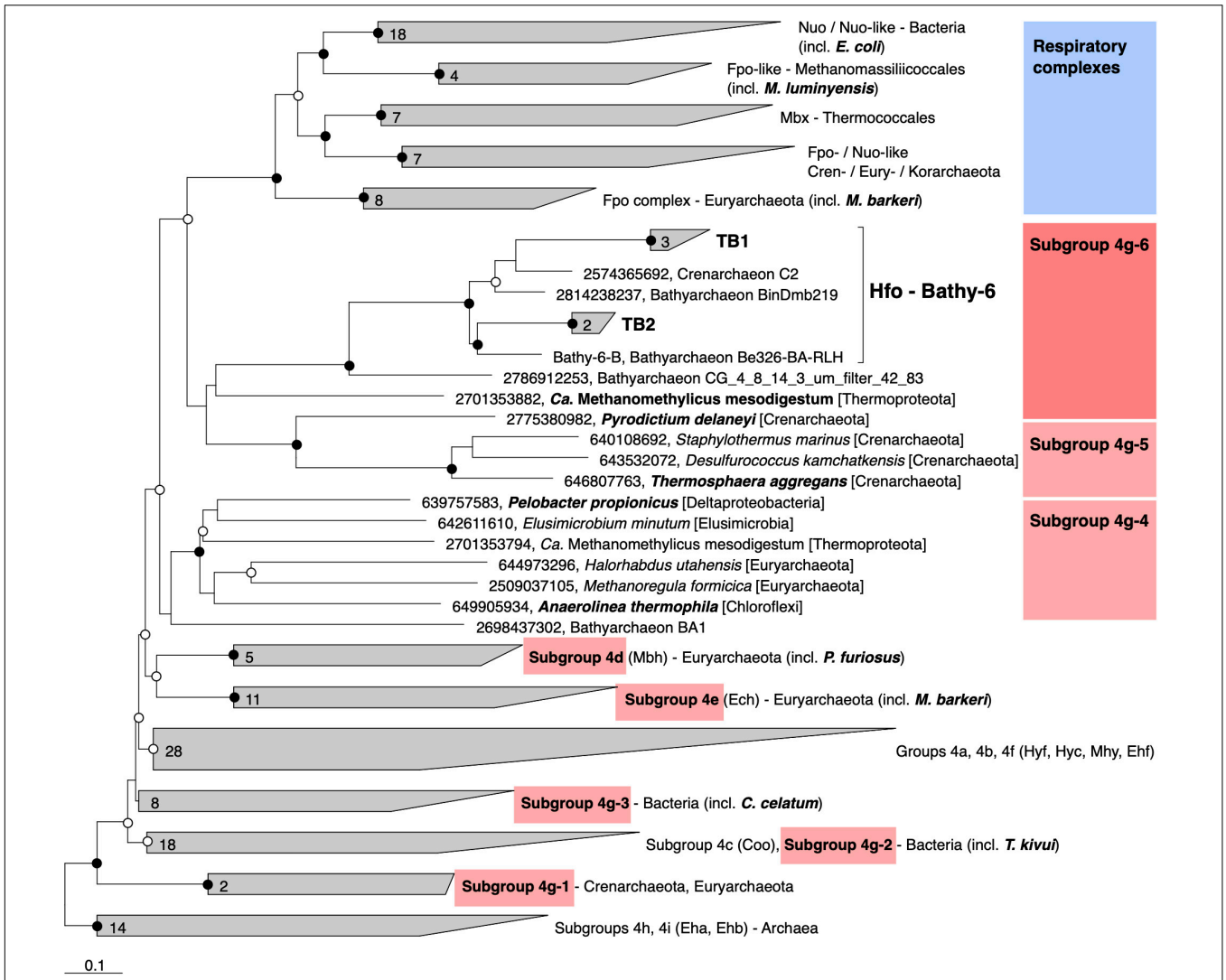

FIGURE 6 | Phylogeny of the catalytic subunit of selected group 4 [NiFe] hydrogenases and their homologs in the respiratory complexes. The maximum-likelihood tree is based on a curated alignment of the deduced amino acid sequences; the scale bar indicates 0.1-amino-acid substitutions per site. SH-aLRT values (• ≥ 95%; ∘ ≥ 80%, 1,000 replications) indicate node support. The genomic context of the highlighted genes is shown in **Figure 5**. Gene numbers indicate IMG/Mer gene IDs.

the formation of H_2 from reduced ferredoxin to the formation of an electrochemical membrane potential (Greening et al., 2016; Søndergaard et al., 2016; Schoelmerich and Müller, 2019). This is in agreement with biochemical data obtained for the Fpo-like 11-subunit complex of methanogenic *Euryarchaeota*, which generate an electrochemical membrane potential during electron transport from reduced ferredoxin to methanophenazine (*Methanosaeta*; Welte and Deppenmeier, 2011) or a so far unidentified electron acceptor (*Methanomassiliicoccales*; Kröninger et al., 2016). The absence of genes involved in the biosynthesis of methanophenazine from all MAGs of Bathy-6 (**Supplementary Table S2**) adds to the evidence that the Hfo of *Bathyarchaeia* is not a respiratory complex but is instead a novel energy-converting hydrogenase that catalyzes the reduction of ferredoxin with H_2 using the electrochemical membrane potential (**Figure 4**).

While Hox and Hfo hydrogenase should provide members of TB2 with the NADH and reduced ferredoxin required to operate the Wood–Ljungdahl pathway, the source of $F_{420}H_2$ as potential electron donor for methylene-H_4MPT reductase (Mer) remains unclear. All phylotypes encode enzymes involved in the biosynthesis of F_{420} (**Supplementary Table S2**), but a complete gene set encoding F_{420}-reducing [NiFe] hydrogenase (FrhABG, subgroup 3a; **Supplementary Figure S5**) is present only in Bathy-6-A. All members of TB2 and several phylotypes of TB1 encode a homolog of FrhB, an iron–sulfur flavoprotein with an F_{420}-binding site, but not the hydrogenase subunits (**Figure 3**). It is possible that FrhB is involved in the reduction of F_{420} via an interaction with HdrABC and an unknown electron donor, as proposed for the methane-oxidizing *Ca.* Methanoperedens spp. (Arshad et al., 2015).

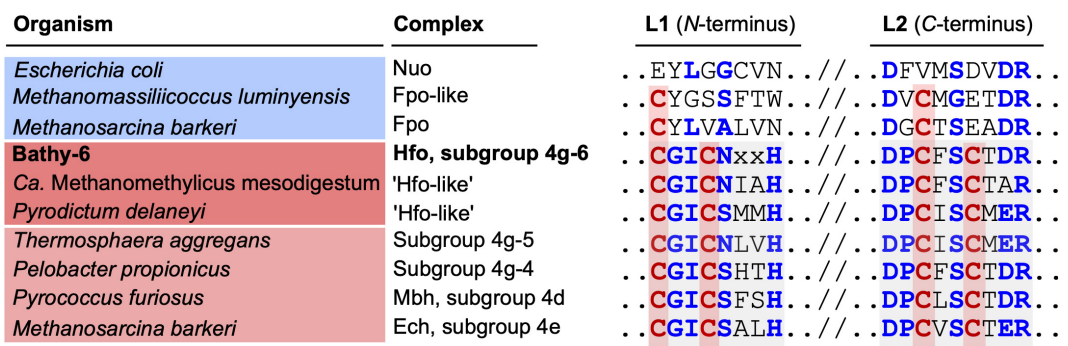

FIGURE 7 | Comparison of the [NiFe]-binding motifs (L1 and L2) in the large subunits of selected group 4 [NiFe] hydrogenases with the corresponding amino acid residues (IUPAC code) of their homologs in the Nuo and Fpo complexes. The shading indicates the typical motifs of [NiFe] hydrogenases (L1 motif: C[GS][ILV]C[AGNS]xxH; L2 motif: [DE][PL]Cx[AGST]Cx[DE][RL]; Vignais and Billoud, 2007). The four cysteine residues that coordinate the [NiFe] cluster are marked in red; other conserved residues are marked in blue.

The only member of subgroup Bathy-6 that encodes a complete FrhABG is Bathy-6-A. It is also the only MAG that encodes a methylviologen-dependent [NiFe] hydrogenase (MvhADG; **Supplementary Figure S5**, subgroup 3c), which forms an electron-bifurcating complex with the soluble heterodisulfide reductase (HdrABC) and catalyzes the hydrogen-dependent reduction of ferredoxin and the heterodisulfide of coenzyme M (CoM) and coenzyme B (CoB) in methanogens (Kaster et al., 2011). The presence of genes encoding HdrABC, MvhADG, and a complete Wood–Ljungdahl pathway in the putatively methanogenic BA1 (Bathy-3) provides strong evidence that BA1 is capable of hydrogenotrophic methanogenesis (Evans et al., 2015). In Bathy-6-A, however, the pathway is incomplete, and the identity of the heterodisulfide reduced by Hdr remains unclear. Interestingly, the same constellation as in Bathy-6 has been recently reported for the bathyarchaeal MAG CR_14 from marine sediments, which represents another, novel subgroup of *Bathyarchaeia* (Farag et al., 2020).

Organic Substances as Electron Donors

Most members of TB1 and all basal lineages of Bathy-6 lack Hox and Hfo (**Figure 3**), which means that they cannot grow lithotrophically with H_2 as electron donor. However, the reduced Fd required to operate reductive acetogenesis, either via the Wood–Ljungdahl pathway (TB2) or by methylotrophy (all phylotypes), could be provided also by the oxidation of organic substrates (**Figure 4**). Such organotrophic acetogenesis is common among bacteria with a homoacetogenic lifestyle (Drake, 1994; Schink, 1994). All Bathy-6 genomes (except Bathy-6-A) encode pyruvate:ferredoxin oxidoreductase (Por) and indolepyruvate:ferredoxin oxidoreductase (Ior), and some also encode 2-oxoglutarate:ferredoxin oxidoreductase (Oor), all of which catalyze the oxidative decarboxylation of 2-oxo acids to their corresponding acyl-CoA esters (**Figure 3**). The 2-oxo-acids would result from the transamination of amino acids via numerous aminotransferases encoded by all genomes; a putative amino acid permease, however, is encoded only in TB2. ATP would be formed via the ADP-dependent acetyl-CoA synthetase, which accepts also other acyl substrates in *P. furiosus* (Mai and Adams, 1996). Such pathways have been shown to operate in other archaea (*P. furiosus, Thermococcus* spp.; Kengen and Stams, 1993; Heider et al., 1996) and in the insect gut-associated bacterium *Elusimicrobium minutum* (Herlemann et al., 2009) during growth on glucose, where they result in a net formation of alanine.

The data compiled by Zhou et al. (2018) suggest that several lineages of *Bathyarchaeia*, including Bathy-6-A; Lazar et al., 2016), have the capacity to ferment various organic carbon compounds. However, genes encoding extracellular peptidases, which are numerous in other *Bathyarchaeia*, seem to be less prevalent in the MAGs of Bathy-6 and Bathy-1 (Feng et al., 2019), which suggests that members of these subgroups are limited to the utilization of amino acids or oligopeptides that are small enough to be transported across the cytoplasmic membrane.

There is no indication that members of Bathy-6 have the capacity to utilize sugars. Like Bathy-6-A (Lazar et al., 2016), all MAGs of TB1 and TB2 encode many genes of the classical Embden-Meyerhof-Parnas (EMP) pathway, including glyceraldehyde-3-phosphate dehydrogenase and phosphoglycerate kinase. However, all MAGs lack hexokinase and the alternative archaeal glycolytic enzymes (Bräsen et al., 2014), and most MAGs lack phosphofructokinase and pyruvate kinase. As all MAGs encode phosphoenolpyruvate synthetase and fructose bisphosphatase, it is likely that the EMP pathway functions only in gluconeogenesis. Sugar transporters were not detected; the role of the lipooligosaccharide ABC transporter encoded by almost all phylotypes from termite guts (except phylotype 9) is not clear (**Supplementary Table S2**). The identification of a cellulolytic system in Bathy-6-A (Lazar et al., 2016) requires verification.

Energy Conservation in TB2

In acetogenic bacteria growing on hydrogen and CO_2, all ATP synthesized by SLP is consumed in the activation of formate. Therefore, energy conservation involves electron-transport phosphorylation, which is driven by the oxidation of reduced ferredoxin via membrane-bound electron-transport complexes (Schuchmann and Müller, 2014; Basen and Müller, 2017). By

contrast, the activation of formate (i.e., the formation of formylmethanofuran) in the archaeal variant of the Wood–Ljungdahl pathway is not ATP-dependent but is instead driven by the reducing power of ferredoxin, yielding a full ATP per acetate produced via SLP. However, thermodynamics dictates that a fraction of this ATP must be reinvested, as a metabolism where the net ATP yield exceeds the free-energy change of the reaction would become endergonic (Thauer et al., 2008).

Fermenting bacteria that lack respiratory chains energize their membrane by operating their ATP synthase in the reverse direction (Buckel and Thauer, 2013). Likewise, members of Bathy-6 that possess a complete Wood–Ljungdahl pathway (i.e., the phylotypes in TB2) might use part of the ATP gained by SLP to generate an electrochemical membrane potential that drives the H_2-dependent reduction of ferredoxin via Hfo (see above). Other energy-converting complexes that would allow generation of reduced ferredoxin, such as the group-4 [NiFe] hydrogenases in acetogenic bacteria and methanogenic archaea (Ech, Künkel et al., 1998; Eha and Ehb, Tersteegen and Hedderich, 1999) or an NADH:Fd oxidoreductase complex (RnfABCDEG, Westphal et al., 2018), were not detected in any member of Bathy-6. If one assumes that the ATPase translocates 4 H^+ per ATP and Hfo translocates only 2 H^+ during electron transport from H_2 to ferredoxin (m = 4, n = 2 in **Figure 4**), production of 2 Fd^{2-} via Hfo would completely consume the energy conserved by SLP (1 ATP). Therefore, it is likely that members of TB2 grow mixotrophically, producing one Fd^{2-} from H_2 (via Hfo) and the other by the oxidation of pyruvate or other 2-oxo acids. An entirely lithotrophic pathway would be feasible if one Fd^{2-} is produced by Hfo and the other, together with $F_{420}H_2$, by flavin-based electron bifurcation (see above), but this would require an additional, unknown electron donor.

It is intriguing that several phylotypes of TB1 and TB2 (**Figure 3**) and also bathyarchaeal MAGs from other subgroups (Evans et al., 2015; Zhou et al., 2018) do not encode an ATP synthase (neither the genes for the archaeal V-type ATP synthase nor those for the bacterial equivalent were detected). While this observation is most likely explained by incomplete genome assemblies, it cannot be entirely excluded that these organisms generate their membrane potential (vital for any organism) by other means. In this case, the Hfo complex (if present) might operate in the reverse direction, using reduced ferredoxin provided by the oxidation of organic substrates to produce H_2 and generate an electrochemical membrane potential, like the energy-converting hydrogenases in fermenting bacteria.

In principle, the entire Wood–Ljungdahl pathway is reversible and can oxidize acetate to CO_2 given the appropriate thermodynamic framework. This has been demonstrated in syntrophic cultures of "Reversibacter"-like microorganisms with hydrogenotrophic partners (Lee and Zinder, 1988; Schnürer et al., 1997) and has been suggested to occur also in *Bathyarchaeia* (Evans et al., 2015; Xiang et al., 2017). However, at least in the termite hindgut, where the hydrogen partial pressure is much higher than in sediments (Ebert and Brune, 1997; Schmitt-Wagner and Brune, 1999) and reductive acetogenesis often prevails over methanogenesis as electron sink (Brauman et al., 1992; Tholen and Brune, 1999; Tholen and Brune, 2000), an anaerobic oxidation of acetate is an unlikely scenario.

Ecological Aspects

Although the proportion of archaeal rRNA in termite hindguts is relatively small (0.9–2.3% of all prokaryotic rRNA; Brauman et al., 2001), methanogenesis represents a substantial hydrogen sink (Brune, 2019). Considering that the proportion of reads assigned to bathyarchaeal MAGs in the hindgut metagenomes of higher termites (0.03–2.5%; avg. 0.69%) is four times higher than that assigned to euryarchaeal MAGs (0.02–0.79%; average, 0.16%; **Supplementary Table S2** in Hervé et al., 2020), the population sizes of *Bathyarchaeia* might be sufficient to contribute significantly to acetogenesis, particularly in soil-feeding species.

However, the substrates of termite gut *Bathyarchaeia* remain open to speculation. While only members of TB2 have the genomic capacity for lithotrophic acetogenesis, almost all members of Bathy-6 have the capacity to ferment amino acids and might employ organotrophic acetogenesis from methylated substrates as an electron sink. This would explain their prevalence in soil- and humus-feeding termites. It has been estimated that soil peptides and other nitrogen-rich humus constituents contribute substantially (20–40%) to the dietary carbon oxidized by soil-feeding *Cubitermes* spp. (Ngugi et al., 2011), which is consistent with the depletion of peptides in soil organic matter during gut transit (Griffiths et al., 2012) and the high ammonia concentrations (up to 130 mM) in the posterior hindgut (Ji and Brune, 2006). An NifDH homolog (pfam00142 and pfam001428) encoded by both TB1 and TB2 is most likely not involved in dinitrogen fixation but rather in a so far unidentified archaeal tetrapyrrole biosynthesis pathway (Ghebreamlak and Mansoorabadi, 2020).

Stable-isotope probing of salt marsh sediments indicated that members of Bathy-8 and Bathy-6 assimilate organic substrates, notably excluding proteins and inorganic carbon (Seyler et al., 2014). Yu T. et al. (2018), however, reported that the addition of lignin to an estuarine sediment sample selectively stimulated the growth of Bathy-8 and the incorporation of carbon from ^{13}C-bicarbonate into archaeal tetraether lipids, which suggests that members of Bathy-8 are methylotrophs that use lignin-derived methyl groups. Together with the potential capacity for methyl group utilization in many bathyarchaeotal MAGs (Seyler et al., 2014; Yu T. et al., 2018; this study), these results explain the observations of Lever et al. (2010), who found that porewater acetate in deep-subseafloor sediments was depleted in ^{13}C relative to sedimentary organic matter and postulated that a substantial fraction of the acetate produced in marine sediments might stem from reductive acetogenesis, fueled by microbial fermentation products, molecular hydrogen, and the methoxy groups of lignin monomers.

The utilization of the methoxy groups of lignin-derived aromatic compounds is a common trait of many acetogenic bacteria (Schink et al., 1992; Drake, 1994). Methoxylated aromatic compounds are demethylated by the hindgut microbiota of termites (Brune et al., 1995), but the organisms responsible for this activity have not been identified. It is

tempting to speculate that termite gut *Bathyarchaeia* are organotrophic (TB1) or mixotrophic (TB2) acetogens that utilize methylated compounds such as lignin derivatives as methyl group donors and reduce CO_2 either with molecular hydrogen and/or with reducing equivalents derived from the oxidation of organic substrates.

It has been speculated that acetogenic archaea might have an energetic advantage over acetogenic bacteria, as they do not have to invest ATP to activate formate (He et al., 2016). However, the net synthesis of ATP is limited by the free-energy change of an acetogenic metabolism, which is independent of its reaction path and requires part of the ATP gained by SLP to be reinvested (e.g., for ferredoxin reduction; see above). Rather, it is feasible that the capacity for methylotrophic acetogenesis, which is less sensitive to low hydrogen partial pressures than hydrogenotrophic acetogenesis, provides an energetic advantage, analogous to the situation in methyl-reducing methanogens (Feldewert et al., 2020). Moreover, it has been argued that long generation times contribute to the difficulties surrounding the enrichment and isolation of *Bathyarchaeia* in the laboratory (Yu H. et al., 2018). In view of the relatively short residence time of organic matter in termite guts (24–48 h; Kovoor, 1967; Bignell et al., 1980), the growth rates of termite gut *Bathyarchaeia* must be high enough to avoid washout – unless they are attached to the intestinal surface.

Taxonomy

Candidatus Termiticorpusculum

Etymology: L. n. *termes -itis*, a worm that eats wood, a termite; L. neut. n. *corpusculum*, a little body, a particle; N.L. neut. n. *Termiticorpusculum*, a little body associated with termites.

Uncultured. Unclassified genus-level lineage in the Bathy-6 subgroup of *Bathyarchaeia* (**Figure 1**; TB1 lineage). Comprises phylotypes 1–7 (**Table 1**).

Habitat: The hindgut of higher termites.

Candidatus Termitimicrobium

Etymology: L. n. *termes -itis*, a worm that eats wood, a termite; N.L. neut. n. *microbium*, microbe; from Gr. masc. adj. *mikros*, small; from Gr. masc. n. *bios*, life; N.L. neut. n. Termitimicrobium, small life(-form) associated with termites.

Uncultured. Unclassified genus-level lineage in the Bathy-6 subgroup of *Bathyarchaeia* (**Figure 1**; TB2 lineage). Comprises phylotypes 8–9 (**Table 1**).

Habitat: The hindgut of higher termites.

CONCLUSION

To date, the nonmethanogenic archaea in termite guts and their potential role in symbiotic digestion have received little attention. Our study provides strong evidence that termite gut *Bathyarchaeia* and other members of the Bathy-6 subgroup are archaeal acetogens; they possess the genomic potential to conserve energy by the production of acetyl-CoA from CO_2 (*Ca.* Termitimicrobium; TB2) and/or possibly methyl groups (almost all members of Bathy-6, including *Ca.* Termiticorpusculum; TB1). As in bacterial acetogens, their energy metabolism is likely mixotrophic or organotrophic. We identified a complete gene set encoding a novel Fpo-like 11-subunit hydrogenase, which closes the evolutionary gap between the ancestral [NiFe] hydrogenases and the respiratory complex I and would enable members of TB2 to grow mixotrophically on H_2. All members of Bathy-6 are probably able to derive reducing equivalents from the oxidation of organic substrates (*viz.*, amino acids) and use reductive acetogenesis as an electron sink.

These findings agree with previous claims concerning the capacity for reductive acetogenesis in other subgroups of *Bathyarchaeia*. However, this is the first time that all genes encoding the Wood–Ljungdahl pathway and the components required for the provision of reducing equivalents and energy conservation are conclusively documented. Although eight of the nine closely related phylotypes of termite gut *Bathyarchaeia* were represented by high-quality MAGs, a complete pathway was detected only in members of TB2 and two more basal lineages from other environments. This underscores the long-standing caution that the mere presence of marker genes of the Wood–Ljungdahl pathway does not qualify an organism as an acetogen, as many of its enzymes are found also in nonacetogenic organisms, where they are involved in the assimilation and interconversion of C_1 metabolites (Drake, 1994).

EXPERIMENTAL PROCEDURES

Metagenome-Assembled Genomes

Data on the MAGs from termite guts are from Hervé et al. (2020). All other MAGs were retrieved from the NCBI Assembly database[1]; accession numbers are listed in **Table 1**. Assembly coverage was determined as described by Hervé et al. (2020). Average nucleotide acid identities (ANIs) were calculated with fastANI (Jain et al., 2018). Protein-coding genes were predicted with Prodigal v2.6.3 (Hyatt et al., 2010).

Genome Phylogeny

A concatenated gene tree of bathyarchaeotal MAGs was constructed using the deduced amino acid sequences of 43 marker genes extracted with CheckM v1.0.8 (Parks et al., 2015). The sequences were aligned using MAFFT v7.305b with the FFT-NS-2 method, and the resulting alignment was filtered using trimAL v1.2 with the gappyout method (Capella-Gutiérrez et al., 2009; Katoh and Standley, 2013). Tree topology was inferred with IQ-TREE (multicore v1.6.11; Nguyen et al., 2015) using the best-fit evolutionary model suggested by ModelFinder under the Bayesian Information Criterion (Kalyaanamoorthy et al., 2017); node support was assessed using the Shimodaira–Hasegawa approximate-likelihood-ratio test (SH-aLRT) with 1,000 resamplings (Anisimova et al., 2011).

Taxonomic classification was done with the GTDB-tk version 0.3.2 using the GTDB release 04-RS89 ([2]Chaumeil et al., 2018).

[1]https://www.ncbi.nlm.nih.gov

[2]https://gtdb.ecogenomic.org/

16S rRNA Gene Phylogeny

SSU rRNA gene sequences in the MAGs and other bathyarchaeotal bins obtained from the original metagenomes (Hervé et al., 2020) were identified using the *ssu_finder* function implemented in CheckM. Sequences were imported into the alignment of rRNA gene sequences in the SILVA SSURef NR database release 132 ([3]Quast et al., 2013) using Arb v6.0.6 (Ludwig et al., 2004). After automatic alignment of the imported sequences using the *PT server* and the *Fast Aligner* tool implemented in Arb, the alignment was manually refined using the Arb editor, considering secondary structure information to identify homologous base positions. After removing sites with more than 50% gaps, the alignment consisted of 1,424 sites with unambiguously aligned base positions. Phylogenetic trees were reconstructed by maximum-likelihood analysis with IQ-TREE using the best-fit evolutionary model (GTR+F+R4) suggested by ModelFinder; node support was assessed using SH-aLRT with 1,000 resamplings. Gene fragments (<1,300 bp) were inserted into the core tree using the *parsimony* tool implemented in Arb.

Gene Discovery and Annotation

For an initial exploration of the genes potentially involved in energy metabolism, bathyarchaeotal MAGs were analyzed using the annotation provided in the IMG/Mer database ([4]Chen et al., 2019). Annotation results were verified, and missing functions were identified with hidden Markov model (HMM) searches, using HMMER v3.1b2 (Eddy, 2011) with a threshold *E*-value of 1E–5; the respective models are listed in **Supplementary Table S3**. The identity of all genes of interest was confirmed using the NCBI Conserved Domain search (Marchler-Bauer and Bryant, 2004) and BLASTp (Altschul et al., 1990). Additionally, Bathy-6-S and Bathy-6-B were annotated with BlastKOALA (Kanehisa et al., 2016). When indicated, closest neighbors were identified by BLAST and aligned using MAFFT v7.305b with the L-INS-i method (Katoh and Standley, 2013). Phylogenetic trees were reconstructed by maximum-likelihood analysis with IQ-TREE (Nguyen et al., 2015) using the best-fit evolutionary model (LG+G+I) suggested by ModelFinder (Kalyaanamoorthy et al., 2017). Node support was assessed using SH-aLRT with 1,000 resamplings (Anisimova et al., 2011).

Analysis of [NiFe] Hydrogenases

Putative [NiFe] hydrogenase genes were identified by HMM searches (see above), using the highly resolved models provided by Anantharaman et al. (2016). Search results were confirmed with HydDB, a web-based tool for hydrogenase classification and analysis ([5]Søndergaard et al., 2016).

The deduced amino acid sequences of the large subunit (LSU) of [NiFe] hydrogenases recovered from the MAGs and their top BLAST hits on the IMG/Mer database were imported into an alignment of NuoD and FpoD homologs (Lang et al., 2015), which was completed with representative members of other hydrogenase classes extracted from HydDB. The alignment was manually refined in the Arb editor. Phylogenetic trees were reconstructed by maximum-likelihood analysis with IQ-TREE (Nguyen et al., 2015) using the best-fit evolutionary model (LG+G+I) suggested by ModelFinder (Kalyaanamoorthy et al., 2017). Node support was assessed using SH-aLRT with 1,000 resamplings (Anisimova et al., 2011).

[3]https://www.arb-silva.de

[4]https://img.jgi.doe.gov/mer/

[5]https://services.birc.au.dk/hyddb/

DATA AVAILABILITY STATEMENT

The original contributions presented in the study are included in the article/**Supplementary Material**, further inquiries can be directed to the corresponding author.

AUTHOR CONTRIBUTIONS

HL and AB designed the study. HL analyzed data and wrote the first draft of the manuscript. VH contributed to the analyses. AB analyzed data and revised the manuscript. All authors edited and approved the final version of the manuscript.

FUNDING

This study was funded by the Deutsche Forschungsgemeinschaft (DFG) in the Collaborative Research Centers SFB 987 and by the Max Planck Society. HL was supported by a doctoral fellowship of the International Max Planck Research School for Environmental, Cellular and Molecular Microbiology (IMPRS-Mic), Marburg, Germany.

ACKNOWLEDGMENTS

The authors thank the Joint Genome Institute for their metagenome sequencing service and for providing the IMG/ER platform.

SUPPLEMENTARY MATERIAL

The Supplementary Material for this article can be found online at: https://www.frontiersin.org/articles/10.3389/fmicb.2020.635786/full#supplementary-material

Supplementary Figure 1 | Average nucleotide identity (ANI) of the MAGs in subgroup Bathy-6. The termite gut *Bathyarchaeia* were assigned to phylotypes based on ANI > 99%. NA indicates ANI values <75%, which are not returned by the fastANI program.

Supplementary Figure 2 | Genome-based phylogeny of termite gut *Bathyarchaeia* illustrating the relationship of lineages TB1 and TB2 to other MAGs in the Bathy-6 subgroup. MAGs mentioned in the text are marked in bold. The maximum-likelihood tree was inferred from a concatenated alignment of 43 proteins using the LG+F+I+G4 model and rooted with selected Crenarchaeota and Euryarchaeota as outgroup. The numbers in circles indicate the phylotypes discussed in the text (**Table 1**). MAGs included in the comparative analysis (**Figure 3**) are shown in bold. The tree was rooted other archaeal genomes as outgroup. The scale bar indicates 10-amino-acid substitutions per site. Node support values (SH-aLRT) are shown in blue. A simplified version of the tree is shown in **Figure 1**.

Supplementary Figure 3 | 16S rRNA-based phylogeny of subgroup Bathy-6, indicating the placement of the sequences from termite guts among those obtained from other environments. The maximum-likelihood tree is based on a curated alignment (1,424 positions) of all sequences in the SILVA database and their homologs retrieved from the bathyarchaeal MAGs (in bold) and the low-quality bins obtained from the termite gut metagenomes (Hervé et al., 2020). The tree was rooted using members of Bathy-5 as outgroup. The scale bars indicate 0.05 nucleotide substitutions per site. Node support values (SH-aLRT) are shown in blue. Branches marked with dashed lines indicate shorter sequences that were added using the ARB parsimony tool. A simplified version of the tree is shown in **Figure 2**.

Supplementary Figure 4 | The methyltransferase-associated corrinoid protein (CoP) of Bathy-6 and its homologs. **(A)** The canonical methyltransferase system of bacteria and archaea. **(B)** Gene neighborhood of the CoP gene of Bathy-6 and selected homologs [for accession numbers, see panel **(C)**]. Colors indicate the presumed functions of the respective gene products **(A)**. Unrooted phylogenetic trees of the methyltransferase-associated CoP genes **(C)** and the associated *mtrH* genes **(D)** of Bathy-6 and their closest relatives (deduced amino acid sequences). Genes that appear in **(D)** are shown in bold. Numbers are IMG/Mer gene IDs. The scale bar indicates 1.0-amino-acid substitution per site. Node support values (SH-aLRT) are shown in blue.

Supplementary Figure 5 | Phylogenetic tree of the catalytic subunit of the Hox hydrogenase of Bathy-6 and its homologs among group 3 [NiFe] hydrogenases. The maximum-likelihood tree is based on deduced amino acid sequences and was rooted [NiFe] hydrogenase sequences of groups 1 and 2. The scale bar indicates 0.5 nucleotide substitutions per site. Node support values (SH-aLRT) are shown in blue.

Supplementary Table 1 | Taxonomic assignment and characteristics of the bathyarchaeotal MAGs from termite guts (from Hervé et al., 2020).

Supplementary Table 2 | Annotation details of the genes that encode the metabolic pathways and other functional markers in the 15 bathyarchaeotal MAGs from termite guts, as discussed in the text (see **Figures 3**, **4**).

REFERENCES

Altschul, S. F., Gish, W., Miller, W., Myers, E. W., and Lipman, D. J. (1990). Basic local alignment search tool. *J. Mol. Biol.* 215, 403–410.

Anantharaman, K., Brown, C. T., Hug, L. A., Sharon, I., Castelle, C. J., Probst, A. J., et al. (2016). Thousands of microbial genomes shed light on interconnected biogeochemical processes in an aquifer system. *Nat. Comm.* 7:13219.

Anisimova, M., Gil, M., Dufayard, J. F., Dessimoz, C., and Gascuel, O. (2011). Survey of branch support methods demonstrates accuracy, power, and robustness of fast likelihood-based approximation schemes. *Sys. Biol.* 60, 685–699. doi: 10.1093/sysbio/syr041

Arshad, A., Speth, D. R., de Graaf, R. M., Op, den Camp, H. J. M., Jetten, M. S. M., et al. (2015). A metagenomics-based metabolic model of nitrate-dependent anaerobic oxidation of methane by *Methanoperedens*-like archaea. *Front. Microbiol.* 6:1423. doi: 10.3389/fmicb.2015.01423

Basen, M., and Müller, V. (2017). "Hot" acetogenesis. *Extremophiles* 21, 15–26. doi: 10.1007/s00792-016-0873-3

Bignell, D. E., Oskarsson, H., and Anderson, J. M. (1980). Distribution and abundance of bacteria in the gut of a soil-feeding termite *Procubitermes aburiensis* (Termitidae, Termitinae). *J. Gen. Microbiol.* 117, 393–403. doi: 10.1099/00221287-117-2-393

Borrel, G., Parisot, N., Harris, H. M., Peyretaillade, E., Gaci, N., Tottey, W., et al. (2014). Comparative genomics highlights the unique biology of Methanomassiliicoccales, a Thermoplasmatales-related seventh order of methanogenic archaea that encodes pyrrolysine. *BMC Genomics* 15:679. doi: 10.1186/1471-2164-15-679

Bowers, R. M., Kyrpides, N. C., Stepanauskas, R., Harmon-Smith, M., Doud, D., Reddy, T. B. K., et al. (2017). Minimum information about a single amplified genome (MISAG) and a metagenome-assembled genome (MIMAG) of bacteria and archaea. *Nat. Biotech.* 35, 725–731.

Bräsen, C., Esser, D., Rauch, B., and Siebers, B. (2014). Carbohydrate metabolism in *Archaea*: current insights into unusual enzymes and pathways and their regulation. *Microbiol. Mol. Biol. Rev.* 78, 89–175. doi: 10.1128/MMBR.00041-13

Brauman, A., Dore, J., Eggleton, P., Bignell, D., Breznak, J. A., and Kane, M. D. (2001). Molecular phylogenetic profiling of prokaryotic communities in guts of termites with different feeding habits. *FEMS Microbiol. Ecol.* 35, 27–36. doi: 10.1111/j.1574-6941.2001.tb00785.x

Brauman, A., Kane, M. D., Labat, M., and Breznak, J. A. (1992). Genesis of acetate and methane by gut bacteria of nutritionally diverse termites. *Science* 257, 1384–1387. doi: 10.1126/science.257.5075.1384

Breznak, J. A., and Switzer, J. M. (1986). Acetate synthesis from H_2 plus CO_2 by termite gut microbes. *Appl. Environ. Microbiol.* 52, 623–630. doi: 10.1128/aem.52.4.623-630.1986

Brune, A. (2014). Symbiotic digestion of lignocellulose in termite guts. *Nat. Rev. Microbiol.* 12, 168–180. doi: 10.1038/nrmicro3182

Brune, A. (2019). "Methanogenesis in the digestive tracts of insects and other arthropods," in *Biogenesis of Hydrocarbons (Book series, Handbook of Hydrocarbon and Lipid Microbiology)*, eds A. J. M. Stams and D. Sousa (Cham: Springer), 229–260. doi: 10.1007/978-3-319-78108-2_13

Brune, A., and Dietrich, C. (2015). The gut microbiota of termites, Digesting the diversity in the light of ecology and evolution. *Annu. Rev. Microbiol.* 69, 145–166. doi: 10.1146/annurev-micro-092412-155715

Brune, A. (2018). "Methanogens in the digestive tract of termites," in *(Endo)symbiotic methanogenic archaea*, eds J. H. P. Hackstein (Cham: Springer International Publishing), 81–101. doi: 10.1007/978-3-642-13615-3_6

Brune, A., Miambi, E., and Breznak, J. A. (1995). Roles of oxygen and the intestinal microflora in the metabolism of lignin-derived phenylpropanoids and other monoaromatic compounds by termites. *Appl. Environ. Microbiol.* 61, 2688–2695. doi: 10.1128/aem.61.7.2688-2695.1995

Bucek, A., Šobotník, J., He, S., Shi, M., McMahon, D. P., Holmes, E. C., et al. (2019). Evolution of termite symbiosis informed by transcriptome-based phylogenies. *Curr. Biol.* 29:21.

Buckel, W., and Thauer, R. K. (2013). Energy conservation via electron bifurcating ferredoxin reduction and proton/Na^+ translocating ferredoxin oxidation. *Biochim. Biophys. Acta* 1827, 94–113. doi: 10.1016/j.bbabio.2012.07.002

Capella-Gutiérrez, S., Silla-Martínez, J. M., and Gabaldón, T. (2009). trimAl, a tool for automated alignment trimming in large-scale phylogenetic analyses. *Bioinformatics* 25, 1972–1973. doi: 10.1093/bioinformatics/btp348

Chaumeil, P. A., Mussig, A. J., Hugenholtz, P., and Parks, D. H. (2018). GTDB-Tk, a toolkit to classify genomes with the Genome Taxonomy Database. *Bioinformatics* 36, 1925–1927. doi: 10.1093/bioinformatics/btz848

Chen, I. A., Chu, K. P., Pillay, A. M., Ratner, J., Huang, M., et al. (2019). IMG/M v.5.0, an integrated data management and comparative analysis system for microbial genomes and microbiomes. *Nucleic Acids Res.* 47, D666–D677.

Collins, G., O'Connor, L., Mahony, T., Gieseke, A., de Beer, D., and O'Flaherty, V. (2005). Distribution, localization, and phylogeny of abundant populations of *Crenarchaeota* in anaerobic granular sludge. *Appl. Environ. Microbiol.* 71, 7523–7527. doi: 10.1128/aem.71.11.7523-7527.2005

Dombrowski, N., Seitz, K. W., Teske, A. P., and Baker, B. J. (2017). Genomic insights into potential interdependencies in microbial hydrocarbon and nutrient cycling in hydrothermal sediments. *Microbiome* 5:106. doi: 10.1186/s40168-017-0322-2

Drake, H. L. (1994). "Acetogenesis, acetogenic bacteria, and the acetyl-CoA 'Wood/Ljungdahl' pathway, past and current perspectives," in *Acetogenesis. Chapman & Hall Microbiology Series (Physiology / Ecology / Molecular Biology / Biotechnology)*, ed. H. L. Drake (Boston, MA: Springer).

Ebert, A., and Brune, A. (1997). Hydrogen concentration profiles at the oxic-anoxic interface: a microsensor study of the hindgut of the wood-feeding lower termite *Reticulitermes flavipes* (Kollar). *Appl. Environ. Microbiol.* 63, 4039–4046.

Eckert, C., Boehm, M., Carrieri, D., Yu, J., Dubini, A., Nixon, P. J., et al. (2012). Genetic analysis of the Hox hydrogenase in the cyanobacterium *Synechocystis sp.* PCC 6803 reveals subunit roles in association, assembly, maturation, and function. *J. Biol. Chem.* 287, 43502–43515. doi: 10.1074/jbc.m112.392407

Eddy, S. R. (2011). Accelerated profile HMM searches. *PLoS Comput. Biol.* 7:e1002195. doi: 10.1371/journal.pcbi.1002195

Evans, P. N., Parks, D. H., Chadwick, G. L., Robbins, S. J., Orphan, V. J., Golding, S. D., et al. (2015). Methane metabolism in the archaeal phylum Bathyarchaeota revealed by genome-centric metagenomics. *Science* 350, 434–438. doi: 10.1126/science.aac7745

Farag, I. F., Biddle, J. F., Zhao, R., Martino, A. J., House, C. H., and León-Zayas, R. I. (2020). Metabolic potentials of archaeal lineages resolved from metagenomes of deep Costa Rica sediments. *ISME J.* 14, 1345–1358. doi: 10.1038/s41396-020-0615-5

Feldewert, C., Lang, K., and Brune, A. (2020). The hydrogen threshold of obligately methyl-reducing methanogens. *FEMS Microbiol. Lett.* 367:fnaa137.

Feng, X., Wang, Y., Zubin, R., and Wang, F. (2019). Core Metabolic Features and Hot Origin of Bathyarchaeota. *Engineering* 5, 498–504. doi: 10.1016/j.eng.2019.01.011

Fillol, M., Auguet, J., Casamayor, E. O., and Borrego, C. M. (2016). Insights in the ecology and evolutionary history of the Miscellaneous Crenarchaeotic Group lineage. *ISME J.* 10, 665–677. doi: 10.1038/ismej.2015.143

Friedrich, M. W., Schmitt-Wagner, D., Lueders, T., and Brune, A. (2001). Axial differences in community structure of Crenarchaeota and Euryarchaeota in the highly compartmentalized gut of the soil-feeding termite *Cubitermes orthognathus*. *Appl. Environ. Microbiol.* 67, 4880–4890. doi: 10.1128/aem.67.10.4880-4890.2001

Friedrich, T., and Scheide, D. (2000). The respiratory complex I of bacteria, archaea and eukarya and its module common with membrane-bound multisubunit hydrogenases. *FEBS Lett.* 479, 1–5.

Galagan, J. E., Nusbaum, C., Roy, A., Endrizzi, M. G., Macdonald, P., FitzHugh, W., et al. (2002). The genome of *M. acetivorans* reveals extensive metabolic and physiological diversity. *Genome Res.* 12, 532–542. doi: 10.1101/gr.223902

Ghebreamlak, S. M., and Mansoorabadi, S. O. (2020). Divergent members of the nitrogenase superfamily, tetrapyrrole biosynthesis and beyond. *ChemBioChem* 21, 1723–1728. doi: 10.1002/cbic.201900782

Godon, J.-J., Zumstein, E., Dabert, P., Habouzit, F., and Moletta, R. (1997). Molecular microbial diversity of an anaerobic digestor as determined by small-subunit rDNA sequence analysis. *Appl. Environ. Microbiol.* 63, 2802–2813. doi: 10.1128/aem.63.7.2802-2813.1997

Greening, C., Biswas, A., Carere, C., Jackson, C. J., Taylor, M. C., Stott, M. B., et al. (2016). Genomic and metagenomic surveys of hydrogenase distribution indicate H2 is a widely utilised energy source for microbial growth and survival. *ISME J.* 10, 761–777. doi: 10.1038/ismej.2015.153

Grieco, M. B., Lopes, F. A. C., Oliveira, L. S., Tschoeke, D. A., Popov, C. C., Thompson, C. C., et al. (2019). Metagenomic analysis of the whole gut microbiota in Brazilian Termitidae termites *Cornitermes cumulans, Cyrilliotermes strictinasus, Syntermes dirus, Nasutitermes jaraguae, Nasutitermes aquilinus, Grigiotermes bequaerti, and Orthognathotermes mirim*. *Curr. Microbiol.* 76, 687–697. doi: 10.1007/s00284-019-01662-3

Griffiths, B. S., Bracewell, J. M., Robertson, G. W., and Bignell, D. E. (2012). Pyrolysis–mass spectrometry confirms enrichment of lignin in the faeces of a wood-feeding termite, *Zootermopsis nevadensis* and depletion of peptides in a soil-feeder, *Cubitermes ugandensis*. *Soil Biol. Biochem.* 57, 957–959. doi: 10.1016/j.soilbio.2012.08.012

Gutekunst, K., Chen, X., Schreiber, K., Kaspar, U., Makam, S., and Appel, J. (2014). The bidirectional NiFe-hydrogenase in *Synechocystis sp.* PCC 6803 is reduced by flavodoxin and ferredoxin and is essential under mixotrophic, nitrate-limiting conditions. *J. Biol. Chem.* 289, 1930–1937. doi: 10.1074/jbc.m113.526376

Harris, R. L., Lau, M. C. Y., Cadar, A., Bartlett, D. H., Cason, E., van Heerden, E., et al. (2018). Draft genome sequence of "*Candidatus* Bathyarchaeota" archaeon BE326-BA-RLH, an uncultured denitrifier and putative anaerobic methanotroph from South Africa's deep continental biosphere. *Microbiol. Resour. Announc.* 7, 1295–e1218.

He, Y., Li, M., Perumal, V., Feng, X., Fang, J., Xie, J., et al. (2016). Genomic and enzymatic evidence for acetogenesis among multiple lineages of the archaeal phylum Bathyarchaeota widespread in marine sediments. *Nat. Microbiol.* 1:16035.

Heider, J., Mai, X., and Adams, M. W. (1996). Characterization of 2-ketoisovalerate ferredoxin oxidoreductase, a new and reversible coenzyme A-dependent enzyme involved in peptide fermentation by hyperthermophilic archaea. *J. Bacteriol.* 178, 780–787. doi: 10.1128/jb.178.3.780-787.1996

Herlemann, D. P. R., Geissinger, O., Ikeda-Ohtsubo, W., Kunin, V., Sun, H., Lapidus, A., et al. (2009). Genomic analysis of "*Elusimicrobium minutum*," the first cultivated representative of the phylum "*Elusimicrobia*" (formerly termite group 1). *Appl. Environ. Microbiol.* 75, 2841–2849. doi: 10.1128/aem.02698-08

Hervé, V., Liu, P., Dietrich, C., Sillam-Dussès, D., Stiblik, P., Šobotník, J., et al. (2020). Phylogenomic analysis of 589 metagenome-assembled genomes encompassing all major prokaryotic lineages from the gut of higher termites. *PeerJ.* 8:e8614. doi: 10.7717/peerj.8614

Hippler, B., and Thauer, R. K. (1999). The energy conserving methyltetrahydromethanopterin:coenzyme M methyltransferase complex from methanogenic archaea, function of the subunit MtrH. *FEBS Lett.* 449, 165–168. doi: 10.1016/s0014-5793(99)00429-9

Hochheimer, A., Linder, D., Thauer, R. K., and Hedderich, R. (1996). The molybdenum formylmethanofuran dehydrogenase operon and the tungsten formylmethanofuran dehydrogenase operon from *Methanobacterium thermoautotrophicum*. Structures and transcriptional regulation. *Eur. J. Biochem.* 242, 156–162. doi: 10.1111/j.1432-1033.1996.0156r.x

Hyatt, D., Chen, G., Locascio, P. F., Land, M. L., Larimer, F. W., and Hauser, L. J. (2010). Prodigal, prokaryotic gene recognition and translation initiation site identification. *BMC Bioinfo.* 11, 119–119. doi: 10.1186/1471-2105-11-119

Ikeda-Ohtsubo, W., Strassert, J. F. H., Köhler, T., Mikaelyan, A., Gregor, I., McHardy, A. C., et al. (2016). '*Candidatus* Adiutrix intracellularis', an endosymbiont of termite gut flagellates, is the first representative of a deep-branching clade of *Deltaproteobacteria* and a putative homoacetogen. *Environ. Microbiol.* 18, 2548–2564. doi: 10.1111/1462-2920.13234

Inagaki, F., Suzuki, M., Takai, K., Oida, H., Sakamoto, T., Aoki, K., et al. (2003). Microbial communities associated with geological horizons in coastal subseafloor sediments from the sea of Okhotsk. *Appl. Environ. Microbiol.* 69, 7224–7235. doi: 10.1128/aem.69.12.7224-7235.2003

Jain, C., Rodriguez-R, L. M., Phillippy, A. M., Konstantinidis, K. T., and Aluru, S. (2018). High throughput ANI analysis of 90K prokaryotic genomes reveals clear species boundaries. *Nat. Comm.* 9:5114.

Ji, R., and Brune, A. (2006). Nitrogen mineralization, ammonia accumulation, and emission of gaseous NH_3 by soil-feeding termites. *Biogeochemistry* 78, 267–283. doi: 10.1007/s10533-005-4279-z

Kalyaanamoorthy, S., Minh, B. Q., Wong, T. K. F., von Haeseler, A., and Jermiin, L. S. (2017). ModelFinder, fast model selection for accurate phylogenetic estimates. *Nat. Methods* 14, 587–589. doi: 10.1038/nmeth.4285

Kanehisa, M., Sato, Y., and Morishima, K. (2016). BlastKOALA and GhostKOALA, KEGG tools for functional characterization of genome and metagenome sequences. *J. Mol. Biol.* 428, 726–731. doi: 10.1016/j.jmb.2015.11.006

Kaster, A., Moll, J., Parey, K., and Thauer, R. K. (2011). Coupling of ferredoxin and heterodisulfide reduction via electron bifurcation in hydrogenotrophic methanogenic archaea. *Proc. Natl. Acad. Sci.* 108, 2981–2986. doi: 10.1073/pnas.1016761108

Katoh, K., and Standley, D. M. (2013). MAFFT multiple sequence alignment software version 7, improvements in performance and usability. *Mol. Biol. Evol.* 30, 772–780. doi: 10.1093/molbev/mst010

Kengen, S. W. M., and Stams, A. J. M. (1993). Formation of L-alanine as a reduced end product in carbohydrate fermentation by the hyperthermophilic archaeon *Pyrococcus furiosus*. *Arch. Microbiol.* 161, 168–175. doi: 10.1007/s002030050038

Kovoor, J. (1967). Etude radiographique du transit intestinal chez un termite supérieur. *Experientia* 23, 820–821. doi: 10.1007/BF02146863

Kreft, J.-U., and Schink, B. (1994). O-demethylation by the homoacetogenic anaerobe *Holophaga foetida* studied by a new photometric methylation assay using electrochemically produced cob(I)alamin. *Eur. J. Biochem.* 226, 945–951. doi: 10.1111/j.1432-1033.1994.00945.x

Kremp, F., and Müller, V. (2020). Methanol and methyl group conversion in acetogenic bacteria, Biochemistry, physiology and application. *FEMS Microbiol. Rev.* 2020:fuaa040. doi: 10.1093/femsre/fuaa040

Kremp, F., Poehlein, A., Daniel, R., and Müller, V. (2018). Methanol metabolism in the acetogenic bacterium *Acetobacterium woodii*. *Environ. Microbiol.* 20, 4369–4384. doi: 10.1111/1462-2920.14356

Kröninger, L., Berger, S., Welte, C., and Deppenmeier, U. (2016). Evidence for the involvement of two heterodisulfide reductases in the energy−conserving system of *Methanomassiliicoccus luminyensis*. *FEBS J.* 283, 472–483. doi: 10.1111/febs.13594

Kröninger, L., Gottschling, J., and Deppenmeier, U. (2017). Growth characteristics of *Methanomassiliicoccus luminyensis* and expression of methyltransferase encoding genes. *Archaea* 2017:2756573. doi: 10.1155/2017/2756573

Kubo, K., Lloyd, K. G., Biddle, J. F., Amann, R., Teske, A., and Knittel, K. (2012). Archaea of the Miscellaneous Crenarchaeotal Group are abundant, diverse and widespread in marine sediments. *ISME J.* 6, 1949–1965. doi: 10.1038/ismej.2012.37

Künkel, A., Vorholt, J. A., Thauer, R. K., and Hedderich, R. (1998). An *Escherichia coli* hydrogenase−3−type hydrogenase in methanogenic archaea. *Eur. J. Biochem.* 252, 467–476. doi: 10.1046/j.1432-1327.1998.2520467.x

Lang, K., Schuldes, J., Klingl, A., Poehlein, A., Daniel, R., and Brune, A. (2015). New mode of energy metabolism in the seventh order of methanogens as revealed by comparative genome analysis of "*Candidatus* Methanoplasma termitum". *Appl. Environ. Microbiol.* 81, 1338–1352. doi: 10.1128/aem.03389-14

Lazar, C. S., Baker, B. J., Seitz, K., Hyde, A. S., Dick, G. J., Hinrichs, K., et al. (2016). Genomic evidence for distinct carbon substrate preferences and ecological niches of Bathyarchaeota in estuarine sediments. *Environ. Microbiol.* 18, 1200–1211. doi: 10.1111/1462-2920.13142

Leadbetter, J. R., Schmidt, T. M., Graber, J. R., and Breznak, J. A. (1999). Acetogenesis from H_2 Plus CO_2 by Spirochetes from Termite Guts. *Science* 283, 686–689. doi: 10.1126/science.283.5402.686

Lee, M. J., and Zinder, S. H. (1988). Isolation and characterization of a thermophilic bacterium which oxidizes acetate in syntrophic association with a methanogen and which grows acetogenically on H_2-CO_2. *Appl. Environ. Microbiol.* 54, 124–129. doi: 10.1128/aem.54.1.124-129.1988

Lever, M. A., Heuer, V. B., Morono, Y., Masui, N., Schmidt, F., Alperin, M. J., et al. (2010). Acetogenesis in deep subseafloor sediments of the Juan de Fuca ridge flank, a synthesis of geochemical, thermodynamic, and gene-based evidence. *Geomicrobiol. J.* 27, 183–211. doi: 10.1080/01490450903456681

Ludwig, W., Strunk, O., Westram, R., Richter, L., and Meier, H. (2004). ARB, a software environment for sequence data. *Nucleic Acids Res.* 32, 1363–1371. doi: 10.1093/nar/gkh293

Mai, X., and Adams, M. W. (1996). Purification and characterization of two reversible and ADP-dependent acetyl coenzyme A synthetases from the hyperthermophilic archaeon *Pyrococcus furiosus*. *J. Bacteriol.* 178, 5897–5903. doi: 10.1128/jb.178.20.5897-5903.1996

Marchler-Bauer, A., and Bryant, S. H. (2004). CD-Search, protein domain annotations on the fly. *Nucleic Acids Res.* 32, W327–W331.

Meng, J., Xu, J., Qin, D., He, Y., Xiao, X., and Wang, F. (2014). Genetic and functional properties of uncultivated MCG archaea assessed by metagenome and gene expression analyses. *ISME J.* 8, 650–659. doi: 10.1038/ismej.2013.174

Mikaelyan, A., Meuser, K., and Brune, A. (2016). Microenvironmental heterogeneity of gut compartments drives bacterial community structure in wood- and humus-feeding higher termites. *FEMS Microbiol. Ecol.* 93:fiw210. doi: 10.1093/femsec/fiw210

Moparthi, V. K., and Hägerhäll, C. (2011). The evolution of respiratory chain complex I from a smaller last common ancestor consisting of 11 protein subunits. *J. Mol. Evol.* 72, 484–497. doi: 10.1007/s00239-011-9447-2

Musfeldt, M., Selig, M., and Schönheit, P. (1999). Acetyl coenzyme A synthetase (ADP forming) from the hyperthermophilic archaeon *Pyrococcus furiosus*, identification, cloning, separate expression of the encoding genes, *acdAI* and *acdBI*, in *Escherichia coli*, and in vitro reconstitution of the active heterotetrameric enzyme from its recombinant subunits. *J. Bacteriol.* 181, 5885–5888. doi: 10.1128/jb.181.18.5885-5888.1999

Nelson, W. C., Tully, B. J., and Mobberley, J. M. (2020). Biases in genome reconstruction from metagenomic data. *PeerJ.* 8:e10119. doi: 10.7717/peerj.10119

Ngugi, D. K., Ji, R., and Brune, A. (2011). _Nitrogen mineralization, denitrification, and nitrate ammonification by soil-feeding termites, a ^{15}N-based approach. *Biogeochemistry* 103, 355–369. doi: 10.1007/s10533-010-9478-6

Nguyen, L., Schmidt, H. A., von Haeseler, A., and Minh, B. Q. (2015). IQ-TREE, A fast and effective stochastic algorithm for estimating maximum-likelihood phylogenies. *Mol. Biol. Evol.* 32, 268–274. doi: 10.1093/molbev/msu300

Ochsenreiter, T., Selezi, D., Quaiser, A., Bonch-Osmolovskaya, L., and Schleper, C. (2003). Diversity and abundance of Crenarchaeota in terrestrial habitats studied by 16S RNA surveys and real time PCR. *Environ. Microbiol.* 5, 787–797. doi: 10.1046/j.1462-2920.2003.00476.x

Ohkuma, M., Noda, S., Hattori, S., Iida, T., Yuki, M., Starns, D., et al. (2015). Acetogenesis from H_2 plus CO_2 and nitrogen fixation by an endosymbiotic spirochete of a termite-gut cellulolytic protist. *Proc. Natl. Acad. Sci.* 112, 10224–10230. doi: 10.1073/pnas.1423979112

Ottesen, E. A., and Leadbetter, J. R. (2011). Formyltetrahydrofolate synthetase gene diversity in the guts of higher termites with different diets and lifestyles. *Appl. Environ. Microbiol.* 77, 3461–3467. doi: 10.1128/aem.02657-10

Parks, D. H., Imelfort, M., Skennerton, C. T., Hugenholtz, P., and Tyson, G. W. (2015). CheckM, assessing the quality of microbial genomes recovered from isolates, single cells, and metagenomes. *Genome Res.* 25, 1043–1055. doi: 10.1101/gr.186072.114

Quast, C., Pruesse, E., Yilmaz, P., Gerken, J., Schweer, T., Yarza, P., et al. (2013). The SILVA ribosomal RNA gene database project, improved data processing and web-based tools. *Nucleic Acids Res.* 41, D590–D596.

Rinke, C., Chuvochina, M., Mussig, A. J., Chaumeil, P., Waite, D. W., Whitman, W. B., et al. (2020). A rank-normalized archaeal taxonomy based on genome phylogeny resolves widespread incomplete and uneven classifications. *bioRxiv [Preprint]*. Available online at: https://doi.org/10.1101/2020.03.01.972265 (accessed on March 10, 2020).

Rosenthal, A. Z., Zhang, X., Lucey, K. S., Ottesen, E. A., Trivedi, V., Choi, H. M. T., et al. (2013). Localizing transcripts to single cells suggests an important role of uncultured deltaproteobacteria in the termite gut hydrogen economy. *Proc. Natl. Acad. Sci. USA* 110, 16163–16168. doi: 10.1073/pnas.1307876110

Schink, B. (1994). "Diversity, ecology, and isolation of acetogenic bacteria," in *Acetogenesis. Chapman & Hall Microbiology Series (Physiology / Ecology / Molecular Biology / Biotechnology)*, ed. H. L. Drake (Boston, MA: Springer).

Schink, B., Brune, A., Schnell, S., and Winkelmann, G. (eds) (1992). "Anaerobic degradation of aromatic compounds," in *Microbial Degradation of Natural Products* (VCH Verlagsgesellschaft: Weinheim), s219–s242.

Schleper, C., Holben, W., and Klenk, H. P. (1997). Recovery of crenarchaeotal ribosomal DNA sequences from freshwater-lake sediments. *Appl Environ Microbiol* 63, 321–323. doi: 10.1128/aem.63.1.321-323.1997

Schmitt-Wagner, D., and Brune, A. (1999). Hydrogen profiles and localization of methanogenic activities in the highly compartmentalized hindgut of soil-feeding higher termites (*Cubitermes* spp.). *Appl. Environ. Microbiol.* 65, 4490–4496. doi: 10.1128/AEM.65.10.4490-4496.1999

Schnürer, A., Svensson, B. H., and Schink, B. (1997). Enzyme activities in and energetics of acetate metabolism by the mesophilic syntrophically acetate-oxidizing anaerobe *Clostridium ultunense*. *FEMS Microbiol. Lett.* 154, 331–336. doi: 10.1111/j.1574-6968.1997.tb12664.x

Schoelmerich, M. C., and Müller, V. (2019). Energy-converting hydrogenases, the link between H_2 metabolism and energy conservation. *Cell Mol. Life Sci.* 77, 1461–1481. doi: 10.1007/s00018-019-03329-5

Schuchmann, K., and Müller, V. (2012). A bacterial electron-bifurcating hydrogenase. *J. Biol. Chem.* 287, 31165–31171. doi: 10.1074/jbc.m112.395038

Schuchmann, K., and Müller, V. (2014). Autotrophy at the thermodynamic limit of life, a model for energy conservation in acetogenic bacteria. *Nat. Rev. Microbiol.* 12, 809–821. doi: 10.1038/nrmicro3365

Schut, G. J., and Adams, M. W. W. (2009). The iron-hydrogenase of *Thermotoga maritima* utilizes ferredoxin and NADH synergistically, a new perspective on anaerobic hydrogen production. *J. Bacteriol.* 191, 4451–4457. doi: 10.1128/jb.01582-08

Seyler, L. M., McGuinness, L. M., and Kerkhof, L. J. (2014). Crenarchaeal heterotrophy in salt marsh sediments. *ISME J.* 8, 1534–1543. doi: 10.1038/ismej.2014.15

Shi, Y., Huang, Z., Han, S., Fan, S., and Yang, H. (2015). Phylogenetic diversity of Archaea in the intestinal tract of termites from different lineages. *J. Basic Microb.* 55, 1021–1028. doi: 10.1002/jobm.201400678

Søndergaard, D., Pedersen, C. N. S., and Greening, C. (2016). HydDB, A web tool for hydrogenase classification and analysis. *Sci. Rep.* 6:34212.

Tersteegen, A., and Hedderich, R. (1999). *Methanobacterium thermoautotrophicum* encodes two multisubunit membrane−bound [NiFe] hydrogenases. *Eur. J. Biochem.* 264, 930–943. doi: 10.1046/j.1432-1327.1999.00692.x

Thauer, R. K., Kaster, A.-K., Seedorf, H., Buckel, W., and Hedderich, R. (2008). Methanogenic archaea, ecologically relevant differences in energy conservation. *Nat. Rev. Microbiol.* 6, 579–591. doi: 10.1038/nrmicro1931

Tholen, A., and Brune, A. (1999). Localization and in situ activities of homoacetogenic bacteria in the highly compartmentalized hindgut of soil-feeding higher termites (*Cubitermes* spp.). *Appl. Environ. Microbiol.* 65, 4497–4505. doi: 10.1128/aem.65.10.4497-4505.1999

Tholen, A., and Brune, A. (2000). Impact of oxygen on metabolic fluxes and *in situ* rates of reductive acetogenesis in the hindgut of the wood-feeding termite *Reticulitermes flavipes*. *Environ. Microbiol.* 2, 436–449. doi: 10.1046/j.1462-2920.2000.00127.x

van der Meijden, P., Heythuysen, H. J., Pouwels, A., et al. (1983). Methyltransferases involved in methanol conversion by *Methanosarcina barkeri*. *Arch. Microbiol.* 134, 238–242. doi: 10.1007/bf00407765

Vanwonterghem, I., Evans, P., Parks, D., Jensen, P. D., Woodcroft, B. J., Hugenholtz, P., et al. (2016). Methylotrophic methanogenesis discovered in the archaeal phylum Verstraetearchaeota. *Nat. Microbiol.* 1:16170. doi: 10.1038/nmicrobiol.2016.170

Vignais, P. M., and Billoud, B. (2007). Occurrence, classification, and biological function of hydrogenases: an overview. *Chem. Rev.* 107, 4206–4272. doi: 10.1021/cr050196r

Vorholt, J. A., Vaupel, M., and Thauer, R. K. (1996). A polyferredoxin with eight [4Fe–4S] clusters as a subunit of molybdenum formylmethanofuran dehydrogenase from *Methanosarcina barkeri*. *Eur. J. Biochem.* 236, 309–317. doi: 10.1111/j.1432-1033.1996.t01-1-00309.x

Welte, C., and Deppenmeier, U. (2011). Membrane-bound electron transport in *Methanosaeta thermophila*. *J. Bacteriol.* 193, 2868–2870. doi: 10.1128/jb.00162-11

Westphal, L., Wiechmann, A., Baker, J., Minton, N. P., and Müller, V. (2018). The Rnf complex is an energy-coupled transhydrogenase essential to reversibly link cellular NADH and ferredoxin pools in the acetogen *Acetobacterium woodii*. *J. Bacteriol.* 200, 357–e318.

Xiang, X., Wang, R., Wang, H., Gong, L., Man, B., and Xu, Y. (2017). Distribution of Bathyarchaeota communities across different terrestrial settings and their potential ecological functions. *Sci. Rep.* 7: 45028.

Yu, H., Wu, C.-H., Schut, G. J., Haja, D. K., Zhao, G., Peters, J. W., et al. (2018). Structure of an ancient respiratory system. *Cell* 173, 1636–1649 e16.

Yu, T., Wu, W., Liang, W., Lever, M. A., Hinrichs, K., and Wang, F. (2018). Growth of sedimentary Bathyarchaeota on lignin as an energy source. *Proc. Natl. Acad. Sci.* 115, 6022–6027.

Zhou, Z., Pan, J., Wang, F., Gu, J., and Li, M. (2018). Bathyarchaeota, globally distributed metabolic generalists in anoxic environments. *FEMS Microbiol. Rev.* 42, 639–655. doi: 10.1093/femsre/fuy023

Conflict of Interest: The authors declare that the research was conducted in the absence of any commercial or financial relationships that could be construed as a potential conflict of interest.

Frontiers in Microbiology

Explores the habitable world and the potential of microbial life

The largest and most cited microbiology journal which advances our understanding of the role microbes play in addressing global challenges such as healthcare, food security, and climate change.

Discover the latest Research Topics

See more →

Frontiers

Avenue du Tribunal-Fédéral 34
1005 Lausanne, Switzerland
frontiersin.org

Contact us

+41 (0)21 510 17 00
frontiersin.org/about/contact